# SIMULATION OF TURBOCHARGED DIESEL ENGINES UNDER TRANSIENT CONDITIONS

By:

MAGED MARZOUK ABDEL-HAMID

Thesis submitted for the degree of
Doctor of Phil osophy in the
University of London

Department of Mechanical Engineering,
Imperial College of Science and Technology,
London S.W.7.

May, 1976.

## ACKNOWLEDGEMENTS

The author wishes to express his sincere thanks to Dr. N. Watson for his advice and kind encouragement while supervising this work.

Thanks are also due to Mr. R.D. Bloxham and the technical staff of the Thermal Power Section for constructing the test facility.

The author gratefully acknowledges the financial support received from the Military Vehicle and Engineering Establishment.

## ABSTRACT

A non-linear digital simulation of turbocharged diesel engines has been developed to predict transient performance. The mathematical model divides the engine into the following component systems: engine thermo-fluid dynamics, turbine, compressor, engine-load dynamics, turbocharger dynamics, governor and fuel injection system.

The quasi-steady "filling and emptying" approach is employed to describe gas flow and changes in thermodynamic conditions. The turbocharger is also treated on a quasi-steady basis, with the aid of steady state performance characteristics. By applying conservation laws (energy, mass and angular momentum) and the ideal gas equation, a set of coupled ordinary differential equations is obtained in the form of an initial value problem. Governing equations are numerically integrated in a simultaneous manner along equal crankangle increments.

The model of the combustion process is based on the fuel burning rate approach. Experimental burning rate curves are correlated to ignition delay, engine speed, and equivalence ratio. Thermodynamic and chemical equilibrium is assumed to govern heat liberation during conditions of over-rich fuel/air mixtures (encountered during transient operation). Ignition delay is related to temperature and pressure of the cylinder charge. Injection delay is taken as the duration of propagation of a pressure wave along the fuel pipe.

Heat transfer to the cylinder walls is evaluated from wall surface and instantaneous gas temperatures; wall temperature being determined from a one-dimensional heat conduction model. The calculation of gas flow through the

valves takes account of instantaneous values of flow area and pressure difference. Friction torque is computed as a function of engine speed and maximum cylinder pressure.

An extensive experimental programme has been carried out to obtain steady state and transient data. A computer-controlled test bed, instrumentation, data-acquisition hardware and software have been developed for this purpose.

Comparisons of experimental and predicted results show favourable agreement; in most cases within the accuracy of the measurements and the component characteristics of the engine system.

Effects of certain parametric variations on transient response are predicted and discussed. It is concluded that the simulation can be useful as a research and development tool, particularly in studying the feasibility of design options aimed at improving transient performance.

*This thesis is to be presented as a final report to the Military Vehicle and Engineering Establishment. Several classified progress reports have already been submitted.*

# LIST OF CONTENTS

# NOTATION

## Symbols

Aeg : effective liner area.

Ag : geometric flow area.

$A_i$ : heat transfer area (surface no. i).

$A_{\ell,i}$ : liner area exposed to gases (liner no. i).

$A_{v,n}$ : flow area for valve no. n.

C1,C2...C6 : constants.

$C_c$ : compressor torque.

$C_d$ : coefficient of discharge.

cd1,cd2 : shape factors for diffusion burning rate distribution.

$C_e$ : engine indicated torque.

$C_f$ : engine friction torque.

$C_L$ : load torque.

cp1,cp2 : shape factors for premixed burning rate distribution.

$C_t$ : turbine torque.

d : cylinder diameter.

e : specific internal energy.

$\dot{E}_{fr}$ : piston friction power added at piston liner interface.

f : fuel/air ratio.

$f_s$ : stoichiometric fuel/air ratio.

F : equivalence ratio ($F = f/f_s$).

$F_t$ : overall equivalence ratio of cylinder contents.

$FBR_t$,$FBR_p$,$FBR_d$: fuel burning rates; total, premixed and diffusion respectively.

$h_{eg}$ : effective heat transfer coefficient.

$h_i$ : instantaneous heat transfer coefficient; surface no. i.

$h_j$ : specific enthalpy; flow passing through section no. j.

ID : ignition delay.

$J_e$ : engine polar moment of inertia.

$J_L$ : load polar moment of inertia.

$J_{tc}$ : turbocharger polar moment of inertia.

$k_s$ : equivalent linear stiffness of governor spring.

$k$ : torsional stiffness.

$\ell$ : connecting rod length.

$\dot{m}_c$ : compressor mass flow rate.

$\dot{m}_f$ : mass flow rate of fuel.

$\dot{m}_{fa}$ : turbine mass flow at full admission.

$\dot{m}_i$ : mass flow rate through turbine sector no. i.

$\dot{m}_j$ : mass flow rate through section no. j.

$\dot{m}_t$ : total mass flow through turbine.

$M$ : mass.

$M_f$ : mass of fuel.

$M_{tr}$ : mass trapped inside cylinder at closure of inlet valve.

$M_{f,t}, M_{f,p}, M_{f,d}$ : total mass of fuel injected and mass of fuel burnt via premixed and diffusion combustion respectively.

$P$ : pressure.

$P_{amb}$ : ambient pressure.

$P_d$ : downstream pressure.

$P_i$ : turbine power; sector no. i.

$P_{max}$ : maximum cylinder pressure.

$P_t$ : total turbine power.

$P_u$ : upstream pressure.

$\dot{Q}$ : rate of heat transfer.

$r$ : crank radius.

$R$ : gas constant.

$R_1, R_2, R_3$ : thermal resistance of the individual heat paths in the conduction model.

$R_u$ : upstream gas constant.

$t$ : time.

$T$ : temperature.

$T_{amb}$ : ambient temperature.

$T_{co}$ : oil temperature.

$T_{cw}$ : cooling water temperature.

$T_{eg}$ : effective gas temperature.

$T_{g}$ : gas temperature.

$T_{hg}, T_{pg}, T_{\ell g}$ : gas exposed, surface temperatures for cylinder head, piston and liner respectively.

$T_{u}$ : upstream temperature.

$T_{w}$ : instantaneous cylinder wall temperature.

$T_{w_{c=0}}$ : hypothetical cylinder wall temperature if thermal capacity is zero.

$u$ : peripheral blade speed for turbine, or liner speed of fuel rack.

$V$ : volume.

$\dot{V}$ : rate of change of volume with respect to time.

$x$ : position of fuel rack in relation to $X_r$.

$X_r$ : reference position of fuel rack.

$y$ : change of governor setting in relation to $Y_r$.

$Y_r$ : reference position of governor set point.

$\alpha$ : thermal time constant for cylinder walls.

$\beta$ : mode of burning proportionality factor; $\beta = \frac{M_{f,p}}{M_{f,t}}$.

$\gamma$ : specific heat ratio.

$\theta$ : crankangle referred to the TDC preceding the expansion stroke in cylinder no. 1.

$\theta_{di}$ : crankangle at dynamic injection.

$\theta_{e}$ : crankangle at the end of burning.

$\theta_{i}$ or $\theta_{ig}$ : crankangle at ignition.

$\theta_{L}$ : angular position of load shaft in relation to the TDC preceding the expansion stroke in cylinder no. 1.

$\theta_{si}$ : crankangle at static injection (nominal injection timing).

$\omega_{n}$ : natural frequency.

$\Omega_{e}$ : angular speed of crank shaft.

$\Omega_{L}$ : angular speed of load shaft.

$\Omega_{tc}$ : angular speed of turbocharger shaft.

$\eta_t$ : turbine efficiency.

$\eta_c$ : compressor efficiency.

$\eta_{tc}$ : turbocharger efficiency.

$\pi$ : 22/7.

$\tau$ : normalised crank angle; $\tau = \frac{\theta - \theta_i}{\theta_e - \theta_i}$.

$\nu$ : u/c turbine blade speed ratio.

$\lambda$ : power input factor (compressor).

$\Delta t$ : injection delay.

$\varepsilon_k$ : accuracy tolerance for numerical iteration.

$\sigma_{(I,J)}$ : standard deviation of variable no. I at crank position no. J.

$\sigma$ : slip factor (compressor).

Abbreviations

A/F : air/fuel ratio.

BDC : bottom dead centre.

BMEP : brake mean effective pressure.

BSAC : brake specific air consumption.

BSFC : brake specific fuel consumption.

IMEP : indicated mean effective pressure.

ISAC : indicated specific air consumption.

ISFC : indicated specific fuel consumption.

MBPF : mode of burning proportionality factor.

nc : total number of cylinders.

TDC: top dead centre.

$var_n(I,J)$ : variable no. I recorded at crank position J, cycle no. N.

$VAR_N(I,J)$ : summation of var(I,J) for N engine cycles.

* Symbols not included above are defined in the text.

** SI units are employed unless otherwise stated.

# CHAPTER 1

# INTRODUCTION

## 1.1 INTRODUCTION AND OBJECTIVES

Present trends indicate that further development of the diesel engine is largely dependent on its association with an exhaust driven turbocharger. Turbocharged diesel engines are now widely used in almost the entire field of operation in which the naturally aspirated engine was once supreme. This relatively recent conversion was inevitable once the merits of turbocharging had been established; a large increase in specific output coupled with a small improvement in fuel consumption. From then onwards, the maximum rating of engines, as governed by the mass of air available for efficient combustion, has been continuously increasing and already experimental engines are being developed to yield a brake mean effective pressure (bmep) of 25-30 bar.

There are many applications when turbocharged diesel engines operate under transient conditions involving rapid increases in fuelling. Severe operational and design difficulties with highly rated engines are being experienced in the following particular cases:

1) Electrical generation units, where large load changes can be extremely rapid and fluctuating.

2) Marine propulsion systems during crash manoeuvres requiring sudden reversing of course.

3) Land traction vehicles where high specific outputs and rapid accelerations are required (e.g. military vehicles).

4) Stand-by generating sets (e.g. for nuclear power plants (49)) which have to start, accelerate to

normal speed, then carry a series of loads within a very short time schedule, or maintain speed when a large load is applied rapidly.

The performance of a turbocharged diesel engine in such duties is dependent not only on the governor response and system inertia, but also on the response of the turbocharger. Unfortunately the improvements in steady state performance, brought about by turbocharging, are accompanied by a deterioration in the transient response, worsening with increased charging. Engines rated at about 14 bar bmep, or above, are very likely to stall in response to 100% stepped load application (48).

Since the turbocharger is powered by the exhaust gas energy, its steady state speed varies with the position of the fuel rack and engine speed. However, quick changes in rack position (at the initiation of a transient) do not result in instantaneous response in turbocharger speed. This is caused by the compressibility of the energy link between engine and turbocharger, and the polar moment of inertia of the latter. The resultant lag between the rates of variation of air flow and fuelling leads to rapid changes in the overall fuel-air ratio inside the cylinders. In transient situations which require large increases in fuel input, excessively rich mixtures are developed and consequently air supply becomes the controlling factor in the response of the engine.

A typical example is a sudden application of load to a speed governed engine. For large loads, the increase in fuel (as specified by the governor in response to the resultant large drop in engine speed) is normally not matched by a proportionate increase in air. In severe cases this

results in poor combustion, dense smoke and deteriorating output. If the power discrepancy between the engine and the load continues, stalling will occur. On the other hand, if the turbocharger accelerates sufficiently fast to meet the increased air requirement, the engine speed will recover. The speed droop, engine recovery time and the possibility of stalling, in addition to the dense exhaust smoke produced, are the important factors in the case of transient load applications.

A similar situation arises when accelerating a turbocharged traction engine, but the problem is probably less acute. This is because the loading torque is dependent on the speed and acceleration of the engine and consequently it builds up with the actual response. In this case limited acceleration and dense smoke may be observed.

It is useful from the point of view of an engine manufacturer and a user to be able to predict accurately the transient performance of a turbocharged diesel engine. It is also important to assess the effects of different design changes, in order to be able to achieve economical designs which meet predetermined operational specifications, in steady and transient modes.

Taking into account the important criteria of turbocharged diesel engines and published accounts of modelling techniques (Section 1.2), it became evident that a basic and generalised theoretical approach was essential. Consequently, the present work was directed primarily towards achieving the following objectives:

1. Developing a non-linear mathematical simulation of a turbocharged diesel engine, capable of predicting the transient response of the engine to various changes

in external conditions, e.g. load and demand speed.

2. Carrying out an experimental investigation on a fully instrumented turbocharged diesel engine during steady and transient operation, together with the development of the necessary data acquisition system and techniques.

3. Investigating the influence of certain parametric variations on the predicted response of the engine.

## 1.2 - PREVIOUS WORK

The turbocharged diesel engine is in effect a compound engine (18) in which the engine itself handles the high pressure end of both compression and expansion, while the exhaust turbine and air compressor deal with the low pressure end. The power to drive the compressor is extracted from the exhaust gases according to the prevailing pressure and enthalpy levels, hence the turbocharger responds to both fuelling and speed changes of the engine. The pressure head on the turbine (which determines the availability of exhaust energy) is reflected back to the crankshaft via the piston (when the exhaust valve is open). The division of the work between the high and low pressure components of the system is related to the charging pressure ratio, which also governs, to a large extent, values of the engine performance variables. This in turn is a resultant of the engine-turbocharger interaction, the complexity of which is attributed to:

1. the non-existence of a mechanical linkage between the engine and turbocharger, the only connection being thermo-gas dynamic, and

2. the difference between the flow characteristics

of the turbocharger and engine; rotary and reciprocating machines respectively.

Dynamic systems are normally classified as linear or non-linear. A major characteristic of the latter is the dependence of its transient response on the magnitude of the input signal. Experimental investigation of engine response to inputs of various magnitudes (73) exhibited this dependence. Obvious sources of non-linearities in engines include: gas compressibility (manifolds in particular), saturation effects (fuel rack touching end points), thermodynamics of engine cycles, especially in cases of rich fuel/air mixtures, and engine friction.

No general method for dealing with all non-linear systems is available (46,82), and exact solutions are only possible in cases of simple non-linearities. Some approximate solutions may be applied to other cases but should be confined to the limited conditions for which they are derived. Ogata (82) and Gibson (46) describe details of methods developed to solve a number of non-linear control systems.

### 1.2.1 Prediction of steady state performance of turbocharged diesel engines

Various methods are available for evaluating engine steady state performance with different combinations of turbocharger components. Clearly the accuracy and reliability of the results depend on the sophistication of the method applied and the accuracy of the available engine and turbocharger data.

Simple techniques (58,102,107) have been developed primarily to establish an approximate match between the engine and turbocharger; with final matching tests being always conducted on the test bed. More detailed computer

programs have been written (13,61) to evaluate the constant speed performance of turbocharged diesel engines. These constitute mathematical simulations of the engine and hence differ greatly from the traditional concept of ideal cycles. Whilst the latter confines individual processes to simple predetermined paths, such as constant pressure or volume, the former imposes no restriction. Differential equations resulting from the application of the laws of conservation of energy and mass, in conjunction with other relations (Chapter 2), are integrated along time or crankangle. Nevertheless, such programmes are based upon a host of simplifications, some of which are introduced due to lack of knowledge or because of computing limitations. A typical example is the assumption of thermodynamic equilibrium inside the cylinders.

A constant speed performance prediction program is typically divided into a number of component parts or models, the most significant of which are enumerated below:

1. The turbocharger compressor.
2. The charge cooler, if fitted.
3. The inlet manifold or air chest.
4. Flow through the inlet and exhaust valves or ports.
5. Properties of the working medium.
6. Heat transfer from the cylinder.
7. The combustion process.
8. The gas-exchange process.
9. The exhaust manifold.
10. The turbocharger turbine.
11. Engine frictional losses.

Table 1.1 presents a brief comparison between four engine simulation programmes (115,61,13,99).

| Investigator | Cylinder | | Manifolds | Gas Properties | Mixing | Turbocharger | Remarks |
|---|---|---|---|---|---|---|---|
| | combustion | heat transfer | | | | | |
| Whitehouse (116) | Experimental heat release curve | Eichelberg model (38) applied to closed cycle only. | Mean pressures and temperatures are considered.<br>Pipe flow heat transfer is applied. | Keenan and Kaye | Pure displacement scavenging | Fixed compressor and turbine operating points | Simulation of turbocharged engine without turbocharger |
| Janota (61) | Experimental heat release curve | Eichelberg model applied over the whole cycle.<br>Wall temperature computed. | Method of filling and emptying. Heat transfer computed via an overall coefficient. | Specific heat related to temperature and fuel/air ratio. | Perfect mixing. | Turbine swallowing capacity curve and fixed efficiency.<br>Fixed compressor flow. | Simple and economical program which proved useful to manufacturers for some time. |
| Benson (13) | Whitehouse heat release model (116) | Annand's model applied over the whole cycle; constants varied with load and speed speed. | Method of characteristics.<br>Constant gas composition.<br>Steady flow friction data. | Specific heat related to temperature and mixture composition with the exception of scavenging process and manifolds. | | Turbine swallowing capacity curve and fixed efficiency.<br>Fixed compressor flow. | Applicable to 2- and 4-stroke turbocharged and non-turbocharged multi-cylinder diesel engines. Useful when wave action is important. |
| Streit (99) | Experimental heat release curve | Woschni's model. Wall temperatures computed. | Method of filling and emptying.<br>Heat transfer using Eichelberg (38) and Zapf's correlations (128). | Internal energy and gas constant related to temperature, pressure and equivalence ratio (Krieger (64)) | Scavenging model | Turbine represented by 2 orifices in series:i) coefficient varying with speed and pressure ratio; ii) efficiency characteristics.<br>Compressor map employed on a steady flow basis. | Engine and turbocharger are interactive. Turbine treated on a quasi-steady basis whilst compressor is considered as a steady flow machine: operation condition updated every engine cycle. |

TABLE 1.1 Major Features of Four Computer Programs for the Prediction of the Steady State Performance of Turbocharged Diesel Engines.

The simplified approach of quasi-steady "filling and emptying" concept, which is most widely used, considers the multi-cylinder engine as a series of control volumes (air chest, cylinders and exhaust manifolds). These are interconnected to one another via variable geometry orifices (representing valves or ports), in conjunction with the compressor and turbine of the turbocharger as boundary conditions. The problem of determining the varying conditions of the gas with time, in each control volume, is treated over the whole cycle as that of simultaneous charging and discharging. Such an analysis generates the pressure pulses known to occur in the exhaust manifolds of pulse-turbocharged diesel engines, but the effects of pressure wave propagation are ignored.

To account for wave effects in the manifolds, equations governing the unsteady gas flow have to be solved with time and space. Performance prediction programs which consider wave effects (13), normally employ the method of characteristics for solving these equations for the exhaust manifold. The manifold arrangement is specified as a set of pipes in which the propagation and reflection of pressure waves is calculated. However, the cylinders and valves are treated according to the quasi-steady filling and emptying concept.

The treatment of the inlet and exhaust manifolds as control volumes, rather than a complex arrangement of pipes, is a major simplification which substantially reduces the complexity of the simulation program and reduces computing costs. Whether the neglect of pressure waves effects significantly influences the accuracy with which engine performance is predicted, depends on the wave reflection time in relation to engine speed (60). Usually these effects

are insignificant with smaller engines and become more important as the size of the manifolds increases.

A typical example of a program based wholly on the method of filling and emptying is that by Janota (61). In this, the compressor operating point and turbine efficiency are fixed and specified at each run. These are changed iteratively by the user until an energy and mass flow balance is achieved between the compressor and turbine. Benson (13) developed a versatile program which provides a large number of useful features (Table 1.1); the most important of which is the evaluation of pressure wave action in the manifolds. However, it consumes considerably more computer time, hence its application is usually limited to cases where effects of pressure waves are particularly important.

Although the program developed by Borman (21) did not include a turbocharger, it advanced the state of the art of engine simulation considerably. He applied, for the first time, the concept of absolute enthalpy and formulated the problem as that of an initial value, in which all the micro-parameters exhibited a cyclic propagation with time. In other words, all internal variables (e.g. pressures, temperatures, etc.) varied periodically with time:

$$Z_i(t) = Z_i(t + \Delta t) \qquad (1.1)$$

where: $\Delta t$ = duration of engine cycle.

Streit (99) extended this method to a pulse turbocharged, opposed piston 2-stroke diesel engine. He treated the interaction between the engine and turbocharger via automatic adjustment of the turbocharger operating conditions until a cycle-averaged energy balance was obtained.

Steady state performance prediction programs have been employed in a wide variety of applications,

examples of which are:

1. Prediction of cylinder pressure diagrams for stress analysis purposes.

2. Prediction of component temperatures.

3. Parametric studies with the objective of optimising certain design concepts, e.g. valve timing.

4. Investigation of the feasibility of a major design option, e.g. single and two-stage turbocharging.

### 1.2.2 Speed regulation (governing)

Continuous control theory was applied to speed governing of diesel engines within the last two decades (74,114) mainly to investigate stability problems and to achieve good speed control. Welbourn et al (114) modelled the engine control loop using linearised equations of motion for the engine and governor, in conjunction with a transport lag, referred to as firing delay.

In these studies the fundamental action of the engine (converting the fuel control signal to shaft torque) was considered equivalent to a continuous time delay. The implication was that fuel input is transformed into output torque a finite period of time after it has been injected. In reality the fuel is injected into the combustion chamber within a very short period of time and any particular injection will produce a power stroke of limited duration each engine cycle. This means that the behaviour of the engine is not of a continuous nature but can be defined at specific instants in time.

Bowns (23) and later Hazell et al (52) considered it more logical to employ sampled data techniques. An equivalent sampled data system was assumed to comprise: a continuous controller, an ideal sampler and a time delay, a pulse controller and an inertial system. The sampling time ($t_s$) was taken as a function of the mean speed ($\Omega_e$) and the number of cylinders (nc):

$$t_s = \frac{120}{nc.\Omega_e} \qquad (1.2)$$

Engine torque was represented by rectangular pulses. The overlap of torque pulses occurring in engines having more than four cylinders was assumed to be dependent only on the number of cylinders.

Bowns (23) carried out extensive frequency response tests on a 3 cylinder, naturally aspirated engine and reported close agreement with predictions. Hazell (52) used a sampled-data model to investigate the frequency domain properties of multi-cylinder engines (up to 8). He concluded that modelling a diesel engine using continuous control theory should be limited to certain ranges of input frequency.

Flower (42) proposed a time-discrete representation of turbocharged diesel engines employing a state space (7) form. He assumed the induced air mass to be proportional to turbocharger speed and that both air and fuel were sampled simultaneously. To account for induction and compression processes, induced air was subjected to a transport lag. Windett and Flower (119) demonstrated experimentally the importance of recognising the discrete nature of a reciprocating engine. By synchronising frequency response measurements on a turbocharged diesel engine with sampling instants, scatter was eliminated and repeatable results were obtained.

### 1.2.3 Models for the dynamic simulation of a turbocharged diesel engine

The dynamic simulation of turbocharged diesel engines received attention only very recently. A study of the performance of turbocharged diesel engines during rapid load changes has been carried out at the University of Manchester (66-68,7). This aimed primarily at developing techniques to improve engine response.

The model developed consisted of two parts:

1) Dynamics of the mechanical components (engine, turbocharger and governor).

2) Thermodynamics and gas flow.

The first part was represented by differential equations, whilst the thermodynamic and gas flow simulation employed steady state experimental data. Relations linking engine power, mass flow, and temperature rise with boost pressure, fuel rate, trapped air/fuel ratio and engine speed, in addition to steady state characteristics of the compressor and turbine, were used. A relative thermal efficiency was defined as the ratio between the indicated mean effective pressure at a given fuelling/cycle/cylinder and trapped fuel/air ratio (A/F), to that at the same fuelling and A/F = 20:1. This was represented by a single curve independent of speed. A family of curves (imep against fuelling and speed; A/F = 20:1) was used in conjunction with the thermal efficiency curve to compute the imep at any fuelling. Friction torque was evaluated as a function of engine speed and peak cylinder pressure (27); the latter being related empirically to fuel supply and a fixed compression pressure.

The breathing characteristics of the engine were evaluated on a steady-flow basis, thus inhibiting possible

differences between inward and outward gas flows. Air flow was computed in two parts; air pumped by pistons and scavenge air. The latter was calculated by considering two orifices in series, the first representing the geometric mean area of the inlet and exhaust valves and the second standing in for the turbine. Pumped air was taken as the product of density at inlet manifold conditions and swept volume. An iteration procedure involving the two orifices and a speed curve on the compressor map was carried out at each instant (known engine and compressor speeds). This yielded air flow, boost and exhaust pressures. However, large discrepancies were observed between the measured and calculated flow rates and a number of constant and varying correction factors were introduced.

Turbine inlet temperature was obtained using the expression:

$$\text{temperature rise from inlet to exhaust manifold} = \text{temperature rise factor} \times \frac{\text{fuel burned}}{\text{total air flow} + \text{fuel burned}}$$

The temperature rise factor, introduced to represent combustion conditions, was taken to increase linearly with fuelling per cycle. To account for possible cases of over-rich mixtures, a cut-off fuel/air ratio of 15:1 was introduced, beyond which a fixed temperature rise was used. Fuelling per cycle was related to rack position by a single curve.

Turbocharger performance was evaluated using steady flow and efficiency characteristics of the compressor and turbine. An apparent turbine efficiency was introduced as a function of compressor pressure ratio, in order to account for the pulsating flow of the exhaust gases.

In a paper by Bowns et al (22), three models were discussed. A quasi-linear approach based on simplified steady state characteristics of the engine and turbocharger was described. This method yielded an overall transfer function for the system in which the gain terms and time constants were dependent on the engine operating condition. Such a model can be useful in stability studies employing small perturbation techniques.

A different approach in which the engine torque was obtained from a diagram efficiency map (function of speed and trapped air/fuel ratio) was used to develop the other two models. The governor loop, filling and emptying delays (manifolds) and the pulsed nature of the exhaust gas were ignored. The first method treated the response as a number of steady state operating points, as in Ledger's simulation (67). The second method calculated air flow and boost pressure during valve overlap. Experimentally-obtained characteristics of air charging efficiency as a function of engine pressure drop and speed were employed in conjunction with boost and exhaust pressures (determined at previous steps).

Other simplified studies have also been conducted by Jamoulle (59), Greenhalgh and Tooth (49), and Egli (37). Jamoulle attempted to predict the influence of certain engine parameters, e.g. heat losses to cylinder walls, ignition delay, etc. Greenhalgh mentioned a simple method of computing engine transient response, which was based on empirical formulations from transient tests. However, no details were given. Egli (37) based a simple model on the evaluation of time constants for various parts of the engine system. This was developed with the objective of comparing different techniques of improving engine response.

## 1.3 OUTLINE OF THE PRESENT WORK

It can be concluded that linearised models (based on either continuous control or sampled data concepts) should be limited to small perturbations in engine speed. Thus these may be only used in speed governing of engines and associated stability studies. Sampled data models are certainly closer to the discontinuous nature of a reciprocating engine; however, a major handicap is imposed by the assumption of constant sampling interval.

Quasi-linear models, which employ steady state characteristics of the engine, constitute a further step towards the dynamic simulation of turbocharged diesel engines. Unfortunately, these rely very heavily on experimental data and employ many major simplifying assumptions. Also, major sources of non-linearities such as: combustion, particularly in cases of over-rich fuel/air mixtures, exhaust energy, manifold filling and emptying effects, etc., are either neglected or greatly simplified. This imposes severe limitations on the prediction capability and use of such models.

Thermodynamic and gas flow processes occurring inside a turbocharged diesel engine are satisfactorily evaluated by (constant speed) engine simulation programs. Since these processes are essentially unsteady regardless of the engine running conditions, such techniques seem potentially suitable for extension to transient operation. However, work is necessary in order to achieve a complete and interactive thermodynamic simulation. A different formulation and solution procedure to the problem is also essential since the periodicity condition (equation 1.1) does not hold during transient operation.

In this work, a non-linear digital simulation of turbocharged diesel engines has been developed for the prediction of transient performance. The four-stroke, direct injection, variable speed engine was considered. However, the simulation program can cater for other types if simple modifications are introduced.

The mathematical model divides the engine into the following components: cylinders and manifolds, exhaust turbine, air compressor, engine load-dynamics, turbocharger dynamics, governor and injection system. The quasi-steady approach, "The Method of Filling and Emptying", is employed to describe gas flow and changes in thermodynamic conditions within the different compartments of the engine. Chapter 2 presents the theoretical analysis of the engine system and the component models used in the simulation. A set of coupled ordinary non-linear differential equations governing the dynamic behaviour of the engine is developed in Chapter 3. This chapter also describes the numerical techniques applied to solve the resultant initial value problem, the general computational procedure and the simulation program.

An extensive experimental programme, involving the building of a computer-controlled test bed and special data logging hardware, has been carried out. Chapter 4 describes the test bed, instrumentation, control and data acquisition hardware and the programmed test procedures developed. A review of the various steady state and transient tests conducted, together with the experimental results obtained, is given in Chapter 5.

The model for the combustion process is based on fuel burning rates derived from experimentally-obtained cylinder pressure traces. This model correlates the

normalised distribution of the fuel burning rate to charge conditions prior to ignition, engine speed and overall equivalence ratio. The development of the model is given in Chapter 6 following a review of the fuel burning rate approach.

Chapter 7 presents an evaluation of the simulation results. This includes comparisons of predictions with measurements of various parameters at steady state and transient running conditions of the engine. The effects of certain parametric variations on transient response are also predicted and discussed. Conclusions and recommendations for further work are given in Chapter 8.

# CHAPTER 2

# THEORETICAL ANALYSIS

## 2.1 INTRODUCTION

Past attempts at engine simulation under transient conditions have largely been restricted by: a) the application of linearised control techniques, b) oversimplification of component characteristics, or c) extensive reliance on experimental steady state data. This chapter provides a theoretical analysis of the direct injection turbocharged diesel engine, forming the basis of a dynamic model developed to simulate the various non-linear multivariable response patterns of the actual engine. The main objective is to define the engine system, specify the mechanical and thermodynamic paths linking its components, and establish the interactions and interrelations between the different variables. The component models, basic equations and assumptions governing the steady state and dynamic performance of the engine are presented.

In the following sections, it will be seen that the simulation accounts for the time discrete behaviour of the diesel engine, which is governed by the intermittent fuel injection and combustion processes and results in successive torque pulses at the crankshaft. Delays imposed by emptying and filling of the manifolds together with the pulsating nature of the gas flow due to the cyclic opening and closure of the valves, are considered. The simulation of the combustion process stresses its nonlinear influence both on the torque developed by the engine and the available exhaust energy, particularly in cases of over-rich fuel air mixtures (encountered during transient operation). The instantaneous rates of flow of gases into and out of the engine are not

necessarily equal and pressures upstream of the cylinders can be higher or lower than downstream pressures (the turbocharger match may result in higher mean exhaust pressures than boost pressure at some conditions). Scavenge air and possibilities of backflow (from cylinder to air chest or from exhaust manifold to cylinder) are catered for in the model.

In order to derive the mathematical simulation, the engine has been subdivided into a number of well-defined interactive component systems which can be treated individually: engine thermodynamics and gas flow, fuel injection, governor, engine-load dynamics, exhaust turbine, air compressor and turbocharger dynamics. Referring to Fig. 2.1, the governor, in most diesel engines, is merely a proportional controller which has its own dynamics. The fuel injection system is essentially a dynamic non-linearity and a sampler which determines the amount of fuel injected per cycle and the injection timing. The fuel sample to an individual cylinder is combined with the air sample induced and the mixture is burned to produce a torque pulse at the crankshaft. The net torque, after deducting friction, drives the engine and load dynamics. After a delay of less than one crankshaft revolution, following the induction stroke, the exhaust gas resulting from this burning process is released to the exhaust turbine. This component has its own dynamics, which is lumped with that of the compressor. The air delivered by the compressor is fed to the inlet manifold from which the induction stroke obtains its charge of air for the combustion process.

The basic configuration of the engine system can be presented in the form of a control loop, Fig. 2.1. The blocks representing various components are connected in a fashion which characterises their functional relationship within the overall system. It is emphasised that the arrows

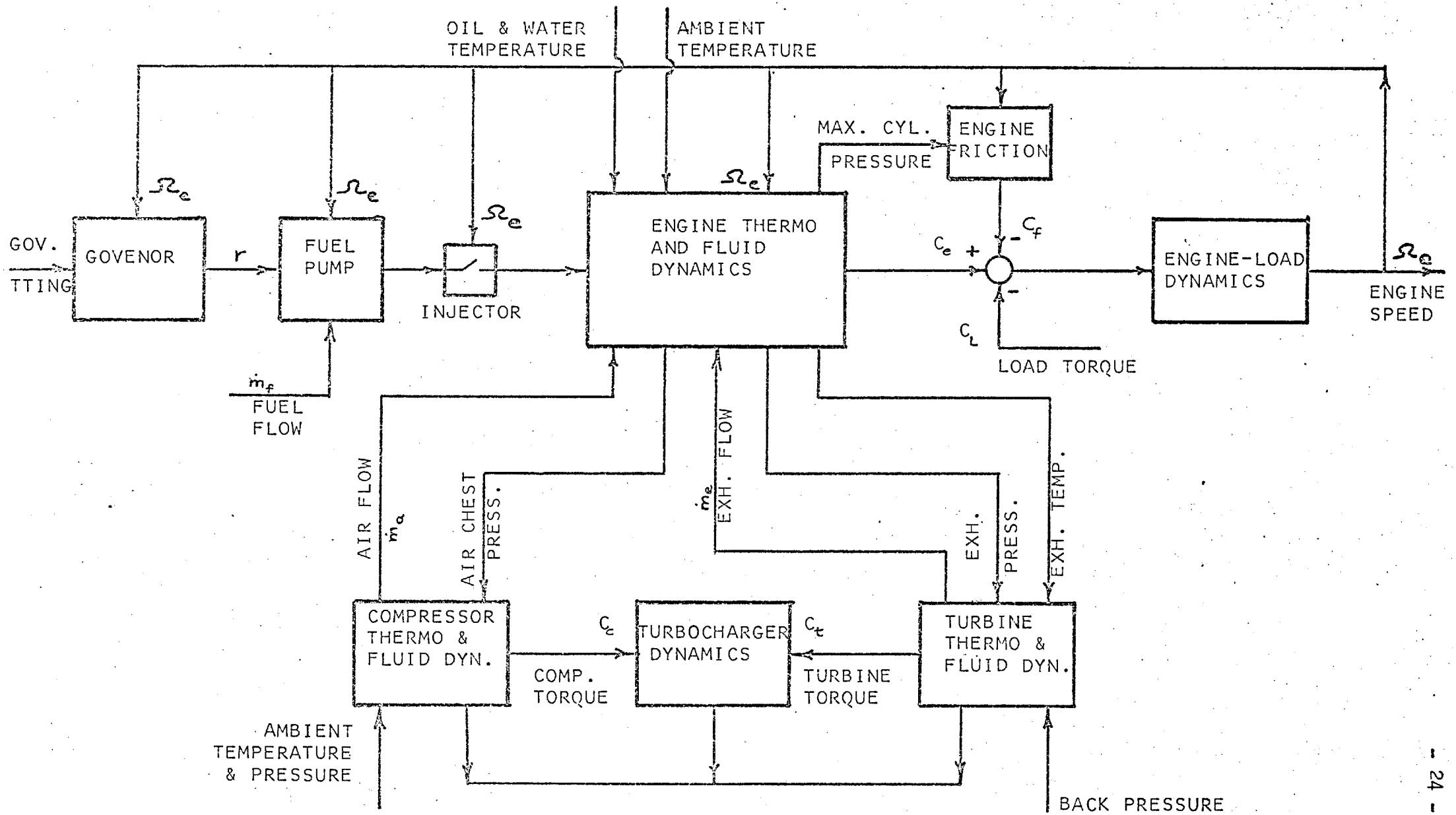


FIG (2.1) BLOCK DIAGRAM FOR A TURBOCHARED DIESEL ENGINE SYSTEM

of the paths connecting one block with another represent the direction of flow of information and not the main source of energy for the system, e.g. rate of flow of exhaust gases between engine and turbine ($\dot{m}_e$) is determined by the turbine.

The external input parameters to the control loop include the load torque, demand speed, ambient temperature and pressure. Resulting outputs comprise: engine speed and the mass flow and temperature of the exhaust gases. Temperatures of the cooling oil and water are assumed constant; experimental data being obtained with closed loop control on coolant temperature (Chapter 4).

Each of the component systems, mentioned earlier, has a significant effect on the events in the engine and subsequently its steady state and dynamic performance. Models were developed to describe their behaviour and to enable their interactions to be evaluated. These will be discussed in detail in the sections that follow.

## 2.2 ENGINE THERMODYNAMICS AND GAS FLOW

### 2.2.1 The Model

Engine thermodynamics and gas flow are described by the behaviour of a system (Fig. 2.2) comprising the following components:

(1) The engine cylinders, each bounded by the gas-exposed metal surfaces, and the inlet and exhaust valves.

(2) The exhaust manifolds, each bounded by the gas-exposed surfaces, the exhaust valves and the turbine entry cross-sections.

(3) The induction manifold (air chest) bounded by

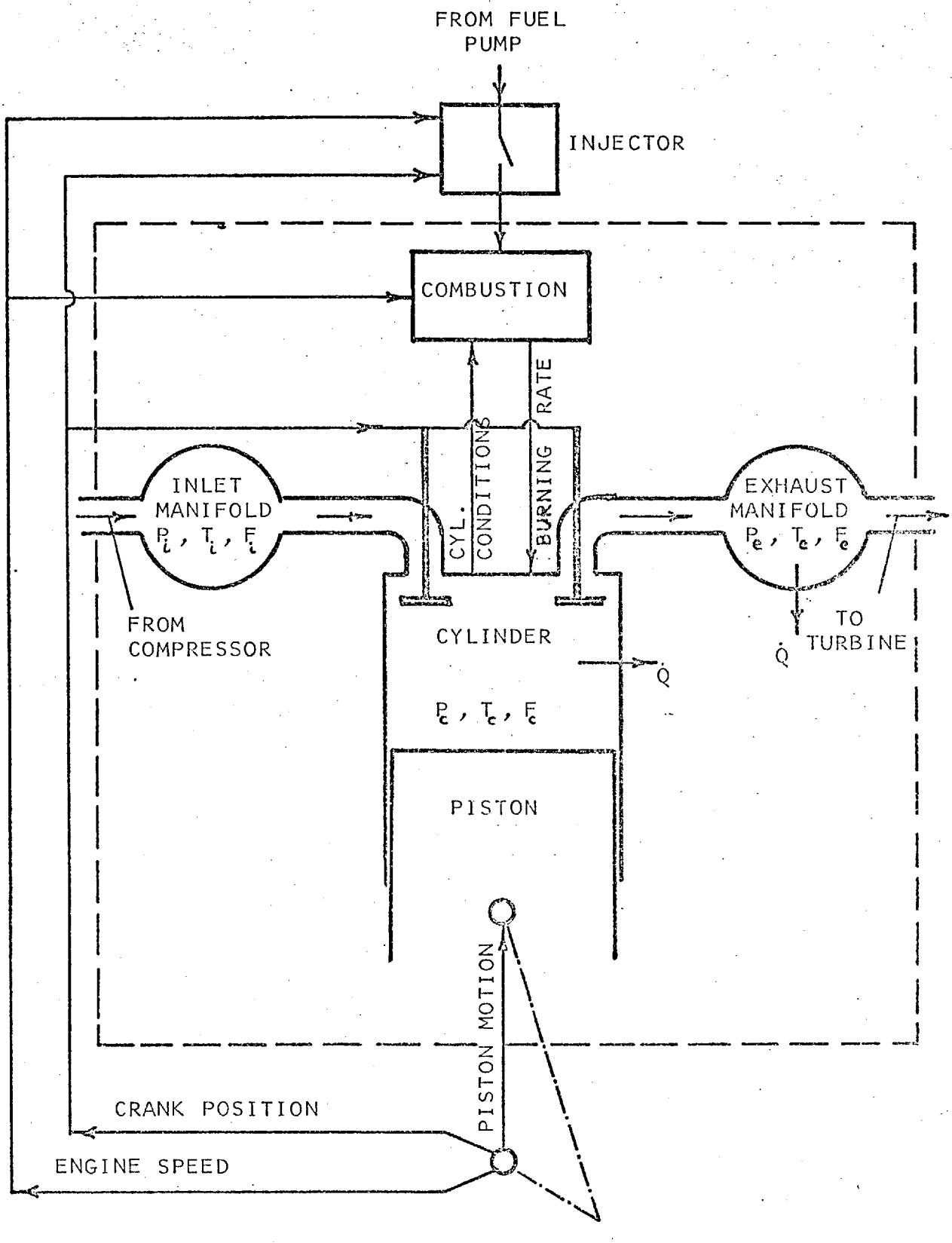


FIG. (2.2) Engine Thermodynamic System

the gas-exposed surfaces, the inlet valves and the compressor inlet cross-section area.

Input signals include: engine speed, crank position, fuel injected/cycle into each cylinder, air mass flow rate into the air chest and the rate of mass flow of exhaust gases permitted by the turbine sectors. The system also outputs the following signals: indicated torque, thermodynamic condition of exhaust gases, pressure in the induction manifold (to be imposed on the compressor) and the maximum cylinder pressure (necessary to determine engine friction).

This system is treated via the simplified approach of the quasi-steady "filling and emptying" concept, commonly applied to steady state engine simulation programs (60,99). The multi-cylinder engine is considered as a series of control volumes, interconnected to one another via orifices simulating valves or ports and coupled by heat and/or mass transfer. Hence the problem of determining the varying conditions of the gas with time, in each control volume, is transformed into a case of a simultaneous step-by-step charging and discharging, governed by instantaneous values of the input signals. For example, conditions in any cylinder are influenced by engine speed, piston position, valve positions, the amount of fuel injected at the last injection and pressures in the inlet and exhaust manifolds (a case of a closed valve suppresses interaction with the manifold it links).

In the thermodynamic model, applicable to all control volumes in this system, thermodynamic equilibrium and ideal gas behaviour are assumed at all times. It is also assumed that individual and control volumes contain homogeneous mixtures of air and products of combustion at every relevant instant. Property gradients and phenomena

such as pressure waves, non-equilibrium compositions, fuel vaporisation before and during combustion, etc. are neglected.

Mixing of two flow streams, of different thermodynamic states and/or different chemical species, is treated as being perfect. To simplify the computational procedure, absolute internal energies and absolute enthalpies, as introduced by Powell (86) are used. This, in conjunction with the equivalence ratio, defined as:

$$F = \frac{\text{fuel air ratio}}{\text{stoichiometric fuel air ratio}} = f/f_s \qquad (2.1)$$

transforms air and products of combustion into one continuous medium whose thermodynamic state is determined by temperature, pressure and equivalence ratio (F = 0.0 for pure air and unity for combustion products of a stoichiometric mixture). The equilibrium thermodynamic properties of the products of combustion of air and diesel fuel are used in the form of analytical expressions function of the thermodynamic state of the medium.

### 2.2.2 Conservation Equations and Mass Transfer

The conservation laws for the spacial average values applicable to any control volume (cylinder or manifold) are as follows:

Energy equation:

$$\frac{d(Me)}{dt} = -p\dot{V} + \sum_i \dot{Q}_i + \sum_j h_j \dot{m}_j \qquad (2.2)$$

where: M = mass inside the control volume,

e = specific internal energy of the medium,

$h_j$ = total (stagnation), specific enthalpy of mass flow entering/leaving through surface j,

p = total pressure inside the control volume,

$\dot{V}$ = rate of volume change,

$\dot{Q}_i$ = rate of heat transfer through surface i,

$\dot{m}_j$ = individual mass flow rate, into or out of the control volume.

Overall continuity equation:

$$\frac{dM}{dt} = \sum_j \dot{m}_j \qquad (2.3)$$

This equation states that the rate of change of the total mass of gases in the control system is equal to the sum of the rates at which mass flows in or out.

Fuel continuity equation:

The conservation of the fuel species can be treated in a similar way, with f denoting fuel:

$$\frac{dM_f}{dt} = \sum_j \dot{m}_{f,j} \qquad (2.4)$$

Fuel is treated mathematically as being injected and burnt instantaneously according to a specified burning rate curve; details are given in the combustion model (Section 2.2.3 and Chapter 6).

Mass transfer:

Extensive studies of flow through engine valves and ports have been carried out by Woods (122), Benson (8-11), Wallace (110-112) and others. A large number of simplifying assumptions (including that of one-dimensional flow) were adopted. Two major groups of factors influencing mass flow rates were reported. The first group was related to the flow restriction itself, e.g. heat transfer (normally neglected), flow separation and secondary flow effects, whilst the second group was introduced by the presence of pressure and rarefaction waves.

It has been shown by several researchers (61,21,13) that the flow may be represented by a one-dimensional quasi-steady model, based on standard steady compressible flow relationships. This ignores the effects of gas inertia and pressure waves and expresses the rate of mass flow of an ideal gas through a flow restriction as:

$$\dot{m} = A_g C_d P_u \sqrt{\frac{2\gamma}{(\gamma-1)R_u T_u}\left[\left(\frac{P_d}{P_u}\right)^{2/\gamma} - \left(\frac{P_d}{P_u}\right)^{\frac{\gamma+1}{\gamma}}\right]} \qquad (2.5)$$

where: $A_g$ = geometric flow area,

$C_d$ = coefficient of discharge determined by steady flow measurements as a function of instantaneous geometric area and pressure ratio $(P_d/P_u)$,

$P_u, T_u, R_u$ = stagnation pressure and temperature and specific gas constant, at upstream conditions,

$P_d$ = stagnation pressure downstream,

$\gamma$ = specific heat ratio at upstream conditions.

At sonic flow rates the pressure ratio reaches the critical value of:

$$\left(\frac{P_d}{P_u}\right)_u = \left(\frac{2}{\gamma+1}\right)^{\gamma/\gamma-1} \qquad (2.6)$$

below which no increase in volumetric flow is possible.

### 2.2.3 Additional Relations

In order to complete the mathematical formulation of the system, the following set of complementary relations is essential:

Thermodynamic properties of combustion products:

The equilibrium thermodynamic properties of the products of combustion of air and diesel fuel (assumed to

be $C_nH_{2n}$) are expressed analytically in the form:

$$e = e(T,P,F) \qquad (2.7)$$

$$R = R(T,P,F) \qquad (2.8)$$

The required formulae for lean fuel/air mixtures ($F \leqslant 1$) including dissociation were taken from Krieger (64). For rich mixtures ($1 < F < 1.6$). other expressions were fitted to data based on (45). Details of the presentation of the properties of products of combustion and air together with the concept of absolute internal energy are given in Appendix A.

Equation of state:

For an ideal gas,

$$pV = MRT \qquad (2.9)$$

Heat transfer:

The rate of heat transfer between a gas exposed surface (i) and the gas is expressed as:

$$\dot{Q}_i = h_i A_i (T_i - T_g) \qquad (2.10)$$

In Section 2.7 it will be shown that, in the case of the cylinder, the coefficient of heat transfer is a function of the thermodynamic properties of the gas and the engine speed or gas velocity. The one-dimensional heat transfer model, employed to obtain the surface temperature, $T_i$, is also described.

Event timing and engine geometry:

The angular position ($\theta$) of the crankshaft times all events, initiates and terminates various processes and governs the instantaneous geometry of each cylinder. It is related to the speed of the engine in the following differential form:

$$\frac{d\theta}{dt} = \Omega_e \qquad (2.11)$$

The cylinder volume $V_{c,i}$ and the liner area exposed $A_{\ell,i}$ are calculated according to the kinematics of a slider crank mechanism:

$$V_{c,i} = \frac{\pi}{4} d_r^2 \left(\frac{\ell}{r} + 1 - \cos\theta - \sqrt{\frac{\ell}{r} - \sin^2\theta}\right) + V_{TDC} \qquad (2.12)$$

$$A_{\ell,i} = \pi dr\left(\frac{\ell}{r} + 1 - \cos\theta - \sqrt{\frac{\ell}{r} - \sin^2\theta}\right) + A_{\ell,TDC} \qquad (2.13)$$

where: $d$ = cylinder bore,

$r$ = crank radius,

$\ell$ = length of connecting rod.

The valve flow area is represented as a numeric function of crank angle:

$$A_{v,n} = A_{v,n}(\theta) \qquad (2.14)$$

Combustion:

A model based on the burning rate approach (64) was developed to simulate the overall thermal effects of the combustion process. This model relates the overall pattern by which the fuel burns inside the cylinder to: the charge conditions at the start of injection, the amount of fuel injected, ignition delay and engine speed. It also determines the rate by which heat is released for the two cases of lean ($F < 1$) and rich ($F > 1$) fuel-air mixtures. Fuel is introduced into the thermodynamic analysis in the form of a mass-burning rate function which starts at the ignition point. All intermediary processes following the start of injection to the end of combustion (spray penetration, atomisation, evaporation, air entrainment, micro-mixing, combustion kinetics, etc.), together with thermodynamic effects on the mean state of the charge, are not explicitly linked to the injection process.

The total rate of burning is considered to be a resultant of two mechanisms, namely: premixed combustion and turbulent diffusion combustion. A mode of burning proportionality factor (MBPF) is introduced to quantify the share of fuel burned by either mechanism:

$$\beta = \frac{M_{f,p}}{M_{f,t}} \tag{2.15}$$

where: $M_{f,t} = M_{f,p} + M_{f,d}$ (2.16)

$M_{f,t}$ = total mass of fuel injected per cycle,

p,d denote premixed and diffusion burning modes respectively.

The mass burning rate is expressed in the following normalised form:

$$FBR_t(\tau) = \frac{\frac{dM_{f,t}}{d\theta}(\theta_e-\theta_i)}{M_f} = \beta.FBR_p(\tau)+(1-\beta)FBR_d(\tau) \tag{2.17}$$

$$FBR_p(\tau) = cp1.cp2.\tau^{cp1-1}(1-\tau^{cp1})^{cp2-1} \tag{2.18}$$

$$FBR_d(\tau) = cd1.cd2.\tau^{cd2-1}EXP(-cd1.\tau^{cd2}) \tag{2.19}$$

where: $FBR(\tau)$ = non-dimensional burning rate distribution,

$\theta_i, \theta_e$ = crank position at ignition and at nominal end of burning,

$\tau = \frac{\theta-\theta_i}{\theta_e-\theta_i}$ = normalised crank angle.

The basic concept of this model is that the explosive pattern of the pre-mixed combustion mode is controlled mainly by the amount of fuel prepared during the ignition delay. Fuel surviving this mechanism, in addition to quantities injected after ignition, is assumed to react according to the diffusion burning pattern, irrespective of the overall equivalence ratio. The use of equilibrium thermodynamic properties automatically takes care of the condition

of the combustion products and governs the amount of heat liberated.

The MBPF was correlated to the ignition delay and the overall equivalence ratio of the charge. The shapes of the component burning rates $FBR_p$ and $FBR_d$ were linked to: ignition delay, engine speed and equivalence ratio using the parameters cp1 and cd1. The total ignition delay was related to the temperature and pressure (T,P) of the charge, following ignition, using Wolfer's formula (121):

$$\theta_{ig} = \theta_{di} + \frac{C1}{p^{C2}} EXP(C3/T) \qquad (2.20)$$

where: $\theta_{ig}, \theta_{di}$ = crank position at the points of ignition and dynamic injection.

Chapter 6 presents details of the combustion model, the experimental data employed together with the correlations established.

Engine torque:

The instantaneous value of the indicated torque $C_e(t)$ is given by:

$$C_e(t) = \frac{1}{\Omega_e(t)} \sum_{i=1}^{nc} \left[ P_i \frac{dV}{dt} \right] \qquad (2.21)$$

where: nc = the number of cylinders.

## 2.3 TURBOCHARGER

Commercial turbochargers consist of a single stage centrifugal compressor and a single stage axial-flow or centripetal turbine mounted on a common shaft. The turbocharger is linked to the engine via the induction and exhaust manifolds; therefore the only interconnection is via the conditions the engine imposes on the compressor dis-

charge and turbine inlet. The turbocharger responds to these conditions by satisfying the airflow requirements of the engine and by imposing its own requirements.

The turbocharger characteristics are different from those of the engine; being rotary and reciprocating machines respectively. Its performance varies over the operational range of the engine and changes with the level of turbocharging. Unlike the mechanically driven supercharger, it responds to changes in fuel input to the engine as well as to engine speed. The matching point attained by the turbocharger at each steady operating point of the engine, depends on the flow characteristics and efficiencies of the turbine and compressor. Cyclic variations in the turbocharger speed due to the non-uniform supply of energy to the turbine depend on the turbocharger inertia and characteristics of the exhaust pulses. During transient operation, the turbocharger's response to changes in the conditions imposed by the engine, is greatly influenced by its dynamics, i.e. polar moment of inertia. The following sections (2.3.1-2.3.3) describe the theoretical treatment employed to model the turbocharger and its dynamic action.

### 2.3.1 Exhaust turbine

The exhaust turbine system, Fig. 2.3, is bounded by the exhaust gas entry cross-section, the exit cross-section and the power transmission shaft. The input signals are the pressure, temperature and equivalence ratio of the gases leaving the exhaust manifold, back pressure and the speed determined by the turbocharger dynamics. The system responds via its two outputs; the shaft torque and the value of the mass flow rate of exhaust gases it permits.

Exhaust turbine operation is classified into two distinct types, namely pulse and constant pressure systems. By releasing exhaust gases from all cylinders into a sufficiently large manifold, constant pressure operation maintains an almost steady gas state at the turbine entry. In pulse operation gases from cylinders of non-interfering exhaust strokes are introduced into narrow and properly arranged pipes, hence pressures and temperatures at the turbine entries are continuously varying. Pressure pulses propagating in these pipes ensure a better utilisation of the relatively high energy potential accompanying the gases at the beginning of exhaust valve opening period.

Quasi-steady analysis:

The continuous variation in the state of the gas in the exhaust manifold of a pulse turbocharged diesel engine leads to a time varying energy potential and complicates the problem of evaluating the turbine instantaneous performance. Furthermore, in the case of multi-entry turbines, partial admission losses are introduced by subjecting adjacent rings or sectors of the turbine to pulsating flows which are continuously out of phase. Attempts at predicting turbine performance are described in several papers (31,106,104,108,109). Empirical methods, based on mean pressures and temperatures, have been reported (20,130) but their accuracy and use are rather limited (98).

With regard to engine simulation applications (55,61, 13 ,99), it was considered most practical to treat the problem as one of quasi-steady flow, i.e. the turbine performs under non-steady flow, at each instant of time, in the same manner as under steady flow. Experimental investigations into the effects of non-steady (pulsating) flow on turbine performance,

and the accuracy of quasi-steady predictions have been carried out on radial (12,105,104,109) and axial flow turbines (30,104). In both cases it was found that quasi-steady flow predictions gave results of varying accuracy. This can probably be attributed to:

1. Variations in the characteristics of the pulses applied, i.e. shape, frequency, amplitude, ratio of wind milling duration to pulse cycle period and phase difference in the case of multi-entry turbines.

2. Variables selected for measurement; transient temperatures were not measured in refs. (12,30,77,104,106 and 109).

3. Measuring techniques used and the resulting accuracy, e.g. torque or power measurement.

4. Methods and assumptions employed in the computation of the turbine instantaneous performance.

It is also appropriate to mention that accurate experimental determination of instantaneous values of turbine efficiency and mass flow rates on a turbocharger operating under actual engine conditions (including varying gas composition) has not yet been possible.

In view of the lack of superior techniques, it was decided to treat the exhaust turbine on a quasi-steady basis, as in the case of almost all programs (60,13,99) developed to evaluate engine steady state performance. However, it is important to stress the need for more work to establish accurately any errors incurred by this method when evaluating mass flow and turbine efficiency. Correction factors may have to be developed in the form of correlations with the major controlling parameters, e.g. pulse characteristics.

Turbine model:

The multi-entry turbine, having n entries, is modelled as n identical mini-turbines mounted on one shaft with the compressor (61). The instantaneous performance of each mini-turbine (representing a turbine ring or sector) is evaluated on a quasi-steady basis using full admission steady flow characteristics. This was shown by Benson (12) to yield better accuracy in comparison with partial admission data. Exhaust gases are assumed to expand through the turbine passages under conditions of thermodynamic equilibrium.

As each turbine ring or sector (mini-turbine) is treated individually, the overall instantaneous turbine mass flow rate and power are taken as the summation of the component values:

$$\dot{m}_t = \sum_{i=1}^{n} \dot{m}_i \qquad (2.22)$$

and

$$P_t = \sum_{i=1}^{n} P_i \qquad (2.23)$$

Since the full admission swallowing capacity of the turbine is normally represented as a function of both pressure ratio and rotational speed parameter,

$$\dot{m}_{fa} = f(P_u/P_d, \frac{\Omega_{tc}}{\sqrt{T_u}}), \qquad (2.24)$$

the instantaneous mass flow rate through any mini-turbine becomes:

$$\dot{m}_i = \frac{1}{n} f(P_u/P_d, \frac{\Omega}{\sqrt{T_u}}) \qquad (2.25)$$

If the instantaneous exhaust pressure ratio falls below the

minimum value corresponding to the current value of the rotational speed parameter, the mass flow is taken to be zero. In the case of axial flow turbines, Janota (61) advocated the use of one swallowing capacity curve independent of turbine speed.

The turbine efficiency is defined as

$$\eta = \frac{\text{actual turbine work}}{\text{maximum possible work (isentropic)}} \qquad (2.26)$$

It should be noted that the turbine efficiency normally referred to in turbocharger applications (61), is based on the total to static isentropic expansion ratio and includes: windage, exhaust casing, bearing, oil pump disc and the pressurisation air leakage losses of the whole turbocharger. This follows from the fact that the actual turbine work is commonly measured from the compressor side. The turbine efficiency is usually represented as a function of blade speed ratio ($\nu = \frac{u}{c}$) and rotational speed parameter ($\frac{\Omega_{tc}}{\sqrt{T_u}}$):

$$\eta_t = \eta_t(\nu, \frac{\Omega_{tc}}{\sqrt{T_u}}) \qquad (2.27)$$

where: $c = \sqrt{2\Delta h_{is}}$

$\Delta h_{is}$ = isentropic enthalpy drop of the exhaust gases,

$u$ = peripheral blade speed.

Therefore, the instantaneous power developed by any mini-turbine is given by

$$P_i = \dot{m}_i \eta_i \Delta h_{is,i} \qquad (2.28)$$

and the total turbine torque becomes:

$$C_t = P_t / \Omega_{tc} \qquad (2.29)$$

## 2.3.2 Air compressor

The turbocharger's centrifugal compressor discharges air into the induction manifold either directly or through an aftercooler. The compressor system is bounded by its inlet and exit flow cross-sections, the casing and the input power shaft. The induction manifold pressure, turbocharger speed and the temperature and pressure of the inlet air constitute its input variables. The output variables are the air mass flow rate and the required shaft torque.

Pulsations created by the periodic induction process of the different cylinders may cause a slight modification to the compressor performance (98). As no reliable non-steady flow analysis (suiting engine simulation purposes) is available (15), the compressor is treated on a quasi-steady basis (28) employing experimentally-obtained steady state performance characteristics. The inclusion of such data, in a program, in the form of a constant compressor speed line (58, 102) is restrictive but may be tolerated when simulating the steady state performance of an engine. It cannot be accepted when predicting transient performance due to the wide operational range involved and thus a full compressor performance map is essential.

It is common practice to represent centrifugal compressor data in the following form:

$$\frac{\dot{m}\sqrt{T_u}}{P_u} = f\left(\frac{P_d}{P_u}, \frac{\Omega_{tc}}{\sqrt{T_u}}\right) \qquad (2.30)$$

and

$$\eta_c = f\left(\frac{P_d}{P_u}, \frac{\Omega_{tc}}{\sqrt{T_u}}\right) \qquad (2.31)$$

where: $\dot{m}$ = mass flow rate,

$P_d, P_u, T_u$ = delivery and inlet pressures and inlet temperature,

$$\eta_c = \text{compressor efficiency}$$
$$= \frac{\text{minimum possible work}}{\text{actual work}} = \frac{\Delta h_{is}}{\Delta h_{act}} \qquad (2.32)$$

Instantaneous values of the compressor mass flow rate and efficiency are determined according to current values of pressure ratio and rotational speed. Subsequently the required shaft power and torque are evaluated:

$$P_c = \dot{m}_c \times \Delta h_{is} / \eta_c \qquad (2.33)$$
$$C_c = P_c / \Omega_{tc} \qquad (2.34)$$

The air delivery characteristics of the turbocharger do not ideally suit automotive applications and a compromise match is normally accepted. As this class of engines covers a large operational range on the compressor map, the normal match often results in slightly negative boost pressures (depression) at light loads. This case has been identified experimentally (Chapter 5) and the mass flow characteristics were extended to a pressure ratio of 0.8, using actual flow measurements. As regards compressor work, it is evident that the efficiency approach becomes meaningless under these conditions and an alternative method is required. The actual process under such abnormal conditions was assumed to take the shape shown in Fig. 2.4, in which compression takes place but the imbalance in the demand and supply of air leads to throttling and subsequent pressure loss. Hence, the compressor power can be evaluated as a function of wheel tip speed (97):

$$P_c = \dot{m}_c \lambda \sigma u^2 \qquad (2.35)$$

where: $u$ = wheel tip speed,

$\lambda, \sigma$ = power input and slip factors, the resulting product was taken to equal 0.9.

### 2.3.3 Turbocharger dynamics

This system comprises the impellers of the exhaust turbine and centrifugal compressor plus their joining shaft.

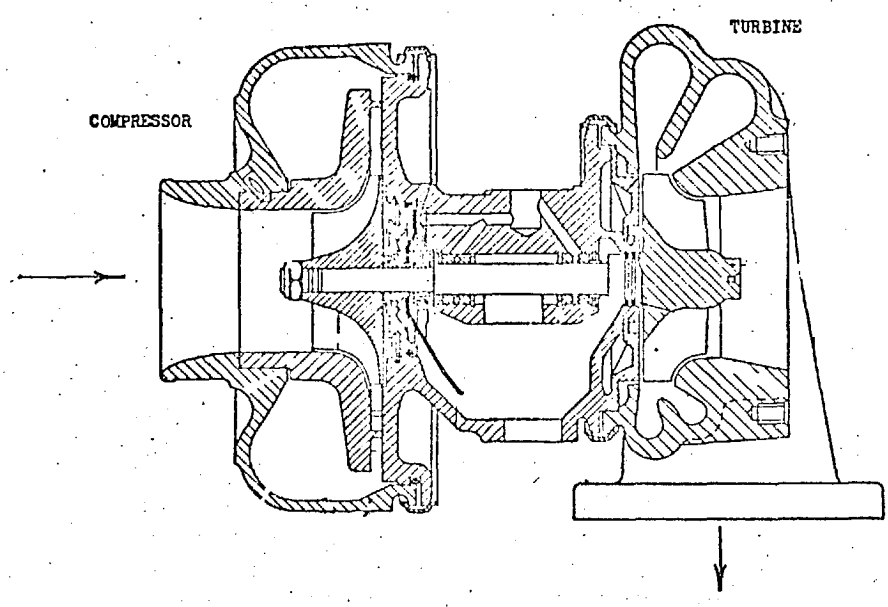


FIG. (2.3) Typical Turbocharger for Automotive Diesel Engines

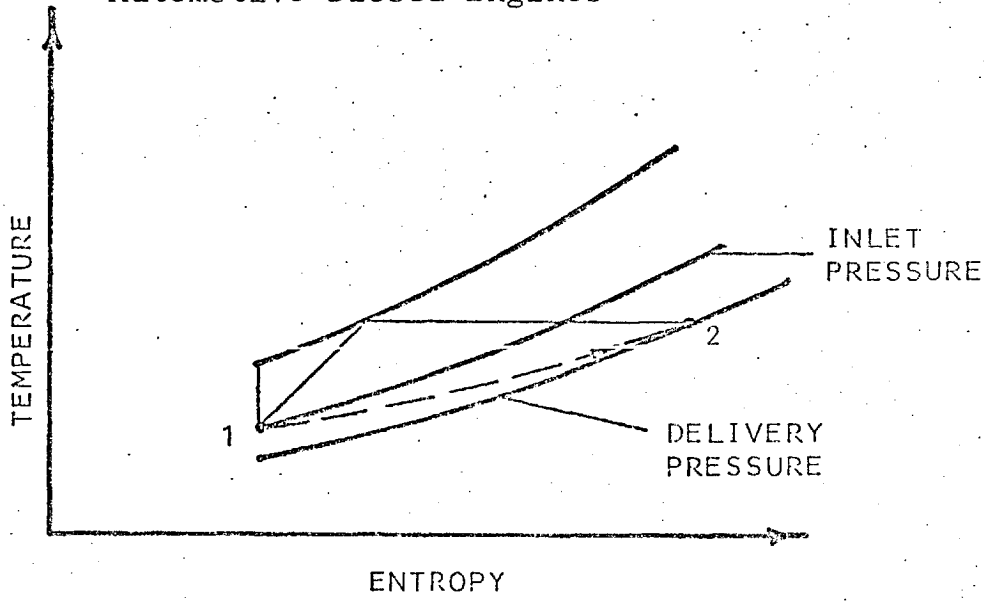


FIG. (2.4) Compressor Operation with Delivery/ Inlet Pressure Ratio Below Unity

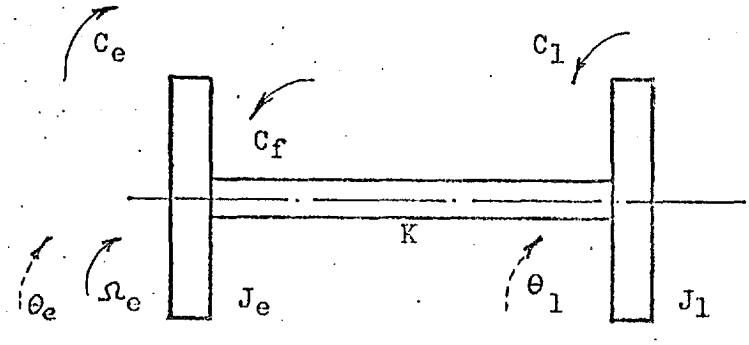


FIG. (2.5) Equivalent System for Engine-Load Dynamics

These are modelled by two discs mounted onto a rigid shaft and subjected to two opposing torques (from the turbine and compressor). As mentioned earlier, the effects of any frictional or resisting torques are accounted for in the turbine efficiency.

Straightforward application of the angular momentum equation gives:

$$\frac{d\Omega_{tc}}{tc} = (C_t - C_c)/J_{t/c} \qquad (2.36)$$

where: $C$ = torque,

$J_{t/c}$ = total polar moment of inertia of turbocharger,

$t,c$ = denote turbine and compressor respectively.

## 2.4 ENGINE LOAD DYNAMICS

The equivalent polar moment of inertia of the engine moving parts and that of the load are represented by two discs connected by a weightless shaft. This system, Fig. 2.5, is continually subjected to the engine developed torque $C_e$ (indicated torque) and opposed by the load and engine friction torques $C_L$ and $C_f$ respectively. It is to be noted that $C_L$ includes windage and other types of friction torques generated inside the loading unit; brake tprque being measured experimentally via the reaction on the dynamometer stator.

Applying the momentum equation in the case of an elastic shaft yields:

$$J_e\dot{\Omega}_e + C_f + K(\theta_e - \theta_L) = C_e \qquad (2.37)$$

and

$$J_L\dot{\Omega}_L + C_L = K(\theta_e - \theta_L) \qquad (2.38)$$

The power transmission shaft is considered sufficiently rigid ($K = \infty$) to neglect the twist and phase shift between the two discs (i.e. $\theta_e = \theta_L$ and $\Omega_e = \Omega_L$). Hence the system can be represented by:

$$(J_e + J_L)\dot{\Omega}_e = C_e - (C_L + C_f) \qquad (2.39)$$

and the instantaneous acceleration takes the form:

$$\frac{d\Omega_e}{dt} = \left[C_e - C_L - C_f\right] \frac{1}{J_e + J_L} \qquad (2.40)$$

Engine friction:

When studying the literature it became apparent that the measurement and analysis of engine frictional losses had not been satisfactorily resolved. This is primarily due to the intransigent problem of direct, accurate measurement of these losses under actual running conditions. The problem of analysis and prediction is further complicated by the fact that the total loss is a summation of losses arising from the operation of various engine components, which respond in various manners to changes in speed, pressure, temperature, etc.

Ideally, the total friction loss is derived by direct measurement of the indicated power (from a cylinder pressure diagram) and the brake power. This may be possible on low speed engines but the considerable problems involved in the case of high speed engines limits the accuracy of this approach and renders it unreliable (75). Measuring frictional losses by direct motoring of the engine yields values different to those under firing conditions. Some of the reasons are: the lower pressure acting on the piston rings and bearings, lower surface temperature (the effect on oil viscosity), greater piston clearance, untrue exhaust blow down.

In the Willan's line method, a plot of gross fuel consumption versus brake output at a fixed engine speed, is extrapolated to zero fuel consumption. The curvature generally experienced in such a plot imposes a limitation on the accuracy of the method. The Morse test, in which individual cylinders are cut out in turn, is basically a motoring procedure, hence similar limitations apply. It has

also been reported (75) that this method disturbs the fuel supply to the firing cylinders.

Based on the above, it was decided to employ the relatively simple correlation developed by Chen (27) and later used by Ledger (67) and others. This formula relates the mean effective pressure equivalent of the rubbing friction to engine speed and the maximum cylinder pressure. Chen's constants were used without any modification:

$$FMEP = 13.7896 + 0.005P_{max} + 1.0858R*\Omega_e \quad (2.41)$$

where: R = crank radius.

The effect of errors in the evaluation of frictional losses is discussed in Chapter 7.

## 2.5 GOVERNOR

An engine governor is a speed sensitive device which automatically controls or limits the speed of the engine via adjustment of the fuel rate. The basic principle is that engine speed is dependent on both load and input fuel rate. To maintain a steady speed, the fuel rate must be adjusted to achieve equality of the power developed by the engine and that required by the load. The governor operates by first measuring speed and detecting differences from the set value (demand speed). It then moves its output shaft (connected to the fuel control rod) in the direction necessary to reduce the error detected. Thus, the governor and the engine form a closed loop to which changes in the set values of load and speed are applied.

A constant speed governor is installed to maintain the engine at a single speed for any load level, whilst the variable speed type is used mainly in automotive engines, to

cover a wide range of speeds. Other types include speed limiting, overspeed-trip, load limiting and load control units.

### 2.5.1 Speed sensing unit

The flyweight speed sensing device is used on most diesel engines. This, shown schematically in Fig. 2.6, consists of a pair of flyweights, located on opposite sides of a shaft, which is positively driven by the engine. The rotating weights produce a centrifugal force opposed and balanced by a spring (referred to as the speeder spring). A rise in speed increases the centrifugal force and the weights move outwards, pushing the speeder rod and causing an increase in the spring force. Therefore, the position of the speeder rod (fuel pump rack) is determined according to the spring force and engine speed.

In order to analyse this system, the two flyweights are assumed to have equivalent masses (m) concentrated at radii of gyration (a) from their pivots. A single equivalent mass (M) is concentrated at the axis and the spring stiffness is denoted by ($K_s$). The equilibrium position can be adjusted by moving the top end of the spring a distance (y) from the original reference position ($Y_r$), i.e. initial spring compression ($Y_r$) corresponds to a reference speed ($\Omega_r$) and a speeder rod position ($x_r = 0$). When setting the equation of motion it is normally assumed (114) that damping is viscous and that the maximum travel of the speeder rod is sufficiently small to justify linearisation ($x = a\theta$). An instantaneous balance of inertia, damping, spring and centrifugal forces gives the following second order differential equation:

$$(2ma^2+b^2M)\ddot{x}+b^2\lambda\dot{x}+b^2k_s(x+y)-2ma^2\Omega_e^2 x = 2mab\ell(\Omega_e^2-\Omega_r^2) \qquad (2.42)$$

where: $\lambda$ = the coefficient of viscous damping.

When rotating steadily at the reference setting $Y_r$, equation (2.42) becomes:

$$2ma\ell\Omega_r^2 = bk_sY_r$$

This explains how the engine speed can be adjusted by simply varying y, i.e. modifying the spring force via shifting the position of its top end.

Dividing equation (2.42) by $(X_t.Y_t.\Omega_m^2)$ and rearranging, the following normalised form is obtained:

$$(2ma^2+b^2M)\ddot{x}+b^2\lambda\dot{x}+b^2k_s(x+\frac{Y_t}{x_t}y)-2ma^2\Omega_m^2\Omega_e^2x$$

$$= \frac{2mab\ell}{x_t}\Omega_m^2(\Omega_e^2-\Omega_r^2) \qquad (2.43)$$

where x, $\dot{x}$, $\ddot{x}$, y, $\Omega_e$ and $\Omega_r$ now denote normalised values and the time dimension appears only in $\dot{x}$ and $\ddot{x}$.

## 2.5.2 Constant speed governing

The operation of a constant speed governor can be described by putting y = 0 in equation (2.43), i.e. fixing the demand speed. The strict limitations (within 5%) normally imposed on speed regulation in constant speed applications, e.g. electric power generation, justify further simplification. By putting $\Omega_e=\Omega_r+w$ and neglecting second order terms, the following form is obtained:

$$(2ma^2+b^2M)\ddot{x}+b^2\lambda\dot{x}+b^2k_sx-(2ma^2\Omega_r^2)x = \frac{4mab\ell}{x_t}\Omega_m^2\Omega_rw \qquad (2.44)$$

### 2.5.3 Variable speed governor

The variable speed governor under consideration, Fig. 2.7, varies from that in Fig. 2.6 in the following two aspects:

1. The speeder spring stiffness is variable.
2. The relationship of the radial motion of the flyweights to that of the speeder rod is exactly linear.

The governor spring is of the leaf type, mounted on a fulcrum pin and loaded via a roller assembly, bearing against an inclined plane, Fig. 2.7. This arrangement results in a variable spring stiffness which increases with the downward motion (y) of the roller (demand speed).

The spring stiffness was considered to be adequately represented by a linear dependence on governor setting (y):

$$k_s = k_1 + k_2 y \qquad (2.45)$$

By substituting into equation (2.43), and rearranging, the governor differential equation takes the form:

$$C1\ddot{x} + C2\dot{x} + (1 + C3y)(x + C4y) - C5\Omega_e^2 x = C6(\Omega_e^2 - \Omega_r^2) \qquad (2.46)$$

Values of the constants C1 to C6 were obtained experimentally (Chapter 5).

## 2.6 FUEL INJECTION SYSTEM

This system includes the fuel pump, delivery valve, fuel pipes and injectors. A thorough analysis (6,47,63,127,126) of the fuel pump and injection system, taking into account wave action in the fuel pipes, was not considered to be justified for this work. The computational time needed for the solution of the differential equations is excessively long.

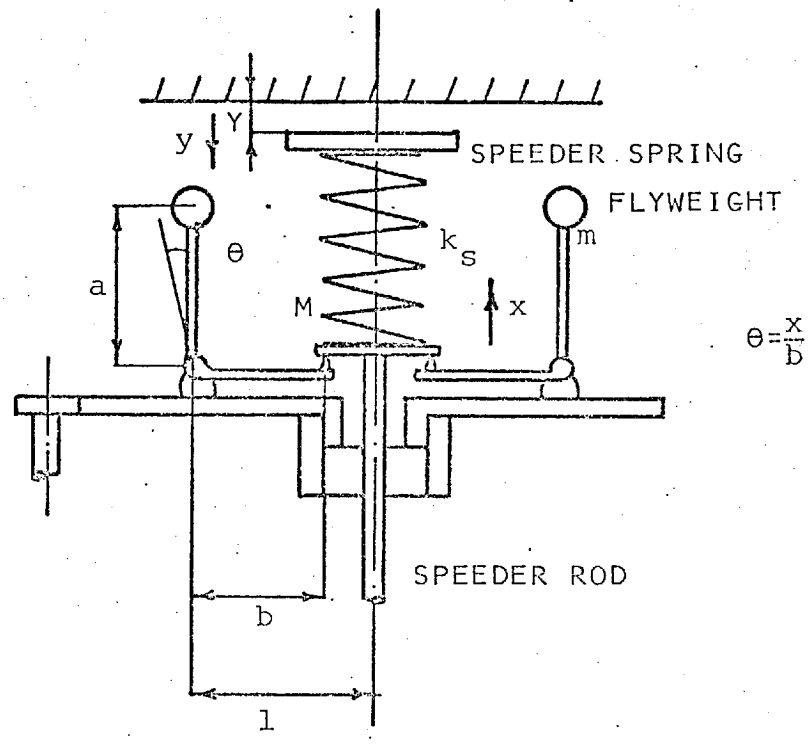


FIG. (2.6) Typical Flyweight Speed Sensing Device

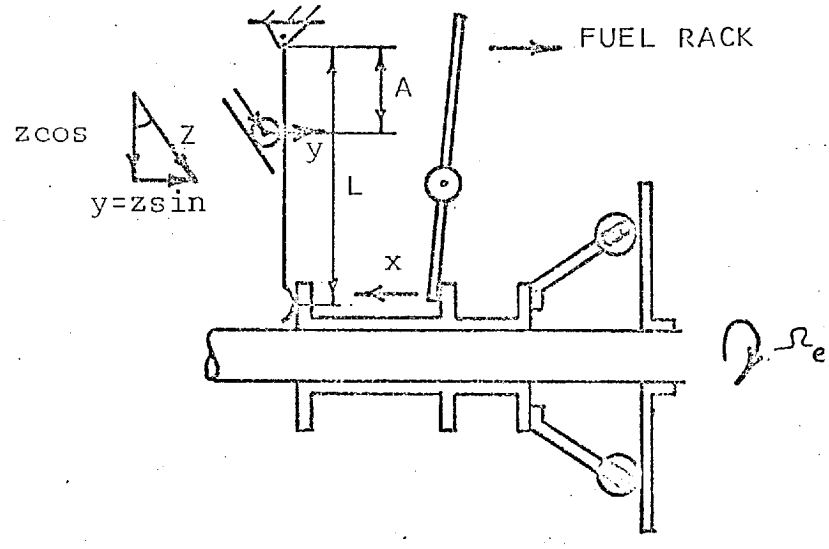


FIG. (2.7) Variable Speed Govenor (with a leaf type Speeder Spring)

Furthermore, a highly accurate prediction of the injection rate diagram preceding each firing is not essential, as combustion is represented by an apparent rate of burning diagram.

Fuel injection can be visualised as a fuel pulse introduced into the cylinder each cycle. This pulse is both modulated in amplitude and duration according to engine speed and rack position. Also, the point of dynamic injection (start of injection) varies with engine speed.

This system was adequately modelled by a dynamic gain element coupled with a sampler. The mass of fuel injected per cycle was correlated (Chapter 5) with rack position (r) and engine speed ($\Omega_e$):

$$M_f = M_f(r, \Omega_e) \qquad (2.47)$$

The sampling instant was taken to coincide with the point of dynamic injection:

$$\theta_{di} = \theta_{si} + \Delta t \Omega_e \qquad (2.48)$$

where: $M_f$ = mass of fuel injected per cycle per cylinder,

$\theta_{di}, \theta_{si}$ = crank position at points of dynamic and static injection,

$\Delta t$ = injection delay, i.e. time lapsing between $\theta_{si}$ and $\theta_{di}$.

Since the engine speed and rack position were unlikely to alter appreciably during this extremely short period (injection duration), this assumption seemed justifiable, particularly in a case of a simple mechanical governor.

## 2.7 HEAT TRANSFER

The heat loss to the cylinder walls is important for two reasons:

1. The effect on the thermodynamic cycle and its efficiency.

2. The influence on the metal temperatures and thermal loading of the components.

It was mentioned earlier that the instantaneous rate of heat transfer between the gases and enclosing walls is evaluated using equation (2.10):

$$\dot{Q} = hA(T_w - T_g)$$

A brief assessment of a number of widely used correlations (Table 2.1) for the coefficient of heat transfer follows, but for a detailed analysis of the subject the reader is referred to Annand ( 4 ) and Lefeuvre (69). The method used for computing the mean cycle temperatures of the gas exposed surfaces is also described. A simplified model for the exhaust manifold heat losses is given.

### 2.7.1 Coefficient of heat transfer in the cylinder

The complexity of the problem of heat transfer between the cylinder gases and gas-exposed surfaces is best illustrated by the fact that despite the numerous investigations that have been carried out in the last four decades, the dependence on many possible parameters is not fully agreed. Within one engine cycle heat transfer occurs by convection in addition to gas and flame radiation. Thus, most of the published correlations describing heat flow in engine cylinders, comprise either one convective term only, or one convective term in conjunction with one or two radiative terms.

Eichelberg's correlation (38) was developed in the late 1930's but is still used due to its simplicity. To achieve greater flexibility, Pflaum (85) introduced a factor

| SOURCE | FORMULA | REMARKS |
|---|---|---|
| Eichelberg (38) | $h = 2.43 \times 10^{-3} (V_p)^{\frac{1}{3}}(PT)^{\frac{1}{2}}$ | $V_p$ = mean piston speed<br>P, T = pressure and temperature of the gas inside the cylinder |
| Pflaum (85) | $h = f(P_{sc}).f(V_p)(PT)^{\frac{1}{2}}$<br>$f(P_{sc}) = 20.44\, a\, (P_{sc}/1.013)^b$<br>$f(V_p) = 6.9 - 5.9 \times (4.5)^{-(0.3215V_p)^{1.8}}$ | $P_{sc}$ = scavenging pressure<br>For piston and cylinder head, a = 2.3 and b = 0.25<br>For liner, a = 0.8 and b = 0.25 |
| Nusselt (80) | $q/A = 1.071 \times 10^{-3}(1 + 1.247V_p)[(P/1.013)^2 T]^{\frac{1}{3}}(T-T_w) + 4.211 \times 10^{-12}(T^4-T_w^4)$ | q = heat transfer rate.<br>$T_w$ = wall temperature.<br>A = heat transfer area. |
| Brilling (25) | $q/A = 1.071 \times 10^{-3}(2.45 + 0.184V_p)[(P/1.013)^2 T]^{\frac{1}{3}}(T-T_w) + 4.211 \times 10^{-12}(T^4-T_w^4)$ | |
| Elser (39) | $Nu = 6.5(1 + 0.5\frac{\Delta s}{Cp})[Re.Pr]^{\frac{1}{2}}$ | $\Delta s$ = increase in specific entropy<br>$C_p$ = specific heat at constant pressure<br>Re = Reynolds number<br>Pr = Prandtl number<br>$\theta$ = crank angle from top dead centre |
| Oguri (83) | $Nu = 6.5(1 + \frac{\Delta s}{Cp})[Re.Pr]^{\frac{1}{2}}[2 + \cos(\theta - 20^\circ)]$ | |
| Annand ( 4 ) | $q/A = 20.44\left[a\frac{k}{D}(Re)^{0.7}(T-T_w) + c(T^4-T_w^4)\right]$ | k = thermal conductivity<br>a = 0.35 to 0.8<br>during compression c = 0<br>during combustion and expansion<br>$c = 1.6 \times 10^{-12}$ for diesel engines<br>$c = 2.1 \times 10^{-13}$ for spark ignition engines |
| Woschni (124) | $h = \frac{0.12793}{D^{0.2}T^{0.53}}(\frac{P}{0.98067})^{0.8}\left[C_1 V_p + C_2 \frac{V_s T_1}{P_1 V_1}(P-P_o)\right]$ | $T_1, P_1, V_1$ = temperature, pressure and cylinder volume at a reference point, e.g. inlet valve closure<br>$V_s$ = maximum cylinder volume<br>Scavenging period: C1 = 6.18, C2 = 0<br>Compression: C1 = 2.28, C2 = 0<br>Combustion and expansion: C1 = 2.28, $C2 = 3.24 \times 10^{-3}$ |
| Sitkei (95) | $h = 0.044(1+b)\left[\frac{P^{0.7}V^{-0.7}}{T^{0.2}} D_e^{0.3}\right]$ | $D_e = \frac{2Dh_e}{D+2h_e}$<br>$h_e$ = height of cylinder space above piston<br>b varies from 0 to 0,4 according to the configuration of the combustion chamber |

TABLE 2.1 A Number of Published Correlations for Heat Transfer from Gases to Cylinder Walls.

related to the scavenging pressure and modified the dependence on mean piston speed. Henien (53) reported better agreement with his measurements when replacing the mean piston speed in the Eichelberg relationship by a calculated instantaneous gas velocity. However, he gave no experimental evidence to support the validity of his assumption. Nusselt's formula (80), later modified by Brilling (25), was based on hot bomb studies.

Elser (39) applied dimensional analysis to obtain his formula, in which he used the mean piston speed as a characteristic velocity in the calculation of the Reynolds number. He reported better agreement with the measurements obtained on a two-stroke engine in comparison with four-stroke. Ouguri (83) later modified Elser's relationship to allow for the cyclic variation of the piston speed, verifying his calculations against experimental data from a four-stroke spark ignition engine.

Annand (4 ) reviewed earlier studies of unsteady heat transfer in the internal combustion engine and concluded that all the formulae failed to meet basic requirements. He criticised Eichelberg, Nusselt and Brilling on the grounds that their formulae were dimensionally incorrect and hence could not be relied upon in representing conditions greatly different from those upon which their tests were based. Elser and Ouguri were criticised for incorrectly replacing the dimensionless group $(\frac{q}{\rho C_p NT})$ by $\Delta S/C_p$. Annand then re-analysed Elser's experimental data and proposed a correlation comprising a Nusselt-Reynolds convection term in addition to a flame radiation term.

Although this was an attempt to produce a flexible and dimensionally correct formula, the inadequate representation of the gas velocity by the mean piston speed was

retained. Moreover, the limits specified for the proportionality constant (a), in the convection term, were quite wide.

Sitkei (95) proposed a formula based on the Nusselt-Reynolds forced convection relationships, and introduced a constant (b) to cater for the effect of the combustion chamber configuration. Knight outlined a method for calculating instantaneous gas velocities and applied pipe flow heat transfer data but predictions for fixed cycles were not in good agreement with measurements. Woschni (123) has also derived a formula using heat transfer data for turbulent flow in pipes. He related gas velocities to the mean piston speed and a term accounting for the additional equivalent turbulence introduced by combustion. The advantage of this formula lies in the distinction between the different rates of heat transfer during compression, combustion and scavenging. This is coupled with the possibility of adjustment to any engine (76) via experimentally determinable constants in the gas velocity expression. In comparisons by Woschni (123) using area averaged, and by Lefeuvre (69) using local, heat transfer rates, Woschni's correlation showed better agreement with experimental data than other formulae.

Based on these facts and because of the above mentioned advantages, Woschni's correlation is used in the simulation. No modification to the original constants was found necessary as the computation of the fuel mass burning rates from experimental pressure diagrams (Chapter 6) showed good agreement with the measured quantity of fuel supplied. However, provision was also made to enable the use of other heat transfer correlations in the simulation, if required, e.g. Annand or Eichelberg.

## 2.7.2 Evaluation of cylinder wall temperatures

A one-dimensional heat balance between the gas and coolant is applied to compute temperatures of the gas-exposed surfaces in the cylinder during steady state operation. The conduction heat transfer model employed here was presented in detail by Borman (21) and later used by Streit (99) in a simulation of a two-stroke turbocharged diesel engine. In order to assess the influence of the cylinder wall temperatures on the transient performance of the engine, the model was extended in a simplified way.

Steady state operation:

The cylinder walls are divided into three regions, namely: cylinder head, liner and piston crown. An equivalent steady rate of heat transfer was assumed through each surface with uniform temperatures and heat transfer coefficients on both sides of each wall. By neglecting the cyclic variation in wall temperature the steady heat transfer rate can be expressed as:

$$\dot{Q} = \frac{T_{eg} - T_c}{R_g + R_m + R_c} \qquad (2.49)$$

where: $R$ = the thermal resistance of each heat path,

$$R_g = \frac{1}{h_{eg} A_{eg}},$$

$$R_m = \frac{x_m}{K_m A_m},$$

$$R_c = \frac{1}{h_c A_c},$$

$h$ = coefficient of heat transfer,

$k$ = thermal conductivity of wall,

$x$ = wall thickness,

and e, g, w, c stand for effective, gas, wall and coolant respectively.

To account for cyclic variation in the gas temperature, the gas side heat transfer coefficient, and in the case of the liner the heat transfer area, the following effective time average quantities are used:

liner effective area:

$$A_{eg} = \frac{\oint A_g(t)dt}{\oint dt} \qquad (2.50)$$

effective heat transfer coefficient:

$$h_{eg} = \frac{\oint A_g(t)h_g(t)dt}{\oint A_g(t)dt} \qquad (2.51)$$

and the effective gas temperature:

$$T_{eg} = \frac{\oint T_g(t)A_g(t)h_g(t)dt}{\oint A_g(t)h_g(t)dt} \qquad (2.52)$$

where $\oint$ denotes the cyclic integral between t and $t+\Delta t$; t and $\Delta t$ being time and the cycle duration respectively.

Analogous heat transfer resistance networks for the piston, liner and cylinder head are shown in Fig. 2.8. The metal thermal resistances $R_2$, $R_4$, $R_5$, $R_7$ and $R_{10}$ are obtained from geometric best estimates. The friction heat flux ($\dot{E}_{fr}$), taken as 50% of all mechanical losses (98), is added at the piston/liner interface. In the case of an effectively oil-cooled piston, the heat path branching off $T_p$ is considered and $R_8$ is estimated. An empirical correlation, suggested by Howarth (56) is used to evaluate the water side heat transfer coefficient and hence resistances $R_1$ and $R_c$:

$$h_w = 0.12695\ \dot{Q}^{0.644} \qquad (2.53)$$

This assumes that nucleate boiling will occur and accordingly relates the heat transfer coefficient to the heat flux. However, any other correlation could be employed.

The temperatures $T_{hg}$, $T_{pg}$ amd $T_{\ell g}$ can be obtained

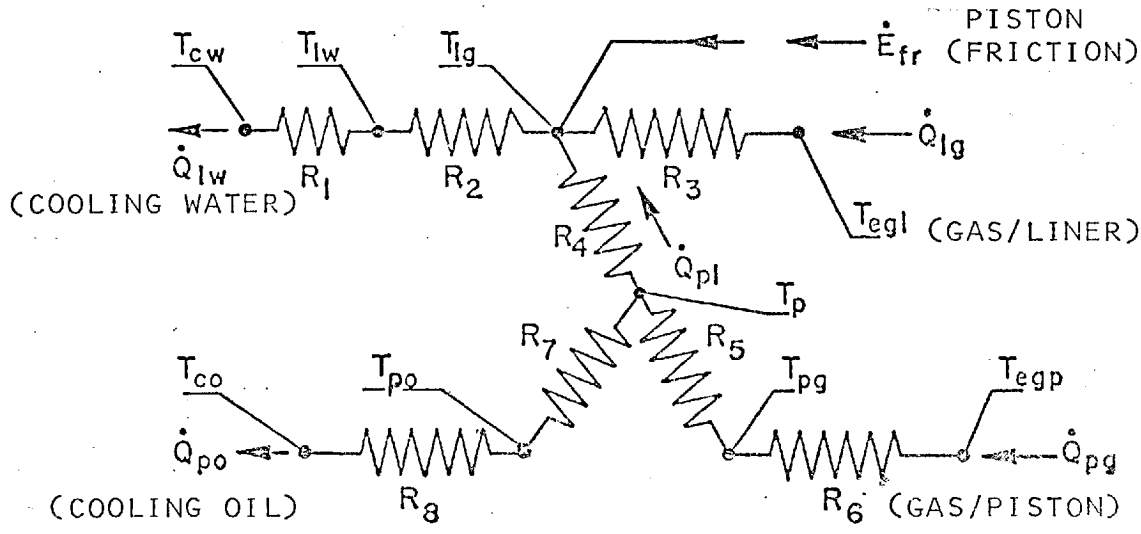


PISTON AND LINER.

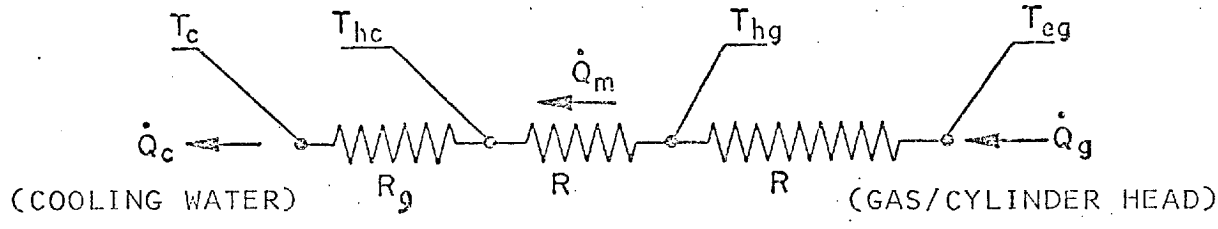


CYLINDER HEAD

FIG. (2.8) Heat Transfer Resistance Networks for Piston, Liner and Cylinder Head

in terms of the resistances, the effective gas temperatures and the friction heat flux ($T_{pg}$ and $T_{\ell g}$ only).

$$T_{hg} = \frac{T_{eg}(R_9+R_{10}) + T_c R_g}{R_9 + R_{10} + R_{11}} \qquad (2.54)$$

$$T_{pg} = \frac{(R_5 T_{egp} + R_6 T_p)}{(R_5 + R_6)} \qquad (2.55)$$

$$T_{\ell g} = R_4\left[\frac{T_p - T_{egp}}{R_5+R_6} + \frac{T_p - T_{co}}{R_7 + R_8}\right] + T_p \qquad (2.56)$$

where

$$T_p = \frac{\dot{E}_{fr} + \frac{T_{eg\ell}}{R_3} + \frac{T_{cw}}{R_1+R_2} + \left[1 + \frac{R_4}{R_3} + \frac{R_4}{R_1+R_2}\right]\left[\frac{T_{egp}}{R_5+R_6} + \frac{T_{co}}{R_7+R_8}\right]}{\frac{1}{R_3} + \frac{1}{R_1+R_2} + \left[1 + \frac{R_4}{R_3} + \frac{R_4}{R_1+R_2}\right]\left[\frac{1}{R_5+R_6} + \frac{1}{R_7+R_8}\right]} \qquad (2.57)$$

At the end of each calculated cycle, the effective gas temperatures, friction flux and the variable thermal resistances are computed. Subsequently, new values for the surface temperatures can be calculated.

Transient operation:

Due to the thermal capacity of the cylinder walls, a step change in the effective temperature of the gas does not result in an instantaneous response in the metal temperature. The time lag experienced is of a greater order of magnitude than the response of the engine to rapid changes in load and/or speed (minutes versus seconds). The calculation of this lag is a difficult exercise and cannot be justified in this application due to the small error involved. However, a simplified method was employed in order to investigate the effect of the thermal capacity of the walls.

The steady state heat transfer model, mentioned earlier, is applied once every engine cycle to provide the

value of the wall temperature for a case of zero thermal capacitance and the actual wall temperature is allowed to follow in an exponential form as given by Sitkei (94):

$$T_w(t_{n+1}) = T_w(t_n) + \left[T_{w_{c=0}}(t_{n+1}) - T_w(t_n)\right](1-e^{\Delta t/\alpha}) \qquad (2.58)$$

where: $T_w$ = actual wall temperature,

$T_{w_{c=0}}$ = wall temperature for a case of zero thermal capacity, c = 0,

$n$ = cycle number,

$\Delta t$ = cycle duration,

$\alpha$ = time constant.

It is important to mention that the steady heat flow treatment as proposed by Borman (21) constitutes a considerable simplification of the actual situation. Nevertheless, the computed temperatures represent some average values indicative of individual surface temperature level but cannot be used for applications such as thermal stress analysis. The treatment postulated for transient operation provides a simple and useful means of investigating the effect of the wall temperature on the response of the engine.

### 2.7.3 Heat losses from the exhaust gases

Several attempts have been made to compute heat losses through the walls of the exhaust manifolds. Borman (21) used Eichelberg's and Zapf's correlations (38, 128) to represent the heat transfer coefficient from the exhaust gases to the manifold walls. Arbitrary constants were used in this case and no experimental support was given. This lack of experimental information led Janota (61) to use a fixed overall heat transfer coefficient accounting for the thermal resistances of the gas, metal and air.

The latter approach was adopted here. However, this assumption may be replaced by a correlation (if available) for the heat transfer coefficient, dependent on the instantaneous conditions of the gas and manifold geometry.

# CHAPTER 3

## NUMERICAL TECHNIQUES AND SIMULATION PROGRAM

### 3.1 INTRODUCTION

This chapter reviews the governing differential equations involved in the simulation and describes the mathematical manipulation necessary for the solution process. The resulting set of first-order non-linear differential equations is presented in the form of a rate of change of an individual state variable, expressed in terms of the remaining variables and their rates. Boundary conditions are also outlined.

The equations are solved numerically along equal increments of crank angle. The numerical methods applied together with the solution procedure are discussed. The general framework of the simulation program is outlined; a brief description of its individual subroutines being given in Appendix B. Also the input data requirements are listed and the resulting output is described.

### 3.2 REVIEW OF GOVERNING EQUATIONS

The theoretical analysis, presented in Chapter 2, shows that the prediction of the transient performance of a turbocharged diesel engine necessitates a continuous evaluation of the interactions between all its individual components. It is therefore essential to select the parameters which define the state of the engine system at any moment, and to develop the differential equations governing their interaction and subsequent variation with time.

The dynamic state of the engine could be conveniently described by the following variables: the temperature,

equivalence ratio and mass of the gases inside each compartment, the rotational speeds of the crankshaft and turbocharger, the linear speed and position of the fuel rack, and the angular position of the crankshaft. The knowledge of values of these variables at time $t_o$ together with the time pattern of the loading torque and demand speed is essential and sufficient to yield the transient response of the engine.

Prior to developing the governing equations, the operational nature of the diesel engine will be reviewed briefly. Most of the processes and events involved are periodic with respect to the crank position, whether the engine speed is constant or varying: piston motion, valve motion, injection and the four basic strokes. The timing of the dynamic injection point, the ignition point and the resultant pressure developed inside each cylinder in relation to top dead centre (TDC), have an important influence on the engine torque and the available exhaust energy. Also the phase difference between the points of static injection and the application of external disturbance (variation in load or demand speed) affects the engine response.

To investigate and analyse the interaction between the different processes, and their influence on the transient behaviour of the engine, it was decided to transform the problem from the time to the crankshaft domain. Such a transformation, in addition to displaying the periodic nature of engine events, simplified the structure of the simulation program. It also reduced the computational effort in the case of a fully iterative algorithm.

By using crank angle as the sole independent variable, equation (2.11) becomes:

$$\frac{dt}{d\theta} = \frac{1}{\Omega_e} \tag{3.1}$$

From the definition of the equivalence ratio, equation (2.1), the mass of burned fuel, $M_f$, present in a mixture of combustion products of mass M, is:

$$M_f = \frac{f_s F}{1+f_s F} M \tag{3.2}$$

Using equations (3.1) and (3.2), the conservation of fuel species, equation (2.4) takes the form:

$$\frac{dM_f}{d\theta} = \frac{1}{\Omega_e} \sum_j \frac{f_s F_{j,u}}{1+f_s F_{j,u}} \dot{m}_j + \frac{dM_{f,t}}{d\theta} \tag{3.3}$$

where: $F_{j,u}$ = equivalence ratio of gases flowing; taken equal to the upstream value ($F_u$).

$\frac{dM_{f,t}}{d\theta}$ = apparent rate of burning of fuel; cylinders only.

Differentiating equation (2.1) with respect to crank angle and substituting for $M_f$ and $dM_f/d\theta$ from equations (3.2) and (3.3) respectively gives:

$$\frac{dF}{d\theta} = \frac{1+f_s F}{f_s M} \left[ (1+f_s F)\left(\frac{\psi_1}{\Omega_e} + \frac{dM_{f,t}}{d\theta}\right) - f_s F \frac{dM}{d\theta} \right] \tag{3.4}$$

where: $$\psi_1 = \sum_j \frac{f_s F_{j,u}}{1+f_s F_{j,u}} \dot{m}_j \tag{3.5}$$

To account for temperature variation, the differential equation developed by Borman (21), for his steady state engine simulation program, is employed. It is based on the law of conservation of energy, equation (2.2) and equations (2.7) to (2.9) after differentiation:

$$M\frac{de}{d\theta} + e\frac{dM}{d\theta} = -p\frac{dV}{d\theta} + \frac{1}{\Omega_e}\sum_i Q_i + \frac{1}{\Omega_e}\sum_j \dot{m}_j h_j \tag{3.6}$$

$$\frac{de}{d\theta} = \frac{\partial e}{\partial \theta}\frac{dT}{d\theta} + \frac{\partial e}{\partial P}\frac{dP}{d\theta} + \frac{\partial e}{\partial F}\frac{dF}{d\theta} \tag{3.7}$$

$$\frac{dR}{d\theta} = \frac{\partial R}{\partial \theta}\frac{dT}{d\theta} + \frac{\partial R}{\partial P}\frac{dP}{d\theta} + \frac{\partial R}{\partial F}\frac{dF}{d\theta} \qquad (3.8)$$

$$\frac{dP}{d\theta} = \frac{MRT}{V}\left[\frac{1}{M}\frac{dM}{d\theta} + \frac{1}{R}\frac{dR}{d\theta} + \frac{1}{T}\frac{dT}{d\theta} - \frac{1}{V}\frac{dV}{d\theta}\right] \qquad (3.9)$$

By manipulating equations (3.6) to (3.9) the terms $\frac{dR}{d\theta}$, $\frac{dP}{d\theta}$ and $\frac{de}{d\theta}$ are eliminated, resulting in:

$$\frac{dT}{d\theta} = \frac{-\frac{P}{M}\frac{dV}{d\theta} + \frac{1}{M}\left[\frac{1}{\Omega_e}\sum_i Q_i + \frac{1}{\Omega_e}\sum_j \dot{m}_j h_j - e\frac{dM}{d\theta} - M\frac{\partial e}{\partial F}\frac{dF}{d\theta}\right] - \psi_4}{\frac{\partial e}{\partial T} + \frac{\psi_3}{\psi_2}\frac{P}{T}\frac{\partial e}{\partial P}} \qquad (3.10)$$

where:

$$\psi_2 = 1 - \frac{P}{R}\frac{\partial R}{\partial P} \qquad (3.11)$$

$$\psi_3 = 1 + \frac{T}{R}\frac{\partial R}{\partial T} \qquad (3.12)$$

$$\psi_4 = \frac{P}{\psi_2}\frac{\partial e}{\partial P}\left[\frac{1}{M}\frac{dM}{d\theta} - \frac{1}{V}\frac{dV}{d\theta} + \frac{1}{R}\frac{\partial R}{\partial F}\frac{dF}{d\theta}\right] \qquad (3.13)$$

The rate of change of mass is provided with the aid of equation (2.3):

$$\frac{dM}{d\theta} = \frac{1}{\Omega_e}\sum_j \dot{m}_j \qquad (3.14)$$

Equations (2.36) and (2.40) describe the rates of change of turbocharger and engine speeds with respect to time. These are transformed into:

$$\frac{d\Omega_{tc}}{d\theta} = \frac{C_t - C_\theta}{\Omega_e J_{tc}} \qquad (3.15)$$

and

$$\frac{d\Omega_e}{d\theta} = \frac{1}{\Omega_e}\frac{C_e - C_L - C_f}{(J_e + J_L)} \qquad (3.16)$$

By considering the linear speed of the fuel rack, u, as an intermediary variable, the governor second-order differential equation is resolved into two first-order equations. Also applying equation (3.1) gives:

$$\frac{dx}{d\theta} = \frac{1}{\Omega_e}u \qquad (3.17)$$

$$\frac{du}{d\theta} = \frac{1}{\Omega_e C1}\left[ C6(\Omega_e^2 - \Omega_r^2) + C5\Omega_2^2 x - C2u - (1 + C3y)(x + C4y) \right] \quad (3.18)$$

The resulting set of $3n_t+5$ ($n_t$ = total number of control volumes) first-order ordinary differential equations (3.1, 3.5, 3.10 and 3.14 to 3.18), must be solved simultaneously in order to obtain the dynamic behaviour of the system. The evaluation of the right-hand side terms, essential for the solution, constitute the major part of the simulation programme and require the use of all remaining relations in Chapter 2.

Boundary Conditions:

It is essential to define the initial and boundary conditions in order to obtain a solution to the set of differential equations developed. Accordingly the following information is required:

1. Ambient temperature and pressure; $T_{amb}$ and $P_{amb}$ for $t \geqslant 0$, plus the turbine back pressure, $P_{to}$.
2. The initial crank position; $\theta_i$.
3. Load torque and governor setting; $C_L(t)$ and $y(t)$ for $t \geqslant 0$.
4. Temperatures of the cooling water and oil; $T_{CW}$ and $T_{CO}$.
5. Values of the state variables at the initial crank position; $T_K$, $F_K$, $M_K$, $\Omega_e$, $\Omega_{tc}$, u and x at $t = 0$; $i = 1, 2, \ldots, n_t$.
6. Wall temperatures and combustion constants for the initial steady state condition.

However, in the case of items 5 and 6, only reasonable estimates are required. This is achieved by

programming the computation to proceed for a number of cycles using fixed values of load and governor setting until the solution converges to an initial steady state point.

## 3.3 NUMERICAL METHODS

The governing equations presented in the previous section constitute an initial value problem comprising m simultaneous first-order differential equations of the form:

$$\frac{dZ_k}{d\theta}(\theta) = f_k(Z_1, Z_2, \ldots, Z_m, \theta) \qquad (3.19)$$

where: $Z_k(\theta_o) = Z_o$

$k = 1, 2, \ldots, m$; m being equal to $3n_t+5$.

It appears essential at this stage to consider the nature of the variables involved, prior to selecting the numerical technique. It is mentioned earlier that conditions inside the cylinders (charge mass, temperature and equivalence ratio) varied periodically in relation to crank angle, even at fixed engine speeds. Moreover, the rates of variation of these thermodynamic conditions are several orders of magnitude faster than the steepest rates of acceleration/deceleration of the engine and turbocharger (the response times of the engine and turbocharger are of the order of one second, whilst large changes in equivalence ratio and temperature occurred in a few ms). Therefore, the numerical solution and the integration step size primarily should satisfy the requirements of equations (3.4), (3.10) and (3.14).

The literature describes several techniques for integrating differential equations, the two most common methods are the Runge-Kutta and the predictor corrector (iterative) techniques. Although neither of the two are superior in all problems(29), Annand (2) indicated that

iterative techniques were more suited to engine simulation (steady state operation). He showed that a fourth order Runge-Kutta method was less efficient than an iterative scheme of the same order of accuracy. Annand also reported that the former method could display numerical instability during the gas exchange process. Furthermore, predictor corrector methods provide an automatic estimate of the truncation error (a property lacked by Runge-Kutta methods), allowing step size optimisation for a fixed accuracy.

Based on the above considerations and experience resulting from simulation of engine steady state performance (21,61,99), a second order predictor corrector method was adopted for the integration of equations (3.5), (3.11) and (3.16). This was of the Euler open type formula for prediction:

$$Z_k(\theta_j) = Z_k(\theta_{j-1}) + \Delta\theta . f_k\left[\underline{Z}(\theta_{j-1}), \ldots\ldots, \theta_{j-1}\right] \qquad (3.20)$$

and the modified Euler closed type integration formula for correction:

$$Z_k^n(\theta_j) = Z_k(\theta_{j-1}) + \frac{\Delta\theta}{2}\left\{f_K\left[\underline{Z}_1(\theta_{j-1}), \ldots, \theta_{j-1}\right] + f_k\left[\underline{Z}_1^{n-1}(\theta_j), \ldots, \theta_{j-1}\right]\right\} \qquad (3.21)$$

The predictor formula (3.20) provided a first approximation $Z_k^o(\theta_j)$, which was essential for the evaluation of a better estimate via the corrector formula. An iterative sequence was evolved by the alternate application of equation (3.21) and subsequent testing for convergence. The difference between two successive iterations, n and n-1, had to be within a specified tolerance $\varepsilon_k$:

$$\left|Z_k^n(\theta_j) - Z_k^{n-1}(\theta_j)\right| \leqslant \varepsilon_k \qquad (3.22)$$

An integration step length of $1^{o}$CA was selected, to cater for the nature of the thermodynamic variables. Streit (99) reported that employing smaller steps did not yield significant improvement in accuracy.

As the chosen step length was very small in comparison with the requirements of equations (3.15) and (3.16), iteration was not essential in this case. Accordingly the Adams Bashforth open type integration formula (51) was used:

$$Z(\theta_j) = Z(\theta_{j-1}) + \frac{\Delta\theta}{24}\left[55f(\theta_{j-1}) - 59f(\theta_{j-2}) + 37f(\theta_{j-3}) - 9f(\theta_{j-4})\right] \qquad (3.23)$$

Equations (3.17) and (3.18) were integrated using the predictor corrector pair (3.20) and (3.21). This was done to provide an accurate description of the governor behaviour during rapid changes in demand speed, particularly close to the end points of the fuel rack travel.

## 3.4 GENERAL SOLUTION PROCEDURE

The solution procedure consisted of integrating the differential equations (Section 3.2) in parallel along equal increments of crank angle. A computational scheme, based on the numerical integration formulae (3.20), (3.21) and (3.23) was employed to compute values of the engine state variables at any crank angle $\theta_j$, using information generated at previous crank positions. This, presented in the form of a flow chart, (Fig. 3.1) comprises the following basic steps:

1. Engine and turbocharger speeds are evaluated using formula (3.23).

2. The current time $t_j$ is calculated by integrating equation (3.1) using formula (3.21); the load torque and governor setting are determined accordingly.

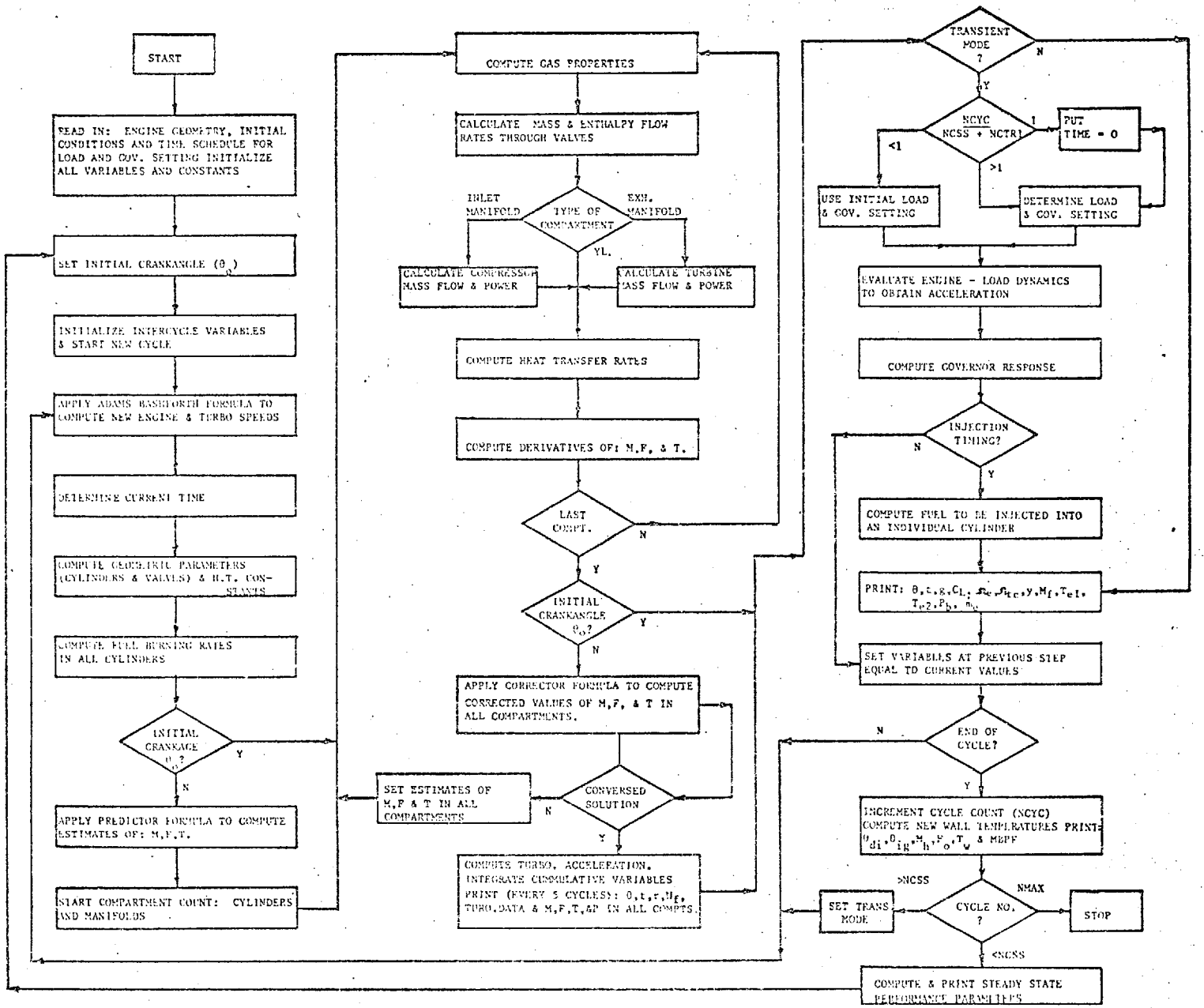


FIG. (3.1) Flow Diagram Showing Overall Sequence of Computations

3. Values of the geometric parameters and fuel burning rates are determined for all cylinders.

4. The predictor formula (3.20) is applied to provide estimates of $M_k$, $F_k$ and $T_k$ in all compartments.

5. Properties of the fluids are evaluated in all compartments.

6. Rates of mass flow of gases and burned fuel species together with the accompanying rates of enthalpy transfer through all flow sections are calculated. Compressor and turbine torques are also evaluated.

7. All rates of heat transfer from the gases are calculated.

8. The rates of change of $M_k$, $F_k$ and $T_k$ in all control volumes are determined using equations (3.14), (3.4) and (3.10) in order.

9. Corrected estimates of $M_k$, $F_k$ and $T_k$ are then evaluated using equation (3.21), and inequality (3.22) is applied to check convergence. A compromise between accuracy and computing time is normally sought when selecting convergence tolerances. Suitable values are $2 \times 10^{-4}$, $5 \times 10^{-4}$ and $9 \times 10^{-4}$ of the maximum steady state values of $M_k$, $T_k$ and $F_k$ respectively. The thermodynamic iteration is restarted from step 5 if the specified tolerances are exceeded in any control volume.

10. The torques developed by the engine and imposed by friction are evaluated. Rates of change of turbocharger and engine speeds are determined using equations (3.15) and (3.16).

11. The governor response (fuel rack position) is evaluated using the predictor-corrector pair, equations

(3.20) and (3.21). An accuracy tolerance of $1 \times 10^{-4}$ of the fuel rack travel is employed.

12. The current crank position is checked against the static injection timing of all cylinders. When necessary, the mass of fuel to be injected is evaluated using equation (2.47).

13. The crank position is then incremented and the sequence is repeated from step 1.

## 3.5 COMPUTER PROGRAM

A computer program has been written to predict the transient response of turbocharged diesel engines to variations in external conditions, i.e. load, demand speed and atmospheric conditions. The program evaluates a number of important aspects of the dynamic and steady state performance of turbocharged and naturally aspirated direct injection diesel engines. Particular reference is given to the influence of the permanently transient thermodynamic conditions within the cylinders and manifolds. The general structure of the program is sufficiently flexible to enable adaptation to different engine types and configurations, such as: indirect injection, 2-stroke, 2-stage turbocharging, etc. The computer code is subdivided into 12 independent subroutines; details of which are described in Appendix B. Each subroutine is assigned one or more tasks; e.g. modelling of engine thermodynamics, simulation of governor behaviour, reading of input data, etc.

The simulation program is based on the theoretical analysis given in Chapter 2 and employs the quasi-steady approach in the treatment of the engine thermodynamics and gas flow. The governing differential equations (Section 3.2) are solved as an initial value problem in conjunction

with the additional algebraic equations in Chapter 2. The general solution procedure is described in Section 3.4.

There are three basic modes of programme operation:

1. NATASP:

In this mode, a naturally aspirated engine with one inlet manifold and a single- or twin-branch exhaust manifold is simulated under steady state or transient running conditions.

2. TURBO:

This mode considers steady state and transient operation of a turbocharged, direct injection diesel engine. Complete turbine and compressor characteristics have to be specified by the user. Since the programme determines its matching point, only an initial estimate of the turbocharger speed is required. Variations in turbocharger speed at a fixed engine speed are computed. Again a common inlet manifold and a single- or twin-entry turbine may be used in this mode.

3. NOZZLE (steady state only):

This mode represents an engine operating under simulated turbocharged conditions; boost conditions are specified and the turbine is replaced by an exhaust nozzle. It is normally used in early design stages to provide approximate turbocharger matching when the turbocharger characteristics are not available.

### 3.5.1 Input data

The following input data is required:

1. Operational mode: NATASP, TURBO or NOZZLE.

2. Integration step size.

3. Required number of steady state and transient cycles (see Appendix B).

4. A detailed geometric specification of the engine.

5. Valve timing and effective valve area against crank angle (or geometric area plus discharge coefficient).

6. Complete compressor and turbine characteristics for the turbocharged mode, together with wheel diameters. Conversely, effective area of exhaust nozzle and boost pressure for nozzle mode.

7. Equivalent polar moment of inertia for engine and turbocharger.

8. Injection timing (static).

9. Values of thermal resistance for the heat flow paths through the cylinder walls (Section 2.7.2) together with estimates of wall temperatures.

10. Ambient pressure and temperature.

11. Initial estimate of fuel injected per cylinder per cycle.

12. Initial crank position in relation to T.D.C. for cylinder number (1), together with estimates of conditions inside all cylinders and manifolds, i.e. temperature, pressure and equivalence ratio.

13. Initial estimates of engine and turbocharger speeds.

14. Time schedule of external disturbances, i.e. load and governor setting (demand speed).

### 3.5.2 Program Output

For steady state operation, the program (3 modes) prints out instantaneous values of pressure, mean gas temperature and equivalence ratio in each cylinder, mass flow rates through the valves, efficiency, torque and mass flow of the turbine and compressor (at specified intervals around the cycle). Cumulative values (complete cycle) of total mass flow and heat transfer for each compartment, plus total work done, trapped mass, trapped equivalence ratio, timing of dynamic injection and ignition, peak pressure and IMEP for each cylinder are printed out at the end of each cycle. In addition, the turbocharger speed, cylinder wall temperatures and overall values of IMEP, ISFC, ISAC, FMEP, BMEP, BSFC, BSAC and turbocharger efficiency are printed.

The above mentioned values are also generated during transient operation (TURBO and NATASP), with the exception of the overall steady state performance parameters, e.g. IMEP, ISFC, etc. Values of engine speed, rack position, fuelling per cylinder per cycle, turbocharger speed, boost pressure, air flow and exhaust temperatures are printed once every injection.

Special plotting subroutines were written to permit a graphical presentation of the data.

### 3.5.3 Computing Requirements and General Remarks

The program has been developed in FORTRAN IV on a CDC 6400 computer. Storage requirement is 22 to 25 k words and the running time is approximately 30 seconds per engine cycle (dependent upon operational mode, step size and engine speed). A typical transient run of 60 engine cycles consumes about 1900 seconds. If reasonable initial

values are given, 4 to 6 cycles will be sufficient for convergence to the initial steady state condition. This process is speeded up by reducing the turbocharger inertia during the steady state computations. Convergence of cylinder wall temperatures normally occurs in 2 to 3 cycles. The initial estimate of engine speed is of particular importance due to the relatively large inertia of the engine and the high gain of the governor.

One of the useful applications of the simulation program is in assessing the effects of design changes on the steady state and transient performance of the engine (examples are given in Section 7.3). The steady state version of the program was made available for teaching and research applications in the Department of Mechanical Engineering at Imperial College. The program is also currently being used (after modification) to predict the steady state performance of a two-stage turbocharged diesel engine.

# CHAPTER 4

# EXPERIMENTAL TECHNIQUES

## 4.1 INTRODUCTION

Difficulties involved in running an engine under controlled transient conditions and handling the measurements required, has limited experimental information on the transient response of a turbocharged diesel engine. English Electric Diesels Ltd. (41) subjected a 1000 hp engine to rapid loads and recorded the following variables with time: brake torque, engine and turbocharger speeds, fuel rack position, boost pressure, exhaust temperature and air flow. Fuel flow was calculated using a relationship between fuelling/cycle/cylinder and rack position based on steady state measurements.

In view of the need for a detailed understanding of the engine thermodynamics and fluid flow during transient operation (a requirement of the simulation), a different experimental approach was employed. Complete cycle diagrams of: cylinder pressure, fuel line pressure, needle lift, boost and exhaust pressures, had to be recorded in addition to the variables mentioned above. It was necessary to record data over a period of 200 engine revolutions following the application of the input signal (rapid change in load and/or demand speed).

The basic requirements of the test programme were as follows:

1. variable control of engine speed and loading torque with time;
2. multichannel (simultaneous) data-logging of sixteen variables;
3. control of the test sequence to ensure repeatability;

4. checking data for effects of faulty instrumentation;

5. data processing and storage.

The advent of computer-controlled engine test beds and the use of computers for data handling made this a feasible programme. In such systems the computer is the nerve centre which directs the sequence of all operations: engine control, data acquisition, on-line data processing and fault detection. The degree of direct digital control (d.d.c.) of the engine depends on the speed and core size of the computer, software capabilities and the data requirements. A compromise design (19) was employed in this work. This consisted of local control of the secondary variables (coolant and oil temperature) and d.d.c. for engine speed and brake torque.

This chapter provides a description of the computer-controlled test bed, built to carry out the transient and steady state tests. Details of the instrumentation used and signal adaptation hardware are given. The digital computer together with the specially built control and data acquisition electronic interfaces are also described. The computer software written to carry out the data-logging and control operations involved in the test procedures developed are presented.

## 4.2 TEST BED

The engine test bed was basically a developed version of the Imperial College computer-controlled test rig (19,62,73). The general arrangement, Figs. 4.1 and 4.2, consisted of the engine coupled to an eddy-current brake, an electrical stepping motor for demand speed variation and an external oil and water cooling system. The engine and

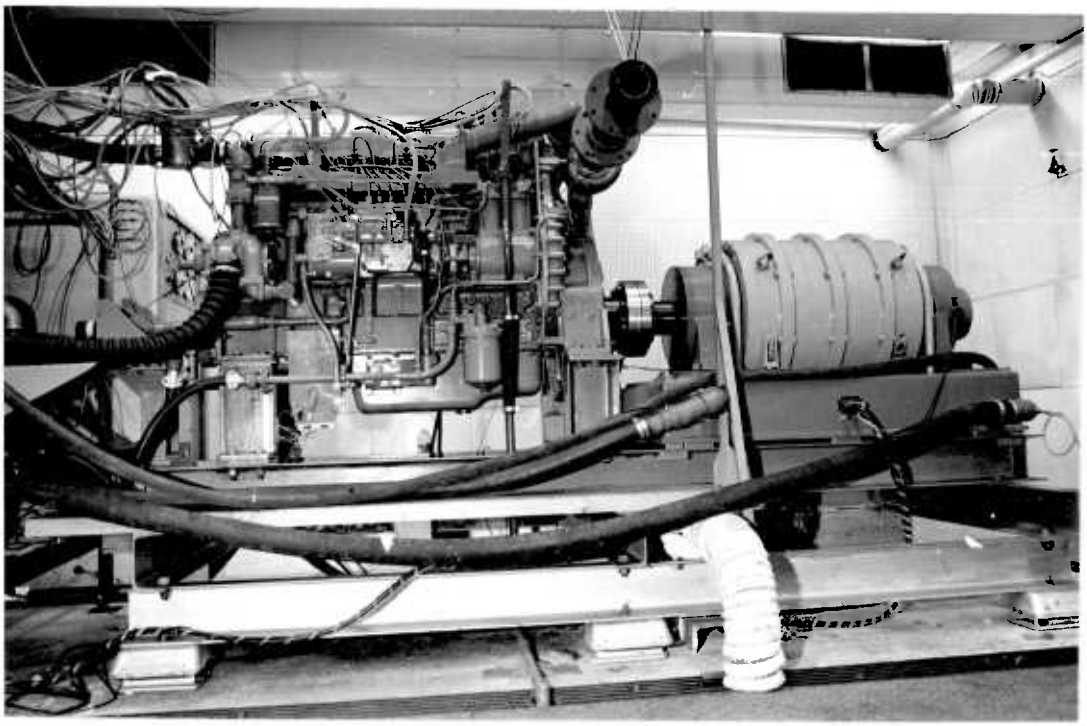

FIG. (4.1) Photograph of Test-Bed Showing Instrumented Engine and Dynamometer.

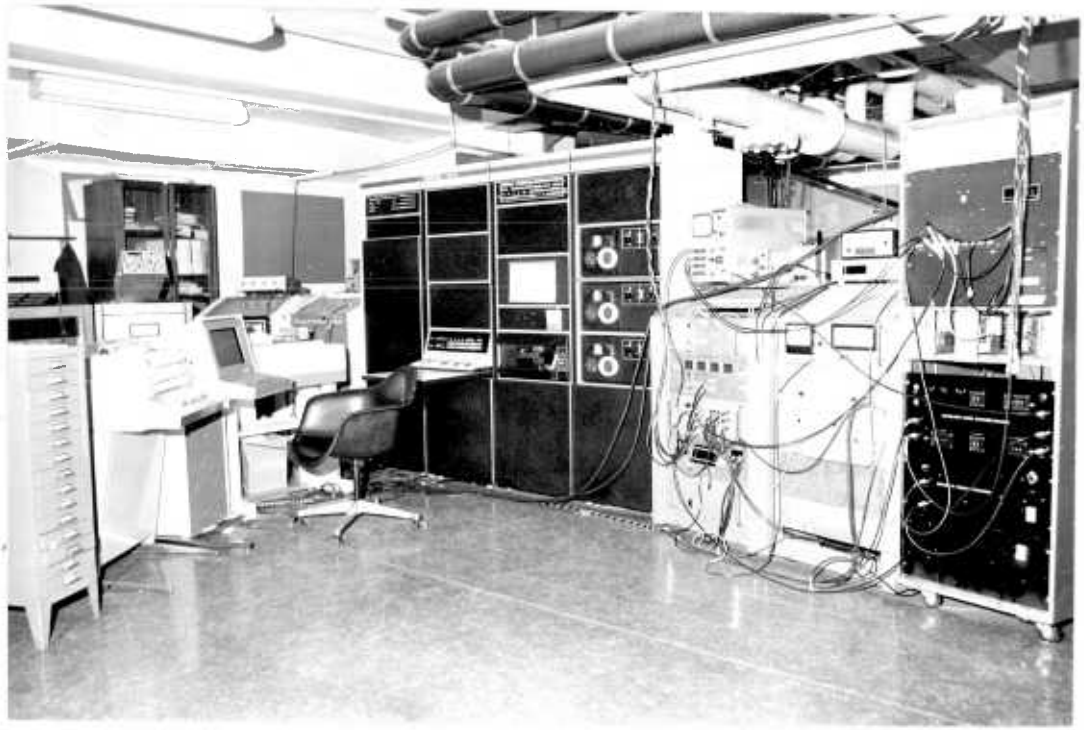

FIG. (4.2) Photograph of Computer-Based Control and Data-Acquisition System.

brake were rigidly fixed to a fabricated steel frame, which was flexibly mounted to a large concrete base. A schematic diagram of the test bed and the control and data lines connecting it to the computer-based control and data acquisition system is shown in Fig. 4.3.

4.2.1 Engine

The experiments were performed on a Leyland 520 series direct injection, turbocharged automotive diesel engine. This was a six cylinder 4-stroke high speed engine built in accordance with the fixed head concept (96). Elimination of the cylinder head high-pressure joint was a radical departure from current design practice, aiming at higher ratings, improved cooling, reduced thermal stress and freedom from restrictions in the cylinder head porting arrangement.

The engine was equipped with an overhead camshaft and directional inlet ports to create air swirl via tangential discharge into the cylinders. The fuel injection system comprised a Simms in-line pump with Leyland 4-hole injectors connected by pipes of equal length. A leaf spring type mechanical governor was included as an integral part of the fuel pump body.

Pulse turbocharging up to delivery pressure ratio of 2.1:1 was effected by a Holset 4LE turbocharger comprising a centrifugal compressor and a dual entry radial exhaust turbine. Two exhaust manifolds separated the gases leaving the two cylinder groups (connecting cylinders 1, 2, 3 and 4, 5, 6).

A boost pressure-sensing fuel control was provided to limit smoke particularly during rapid increases in fuel

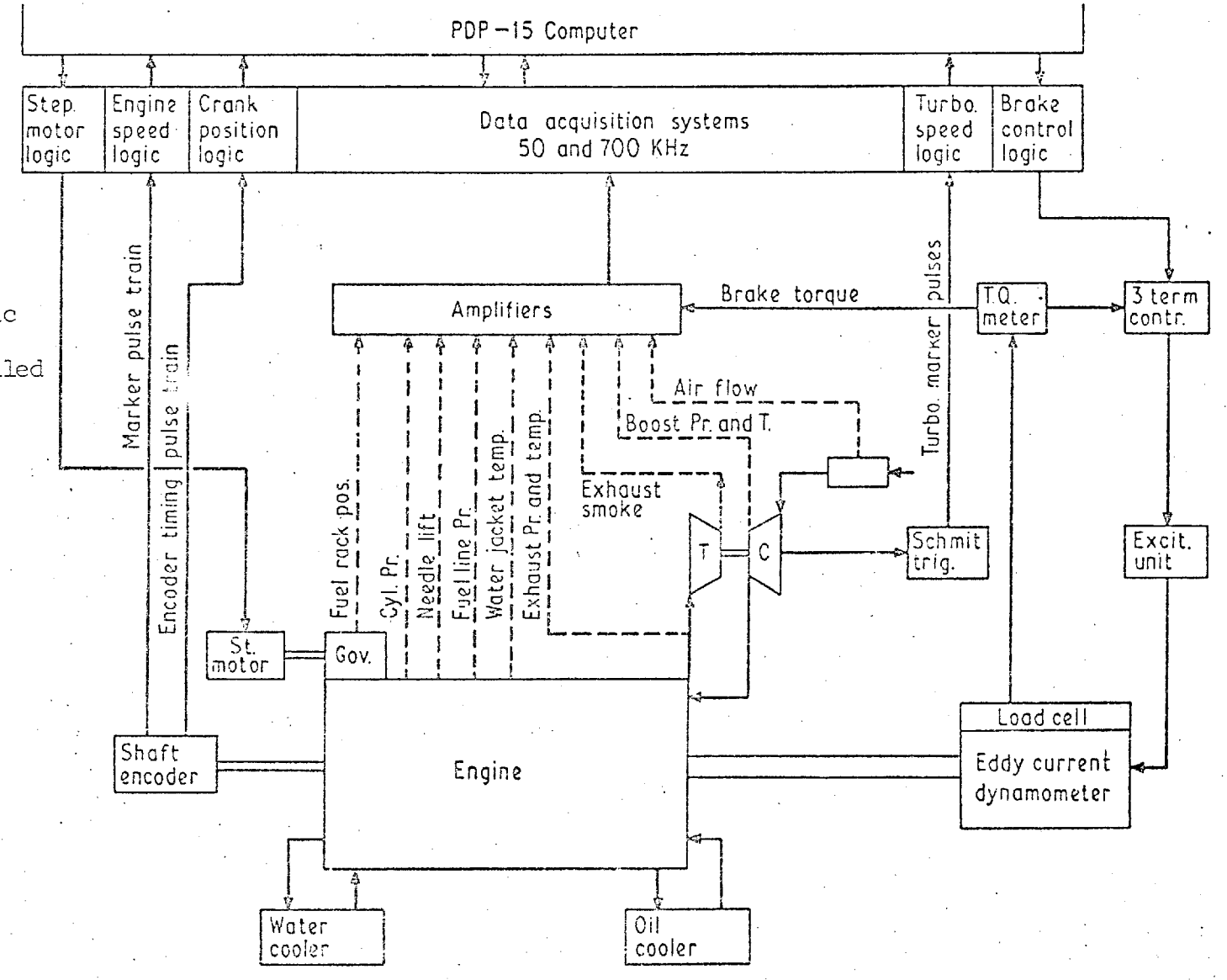


FIG. (4.3) Schematic of Computer Controlled Test-Bed and Data Logging Facility

injection at low speeds. However, all tests were carried out without the controller, hence no limit, other than the fixed maximum fuelling point, was imposed on the fuel input.

The principal engine data together with other particulars are given in Appendix C.

4.2.2 Load

The engine was loaded by a Vibro-meter eddy current dynamometer (type 3WD/25) capable of a maximum torque of 1520 NM at 1800 rev/min. The low inertia of the brake's cylindrical rotor together with its thyristor drive unit ensured a rapid overall response.

The braking power rose progressively with speed according to the degree of excitation (Fig. 4.4). The nominal power of the brake was fixed for thermal reasons, this being reached at 100% excitation and speed $\Omega_g$ (1800 rev/min.). A thermal safety switch was included to intervene if this was exceeded. At speeds above $\Omega_g$, maximum excitation was reduced and the torque characteristic was determined by the brake power and speed; nominal (maximum) torque was obtained at 100% excitation and $\Omega_g$.

The size of the brake was selected such that its maximum torque envelope completely enclosed the engine operational range. Power dissipation in the form of generated heat was carried away by cooling water which flowed inside the stator jacket.

The brake excitation unit, a thyristor-controlled voltage stabilizer, supplied the stator coil with a highly stable direct current to maintain a fixed field strength. Manual control of the output was possible via a ten-turn potentiometer whilst an externally fed d.c. voltage permitted

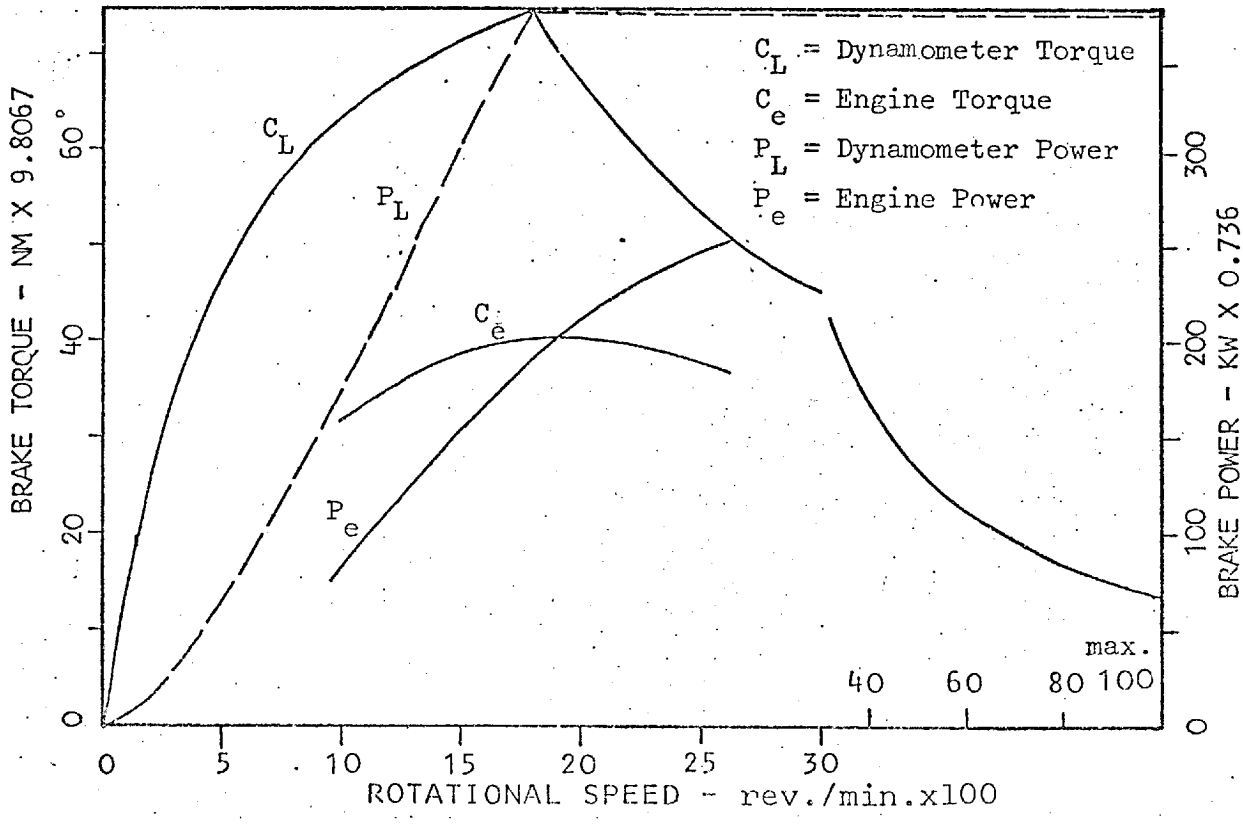


FIG. (4.4) Torque and Power Characteristics of Dynamometer

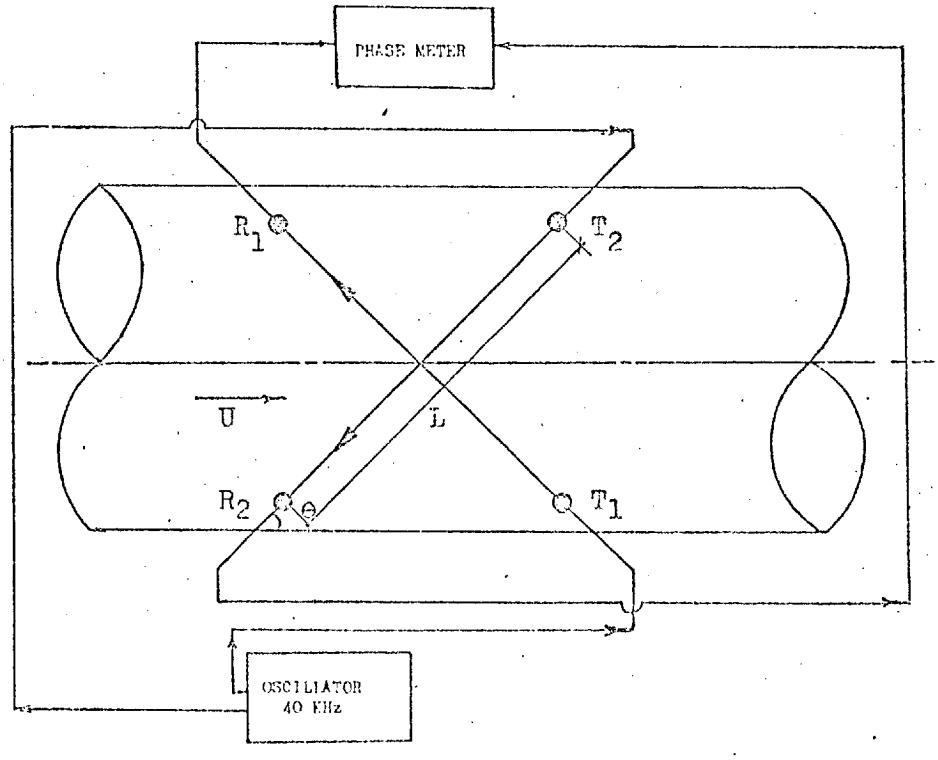


FIG. (4.5) General View of Ultrasonic Air Flowmeter

an alternative remote control. Continuous monitoring of the brake torque was achieved by a load cell, embodied in the dynamometer, together with an appropriate meter.

### 4.2.3 Speed adjustment

A digital stepping motor was used to drive the governor control via a reduction gear box, combining fast adjustment of the engine demand speed with a fine resolution. The permanent magnet motor (Sigma 3437 D200-F075) was of the dual angle type, capable of rotating at two step sizes ($1.8^{o}$ and $0.9^{o}$) at speeds up to 3850 step/s ($0.9^{o}$). A gear reduction ratio of 56.25:1 was selected to give a governor set point resolution of 1/2000 of full range. This allowed a change from minimum to maximum demand speeds in less than 0.6 second.

### 4.2.4 Cooling and temperature control

Both the oil and cooling water were passed through external heat exchangers. The temperatures were controlled via a by-pass system using Sarco TW3 diversion valves. These fully modulated valves responded to the temperature of a sensor via oil-filled capillary tubing. Thus a proportion of the flow was cooled to maintain the temperature within $\pm 1^{o}C$ of the set value.

## 4.3 INSTRUMENTATION

The measuring requirements of the experimental programme were as follows:

a) External variables: engine speed, brake torque, fuel flow, air flow, exhaust smoke, crank angle and real time.

b) Internal variables: cylinder pressure, boost pressure, exhaust pressure, fuel line pressure, needle lift, turbocharger speed, inlet air temperature (manifold), turbine entry temperatures, and fuel rack position.

c) Safety variables: oil pressure and temperature, plus cooling water inlet and exit temperatures.

A description of the measuring techniques, transducers and signal adaptation equipment follows. This is limited to variables recorded by the computer-based data acquisition system. Simple conventional instruments, e.g. temperature gauges, are not discussed.

### 4.3.1 Pressures

Cylinder pressure:

Brown (26) reported that water-cooled piezoelectric pressure transducers are superior to other types with respect to thermal shock, vibration sensitivity, linearity and natural frequency. Strain gauge transducers have excellent performance but can suffer from temperature and vibration effects and have poor linearity. In the case of the balanced disc type, the cylinder pressure diagram is built up point by point over a large number of cycles; a lengthy procedure suitable only for steady state operation.

In view of the above, a water-cooled piezoelectric pressure transducer (AVL 12QP 500C) was used. Errors due to drift of the transducer output were minimised by keeping all electrical connections spotlessly clean (to reduce charge leakage) and by limiting the test duration to a few seconds. The standard deviation of the pressure during the intake stroke was used as a criterion for checking drift during

steady state tests. This was computed for fifty engine cycles and if it exceeded 7 $KN/m^2$ the test was abandoned and repeated. The datum of the cylinder pressure diagram was obtained by relating it to boost pressure measured at the bottom dead centre (BDC) following the intake process.

The effects of thermal shock were reduced (26) by recessing the transducer by 4 mm. Static calibration difficulties were overcome by connecting the transducer to a high impedance charge amplifier (Kistler E568) and using the on-line data logger and computer to record the output continuously for five seconds following a pressure application. The amplifier gain was selected to permit maximum signal resolution (most of the 10 V range of the data logger) with sufficient positive zero offset to prevent the occurrence of negative values.

Manifold pressures: (exhaust and intake)

Water-cooled strain gauge pressure transducers were used for measuring transient pressures in the exhaust and intake manifolds. The piezoelectric type was not chosen as drift could cause serious error in proportion to the relatively low pressures involved. A Philips (PR9370 series) transducer was used. It consisted of a water-cooled pressure diaphragm, which was mechanically linked to a rosette type strain gauge (4 arm bridge). Pressure on the flush-mounted diaphragm caused the bridge to become unbalanced and gave an output proportional to the applied pressure.

Bridge amplifier units (Bryans Southern Instruments, type MO 4/900) were used to supply the bridge with the exciting voltage (4 V), amplify the output and balance the

bridge. The transducer had a measuring range of 0 to 5 bar and a natural frequency of 7 KHz. Static calibration was carried out for each transducer together with its corresponding amplifier.

Injection pressure:

It was intended to measure the injection pressure at the bottom of the injector gallery. The nozzle holder body was drilled and fitted with an Intersonde VT series miniature strain gauge pressure transducer, capable of measuring pressures up to 700 bar with reasonable linearity (± 1.0%). Excellent injection pressure records were obtained using this transducer but unfortunately its life was too short.

As an alternative, but less satisfactory, technique the pressure was measured in the fuel line prior to the injector, using a standard AVL strain gauge transducer (type 31DPS00 E.2). The major drawback of the method resulted from the distance (about 25 cm) separating the measuring point from the injector seat. Subsequently the output signal could not always be considered a truthful picture of the actual valve pressure due to pressure wave effects. Errors were found to increase at part loads; very low pressures were observed immediately following valve opening.

### 4.3.2 Angular and linear displacements

The technique employed for measuring crank angle was first presented by Bloxham et al (19). This constituted a significant improvement in accuracy in comparison with earlier methods (magnetic and photo-electric, etc.). A commercial, heavy duty, optical position encoder (Ferranti, type 28 H2/M4) was used. This was coupled directly to the front of the engine crank shaft by a miniature carden shaft

with flexible (but torsionally stiff) couplings. The device was based on a Moire-fringed glass disc with a solid state light source and light sensitive pick-up on either side. As the disc rotated, the resulting pattern (alternate illuminated and dark lines) produced an approximately sinusoidal output. Processing logic transformed the signal into a square-wave output (digitizer pulse) having a period of $\frac{1}{4}^{o}$. An additional track gave a "once per revolution" marker pulse for absolute position indication.

Determination of the position of T.D.C. in relation to the marker pulse under dynamic conditions was carried out as follows: the engine was run at various speeds with number (1) cylinder motored (zero fuelling). Mean cylinder pressure diagrams were obtained by recording and averaging fifty consecutive cycles and the maximum points were taken as the dynamic positions of the T.D.C. This showed a maximum variation of $\frac{1}{2}^{o}$ over the total speed range 1000-2500 rev/min. Potential error caused by the lack of firing conditions (e.g. lower heat transfer) was investigated using the cycle simulation program and was found to be insignificant.

Injector needle lift:

Needle lift was measured using an inductive nozzle pin displacement transducer (Vibrometer type NH1-100/B). This consisted of a pin core moving inside an inductive coil in the form of a half bridge circuit with a separating air gap of approximately 0.2 mm. A carrier frequency (100 KHz) measuring bridge (AVL type 100-TR1/A) was used in conjunction with the transducer, permitting measurement of high frequency signals (up to 20 KHz). Because of the extremely low weight of the pin core, the mass of the nozzle pin was practically unchanged. An operational amplifier was included to magnify

the transducer output to span most of the data logger voltage range (0-10 V).

The transducer was calibrated statically using a micrometer and digital voltmeter. This was checked dynamically at running conditions when the nozzle pin moved from stop to stop (full lift); linearity was within ±1%.

Fuel pump rack position:

A Penny and Giles displacement sensor type LVDT-1315 was used for measuring the instantaneous fuel rack position. This robust inductive transducer was selected in preference to potentiometers to ensure high resolution together with longer life (no sliding electrical contacts). It was totally self-contained with integral solid state oscillator and demodulator, and gave a d.c. voltage output directly proportional to shaft displacement. An output of 0.10 V was available over a stroke of 2.5 cm with a linearity within ±0.5%.

The transducer was mounted adjacent to the fuel pump, with its axis parallel to the fuel rack. A small opening was made in the pump casing to link the transducer shaft to the fuel rack. The output signal was fed directly to the off-line data logger (Section 4.4.3).

### 4.3.3 Speeds

Engine speed was measured by two devices. The dynamometer was fitted with a 60 tooth gear wheel, a magnetic pick-up and an analogue r.p.m. indicator. This was used for visual indication purposes only. A more accurate means of speed measurement was achieved by electronic processing of the shaft encoder marker pulse together with a 25 KHz pulsed wave source. This method (described in Section 4.4.3) was

used during all the steady state and transient tests.

The turbocharger speed was also measured using the second technique. A Cussons-Ricardo magnetic pick-up was installed to monitor the rotation of a magnetized nut fitted to the compressor end of the turbocharger shaft. This produced an approximately sinusoidal signal with a frequency proportional to the turbocharger speed. A Schmidt trigger circuit was used to transform the signal into a square-wave prior to its processing in conjunction with 500 KHz pulsed wave.

### 4.3.4 Temperatures

Steady state temperature measurements were carried out using sheathed thermocouples: chromel/alumel for exhaust gases at the two turbine entries, and copper/constantin for the inlet manifold and cylinder block water temperature (around number (1) cylinder). For the transient tests, fast response chromel/alumel thermocouples were inserted in the exhaust and inlet manifolds. Wires having a diameter of 0.12 mm and no outer sheaths were used.

The thermocouples were connected to cold junctions placed in a thermostatically-controlled 'fridge. The output leads were connected permanently to specially-built, fixed gain amplifiers feeding the on-line data logger (Section 4.4.3). Since no corrections for radiation effects were made, the accuracy of the exhaust temperature measurements was limited.

### 4.3.5 Air flow

It was originally planned to use an ultrasonic flow meter to measure air flow. A unit was built, in collaboration with Thompson (101). This was calibrated on a

steady flow rig, and installed upstream of the compressor entry. Basically two pairs of ultrasonic transducers were employed, one of which transmitted/received upstream of the flow and the other downstream. The upstream signal was retarded by a flow velocity component, while the downstream one was accelerated (Fig. 4.5). The two transmitters were excited by a highly stable 40 KHz sinusoidal wave source.

By considering the time (t) taken by the signal to cross the flow:

$$t = \frac{1}{C \pm u\cos\theta} \qquad (4.1)$$

where: L = acoustic path length,

C = velocity of propagation of wave in air,

u = mean flow velocity,

$\theta$ = angle enclosed between the wave and flow.

the time lag between the two signals could be obtained:

$$\Delta t = \frac{2uL\cos\theta}{C^2 - u^2\cos^2\theta} \qquad (4.2)$$

The unit design combined low flow velocities and a large angle ($\theta$). Hence $u^2\cos^2\theta$ was neglected in comparison with $C^2$ and the mean flow velocity (u) took the form:

$$u = K.\Delta\phi \qquad (4.3)$$

where: $K = C^2/2Lf\cos\theta$ ; obtained by calibration,

$\Delta\phi$ = resulting phase lag between two signals,

f = wave frequency employed.

Therefore, by measuring the phase lag ($\Delta\phi$) between the two signals, the mean flow velocity could be obtained.

The resulting two signals were squared using high speed operational amplifiers to minimize errors caused by amplitude variations. The outputs were fed to a flip/flop

which yielded a constant amplitude pulsed wave with identical frequency (40 KHz) but of a width proportional to the aforementioned phase lag. This was integrated, amplified and filtered prior to data logging.

The flow meter required extreme care in setting up, in addition to repeated checking for signal drift. Unfortunately time did not allow further development work to improve measuring repeatability and hence an alternative method of flow measurement was later used. Air flow measurement during transient tests was achieved using a hot-wire anemometer. A short intake pipe with a venturi (B.S. 726/1957) flow straightener and hot-wire probe was fitted at the compressor inlet. The venturi flow meter was included to check the calibration of the hot-wire anemometer under actual flow conditions (steady state operation). Full calibration tests were conducted in the same manner, but with a large damping chamber preceding the compressor.

### 4.3.6 Fuel flow

Steady state measurements of the engine's overall fuel consumption were carried out using conventional mass balance system. A check was made on the distribution of fuel between individual cylinders. Each injector was allowed to discharge in turn into a measuring vessel (at ambient pressure), at the same running condition. Variation was found to be within 1.5%.

The measurement of fuel flow during transient operation was achieved indirectly. It was originally intended to compute and integrate injection rate diagrams during a transient run (using needle lift, injection and cylinder pressure diagrams). Steady flow test data for the injector

(35) was used to obtain a relationship between the nozzle coefficient of discharge, needle lift and injection pressure difference, Fig. 4.6. This technique, though ideal for the application, was abandoned when the miniature pressure transducer fitted into the nozzle holder failed, and an accurate fuel pressure diagram was no longer available.

Ledger (67) used an experimental relationship between the quantity of fuel injected and pump rack position (based on steady state measurements) to evaluate fuel flow under transient conditions. The same method was used but was extended to include the effects of engine speed variation.

### 4.3.7 Brake torque

The loading torque (brake) was measured via a strain gauge load cell resisting rotation of the dynamometer stator. A torque metering unit energized the bridge and amplified the output signal prior to its indication. The resulting output was also available for recording or as a feedback signal for closed loop torque control of the dynamometer. This output was filtered prior to recording to eliminate the effects of torque variation during an engine cycle and vibration.

The torque transducer and the meter were standard devices supplied by the dynamometer manufacturer. The complete torque measurement system was calibrated statically using a torque arm and static weights.

## 4.4 CONTROL AND DATA ACQUISITION SYSTEM

### 4.4.1 Computer

The digital computer used was a 16 K word PDP15 produced by Digital Equipment Corporation. It had a 18-bit

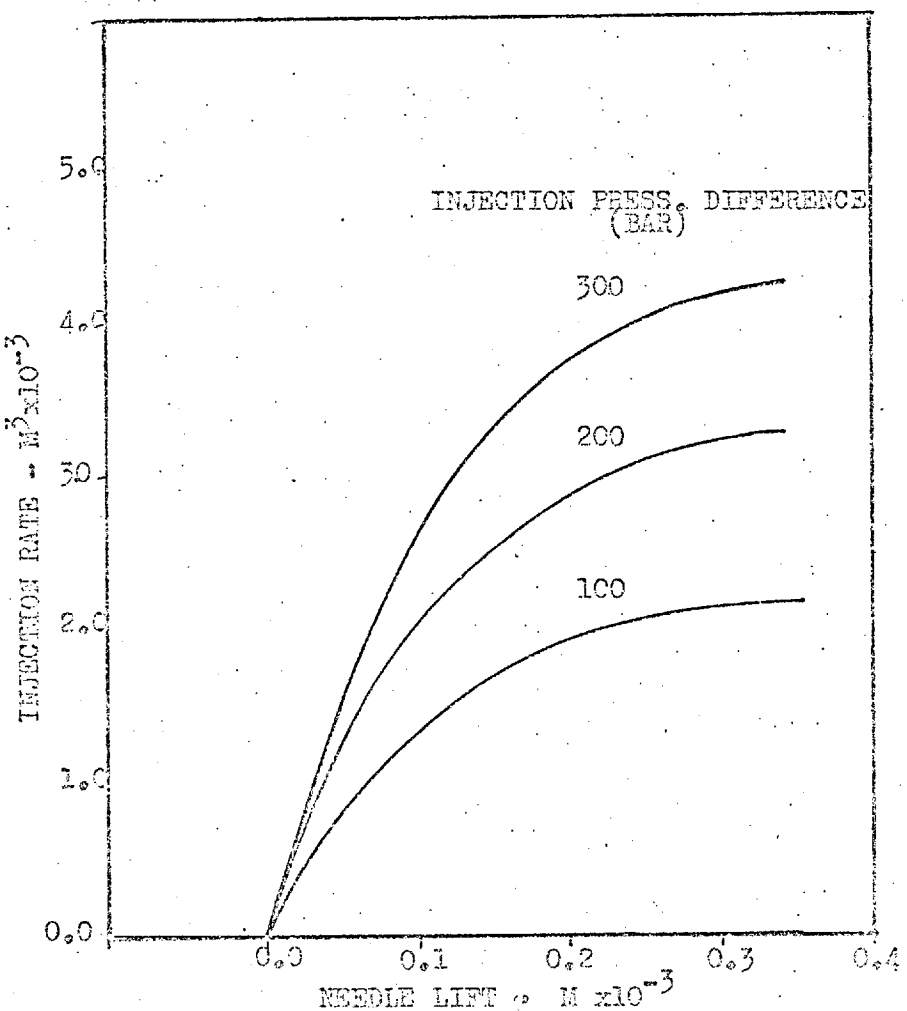


FIG. (4.6) Steady State Flow Data for Leyland Injector

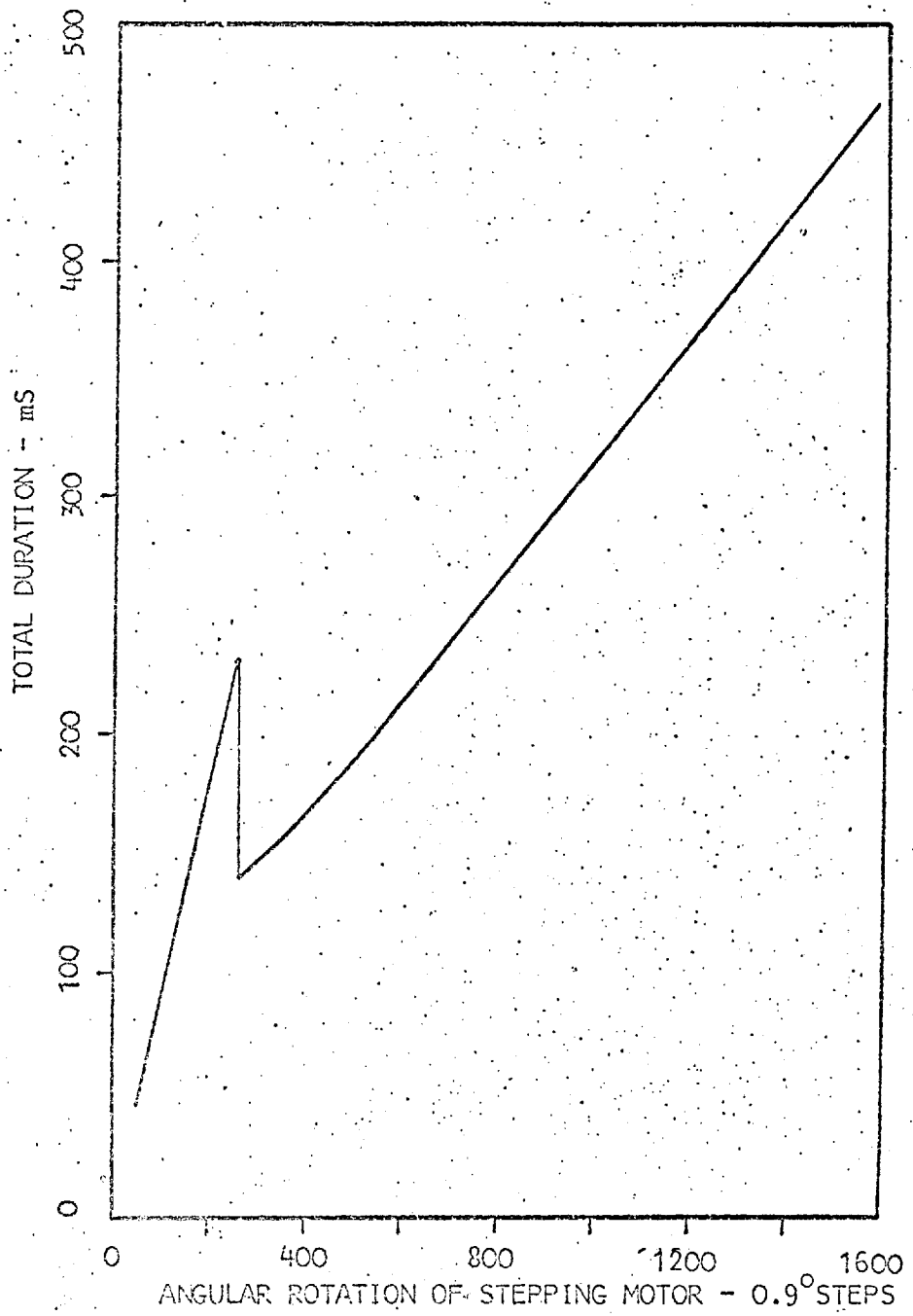


FIG. (4.7) Calibration Curve for Stepping Motor Drive Unit

word length, 0.8 μs cycle time and a 256 K word fixed disc. Peripherals included three dectape units, a paper tape punch and a reader, a teleprinter, a serial printer and a visual display unit. Languages, such as FORTRAN IV, could be used but the majority of the software was written in low-level language, MACRO15.

The computer communicated with the engine via a complex package of electronics, known as the interface, Fig. 4.3. This handled analogue and digital signals and performed all necessary conversion and information transfers for control, supervision and the input/output of experimental data. All interface control operations were carried out using programme controlled transfers (34). These were input /output instructions which selected the device and specified the exact nature of the function to be executed.

### 4.4.2 Control interface

Engine speed demand:

The governor stepping motor (Section 4.2.3) was used in conjunction with a drive unit (Unimatic, model USD853) issuing control pulses at the following rates:

| Stepping rate (0.9° step/s) | Mode | Control |
|---|---|---|
| 80 | inching | manual |
| 1087 | low speed | computer ($\leqslant$ 256 steps) |
| 3850 | high speed | computer ($>$256 steps) |

The acceleration and deceleration periods necessary in the case of the high speed mode, were controlled by logic circuitry in the drive unit. The variation of the mean stepping speed with the input number of steps was established experimentally (Fig. 4.7).

The drive unit was fed command words from the computer via a digital buffer. Each word was programmed to contain two instructions: the required number of $0.9^{o}$ steps and the direction of motor rotation. This was transferred to a binary downcounter where the logic circuitry determined the operational mode (pulse frequency and direction of rotation). Stepping pulses going to the motor were also fed back to the downcounter enabling it to record the number of steps executed. An electronic flag, which was set only when the counter was cleared, was included to prevent computer intervention before the completion of the previously instructed change in governor set point.

Brake torque:

Control of the brake torque was achieved via a locally-closed analogue loop. A control and linearisation unit (three-term controller) was used to close the loop formed by the brake excitation unit, the brake itself and its torque meter (Fig. 4.8). This was a transistorized control amplifier which minimized variations in brake torque due to thermal influences or engine speed changes, and compensated for the non-linear relationship between the excitation current and braking torque. Computer control was achieved by programming the set point voltage (equivalent to a certain torque demand) of the three-term controller. A 10-bit digital to analogue convertor (DAC) was used to convert the computer word (representing torque) into the set point voltage required.

Optimal values of the controller gain together with differential and integral correction terms were established via a systematic series of step changes in torque. These were determined to compromise between maximum set

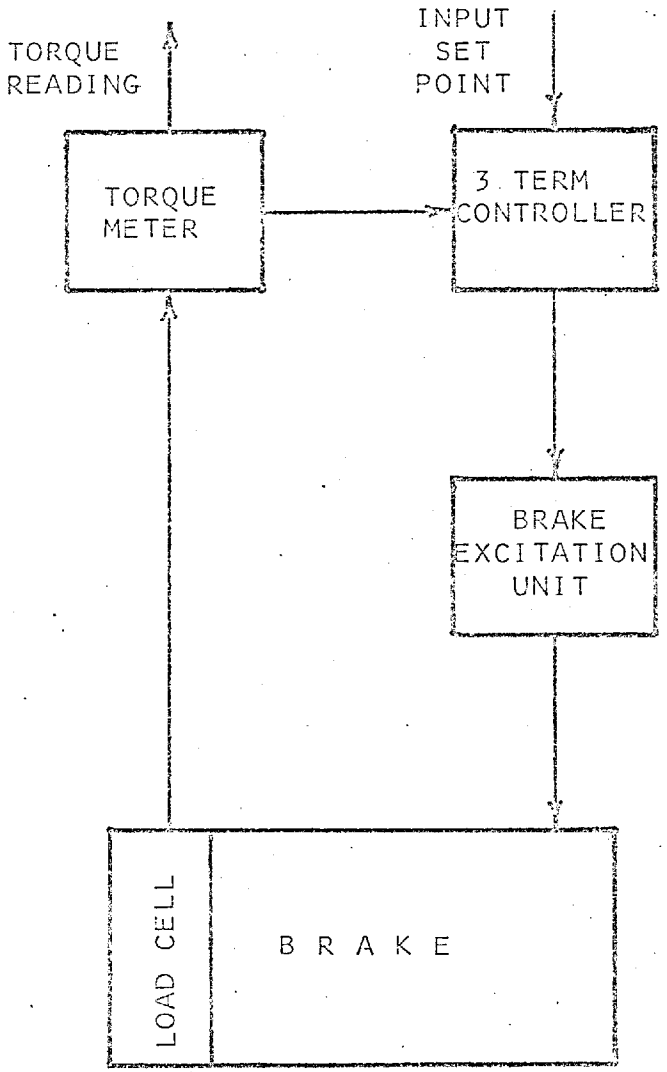


FIG. (4.8) Brake Control Loop

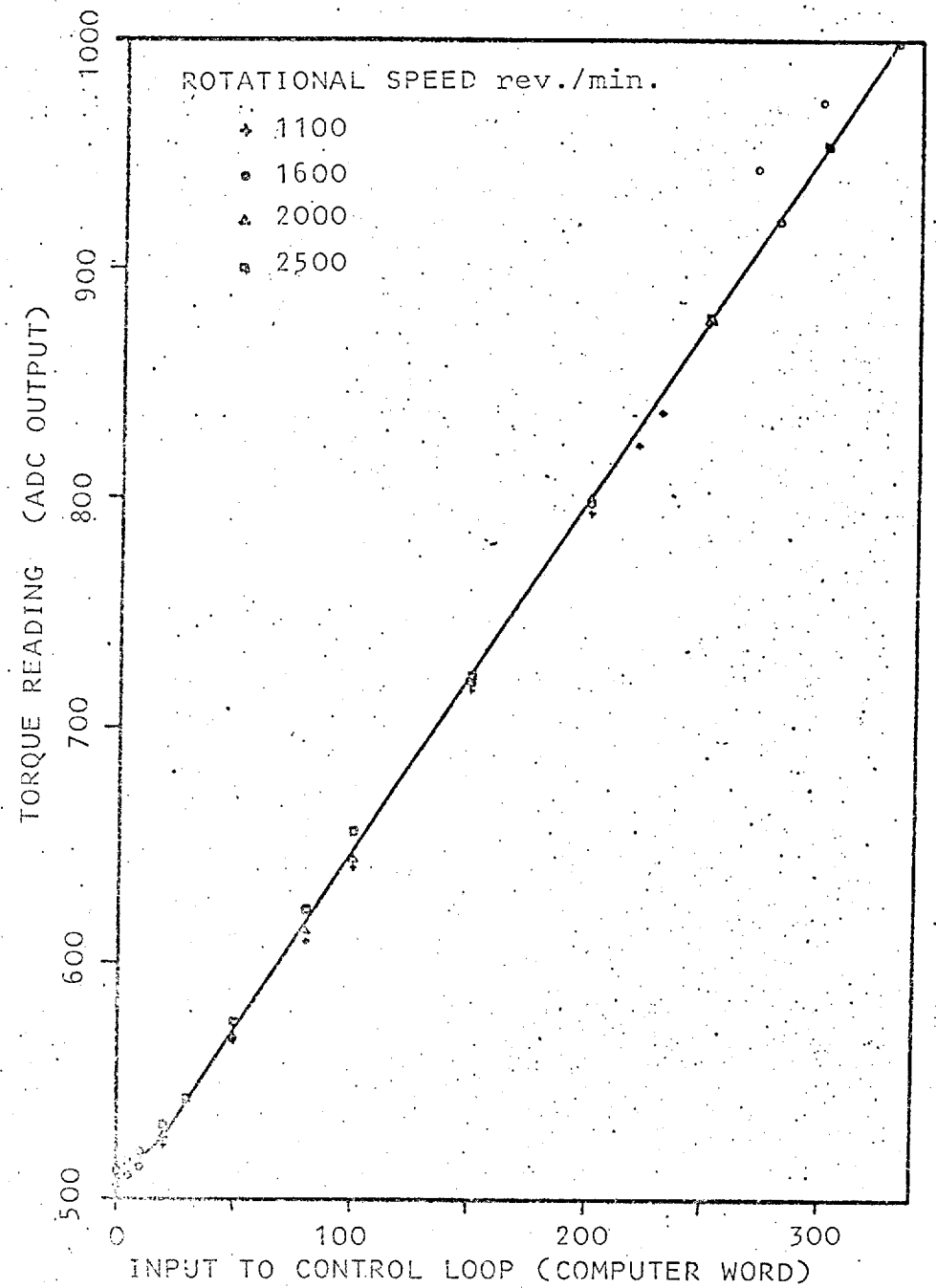


FIG. (4.9) Calibration Curve of Brake Control Loop

point resolution, minimal torque rise time with stability and freedom from oscillations.

Calibration of the torque control loop, Fig. 4.9, yielded an input/output relationship which was practically linear (95% of full range) and independent of speed. This allowed any torque-time schedule to be programmed independent of speed.

### 4.4.3 Data acquisition interface

Engine speed:

A 12-bit counter registered the number of pulses, from a 25 KHz crystal clock, between successive crankshaft revolution marker pulses (Section 4.3.2). This was updated automatically once per revolution. Thus engine speed (reciprocal of measured interval) was continuously available to the computer, and was not susceptible to common errors introduced by conventional techniques, e.g. tachometer ripple.

Logic circuitry, including a digital buffer to store the counter contents following the arrival of a new marker pulse, eliminated the possibility of the computer reading an incomplete interval. Measurement of speed variation within a cycle would have been possible if a higher clock frequency was used in conjunction with the digitizer pulses (Section 4.3.2).

Revolution counting:

A digital counter incremented by the marker pulses was included to allow serial counting of the number of crankshaft revolutions (two times number of cycles) following any specified instant. This was essential for checking the

synchronization of data logging with the firing revolution, particularly during transient tests.

Turbocharger speed:

Turbocharger speed was measured via an electronic package identical to that for engine speed. A 500 KHz clock frequency was used to ensure a reasonable resolution at high speeds (1/350 at 80,000 rev/min. and 1/2800 at 10,000 rev/min.).

On-line data logger:

This data logger was basically a medium speed analogue to digital convertor (ADC) which converted analogue signals varying between -5 to +5 volts into 10-bit binary digits. The unit was capable of servicing up to 32 different input variables one by one. Input channel multiplexing (selection) was controlled by the computer via an addressable sequence generator and analogue switches AS8 and AS4 (Fig. 4.10). A sample and hold amplifier (SHA) sampled the signal and maintained its voltage level during the duration of conversion (normally about 10 μs).

Sampling was timed by an external pulse train whose period was a multiple of that of the digitizer pulse. When a timing pulse was received, the SHA tracked the multiplexed variable for 2.5 μs (acquisition time), after which conversion started. The ADC contents resulting from conversion were then shifted to a digital buffer raising a flag to indicate a state of readiness for computer reading. The computer was programmed to await this flag to ensure rapid data transfer. Following this, the data logger was reset to enable the repetition of the same sequence at the next timing pulse. The same variable would be continuously

FIG. (4.10) Schematic of On-Line Data Logger

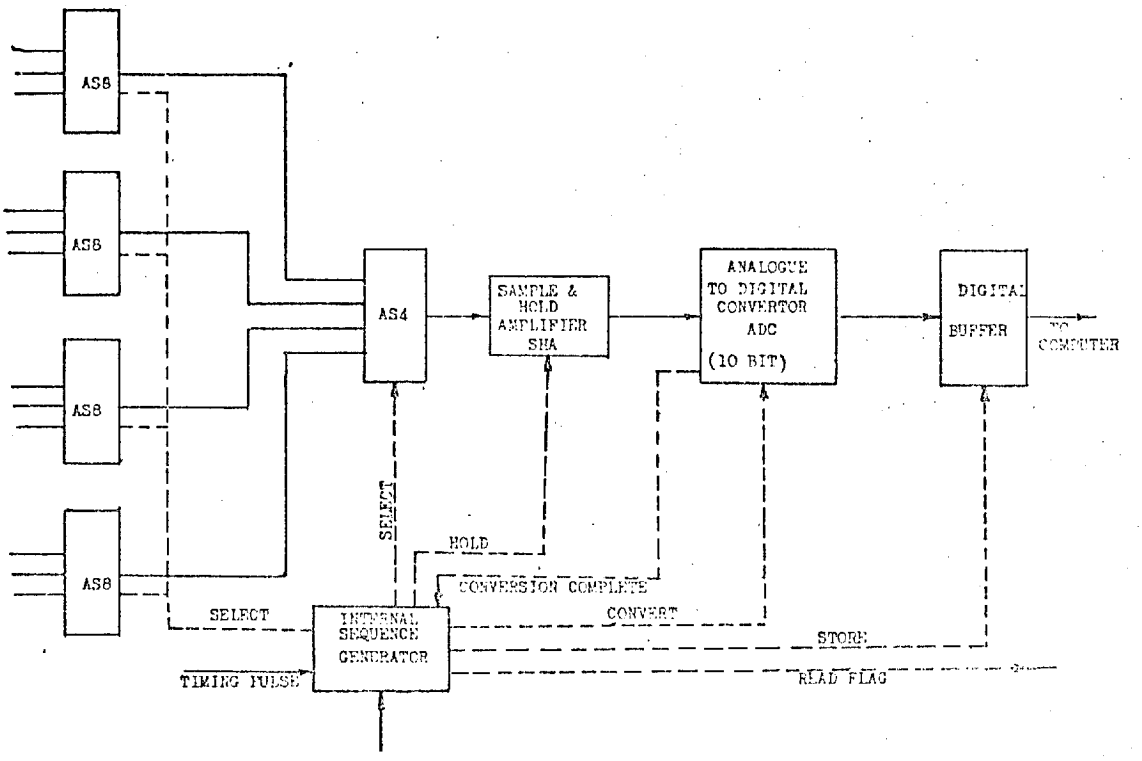


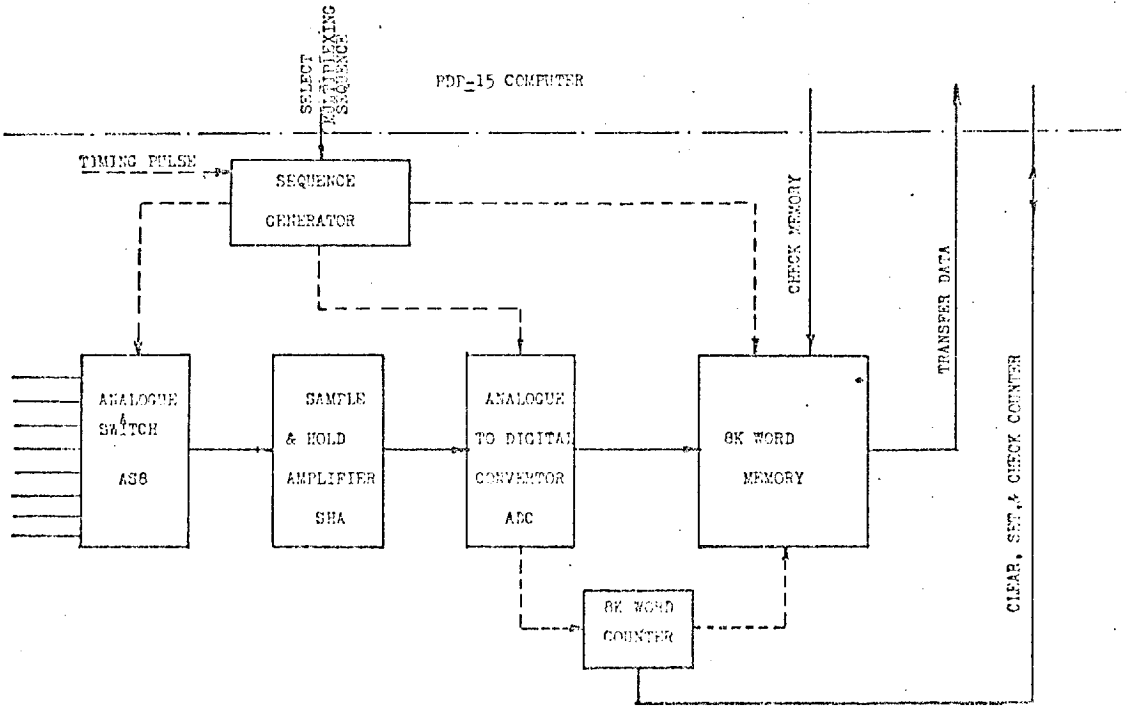


FIG. (4.11) Schematic of Off-Line Data Logger

accessed unless a different input channel was selected by the computer.

Experience with this system confirmed that reliable data acquisition could be effected at rates up to 50 KHz; faster rates resulted in synchronization problems.

Off-line data logger:

A schematic block diagram of the off-line data logger is presented in Fig. 4.11. The unit was similar in concept to the on-line data logger previously described, but it was equipped with its own 8 K word memory to allow temporary data storage.

The system featured a fast ADC (1.2 μs), used in conjunction with a sample and hold amplifier and an 8 input multiplexer, all compatible with the ADC speed. An addressable sequence generator controlled the following:multiplexing sequence, sampling, conversion and subsequent storage into the 8 K word store. Timing pulses were supplied by the data logging control unit, described in the following section. Data transfer from the ADC to the 8 K store was executed automatically and the number of conversions stored was determined by a programmed indexing counter. Access to the memory was disabled when the required word count was achieved. The multiplexing facility enabled the repetitive selection of a single channel or the sequential selection of either two, four or eight channels of data.

The 8 K store was a rotating memory system, preceded by a first in first out 256 word buffer. The buffer (analagous to an accumulator in hydraulic applications) enabled varying data transfer rates to be handled by the memory. Data acquisition at rates up to 700 KHz was

possible. The recording mode was initiated by the computer via an instruction which cleared the memory and downcounter. This was followed by selection of the multiplexing sequence, enabling the recording mode and setting of the downcounter. The data logger was then left to record the data whilst the computer was completely free to execute other operations (such as dynamometer control). The computer was programmed to interrogate the data logger flag for completion of recording, after which play-back started. Data transfer from the 8 K store to the computer memory was carried out on a word by word basis.

Data logging control unit (DLCU):

This package was built primarily to enable the computer to synchronize control and data acquisition with the angular position of the engine crankshaft (an essential requirement of data logging during transient operation). By manipulating the marker and digitizer pulse trains (once and 1440 times per crankshaft revolution), the two data loggers were forced to sample analogue signals in intermittent batches. This intermittency gave the computer sufficient time to execute its diverse control and data handling operations. It also reduced the data storage requirements.

Sufficient operational flexibility was ensured by designing the unit to allow:

1. variation of sampling rates of analogue signals (e.g. cylinder pressure) in relation to engine speed;
2. sampling a batch from one engine cycle, then missing a preset number of cycles (N);
3. recording discrete parts of individual cycles.

Fig. 4.12 shows a schematic block diagram of the basic control circuits of the unit. By dividing the marker pulse by 2 (D1), a "once per cycle" pulse was obtained. Further division of this new pulse train by N using the variable divider D2 yielded a master timing pulse once every N engine cycles (i.e. missing N-1 cycles). N was manually preset from 1 to 99 according to the requirements and complexity of the test.

A 4 decade manually presettable counter (DEL) delayed data logging by a predetermined crank angle increment from the master pulse, thus allowing the repetitive recording of any specified portion of the cycle, e.g. injection duration etc. The effective data-logging frequency (at any engine speed) was adjusted by D3 which enabled the sampling interval to be increased by up to 99 times the digitizer pulse period ($\frac{1}{4}^{o}$ CA).

The outputs from the DLCU were in the form of two intermittent pulse batches timing the sampling and conversion of the two data loggers. An electronic flag (set once every N engine cycles) was continuously interrogated by the computer and hence it timed all the data logging and control operations. Accordingly, a transient test could be repeatedly initiated from the same crank position.

The number of timing pulses per sequence issued to the off-line data logger was controlled by initial setting of C2. The master counter (C1) limited the maximum number of digitizer pulses processed per data logging sequence, i.e. every N engine cycles, This was never to exceed N times number of digitizer pulses per cycle. By setting C2 to a number larger than that of C1 a longer batch of sampling pulses could be provided to the on-line data logger.

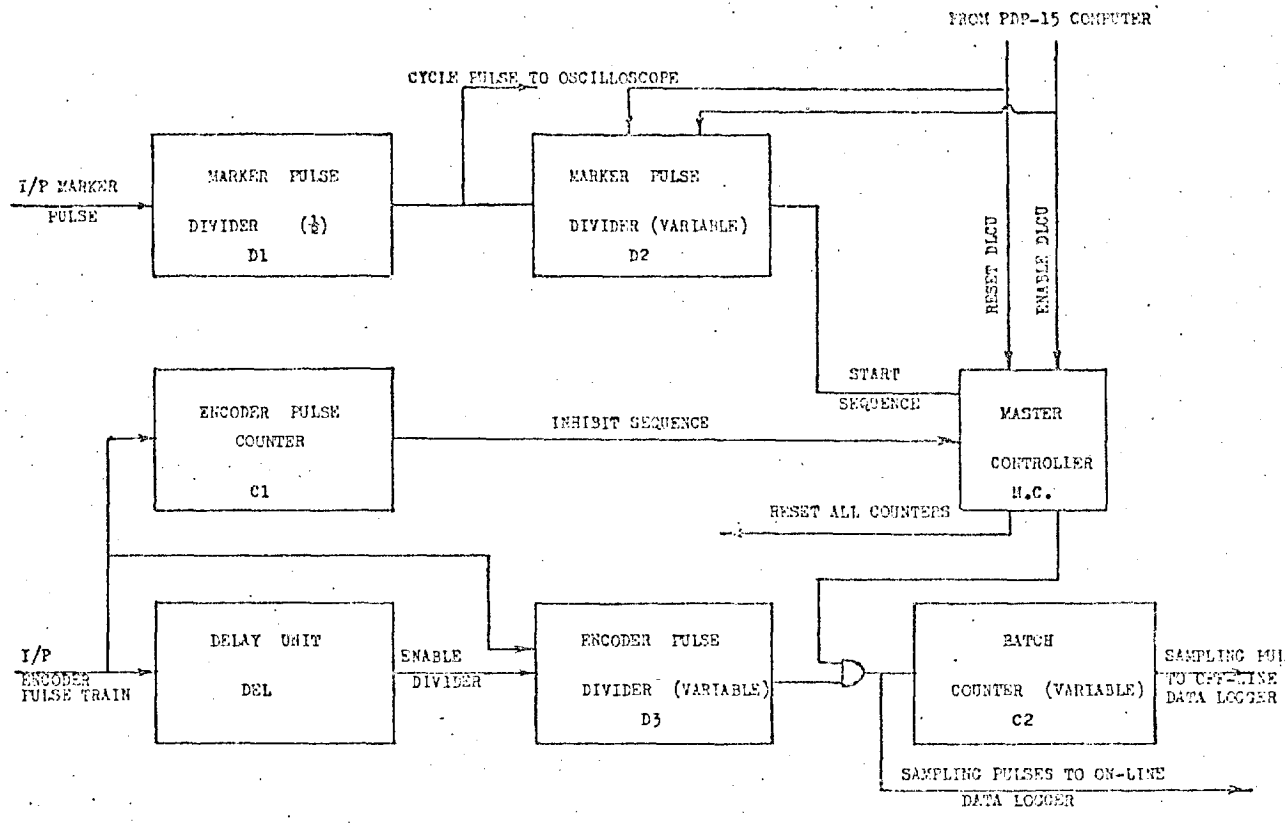


FIG. (4.12) Block Diagram of Data Logging Control Unit (DLCU)

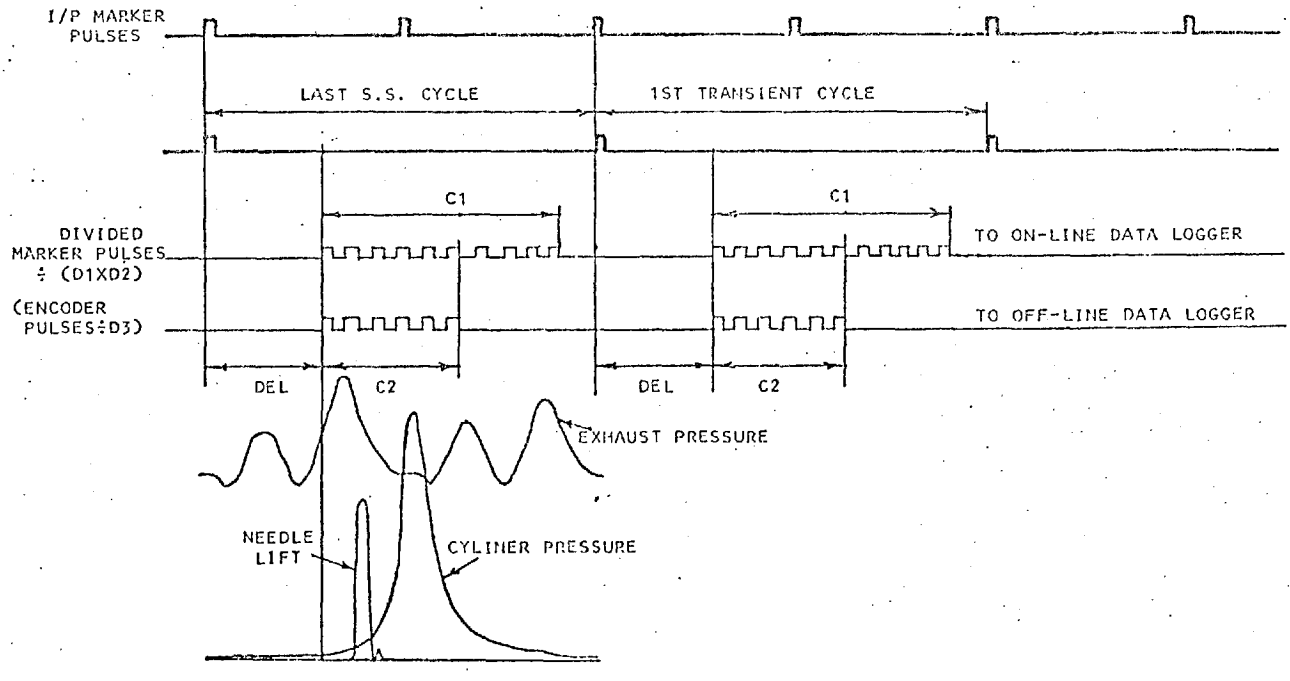


FIG. (4.13) Time Diagram for the Sequence of Operations of the DLCU

The sequence of operations of the DLCU, illustrated by the time diagram in Fig. 4.13, was directed by the master controller MC. This cleared all counters, dividers and delays in addition to starting the sequence. The DLCU could be enabled/disabled both by the computer and manually. Initial synchronisation with the firing TDC of No. (1) cylinder was enabled by a push button.

A pulse multiplier was also included to provide four or eight pulses (2.5 μs apart) for each pulse emitted on the off-line data logger channel. This option permitted the off-line data logger (at each crank position) to sample four or eight different variables practically simultaneously.

## 4.5 PROGRAMMED TEST PROCEDURES

The basic requirements of the programmed test procedures comprised:

1. Controlling engine operation (speed and load).
2. Logical sequencing of test events.
3. Data-acquisition, sorting, processing and/or recording.
4. Safety monitoring, e.g. overspeed.
5. Providing the operator with over riding authority.

To maximize the utilization of the computer-controlled system, the software was written in accordance with the following guidelines:

1. Core requirements and execution time being minimal.
2. Simplicity and logical segmenting to reduce development efforts.
3. Flexibility and ease of expansion to accommodate other possible testing requirements.

4. Maximal usage of the conversational mode to provide computer-operator interaction.

Based on the above considerations and the fact that the majority of the operations were executed in real time (on-line), a fast and efficient symbolic assembler language (MACRO 15) was extensively employed. The use of higher level languages (FORTRAN IV) was limited to off-line data processing and analysis.

### 4.5.1 Control and data logging software

General framework:

Bloxham et al (19) reported a software structural framework to reconcile the diverse programming objectives of a computer-based engine test facility. This was accepted as a basic strategy and a modular architecture, Fig. 4.14, was developed in five levels. Each separately compiled module incorporated a common data transfer link accessible to modules of higher levels only.

Each subroutine in the first level (lowest) was assigned a specific and frequently requested task, e.g. incrementing the governor stepping motor, adjusting the brake torque etc. The second level sub-programs pre-processed measured data or messages sent from level 1 to higher levels. Control of engine operation was carried out by subroutines in level 3. These received input information from level 5 together with feed-back measurements or fault messages from level 2 and accordingly issued corrective instructions to the device actuating modulus (level 1).

Modules controlling data logging during steady state and transient operation were positioned in level 4. Temporary and permanent recording onto disc or dectapes

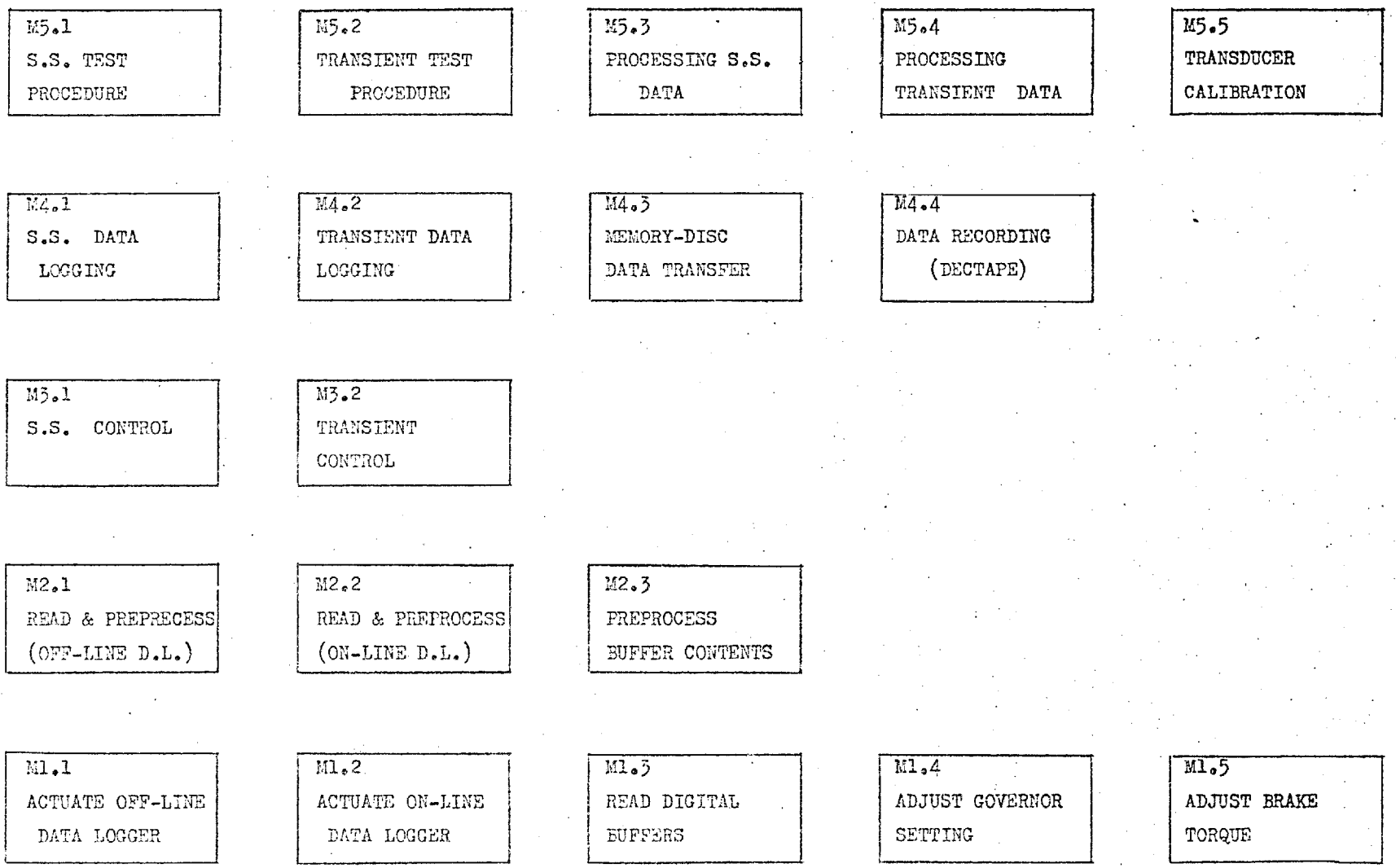


FIG. (4.14) General Architecture of Control and Data-Acquisition Software

was effected via routines embodied in the same level. The top level contained managerial programs for the execution of the steady state and transient test procedures. Level 5 also included programs for the calibration of the instrumentation and for data processing.

In essence, this framework permitted an upward transfer (level 1 to 5) of measured data and device state messages, whilst instructions and interrogations moved downwards. Higher level modules called lower level ones with the exception of the top two levels where communication on the same level was possible in some cases. The independence of each module and the simplicity of simulating its interaction with the software and hardware systems was very beneficial, particularly during the development stages and in cases of fault detection.

Device actuation and handling:

Device identification was possible with the aid of unique device selection codes; appropriate input/output pulses (34) were generated by the central processor in order to initiate specific operations. For an "out" transfer the program read a data word from the computer memory, selected a device and transmitted the data to it. The process was reversed in the case of an "in" transfer. Separate modules were written for the actuation and handling of the various devices interfaced to the computer.

Module 1.1 was written to actuate the off-line data logger, by executing all the steps necessary for starting either of its two operational modes (recording and play-back). Transferring the recorded measurements from the logger memory to the computer was carried out by M2.1,

as this involved sorting and exclusion of redundant data, e.g. needle lift and fuel line pressure prior to or after injection. M2.1 catered for the two multiplexing sequences employed during the work (four and eight input channels). Actuation of the on-line data logger and the transfer and pre-processing of the measurements were carried out by M1.2 and M2.2 respectively.

The contents of the following registers: engine speed, turbocharger speed and crankshaft revolutions, were read by M1.3. These were converted into speeds and serial cycle number via M2.3.

M1.4 and M1.5 were written to adjust the demand speed and brake torque respectively. The former transmitted the number of steps and direction of rotation of the stepping motor into the digital buffer of the drive unit (Section 4.4.2). The latter varied the value of the set point to the dynamometer control loop.

Control of engine operation:

Control of the steady state and transient operation of the engine was made possible via sub-programs M3.1 and M3.2, which were originally developed by Willis (118) and the author (73) during earlier work on a naturally aspirated diesel engine. The two modules were adapted to the test bed used in the present work after establishing the necessary control characteristic experimentally (Section 5.2.7).

Basically M3.1 adjusted the running condition of the engine by imposing one change in brake torque preceded and followed by a series of alternate speed corrections and time delays. By employing proportional control coupled with damping (attenuating the corrective action), fast adjustment was achieved without inducing violent strains or instability.

M3.2 was available for the execution of various rates of linearly increasing or decreasing combinations of speed and load under closed loop control. This module was not used as the present study was primarily directed towards the investigation of the engine rèsponse to rapid changes in load and/or demand speed under open loop control. Input signals were limited to step changes in the set point values of the brake torque and governor setting with no computer corrective action. Intervention of the computer was only allowed in emergency cases, e.g. engine overspeed.

Data storage:

M4.3 was written to provide a sufficiently fast means of transferring data from the computer memory to the disc. This was essential for data acquisition during transient tests when the storage capacity of the computer memory was limited to 6K words against a requirement of about 40K measurements. The use of magnetic tapes was not feasible, due to their relatively slow data handling characteristics (duration of a transient test varied between 6 and 12 seconds).

The DOS-15 software package (33), supplied by the computer manufacturer, simplified the task of programming input/output operations by providing an interface between the user programs and the physical devices. Data transfer between the computer memory and disc was normally carried out by DOS-15 macros (recursive instruction sequences) which automatically catered for file structuring and addressing functions. By measuring the time duration necessary to record a block of 4K words on to the disc, the data transfer rate was found not to exceed 4 KHz. This was due to the time consumed by the numerous interrogations and searching operations imposed by the wide range of facilities offered in the DOS-15 package.

To speed up the process, total freedom in data structuring of the disc was essential. Hence a macro which permitted non-directoried input/output capability at the device level (independent of the DOS-15 file structuring facility) had to be used. The macro "TRAN" (33) allowed user-designed file structuring via addressing of the individual blocks on the disc by their physical locations.

Very limited information about the use of "TRAN" was available, since in this case the burden of data structuring, interpretation, checking and packing lay with the user. Subsequently the development of M4.3 involved a great deal of experimentation. The final version used was capable of transferring data in batches of 4K words each at a rate of 45 KHz. The use of this module necessitated specifying the direction of data transfer (memory to disc or reverse), the address of the memory block set to accommodate the data and batch length in 18 bit binary words. The batch serial number was also essential to determine the corresponding physical location on the disc.

Magnetic tapes were employed for permanent mass storage of data for future analysis. M4.4 was written to strobe and record the contents of a specific block in the computer memory, on to dectape unit 2. Data from different test runs were recorded under unique file names, addressable via the tape directory.

Recording was effected in a binary form employing a sequential format, thus ensuring efficiency and compatability with the Fortran IV analysis programmes M5.3 and 5.4. By considering each physical data block on the tape (251 words) as a separate record, segmented retrieval of the data was possible. This was necessary for the processing and analysis

of long data files which exceeded the core size of the computer (transient measurements). M4.3 was programmed to compute the file length according to the amount of data to be recorded.

Data processing:

Two Fortran IV programmes (M5.3 and 5.4) were written to process the experimental data and reduce them to a form suitable for either further analysis (e.g. computation of burning rate curves from steady state cylinder pressure records), or for comparison with predictions of the simulation programme. Raw data recorded on dectapes were retrieved sequentially and the following operations were carried out:

1. Data scaling: raw measurements were scaled from volts to physical units using appropriate transducer calibration constants.

2. Data offsetting.

Readings from the strain gauge pressure transducers were transformed to absolute pressures by adding atmospheric pressure. The absolute pressure inside the cylinder was obtained by assuming equal instantaneous pressures inside the cylinder and inlet manifold at the BDC, following the intake stroke. In the case of needle lift, a dynamic datum was evaluated by averaging 20 readings prior to the start of fuel injection.

3. Computation of mean values and standard deviations.

This was undertaken in the case of steady state data to obtain averaged values. Standard deviations were used in the smoothing procedure applied to the cylinder pressure diagram, prior to evaluating the fuel burning rate curve.

### 4.5.2 Steady state test procedure

Steady state engine data was essential to achieve the following objectives:

1. Modelling the combustion process via the fuel burning rate approach (Chapter 6).
2. Determination of the fuel injection system characteristics.
3. Validation of the steady state predictions of the simulation program (Chapter 7).

A test procedure, comprising two operational modes, was programmed and employed to conduct all the steady state experiments. This is shown in the form of a flow chart in Fig. 4.15.

Mode (1) catered for the requirements of the first two objectives. It provided records of the cylinder pressure, fuel line pressure, needle lift and position of the fuel pump rack. These were logged simultaneously (i.e. from the same cycles) at a sampling interval of $\frac{1}{2}^{o}$CA. Mode (2) met the requirements of the third objective by yielding crank angle records of air flow and pressures in the inlet and two exhaust manifolds in addition to those obtained via Mode(1). A sampling interval of $1^{o}$CA was used. The two modes also provided averaged values of brake torque, engine and turbo-charger speeds and temperatures of: (a) exhaust gases at the two turbine entries, (b) air in the inlet manifold, and (c) cooling water around the instrumented cylinder.

In both data logging modes, measurements were obtained along a complete engine cycle and averaged over 50 cycles. Standard deviations were computed at each crank position in Mode(2)(necessary for the computation of a fuel

burning rate). Data logging was enabled once every four cycles to allow sufficient time for inter-cycle operations. These consisted of data transfer to computer memory, sorting of different variables and exclusion of redundant information, adding and squaring of values measured at the same crank position. Such operations were essential to cut down the requirement of computer memory by a factor of $\frac{1}{2N}$ and $\frac{1}{N}$ in the case of Modes(1)and(2)respectively; N being the number of cycles logged.

The testing procedure began by requesting (from the operator) values of the engine speed and brake torque. This information was input via a tele-type and accordingly the computer adjusted the engine operating point using M3.1. A time delay, normally lasting five minutes, was enforced to ensure settling to a steady state condition. Meanwhile messages appeared on the visual display unit (VDU) screen to check the tape recording unit and to set the DLCU sampling parameters according to the required data logging mode:

| | Mode 1 | Mode 2 |
|---|---|---|
| Sampling interval $^{o}$CA | $\frac{1}{2}$ | 1 |
| Number of samples/variable | 1440 | 720 |
| Number of variables at each crank position | 4 | 8 |
| Cycle intermittency | 1 in 4 | 1 in 4 |

Measurement of fuel flow rate, ambient pressure and temperature together with manometer readings of pressures inside the engine manifolds were also taken in this period.

Following the settling delay, all data arrays were initialized, the DLCU and off-line data logger were

set and started. The computer then awaited the DLCU flag, emitted at the arrival of the first crank position marker pulse which started the data logging sequence. This was followed by clearing the revolution counter and reading the variables connected to the on-line data logger together with engine speed, revolution counter and turbocharger speed. The computer then paused until the end of the engine cycle, awaiting the completion of the high speed data acquisition of the crank angle records (8K memory downcounter flag). Subsequently contents of the off-line data logger were read and sorted by the computer on a word by word basis and the following summations were evaluated:

for the two modes:

$$VAR_N(I,J) = VAR_{N-1}(I,J) + var_N(I,J) \qquad (4.4)$$

for Mode(1)only:

$$VAR^2_N(I,J) = VAR^2_{N-1}(I,J) + var^2_N(I,J) \qquad (4.5)$$

where: var(I,J) = recorded variable,

N = cycle number,

I = variable number, e.g. 1,2, denoting cylinder pressure, fuel line pressure etc.,

J = crank position.

The off-line data logger was reset and started and the same sequence was repeated at the following marker pulse until fifty engine cycles had been acquired. Subroutine M4.3 was then employed to write the resulting data on to a dectape under a unique file name specifying the test run executed.

The data measured was displayed on the VDU to check for freedom from errors caused by faulty instrumentation. Fortran sub-programs were used to calibrate the raw data

(in the form of volts) and computer mean values and standard deviations:

$$\overline{VAR}(I,J) = VAR/I,J)/N \tag{4.6}$$

$$\sigma(I,J) = \frac{VAR^2(I,J)}{N-1} - \frac{N}{N-1}(VAR(I,J))^2 \tag{4.7}$$

The cylinder pressure diagram was checked for drift with the aid of its standard deviation during the compression stroke; values exceeding 7 $KN/M^2$ were considered unacceptable. Synchronization of data logging with crank position was checked by the readings of the revolution counter.

Any defective set of data was deleted and the test run repeated after correcting the fault. Data collected from a number of test points was later output in the form of punched paper tape for further use on a larger computer.

4.5.3 Transient response test procedure

The transient test basically consisted of applying a rapid change in load and/or demand speed followed by detailed recording of the engine response, namely:

1. Data logging complete cycle traces of the pressures in: cylinder no. (1), induction and exhaust manifolds, fuel line pressure, needle lift, fuel rack position and air flow.

2. Measuring the following variables once every five cycles: engine and turbocharger speeds, brake torque, temperatures of the exhaust gases at both entries of the turbine, the air in the induction manifold and cooling water around the instrumental cylinder.

Fig. 4.16 presents a flow chart of the test procedure, in which all operations were carried out under computer control. The main driving programme M5.2 started the sequence

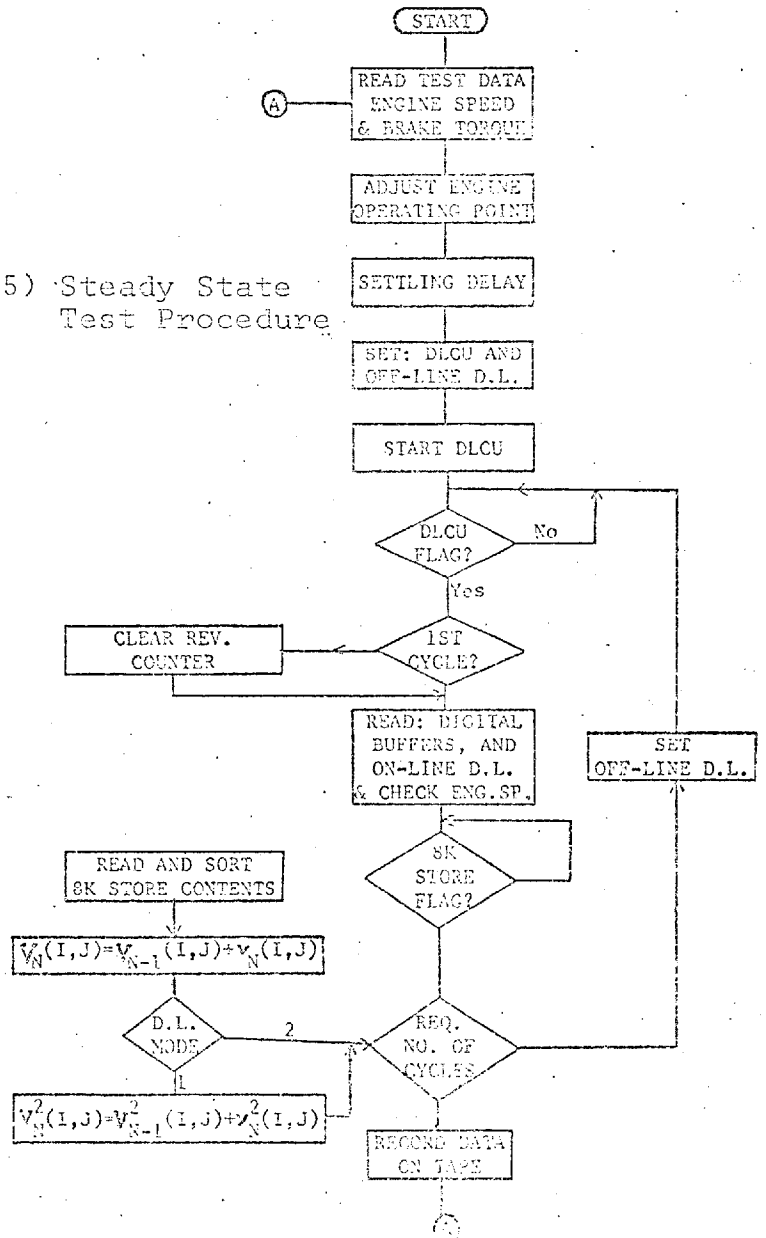


FIG. (4.15) Steady State Test Procedure

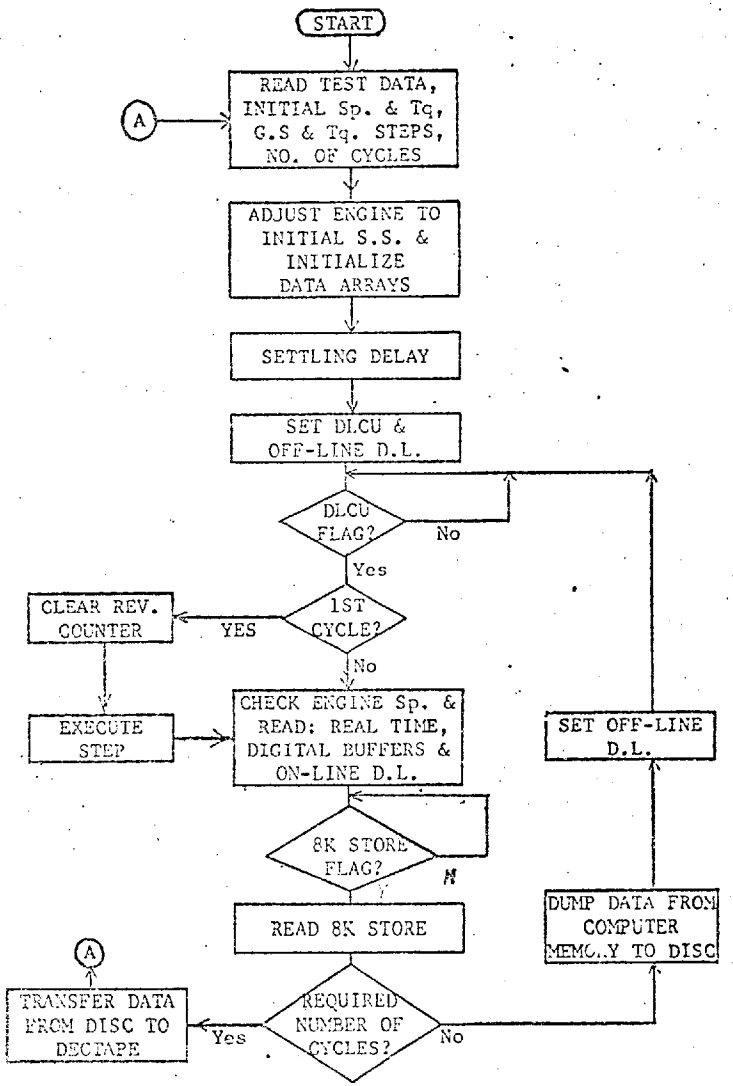


FIG. (4.16) Transient Operation Test Procedure

by requesting the operator to type in the test specification;

- initial speed and load,
- change in brake torque (magnitude and direction),
- change in demand speed (magnitude and direction),
- number of cycles to be recorded,
- file name selected to identify the data recorded.

Having received the necessary information, M3.1 was used to adjust the engine to the specified initial condition. This was followed by a settling delay (73), to ensure starting the transient from a true steady state. Meanwhile reminding messages were output to the operator (via the visual display unit) to set the sampling parameters of the DLCU (Section 4.4.3) and to check dectape unit 2 (used for permenant recording of the measured data).

At the end of the settling delay, control was transferred to M4.2 to initiate the data logging sequence. M4.2 reset the DLCU and called M1.1 to actuate the off-line data logger (Section 4.4.3). The 1 to 8 input channel multiplexing sequence was selected and the memory downcounter set to control the number of measurements sampled per batch (8 channels x 720°CA). M4.2 directed the computer to activate the DLCU and await the assertion of its flag, i.e. indicating the arrival of the divided crank marker pulse. The moment the DLCU flag came up (once every five cycles), both off-line and on-line data loggers were automatically activated and the DLCU controlled the flow of the sampling pulses according to the preset values of the sampling parameters (sampling interval, batch length, delay in relation to marker pulse and cycle intermittency).

In the case of the first cycle of the test, the revolution and real-time registers were cleared, reactivated

and control was then transferred to the main program M5.2 to execute the initially specified step changes in brake torque and governor setting (using M1.5 and 1.4 respectively). M4.2 was then recalled to direct the data logging operations:

1. Reading the digital registers containing real time, engine speed, turbocharger speed and revolution count;

2. Reading the variables sampled by the on-line data logger; brake torque and temperatures;

3. Transferring the contents of the 8K store of the off-line data logger to the computer memory.

After executing the first two items, the computer paused until the end of the current engine cycle to allow the off-line data logger to acquire the necessary cycle records. M2.1 was employed to transfer the contents of the 8K store to the computer memory after sorting the measurements and excluding the redundant parts of the cycle. The data collected was rapidly transferred to the disc (at a rate of 45 KHz) using M4.4.

The same sequence of data logging operations was repeated every five engine cycles. The contents of the 8K store were considered only at the following cycles: 1, 6, 11, 16, 31, 51, 71, 91, 111 and 131; permitting a longer interval at the later stages of the transient response test in order to cover a longer duration within a preset maximum amount of data (40K). At the end of the test M4.3 was employed to transfer the data accumulated on the disc to a magnetic tape for permanent storage (this being too slow an operation to conduct concurrently with data logging).

The complete test sequence covering 135 engine cycles was achieved in approximately 30 seconds, excluding

the initial settling delay. A Fortran program was later used to process the data recorded and to punch it out on standard paper tape for further analysis and plotting using a CDC 6400 computer.

# CHAPTER 5

# EXPERIMENTAL RESULTS

## 5.1 INTRODUCTION

This chapter reports the experimental programme carried out during the present work, including the tests conducted and results obtained. Preliminary tests were executed to establish the control characteristics of the engine-dynamometer combination and to evaluate the numeric parameters of the governor model.

Steady state tests covering the entire operational range were then conducted. The objectives were:

1. To obtain basic data for modelling the combustion process (Chapter 6).
2. To determine the characteristics of the fuel injection system.
3. To provide measurements to validate the steady state predictions.

Finally, three types of transient tests were carried out at various initial conditions. The data recorded during the resulting unsteady running conditions was required for comparisons with predictions of the simulation program.

## 5.2 PRELIMINARY TESTS

A series of 138 preliminary transient tests were conducted to establish the control characteristics of the engine and governor. These tests covered the entire operational range and comprised:

1. Equal step changes in governor setting (0.1 full range) at constant load levels.

2. Step changes in load (starting from zero), at constant demand speeds.

Brake torque, engine speed, fuel rack position and turbocharger speed were recorded at intervals of 0.1 second during the transient response period. Fifty measurements were taken at the initial and final steady state conditions, in order to yield mean values and standard deviations.

5.2.1 Variation of engine speed with load and governor setting

Computer control of the engine during steady state and transient operation (Section 4.2.2) was based on a quasi-linear approach (73), in which a change in engine speed consisted of a linear sum of partial changes caused by increments in brake torque and governor setting:

$$d\Omega_e = \left(\frac{\partial \Omega_e}{\partial C_L}\right)_y dC_L + \left(\frac{\partial \Omega_e}{\partial y}\right)_{C_L} dy \qquad (5.1)$$

The measured variation of engine speed with load ($C_L$) and governor setting (y), Fig. 5.1, was used to establish values of the partial rates of change, averaged over the entire operational range:

$$\left(\frac{\partial \Omega_e}{\partial C_L}\right)_y = -0.278 \quad \frac{\text{rev/min}}{\text{N.M}} \qquad (5.2)$$

$$\left(\frac{\partial \Omega_e}{\partial y}\right)_{C_L} = 2.142 \quad \frac{\text{rev/min}}{0.001/y_{fr}} \qquad (5.3)$$

where: $y_{fr}$ = full range change in governor setting.

Any deviations from the above-mentioned representation were catered for by the corrective action of the control software (M3.1 and M3.2 in Section 4.2.2).

### 5.2.2 Evaluation of parameters in governor model

The mathematical representation of the governor system has been established in Section 2.5.3, but the numerical values of the parameters involved were not known. However, Garg et al (43) have shown that in similar dynamic problems, unknown parameters can be estimated from observed input-output data for the system. The estimation problem was posed in terms of a criterion function (36), the minimisation of which yielded the best estimate.

This concept was applied in two stages. First the steady state form of equation (2.48):

$$(1 + C3y)(x + C4y) - C5\Omega_e^2 x = C6(\Omega_e^2 - \Omega_r^2) \qquad (5.4)$$

was fitted to the measured steady state characteristics of the governor, Fig. 5.2. A non-linear curve fitting procedure (79), which minimised the sum of the squares of deviations in rack position, was applied to yield values of C3, C4, C5 and C6.

Thus only the dynamic parameters remained unknown, i.e. coefficients of the inertia and viscous damping terms, C1 and C2 respectively. These were evaluated by curve-fitting the full mathematical representation, equation (2.48), to a number of measured transient responses and averaging the resultant values. Subsequently the final form of the governor mathematical representation was:

$$\ddot{x} + 81\dot{x} + (1383.4 + 379.9y + 527.8\Omega_e^2)x + (8385 + 2302.5y)\, y = 7946.5(\Omega_e^2 + \Omega_r^2) \qquad (5.5)$$

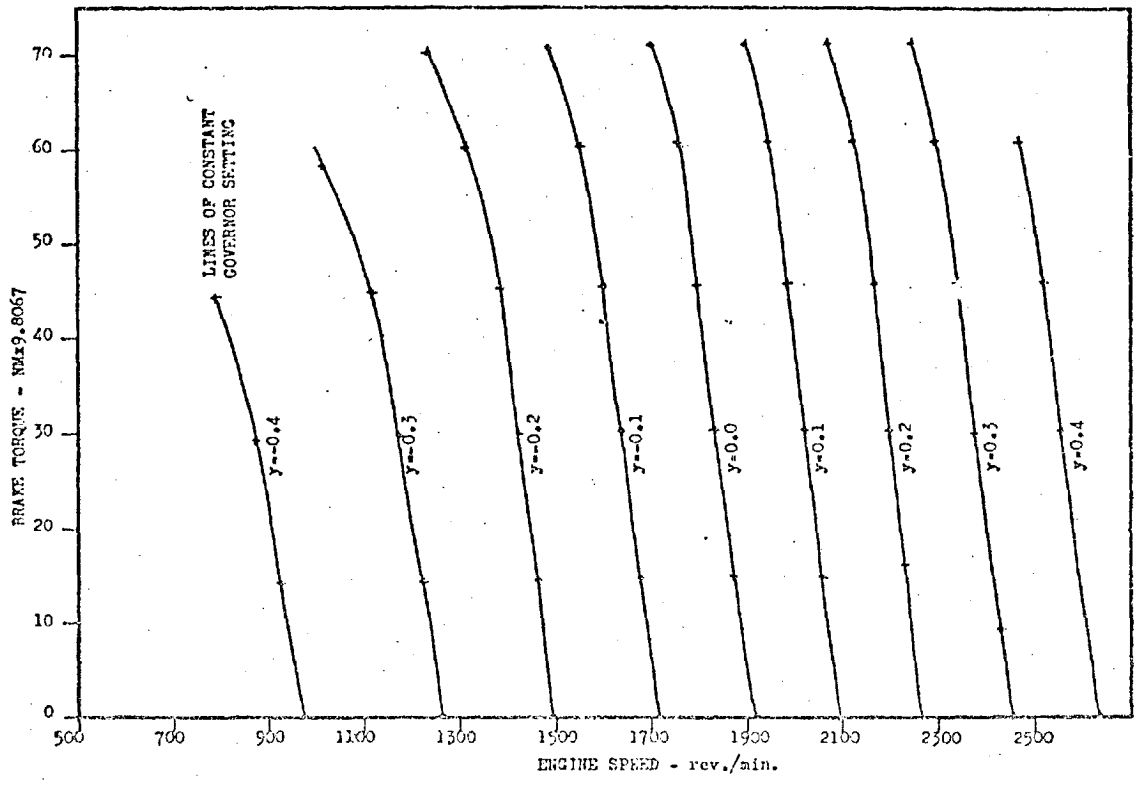


FIG. (5.1) Steady State Speed-Load Characteristics of the Engine at Constant Govenor Settings

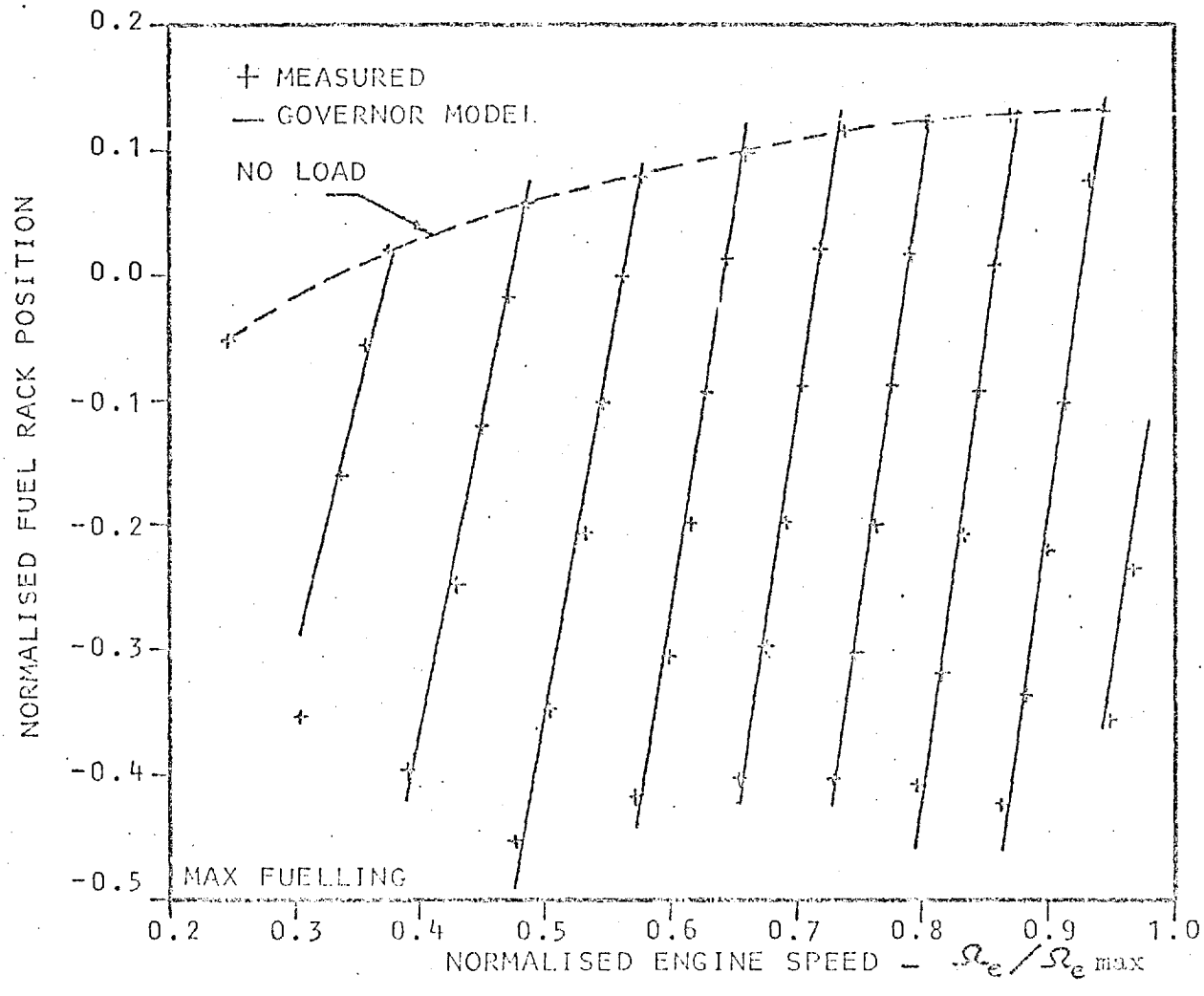


FIG. (5.2) Govenor Steady State Characteristics

## 5.3 STEADY STATE MEASUREMENTS

### 5.3.1 Basic data

A series of 22 steady state tests was undertaken to cover the load and speed range of the engine. These were run at four engine speeds (1000, 1500, 2000 and 2500 rev/min.) and loads from 0 to 11.26 bar (bmep). Details of the test points are listed in Table 5.1 under unique case numbers. The instrumentation, data-logging system and techniques employed during the tests, are described in detail in Chapter 4.

Standard production test data were obtained at each operating condition together with supplementary measurements. These included crankangle records (averaged over 50 cycles) for the needle lift and the pressures inside the cylinder, air chest, exhaust manifold and fuel line pressure. Typical sets of the records obtained are shown in Figs. 5.3-5.6.

The cylinder pressure diagram is plotted together with its standard deviation curve. It is interesting to note the variation in the latter in relation to the different processes occurring inside the cylinder. It maintains very low values along suction and compression until the ignition point, when it rises rapidly to high values during the premixed combustion period. This is followed by a gradual descent during the remaining part of the combustion duration, attaining low values in the second half of the expansion and exhaust strokes.

The relatively high standard deviations shown by the cylinder pressure during combustion, are caused mainly by pressure waves generated as a result of the heterogeneous burning of the fuel droplets. Another minor cause is the

| Case No. | Engine speed rev/min | B.M.E.P. bar | Turbocharger speed rev/min | Boost pressure $KN/m^2$ | Air/fuel ratio |
|---|---|---|---|---|---|
| SS11 | 1000 | 0.0 | 10,336.68 | 100.0 | 132.58 |
| SS12 | 1000 | 224.62 | 13,856.36 | 102.0 | 55.38 |
| SS13 | 1000 | 450.0 | 18,957.24 | 106.96 | 34.87 |
| SS14 | 1000 | 668.61 | 24,231.16 | 112.8 | 24.82 |
| SS15 | 1000 | 901.50 | 30,620.62 | 121.3 | 17.57 |
| SS21 | 1500 | 0.0 | 18,120.78 | 99.9 | 106.36 |
| SS22 | 1500 | 225.38 | 19,752.14 | 101.0 | 49.45 |
| SS23 | 1500 | 453.76 | 26,076.02 | 109.9 | 32.66 |
| SS24 | 1500 | 691.15 | 33,931,74 | 122.3 | 25.93 |
| SS25 | 1500 | 909.01 | 41,524.34 | 133.5 | 21.00 |
| SS26 | 1500 | 1104.34 | 48,248.38 | 150.0 | 18.82 |
| SS31 | 2000 | 0.0 | 24,426.26 | 100.4 | 80.90 |
| SS32 | 2000 | 225.38 | 28,615.64 | 106.9 | 45.65 |
| SS33 | 2000 | 450.75 | 37,753.46 | 122.2 | 33.86 |
| SS34 | 2000 | 676.13 | 45,154.34 | 139.0 | 27.79 |
| SS35 | 2000 | 901.50 | 53,134.70 | 158.8 | 24.41 |
| SS36 | 2000 | 1126.88 | 60,163.24 | 179.7 | 21.83 |
| SS41 | 2500 | 0.0 | 31,470.50 | 102.3 | 63.39 |
| SS42 | 2500 | 214.85 | 38,466.08 | 115.1 | 41.57 |
| SS43 | 2500 | 450.75 | 49,849.88 | 129.9 | 32.95 |
| SS44 | 2500 | 676.13 | 58,486.00 | 164.5 | 28.09 |
| SS45 | 2500 | 901.50 | 66,356.66 | 195.3 | 24.49 |

TABLE 5.1

STEADY STATE TESTS

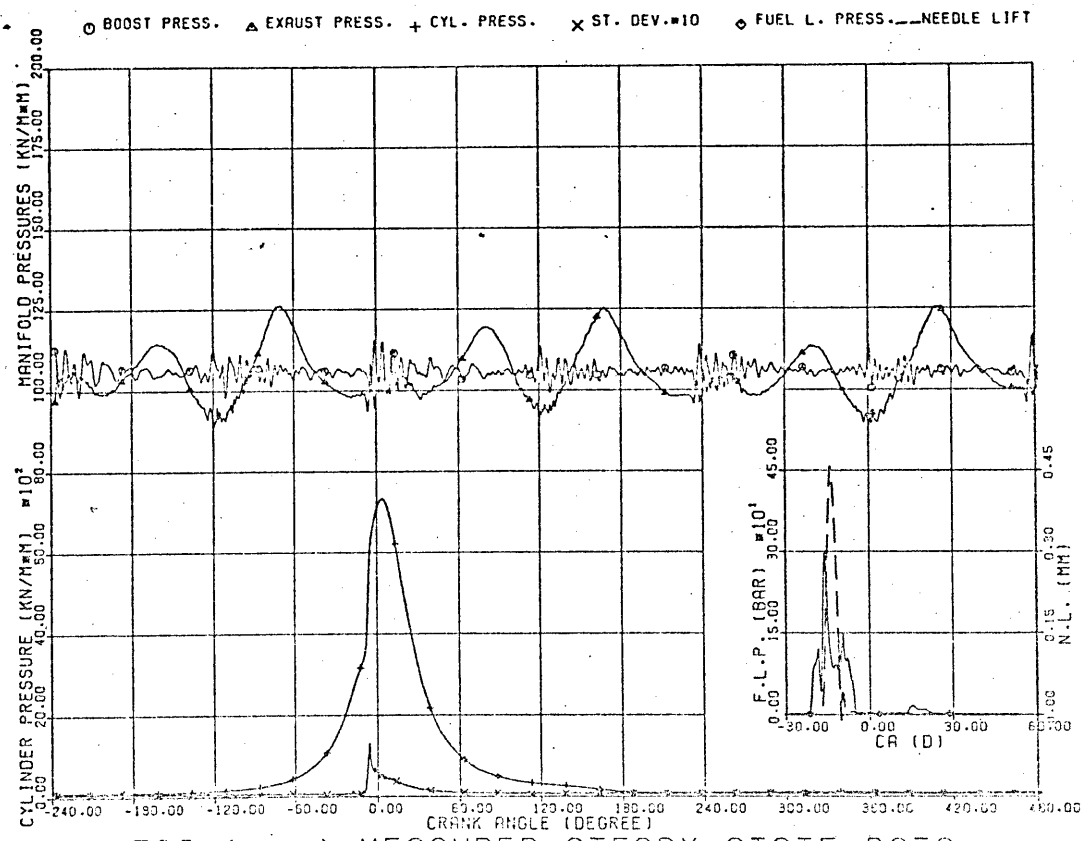


FIG.(5.3,a) MEASURED STEADY STATE DATA

ENGINE SPEED= 1000.0 RPM, BMEP= 450.0 KN/(M*M)

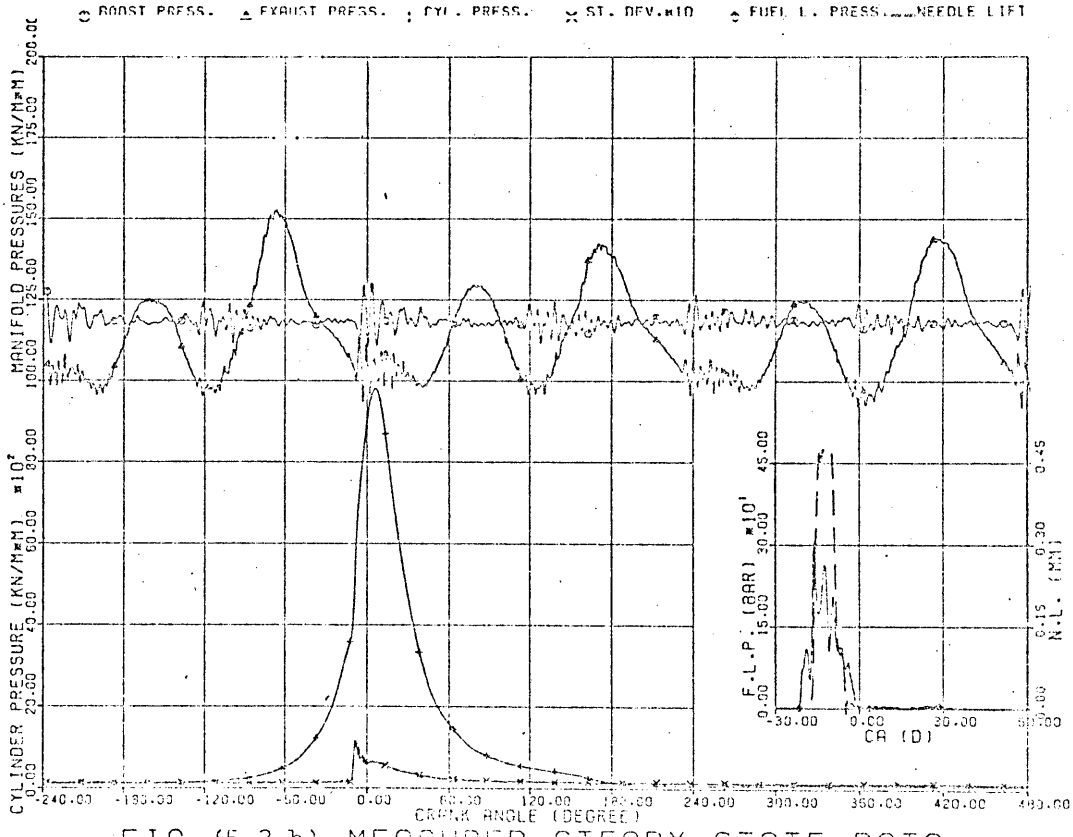


FIG.(5.3,b) MEASURED STEADY STATE DATA

ENGINE SPEED= 1000.0 RPM, BMEP= 901.5 KN/(M*M)

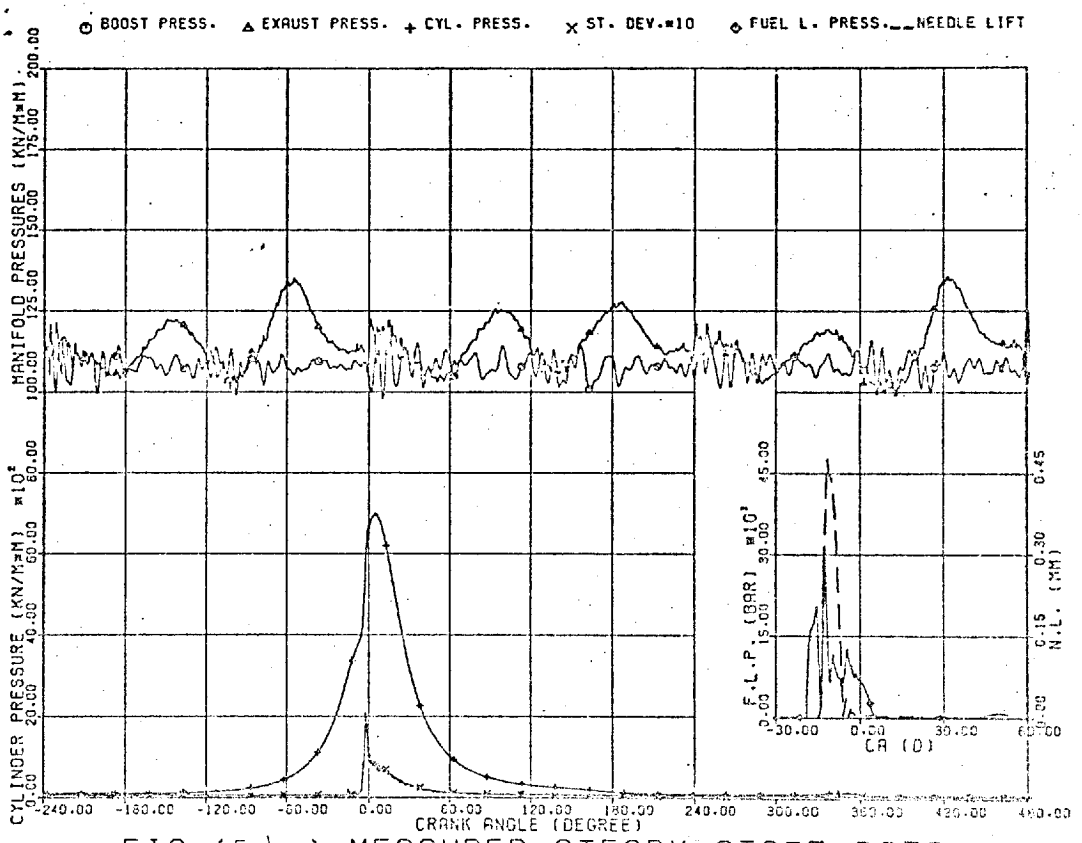


FIG.(5.4,a) MEASURED STEADY STATE DATA

ENGINE SPEED= 1500.0 RPM, BMEP= 453.8 KN/(M*M)

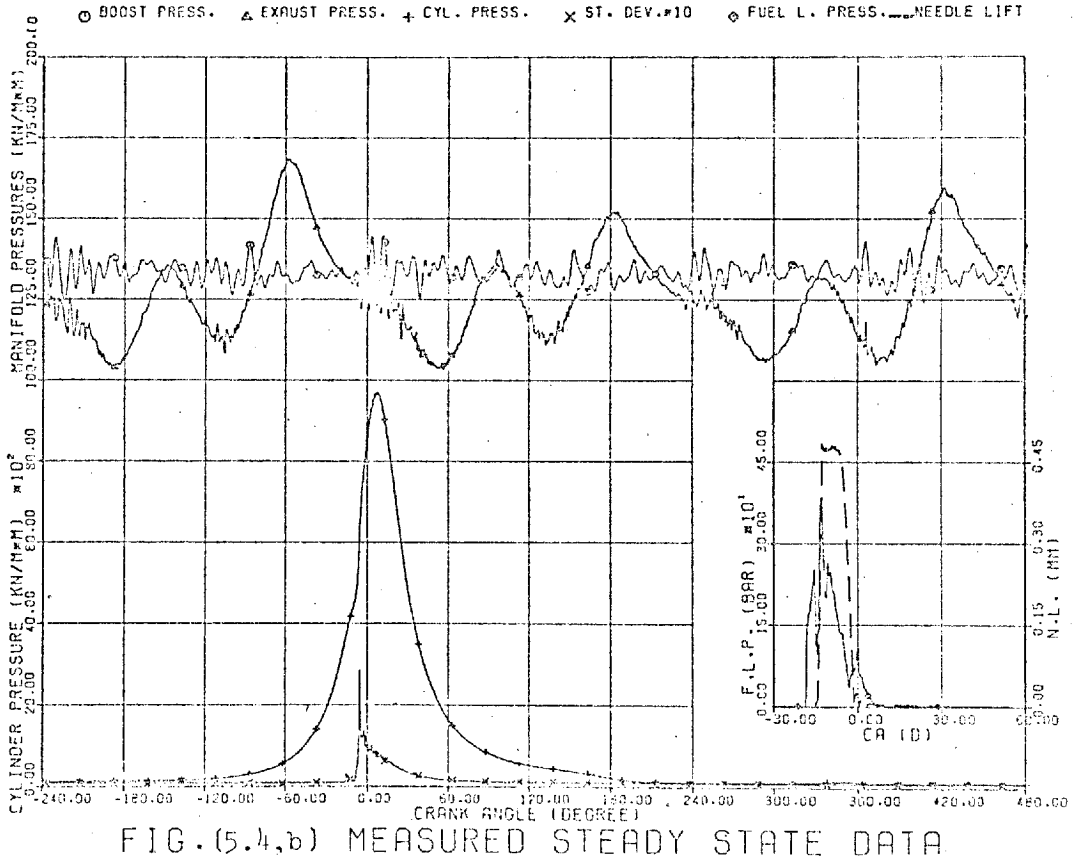


FIG.(5.4,b) MEASURED STEADY STATE DATA

ENGINE SPEED= 1500.0 RPM, BMEP= 901.5 KN/(M*M)

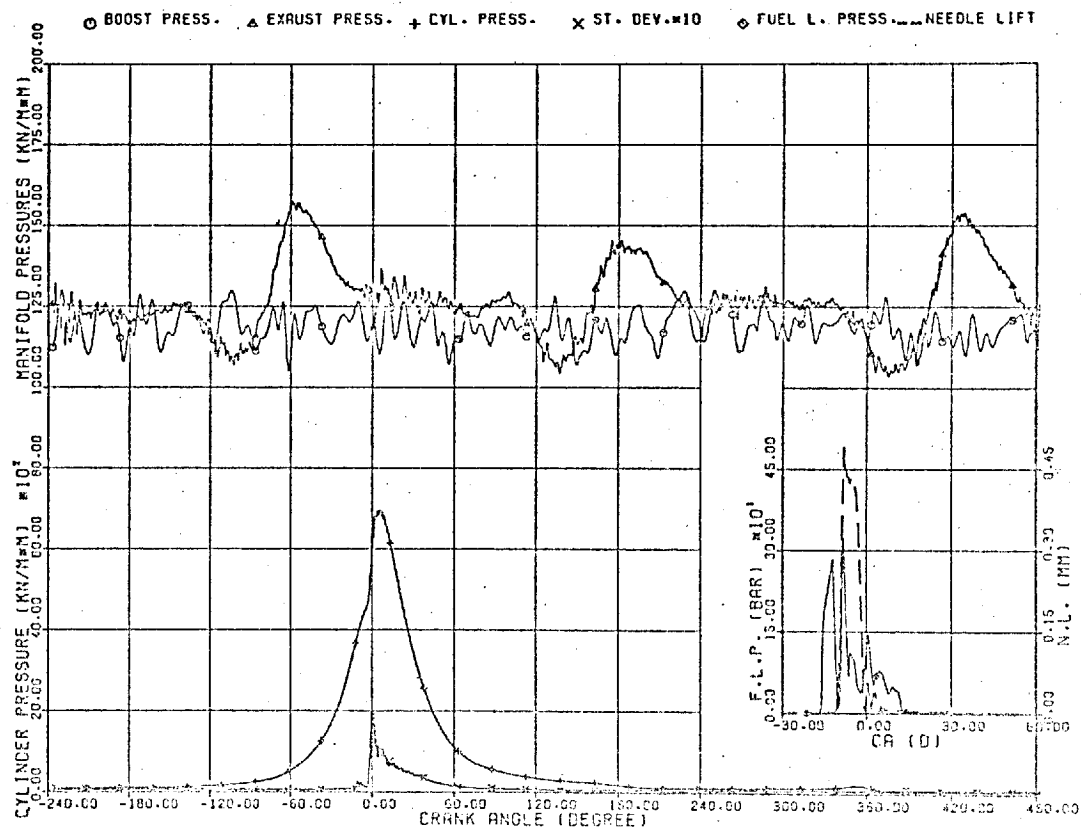


FIG.(5.5,a) MEASURED STEADY STATE DATA

ENGINE SPEED= 2000.0 RPM, BMEP= 450.8 KN/(M*M)

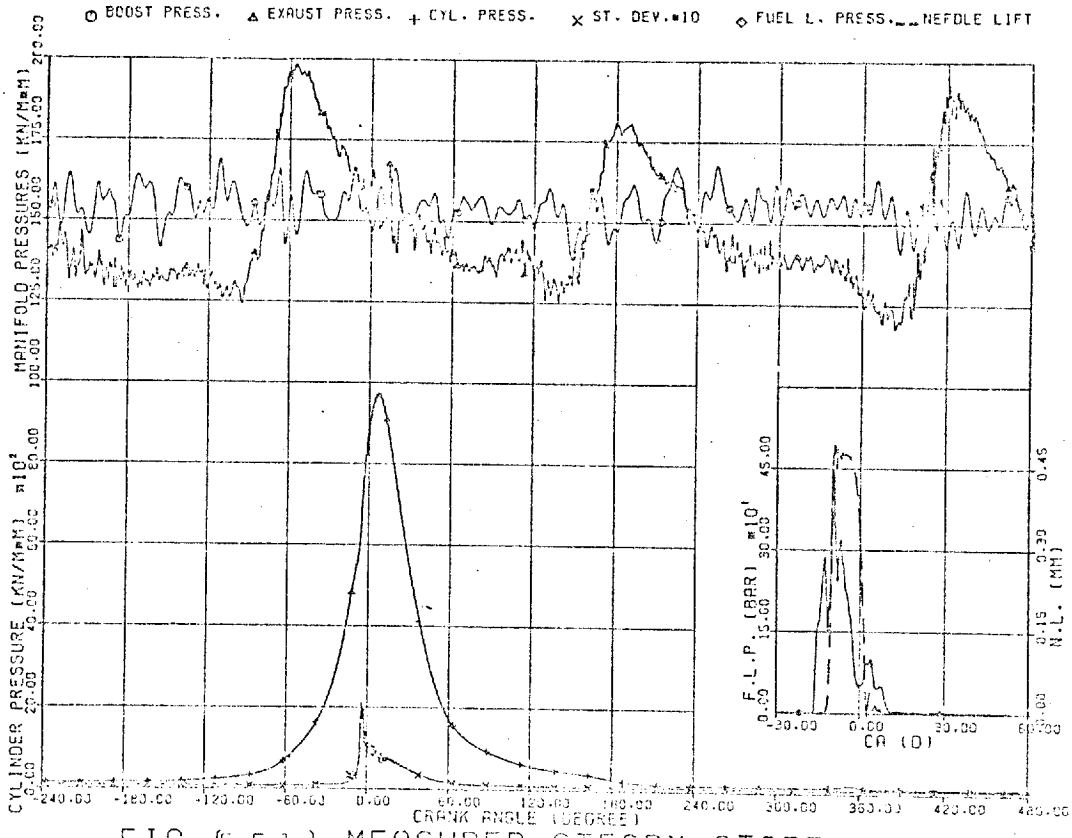


FIG.(5.5,b) MEASURED STEADY STATE DATA

ENGINE SPEED= 2000.0 RPM, BMEP= 901.5 KN/(M*M)

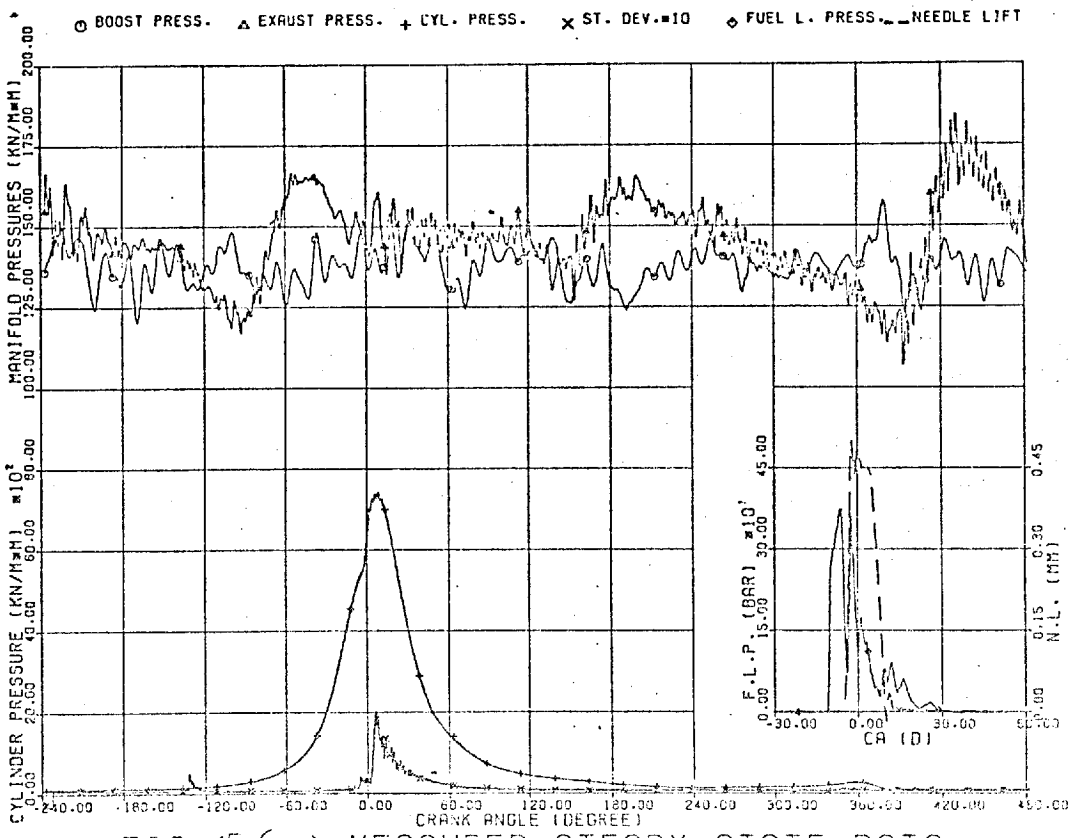


FIG.(5.6,a) MEASURED STEADY STATE DATA

ENGINE SPEED= 2500.0 RPM. BMEP= 450.8 KN/(M*M)

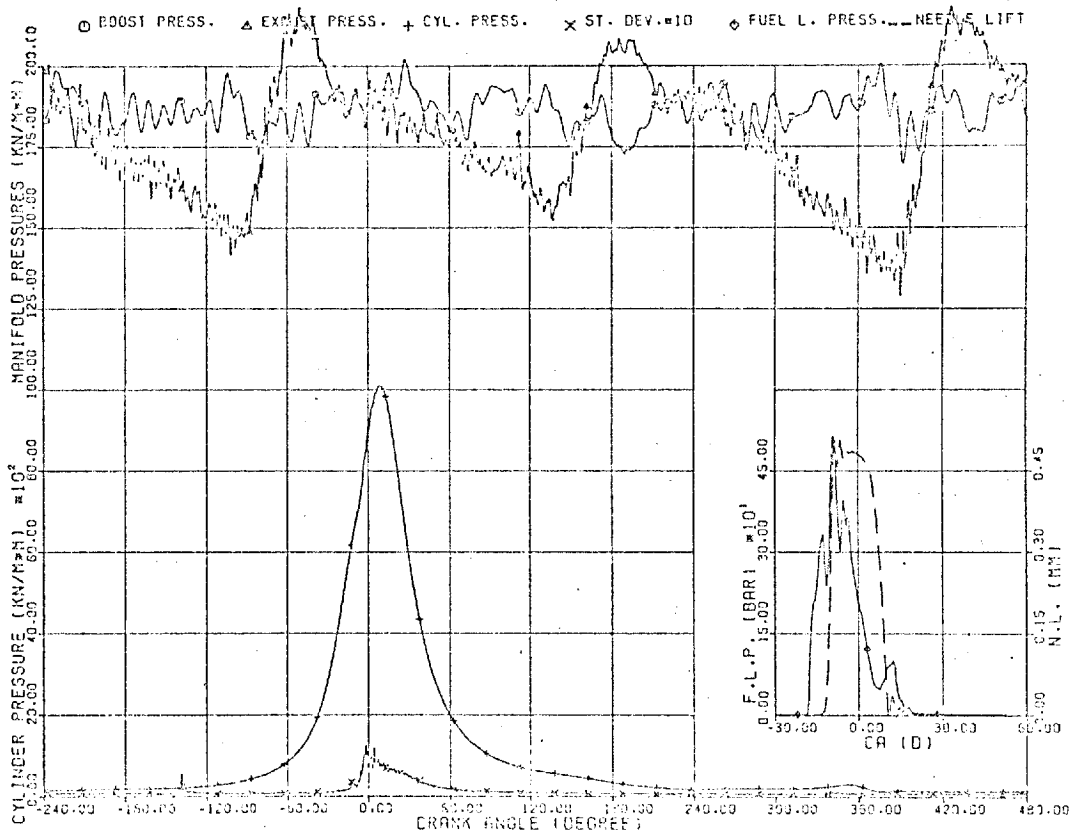


FIG.(5.6,b) MEASURED STEADY STATE DATA

ENGINE SPEED= 2500.0 RPM. BMEP= 901.5 KN/(M*M)

cyclic variation in cylinder pressure (120). Since, for any crank position, the degree of variation in cylinder pressure is described by the corresponding value of standard deviation, the latter was employed to govern the local smoothing of the cylinder pressure curve. This was essential for the computation of fuel burning rates (Chapter 6 and Appendix D). Also, the value of the standard deviation at B.D.C. (prior to compression) was used to check drift in the pressure signal (Chapter 4).

Transient pressures in the exhaust manifold were measured close to the exhaust port of the instrumented cylinder (no. 1). All pressure records basically exhibited three pairs of pulses every two revolutions of the crankshaft. Clearly, each pair corresponded to the exhaust stroke of one of the three cylinders connected to the exhaust manifold under consideration. An individual pair of pulses could be seen to comprise a blowdown pulse which was followed by a secondary pulse. The former, as suggested by its name, was a result of the sudden release of gases from the cylinder at the opening of the exhaust valve. On the other hand, the secondary pulse was caused by the piston motion during the exhaust stroke.

At low loads, the secondary pulse exhibited a higher amplitude and became more dominant with increase in engine speed. As load was increased, blowdown pulses of high peaks were generated, due to the rise in cylinder pressures. Also with increase in flow rates (towards maximum power), the two pulses tended to merge.

The boost pressure trace displayed oscillations which increased with engine speed. At low speeds, six individual bands of oscillations were observed to coincide

with the opening of the inlet valves of the individual cylinders. This indicated that the fluctuations recorded were probably true rarefaction and pressure waves which were initiated by opening and closure of the inlet valves. A further support was the increase in amplitude seen to occur at higher engine speeds (21). On the other hand, engine vibration might have introduced a small part of the fluctuations observed. However, the mean values of the boost pressure (integrated over 720°CA for 50 engine cycles) showed close agreement with manometer readings.

Very low boost pressures were observed during part load operation at all engine speeds; negative gauge values being obtained at no load (cases SS11, SS21, SS31 and SS41). In order to run the simulation program (Chapter 3) with such operating conditions, it was necessary to extend the compressor flow characteristics to similar levels of pressure ratio below unity. This was carried out using measurements of air flow, boost pressure and turbocharger speed which were obtained during the same engine tests.

### 5.3.2 Characteristics of the fuel injection system

If the fuel injection system (jerk pump) were to operate sufficiently slowly, the pump delivery period would coincide with the injection valve opening. Also, the fuel pressure during delivery would be the same as the nozzle opening pressure. In general, the time available for injection, in relation to the length of the pipe between the fuel pump and nozzle seat, is so short that the process is dominated by wave action. This is caused by the finite speed of propagation of pressure waves (speed of sound). It follows that the length of the fuel pipe between the pump and

injector causes a delay between an impulse leaving the pump and that reaching the injector. This delay, represented by the period of time between the points of static and dynamic injection, was evaluated from the experimental data. Figure 5.7a displays values of the injection delay which were obtained at all the test points. These can be seen to be best represented by a fixed delay of 0.9 ms. Hence, the timing of the start of injection was related to the static injection point as follows:

$$\theta_{di} = \theta_{si} + 0.0054\Omega_e \qquad (5.6)$$

where: $\Omega_e$ = engine speed in rev/min.

$\theta_{si}, \theta_{di}$ = crank positions of the static and dynamic injection points respectively.

Regarding the amount of fuel injected per cycle, it was originally planned to correlate the area under the fuel injection rate curves (steady state) with rack position and engine speed. This was considered as a useful means of measuring fuel flow during transient operation. However, it was mentioned in Section 4.3.7 that this technique was abandoned due to inaccuracies in the injection pressure measurements.

As an alternative, the fuelling per cycle per cylinder was evaluated from overall fuel consumption measurements. The resultant variation in fuelling with rack position and engine speed is shown in Fig. 5.7b. This was represented mathematically by:

$$M_f = -1.949 + 0.1279 \times 10^{-2}\Omega_e - 0.2525 \times 10^{-6}\Omega_e^2 + (4.513 - 0.2872 \times 10^{-2}\Omega_e + 0.6312 \times 10^{-6}\Omega_e^2)(r - 0.5) - (1.9915 - 0.2084 \times 10^{-2}\Omega_2 - 0.5156 \times 10^{-6}\Omega_e^2)(r - 0.5)^2 \qquad (5.7)$$

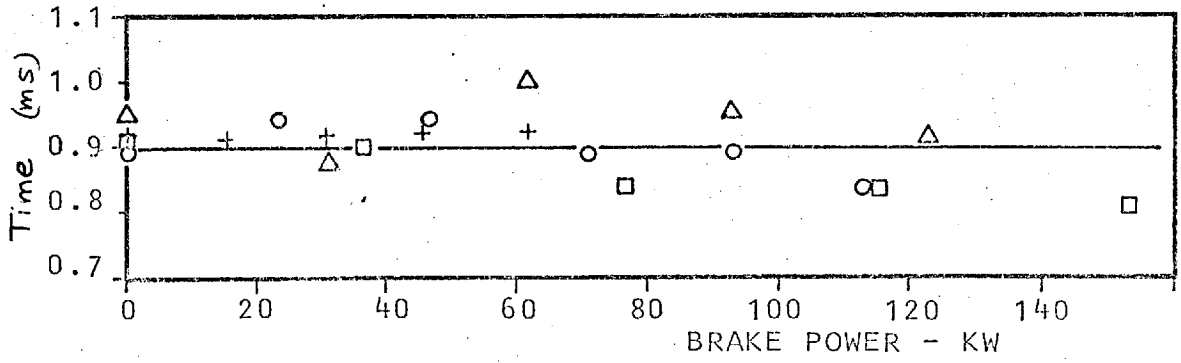


FIG. (5.7,a) Measured Injection Delay

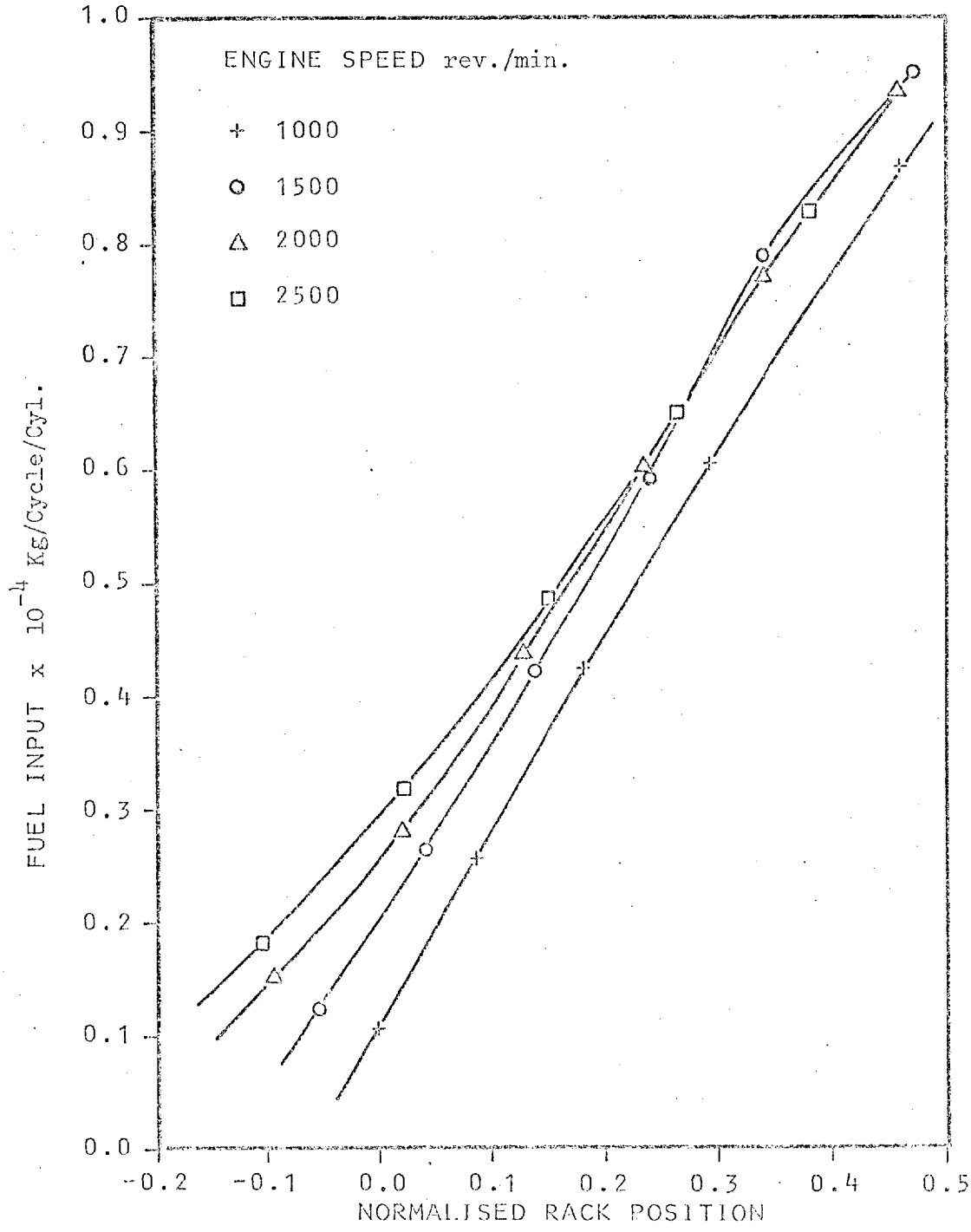


FIG. (5.7,b) Fuel Injection System Characteristic

## 5.4 DETAILED BEHAVIOUR DURING TRANSIENT OPERATION

A series of 24 transient tests were carried out to obtain detailed information about the engine behaviour under unsteady running conditions. These tests are listed in Table 5.2, giving the applied input changes in load and/or governor setting and the resultant variations in engine speed. Also a schematic representation in relation to the torque speed envelope of the engine is given in Fig. 5.8. The test procedure employed is described in Section 5.2.4.

Fourteen of the tests were later repeated using improved instrumentation, namely:

1. fast response thermocouples, and

2. hot wire anemometer for air flow measurements.

An optical smoke meter was employed in the tests repeated to measure the smoke density in the exhaust. Also a magnetic pickup was mounted close to the flywheel to check the position of the dynamic T.D.C.

The new thermocouples showed a marked improvement in response and the use of the hot-wire technique proved more reliable and consistent than the ultrasonic air flow-meter (Section 4.3.5). The exhaust smoke measurements demonstrated the feasibility of the method, but further development work and calibration tests are needed. In the case of T.D.C. shift, this was found to be very small; less than the sampling interval used ($1^{\circ}$CA). The repeat tests also revealed some inaccuracy in the torque measurements which could be attributed to fluctuations in the output of the measuring load cell (Section 4.2.2). These fluctuations were caused by torque pulses generated by the firing of individual cylinders in addition to lateral vibrations transmitted from the engine to the dynamometer base.

| Case No. | Initial Condition | | | Final Condition | | |
|---|---|---|---|---|---|---|
| | Load (BMEP) BAR | Governor setting | Engine speed rev/min | Load (BMEP) BAR | Governor setting | Engine speed rev/min |
| TR1 | 0.05 | -0.391 | 999 | 6.30 | -0.391 | 816 |
| TR2 | 0.04 | -0.391 | 997 | 7.36 | -0.391 | 772 |
| TR3 | 0.09 | -0.200 | 1501 | 6.50 | -0.200 | 1368 |
| TR4 | 0.16 | -0.201 | 1498 | 10.09 | -0.201 | 1242 |
| TR5 | 0.05 | 0.046 | 1997 | 6.79 | 0.046 | 1875 |
| TR6 | 0.20 | 0.045 | 1995 | 11.30 | 0.045 | 1777 |
| TR7 | 0.02 | 0.320 | 2483 | 6.86 | 0.320 | 2362 |
| TR8 | 0.02 | 0.317 | 2479 | 11.32 | 0.317 | 2092 |
| TR9 | 0.02 | -0.390 | 1004 | 0.112 | 0.110 | 2112 |
| TR10 | 0.02 | -0.390 | 998 | 0.04 | 0.312 | 2471 |
| TR11 | 4.49 | -0.360 | 1001 | 4.62 | 0.138 | 2083 |
| TR12 | 4.46 | -0.360 | 999 | 4.64 | 0.340 | 2442 |
| TR13 | 9.28 | -0.300 | 998 | 9.55 | 0.200 | 2109 |
| TR14 | 1.32 | -0.322 | 2467 | 1.44 | -0.173 | 1529 |
| TR15 | 0.04 | -0.391 | 1000 | 6.79 | 0.106 | 1989 |
| TR16 | 0.04 | -0.391 | 998 | 11.32 | 0.110 | 1882 |
| TR17 | 0.04 | -0.390 | 1006 | 11.32 | 0.112 | 2230 |
| TR18 | 0.04 | -0.200 | 1498 | 6.50 | 0.295 | 2325 |
| TR19 | 0.07 | -0.200 | 1497 | 8.65 | 0.290 | 2286 |
| TR20 | 0.99 | -0.384 | 999 | 5.40 | 0.310 | 2340 |
| TR21 | 0.18 | -0.050 | 2000 | 5.74 | -0.460 | 547 |
| TR22 | 0.22 | 0.050 | 1997 | 5.27 | -0.210 | 1353 |
| TR23 | 0.02 | 0.310 | 2463 | 11.28 | 0.052 | 1775 |
| TR24 | 0.74 | 0.338 | 2495 | 4.35 | -0.365 | 886 |

TABLE 5.2

TRANSIENT TESTS

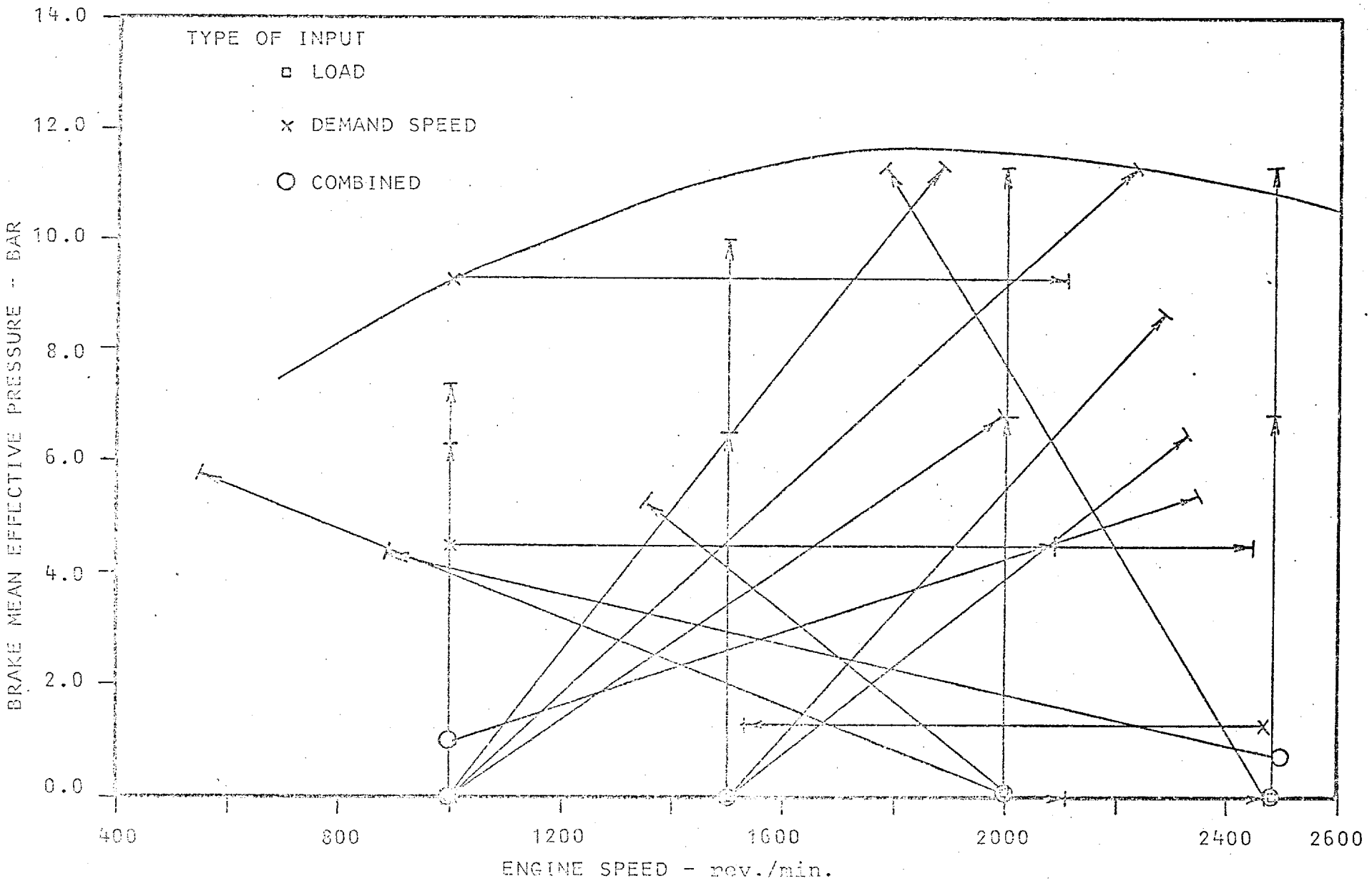


FIG. (5.8) Schematic Representation of Input Signals in Relation to Maximum Torque Curve

The amount of data collected during the tests was formidable and it is impossible to present all but examples: the data obtained from tests TR6, TR8, TR11, TR13 and TR18 are displayed graphically in Figs. 5.9 - 5.13. More experimental transient data is given in Chapter 7.

The overall response curves comprise variations in engine speed, turbocharger speed, fuel rack position, exhaust temperature (at one turbine entry sector), maximum cylinder pressure, air flow and boost pressure. These are plotted against time, in conjunction with the imposed changes in load and governor setting. A curve showing cycle number from the start of the transient period is also included.

The crank angle traces obtained from the same tests included pressures in cylinder no. 1 and in the exhaust manifold connected to it, plus the corresponding fuel line pressure and needle lift. Similar records of boost pressure, air flow and fuel rack position were also recorded, but are not shown. The working line of the engine during the transient period is also displayed on the compressor performance map.

It would appear that this was the first time in which such detailed data was measured during engine transient operation. Apart from asserting the viability of the data logging techniques developed, it provided a useful fund of information (which was not previously available) about the behaviour of the engine internal variables. Clearly this enables further insight into the interrelationships between the various parameters and the resultant influence on the response of the engine.

Cases TR6 and TR8 show the transient response of the engine to a load increase of 11.3 bar (bmep) at two different initial speeds. It may be observed that the load

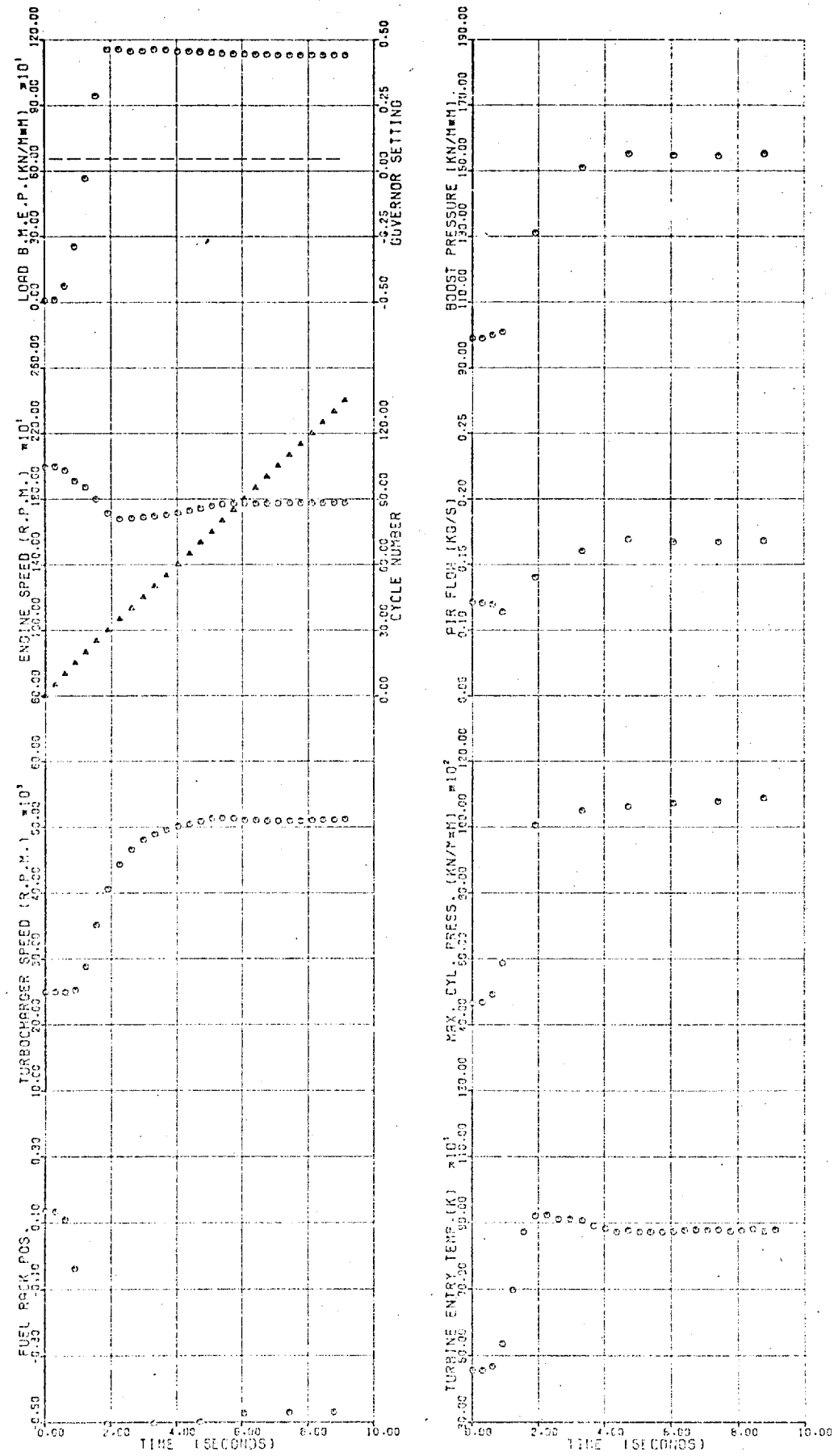


FIG(5.9.a) TRANSIENT CASE TR6

| | LOAD (BMEP BAR) | GOV. SETTING | ENG. SPEED (RPM) |
|---|---|---|---|
| INITIAL | 0.1 | 0.046 | 1994.0 |
| FINAL | 11.3 | 0.046 | 1777.0 |

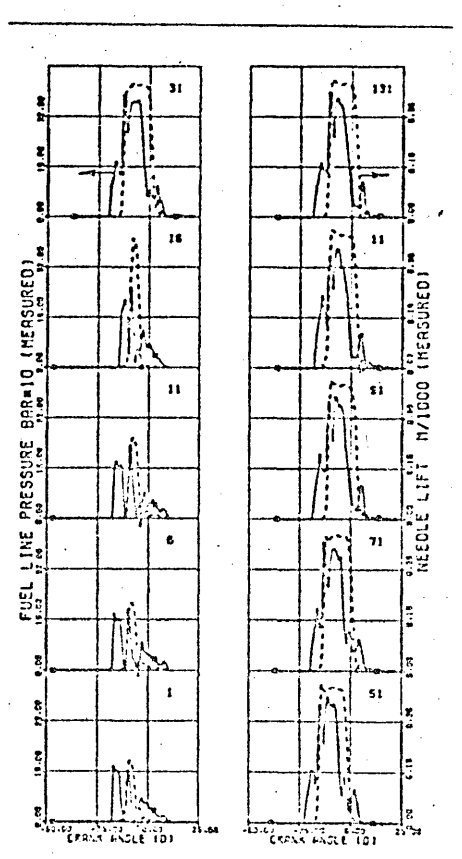


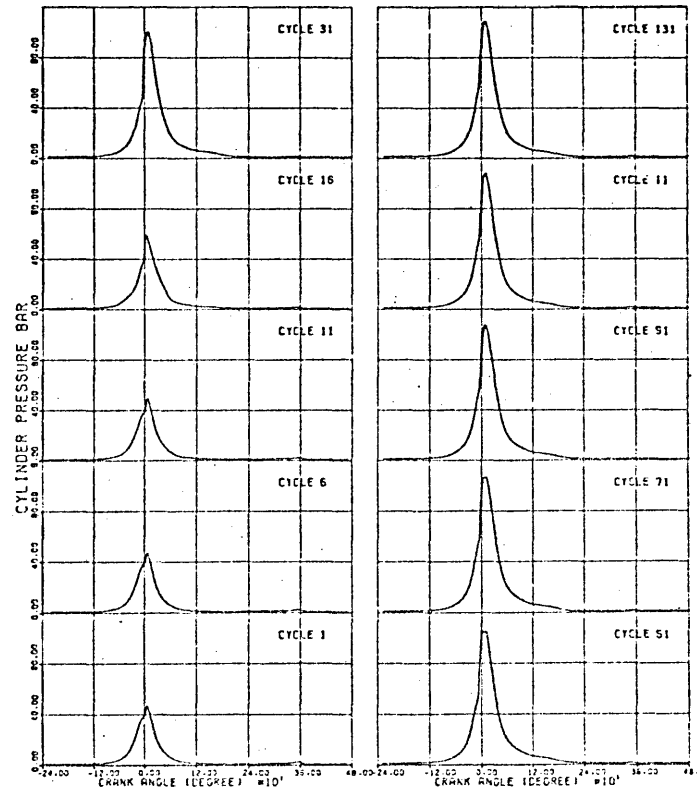


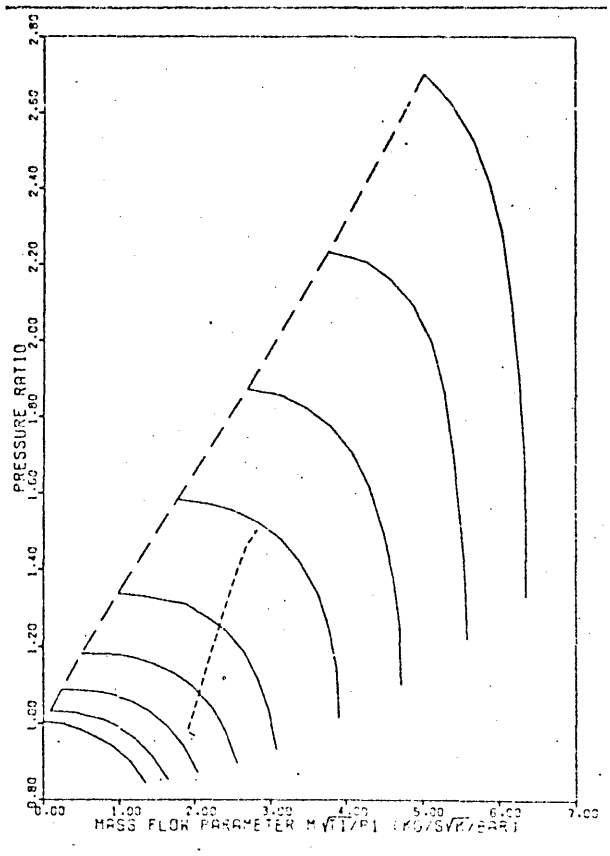


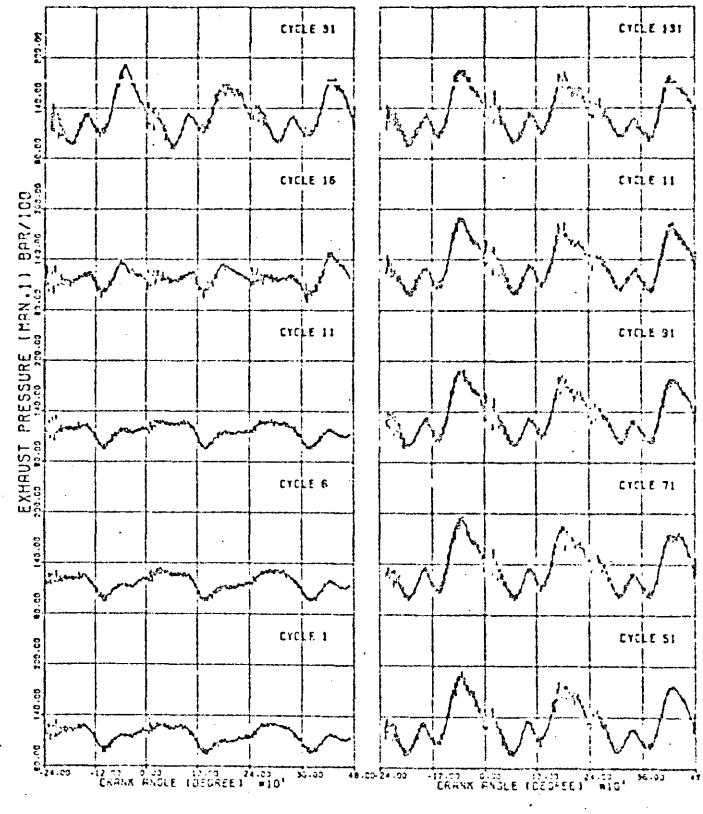


FIG(5.9.b) TRANSIENT CASE TR6

| | LOAD (BMEP BAR) | GOV. SETTING | ENG. SPEED (RPM) |
|---|---|---|---|
| INITIAL | 0.1 | 0.046 | 1994.0 |
| FINAL | 11.3 | 0.046 | 1777.0 |

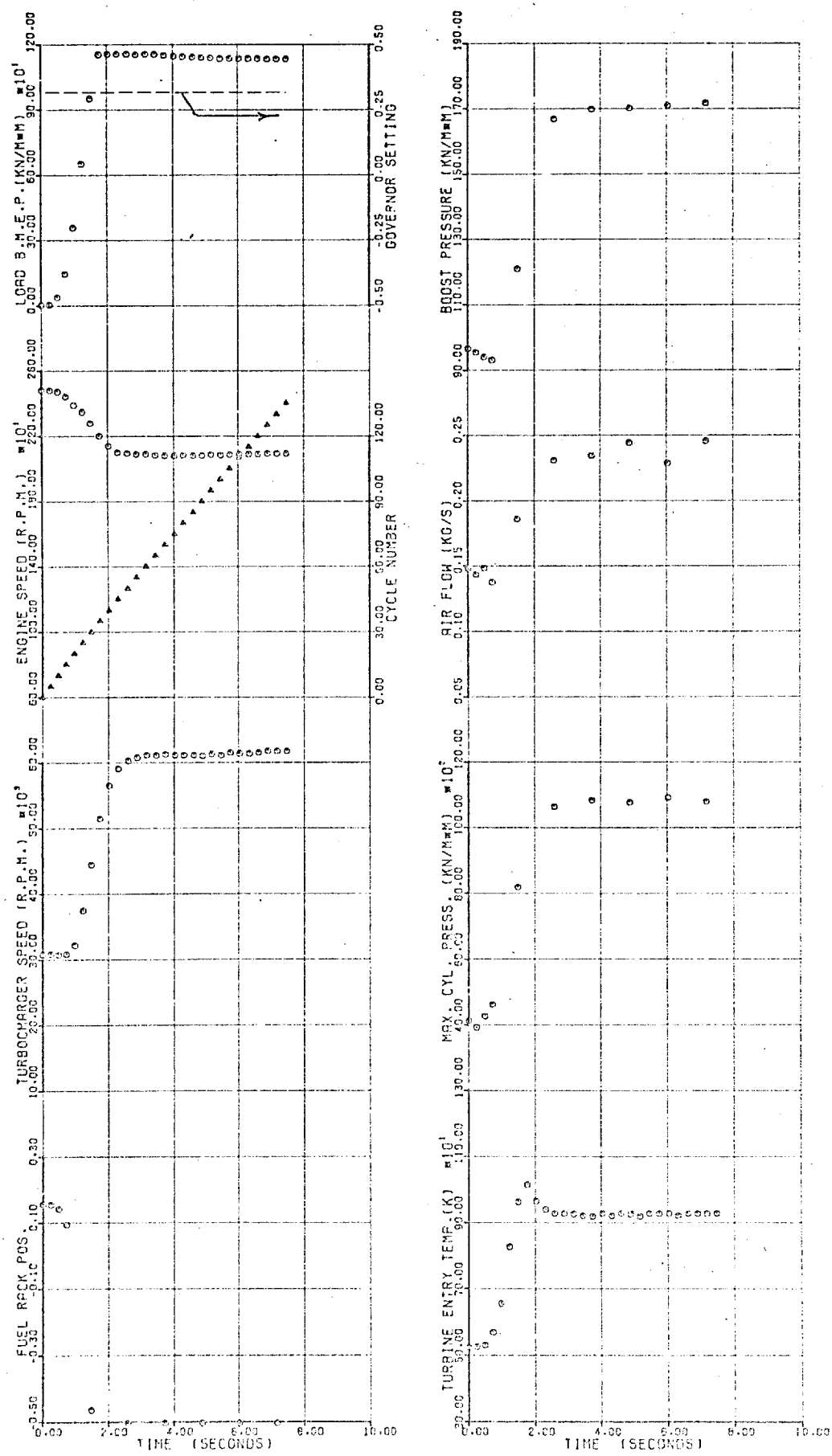


FIG (5.10,a) TRANSIENT CASE TR8

| | LOAD (BMEP BAR) | GOV. SETTING | ENG. SPEED (RPM) |
|---|---|---|---|
| INITIAL | 0.0 | 0.317 | 2479.0 |
| FINAL | 11.3 | 0.317 | 2092.0 |

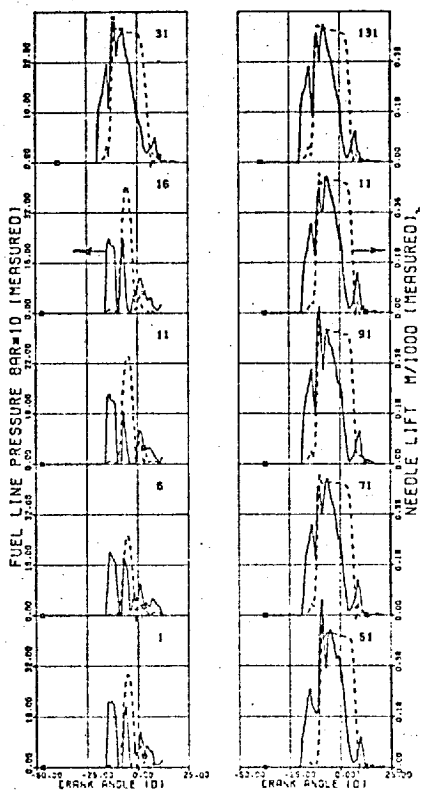


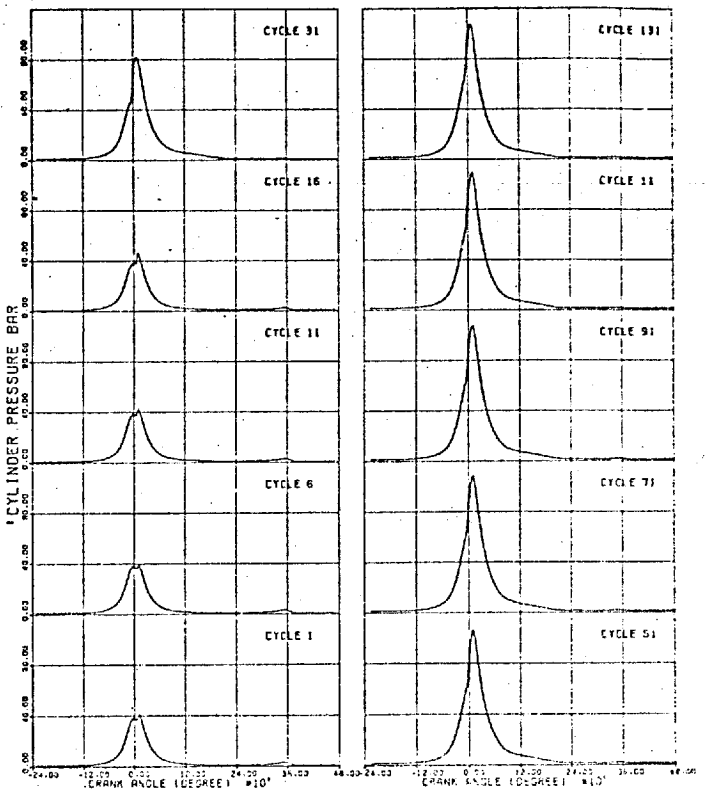


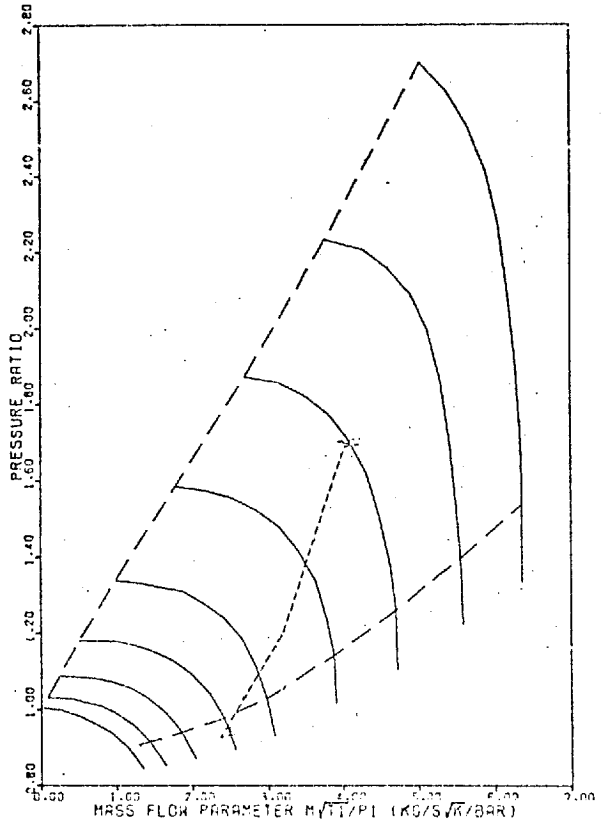


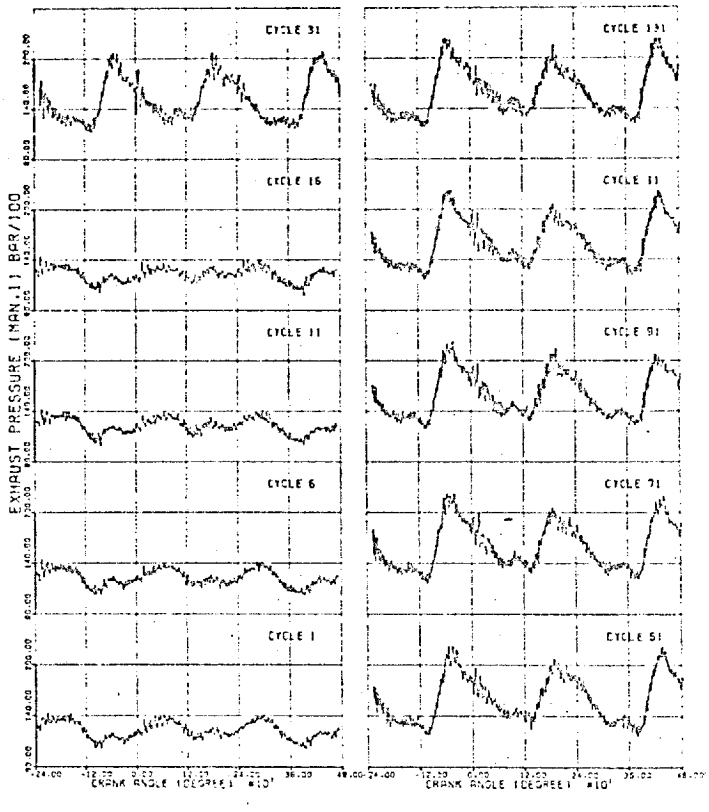


FIG(5.10.b) TRANSIENT CASE TR8

| | LOAD (BMEP BAR) | GOV. SETTING | ENG. SPEED (RPM) |
|---|---|---|---|
| INITIAL | 0.0 | 0.316 | 2479.0 |
| FINAL | 11.3 | 0.316 | 2092.0 |

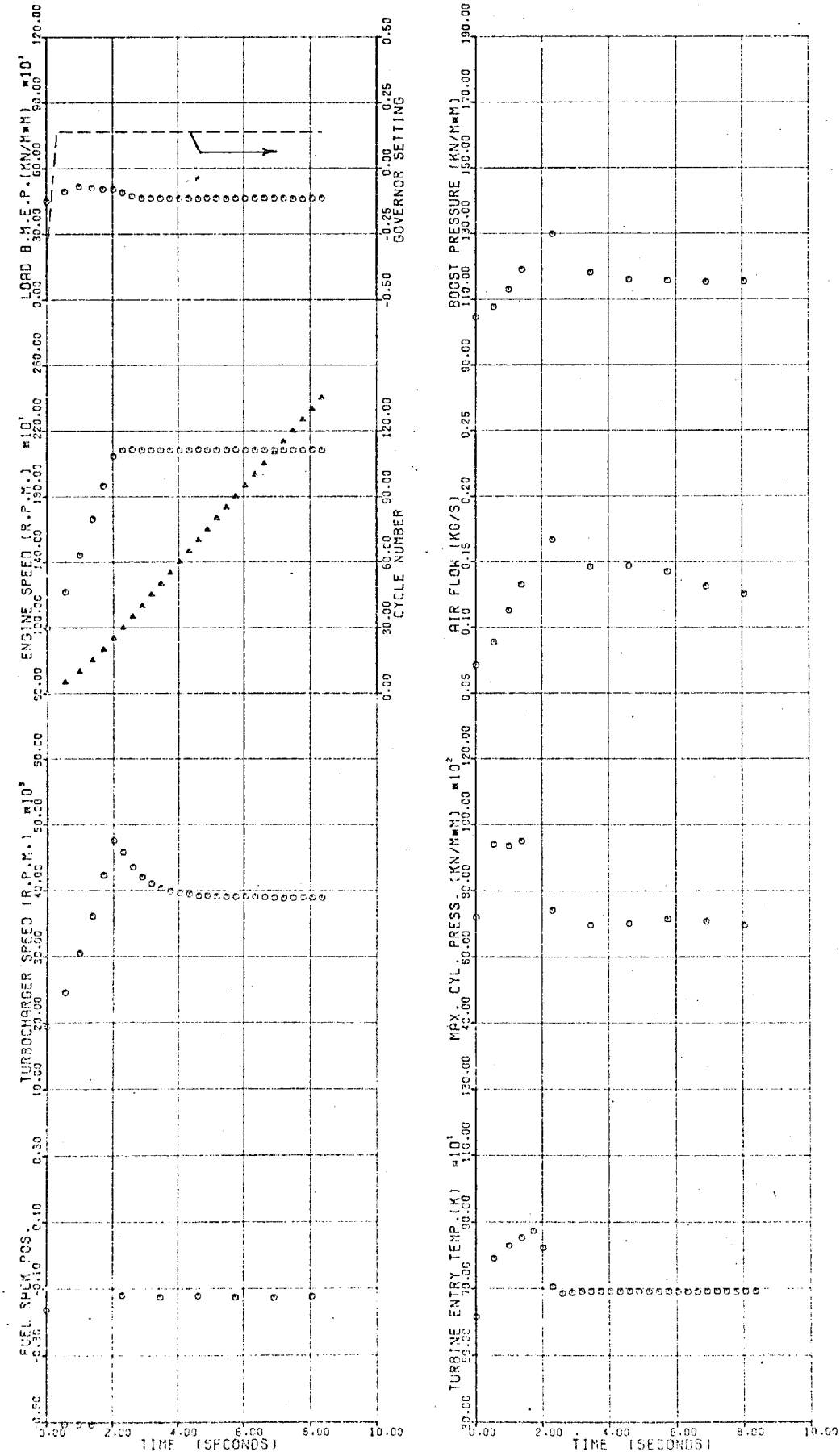


FIG(5.11,a) TRANSIENT CASE TR11

| | LOAD (BMEP BAR) | GOV. SETTING | ENG. SPEED (RPM) |
|---|---|---|---|
| INITIAL | 4.5 | -0.360 | 1001.0 |
| FINAL | 4.6 | 0.138 | 2083.0 |

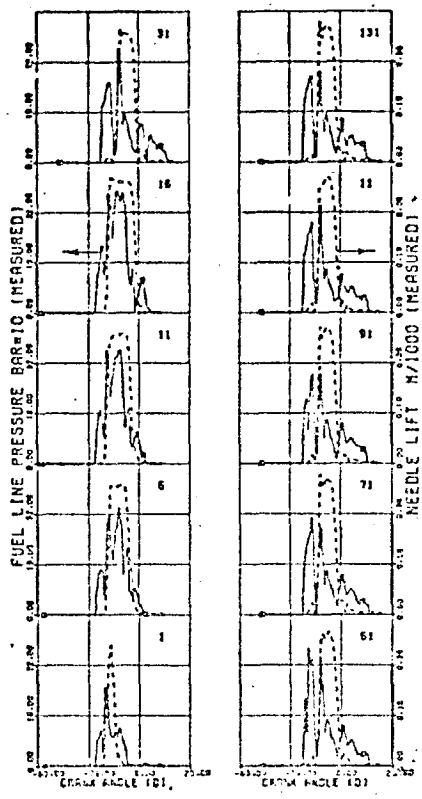


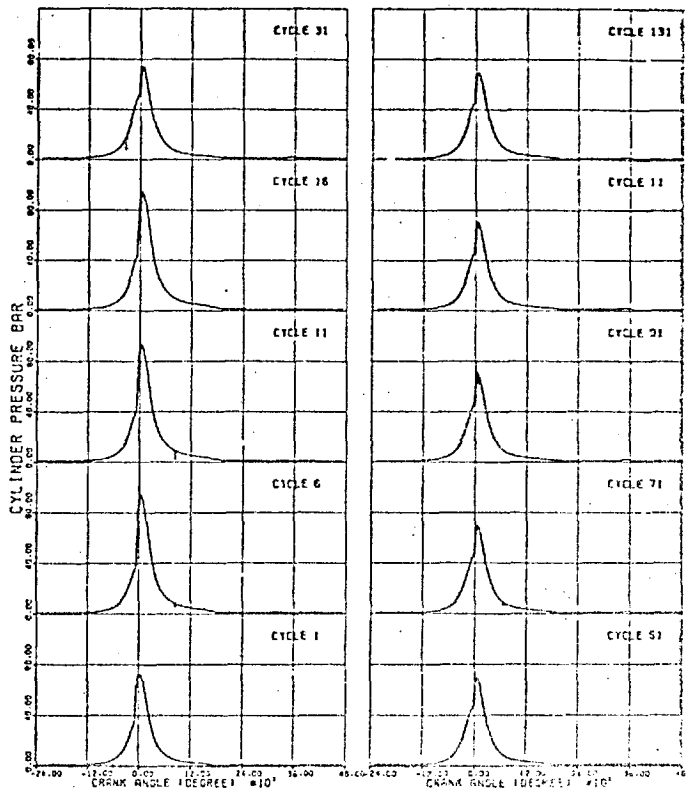


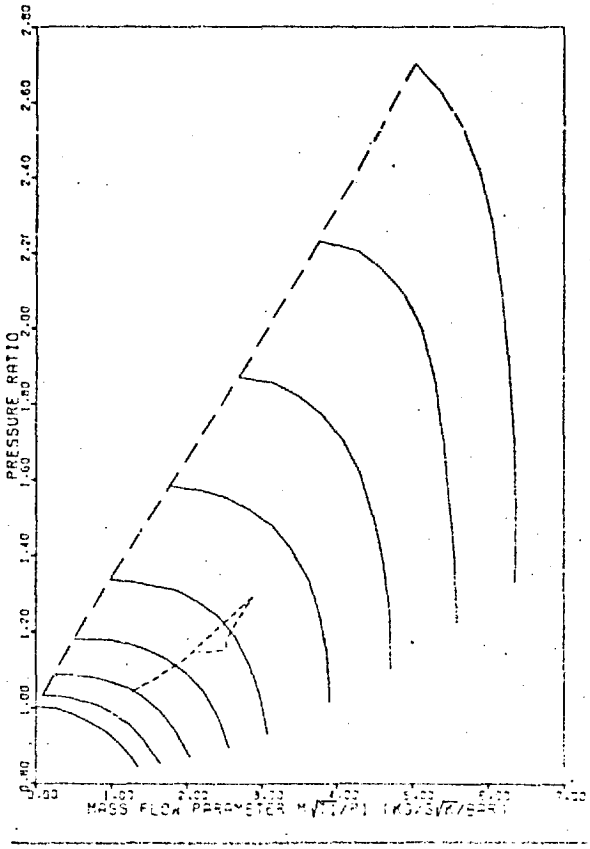


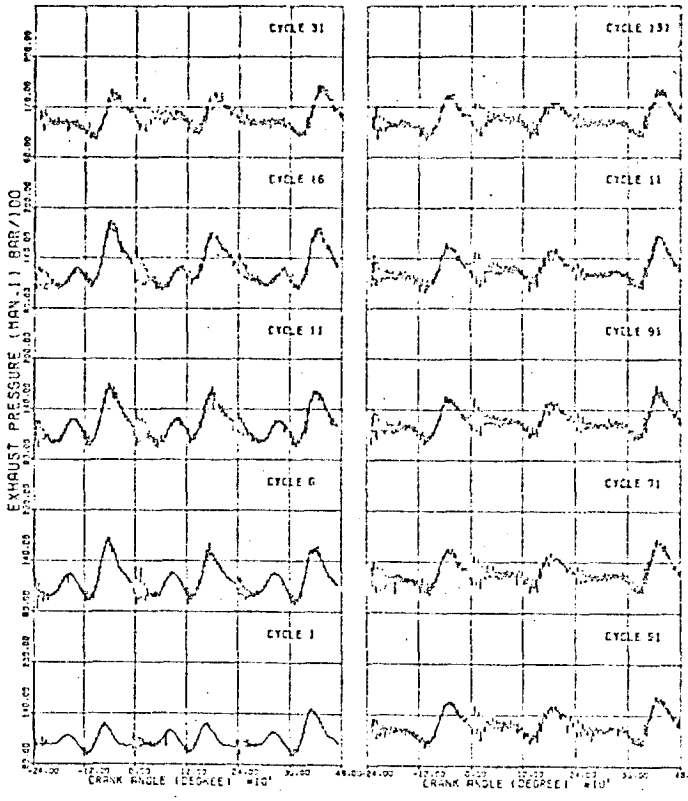


FIG(5.11,b)TRANSIENT CASE TR11

| | LOAD (BMEP BAR) | GOV. SETTING | ENG. SPEED (RPM) |
|---|---|---|---|
| INITIAL | 4.5 | -0.360 | 1001.0 |
| FINAL | 4.6 | 0.138 | 2083.0 |

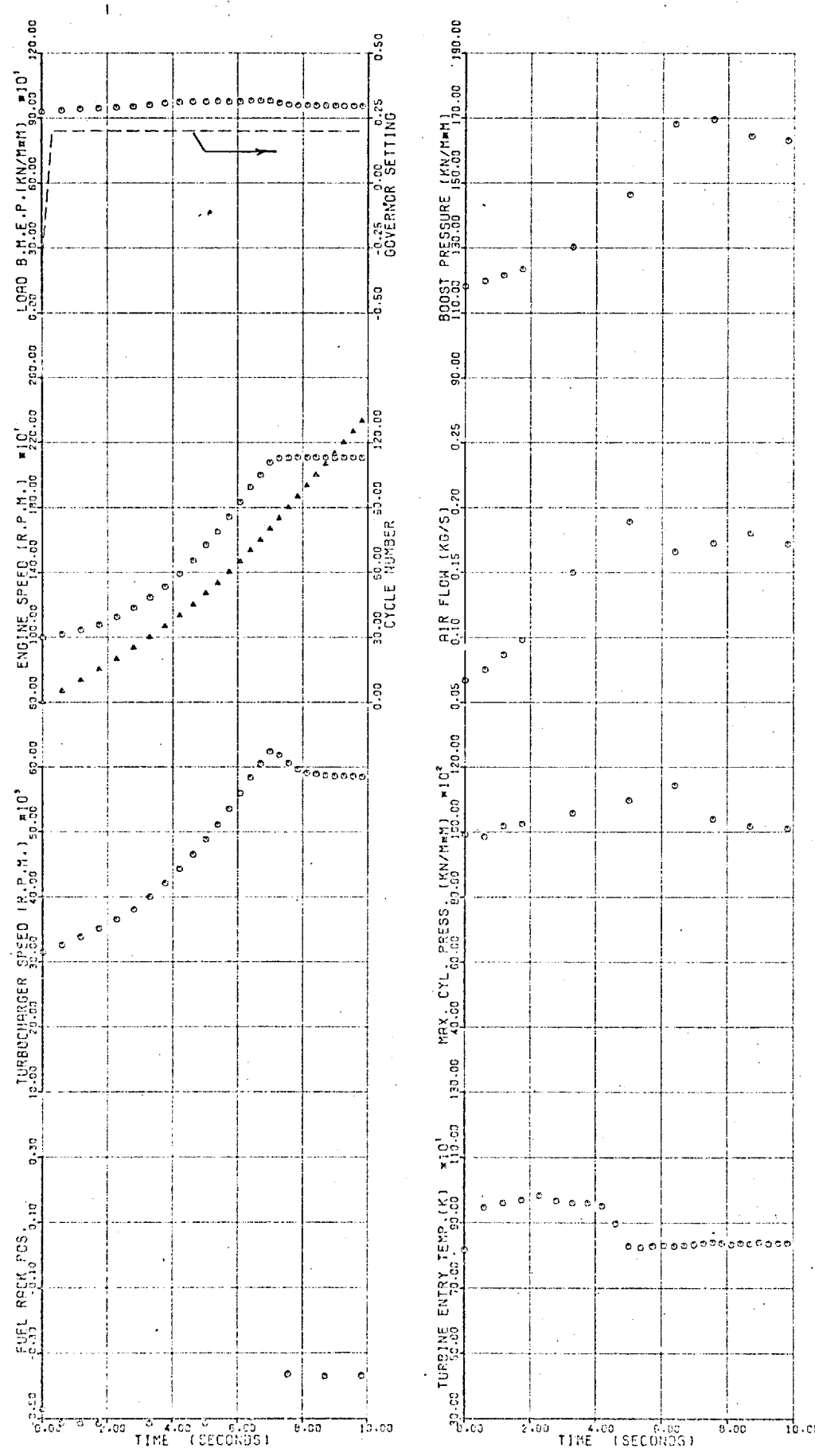


FIG(5.12a) TRANSIENT CASE TR13

| | LOAD (BMEP BAR) | GOV. SETTING | ENG. SPEED (RPM) |
|---|---|---|---|
| INITIAL | 9.3 | -0.302 | 998.0 |
| FINAL | 9.6 | 0.200 | 2109.0 |

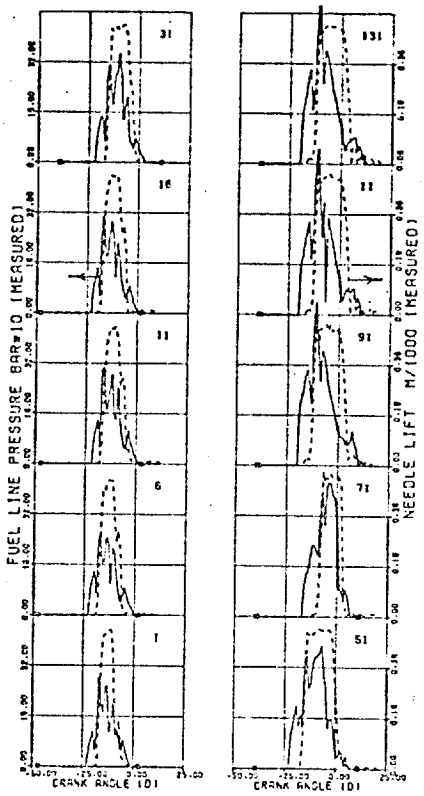


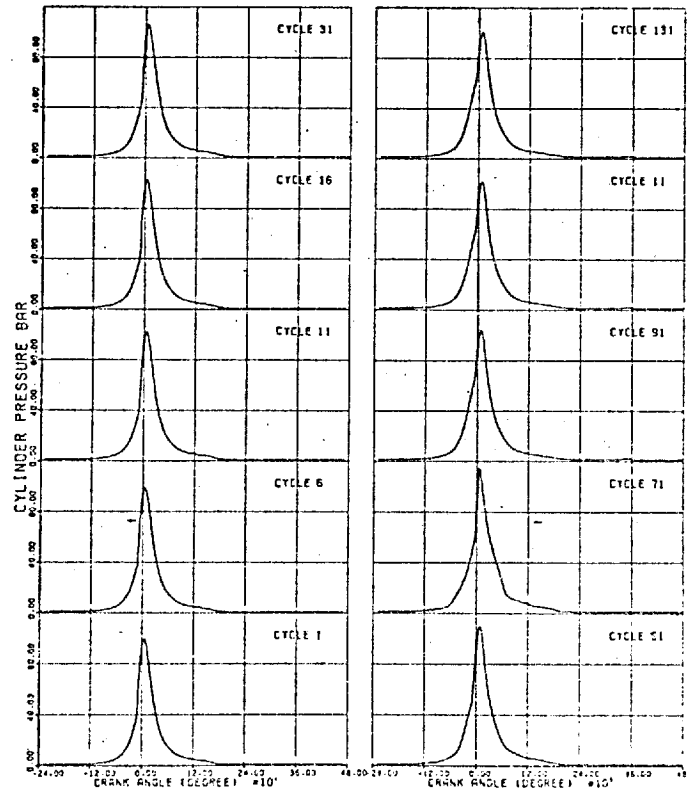


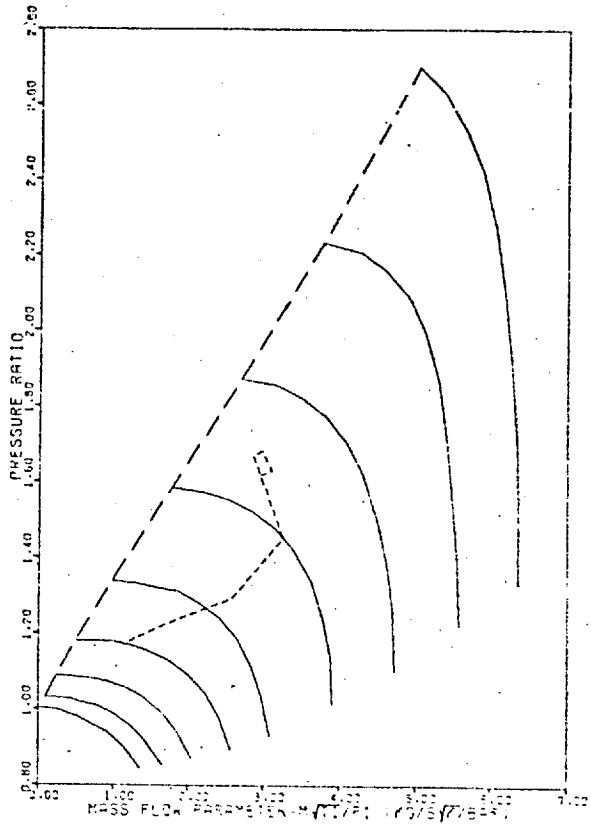


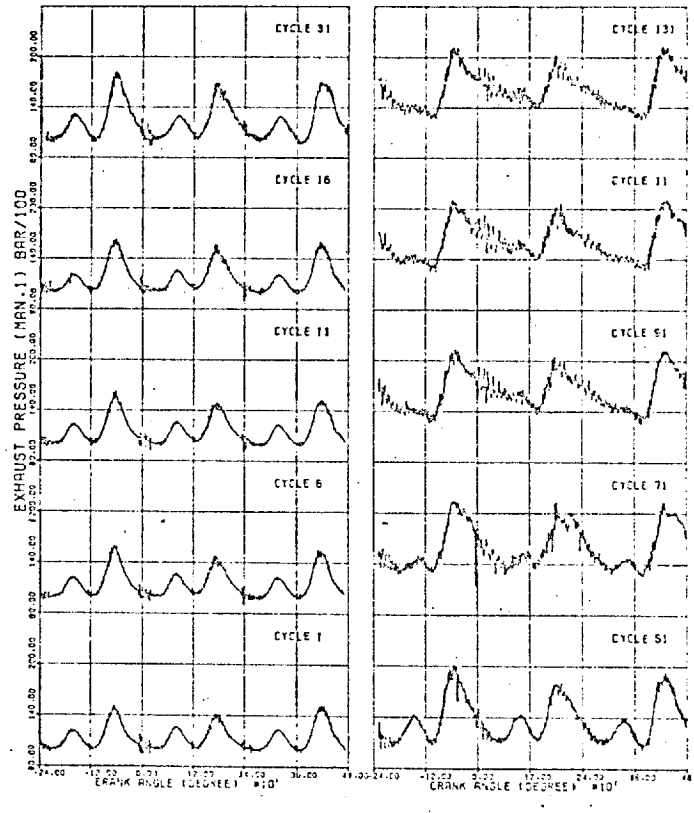


FIG(5.12,b)TRANSIENT CASE TR13

| | LOAD (BMEP BAR) | GOV. SETTING | ENG. SPEED (RPM) |
|---|---|---|---|
| INITIAL | 9.3 | -0.302 | 998.0 |
| FINAL | 9.6 | 0.191 | 2109.0 |

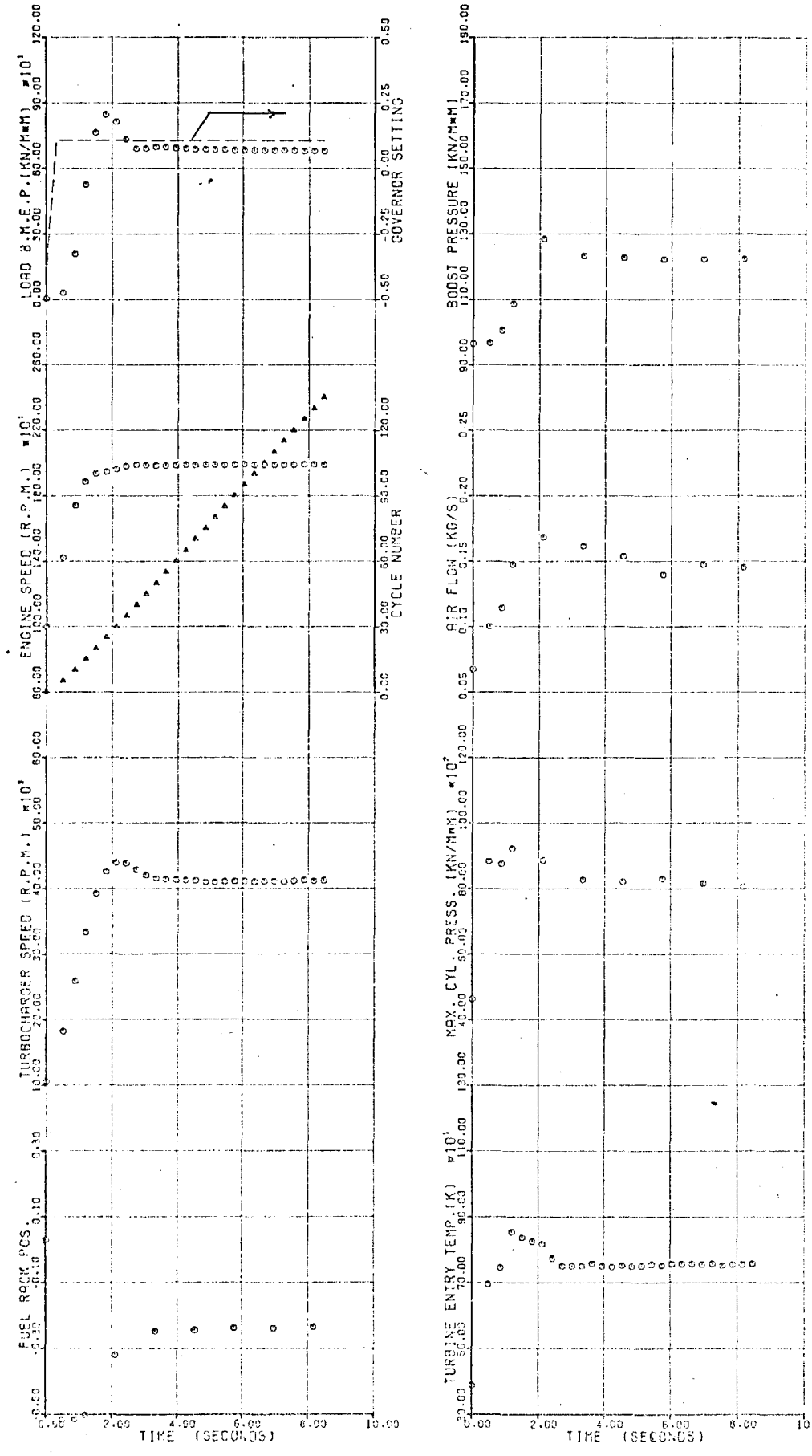


FIG(5.13.a) TRANSIENT CASE TR18

| | LOAD (BMEP BAR) | GOV. SETTING | ENG. SPEED (RPM) |
|---|---|---|---|
| INITIAL | 0.0 | -0.391 | 1000.0 |
| FINAL | 6.8 | 0.106 | 1989.0 |

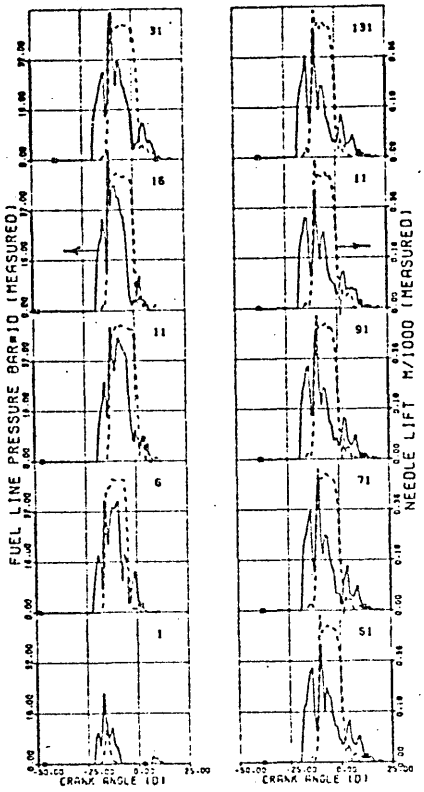


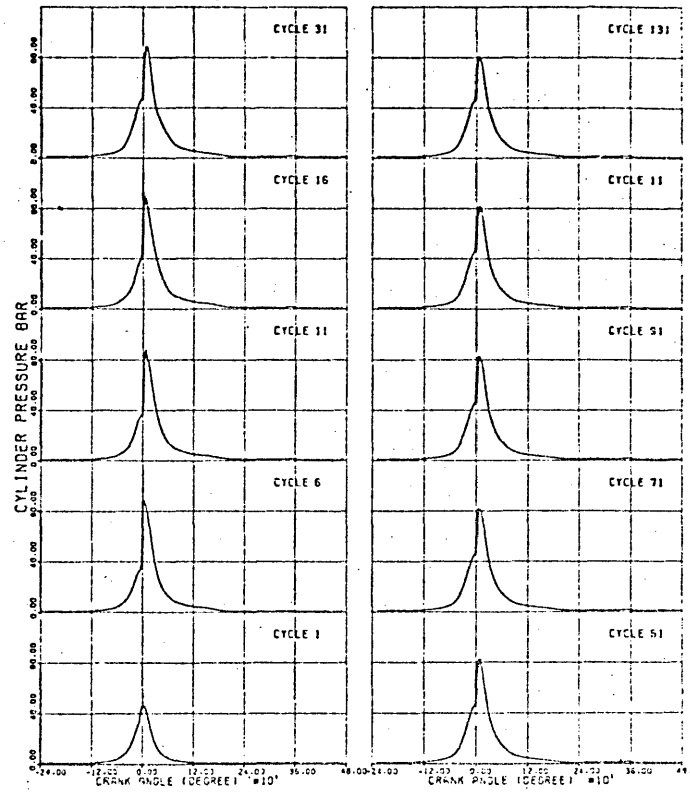


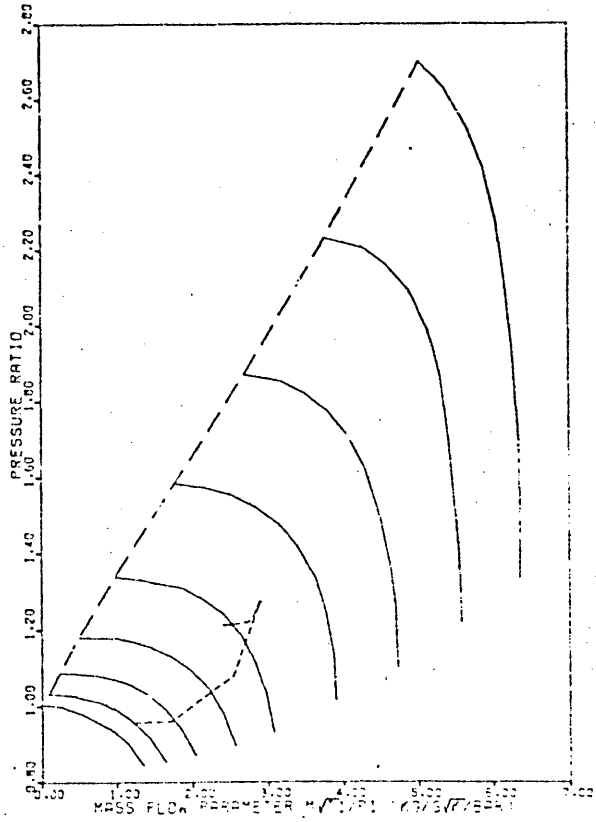


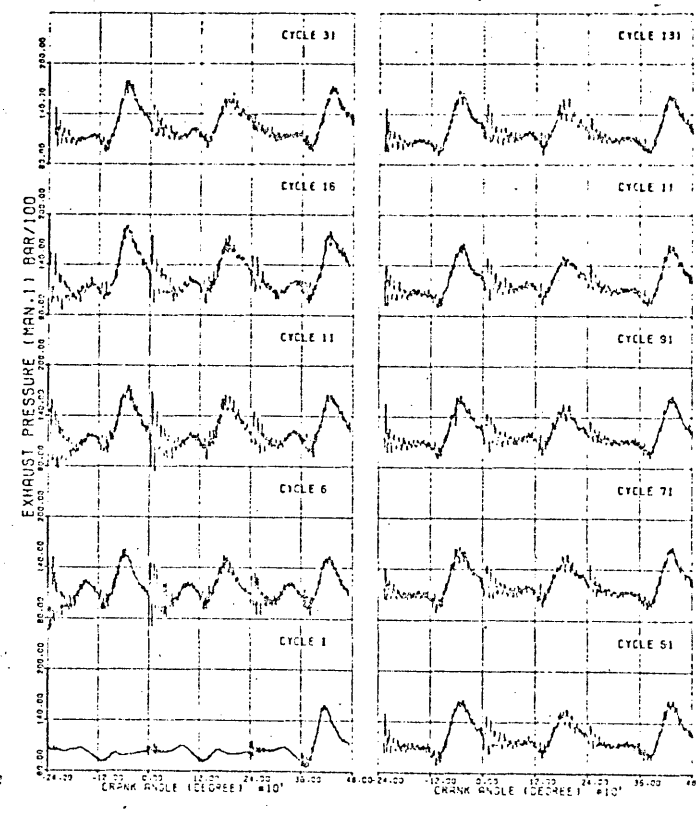


FIG(5.13b) TRANSIENT CASE TR18

| | LOAD (BMEP BAR) | GOV. SETTING | ENG. SPEED (RPM) |
|---|---|---|---|
| INITIAL | 0.0 | -0.391 | 1000.0 |
| FINAL | 6.8 | 0.106 | 1989.0 |

took about 11 engine cycles to show an appreciable rise. Following the resultant decrease in engine speed, the governor quite rapidly moved the fuel rack to the maximum fuelling position (no boost controlled rack limiter was fitted). Case TR8 (higher engine speed) exhibited faster governor response, hence maximum fuelling was attained earlier. This was also shown in the form of a higher overshoot in exhaust temperature. The turbocharger speed also responded much faster; showing a rise time of 2.65 compared with 4.05 in case TR6. Clearly this was reflected in the response of air flow and boost pressure.

Case TR8 displayed a continuous decrease in engine speed without any undershoot and recovery. The final steady state speed showed a large drop in comparison with case TR6 (15.6% and 10.9% respectively). This was caused by the fact that the load in case TR8 was slightly in excess of the maximum brake torque of the engine at the initial speed (see Fig. 5.8).

Cases TR11 and TR13 are examples of the response of the engine to a sudden increase in demand speed (0.5 full range) at two load levels (4.5 and 9.3 bars respectively). Again the governor showed very quick response in varying the rack position. As expected, case TR11 produced a faster engine response*, the rise time of engine speed was 2.0 s compared with 7.0 s for TR13. The percentage overshoot in turbocharger speed was also larger in the former case. This also applied to the exhaust temperature, peak cylinder pressure, air flow and boost pressure, and resulted from the larger percentage increase in fuelling shown in case TR11.

* Similar behaviour was reported by the author in an earlier work (73) on a naturally aspirated diesel engine.

Case TR18 shows the engine response to a combined increase in load and demand speed. Since the change in demand speed was executed faster than load, the initial stages of the transient response were similar to case TR11.

The variation in exhaust temperature during transient operation was controlled mainly by the rack motion and air flow. The quick initial rises in temperature were caused by the rapid increases in fuelling. Whilst sharp drops (TR11, TR13 and TR18) were brought about by the quick response of the governor, gradual reductions were due to the increase in air flow (TR6 and TR8).

In general, the peak cylinder pressure followed the quick response of the governor (reflected in the needle lift diagrams). In other words, the air supply appeared to have a less dominant role than fuelling. This was more obvious in the cases where large increases in fuelling were achieved very rapidly whilst air flow lagged behind (cases TR11 and TR18). Despite the resultant development of very rich fuel-air mixtures, this appeared to have very little effect on the initial phases of combustion which controlled the peak cylinder pressure, i.e. premixed burning. However, in case TR13, the peak pressure rose mainly due to the increase in trapped mass, which followed the rise in air flow; fuelling was fixed at the maximum value.

# CHAPTER 6

# COMBUSTION

## 6.1 INTRODUCTION

The reliable prediction of the consequences of any changes in design or operational conditions on the performance of a diesel engine, would be an invaluable aid to engine manufacturers. In general, diesel combustion and the associated thermo-fluid dynamic processes are at present too complex for analytical prediction. Whilst progress is being made towards achieving this long term objective, the simplifying concept of an overall rate of heat release (due to combustion) is widely applied in engine performance prediction programs.

The present chapter describes a model developed to simulate the overall effects of the compression ignition combustion process and its dependence on the operational conditions of the engine. The model, which is tailored primarily for engine simulation applications, employs the fuel burning rate and thermodynamic equilibrium concepts to determine the heat released inside the cylinder. The characteristics of the apparent burning rate of the fuel are correlated with the major controlling parameters; values of which are determined at the ignition point. The correlations established, together with the ignition delay formula, are based on experimental data obtained from steady state tests (Section 5.3). The proposed model is necessary to describe the non-linear effects of combustion on the instantaneous engine torque, particularly during transient operation when excessively over-rich fuel/air mixtures are developed.

The processes involved in diesel combustion are outlined briefly to illustrate the complexity of the problem

of detailed modelling. The fuel burning rate approach (heat release) and the technique employed to obtain a fuel burning rate curve from an experimental cylinder pressure record are also described.

## 6.2 THE COMPRESSION IGNITION COMBUSTION PROCESS

Combustion inside a diesel engine cylinder is normally considered to commence at the dynamic injection point and to comprise an ignition lag followed by a period of heat release. The length of the ignition delay period is of considerable importance, since it affects the development of the processes following ignition and hence the rate of heat release and pressure rise. This period is usually subdivided into 'physical' and 'chemical' parts. The former part represents the time between the start of injection and attainment of preflame reactions. It is known to involve the following processes: fuel-jet breakup, air entrainment, fuel evaporation and partial mixing of fuel vapour and air. The chemical delay follows, encompassing pre-ignition reactions which oxidise the hydrocarbon fuel-air mixture at a continuously increasing rate until full ignition occurs.

The duration of ignition delay is influenced by the chemical and physical properties of the fuel, the temperature and pressure of the compressed air, the degree of fuel atomisation, the nature and degree of swirl, combustion wall temperature, etc. Due to the highly heterogeneous state of the fuel-air mixture, and the fact that injection takes a finite time, the physical and chemical delays overlap from one point to another within the cylinder. It follows that no clear distinction between the parameters influencing the two compounds is possible (125). However,

chemical delay does reduce greatly with increasing temperature and slightly with pressure. The physical delay period is also reduced by employing high injection pressures, high turbulence (72) in addition to higher compression temperatures (84). However, the change due to reduced physical delay may be offset by an increase in the amount of combustible (prepared) fuel-air mixture accompanying increased injection pressures and turbulence.

Once ignition takes place, the combustion mechanisms accelerate swiftly, resulting in a rapid rate of pressure rise. Clearly, the combustion rate will depend on the amount of fuel available in the cylinder at the time of ignition, which in turn is governed by the delay period. The first appearance of a flame following ignition is (as was noted by many workers) of the non-luminous, premixed type and the highest rate of heat release is normally associated with this relatively short period of uncontrolled premixed combustion. Lyn (70) reported that this phase of premixed burning is very rapid and normally lasts only 5 to 7 crankangle degrees. This initial period is followed by the main period of heat release which usually extends more than 30 degrees. The nature of the flame changes (1, 5) and fuel-air reactions are governed by turbulent diffusion. The burning rate will be controlled by the mixing pattern, which is dependent on purely mechanical and physical processes (viscous and turbulent shear, pressure and temperature gradients, diffusion, etc.). Some further heat release can be observed beyond this main diffusion-controlled period, but its effect is normally relatively small.

From the above brief discussion, it is clear that

the combustion of fuel sprays in an engine cylinder is a very complex phenomenon in which the processes of fuel atomisation, evaporation, mixing and chemical kinetics are interrelated in a relatively unknown manner (44). Simulation of this phenomenon requires the development of sophisticated models for: air motion, fuel spray penetration, atomisation, evaporation, air entrainment, chemical kinetics, turbulent diffusion, etc. To cater for the spatial and temporal variations in composition, burning rate, pressure and temperature, such a simulation should be three-dimensional and unsteady. All attempts (to date) in this direction have yielded qualitative rather than quantitative explanations of combustion (125). Furthermore, if such a procedure was available, the computations involved would certainly be too lengthy to justify their inclusion in a transient response simulation programme.

It is inevitable, therefore, that major simplifications must be made, to arrive at some general workable relationship for an analytical model of heterogeneous burning in diesel engines. A relatively successful approach (serving engine performance prediction programmes primarily) has been the representation of the overall thermal effects of the combustion processes by an apparent rate of heat release (or fuel burning) pattern (99).

## 6.3 THE APPARENT BURNING RATE APPROACH

A simple single-zone combustion model has been widely applied in cycle analysis programs (99,115). This considers the cylinder contents to be a homogeneous mixture of ideal gases which are always at thermodynamic equilibrium and are free of any property gradients. Combustion is

modelled by a uniformly distributed source which emits instantly burning fuel at a rate equivalent to a specified time-varying pattern, known as the apparent rate of burning (AROB).

Provided that a suitable AROB curve is used, good agreement between computed and measured engine performance can be achieved. At the present time, estimation of the AROB curve is a matter of experience (with the type of engine under consideration). Consequently a serious limitation is imposed on the predictive capability of cycle analysis programs.

### 6.3.1 Analytical burning rate functions

Analytical functions describing the pattern of the AROB (e.g. triangular (71) and more complex alternatives) have been used by many researchers. The Wiebe function (117) is the most widely used expression:

$$\frac{M_{fb}}{M_{ft}}(\tau) = 1 - \exp\left[-CW1\ \tau^{CW2}\right] \qquad (6.1)$$

where:
- $M_{ft}$ = total mass of fuel injected per cycle,
- $M_{fb}$ = mass of fuel burned up to $\tau$,
- $\tau$ = normalised crank angle, $\tau = \frac{CA - CAIP}{CAEB-CAIP}$,
- CA = current crank angle referred to firing TDC,
- CAIP = CA at ignition,
- CAEB = CA at which burning ends,
- CW1, CW2 = shape constants.

The resulting AROB (the first derivative of equation (6.1)) is represented by a smooth continuous curve which is similar to the Arrhenius function:

$$AROB(\tau) = M_{fb}(\tau) = \frac{M_{ft}}{(CAEB-CAIP)} CW1.CW2\ \tau^{(CW2-1)}.$$
$$\exp\left[-CW1\ \tau^{CW2}\right] \qquad (6.2)$$

This expression was originally (117) based on the burning of homogeneous mixtures; a condition closer to spark ignition engines rather than diesel.

Nevertheless, it is considered useful as a basic shape for the substitute heat release diagram in diesel engines. It is also simple to handle mathematically, using the two shape parameters CW1 and CW2, which control the percentage of fuel injected that burns and the initial rate of rise respectively. Virtually complete burning (99.9%) is achieved if CW1 = 10, whilst CW2 normally varies between 1.4 and 2.6.

The influence of the shape of the analytical AROB functions on the characteristics of the simulated combustion process was studied by Lyn (71) and Lange (65).

### 6.3.2 Burning rates from injection rates

Lyn (70) was one of the first to relate the AROB to injection characteristics. He proposed a graphical method which subdivided the injection rate diagram into elements of equal duration. Fuel elements were assumed to enter the combustion chamber and mix with air successively, each becoming ready for burning according to a specified (triangular) pattern. Fuel mixing during the (specified) ignition delay period was added to the total rate of mixture preparation diagram, thus leading to a high initial burning rate. The high degree of empiricism involved greatly limited the applicability of the method.

In order to account for the later decrease in burning rate, Austen and Lyn ( 5 ) used a modified model based on the burning of single fuel droplets in free air. The burning time of each fuel element injected was allowed to increase progressively. This model appears to be an analytical extension of Lyn's method (70).

Nagao et al (78) used the same incremental injection approach and assumed that each element burned completely within $1^{o}$ CA following its ignition delay period. The vaporisation rate and ignition delay were computed for each fuel element injected, using single droplet theory and Wolfer's formula (121) respectively. The model gave no explicit consideration to droplet size distribution or droplet mean diameter and it is doubtful if it could be applied to predict realistic burning rate curves.

Shipinski et al (91) attempted to correlate heat release with fuel injection by fitting the Wiebe function to experimentally-obtained heat release curves. The resultant Wiebe constants were related to the fraction of fuel injected during the ignition delay period and the overall air/fuel ratio. Ignition delay was represented by a modified version of Wolfer's formula. The poor results of this correlation attempt prevented its use in engine simulation programs.

A spray droplet burning model based on single droplet theory was presented by Shipinski et al (91,92), in which the Sauter mean diameter and droplet size distribution were calculated according to the proposals of Knight (63) and Tanasawa (100) respectively. The ignition delay for each element was determined by a Wolfer type formula and a single droplet burning was introduced. Fairly reasonable

agreement with experimental data was shown if this coefficient was related to either fuel/air ratio or gas temperature.

A simple empirical model, linking the cumulative fuel injection and burning histories, was reported by Whitehouse et al (116). The rate of mixture preparation was related to the surface area of fuel droplets and the partial pressure of oxygen. An Arrhenius type expression was used to describe the heat release pattern during the initial premixed combustion phase (starting from the injection point). This model was developed primarily to suit the requirements of steady state cycle analysis programs, but it had to be tailored to yield reasonable results over a limited working range.

### 6.3.3 Burning rates from experimental pressure diagrams

The first attempt to obtain an apparent burning rate from a pressure-crank angle diagram was probably that of Schweitzer (90). The fact that the resultant burning rate curves were used for comparisons only, reduced the significance of the very crude simplifications that he employed.

Austen and Lyn ( 5 ,70,71) carried out an extensive experimental study of heat release in diesel engines, employing a balanced pressure indicator for cylinder pressure measurement. They neglected the molar change in the cylinder contents due to combustion and computed the internal energy of the charge according to Gilchrist's data (50). The total heat transferred to the walls was taken as the difference between the calorific content of the fuel input, the heat recovered as work, and the change in internal energy of the gas. In fact, this process concealed errors in the heat

release calculations. An additional error resulted from the assumption that heat was transferred at a uniform rate, even though it actually increased, during combustion in particular. Whitehouse et al (116) indicated that an irregular AROHR could be obtained from the cylinder pressure diagram due to insufficient measurement accuracy.

With the introduction of detailed mathematical simulations of engine cycles (21,115), methods of obtaining more accurate burning rate curves have improved. Descriptions of the assumptions, equations and solution procedures are given in the literature (21,64,124). The method reported by Krieger and Borman (64) employs probably the most refined mathematical formulation. Further development of the procedure, particularly relating to smoothing and numerical differentiation of the pressure diagram, was reported by Streit and Borman (99).

Basically, the Krieger-Borman method (64) conducts an instantaneous energy balance of the cylinder contents during the closed cycle period. In this, the equations for conservation of energy and mass (air and fuel) are solved in conjunction with the equation of state and mathematical expressions for the gas properties, to yield the fuel burning rate as a function of crank angle (or time):

$$\frac{dM_f}{d\theta} = \frac{-p\frac{dV}{d\theta} - \frac{dP}{d\theta}.M.\frac{\partial e}{\partial P} + \frac{1}{\Omega e}\Sigma Q_i - \psi_1.\psi_2.M}{e - h_f + \psi_3\frac{\partial e}{\partial F} - \psi_2(1 + \frac{\psi_3}{R}\frac{\partial R}{\partial F})} \qquad (6.3)$$

where: $$\psi_1 = (\frac{1}{P} - \frac{1}{R}\frac{\partial R}{\partial P})\frac{dP}{d\theta} + \frac{1}{V}\frac{dV}{d\theta} \qquad (6.4)$$

$$\psi_2 = \frac{\frac{\partial e}{\partial T}}{\frac{1}{T} + \frac{1}{R}\frac{\partial R}{\partial T}} \qquad (6.5)$$

$$\psi_3 = \frac{(1 + f_s.F_o)M}{f_s.M_o} \qquad (6.6)$$

$\frac{dM_f}{d\theta}$ = mass fuel burning rate; Kg/$^o$CA.

$Q_i$ = instantaneous heat transfer rate through surface i; KW.

$M_o, F_o$ = charge mass and equivalents ratio prior to injection.

$h_f$ = absolute fuel enthalpy.

In addition to the experimental cylinder pressure diagram and its first derivative, the following data are required for the solution: engine geometry, an estimate of charge mass and composition prior to injection, and an estimate of the cylinder wall temperatures. In order to achieve optimal accuracy when applying the method, the input data together with other factors must be carefully examined for possible errors. Appendix D presents an analysis of the influence of individual factors on accuracy.

## 6.4 COMBUSTION MODEL

An empirical model was developed to simulate the combustion process during steady state conditions and a succession of engine cycles during transient operation (including cases of over-rich fuel/air mixtures). Basically a relatively simple hypothesis of the process was introduced in order to obtain a reasonable simulation of its major characteristics via manageable analytical expressions.

The combustion process was considered to start at the dynamic injection point and to comprise two distinct phases; ignition delay and heat generation. The evaluation of the injection delay period, which relates the dynamic and static injection points, was described in Sections 2.6 and 5.3.2. The total length of the ignition delay period was

related to the mean cylinder gas temperature and pressure during delay, by the following semi-empirical expression (44):

$$I.D. = \frac{a_1}{P_1^{a_2}} EXP(a_3/T) \qquad (6.7)$$

where: $P$, $T$ = arithmetic mean cylinder gas pressure and temperature during delay,

$a_1, a_2, a_3$ = empirical constants.

The heat emission period encompassed two different modes of burning; "premixed" and "diffusion" burning. The two mechanisms were assumed to begin at the ignition point and to proceed concurrently for a small portion of the heat emission period during which the amount of fuel/air mixture prepared prior to ignition was exhausted. Following this point, burning was considered to progress in accordance with a rate stipulated solely by diffusion burning.

Accordingly, the instantaneous rate of burning was expressed mathematically as the sum of two components:

$$\frac{dM_{f,t}}{d\theta} = \frac{dM_{f,p}}{d\theta} + \frac{dM_{f,d}}{d\theta} \qquad (6.8)$$

where: $\frac{dM_f}{d\theta}$ = fuel mass burning rate with respect to crank angle,

$\theta$ = crank angle,

$t, p, d$ = total, premixed and diffusion respectively.

In order to quantify the share of fuel burned by either mechanism, a mode of burning proportionality factor (MBPF) was introduced. This expressed the cumulative fuel consumed by premixed burning as a fraction of the total amount of fuel injected per cycle ($M_{f,t}$):

$$\beta = \frac{M_{f,p}}{M_{f,t}} \qquad (6.9)$$

where: $M_{f,t} = M_{f,p} + M_{f,d}$ (6.10)

Consequently, a non-dimensional form of fuel burning rate was obtained using equations (6.8) to (6.10):

$$FBR_t(\tau) = \beta.FBR_p(\tau) + (1-\beta).FBR_d(\tau) \quad (6.11)$$

where: $FBR(\tau)$ is the non-dimensional burning rate distribution, $FBR_k(\tau) = \dfrac{\frac{dM_{f,k}}{d\theta}(\tau).(\theta_e-\theta_i)}{M_{f,k}}$; k = t,p or d.

$\theta_i, \theta_e$ = crank position at ignition and end of burning.

$\tau$ = normalised crank position; $\tau = \dfrac{\theta - \theta_i}{\theta_e - \theta_i}$.

In doing so, the rate of burning was expressed as the sum of two component dimensionless distributions, weighted by the MBPF (Fig. 6.1). This weighting factor (the proportion of total fuel per cycle burned after being premixed) was considered to be mainly controlled by the length of the ignition delay period and the trapped equivalence ratio (i.e. the overall equivalence ratio of charge at the end of combustion).

The relationship between the fuel burning rate and the resultant heat release rate was based on the assumption that thermodynamic and chemical equilibrium existed. All the fuel injected into the cylinder was assumed to react (not necessarily completely), irrespective of the equivalence ratio. For lean mixtures ($F<1$), and in the absence of dissociation effects, the two rates were directly proportional. In the case of richer fuel mixtures, this linear relationship was considered to hold until either dissociation started or the charge equivalence ratio exceeded unity. Beyond the stoichiometric fuel/air ratio, any increase in the amount of reacting fuel would lead to a reduction in the

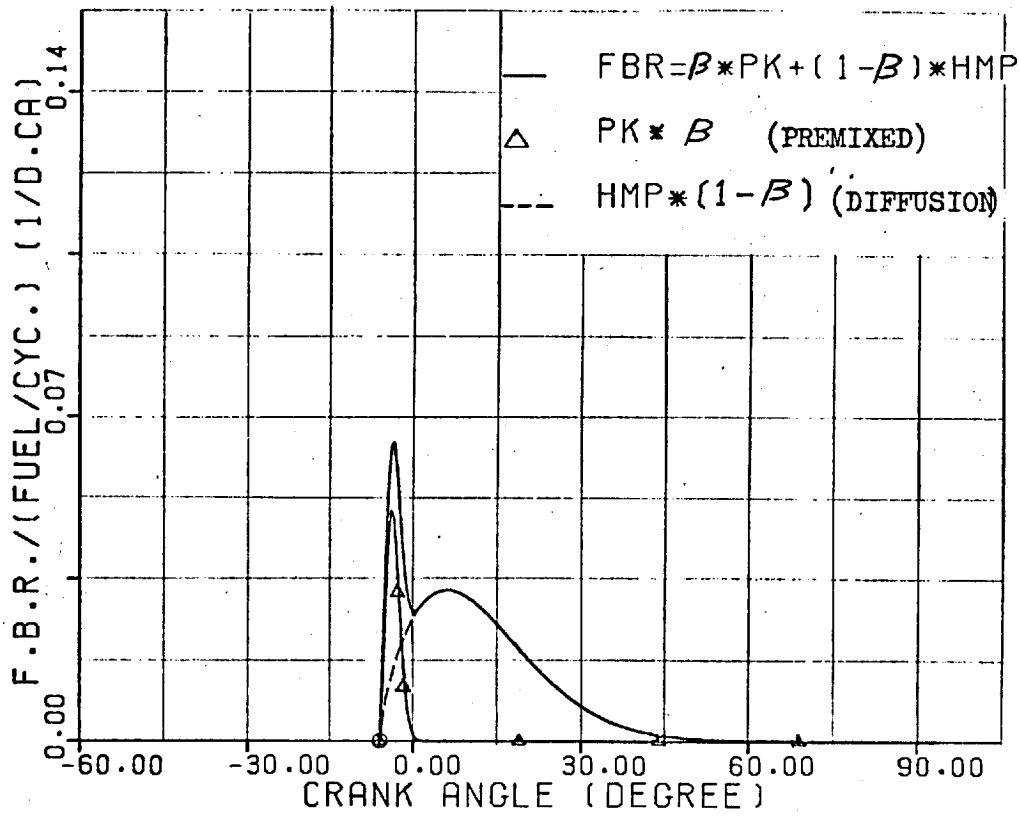


FIG.(6.1) Fuel Burning Rate Distribution.

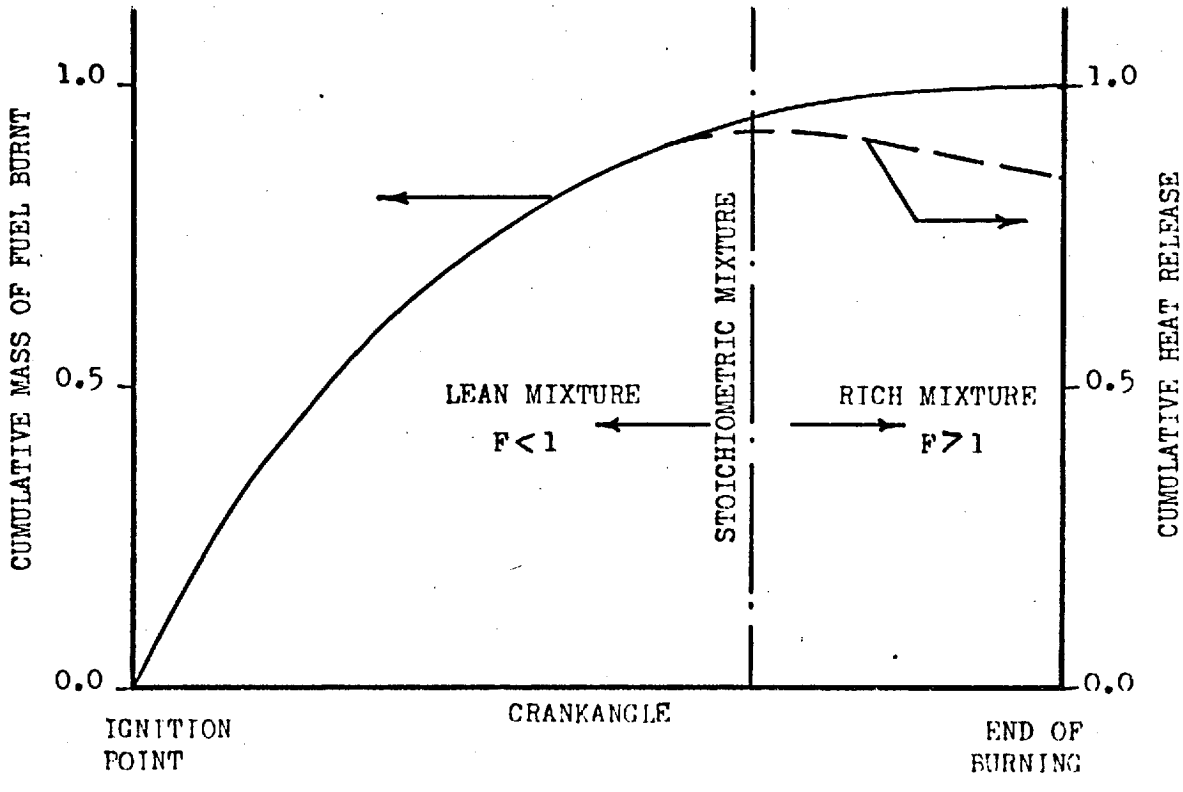


FIG.(6.2) Cumulative Mass of Fuel Burnt and Heat Release.

cumulative heat release (Fig. 6.2). Dissociation affects the above-mentioned relationship in regions of high temperatures, low pressures, and when the equivalence ratio is close to unity, i.e. stoichiometric conditions.

The variation of absolute internal energy and gas constant for combustion products of diesel fuel are shown diagrammatically in Appendix A . The sudden alteration in the rates of change of the two variables with respect to equivalence ratio (occurring around F = 1) explains the change in the relationship between the mass of fuel burned and the resultant heat release. Furthermore, it can be seen that the application of the concept of absolute internal energy (Section 2.2) is most useful in simplifying the problem.

The shapes of the component burning rate distributions were selected in the light of the actual burning rate curves (Section 6.5). The objective was to achieve a reliable correlation between the important characteristics of the total rate of burning pattern and the engine operating parameters. Subsequently, extensive trials were carried out employing different mathematical expressions. The best representation of the experimental curves was achieved using the following two functions:

$$FBR_p(\tau) = cp1.cp2.\tau^{cp1-1}.(1-\tau^{cp1})^{cp2-1} \qquad (6.12)$$

$$FBR_d(\tau) = cd1.cd2.\tau^{cd2-1}.\exp(-cd1\tau^{cd2}) \qquad (6.13)$$

where: cp1, cp2, cd1 and cd2 are shape factors.

With large values of cp2, the first function (equation (6.12)) is capable of producing very steep rates of rise and decay which result in a sharp peak similar to that

brought about by actual premixed burning. In addition to the possibility of controlling the timing of the peak via cpl, the area under the first distribution (equation 6.12) is, as required, equal to unity:

$$\int_0^1 FBR_p(\tau) = \left[1 - (1 - \tau^{cpl})^{cp2}\right]_0^1 = 1 \qquad (6.14)$$

The characteristics of the Weibe function, which was selected to represent diffusion burning (equation 6.13), were discussed in Section 6.2.1.

It is appropriate to mention that the formulation of the combustion model, as given by equations (6.11) to (6.13), provided a high degree of flexibility. Burning rate curves varying between the two extremes of zero and 100% premixed combustion could be represented by simply altering the value of $\beta$. Furthermore, changes in burning rate with engine running conditions could be described by correlating the constants $\beta$, cpl, cp2, cd1 and cd2 with engine operating parameters.

The following section presents an analysis of the steady state experimental combustion data with the objective of evaluating the model constants and correlating them with the engine operating parameters.

## 6.5 ANALYSIS AND CORRELATION OF EXPERIMENTAL DATA

The basic combustion data considered here was obtained through processing steady state engine measurements (described in Section 5.3). A Fortran program was written to compute the rates of fuel injection and burning from experimental records of fuel line pressure, needle lift and cylinder pressure. It also yielded a first derivative of the needle lift diagram to enable an accurate determination of the point of dynamic injection.

Fuel burning rates were computed from smoothed cylinder pressure diagrams according to the Krieger-Borman method (64), which was described in Section 6.3.3. The smoothing and numerical differentiation of the pressure diagrams was carried out by a spline function subroutine which was adapted from an original version used by Streit (98). The degree of smoothing was varied with crank angle according to the recorded standard deviation of the cylinder pressure curve.

By processing all the experimental data obtained, a reliable set of 21 burning rate diagrams was established. This gave a complete picture of the variations in the combustion process over the entire engine operating range (the operating points chosen covered speeds from 1000 to 2500 rev./min. and loads from zero to 11.27 bar bmep). A typical set of the results, as obtained at each running condition, is shown diagrammatically in Fig. 6.3.

### 6.5.1 Ignition delay

The ignition delay data is presented graphically in Fig. 6.4. The length of the delay period (ms) together with the arithmetic mean values of the charge pressure (measured) and temperature (computed), during the delay, are plotted versus bmep for different engine speeds. Clearly delay reduces with increased pressure and temperature.

Since the requirement was an ignition delay correlation for prediction applications (to be used in an engine simulation program), it was decided to take the starting point of the burning rate diagram as an indication of the ignition point. Other definitions of the ignition point (40,89,24) were unsuitable since they are based on

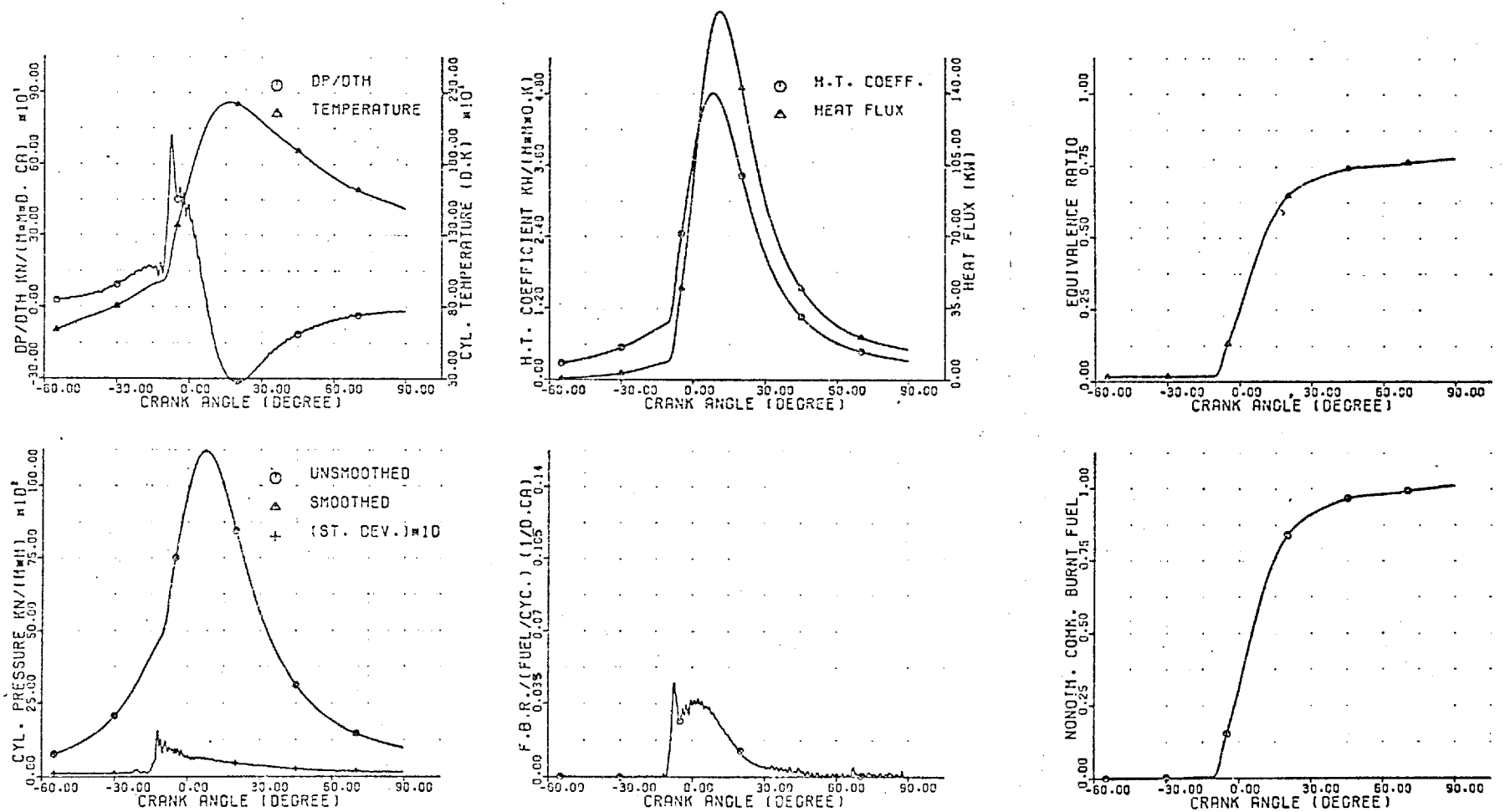


FIG.(6.3) Typical Results from a Burning Rate Computation.

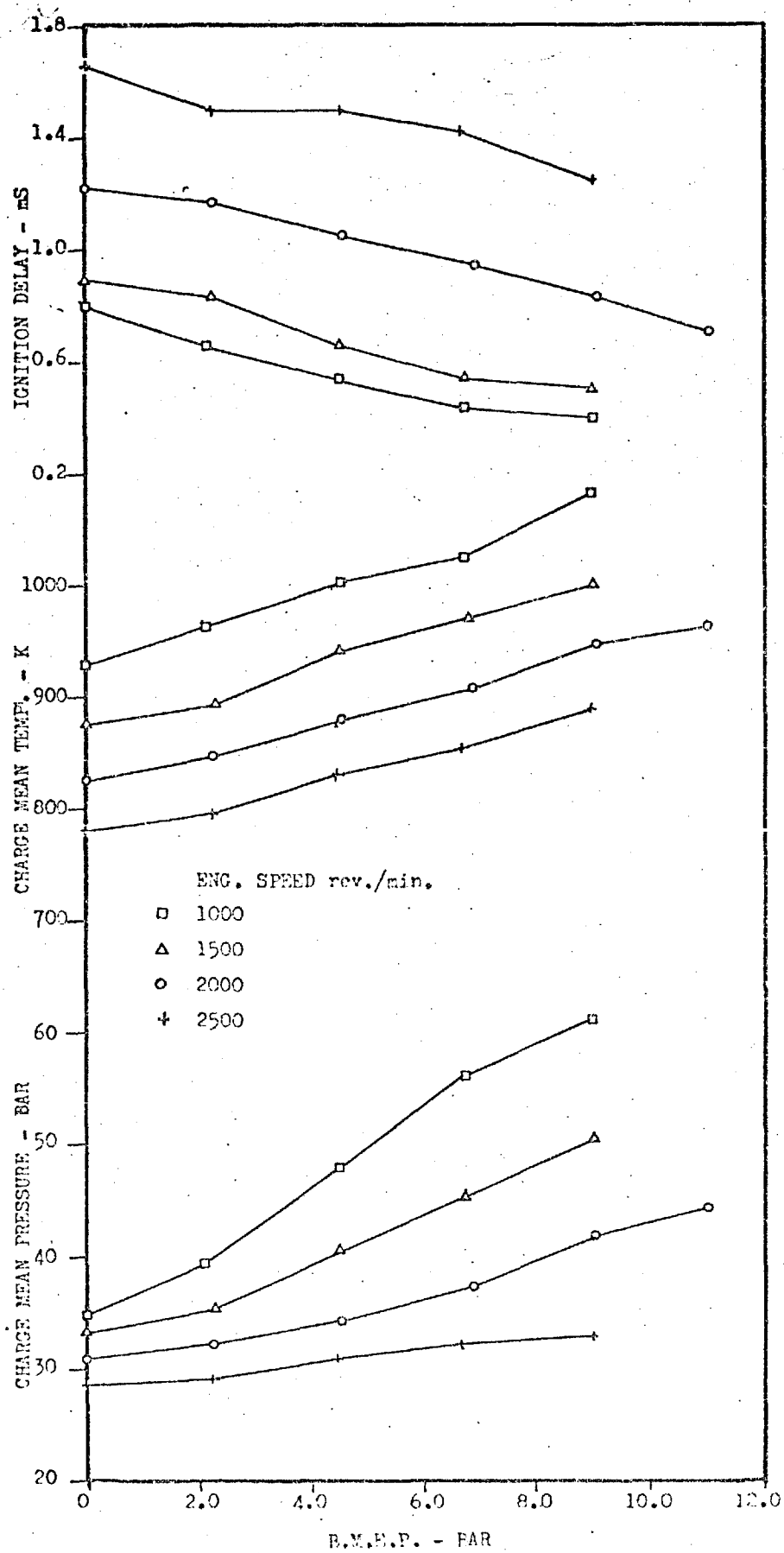


FIG.(6.4) Ignition Delay, Mean Temperature and Pressure of Charge as Function of BMEP and Engine Speed.

either flame visibility, reaction temperature, or changes in the shape of the pressure diagram. The dynamic injection point, which initiates the ignition delay period, was considered to be the moment when the injector needle started to rise. This was determined via the first derivative of the needle lift diagram (56).

Correlations developed by several researchers, Table 6.1, were checked against experimental data. In Fig. 6.5, Ilmari's formula (56) shows significant deviation as it was based on a swirl chamber type engine, in which the swirl rate and fuel impingement were relatively high. The overestimation shown by Sitkei's (93) representation, Fig. 6.5, appears to be partly due to the constant value of 0.5 ms taken to represent physical delay. Wolfer (121), Schmidt (89) and Zimmerman (129) used the same basic formula to represent bomb test data and reported different values for the coefficients. Fairly close agreement is obtained by Wolfer's formula with the exception of some overestimation at low speed conditions, Fig. 6.5. Lyn (72) suggests that overestimation is due to the fact that bomb tests are carried out at relatively low temperature. He reported that the effects of air velocity on the fuel evaporation rate become noticeable at lower compression temperatures. Hence, at low temperatures, the low air velocity in the bomb results in a longer delay than would be normal in an engine.

By fitting the Wolfer type of formula to the experimental data, a better representation was achieved, as shown in Fig. 6.5. Ignition delay was found to be best described by:

$$ID = 3.52 \frac{EXP(2100.8/T)}{p^{1.0218}} \text{ ms} \qquad (6.15)$$

| Investigator | Correlation | Notation and Units |
|---|---|---|
| Ilmari (57) | $I.D. = \frac{0.156}{p^{\frac{1}{3}}} \times 10^{8} \left(\frac{T}{10000}\right)^{11} \cdot Exp\left(\frac{10000}{T}\right)$ | I.D. = ignition delay; ms. |
| Sitkei (93) | $I.D. = 0.5 + \frac{0.133}{p^{0.7}} Exp\left(\frac{375648}{RT}\right) + \frac{4.63}{p^{1.8}} Exp\left(\frac{37564.8}{RT}\right)$ | T = mean temperature; $^{o}K$. |
| Schmidt (89) | $I.D. = \frac{0.0646}{p^{1.08}} Exp\left(\frac{6330}{T}\right)$ | P = mean pressure; bar. |
| Wolfer (121) | $I.D. = \frac{0.429}{p^{1.19}} Exp\left(\frac{4650}{T}\right)$ | $T_*, P_*$ = temperature and pressure at start of injection. |
| Zimmerman (129) | $I.D. = \frac{0.392}{p^{1.05}} Exp\left(\frac{4650}{T}\right)$ | |
| Tsao (103) | $I.D. = \left(\frac{8.48}{P_*} + 0.415\right)\left[\left(-\frac{20.17}{T_*} + 0.0222\right)N + \left(\frac{26361.1}{T_*} - 26.66\right) + \left(0.0018T_* - 1.45\right)\left(\frac{1000-N}{60}\right)\right]$ | R = universal gas constant = 8.314 KJ/kmole $^{o}K$. N = engine speed; rev./min. |

TABLE 6.1

A Number of Published Ignition Delay Correlations

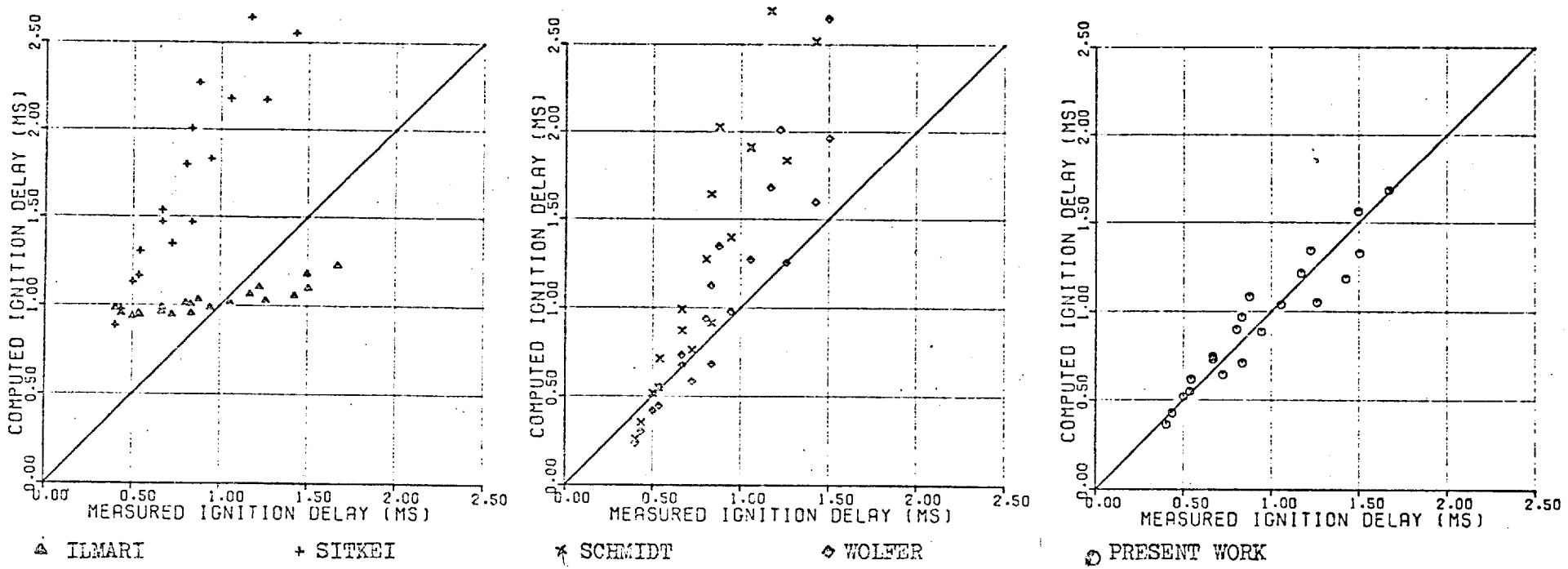


FIG.(6.5) Comparison of Ignition Delay Formulae with Aid of Experimental Data.

6.5.2 Burning rate

The resulting experimental fuel burning rate curves are presented in Figs. 6.6(a) and (b), in the form of normalised rates versus crank angle, at five engine loads and four speeds (covering the whole operating range of the engine).

The following observations can be made:

1. Burning appears to proceed in two distinct patterns, supporting the discussion of Section 6.4.

2. The initial peak appears to increase with reduced load and/or speed, suggesting a relationship with ignition delay and equivalence ratio.

3. Burning duration appears to increase with BMEP at a constant engine speed.

4. Determination of the ignition point is relatively simple but an exact definition of the crank position at which burning ceases is not possible in most cases, particularly at high load. This is due to the almost asymptotic shape of the curve towards the end of burning in addition to the ripples superimposed.

To quantify these trends, the coefficients in equation (6.11) were evaluated for each of the above curves, using non-linear curve fitting techniques. A special minimization computer program (79) was used after being specifically adapted for this application. Input data consisted of initial estimates of the coefficients (representing a hypothetical minimum sum of deviations) in addition to the experimental burning rate curves in numerical form. The program then proceeded to improve the fit by modifying

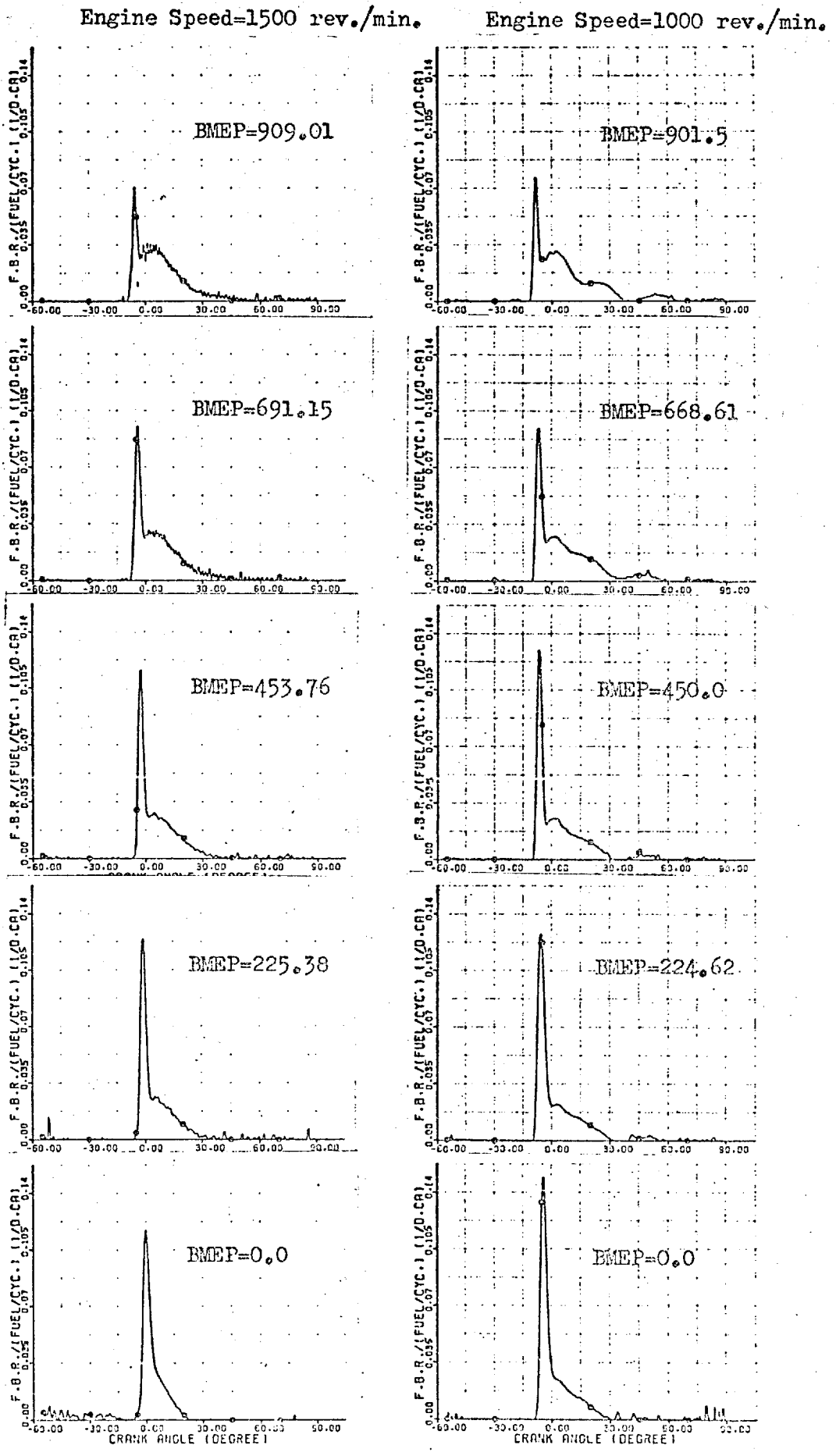


FIG.(6.6,a) Experimental Fuel Burning Rate Curves.

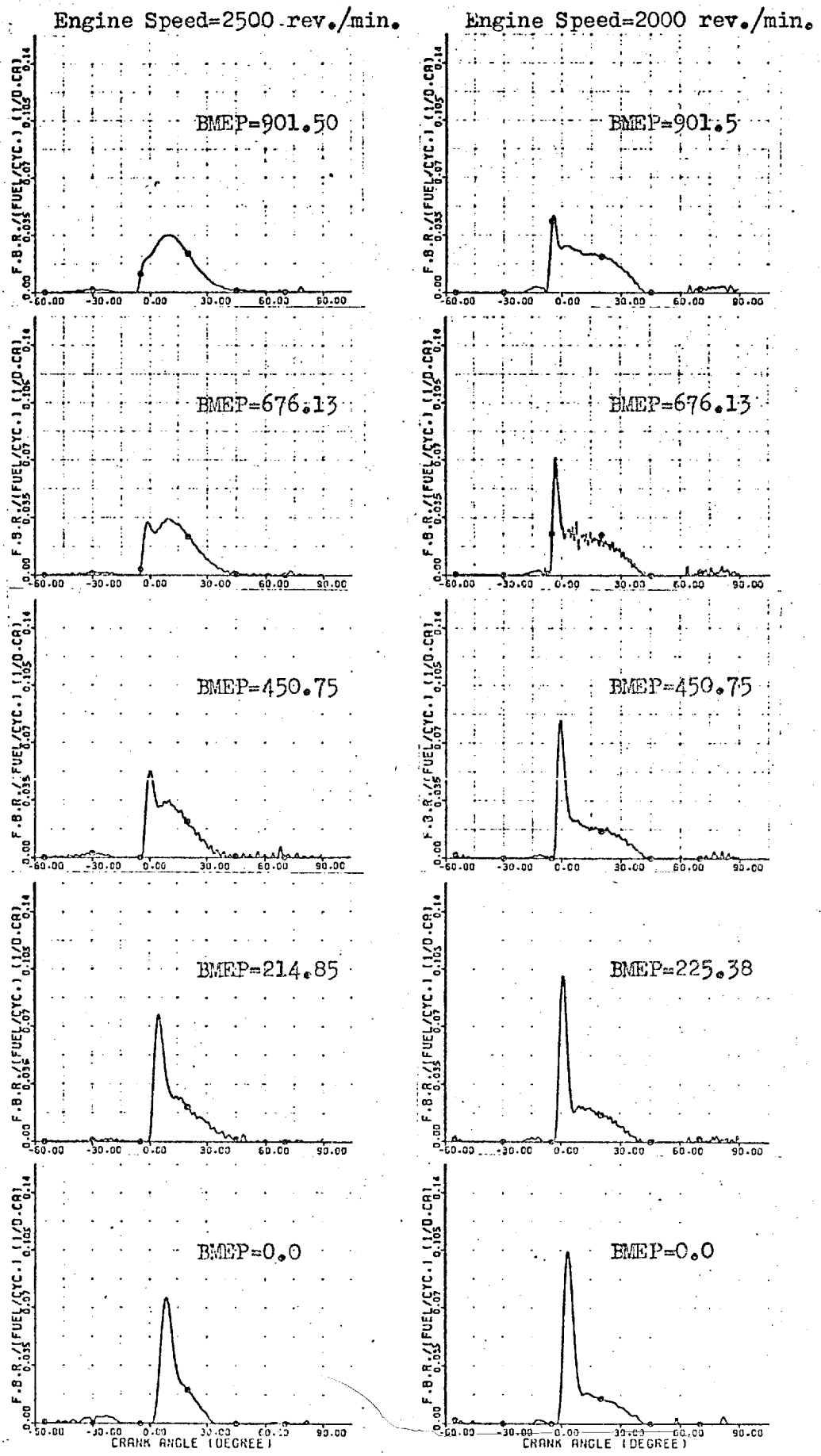


FIG.(6.6,b) Experimental fuel Burning Rate Curves.

values of the coefficients in an iterative manner, according to the algorithm developed by Powell (87).

It was decided to allow the actual burning duration to be determined by the values of coefficients obtained by curve fitting. Thus a relatively long nominal duration of $125^{o}$ (starting from ignition and covering most of the expansion stroke) was used as a datum. This was essential to enable crank angle (or time) to be non-dimensionalised.

Experiment showed that the representation of the initial peak improved with high values of cp2 (in equation 6.12), up to a limit of cp2 = 5000, with marginal benefit thereafter. The value of coefficient cp2 was then fixed, and the curve fitting process repeated to obtain the mode of burning proportionality factor $\beta$ and the remaining coefficients cp1, cd1 and cd2.

By cross-plotting the resulting values of the coefficients of the diffusion burning distribution cd1 and cd2, a clear dependence was observed, Fig. 6.7. This was represented by the following relationship:

$$cd2 = 0.791(cd1)^{0.2477} \qquad (6.16)$$

It followed that the development of the burning rate pattern across the engine operating range was now controlled by only three parameters. These were the mode of burning proportionality factor and one shape factor for each of the two modes, i.e. cp1 and cd1.

The variation of the MBPF with load and engine speed is presented graphically in Fig. 6.8. A clear trend of decrease in the proportion of premixed burning with increase in load and speed may be seen to exist. This was later considered in conjunction with the variation of trapped

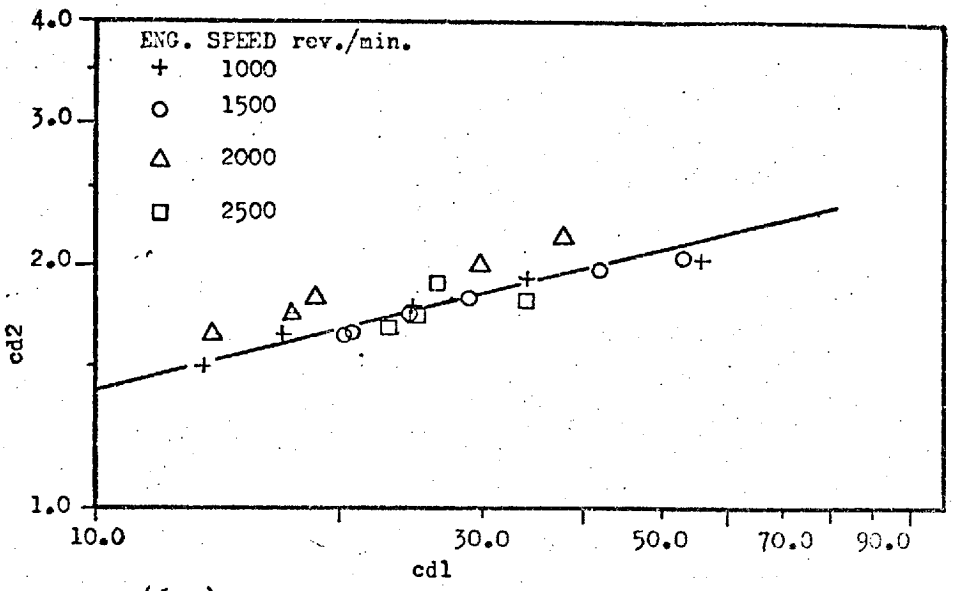


FIG.(6.7) Interdependence of the Coefficients of the Diffusion Burning Rate Distribution.

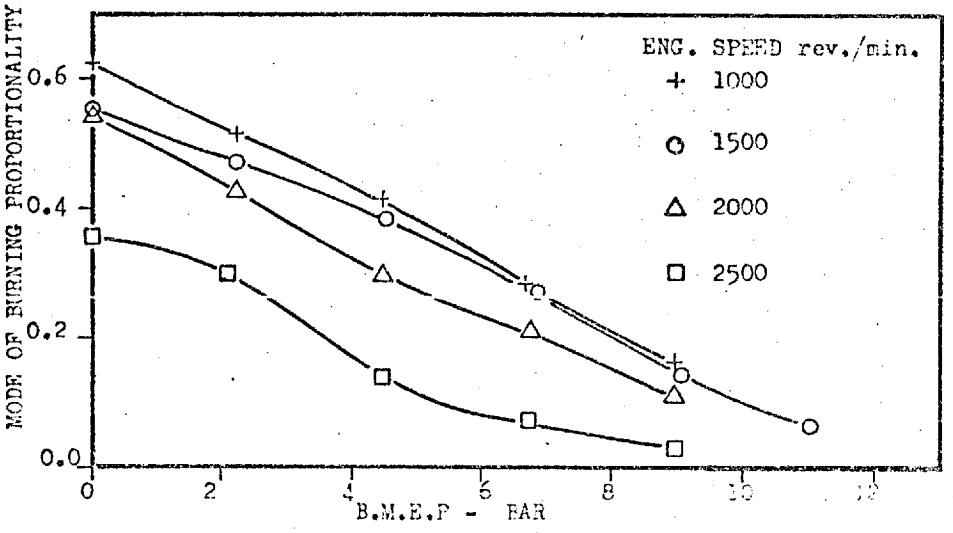


FIG.(6.8) Variation of MBPF with BMEP and Engine Speed.

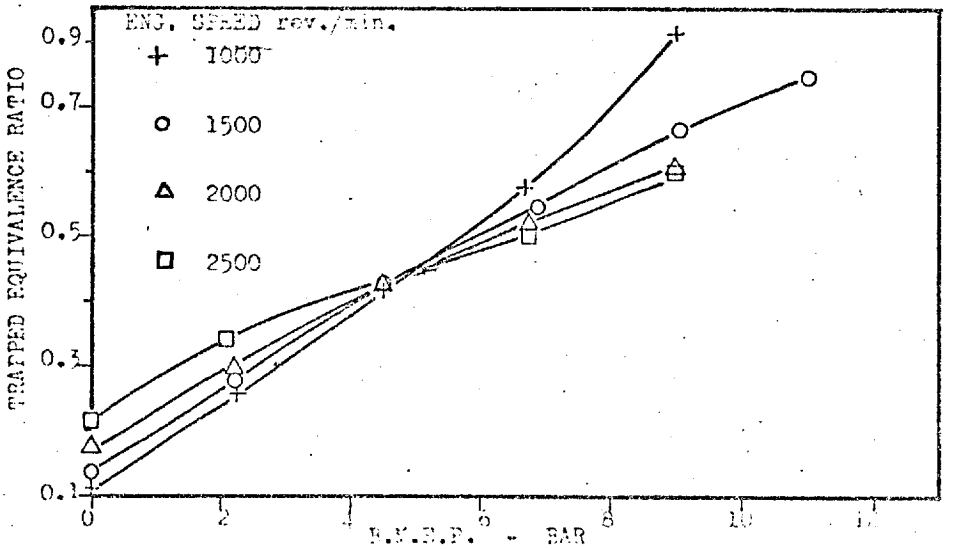


FIG.(6.9) Variation of Trapped Equivalence Ratio with BMEP and Engine Speed.

equivalence ratio and ignition delay, as depicted in Figs. 6.9 and 6.4 respectively. In doing so, it was established that the MBPF decreased with reducing ignition delay and increasing equivalence ratio (as was suggested earlier in Section 6.4). This relationship, Fig. 6.10, was determined by curve fitting:

$$\beta = 1.0 - 0.9259 \frac{F^{0.3708}}{I.D.^{0.2613}} \qquad (6.17)$$

The shape factors cp1 and cd1 were found to be best represented as follows:

$$cp1 = 2.0 + 1.25 \times 10^{-8}(I.D. \times \Omega_e)^{2.4} \qquad (6.18)$$

$$cd1 = \frac{14.2}{F^{0.644}} \qquad (6.19)$$

The first correlation, Fig. 6.11, indicates that in the case of premixed burning, the position of the peak retards in relation to the ignition point with increases in ignition delay and/or speed. This seems to indicate that the resultant increase in the amount of combustible mixture prepared during ignition delay lengthens the duration of premixed burning. On the other hand, equation (6.19), depicted graphically in Fig. 6.12, shows the diffusion burning coefficient cd1 to decrease with increase in equivalence ratio. This can be seen to provide a means of relating the actual duration of combustion to equivalence ratio; richer fuel-air mixture results in longer burning durations. An attempt has been made to relate cd1 to other relevant parameters such as engine speed and density ratio; however, scatter in the data prevented the identification of any positive trends. Fortunately this had very little effect on the accuracy of the predictions made by the correlations.

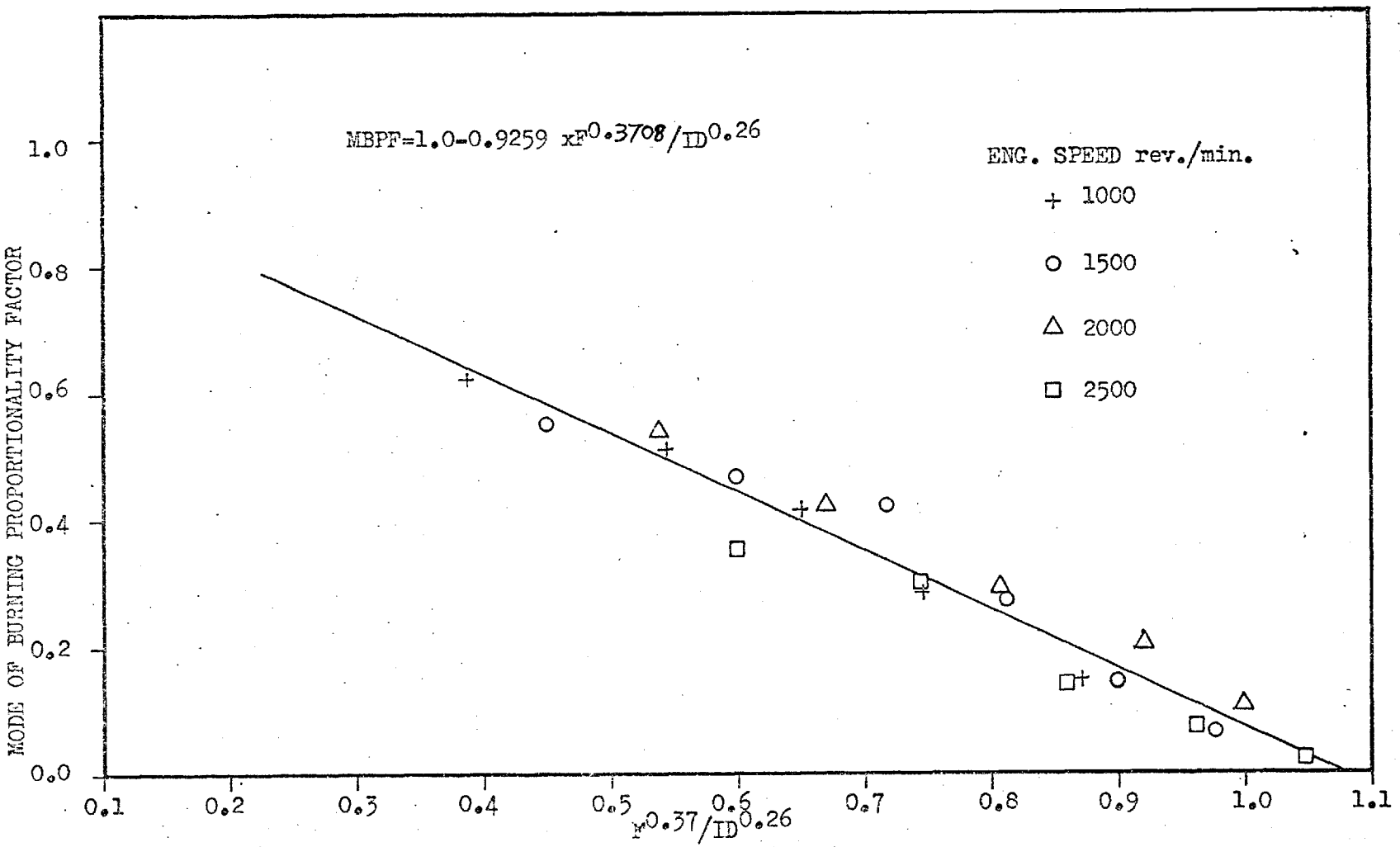


FIG.(6.10) Mode of Burning Proportionality Factor (MBPF) as a function of Ignition Delay and Trapped Equivalence Ratio.

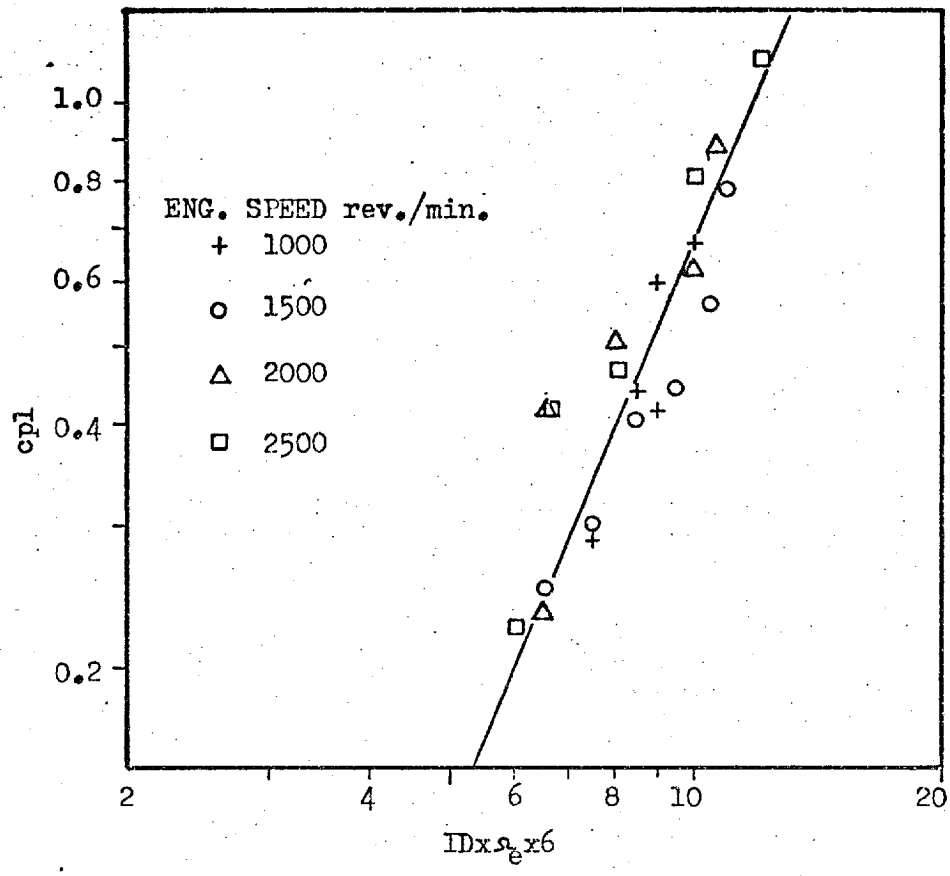


FIG.(6.11) cpl as a Function of Igniton Delay and Engine Speed.

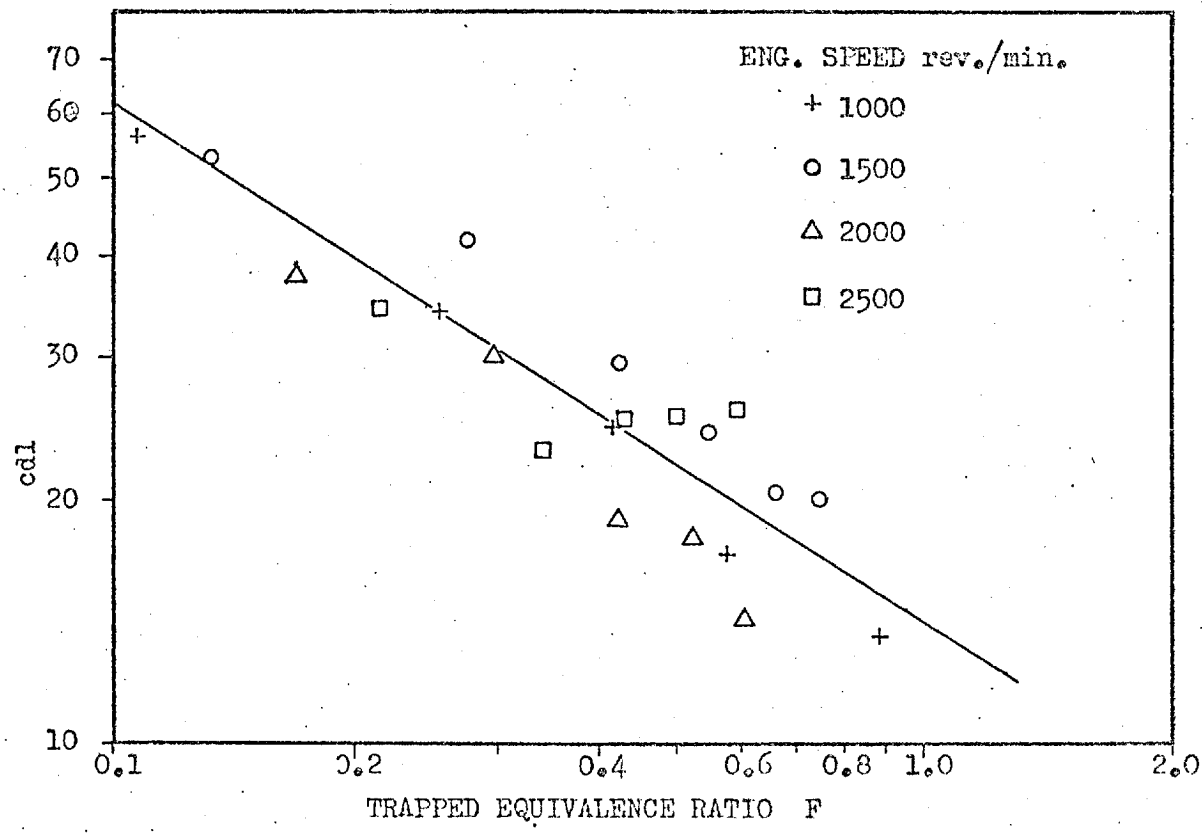


FIG.(6.12) Variation of cdl with equivalence Ratio

Figs. 6.13(a) and (b) display predicted and actual burning rate curves at 20 different running conditions. The comparisons show a favourable agreement over the entire operating range of the engine.

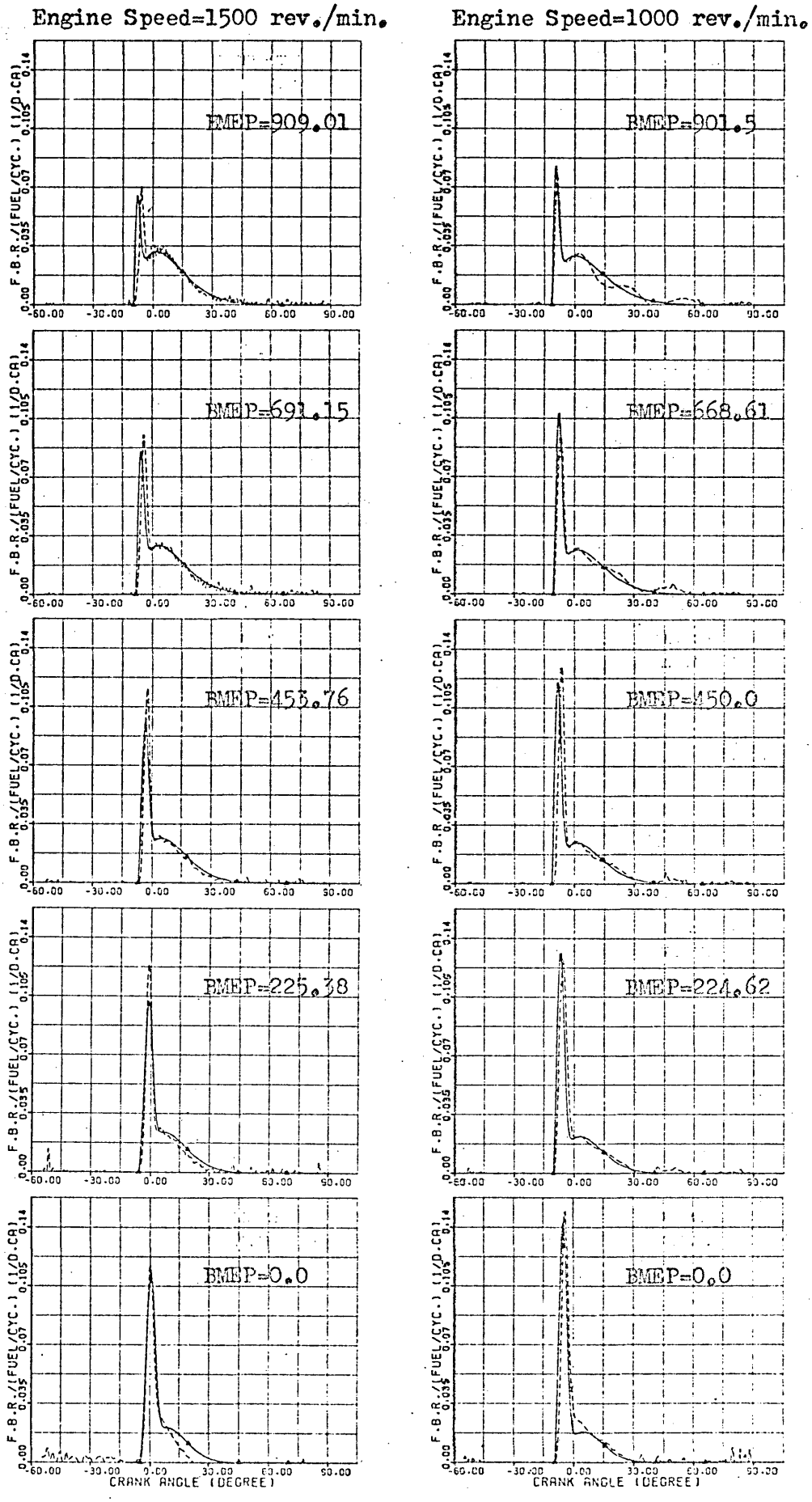


FIG.(6.13,a) Comparison of Predicted and Experimental Fuel Burning Rate Curves.

Predicted ___ Experimental___

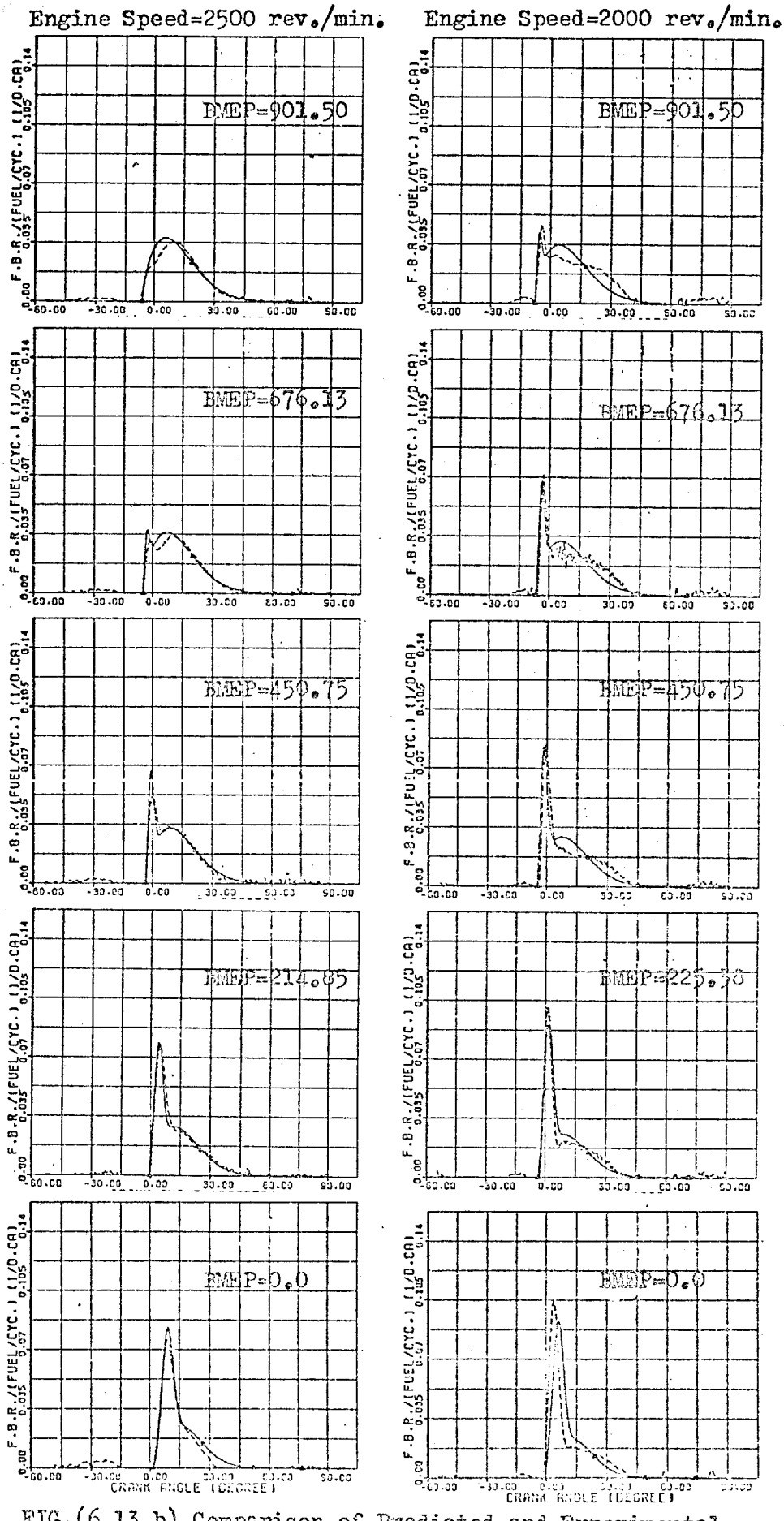


FIG.(6.13,b) Comparison of Predicted and Experimental Fuel Burning Rate Curves.

Predicted ——  Expermental - - -

# CHAPTER 7

# EVALUATION OF SIMULATION RESULTS

## 7.1 INTRODUCTION

Any mathematical simulation of an actual system must be representative of the major processes involved and should be evaluated according to the accuracy with which it reproduces the behaviour of the system. This chapter demonstrates the validity of the simulation program developed via comparisons between predicted and measured data. The usefulness of the program in studying the effects of various design parameters on the transient performance of the engine, and in understanding the interactions between the engine and turbocharger is also discussed. This is of particular interest to engine manufacturers, as large savings in time and cost can be achieved if such a simulation program were to be employed early in the design stage.

The work reported here is basically divided into three parts, namely:

1. Evaluation of the steady state predictions with the aid of experimental data.

2. Validation of the predictions of engine transient response against measured data.

3. Parametric studies to demonstrate the capabilities of the model in ascertaining the effect of various design changes on the engine's transient performance.

## 7.2 EVALUATION OF STEADY STATE PREDICTIONS WITH THE AID OF EXPERIMENTAL MEASUREMENTS

An extensive series of program runs has been carried out in order to assess the ability of the simulation to predict the steady state performance of a turbocharged diesel engine. Initially 22 runs were executed to compute performance data at those running conditions at which experimental measurements had been taken. These covered a range of engine tests from 1000-2500 rev./min. and zero to full load (11.27 bar bmep). The experimental data obtained for comparison with the predictions is described in detail in Chapter 5.

In these tests the simulation program was run in the steady state mode, in which the models for the engine-load dynamics, governor and fuel injection system were disabled. At each running condition, the measured engine speed and fuelling rate (amount of fuel injected/cylinder/cycle) were entered as input data and were held constant. The program then proceeded to solve the thermo-gas dynamic equations in conjunction with the dynamics of the turbo-charger until convergence was achieved. This normally took five engine cycles, after which detailed information of the engine steady state performance was printed out.

A typical set of predicted steady state data is shown in Fig. 7.1 a-c. Predicted crankangle histories of the cylinder pressure, exhaust pressure (in the manifold connected to the instrumented cylinder) and boost pressure are given in Fig. 7.1a for a complete cycle. The exhaust pressure exhibits three basic pulses (240$^{o}$CA apart) which are produced by the cyclic discharge of exhaust gases from the three cylinders connected to the same manifold. The

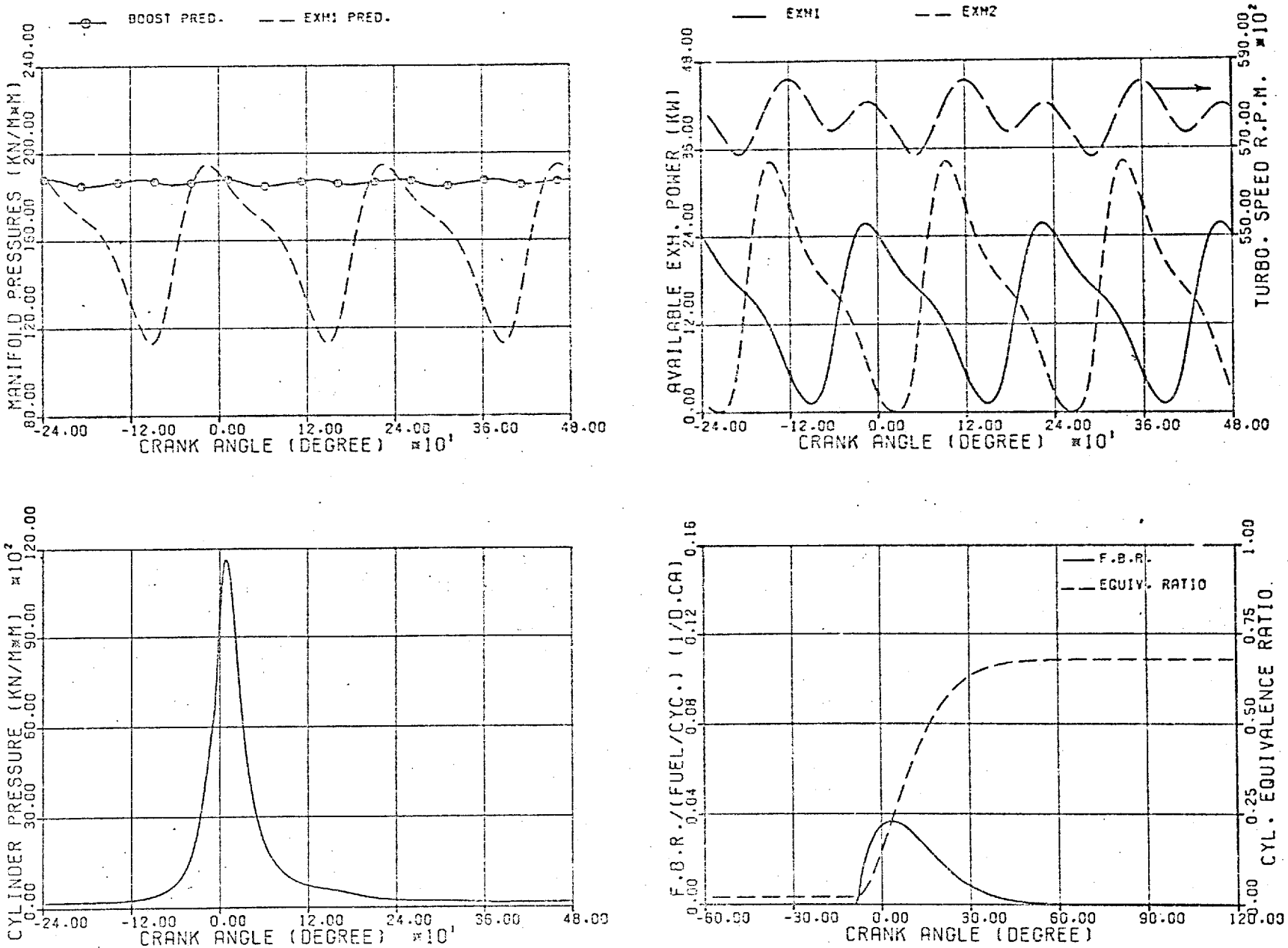


FIG. (7.1,a) Typical Predicted Steady State Data, Engine Speed = 2000 rev./min, BMEP = 11.0 BAR
Cylinder Pressure, Manifold Pressures, Fuel Burning Rate, Equivalence Ratio and Available Exhaust Power

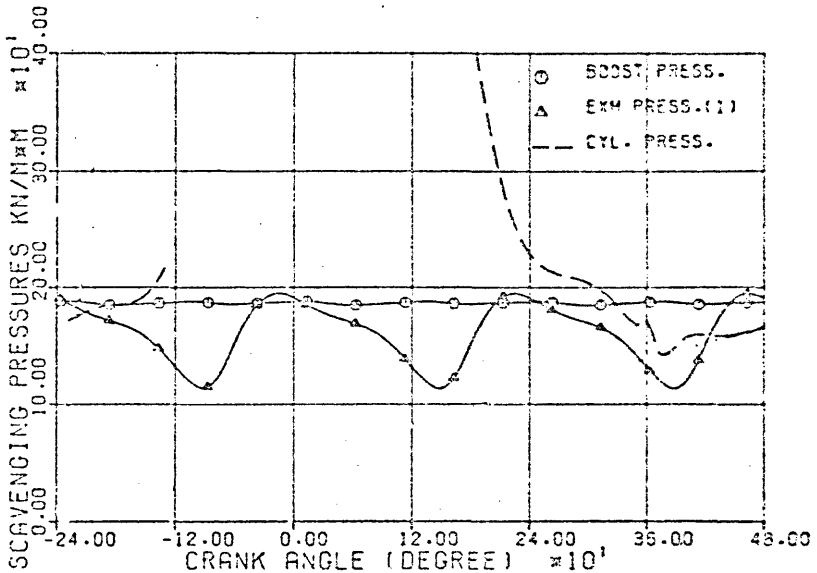


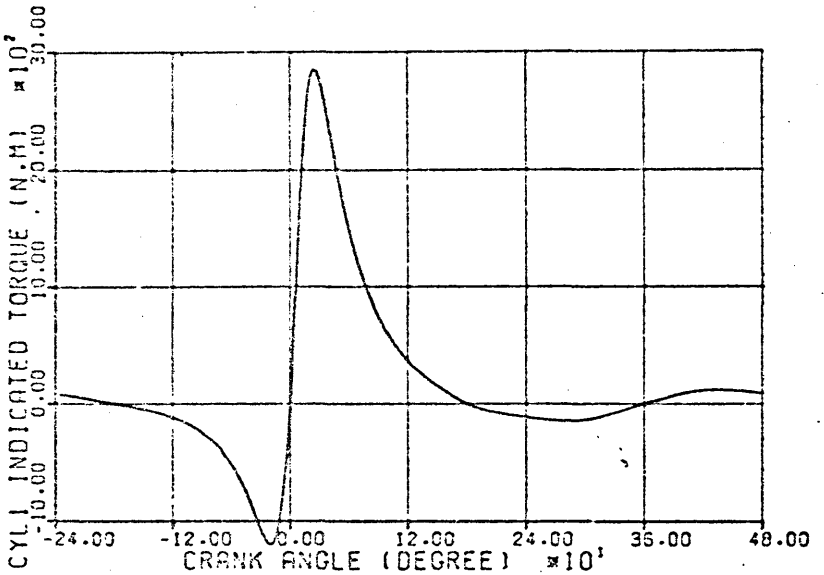


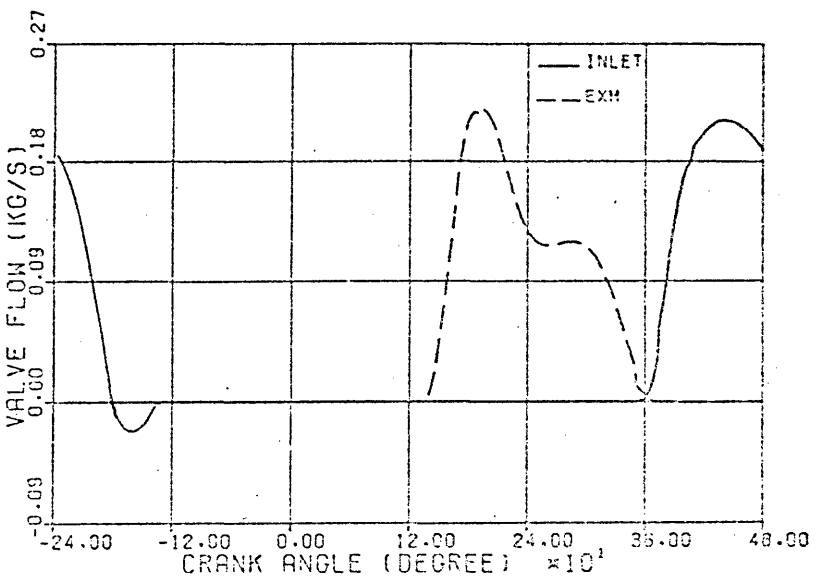


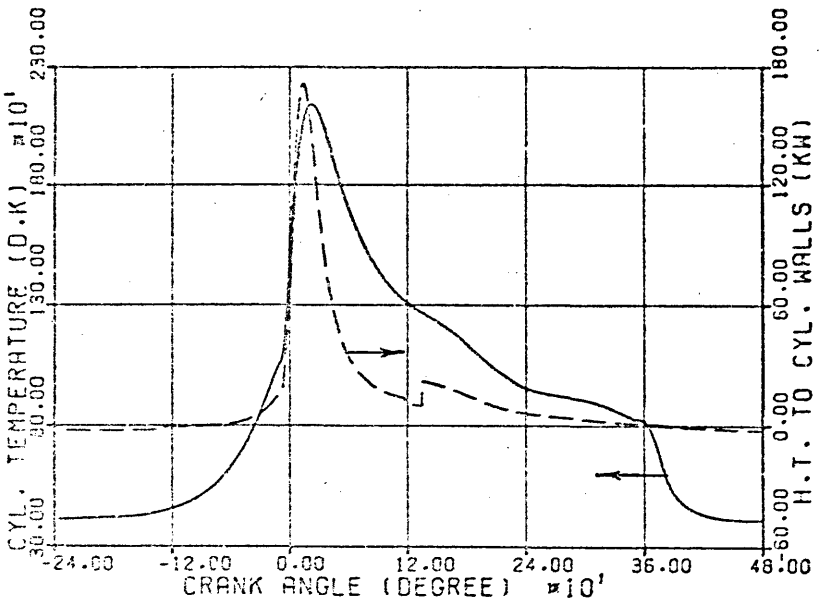


FIG. (7.1,b) Typical Predicted Steady State Data, Engine Speed = 2000 rev./min. BMEP = 11.0 BAR
Valve Flow, Scavenging Pressures, Cylinder Temperature, Heat Transfer Rate and Indicated Torque

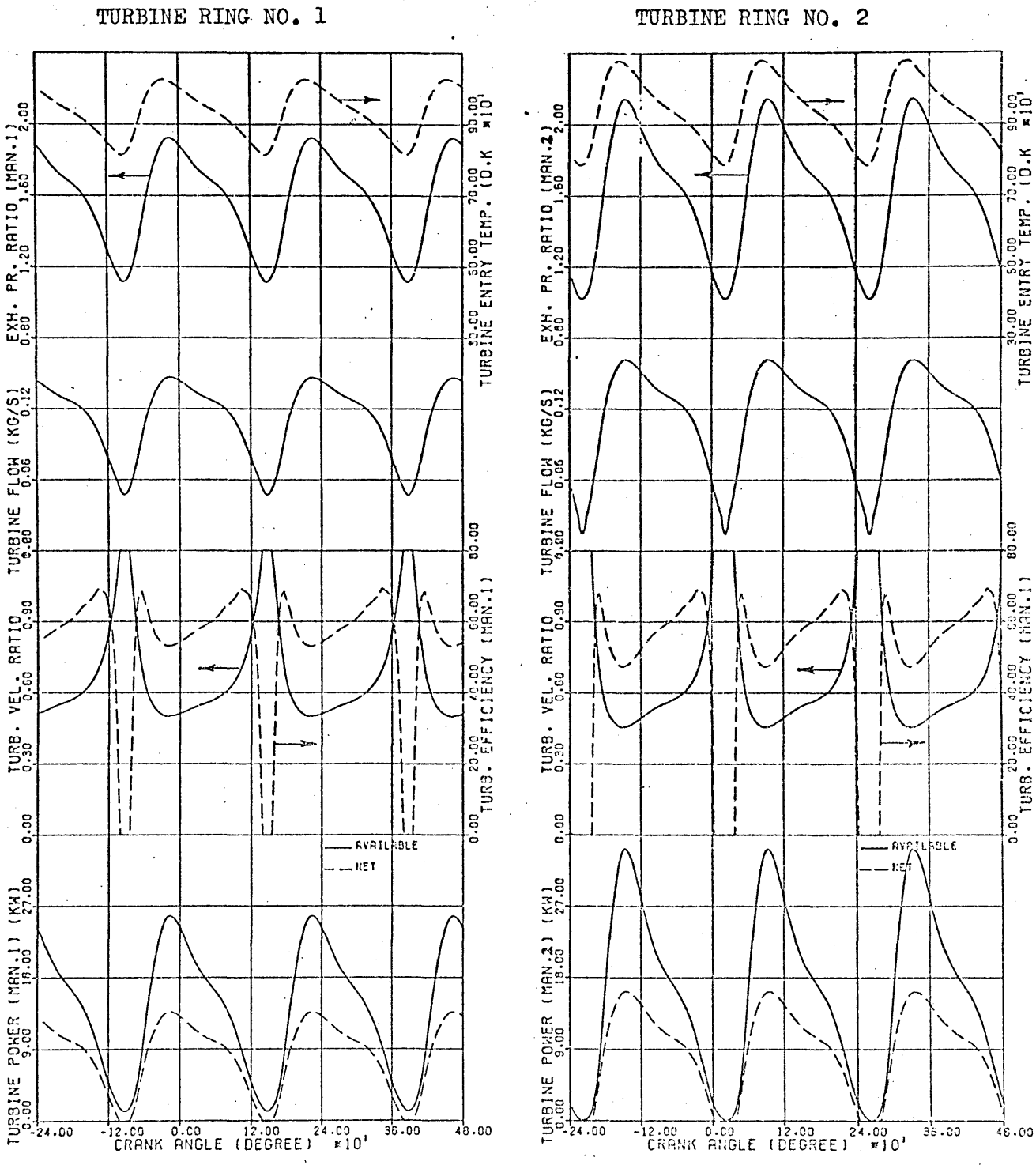


FIG. (7.1,c) Typical Predicted Steady State Data (Turbine Performance).
Engine Speed = 2000 rev./min, BMEP = 11.0 BAR

crankangle distributions of the available exhaust energy and turbine speed are presented. The smaller manifold, which collects gases from the three cylinders close to the turbine, exhibits power pulses of greater amplitude due to the larger fluctuation in pressure and temperature. The normalised fuel burning rate curve generated by the combustion model and the distribution of charge equivalence ratio is also plotted.

Fig. 7.1b shows crankangle distributions of cylinder and manifold pressures during the induction and exhaust strokes, gas flow rates through the valves, cylinder temperature, heat transfer rate to the cylinder walls and indicated torque for one cylinder. In this particular running condition, the flow of the gases through the exhaust valve exhibits an initially high peak which is followed by a duration of nearly constant flow. The inward flow of fresh air (through the inlet valve) shows a wider and lower peak with gradual rates of acceleration and deceleration. A short period of backflow is shown immediately before valve closure.

It can be seen that the effects of the different processes occurring inside the cylinder are clearly reflected on the shape of the temperature and heat flow distributions. The heat transfer rate shows a sharp rise following the increase in gas velocities at exhaust valve opening. The reversal of the direction of heat flow during the induction stroke (the charge is heated by the cylinder walls) is due to the negative temperature differential between the walls and incoming air. This limits the mass of air trapped at inlet valve closure.

Fig. 7.1c depicts the crankangle distributions of: exhaust temperature, turbine expansion ratio, turbine

velocity ratio and efficiency, plus the available and net turbine power. These are presented for the two turbine sectors along a complete engine cycle.

Comparisons between the computed and measured steady state performances of the engine are shown in Figs. 7.2 to 7.5. The variables compared include: indicated and brake mean effective pressures (imep and bmep), indicated and brake specific fuel consumptions (isfc and bsfc), fuel/air ratio, peak cylinder pressure, mean pressures and temperatures inside the induction and exhaust manifolds and turbocharger speed. Measured and computed quantities are plotted against fuelling rate for four engine speeds, namely: 1000, 1500, 2000 and 2500 rev./min.

In this representation, the fuelling rate was taken as the abscissa in preference to bmep for two reasons:

1) If the bmep was used, deviations between the computed and measured values would be seen in both the vertical and horizontal directions, thus complicating the analysis. Deviations in the horizontal direction are introduced by possible errors in the evaluation of engine friction.

2) During transient operation, the bmep developed by the engine cannot be considered as an independent variable as in the case of the fuelling rate.

It may be seen that despite considering the entire operational range of the engine, agreement between prediction and experiment is generally good. While small discrepancies exist between the predicted and experimental values, the effects of changes in the engine operating conditions are accurately represented in the predictions. Agreement between

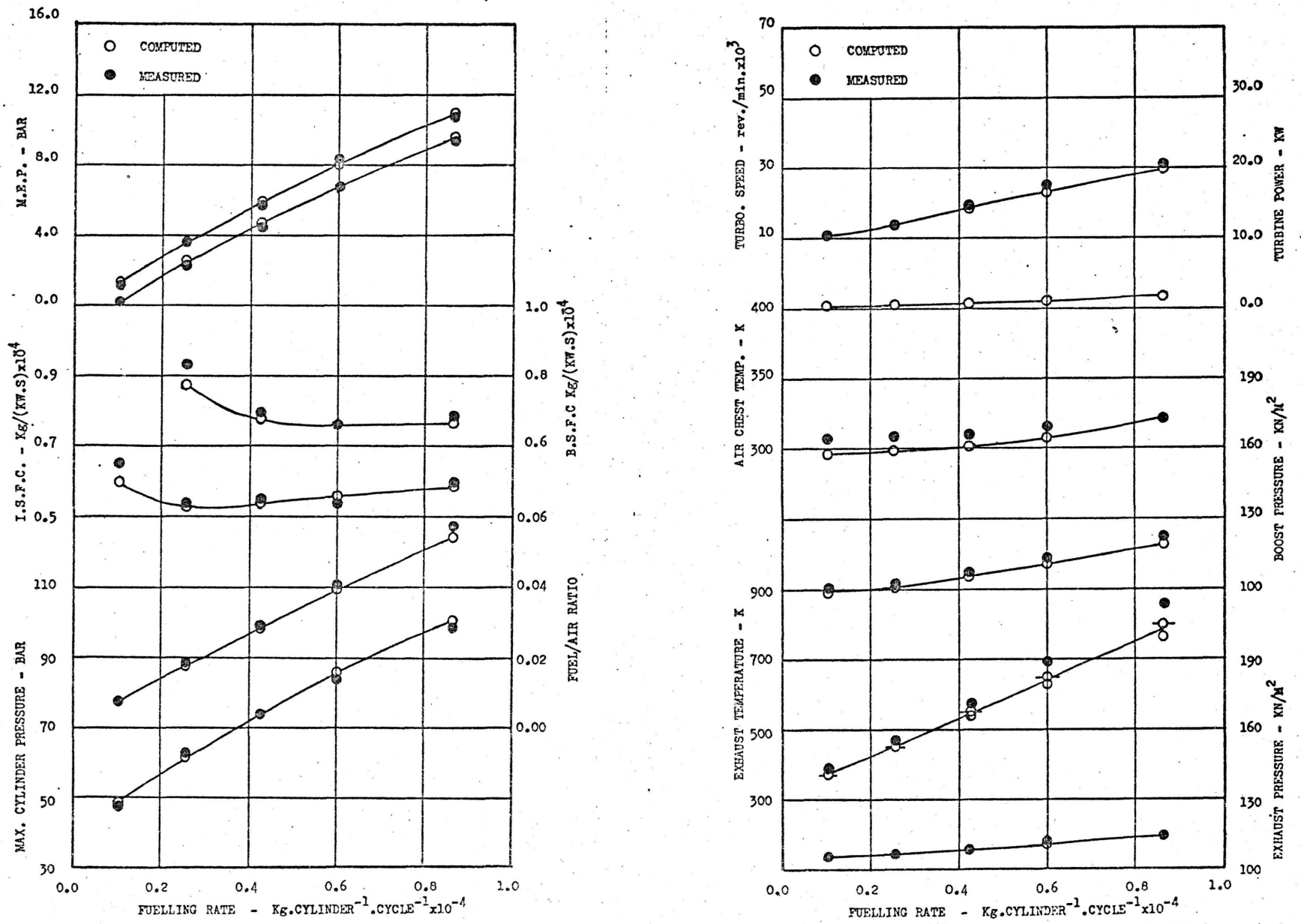


FIG. (7.2) Comparison of Experimental and Computed Steady State Data. Engine Speed = 1000 rev./min.

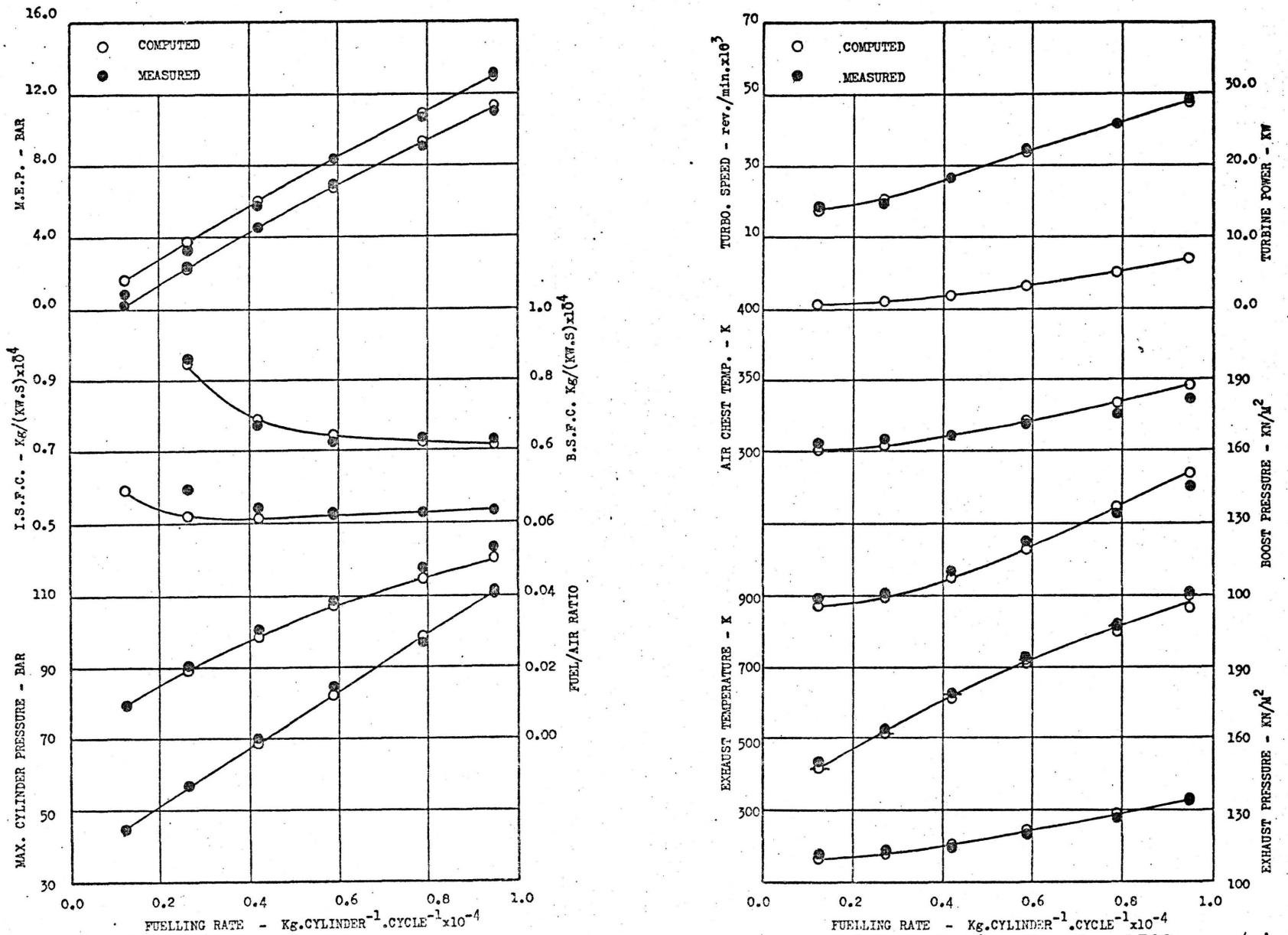


FIG. (7.3) Comparison of Experimental and Computed Steady State Data. Engine Speed = 1500 rev./min.

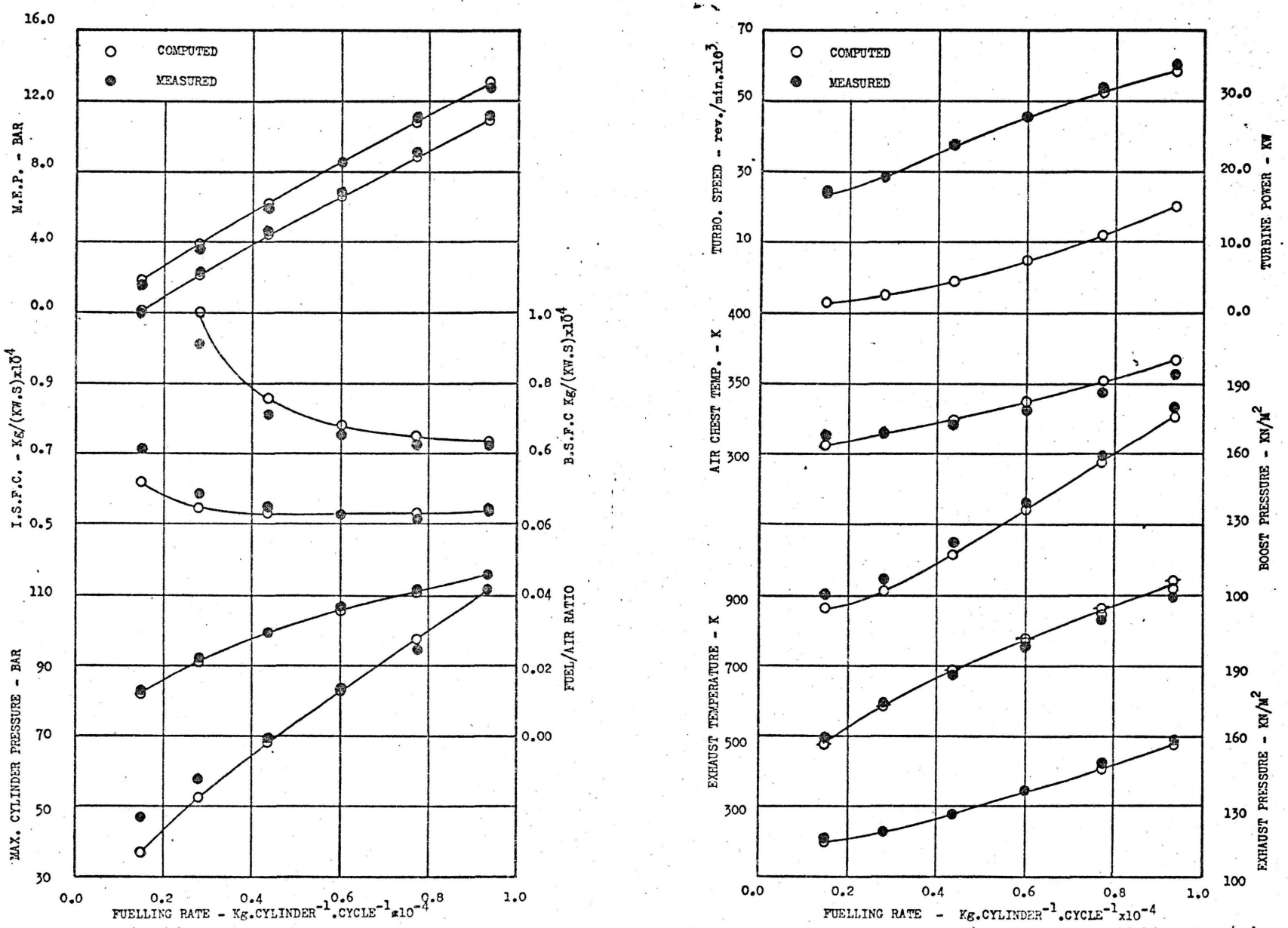


FIG. (7.4) Comparison of Experimental and Computed Steady State Data. Engine Speed = 2000 rev./min.

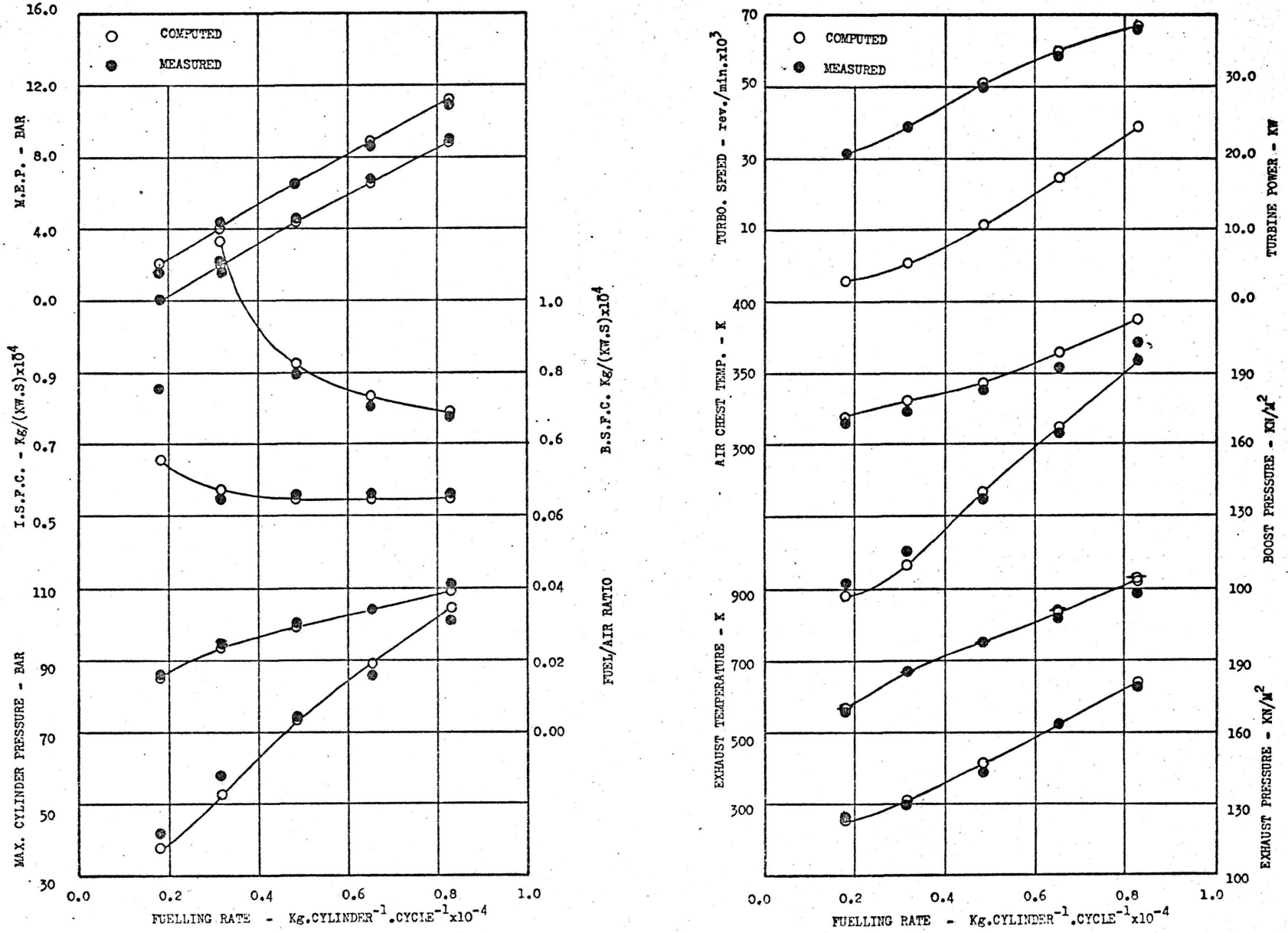


FIG. (7.5) Comparison of Experimental and Computed Steady State Data. Engine Speed = 2500 rev./min.

the computed and measured quantities can be seen to improve with increase in load; most of the deviations occurring at low loads (below 0.2 full load). This is understandable as the percentage errors in the measurement of most variables increase with reduction in load (fixed data logging resolution). Other errors are introduced at low loads due to fluctuation in engine speed and cyclic variations. Computational inaccuracies are also possible at such conditions due to the extension of the compressor and turbine performance characteristics to very low pressure ratios (data normally supplied by the turbocharger manufacturer does not cover this range ), plus errors in engine friction.

The general trend is predicted correctly for both the indicated and brake mean effective pressures at all speeds, with the latter showing closer agreement with experiment. The maximum deviation in imep is 5.3%, occurring at no load and an engine speed of 1500 rev./min. Obviously this accounts for the increased discrepancy in the isfc curve at the same running condition. At a constant speed, both the predicted and measured specific fuel consumption depict a reducing trend with increase in fuelling rate. This is due to the rise in the maximum pressures and temperatures inside the cylinders. Predictions of the isfc and bsfc are in good agreement with measurements at above 20% full load. The variation of the sfc with engine speed (at constant fuelling) is also predicted correctly.

The simulation results underestimate the fuel/air ratio by 0-5.3% due to overestimating air flow. This could be caused by inaccuracies introduced by one or more of the following factors: compressor flow characteristics, swallowing capacity of turbine, effective flow areas of

inlet and exhaust valves, systematic error in the measurement of air flow and the approximation of gas flow by a quasi-steady treatment. An overestimate of air flow could result in predicting a low exhaust temperature, e.g. at low engine speeds (1000 and 1500 rev./min.). However, the fact that predicted mean exhaust temperatures exceed the measured values, suggests that other factors must be considered.

The computed exhaust temperatures show two values at each running condition with a difference increasing with load. The higher and lower values are the mass and time-averaged temperatures respectively. Borman (21) indicated that the measured exhaust temperatures should be enclosed by the two predicted values. Measurements of exhaust gas temperatures (described in Chapter 5) were taken by sheathed thermocouples placed at the two entries of the turbine and no compensation for radiation effects was considered. Thus the values recorded are below the true stagnation temperatures. Furthermore, these values are a function of the thermal capacity of the thermocouple, the thermal resistance of the sheath, the flow velocity of the exhaust gases (the heat transfer coefficient varies with gas velocity) and the frequency and shape of the exhaust temperature pulse.

The computed and measured temperatures of the air inside the induction manifold, plotted in Figs. 7.2-7.5, exhibit the same trends. The computed values show a small overestimate at high speeds, which is possibly caused by the prediction of a very short period of backflow through the inlet valve immediately after opening (i.e. flow from the cylinder into the induction manifold). The predicted and measured boost pressures show a close agreement in most cases. An even closer agreement is to be noted in the

comparison between the measured and the computed turbocharger speeds.

The variation of turbine power with load at the four engine speeds, as computed by the program, is also shown. The turbine power (expressed as a percentage of engine brake power) increases with engine output, up to a maximum of 19.5% at full power.

Computed and measured average exhaust pressures also show good agreement. However, it should be borne in mind that the measured and computed values do not always represent the same quantity. Measurements under pulsating flow, using a normal U-tube manometer, may not necessarily give the correct mean pressures. Also deviations between the predicted and actual pulsating pressure traces introduce errors in the mean pressures computed. Hence comparisons between the pressure records are necessary.

Figures 7.6-7.9 show comparisons of computed and measured pressure records inside number (1) cylinder and the exhaust manifold connected to it, at four engine speeds (1000, 1500, 2000 and 2500 rev./min.) and two loads. The agreement is excellent in the case of the cylinder pressure with the exception of the no-load conditions at the two higher speeds, at which lower and retarded peak pressures are predicted. The underestimation of peak pressures at low loads for the two high speeds was previously seen in Figs. 7.4 and 7.5. Apparently this is caused by an over-estimation of ignition delay and to a lesser extent, the injection lag. The former results mainly from low compression pressures and temperatures which are caused by the prediction of low boost pressures.

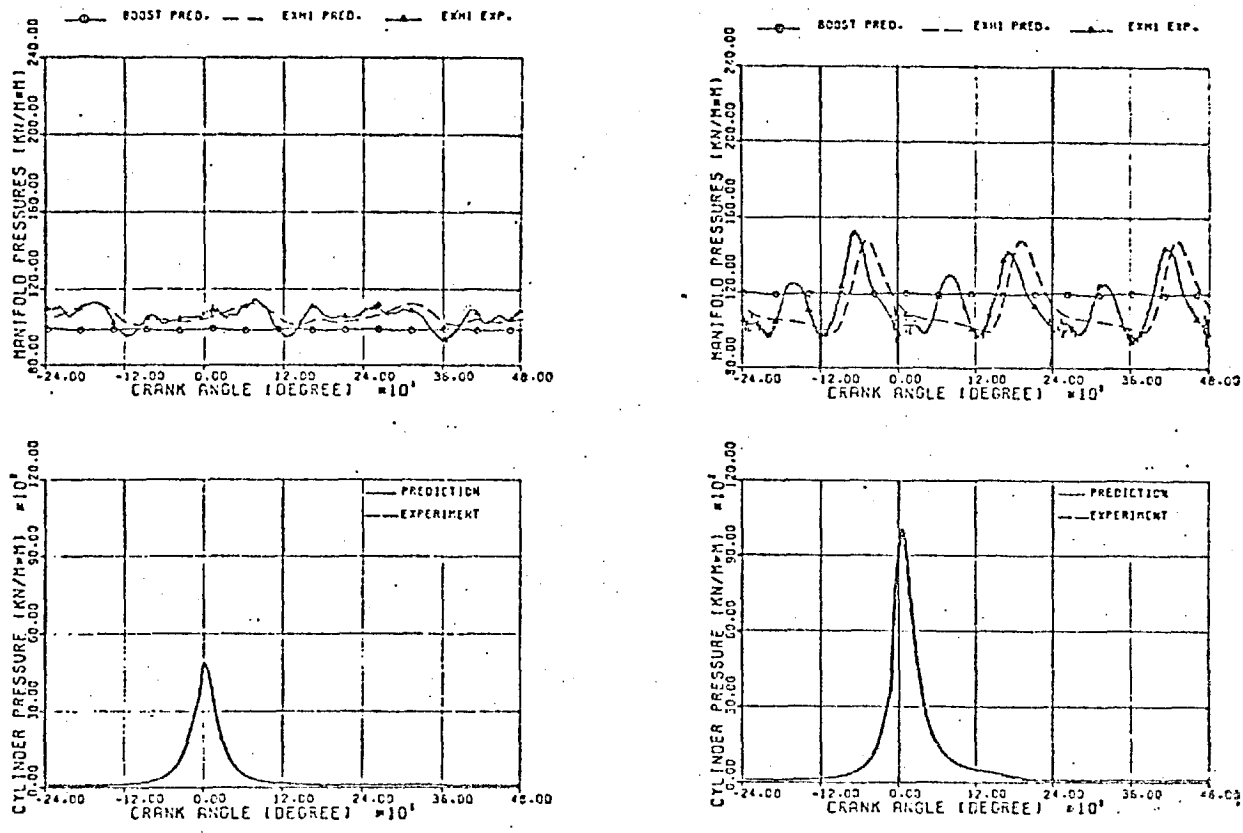


FIG. (7.6) Experimental and Predicted Pressure Histories in the Cylinder and Manifolds. Engine Speed = 1000 rev./min. BMEP = 0 and 9.0 BAR

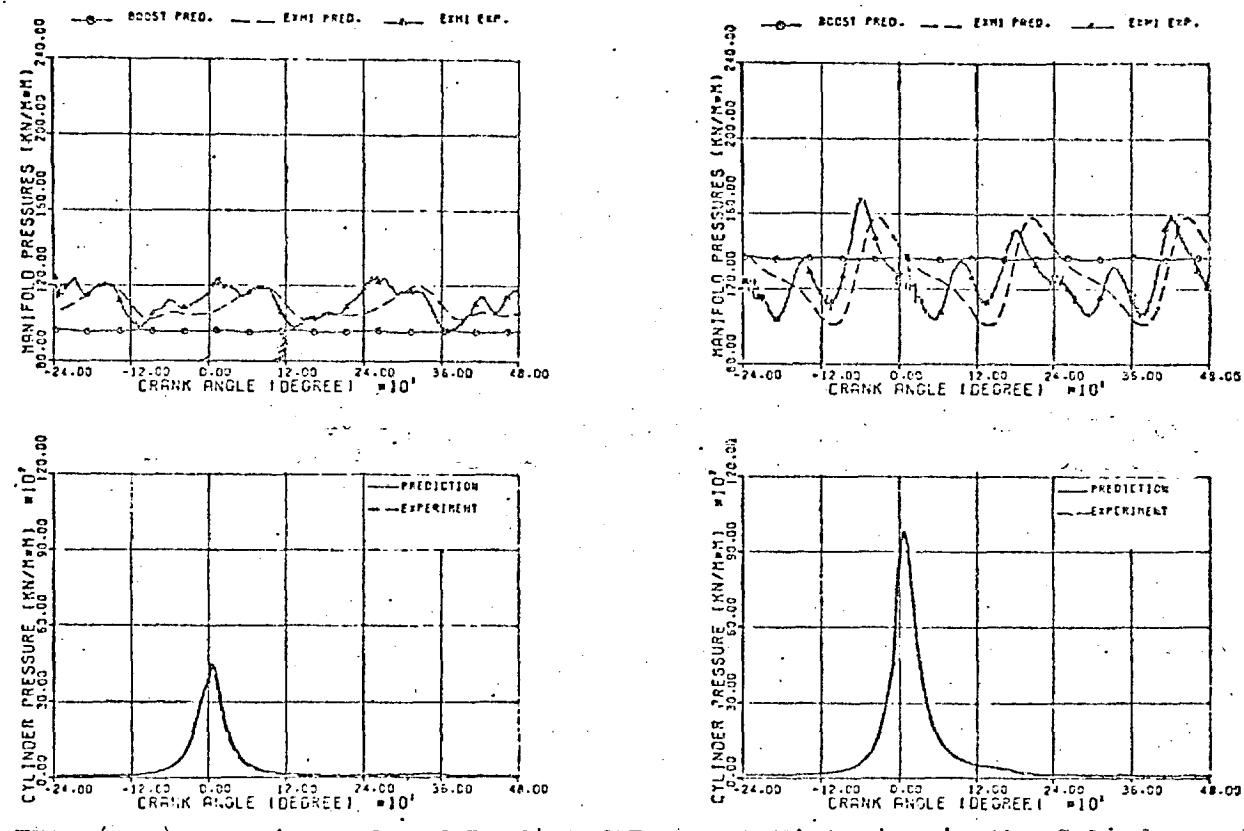


FIG. (7.7) Experimental and Predicted Pressure Histories in the Cylinder and Manifolds. Engine Speed = 1500 rev./min. BMEP = 0 and 9.0 BAR

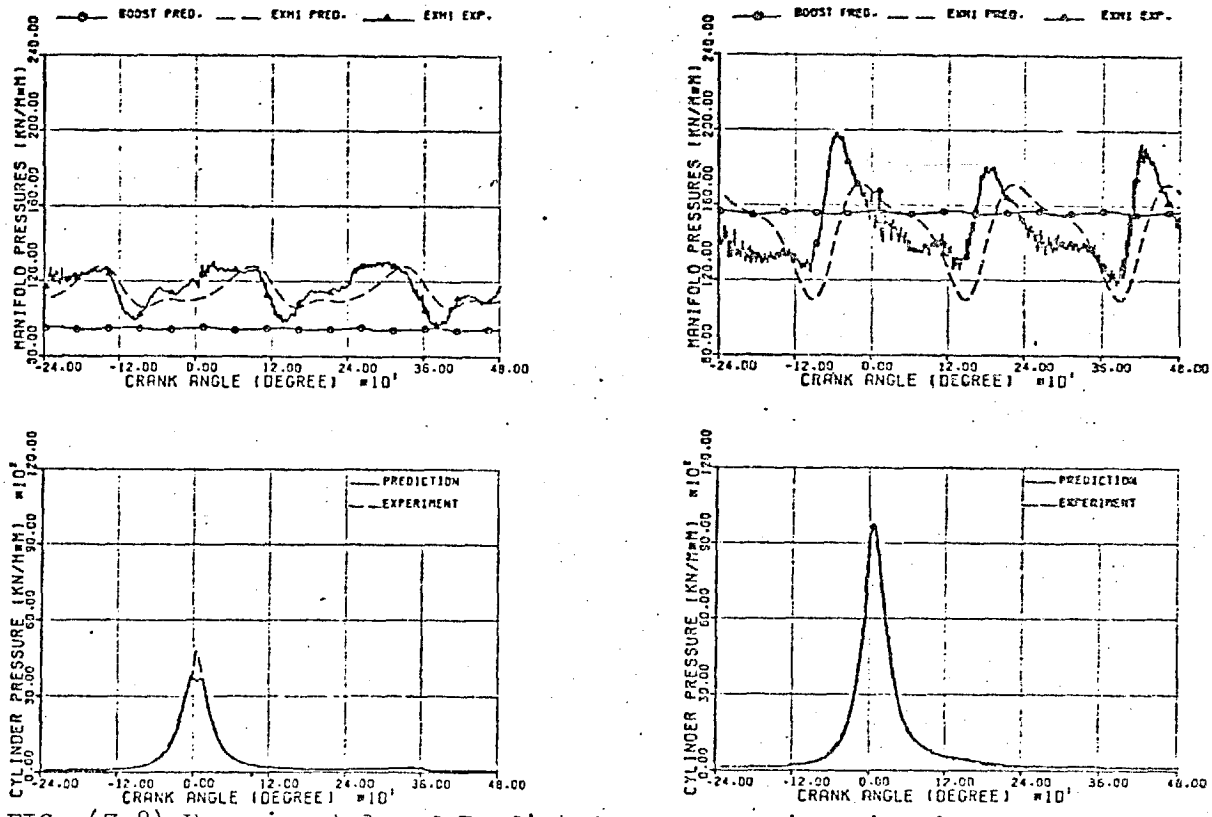


FIG. (7.8) Experimental and Predicted Pressure Histories in the Cylinder and Manifolds. Engine Speed = 2000 rev./min. BMEP = 0 and 9.0 BAR

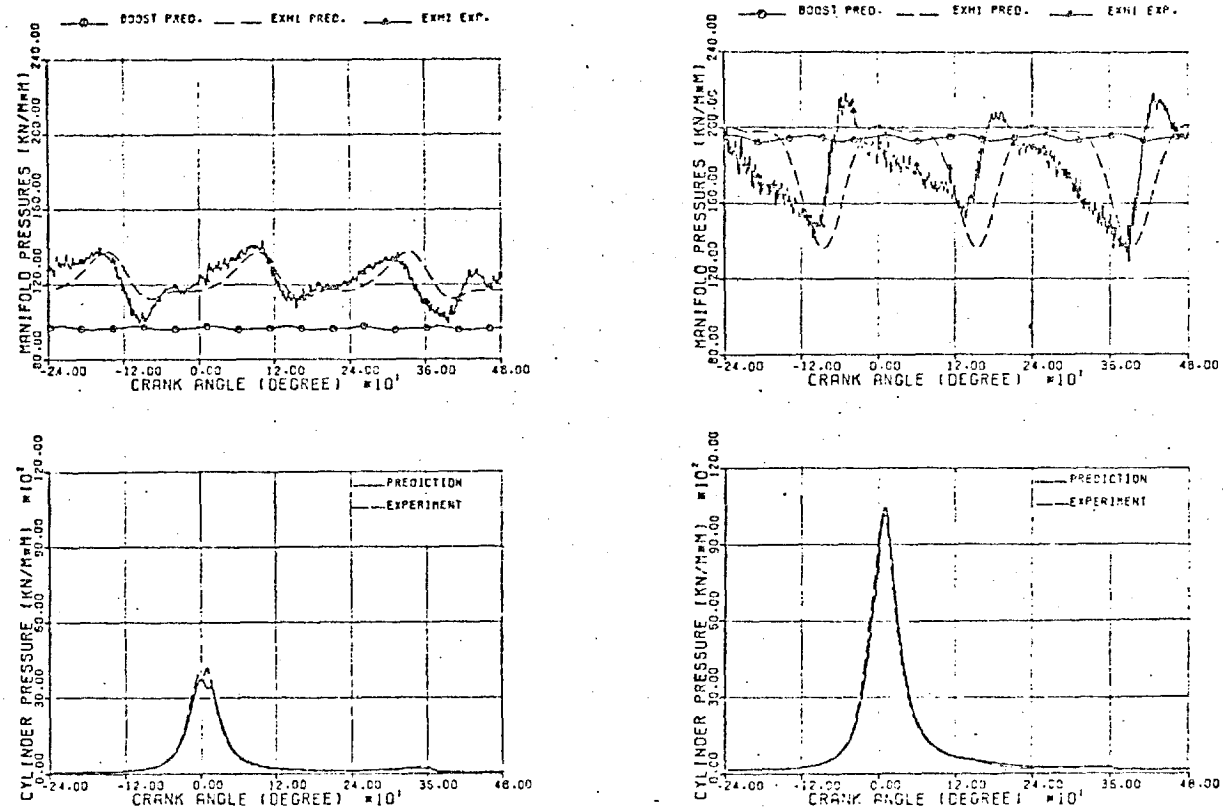


FIG. (7.9) Experimental and Predicted Pressure Histories in the Cylinder and Manifolds. Engine Speed = 2500 rev./min. BMEP = 0 and 9.0 BAR

Measured cylinder pressures exhibit faster rates of decay at the beginning of the exhaust valve opening period due to pressure wave phenomena. As pressure waves are not considered in the present simulation, the computed pressure during the gas exchange only approximates to the actual conditions. It may also be observed that the difference between the computed and measured rates of pressure decay increases with load. This is caused by the rise in release pressures.

Although good agreement between the computed and measured exhaust pressures exists at low loads, the results are not as good at higher loads. This appears to be a result of pressure wave action (not included in the simulation). Note that the measured exhaust pressures display three pairs of pulses every 720°CA (Chapter 5). Each pair consists of a blow down pulse and a secondary pulse (caused by piston displacement). The relative importance of blow down increases with load due to the rise in release pressures.

The phase difference between predicted and measured exhaust pressures should have no direct effect on turbine performance, but would probably slightly affect the engine airflow and imep. On the other hand, discrepancies in absolute value (e.g. the reduced prediction of the secondary pulse at low engine speeds) could have some influence on the turbine flow, hence power. This is probably offset partially by the prediction of relatively wider blowdown pulses.

The negative pressure difference across the engine, which was observed experimentally at low loads (Chapter 5), is reproduced by the model. This is seen to reverse with increase in load, giving boost pressures which are higher than exhaust pressures during the gas exchange period. It

may also be observed that the predicted boost pressure shows six small pulsations every 720°CA, which result from the suction strokes of the six cylinders. The amplitudes of these pulsations appear to increase with load and engine speed.

Illustrations of the effect of load and engine speed on the scavenging pressure and the rates of gas flow through the inlet and exhaust valves are presented in Figs. 7.10 and 7.11. It is obvious that the time history of the pressures upstream and downstream of a valve, and the instantaneous rate of flow through it, are interactive. This is particularly apparent in the case of the exhaust valve. The instantaneous rate of flow of gas through the exhaust valve exhibits two distinct peaks at most running conditions. The first peak (blowdown) is initiated by high release pressures in the cylinder and relatively low exhaust pressures at the instant of valve opening. On the other hand, the second peak is due to the piston displacement during the exhaust stroke. The magnitude of the blowdown flow increases with both load and speed, following the increase in cylinder pressure. The second peak increases with load and, to a larger extent, with speed (because of the increase in piston velocity).

The time distribution of the rate of flow of air through the inlet valve exhibits a single peak at all operating conditions. The magnitude of this peak increases with engine output whilst the rates of acceleration/deceleration of the flow rise with engine speed. During the intake process, the pressure inside the cylinder is normally below that of the induction manifold, thus causing fresh air to flow into the cylinder. However, in practice, the

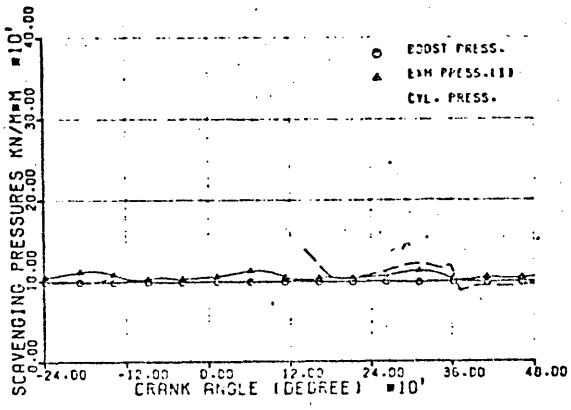


BMEP=0.0 BAR

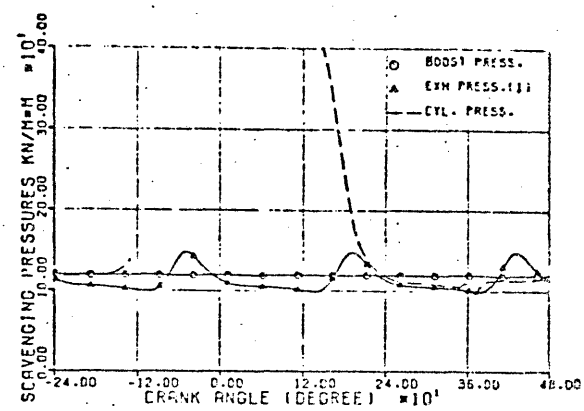


BMEP=9.0 BAR

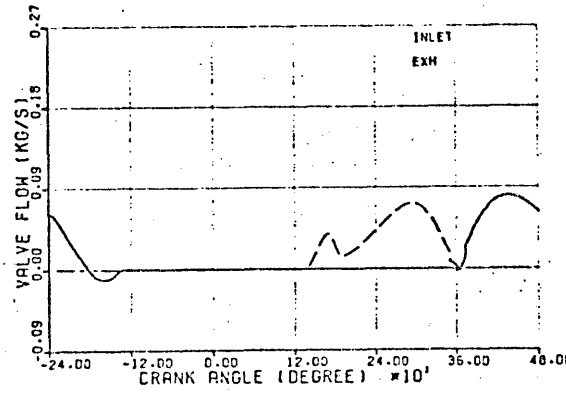


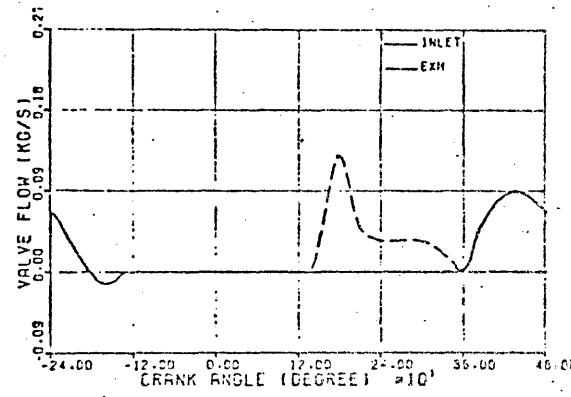


FIG.(7.10) Computed Scavenging Pressures and Valve Flow.
Engine Speed=1000 rev./min.

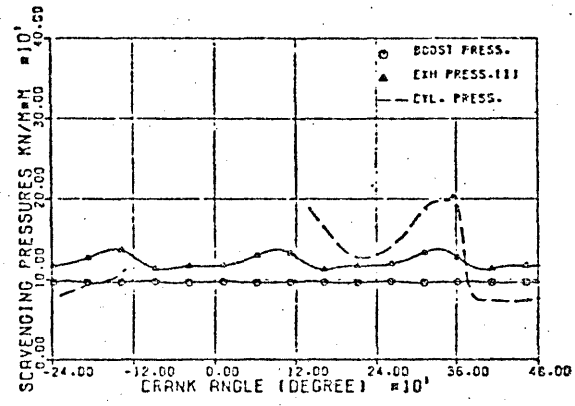


BMEP=0.0 BAR

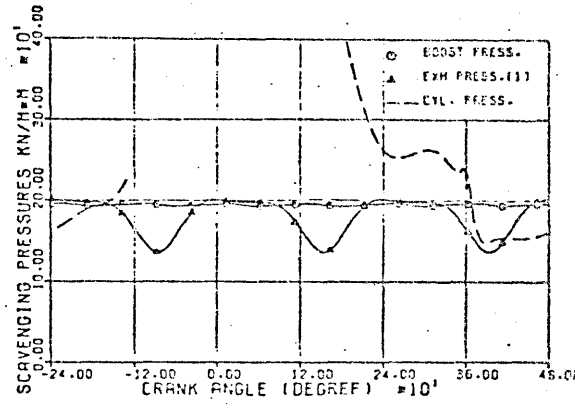


BMEP=9.0 BAR

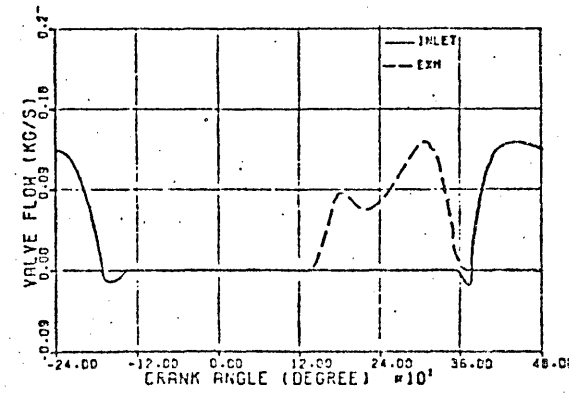


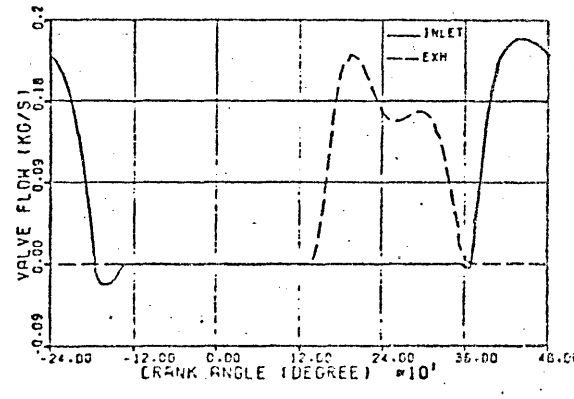


FIG.(7.11) Computed Scavenging Pressures and Valve Flow.
Engine Speed=2500 rev./min.

cylinder pressure may exceed the air receiver pressure at the beginning or towards the end of the inlet valve opening period. Under such conditions backflow (from the cylinder into the air chest) will occur. This pollutes and heats the contents of the air chest, shortens the effective intake process, reduces the trapped mass of the charge (at inlet valve closure) and increases the charge temperature. If backflow occurs at the beginning of the inlet valve opening, its effect on the fresh air will be worse; the cylinder being full of hot residual gases from the previous firing.

Reversed intake flow prior to valve closure was found to occur in all running conditions, thus indicating a late closure timing ($50^{o}$ABDC). The more serious type of reversed flow (occurring at inlet valve opening) was only predicted at high speeds. This probably explains the small overestimation in the predictions of the air temperatures in the induction manifold. Early backflow appears to be reduced with increase in load, but this might not necessarily apply to its effect on the incoming fresh air (temperature of the residual gases rises with load).

Figures 7.12 and 7.13 show variations in the shape of the computed fuel burning rate and charge equivalence ratio with the operating conditions of the engine. The shape of the fuel burning rate curve is seen to follow the experimental observations very closely. It was shown in the previous chapter that if the injection and ignition points are determined accurately, good agreement between the predicted and experimental fuel burning rates is obtained.

The distribution of the indicated torque developed by cylinder no. (1) is presented in Fig. 7.14 for zero and 9.0 bar bmep at engine speeds of 1000 and 2500 rev./min.

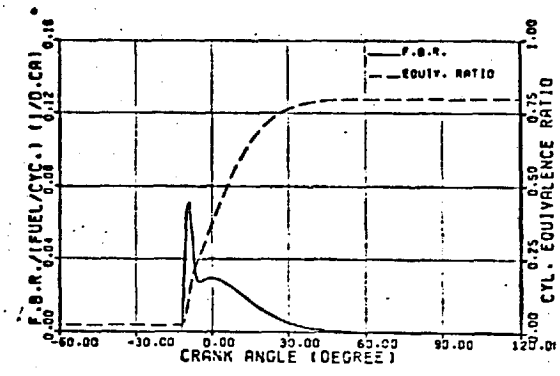


Engine Speed=1000 rev/min BMEP=9.0 BAR

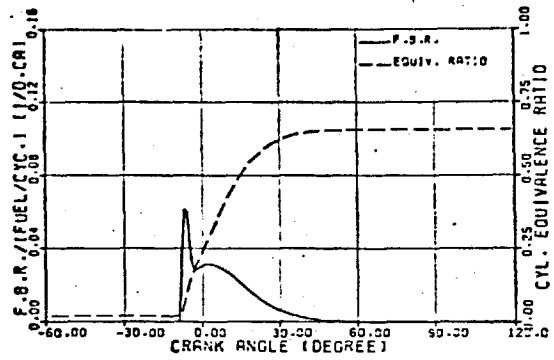


Engine Speed=1500 rev/min BMEP=9.0 BAR

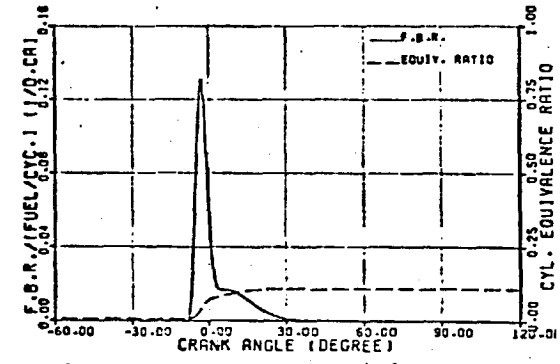


Engine Speed=1000 rev/min BMEP=0 BAR

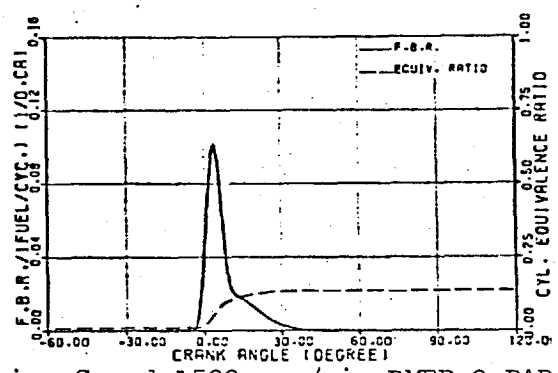


Engine Speed=1500 rev/min BMEP=0 BAR

FIG. (7.12) Fuel Burning Rate and Equivalence Ratio Distributions

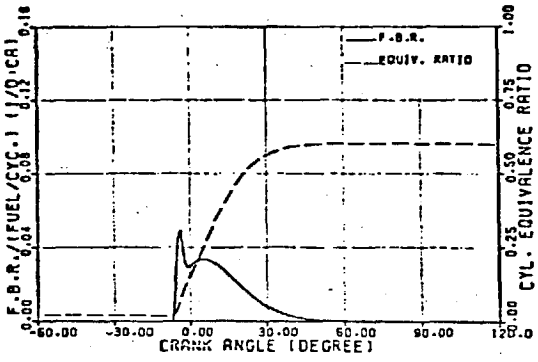


Engine Speed=2000 rev/min BMEP=9.0 BAR

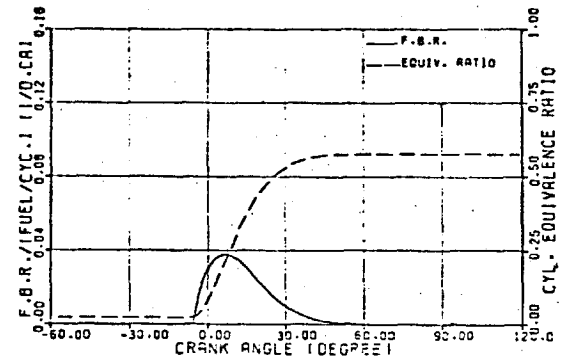


Engine Speed=2500 rev/min BMEP=9.0 BAR

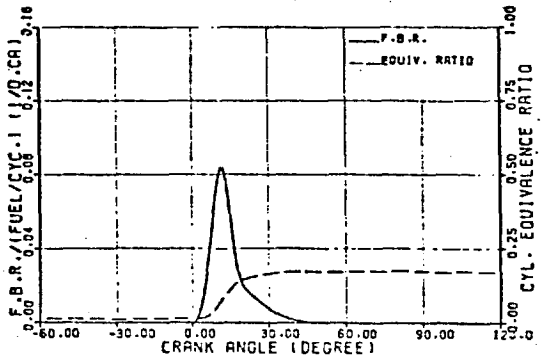


Engine Speed=2000 rev/min BMEP=0 BAR

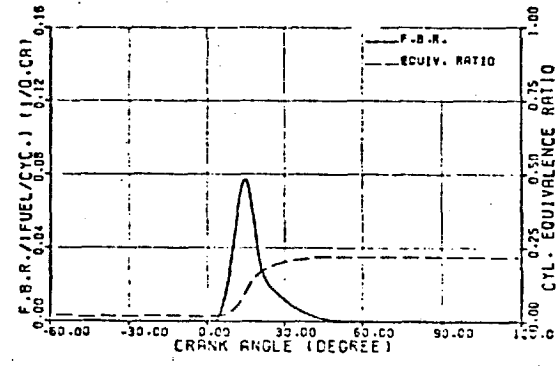


Engine Speed=2500 rev/min BMEP=0 BAR

FIG. (7.13) Fuel Burning Rate and Equivalence Ratio Distributions

The variation in the instantaneous performance of the exhaust turbine is shown in Fig. 7.15 for a complete engine cycle. Two representative cases were selected, namely 9.0 bar bmep at 1000 and 2500 rev./min. These are illustrated for the same turbine sector through which gases released by the no. (1) cylinder flow. The pulsations in the exhaust temperature and turbine expansion ratio are shown together with the resulting distributions of turbine flow, velocity ratio and efficiency. The instantaneous available exhaust gas energy and the net power, that is extracted by the turbine, are also depicted.

The windmilling periods shown in the low speed case should be observed. The reduced exhaust pressures occurring in such periods cause the gas flow and the available exhaust energy to diminish considerably (reaching zero momentarily). At low engine speeds the reduced air flow coupled with the low frequency of the exhaust pulses constitute the major cause of the low exhaust pressure periods. This is also accompanied by a considerable variation in the velocity ratio and subsequently the instantaneous turbine efficiency. Fortunately, in such cases, the turbine efficiency reaches a minimum when the available power at the turbine is also at its lowest value.

The variation of the overall and component mean efficiencies of the turbocharger with fuelling (load) is depicted in Fig. 7.16, for four different engine speeds. It can be seen that the turbine efficiency increases with engine speed with a small variation in load. This is basically caused by the dependence of the mean turbine efficiency on the level of the exhaust pressure and the pulse frequency. On the other hand, the compressor efficiency

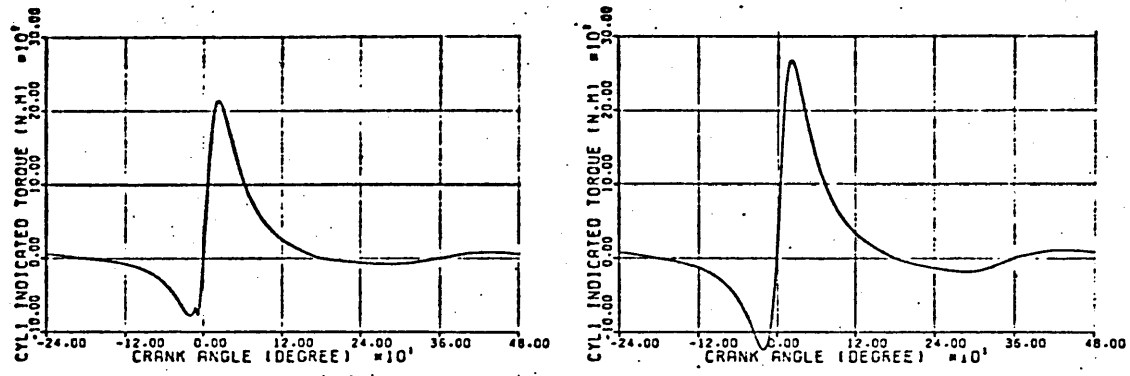


Eng. Speed=1000 rev/min BMEP=9.0 BAR Eng. Speed=2500 rev/min BMEP=9.0 BAR

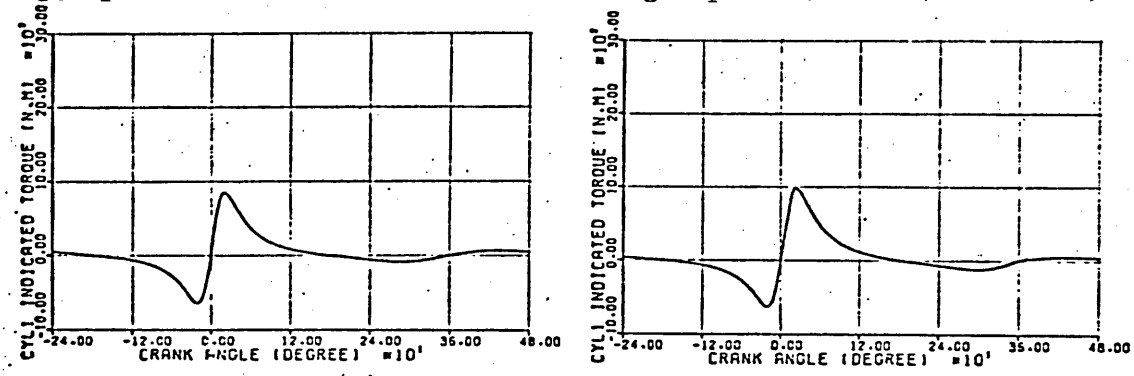


Eng. Speed=1000 rev/min BMEP=0.0 BAR Eng. Speed=2500 rev/min BMEP=0.0 BAR

FIG. (7.14) Variation of Indicated Torque with Crankangle (Cylinder No. 1)

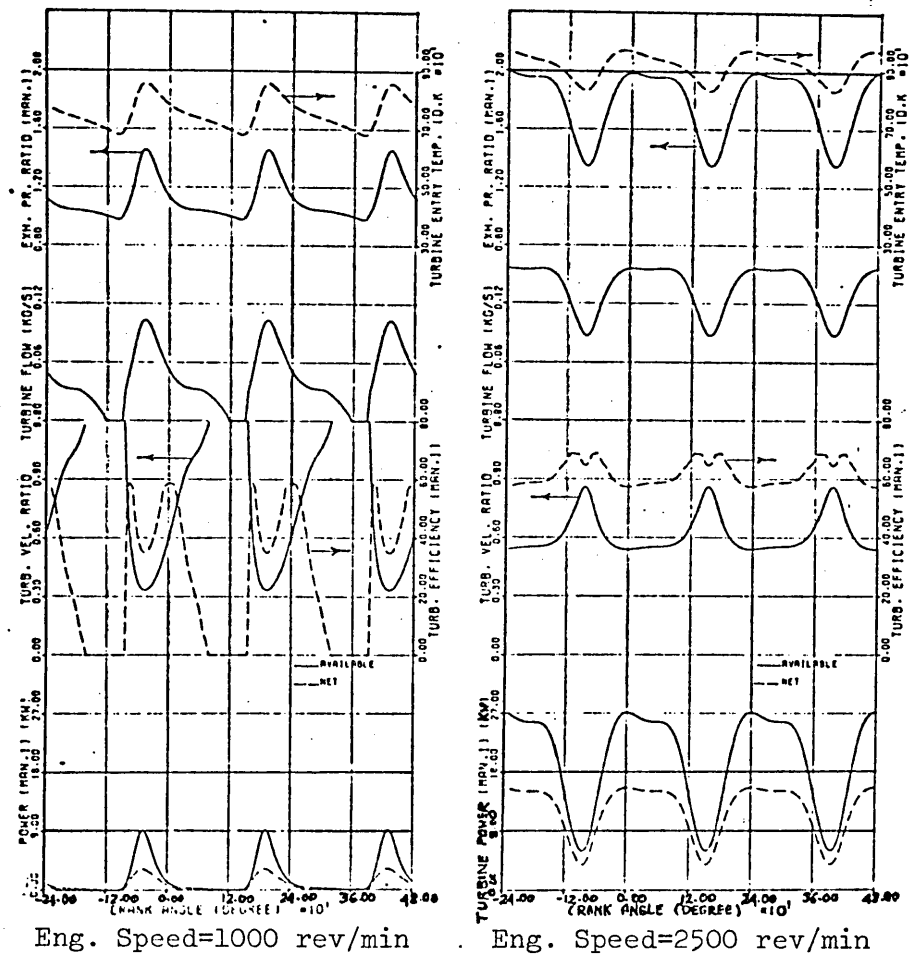


Eng. Speed=1000 rev/min Eng. Speed=2500 rev/min

FIG. (7.15) Variation of Turbine Performance with Crankangle at 9.0 BAR BMEP (Ring 1: Connected to Cylinders 1, 3 and 5)

shows a clear dependence on load. The overall efficiency of the turbocharger (the product of the two component efficiencies) increases with both load and engine speed (excluding the lowest speed at low loads). This indicates that the optimal engine-turbocharger matching point is close to maximum power.

The ability of the program to predict surface temperature trends correctly is demonstrated in Fig. 7.17. Calculated values of the mean temperatures of the liner, piston, and cylinder head surfaces exposed to the gases are plotted for four engine speeds and various fuel inputs (loads). Although no experimental data was available for comparison, the surface temperatures follow a uniform trend without any irregularities. Temperatures are seen to increase with fuel input and to a lesser extent with engine speed. The rise in metal temperatures with fuelling rate, at a fixed speed, is due to the increase in the mean heat flux from the gases to the walls. This is a result of increases in the mean values of the gas temperature and gas/wall coefficient of heat transfer which are brought about by higher rates of heat liberation. Engine speed influences the coefficient of heat transfer via the degree of turbulence it imposes on air motion within the cylinder; this being described by the characteristic velocity term in the heat transfer correlation (Section 2.7). A minor effect of increasing engine speed is also the increase in inlet air temperature.

The calculated surface temperatures are relatively low in comparison with other turbocharged diesel engines (94), which suggests underestimation of the thermal resistances of the different flow paths in the heat conduction model

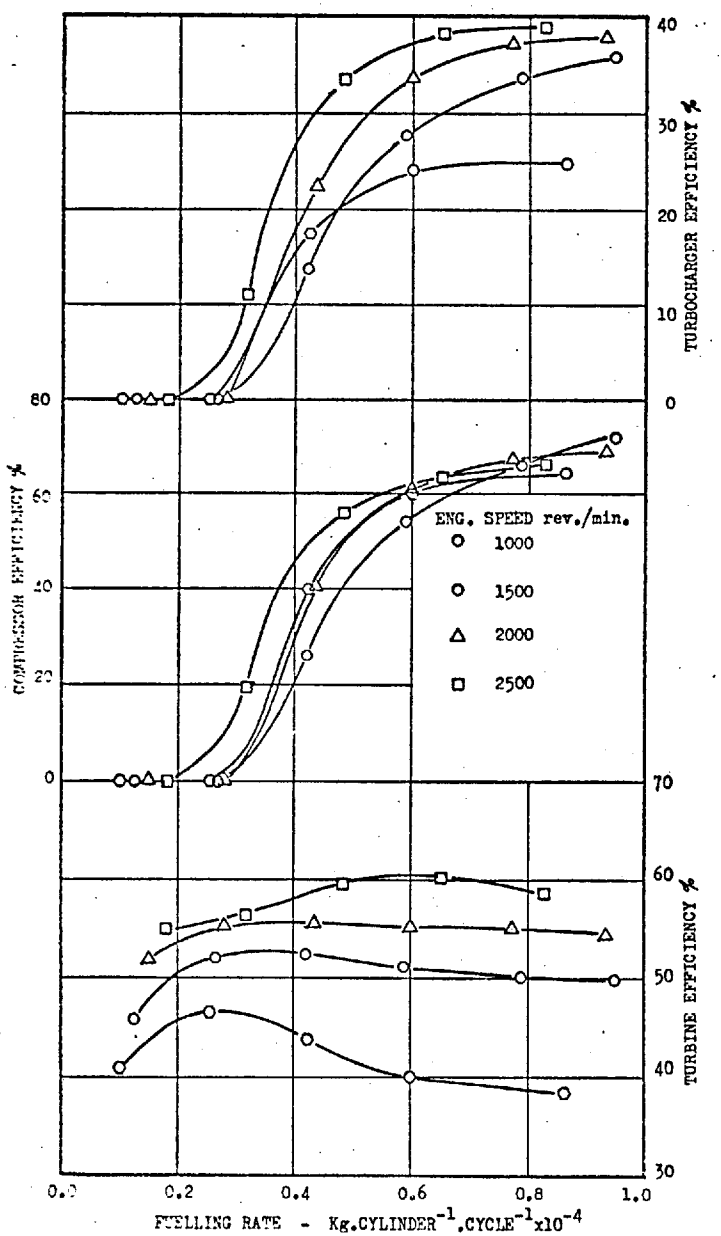


FIG. (7.16) Overall and Component Efficiencies of Turbocharger

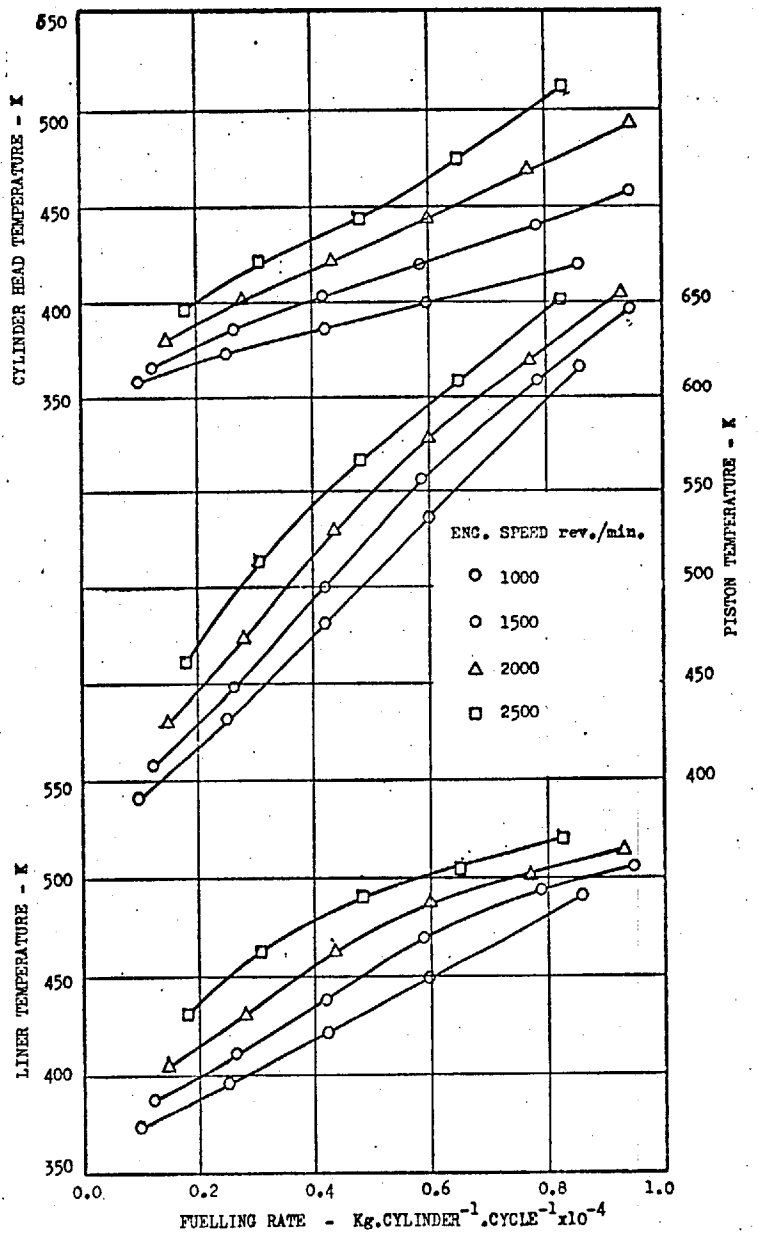


FIG. (7.17) Computed Mean Surface Temperatures Inside the Cylinder

(Section 2.7). This can be caused by an overestimation of the heat transfer coefficient on the coolant side, particularly at low loads, and the assumption of a clean metal coolant surface, i.e. no deposits or rust.

No modifications were made to the thermal resistances as no measured surface temperatures were available for validation purposes. However, it is acknowledged that lower wall temperatures result in higher air consumption due to improved volumetric efficiency.

Heat losses from the exhaust gases have been computed using a constant overall coefficient of heat transfer between the gases and ambient air (Section 2.7). In order to assess the effect of this assumption on the simulation results, the coefficient of heat transfer was increased by 50% and the program was re-run for a number of operating conditions. Comparisons of the original and new predictions are presented in Fig. 7.18. A very slight reduction in the computed mean exhaust temperatures and pressures together with very small changes in the boost and peak cylinder pressures can be observed. However, the effect on the computed overall performance figures of the engine is insignificantly small. Although this supports the assumption employed, it is believed that the development of a heat transfer correlation for pulsating flows in exhaust manifolds would be most useful.

## 7.3 COMPARISON OF PREDICTED AND MEASURED TRANSIENT DATA

Before drawing comparisons between predicted and measured transient data, it is appropriate to consider the output characteristics of the simulation. Figures 7.19a-b display the predicted engine transient response to a rapid increase in load. The input signals to the model are shown

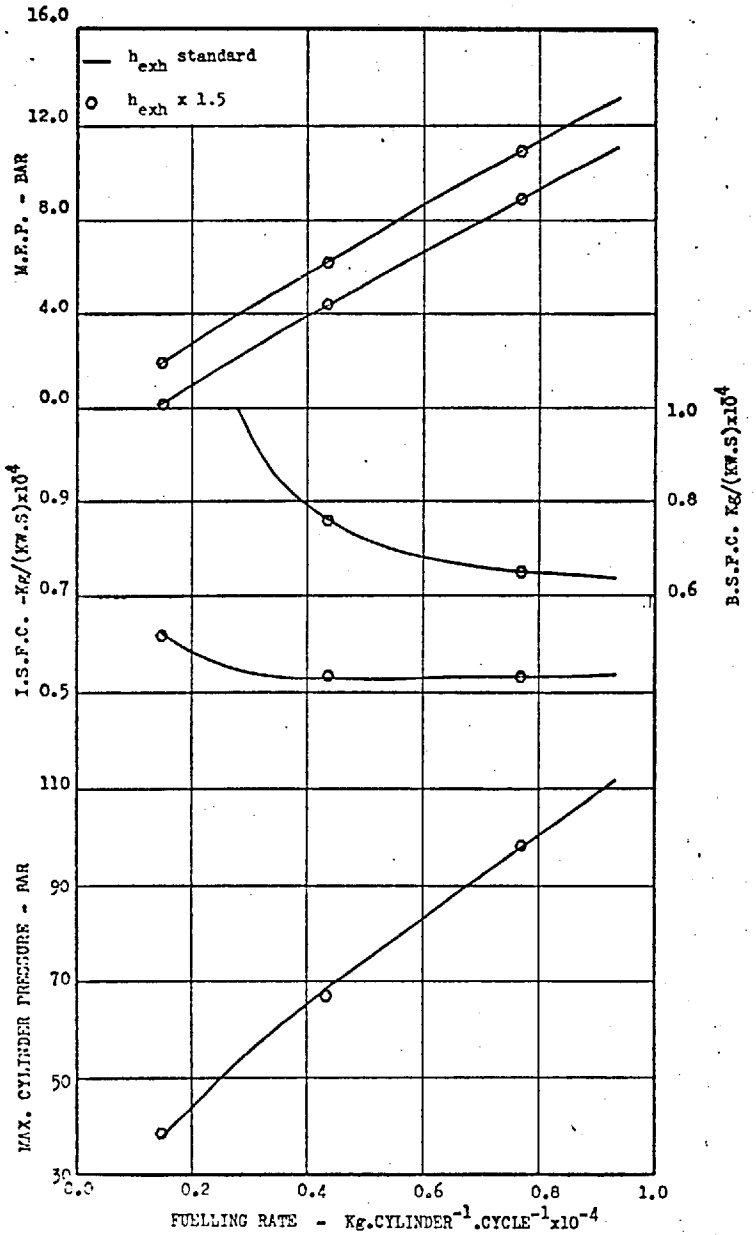


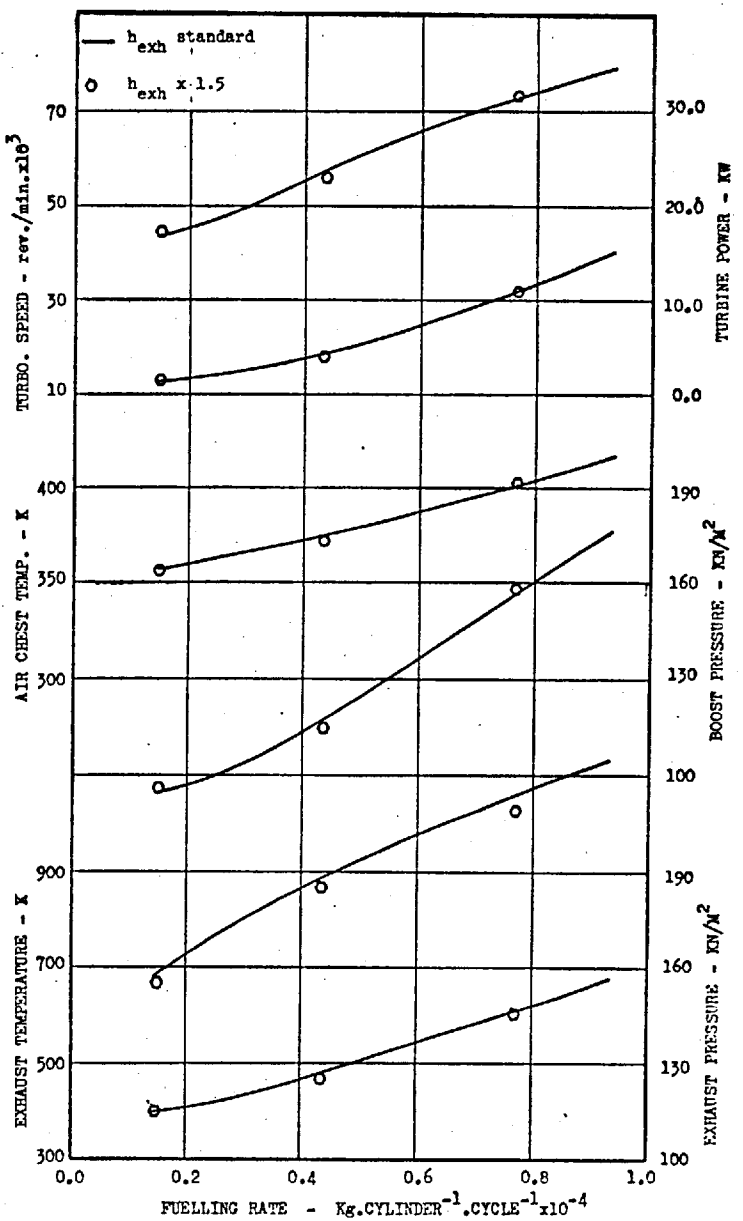


FIG. (7.18) EFFECT OF HEAT LOSSES FROM THE EXHAUST GASES

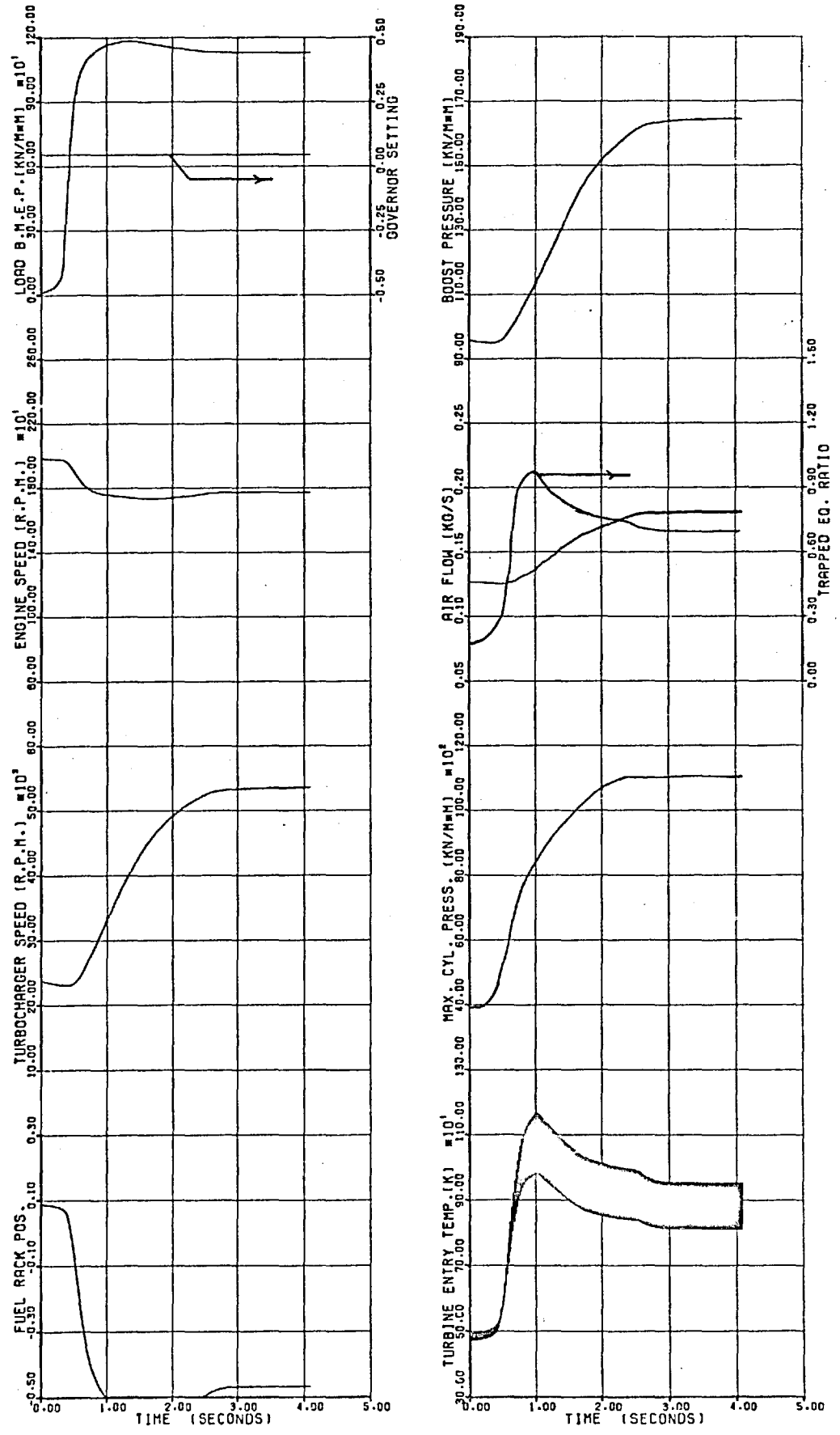


FIG. (7.19,a) TRANSIENT RESPONSE TO RAPID LOADING

| | LOAD (BMEP BAR) | GOV. SETTING | ENG. SPEED (RPM) |
|---|---|---|---|
| INITIAL | 0.1 | 0.045 | 1980.4 |
| FINAL | 11.3 | 0.045 | 1772.7 |

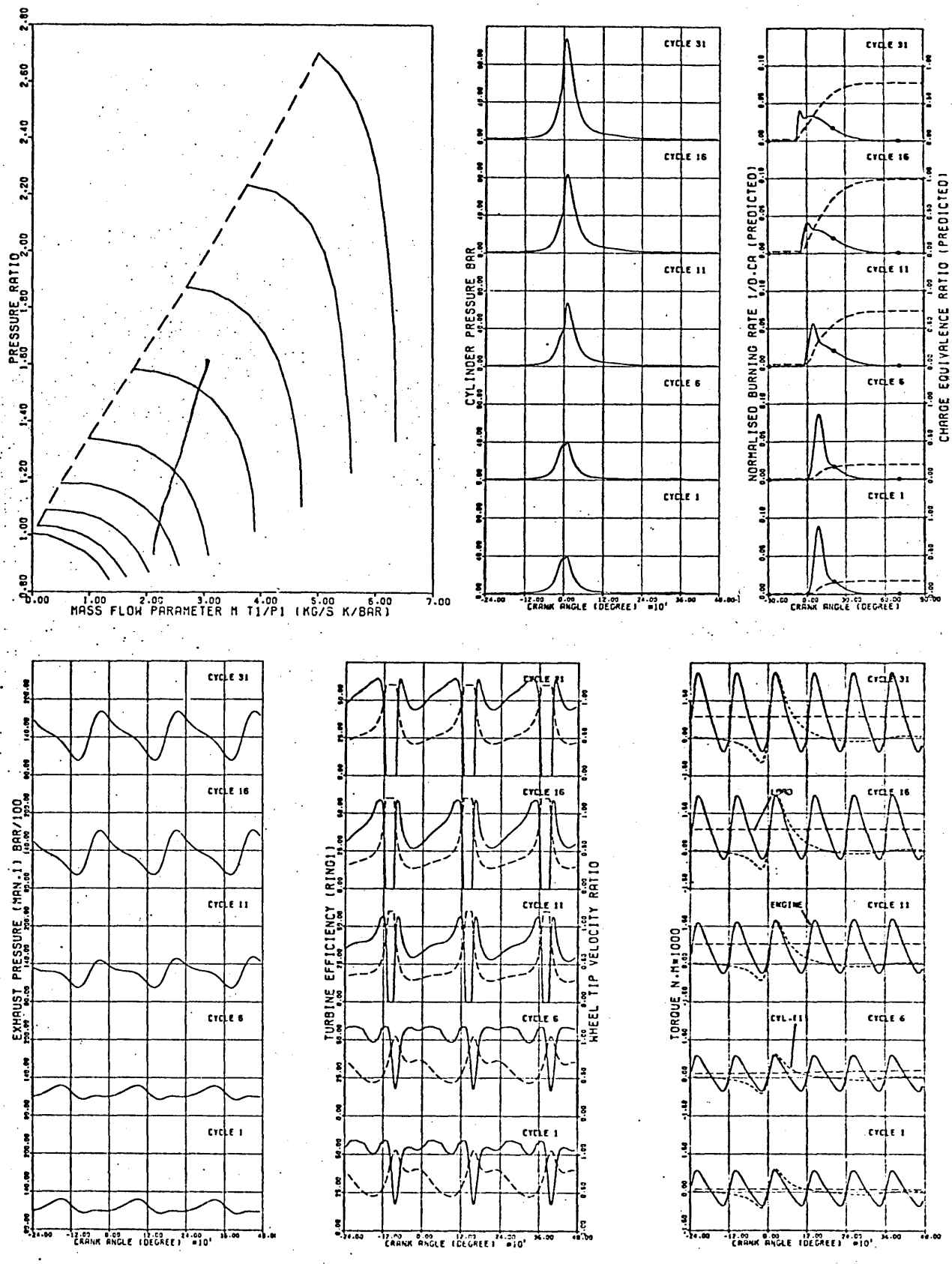


FIG. (7.19,b) Transient Response to Rapid Loading

at the top left of Fig. 7.19a. The resulting response of engine and turbocharger speeds, fuel rack position (governor (output), boost pressure, air flow, trapped equivalence ratio (overall), maximum cylinder pressure and exhaust temperature are also plotted in the same figure. The exhaust temperature exhibits a wide trace at high load due to the pulsation.

In this particular case, the model shows clearly the lag of the turbocharger due to its inertia. The governor response can be seen to be very rapid up to the point when the fuel rack hits the maximum fuelling stop. As a result of the large phase difference between responses of fuelling (governor) and the turbocharger, the overall equivalence ratio of the cylinder charge increases very quickly, approaching the stoichiometric ratio (F = 1). The mixture strength becomes over-rich in fuel momentarily, after which it becomes leaner (the increase in fuel supplied is limited by the maximum fuelling stop whilst the air flow continues to increase gradually). The relatively rapid drop in equivalence ratio, which occurs 2.3 seconds from the start, follows the decrease in fuelling. This results from the departure of the fuel rack from its end position, due to the recovery in engine speed. The trapped equivalence ratio gradually attains a new steady state value with all the other variables following suit.

The variation of mean exhaust temperature with time seems very similar to that of the equivalence ratio. However, the availability of the exhaust energy (for transformation into useful turbine work) is heavily dependent on pressure levels in the exhaust manifolds. This in turn is influenced by events occurring inside the cylinder (mass of

charge trapped at valve closure, combustion and heat tranfer) via the release pressures.

The response of the maximum cylinder pressure curve is rapid during the early stages, due to the quick increase in fuelling. The rate of increase is later reduced as the equivalence ratio attains its peak value. The pressure continues to rise and the rate is further reduced when the fuel rack moves away from the maximum fuelling position.

Figure 7.19b shows (diagrammatically) the working line of the engine during transient operation, superimposed on the compressor characteristic. The initial steady state operating point is identical to the no-load steady state case at 2500 rev./min. shown in Section 7.2. The boost pressure is initially below the ambient pressure and builds up with air flow. As expected, the gradient of the working line exceeds that of the steady state operational line at the same initial speed. Obviously this results from the reduction in engine speed as load is applied. The variation of turbine velocity ratio and efficiency within one engine cycle is shown (in the same figure) for five individual cycles along the transient period.

Predicted crankangle diagrams of pressures inside the cylinder and exhaust manifold (connected to the same cylinder) are presented in Fig. 7.19b for a succession of cycles during the transient period. A comparison of such pressure records with measured ones (Chapter 5) would illustrate the validity and power of the simulation. This would also yield useful information for performance development and improvement.

The fuel burning rate and equivalence ratio predicted during the same cycles are also shown. Note the

changes in the timing, shape and duration of combustion. The ignition point can be seen to be advancing gradually, following the reduction in engine speed and the increase in boost pressure and temperature. The increase in fuelling per cycle, hence overall equivalence ratio, leads to a rise in the proportion of diffusion-controlled burning and an increase in combustion duration (Chapter 6).

The variation of instantaneous engine (developed) torque, in comparison with the load torque is shown for the same cycles selected during the transient period. The shape and amplitude of the torque pulsations are dependent on the cylinder pressures and engine geometry (equation 2.21). Accordingly, all the interactions and non-linearities involved in the thermodynamics of the engine and gas flow have a bearing on the torque developed, e.g. trapped mass of charge, engine speed, injection point, cylinder temperature and pressure prior to injection, overall equivalence ratio, gas flow through the valves, etc. In the case considered, the engine torque rises (amplitude and mean cyclic value) with cylinder pressure, following the increase in fuelling; the equivalence ratio always being below unity. The discrepancy between the torque developed and the load, determines the change in engine speed.

Other variables such as exhaust equivalence ratio, instantaneous torques of the turbine and compressor, mass flow rates through the valves, etc. can also be plotted if required.

A further illustration of the capabilities of the simulation program is the prediction of frequency response (a typical application in diesel engines is stability studies for speed governing). Frequency response testing

is one of the conventional methods available for analysis and design of control systems. The dynamic characteristics of any system are normally determined by varying the frequency of a sinusoidal input signal over a certain range, and studying the resulting response. Although the frequency response of a system represents a qualitative picture of the transient response, an indirect correlation between the two exists (82).

Figure 7.20 displays the predicted frequency response data, in which the engine model is subjected to the following sinusoidal load:

$$C_L(t) = a1(1+a2)\sin(\frac{2\pi}{a3}t) \qquad (7.1)$$

where constants a1, a2 and a3 represent the mean load, amplitude/mean load ratio and the period of the sinusoidal input. These were taken as 6.76 bar (bmep), 60% and 0.5 second respectively. It is important to note the differences in the ratio between the percentage change in the individual parameters, and that of the input signal. In the example considered, these ratios were 0.037, 0.782, 0.284, 0.028, 0.036 and 0.018 for engine speed, rack position, exhaust temperature, turbocharger speed, air flow and boost pressure respectively. The rack motion and the exhaust temperature show very high ratios relative to the other parameters. This indicates that the governor gain, which is defined as the ratio of the percentage changes in rack motion and engine speed, is very large relative to other components of the engine system. As a result, the transient response in fuelling and hence exhaust temperature is always much faster than that of air flow.

As mentioned in Chapter 5, the experimental transient response program included three basic types of tests, namely:

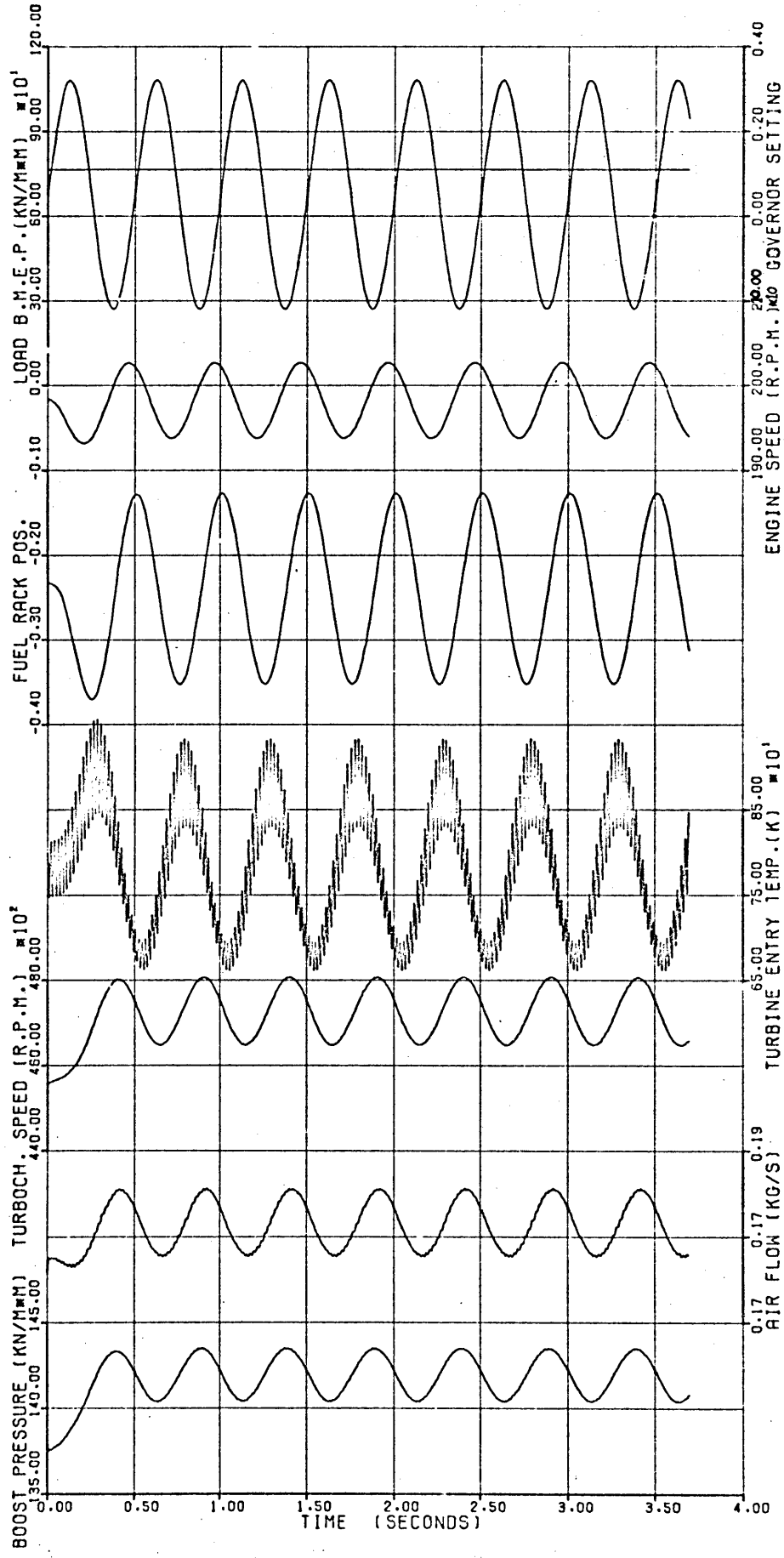


FIG (7.20) FREQUENCY RESPONSE TO SINUSOIDAL LOADING

MEAN LOAD = 6.76 BAR (BMEP), AMPLITUDE = 60%,
FREQUENCY = 2.HZ

1. A step input to the dynamometer.

2. A rapid change in the governor setting (demand speed).

3. A simultaneous combination of the inputs 1 and 2 above.

Since the actual dynamometer output was not sufficiently rapid to constitute an ideal step, it was decided to employ the measured load torque as an input signal to the model. Errors in the torque measurements (mainly due to vibrations transmitted to the torque transducer) were found to be of the order of 4%. Obviously this introduced discrepancies between predictions and experimental data; however, the resulting discrepancies were small in most cases.

The variation in demand speed with time, that is, the exact shape of the input signal to the governor, depended on the magnitude of the input charge (Section 4.4.2). Subsequently the duration of the change in demand speed was determined from the calibration of the stepping motor drive unit, Fig. 4.7. The input signal to the model was considered to be an ideal ramp which had a gradient equal to the mean rate of change (i.e. mean angular speed of the stepping motor). This assumption constituted a minor approximation of the variation in demand speed, particularly in the first 30 milliseconds during which the motor accelerated to the high speed mode.

Table 5.2 gives the details of the transient tests carried out experimentally. Eleven of these transient cases have been predicted and compared with the measured data. Comparisons are shown in Figs. 7.21 to 7.31. Mostly tests involving large changes of input signals (load or demand

speed) were selected, because it was felt that if good agreement could be achieved under such conditions, then the response to smaller inputs should also be predicted reasonably accurately. The cases selected comprise: four load changes, three cases of changes in demand speed, and four of combined inputs.

It should be noted that the comparisons comprise a representative number of transient situations, each of which covers almost the entire load or speed range of the engine. Bearing in mind the accuracy constraints imposed by the data used (e.g. turbocharger characteristics, governor representation, inertias of engine and turbocharger and the load measurements, etc.), the agreement between predictions and measurements is considered to be satisfactory. It can also be observed, that despite minor discrepancies in some cases, the basic trends of the different parameters are reproduced by the model.

Figures 7.21 to 7.24 show cases of engine transient response to a load increase at four fixed demand speeds. Good agreement can be seen; however, the model shows a slightly slower response in engine speed and subsequently rack travel. Agreement in the final steady state values of the two variables is satisfactory with the exception of case TR4 where engine speed is overestimated. In this particular case the maximum torque measured was found to be underestimated by about 4%.

Moving from the case of lowest demand speed (TR2) to the highest (TR8), it is easy to observe that the rise time of the turbocharger speed is reduced by a factor of four. In other words, the turbocharger accelerates

faster at higher engine speeds. This can be seen to be true in both the experimental and predicted responses. The same observation applies to the boost pressure in the four cases and to air flow in cases TR6 and TR8. Measured air flow during the two low demand speed tests does not show a noticeable rise, which is probably a result of the counter-action of the effects of increased fuelling (hence turbocharger speed) and reduced engine speed. The model produces a small reduction in air flow in case TR2. Regarding the end point values of the turbocharger speed, boost pressure and air flow, it is seen that the predictions and measurements are very close. Case TR8 is an exception; the model predicts slightly higher values.

The variation with time of the overall equivalence ratio of the air/fuel mixture inside the cylinder, is a resultant of the rates of change of fuelling and air flow. Despite the relatively fast response of the turbocharger in case TR8, the simulation predicts an equivalence ratio above unity, i.e. over-rich mixture. Apparently this is brought about by the fast response of the governor at high engine speeds. This can be understood by referring to equation (2.46) (Chapter 2) which indicates that the natural frequency of the governor increases with governor setting, i.e. demand speed.

The measured and predicted responsesof the exhaust temperature are very similar and the timing of the peak value shows very close agreement. Nevertheless, the final steady state values are underestimated at low speeds. The same trend was observed in the comparisons of the steady state results and was discussed in the previous section.

Comparisons of the cylinder pressures, in particular peak values, show a large dependence on governor response, i.e. the fuelling per cycle. This also applies, but to a lesser extent, to exhaust pressures. If we consider case TR2 as an example, it can be seen that, at cycle 11, the predicted governor response lags behind the experimental curve whilst a slight lead is shown at cycle 31. The subsequent effect on fuelling results in an early underestimation of the cylinder and exhaust pressures, followed by a small overestimation at cycle 31.

With changes in demand speed at fixed loads, the experimental and model responses agree favourably, e.g. see engine speed curves. The model responds slightly faster, particularly in case TR11. The computed turbocharger speed follows the experimental curve very closely in cases TR10 and TR11, showing a similar overshoot. The model predicts a faster deceleration of the turbocharger in case TR14. The response of the governor model (fuel rack position) is very similar to the measured data, but the former exhibits a faster rate of change. This causes a quick change in fuelling and subsequently rapid changes in the thermodynamic conditions of the cylinders and exhaust manifolds.

A sudden increase in the trapped equivalence ratio, coupled with a rapid rise in the peak cylinder pressure, occurs in cases TR10 and TR11. This is also accompanied by a rapid rise in temperatures and pressures of the exhaust gases. The model predicts the same trends but shows steeper rises in the maximum cylinder pressure and exhaust temperature. The former reaches a peak value, only two cycles from the start of the transient. It then drops faster than the measured pressures (cycles 2 to 16). On the other hand,

the computed exhaust temperature continues to rise but with a reduced rate in comparison with the first two cycles. A further steep drop in peak pressure and exhaust temperature occurs in both the experimental and computed curves between cycles 17 and 21. This is caused by the reduction in fuelling imposed by the response of the governor to the rise in engine speed. The resulting reduction in exhaust energy reverses the initial acceleration of the turbocharger and so its speed begins to fall. Subsequently air flow and boost pressure are reduced after an initial rise. The computed and measured curves agree favourably and hence a close agreement can be seen in the engine working lines on the compressor map.

The underestimation of the maximum cylinder pressures and the overestimation of exhaust temperatures between cycles number 2 and 16 can be explained as follows: the computed and experimental cylinder pressure diagrams show very good agreement during the compression stroke. Also, the ignition point, which is seen to retard with engine speed, is predicted correctly. On the other hand, the fuel burning rate diagrams generated by the combustion model during the cycles considered exhibit a rapid decay in premixed burning and hence a simultaneous increase in diffusion burning. In other words, the mode of burning proportionality factor (Chapter 6) which governs the percentage of fuel burnt by each of the two mechanisms is reducing rapidly. This suggests that, in the case of over rich fuel/air ratios ($F > 1$), equation (6.17) probably overestimates the dependence of the mode of burning proportionality factor on equivalence ratio. The response in trapped equivalence ratio in case TR11 shows a lower peak in comparison with

case TR10. Following from the above argument this results in the reduced discrepancy in cylinder pressures, exhaust temperatures and pressures shown in the former case. Richer fuel/air mixtures are produced in case TR10 because it starts from an initially low load and achieves a maximum fuelling condition in almost the same time as case TR11.

The sudden reduction of demand speed (case TR14) simulates a situation of engine shutoff, in which the governor responds quickly to reduce the input fuel. The rack attains the zero fuelling position after only one cycle duration, hence the spill valve opens very early and prevents the fuel line pressure from building up to the injector opening pressure. It follows that the needle does not lift and no fuel is injected. As a result no combustion occurs inside the cylinders up to cycle number 53 and motored cylinder pressure diagrams are produced. Obviously exhaust temperatures and pressures fall and the turbocharger speed reduces.

A relatively faster deceleration of the turbocharger is predicted due to an underestimation of the turbine power. This is brought about mainly by the simplification of the turbine flow characteristics, due to the limited data available. A single swallowing capacity curve was employed. This in effect overestimates the effective area of the turbine, when running at very low pressure ratios and medium speeds.

Comparisons of predicted and measured response data for combined changes in load and demand speed are shown in Figs. 7.28 to 7.31. The first three cases (TR15, TR16, TR19) consider the engine transient response to increases in the two inputs, whilst case TR23 depicts the response to a reduction in demand speed with an increase in load.

Good agreement between the computed and measured engine speed curves can be observed. Of particular interest is the response of all the parameters during the early stages of the transient (first 16 cycles). This shows a very similar behaviour to a situation where a rapid change in demand speed is imposed at a constant load. This similarity arises from the fact that the load increases very slowly relative to the input variation in governor setting.

For the later stages of the transient period, the computed response of the turbocharger lags slightly. In cases TR15, TR16 and TR19 this appears to result from the fast response of the governor model. As the engine speed approaches the required value, the dynamics of the governor attain a new balancing point, hence the fuel rack is forced to move away from the maximum fuelling position. The resulting decrease in engine torque is seen to coincide with a marked rise in load, and so the engine speed begins to reduce. Again the decrease in speed feeds back to the governor. This responds quickly by reversing the direction of rack travel in order to increase fuelling. The relatively fast response of the governor, which was mentioned earlier, leads to an increased oscillation in rack motion. Subsequently the momentary reduction in fuelling is overrated and a larger dip in exhaust temperature is predicted between cycles 16 and 21. A simultaneous reduction in exhaust pressure also occurs.

Slightly higher end point engine speeds are predicted in cases TR16 and TR19. The same applies to the turbocharger speed and boost pressure. In both cases the measured rack position is seen to bear continuously against the maximum fuelling stop whilst the model rack remains clear off the stop by 3% of its full range travel.

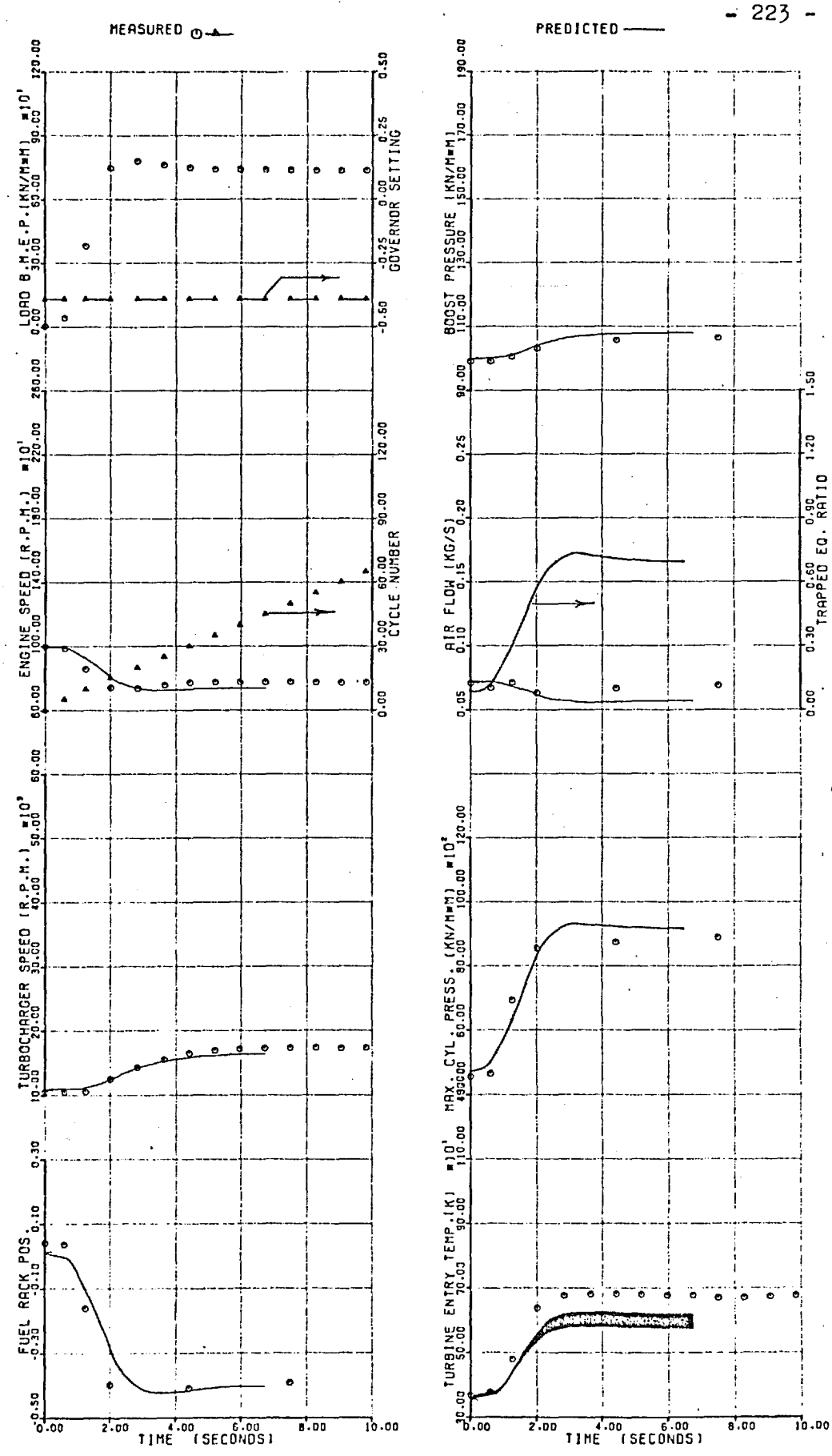


FIG(7.21,a)TRANSIENT CASE TR2

| | LOAD (BMEP BAR) | GOV. SETTING | ENG. SPEED (RPM) |
|---|---|---|---|
| INITIAL | 0.0 | -0.391 | 997.0 |
| FINAL | 7.4 | -0.391 | 772.0 |

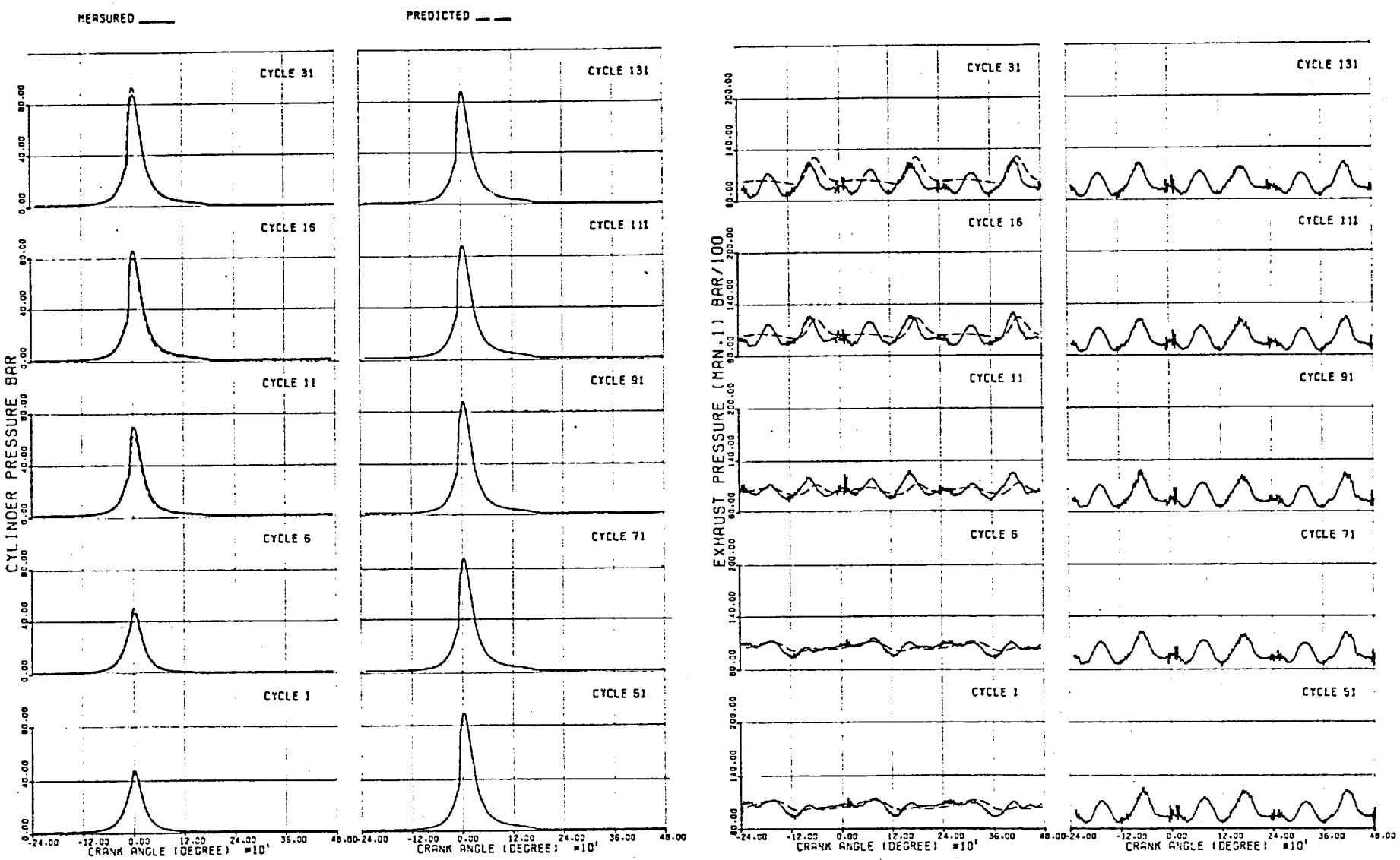


FIG (7.21b) TRANSIENT CASE TR2

| | LOAD (BMEP BAR) | GOV. SETTING | ENG. SPEED (RPM) |
|---|---|---|---|
| INITIAL | 0.0 | -0.391 | 997.0 |
| FINAL | 7.4 | -0.391 | 772.0 |

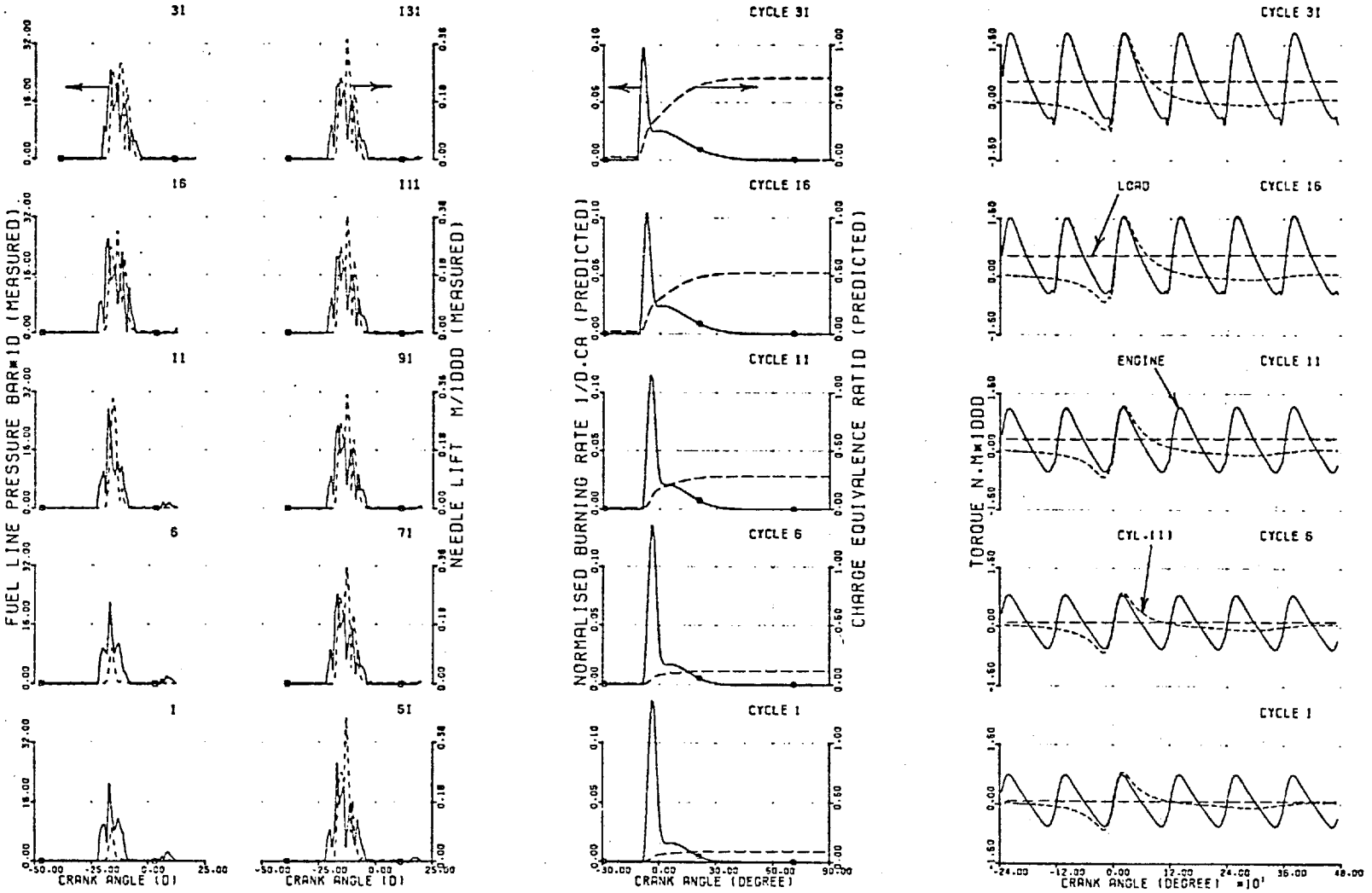


FIG(7.21,c)TRANSIENT CASE TR2

| | LOAD (BMEP BAR) | GOV. SETTING | ENG. SPEED (RPM) |
|---|---|---|---|
| INITIAL | 0.0 | -0.391 | 997.0 |
| FINAL | 7.4 | -0.391 | 772.0 |

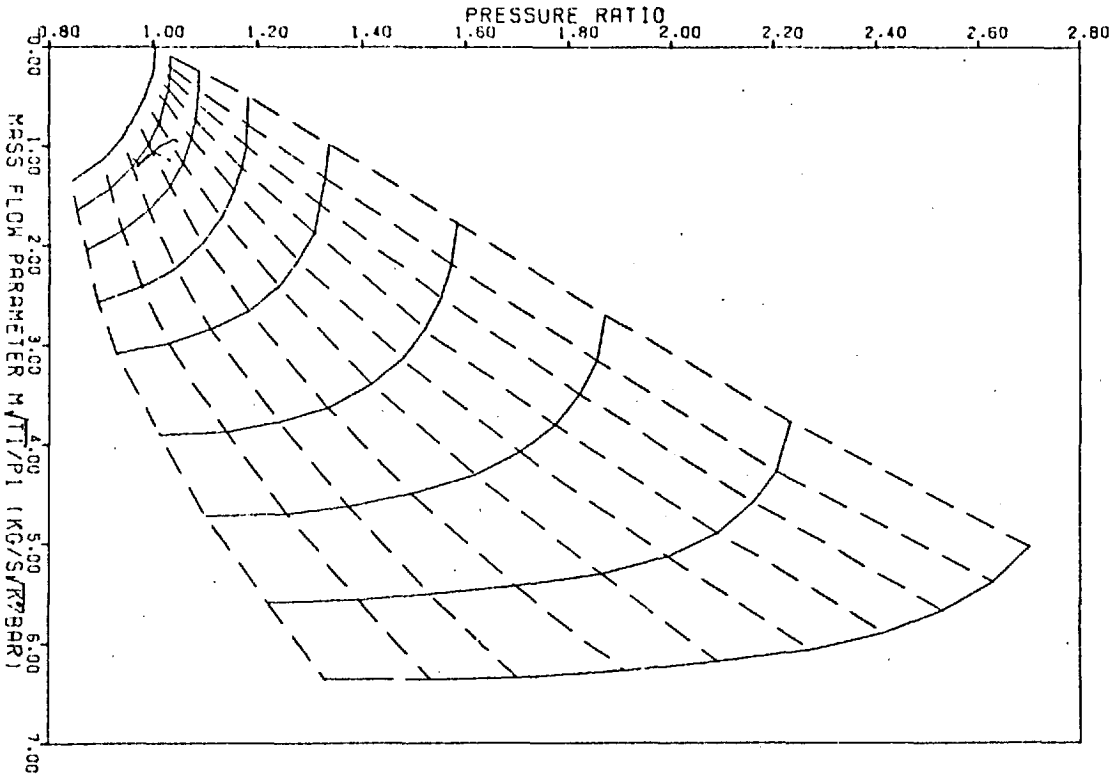


FIG. (7.21,d) TRANSIENT CASE TR2

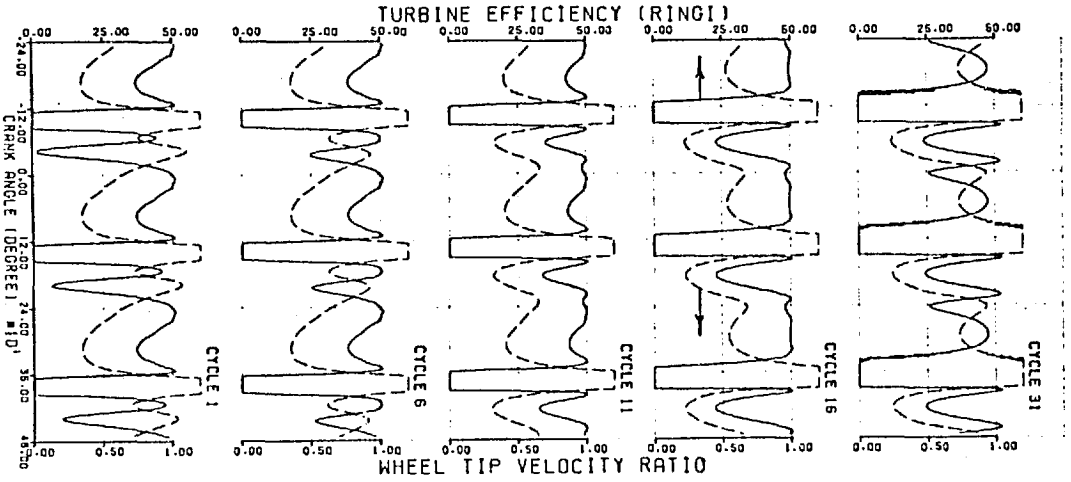

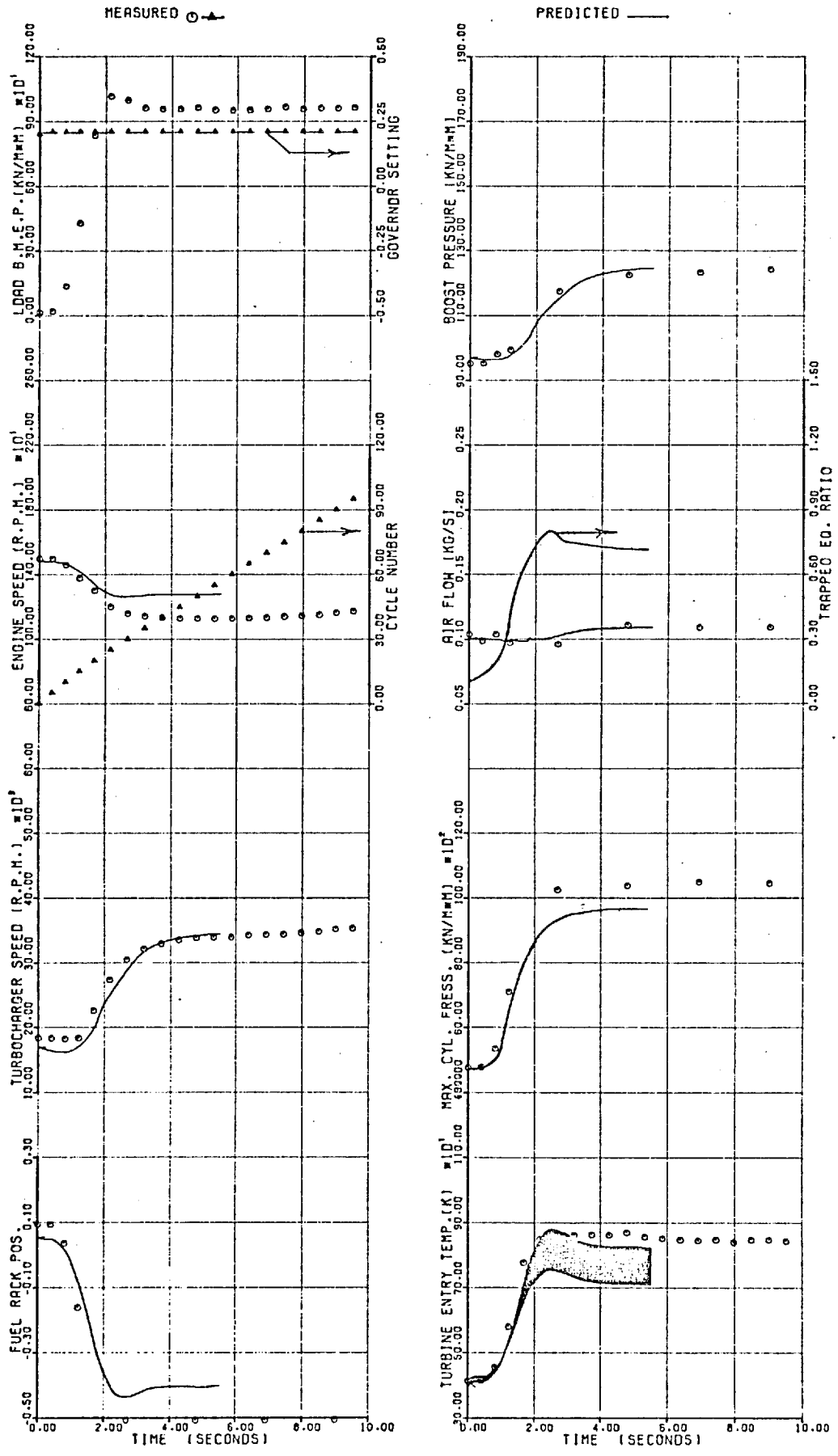


FIG(7.22,a) TRANSIENT CASE TR4

| | LOAD (BMEP BAR) | GOV. SETTING | ENG. SPEED (RPM) |
|---|---|---|---|
| INITIAL | 0.15 | 0.201 | 1498.0 |
| FINAL | 10.09 | 0.201 | 1242.0 |

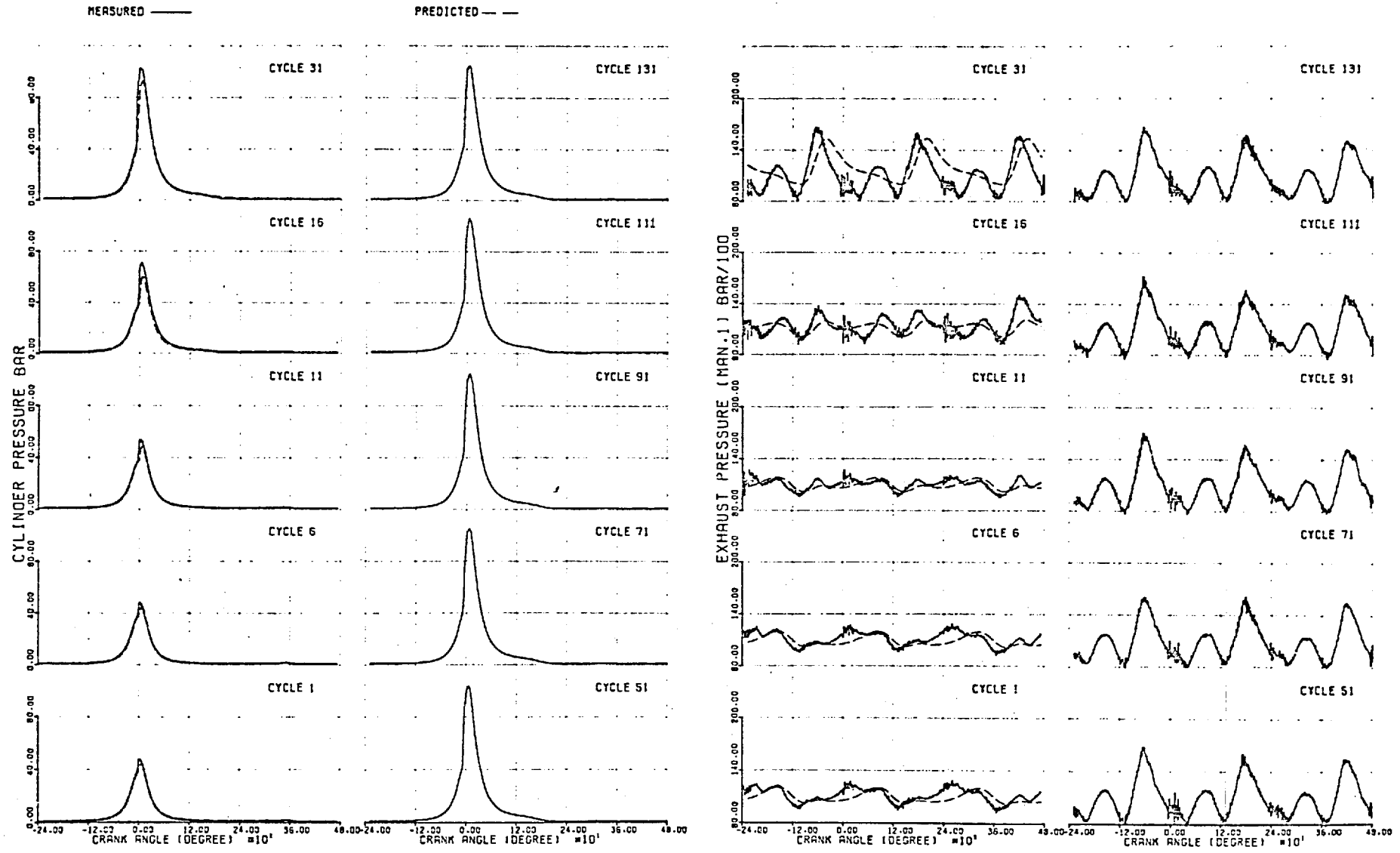


FIG(7.22b)TRANSIENT CASE TR4

| | LOAD (BMEP BAR) | GOV. SETTING | ENG. SPEED (RPM) |
|---|---|---|---|
| INITIAL | 0.15 | 0.201 | 1498.0 |
| FINAL | 10.09 | 0.201 | 1242.0 |

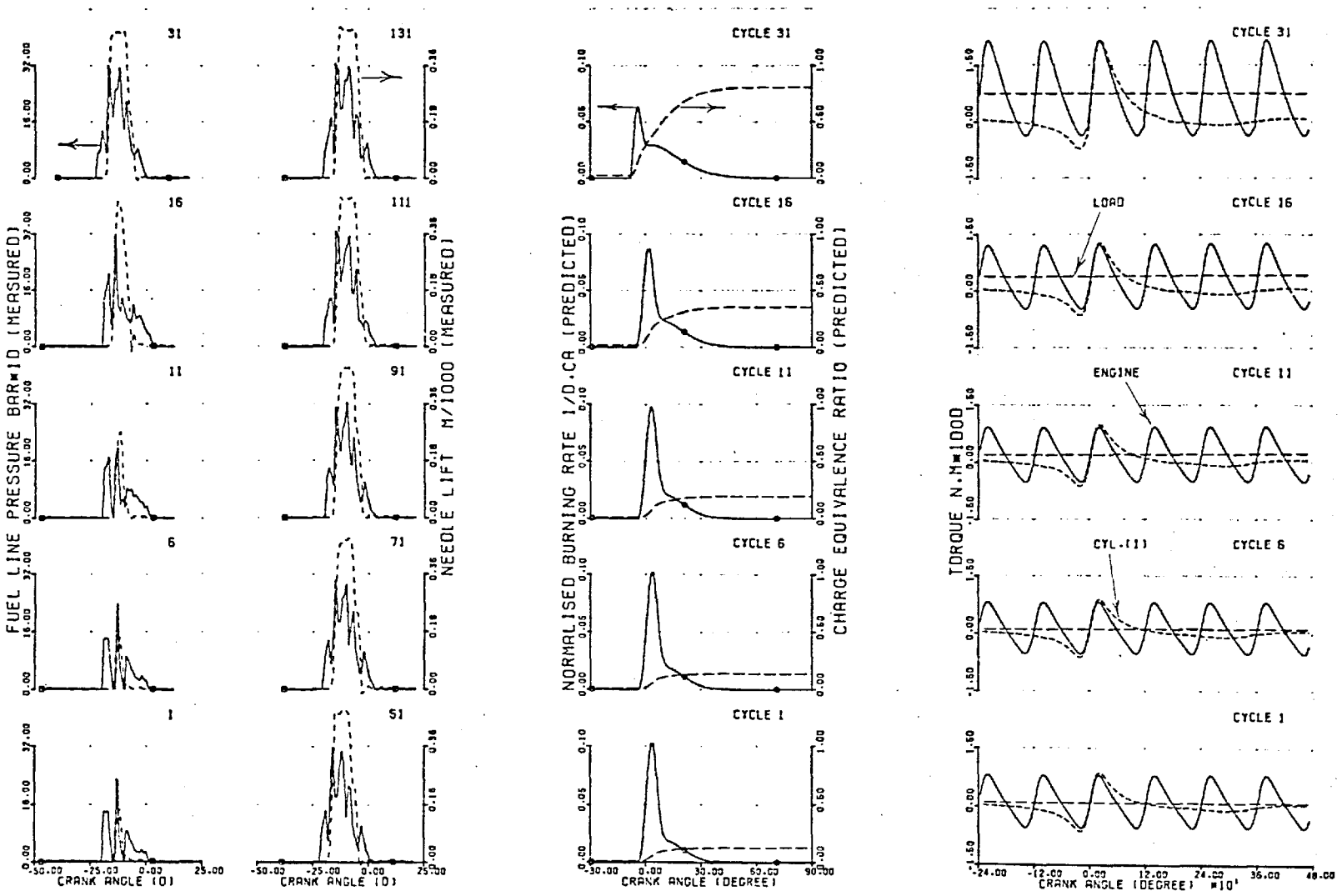


FIG(7.22c)TRANSIENT CASE TR4

| | LOAD (BMEP BAR) | GOV. SETTING | ENG. SPEED (RPM) |
|---|---|---|---|
| INITIAL | 0.15 | 0.201 | 1498.0 |
| FINAL | 10.09 | 0.201 | 1242.0 |

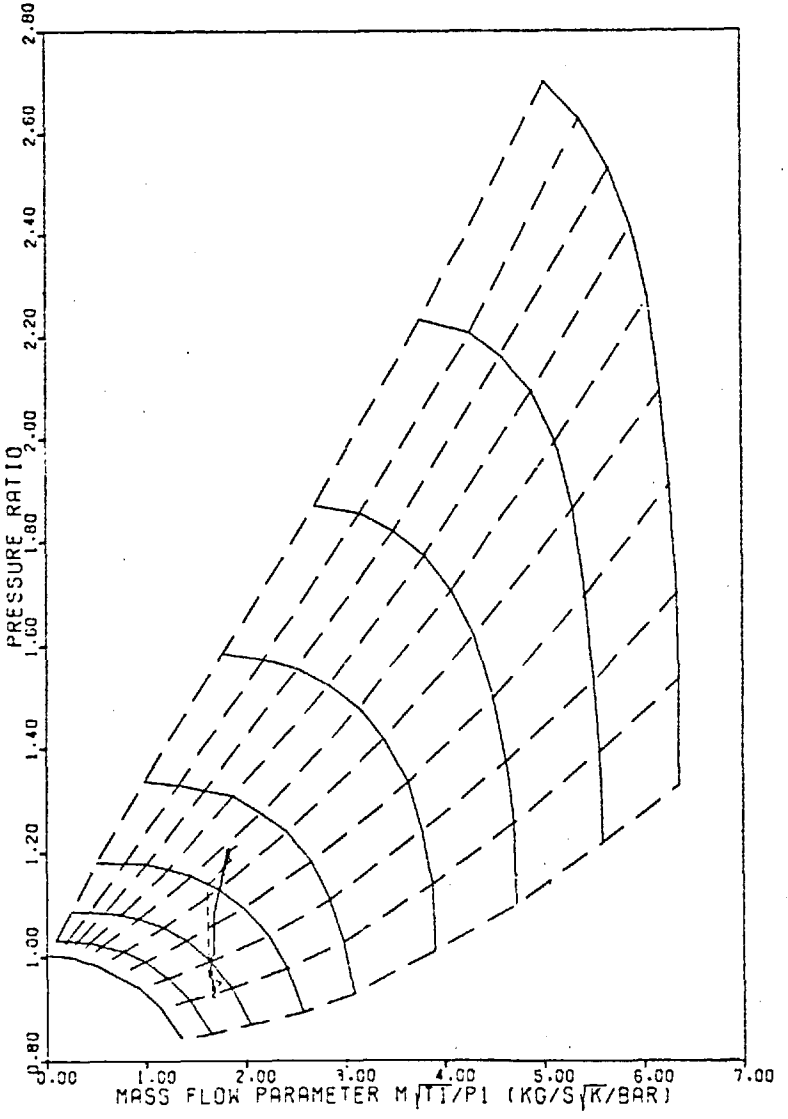


FIG. (7.22,d)

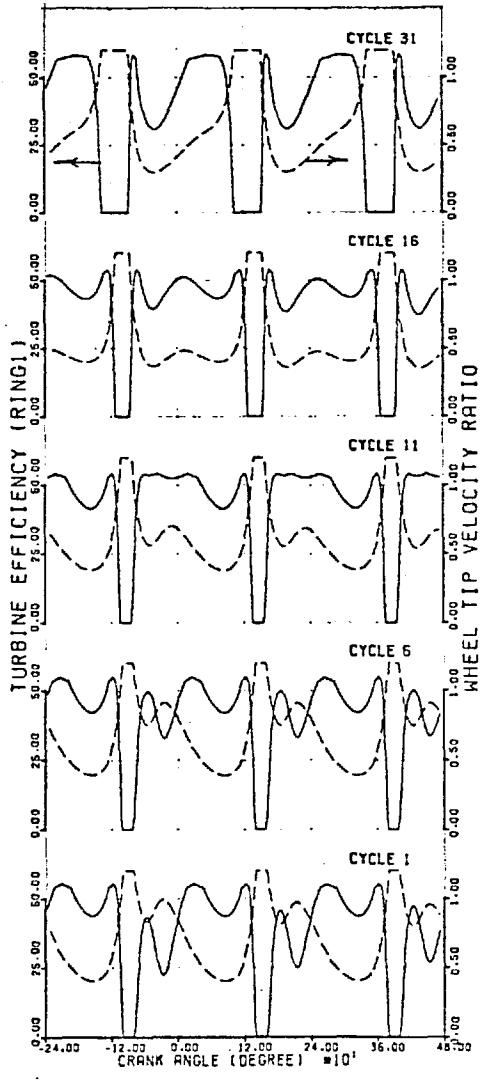


TRANSIENT CASE TR4

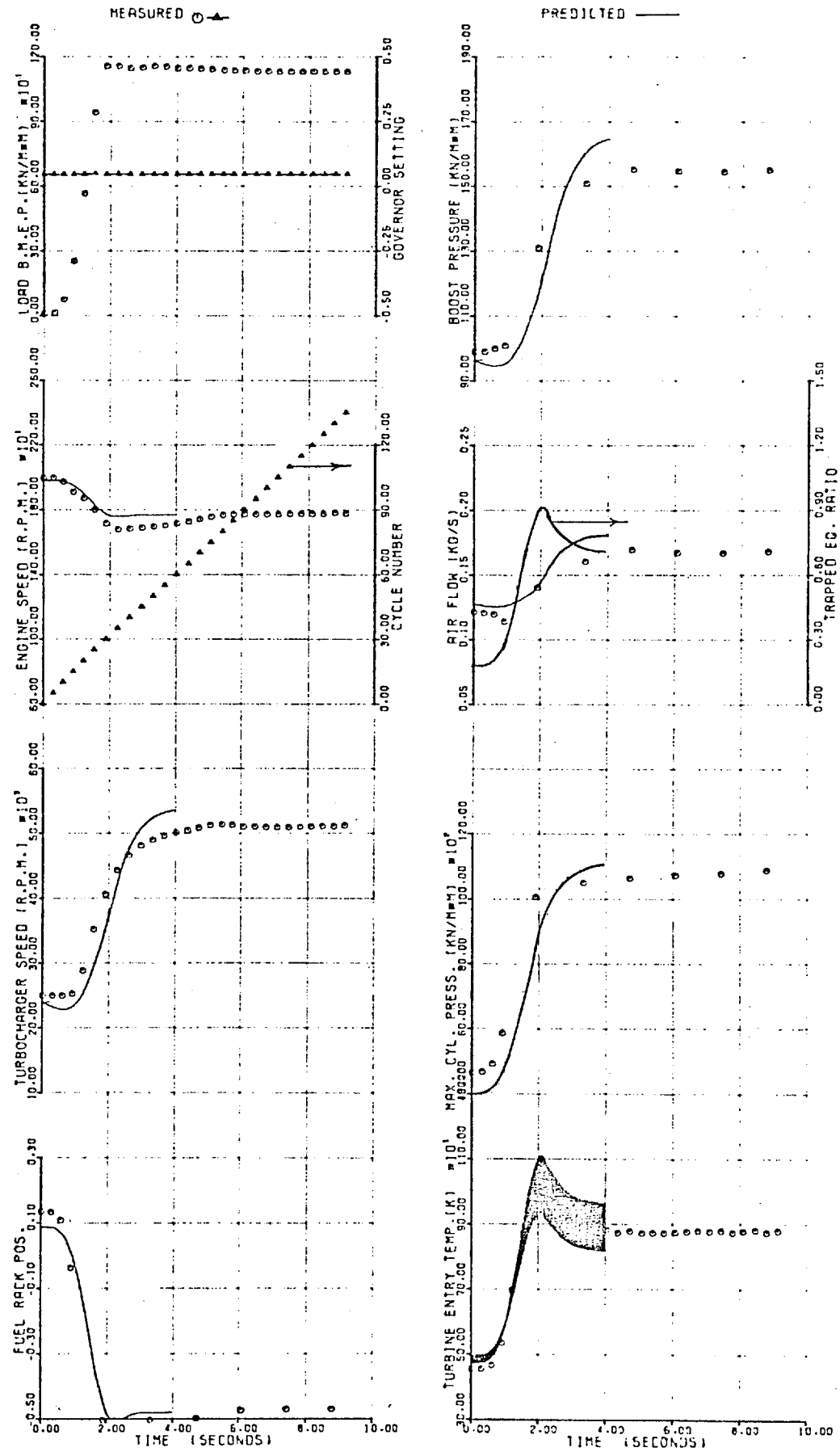


FIG(7.23,a) TRANSIENT CASE TR6

| | LOAD (BMEP BAR) | GOV. SETTING | ENG. SPEED (RPM) |
|---|---|---|---|
| INITIAL | 0.1 | 0.046 | 1994.0 |
| FINAL | 11.3 | 0.046 | 1777.0 |

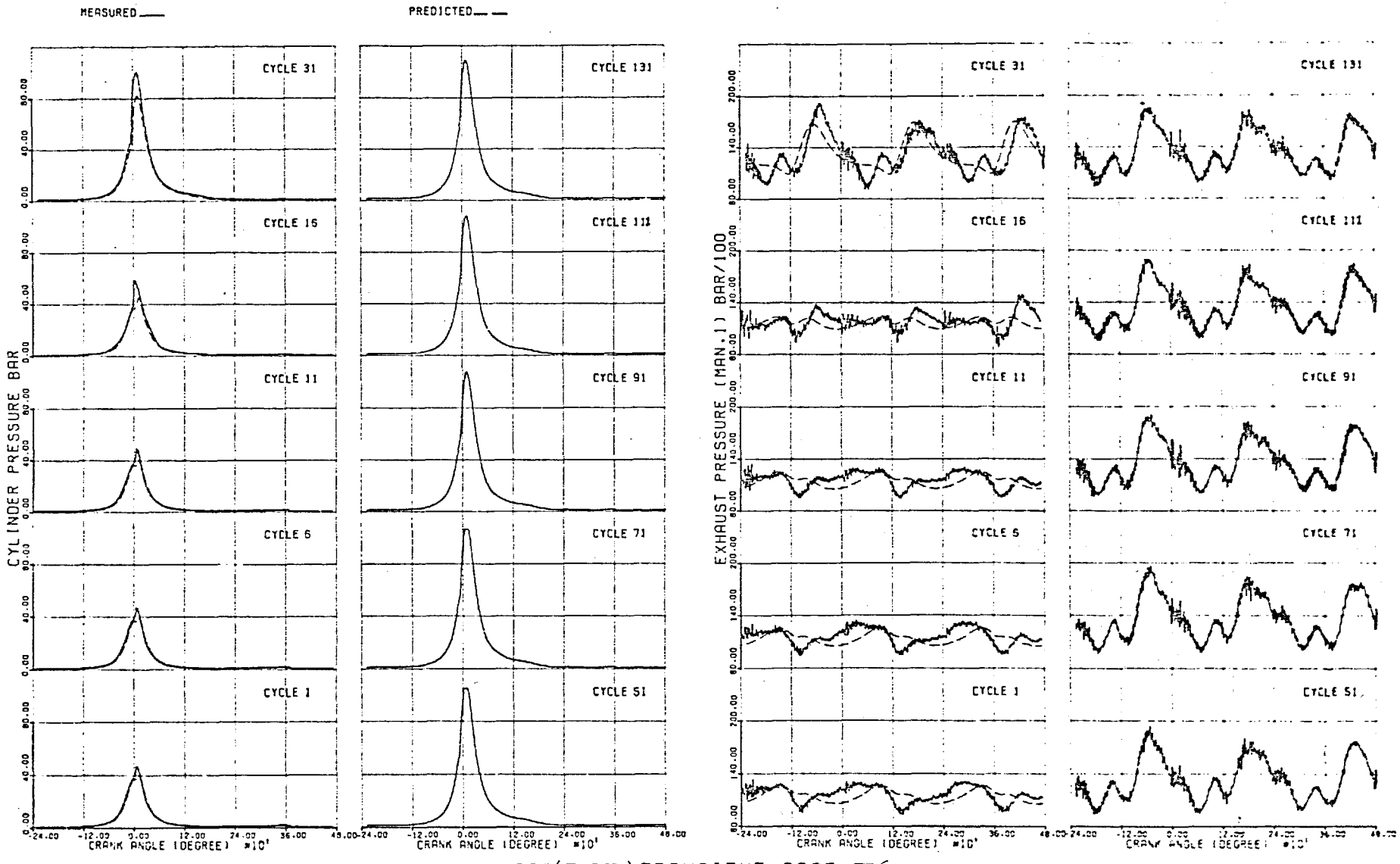


FIG(7.23b) TRANSIENT CASE TR6

| | LOAD (BMEP BAR) | GOV. SETTING | ENG. SPEED (RPM) |
|---|---|---|---|
| INITIAL | 0.1 | 0.046 | 1994.0 |
| FINAL | 11.3 | 0.046 | 1777.0 |

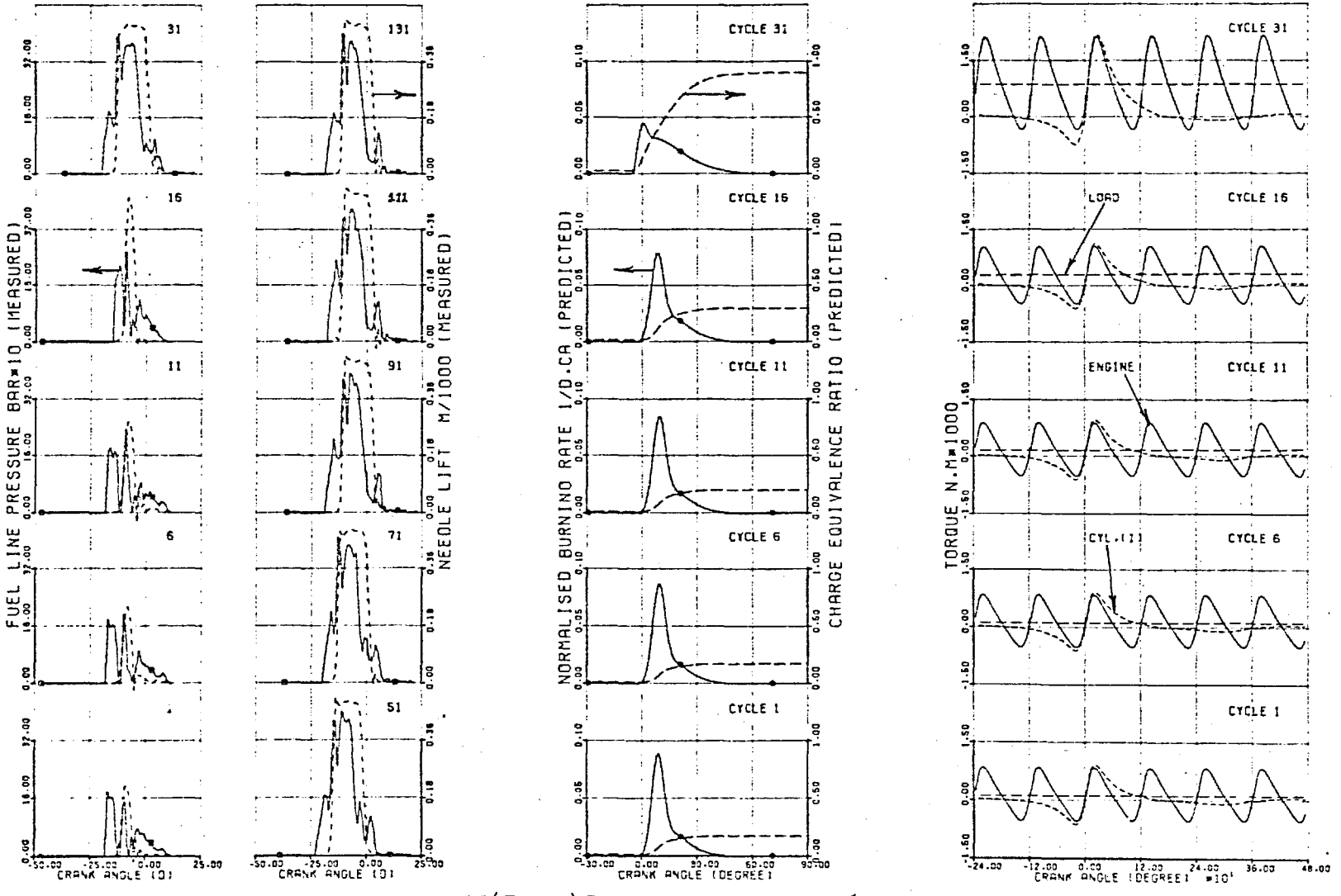


FIG(7.23c) TRANSIENT CASE TR6

| | LOAD (BMEP BAR) | GOV. SETTING | ENG. SPEED (RPM) |
|---|---|---|---|
| INITIAL | 0.1 | 0.046 | 1994.0 |
| FINAL | 11.3 | 0.046 | 1777.0 |

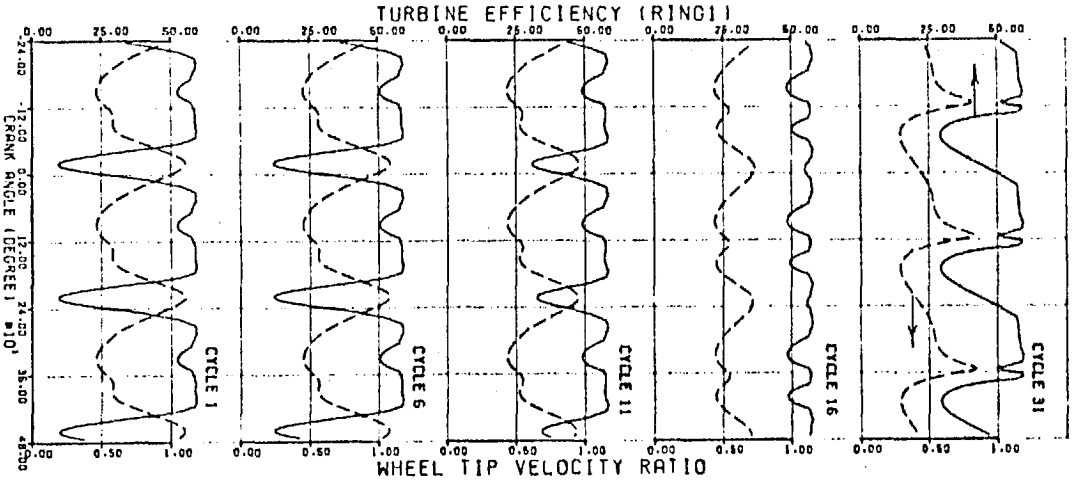


TRANSIENT CASE TR6

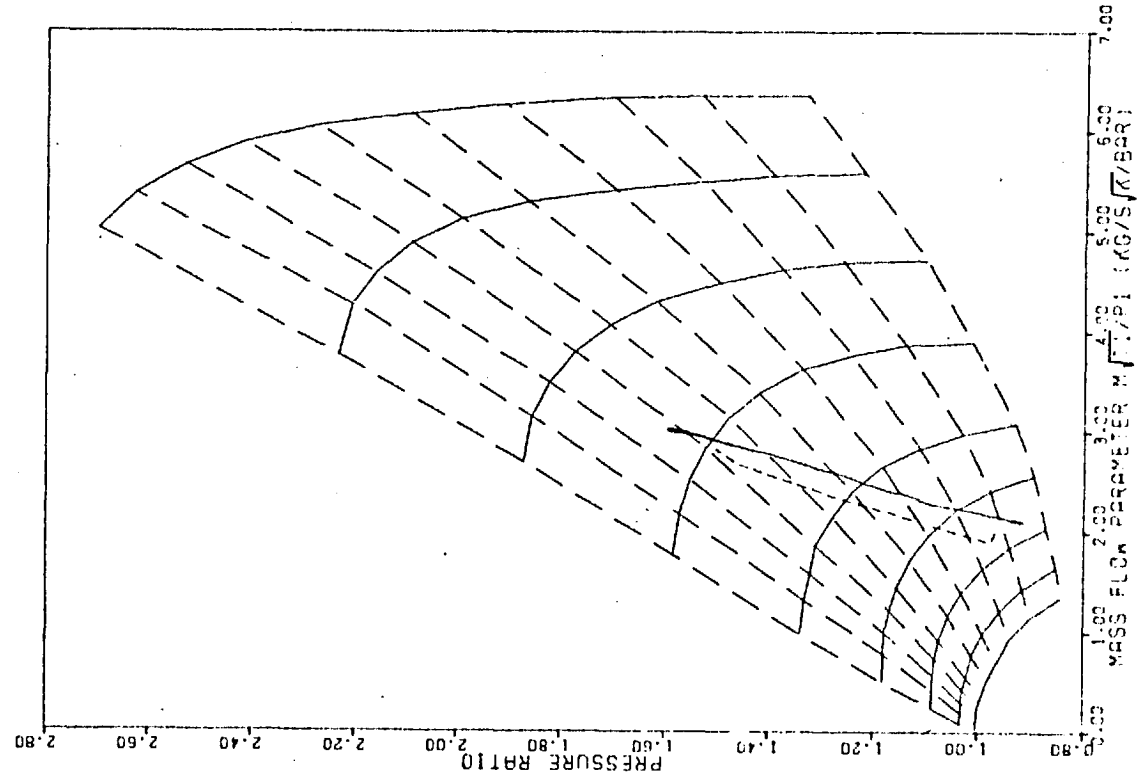


FIG. (7.23,d)

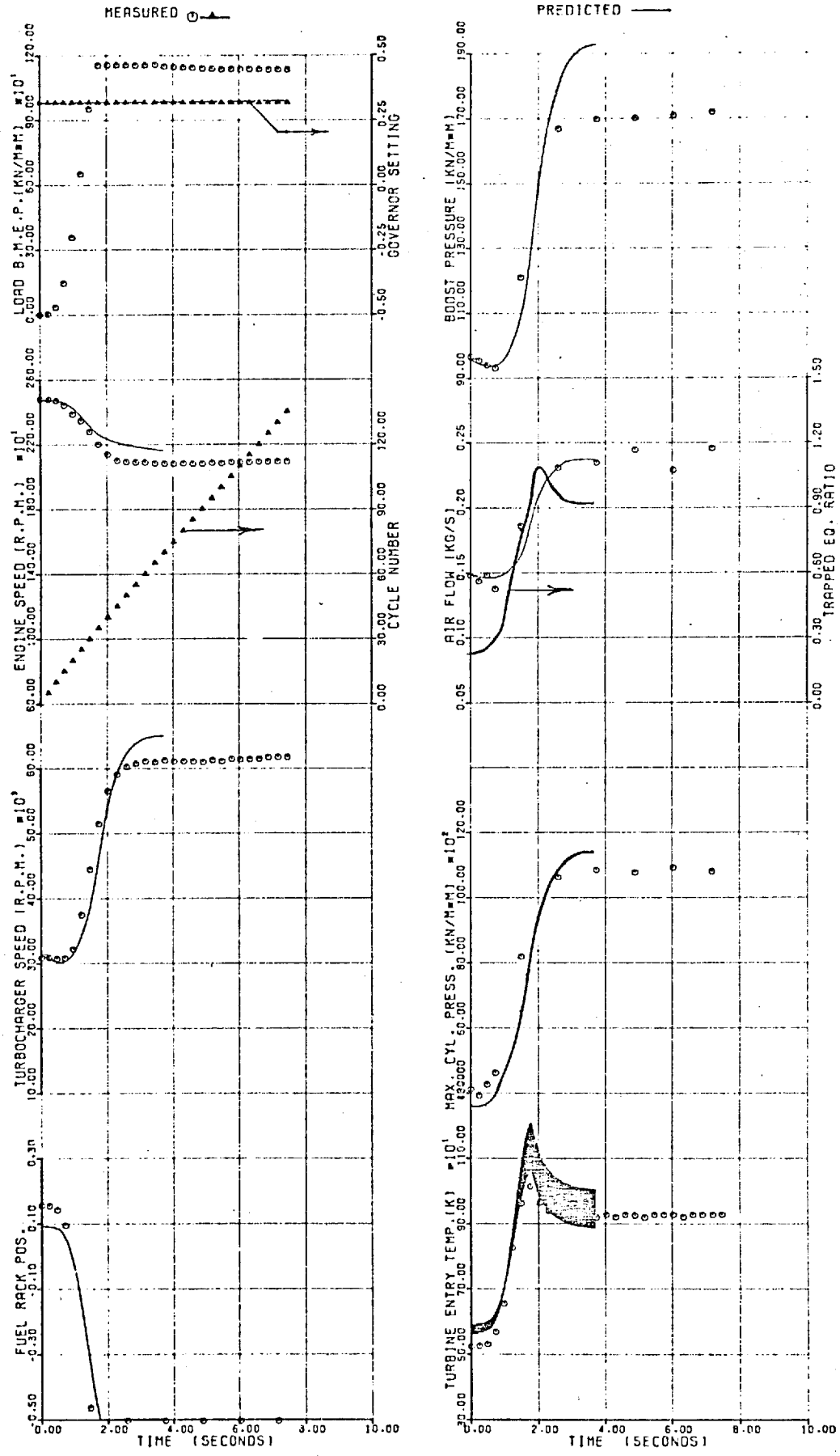


FIG(7.24,a)TRANSIENT CASE TR8

| | LOAD (BMEP BAR) | GOV. SETTING | ENG. SPEED (RPM) |
|---|---|---|---|
| INITIAL | 0.0 | 0.317 | 2479.0 |
| FINAL | 11.3 | 0.317 | 2092.0 |

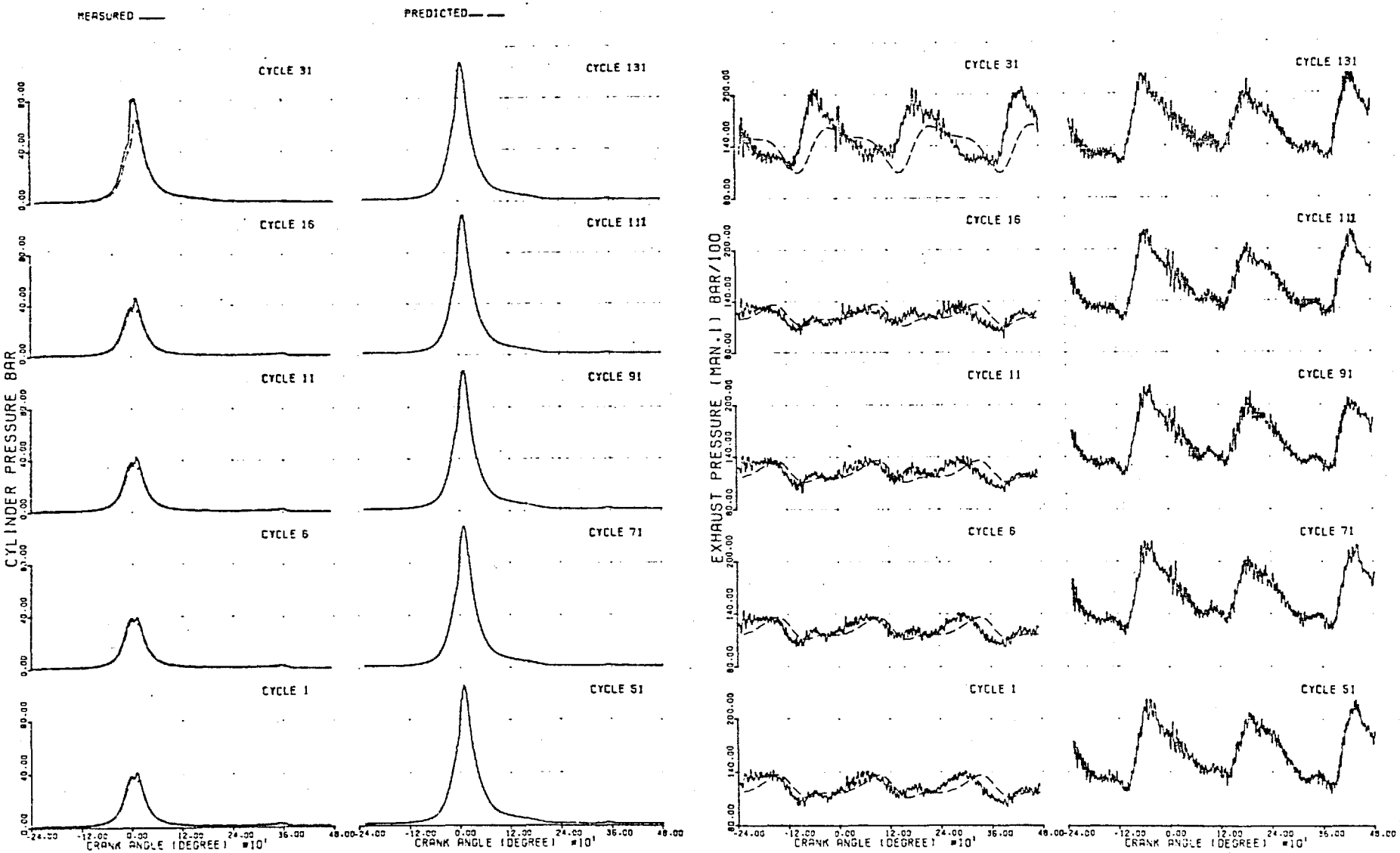


FIG(7.24b) TRANSIENT CASE TR8

| | LOAD (BMEP BAR) | GOV. SETTING | ENG. SPEED (RPM) |
|---|---|---|---|
| INITIAL | 0.0 | 0.317 | 2479.0 |
| FINAL | 11.3 | 0.317 | 2092.0 |

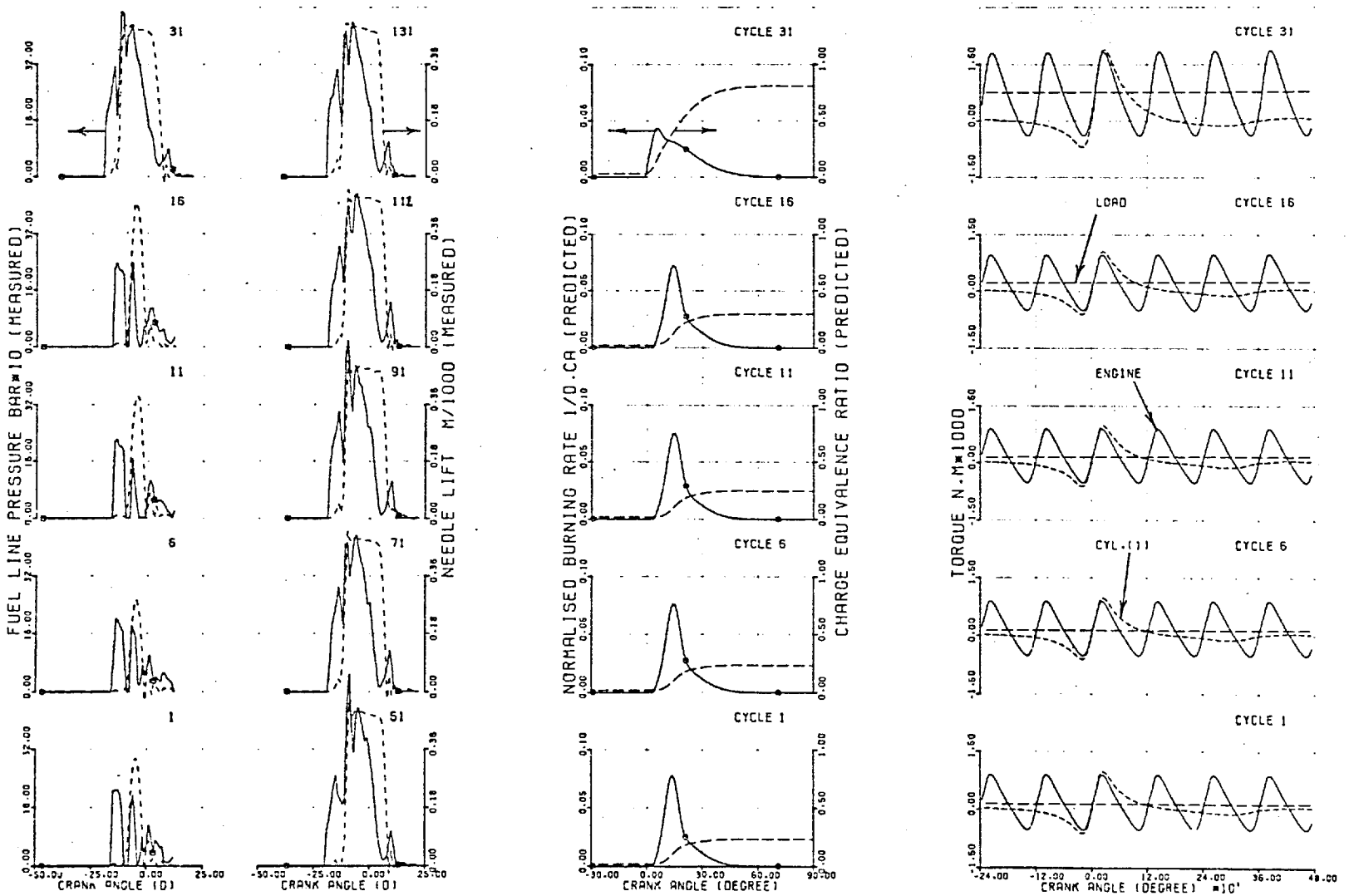


FIG (7.24c) TRANSIENT CASE TR8

| | LOAD (BMEP BAR) | GOV. SETTING | ENG. SPEED (RPM) |
|---|---|---|---|
| INITIAL | 0.0 | 0.317 | 2479.0 |
| FINAL | 11.3 | 0.317 | 2092.0 |

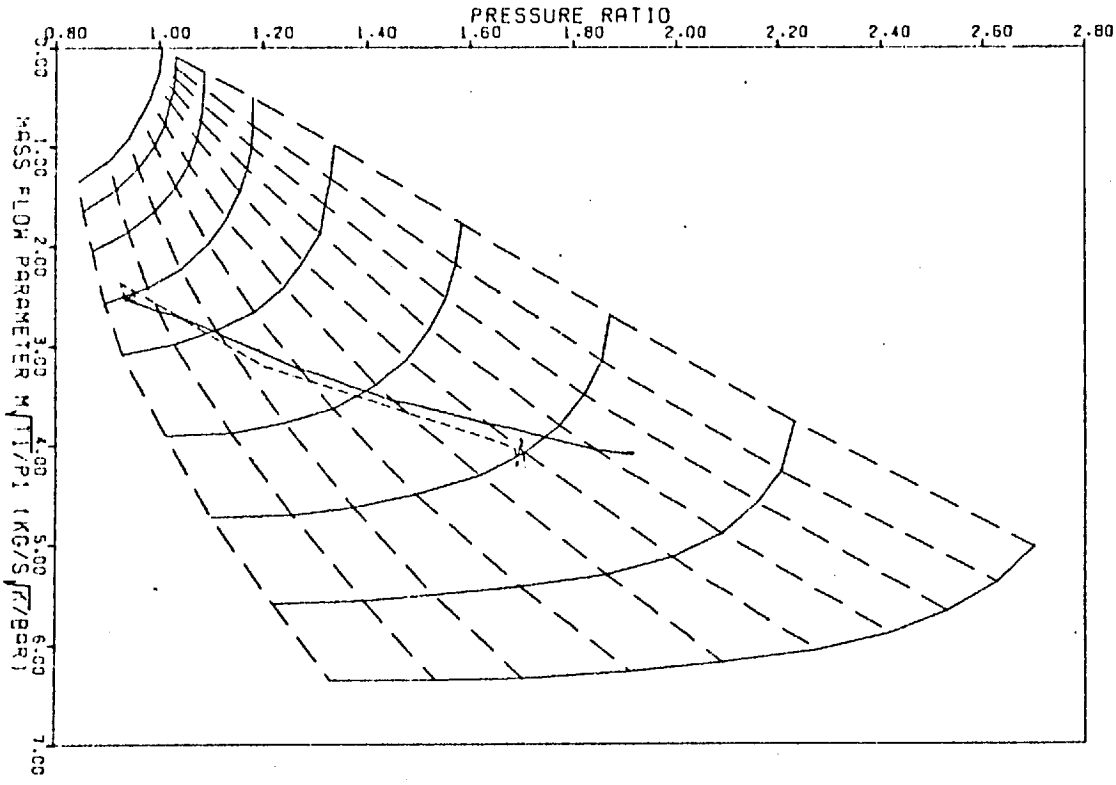


FIG. (7.24,d) TRANSIENT CASE TR8

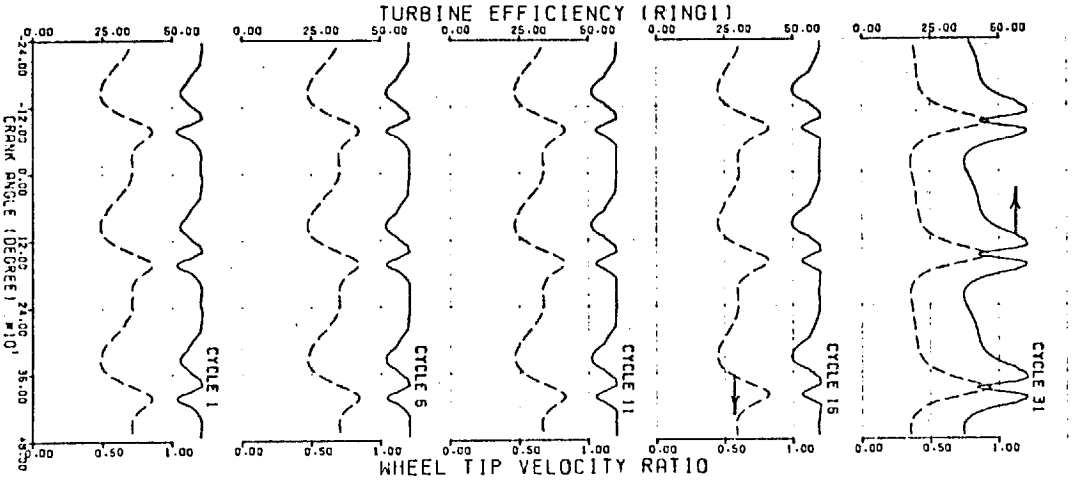

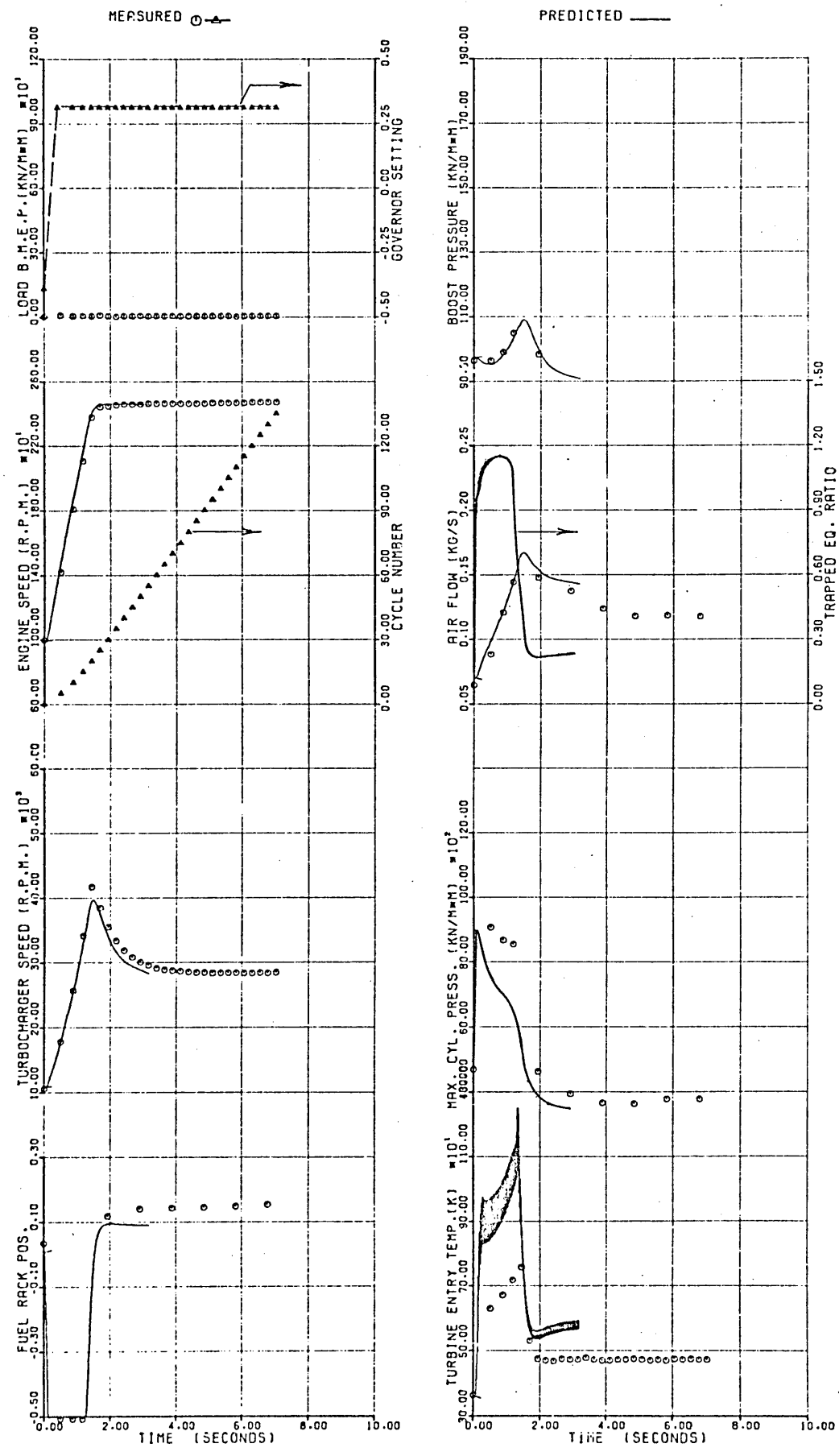


FIG(7.25,a) TRANSIENT CASE TR10

| | LOAD (BMEP BAR) | GOV. SETTING | ENG. SPEED (RPM) |
|---|---|---|---|
| INITIAL | 0.0 | -0.391 | 998.0 |
| FINAL | 0.0 | 0.312 | 2471.0 |

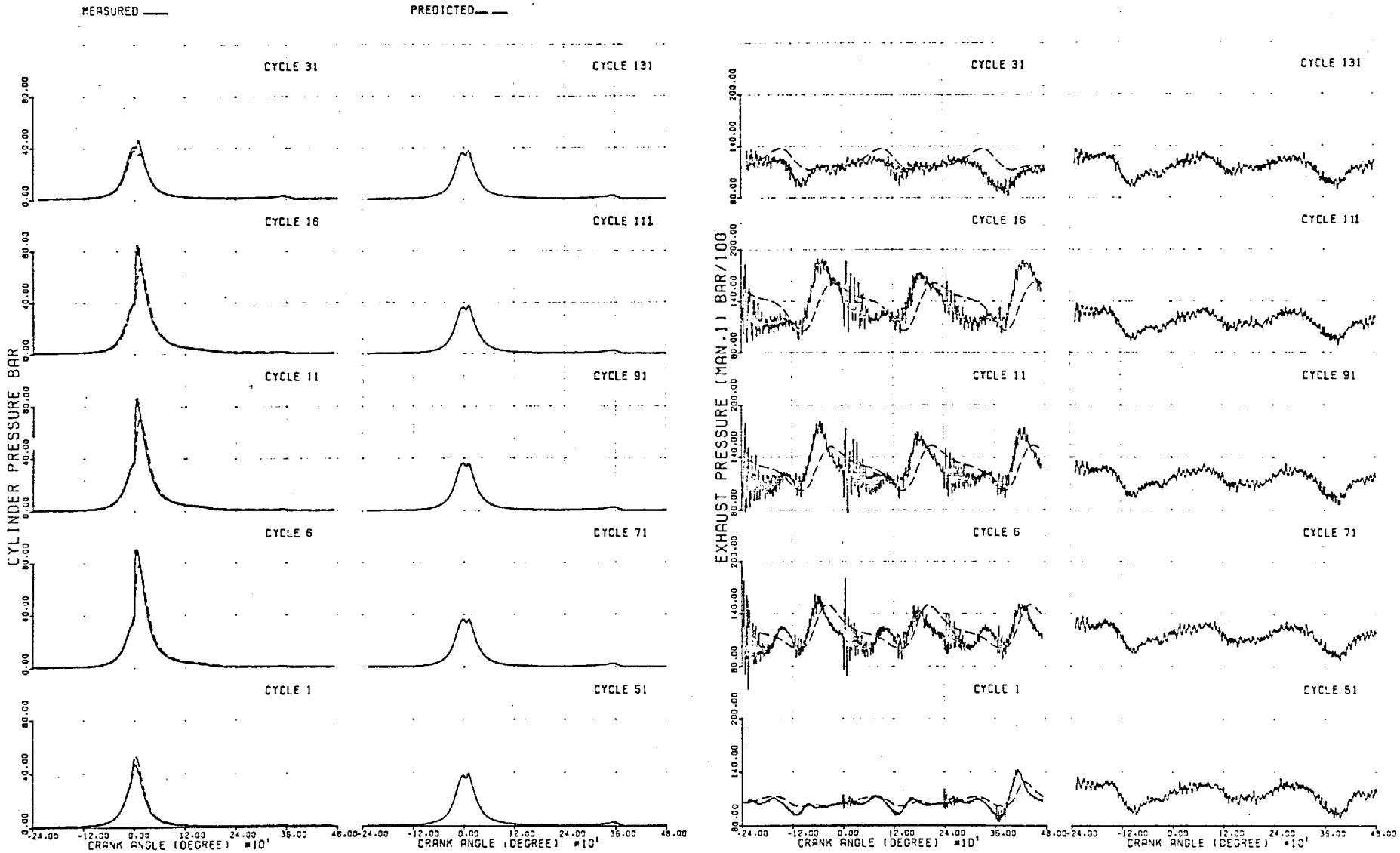


FIG (7.25b) TRANSIENT CASE TR10

| | LOAD (BMEP BAR) | GOV. SETTING | ENG. SPEED (RPM) |
|---|---|---|---|
| INITIAL | 0.0 | -0.391 | 998.0 |
| FINAL | 0.0 | 0.312 | 2471.0 |

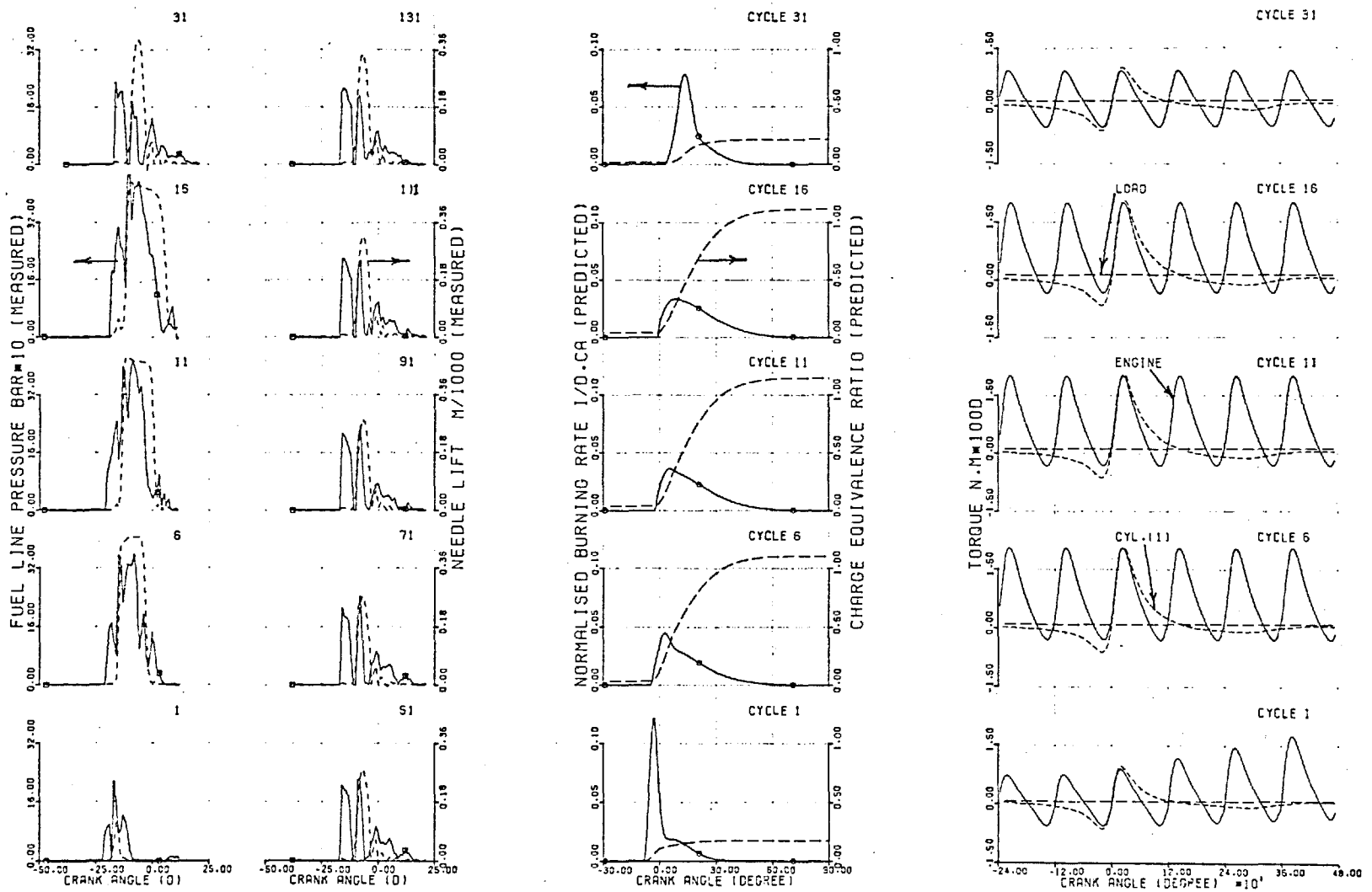


FIG(7.25c) TRANSIENT CASE TR10

| | LOAD (BMEP BAR) | GOV. SETTING | ENG. SPEED (RPM) |
|---|---|---|---|
| INITIAL | 0.0 | -0.391 | 998.0 |
| FINAL | 0.0 | 0.312 | 2471.0 |

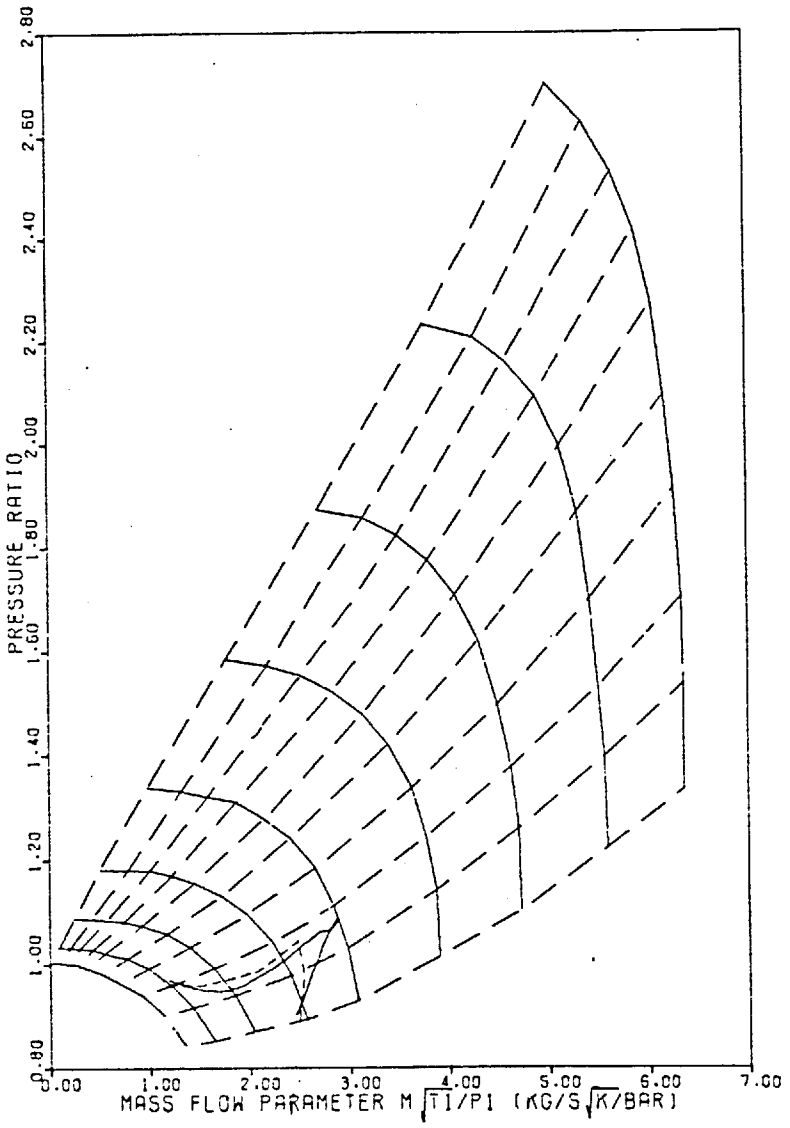


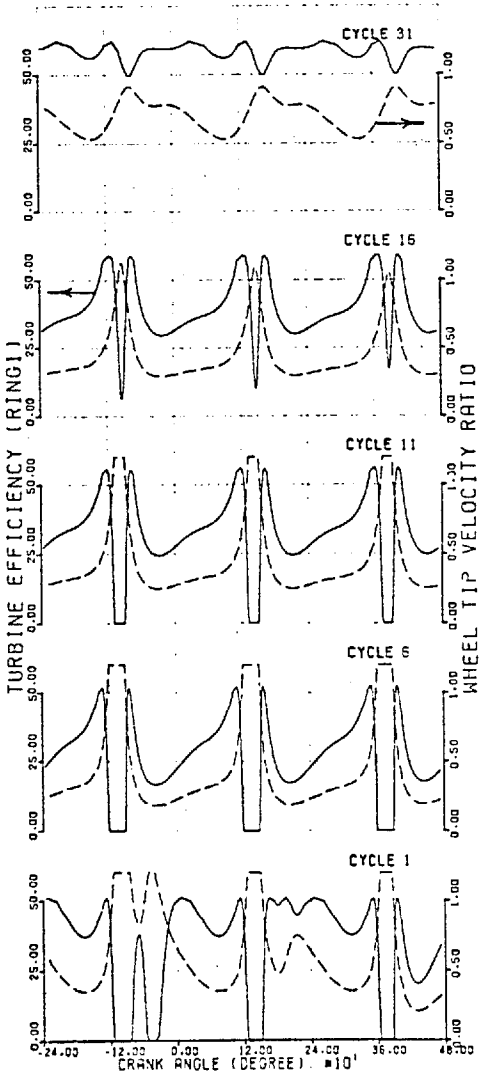


FIG. (7.25,d) TRANSIENT CASE TR10

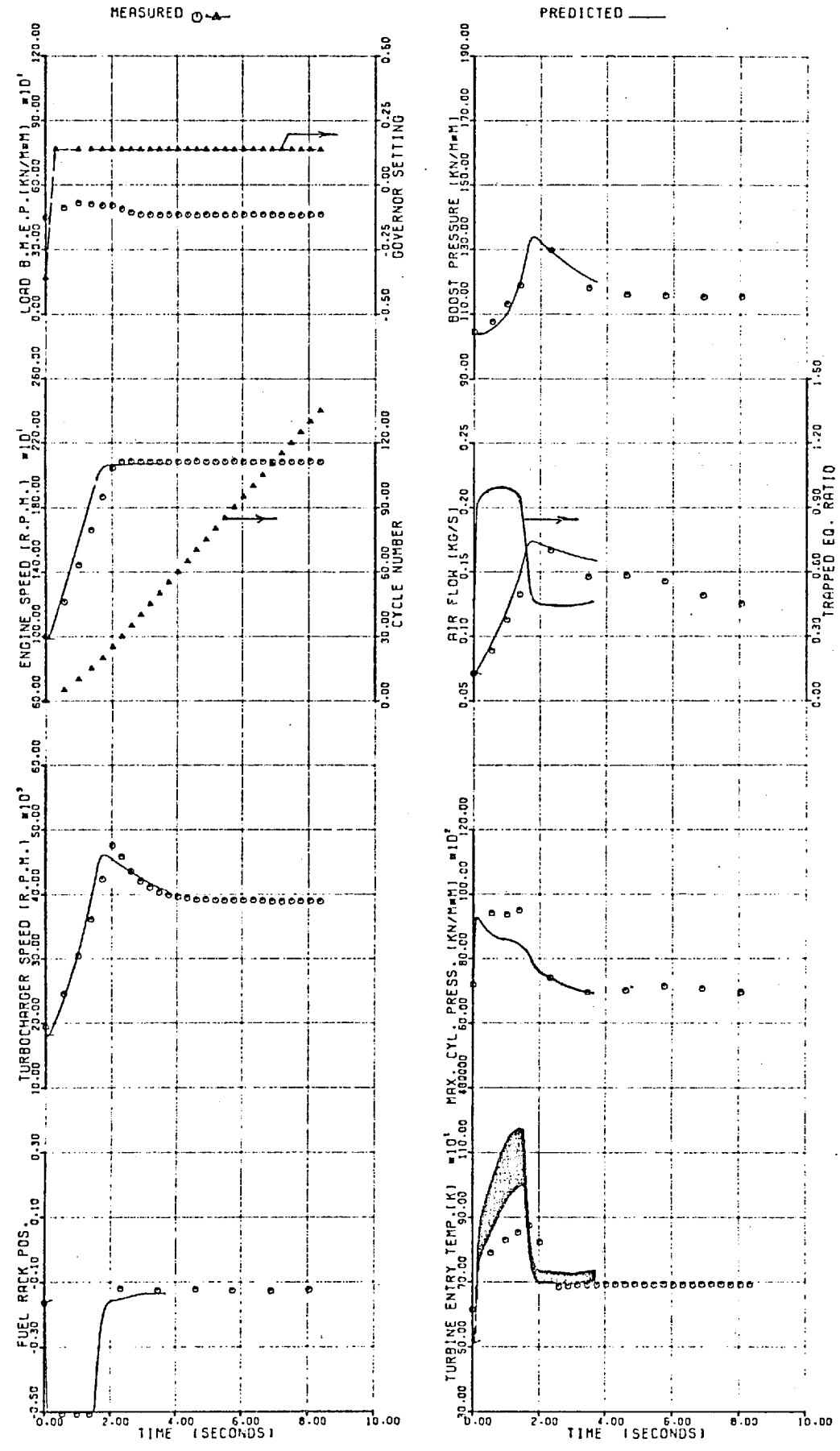


FIG (7.26a) TRANSIENT CASE TR11

| | LOAD (BMEP BAR) | GOV. SETTING | ENG. SPEED (RPM) |
|---|---|---|---|
| INITIAL | 4.5 | -0.360 | 1001.0 |
| FINAL | 4.6 | 0.138 | 2083.0 |

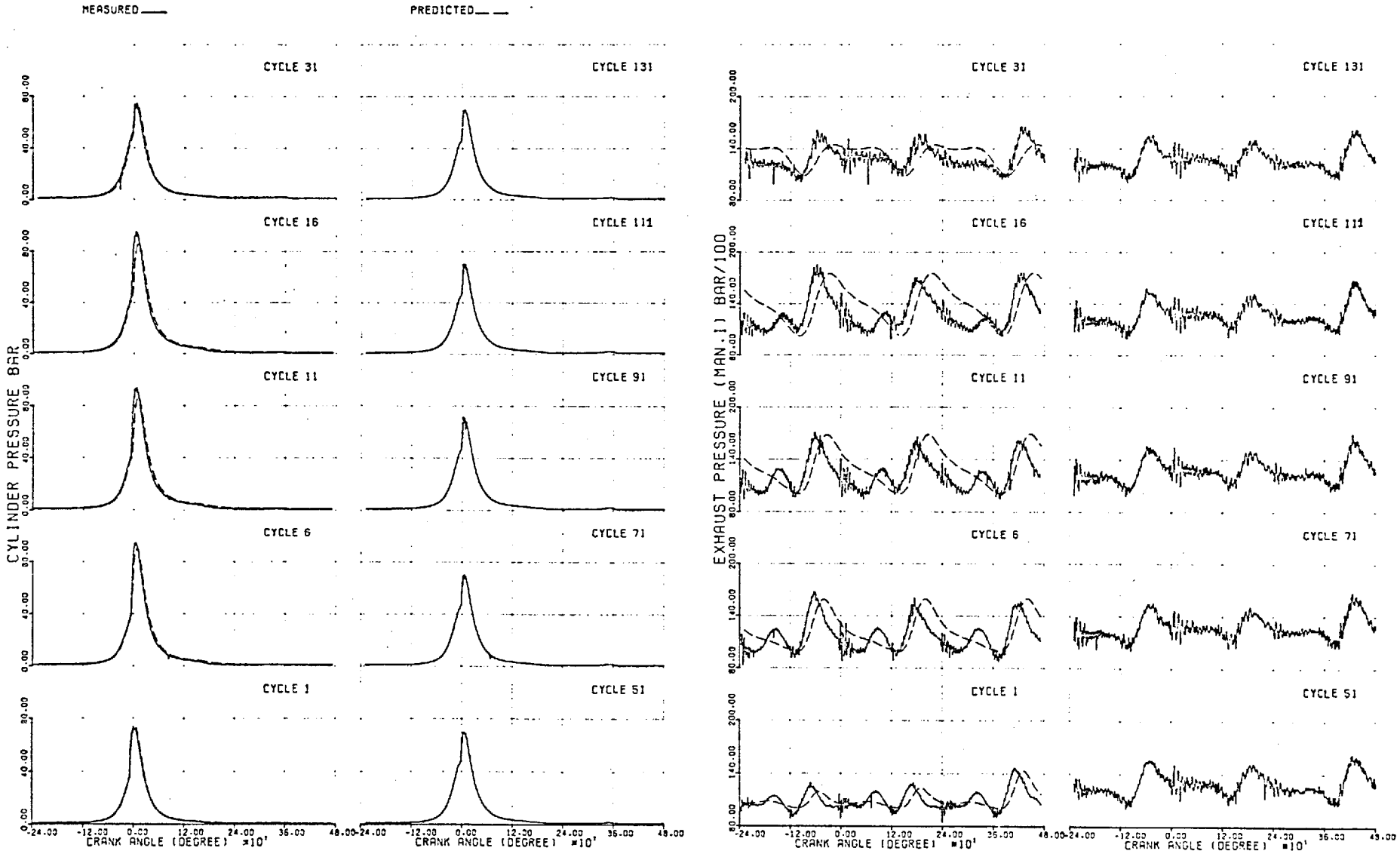


FIG(7.26b)TRANSIENT CASE TR11

| | LOAD (BMEP BAR) | GOV. SETTING | ENG. SPEED (RPM) |
|---|---|---|---|
| INITIAL | 4.5 | -0.360 | 1001.0 |
| FINAL | 4.6 | 0.138 | 2083.0 |

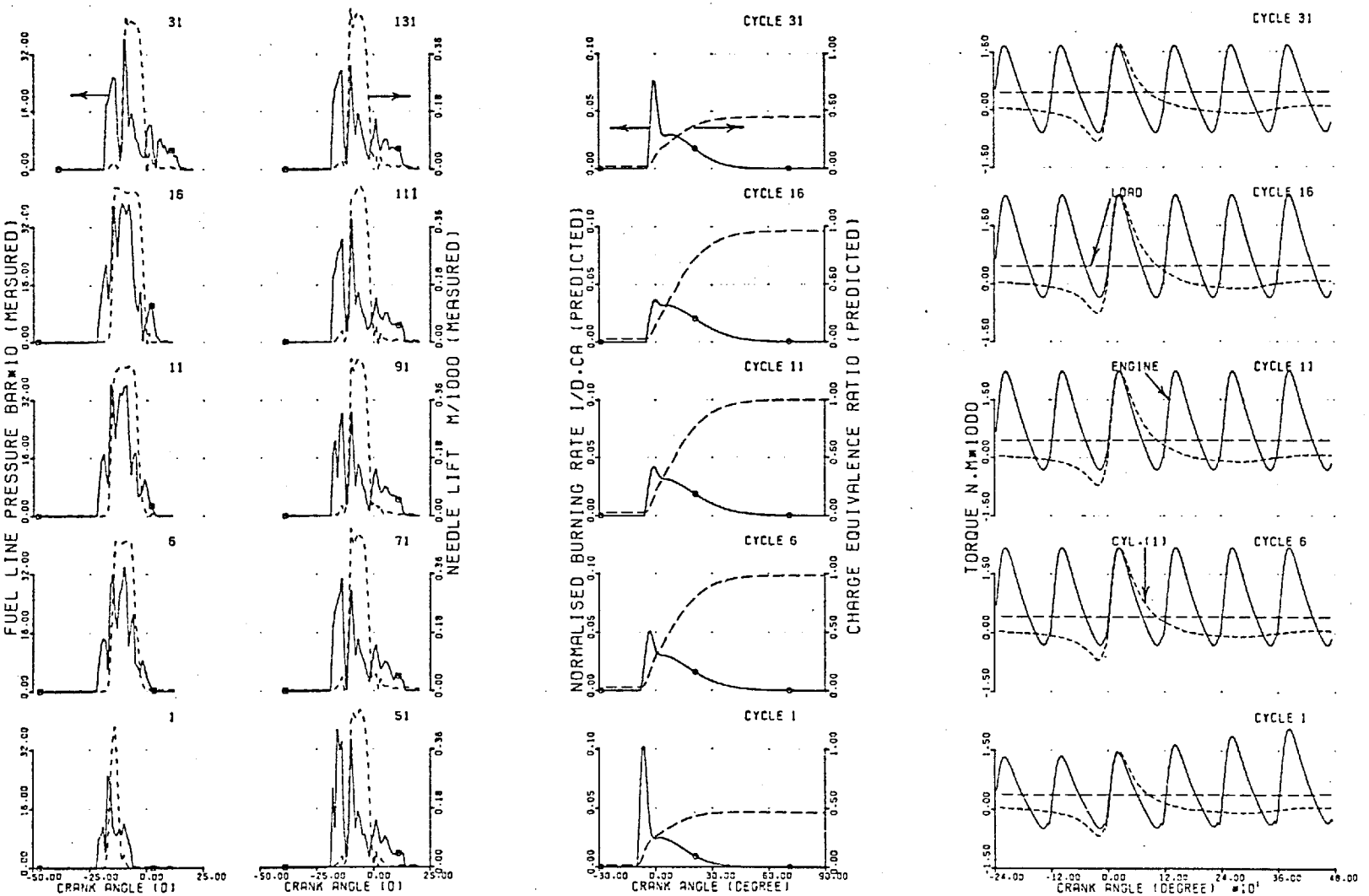


FIG(7.26c)TRANSIENT CASE TR11

| | LOAD (BMEP BAR) | GOV. SETTING | ENG. SPEED (RPM) |
|---|---|---|---|
| INITIAL | 4.5 | -0.360 | 1001.0 |
| FINAL | 4.6 | 0.138 | 2083.0 |

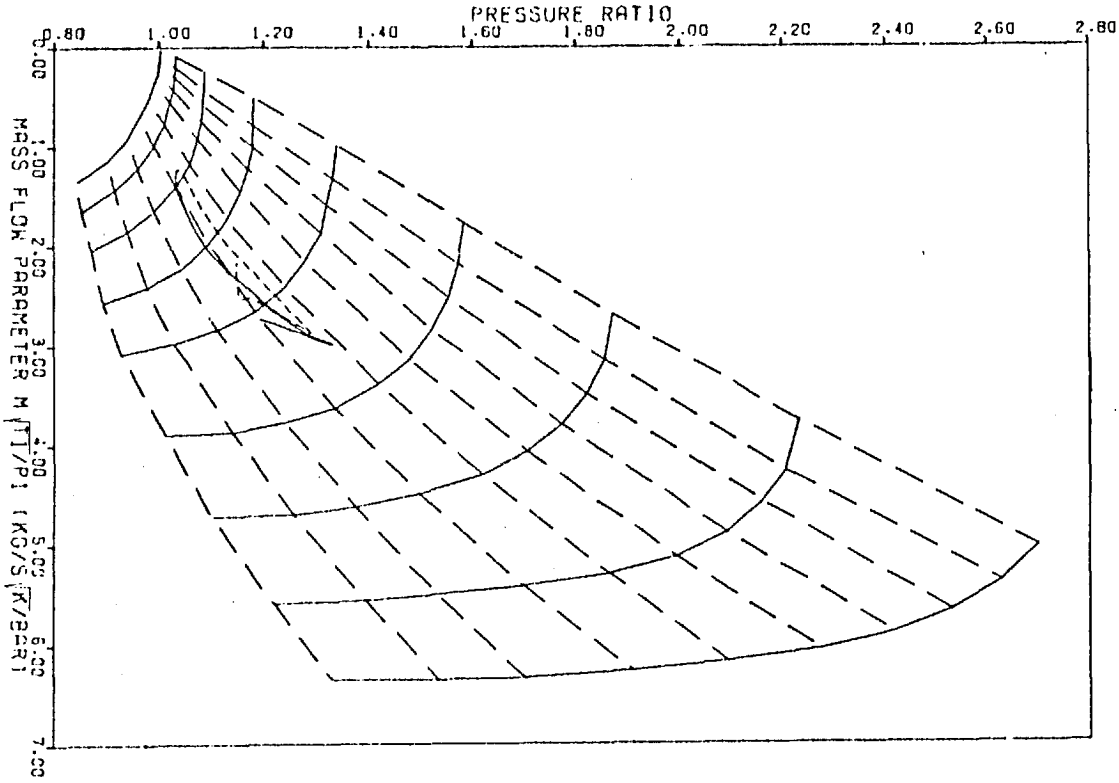


FIG. (7.26,d)

TRANSIENT CASE TR11

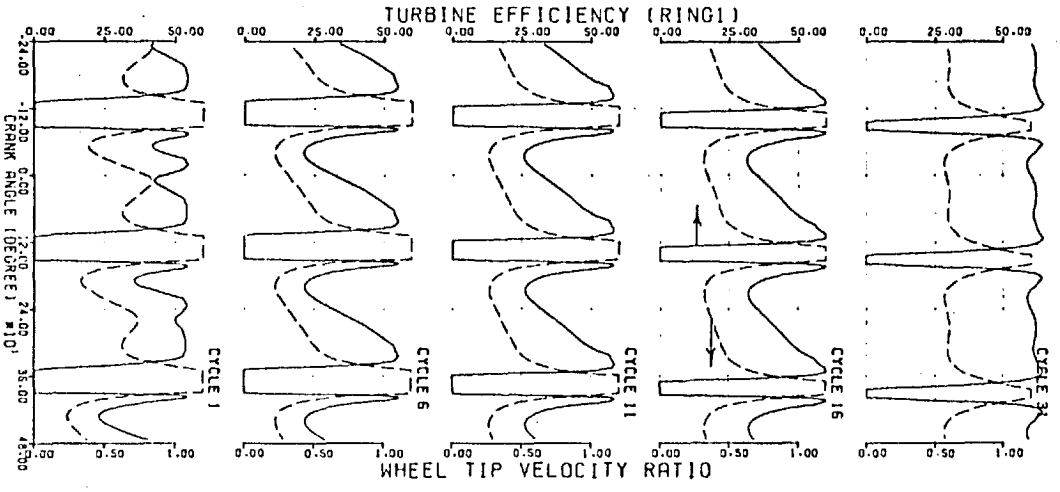

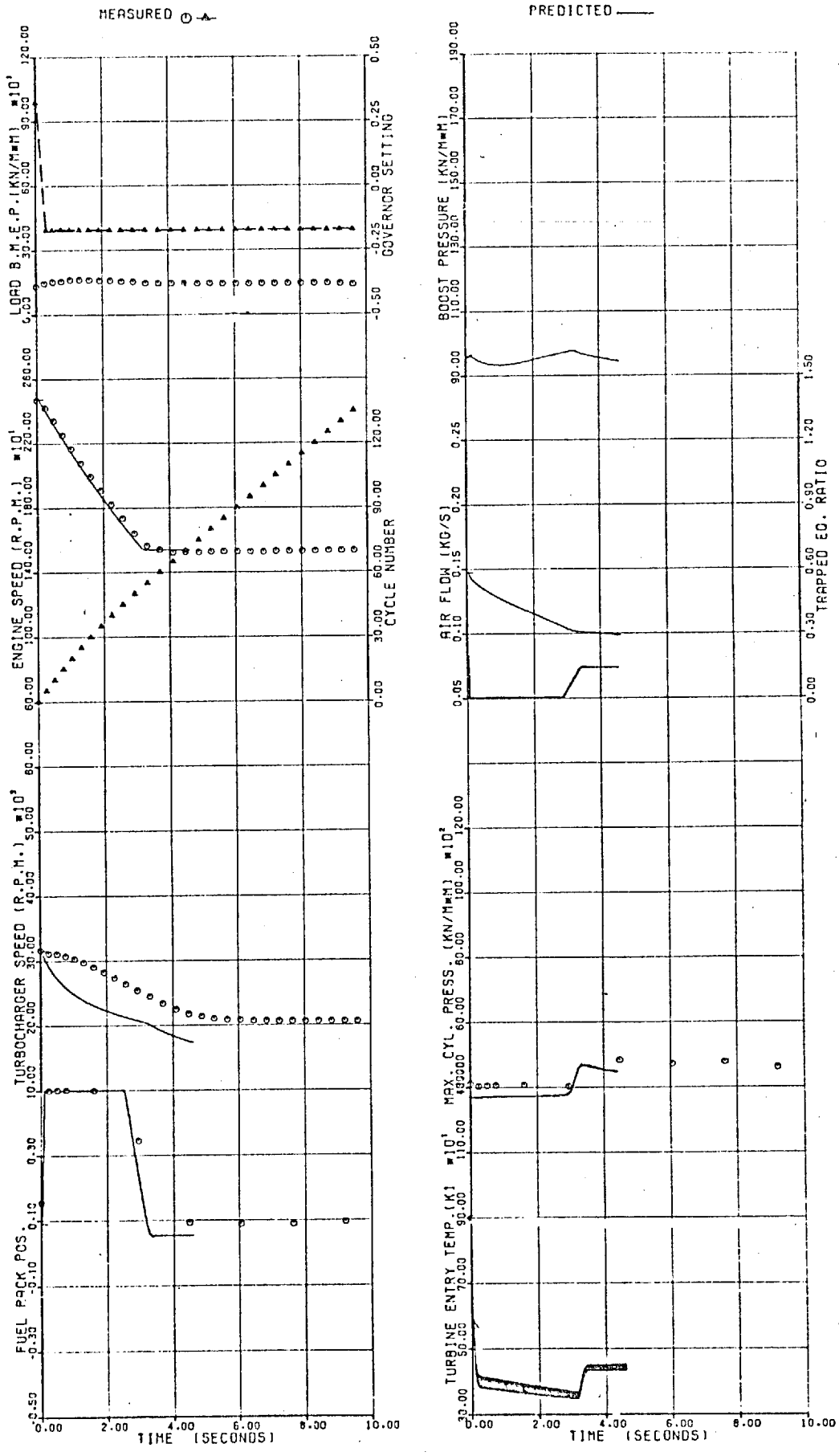


FIG(7.27,a) TRANSIENT CASE TR14

| | LOAD (BMEP BAR) | GOV. SETTING | ENG. SPEED (RPM) |
|---|---|---|---|
| INITIAL | 1.3 | 0.322 | 2467.0 |
| FINAL | 1.4 | -0.173 | 1532.0 |

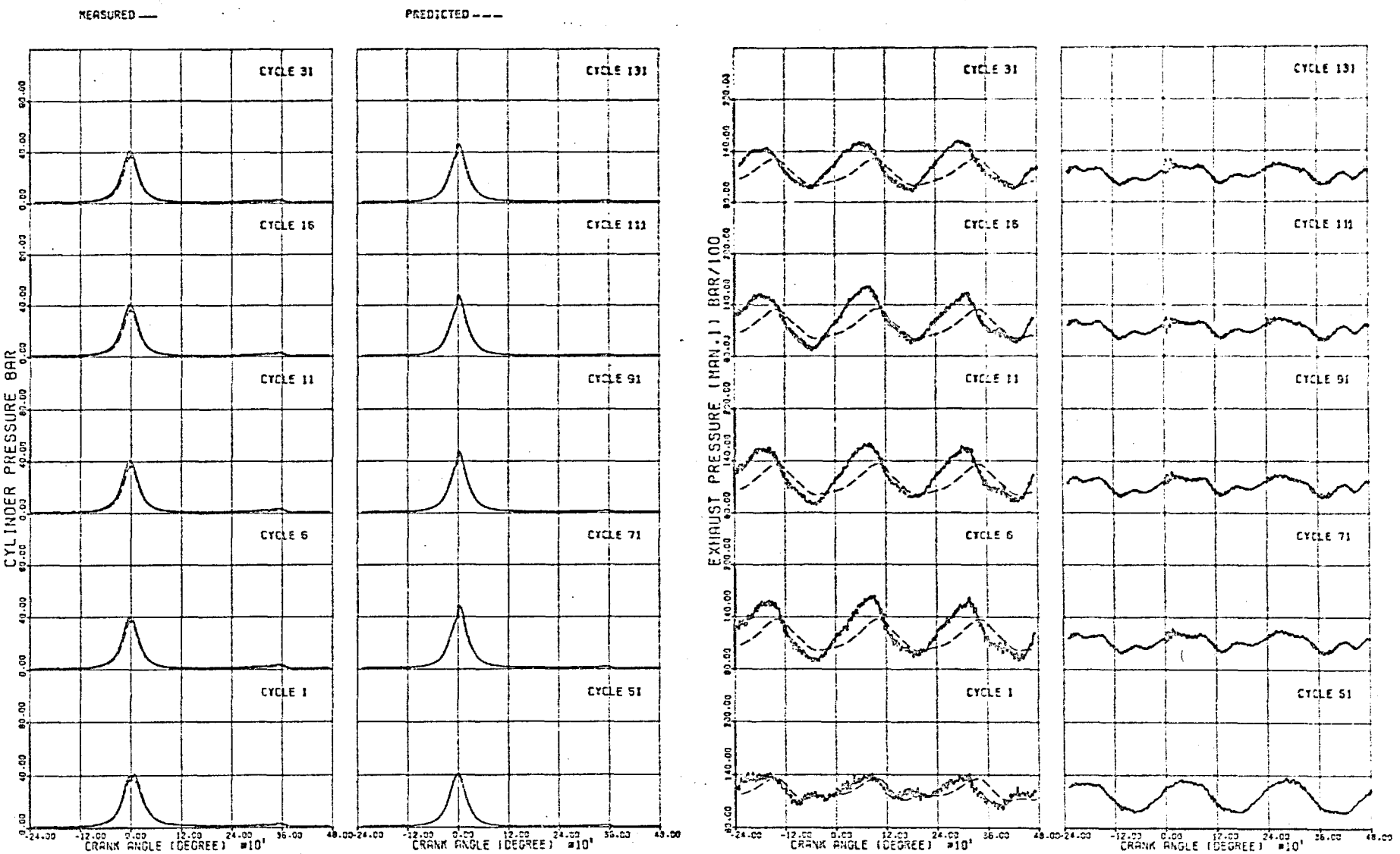


FIG(7.27b)TRANSIENT CASE TR14

| | LOAD (BMEP BAR) | GOV. SETTING | ENG. SPEED (RPM) |
|---|---|---|---|
| INITIAL | 1.3 | 0.322 | 2467.0 |
| FINAL | 1.4 | -0.173 | 1532.0 |

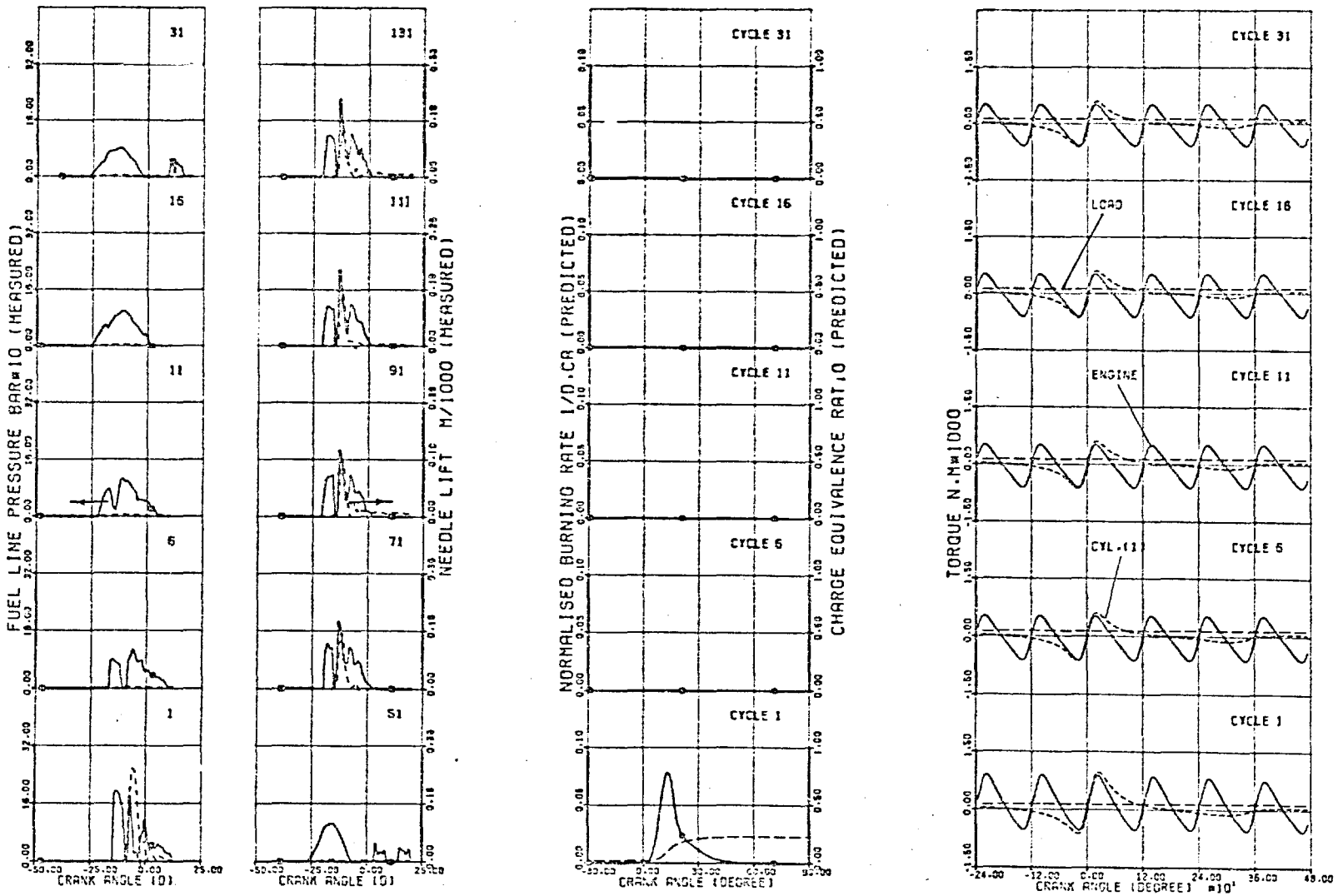


FIG(7.27c)TRANSIENT CASE TR14

| | LOAD (BMEP BAR) | GOV. SETTING | ENG. SPEED (RPM) |
|---|---|---|---|
| INITIAL | 1.3 | 0.322 | 2467.0 |
| FINAL | 1.4 | -0.173 | 1532.0 |

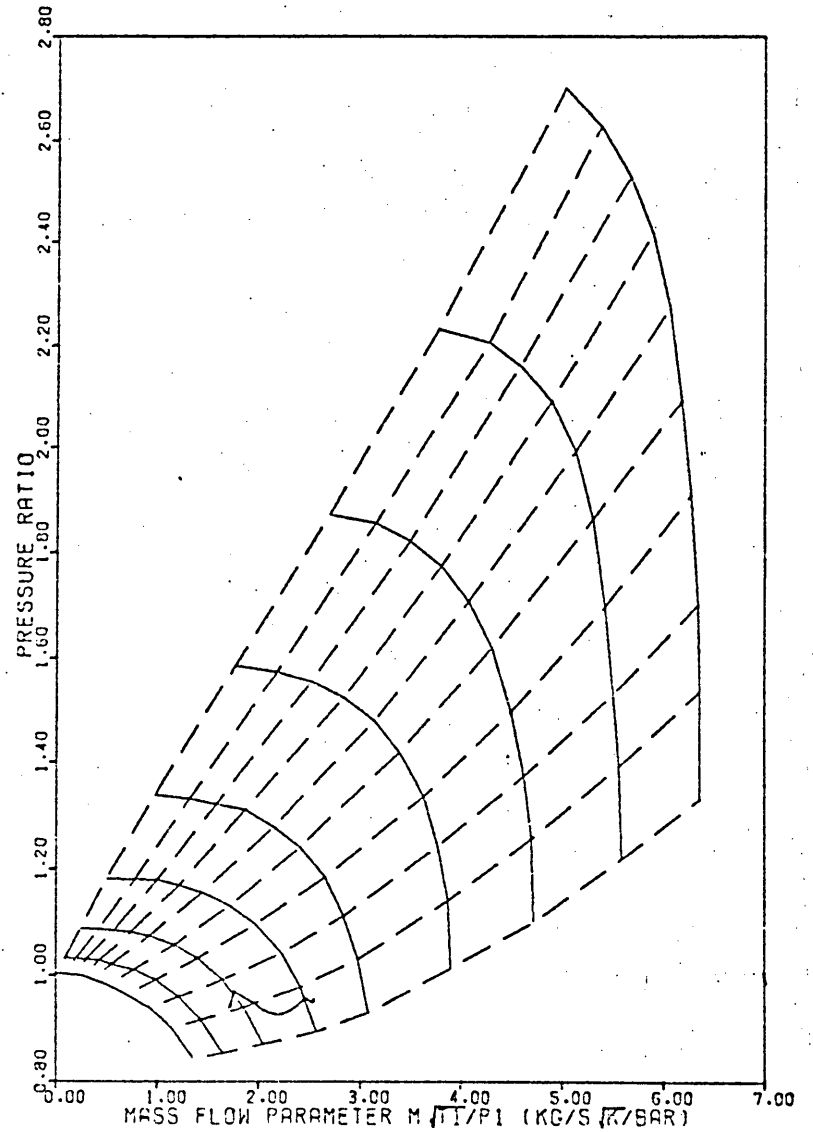


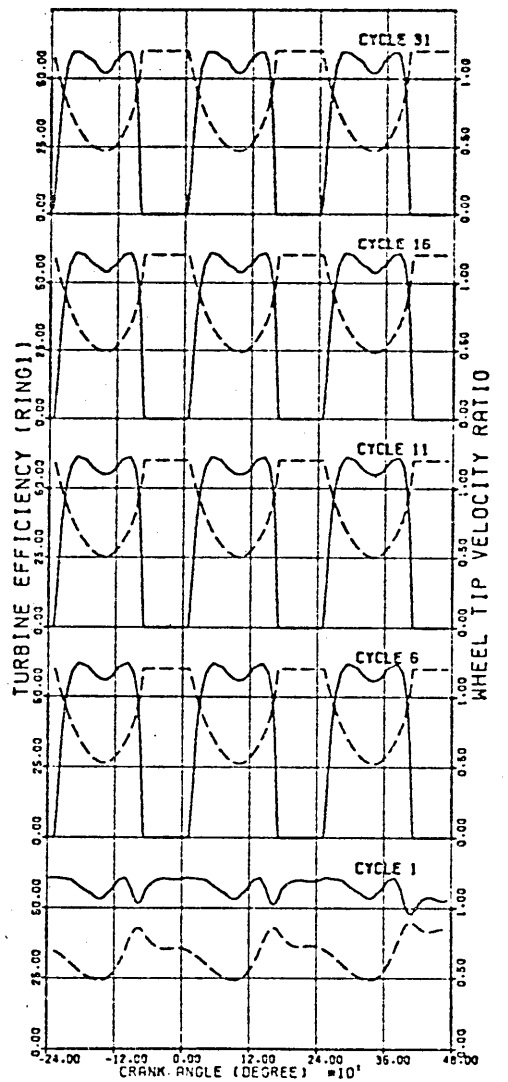


FIG. (7.27,d) TRANSIENT CASE TR14

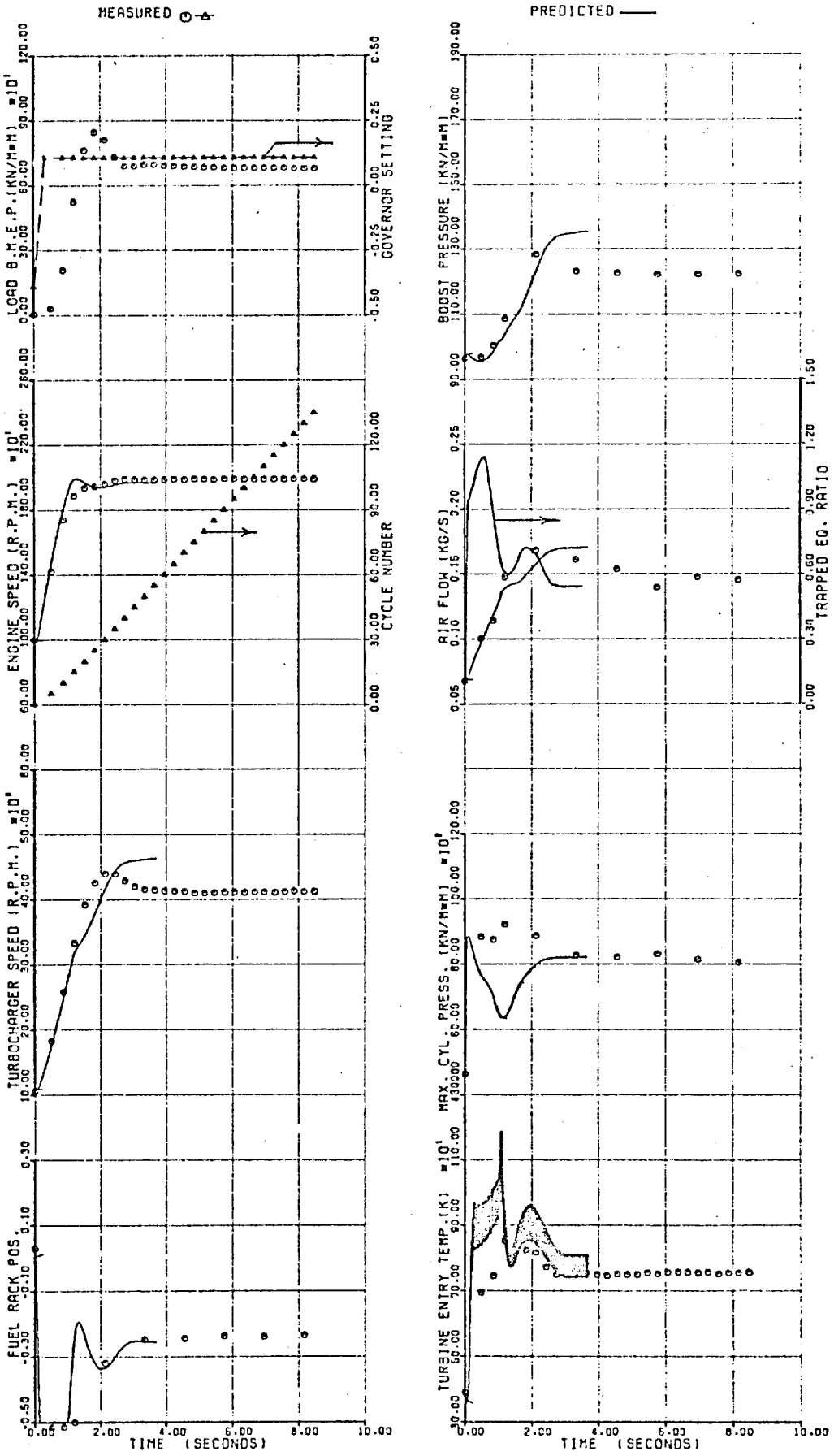


FIG(7.28,a) TRANSIENT CASE TR15

| | LOAD (BMEP BAR) | GOV. SETTING | ENG. SPEED (RPM) |
|---|---|---|---|
| INITIAL | 0.0 | -0.391 | 1000.0 |
| FINAL | 6.8 | 0.106 | 1989.0 |

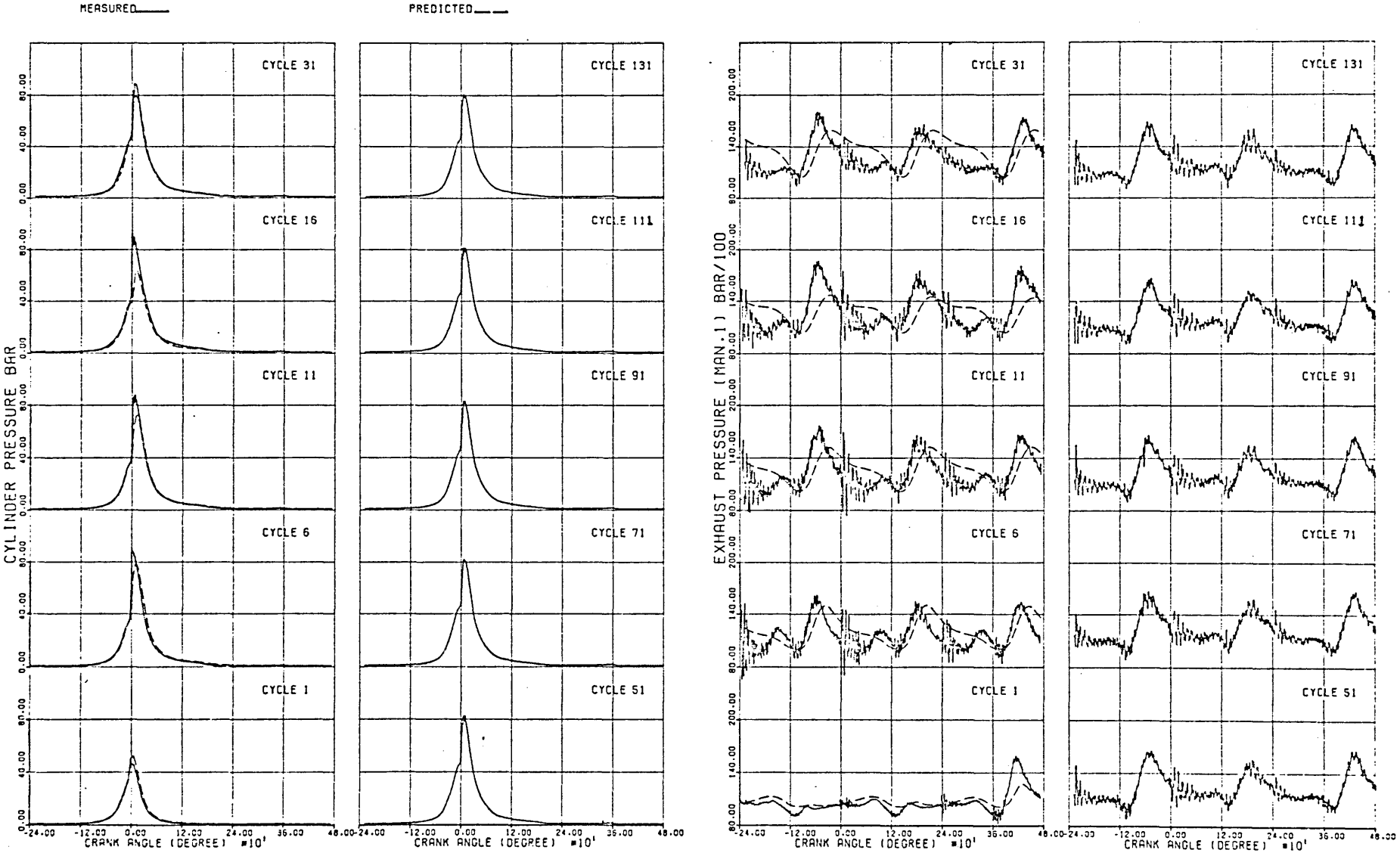


FIG(7.28b) TRANSIENT CASE TR15

| | LOAD (BMEP BAR) | GOV. SETTING | ENG. SPEED (RPM) |
|---|---|---|---|
| INITIAL | 0.0 | -0.391 | 1000.0 |
| FINAL | 6.8 | 0.106 | 1989.0 |

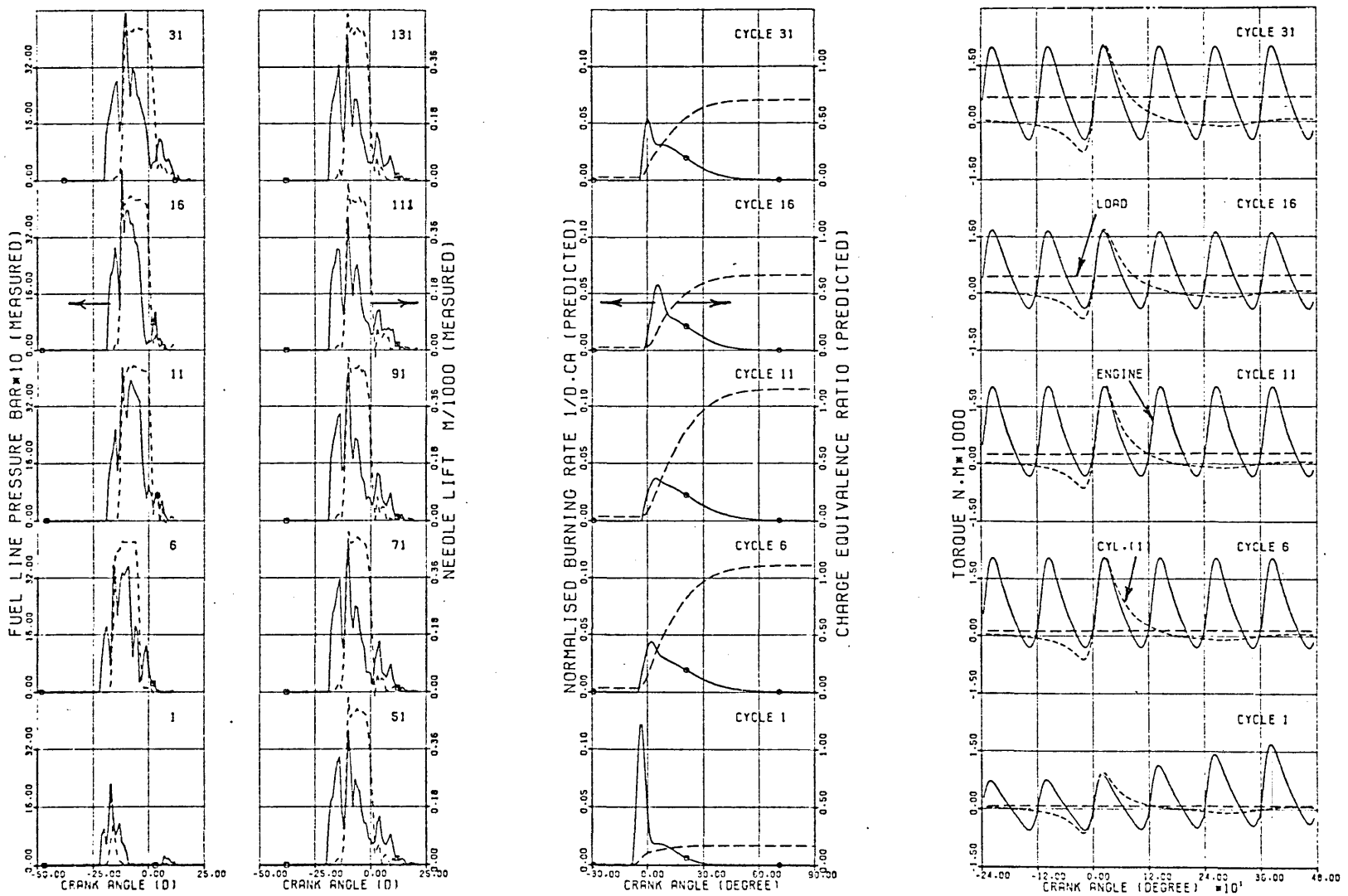


FIG(7.28c)TRANSIENT CASE TR15

| | LOAD (BMEP BAR) | GOV. SETTING | ENG. SPEED (RPM) |
|---|---|---|---|
| INITIAL | 0.0 | -0.391 | 1000.0 |
| FINAL | 6.8 | 0.106 | 1989.0 |

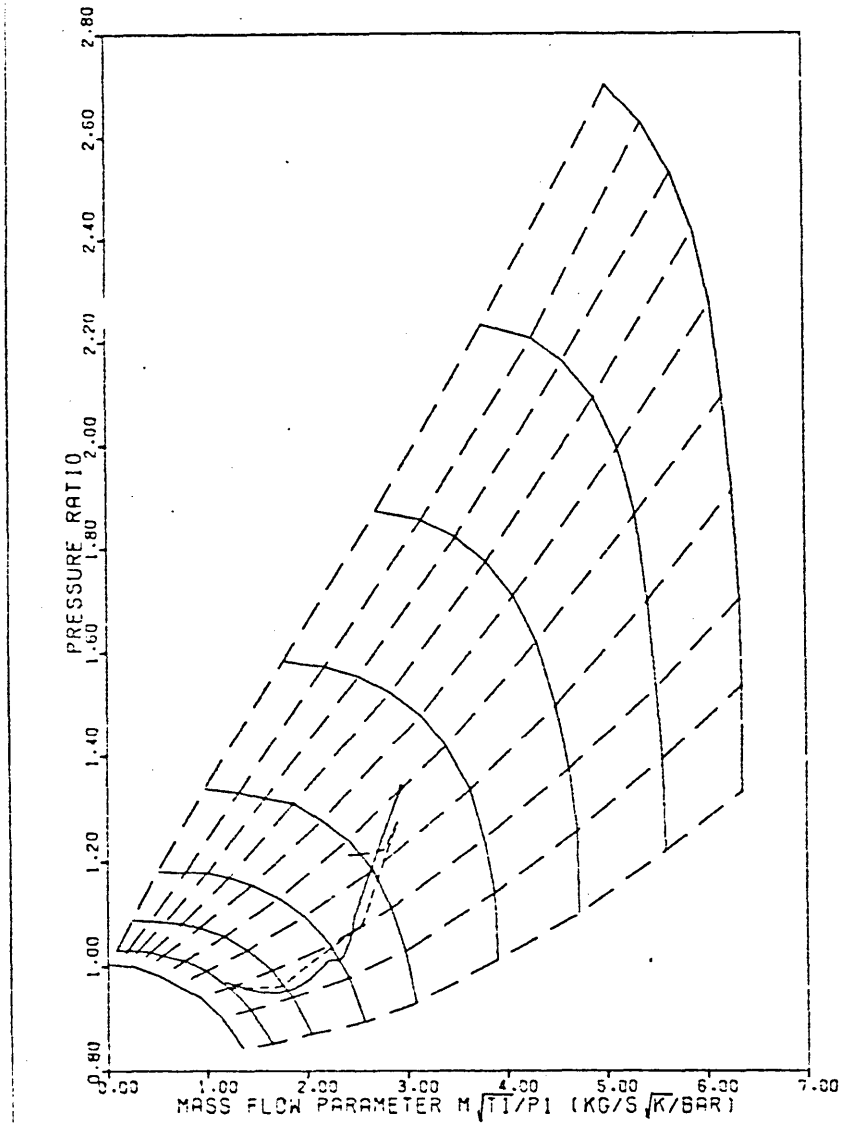


FIG. (7.28,d)

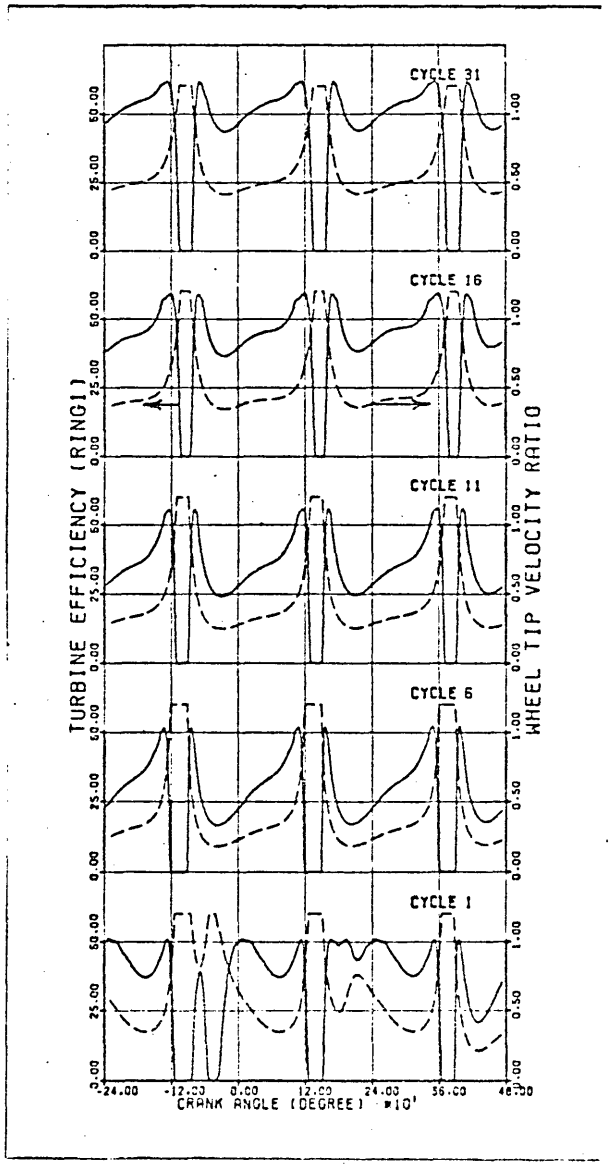


TRANSIENT CASE TR15

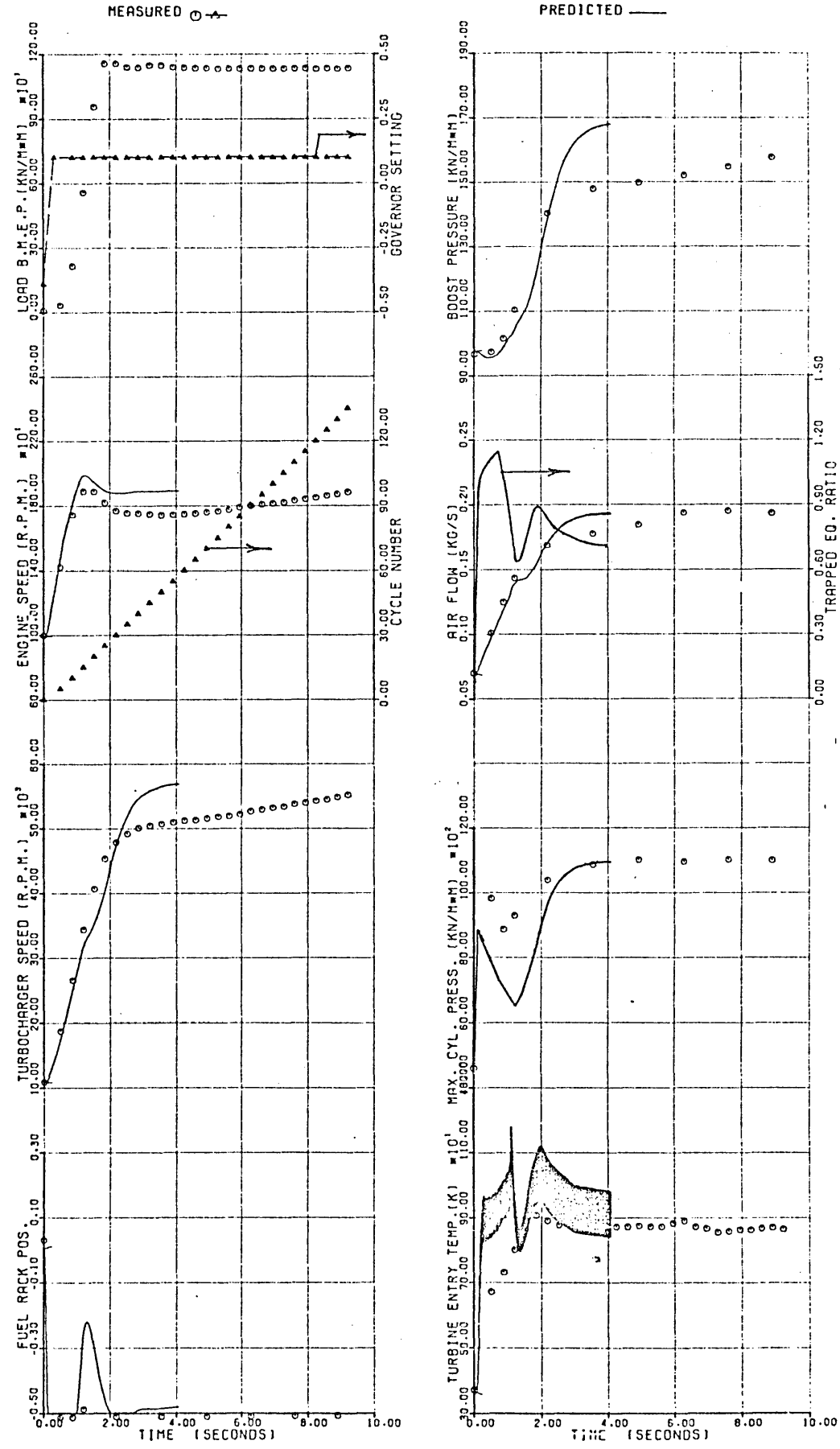


FIG(7.29,a) TRANSIENT CASE TR16

| | LOAD (BMEP BAR) | GOV. SETTING | ENG. SPEED (RPM) |
|---|---|---|---|
| INITIAL | 0.1 | -0.391 | 998.0 |
| FINAL | 11.3 | 0.100 | 1882.0 |

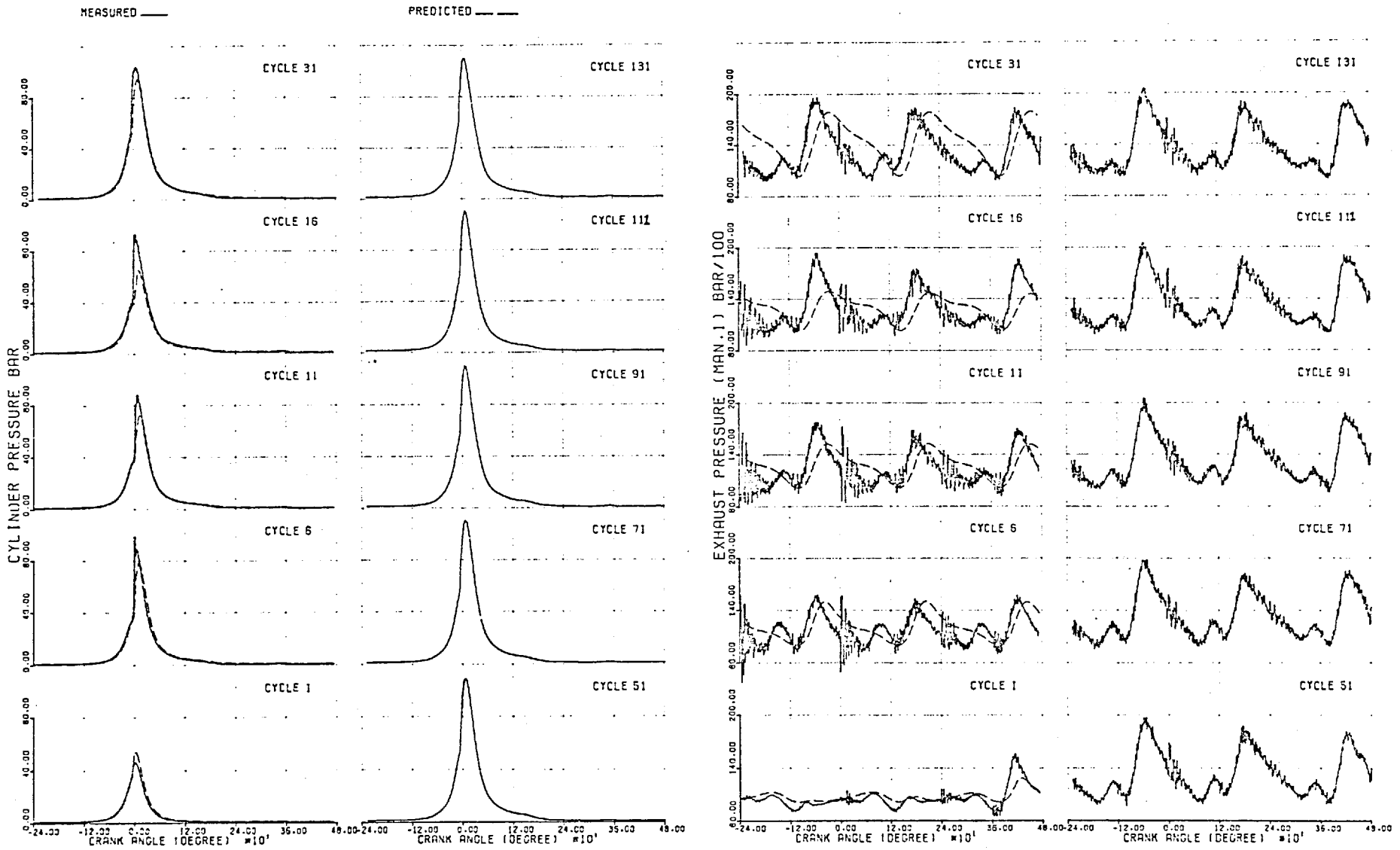


FIG(7.29b)TRANSIENT CASE TR16

| | LOAD (BMEP BAR) | GOV. SETTING | ENG. SPEED (RPM) |
|---|---|---|---|
| INITIAL | 0.1 | -0.391 | 998.0 |
| FINAL | 11.3 | 0.100 | 1882.0 |

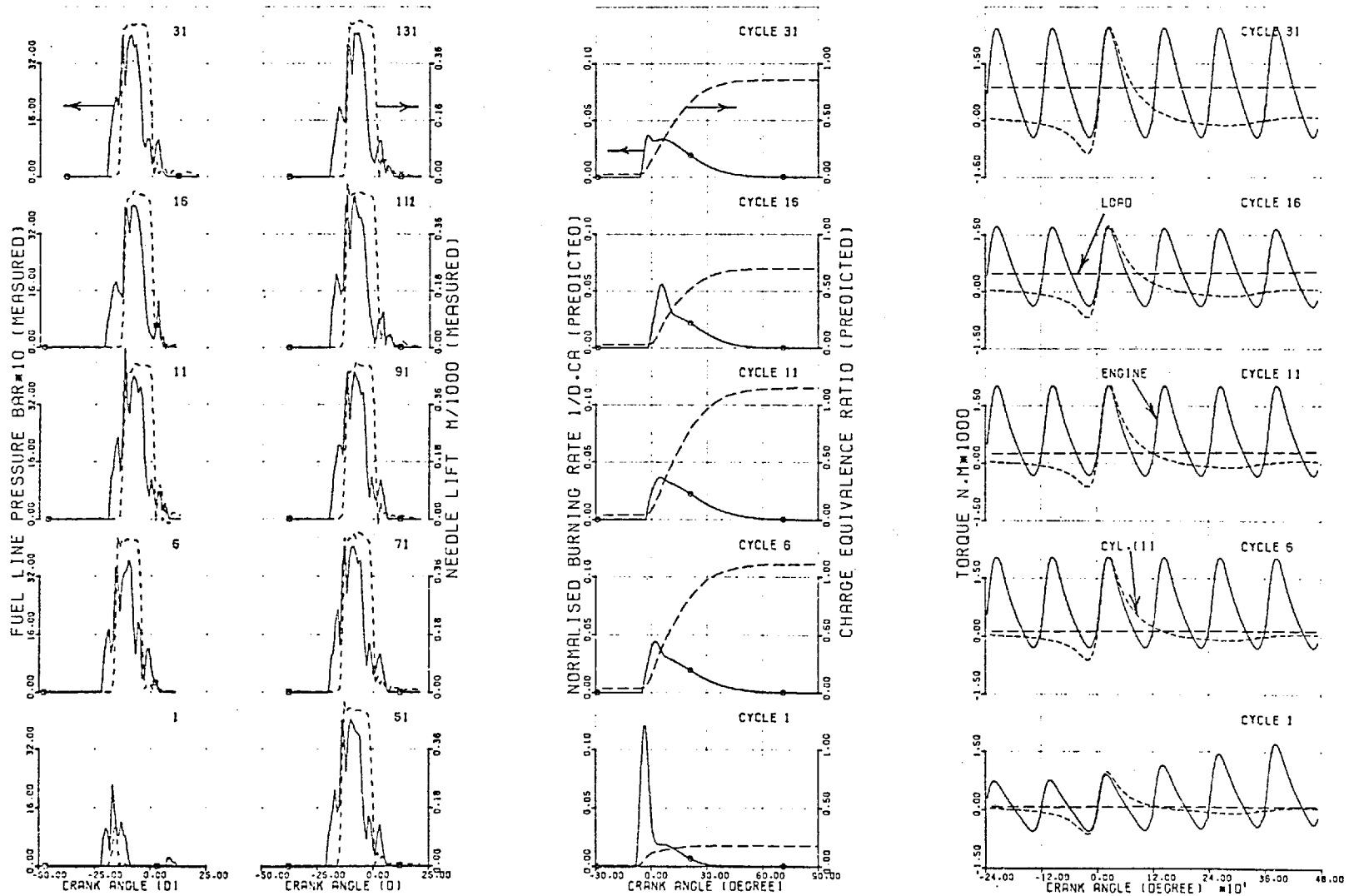


FIG(7.29c)TRANSIENT CASE TR16

| | LOAD (BMEP BAR) | GOV. SETTING | ENG. SPEED (RPM) |
|---|---|---|---|
| INITIAL | 0.1 | -0.391 | 998.0 |
| FINAL | 11.3 | 0.100 | 1882.0 |

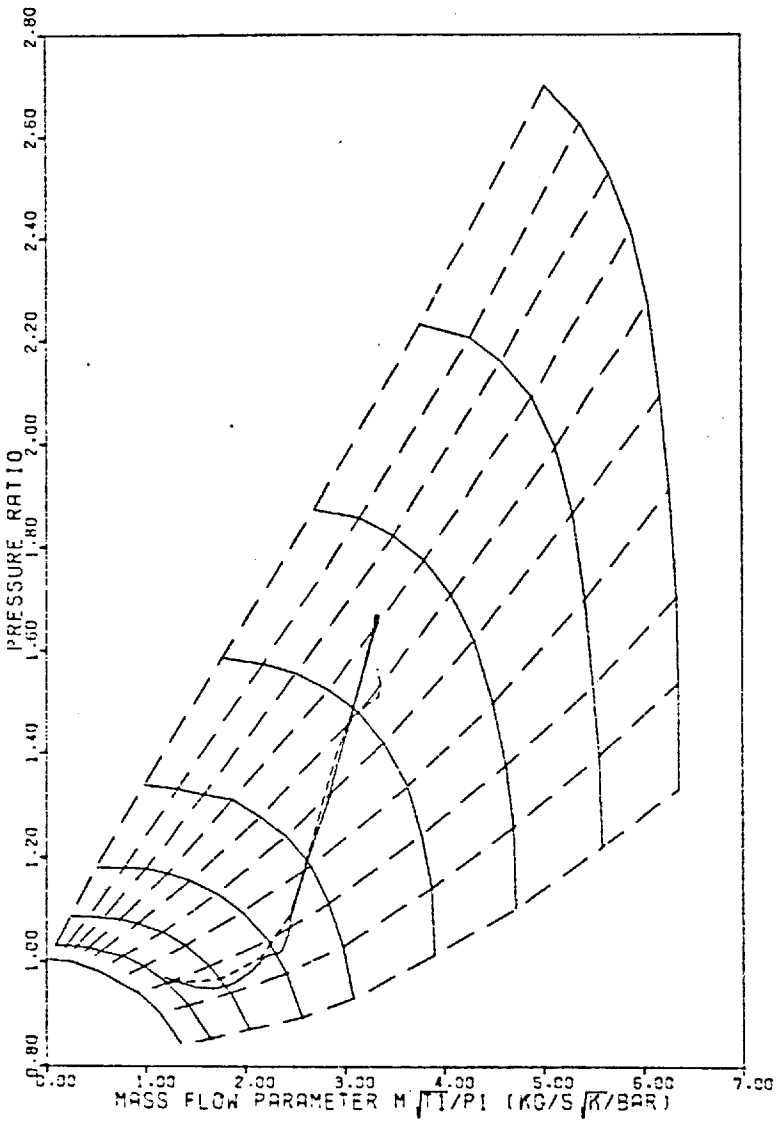


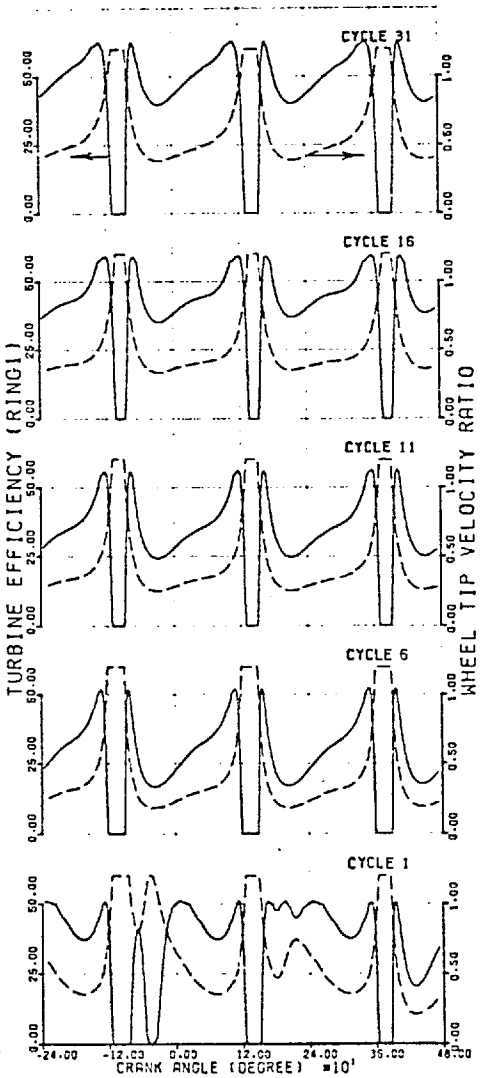


FIG. (7.29,d) TRANSIENT CASE TR16

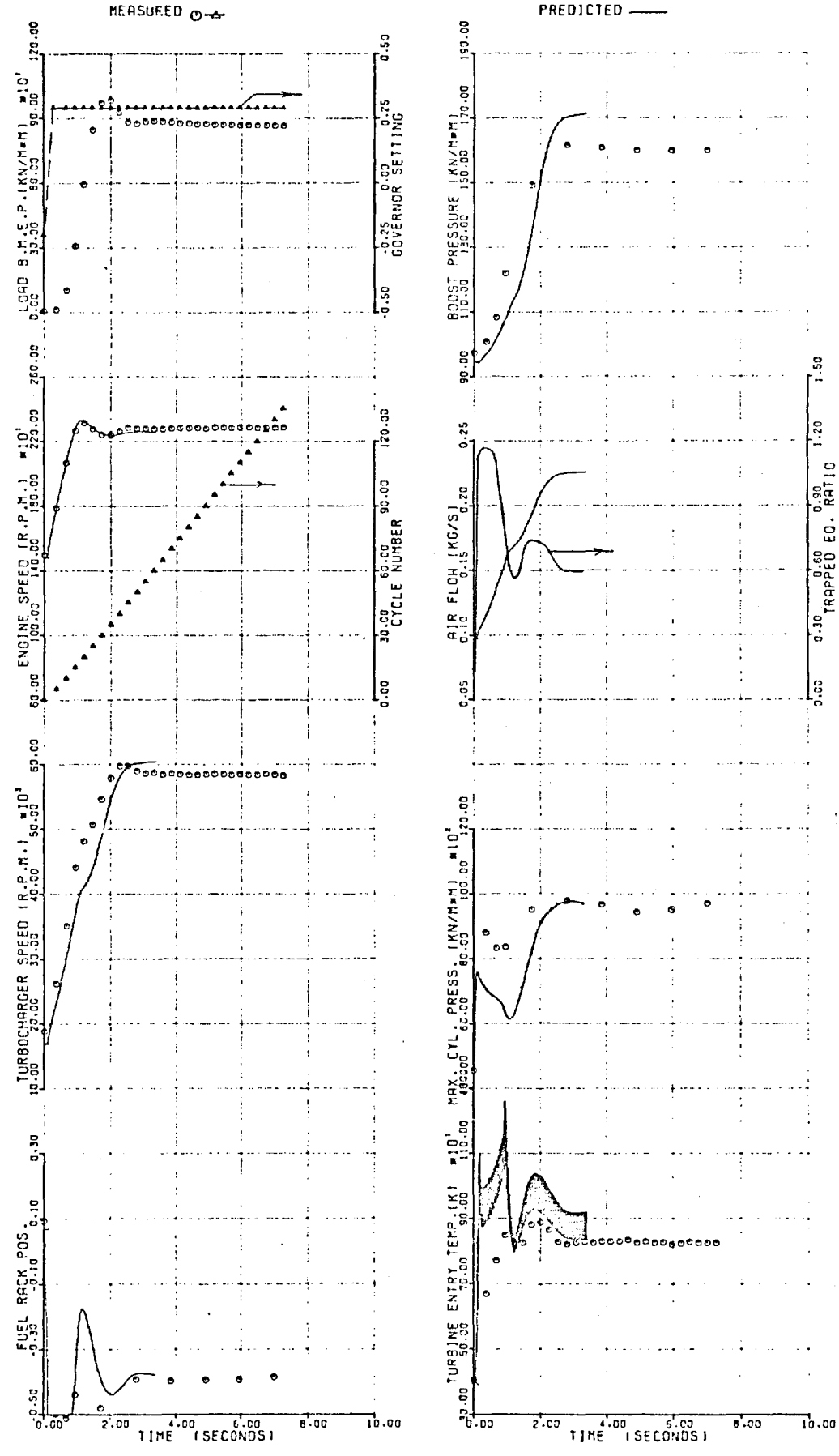


FIG(7.30,a) TRANSIENT CASE TR19

| | LOAD (BMEP BAR) | GOV. SETTING | ENG. SPEED (RPM) |
|---|---|---|---|
| INITIAL | 0.1 | -0.200 | 1497.0 |
| FINAL | 8.7 | 0.290 | 2286.0 |

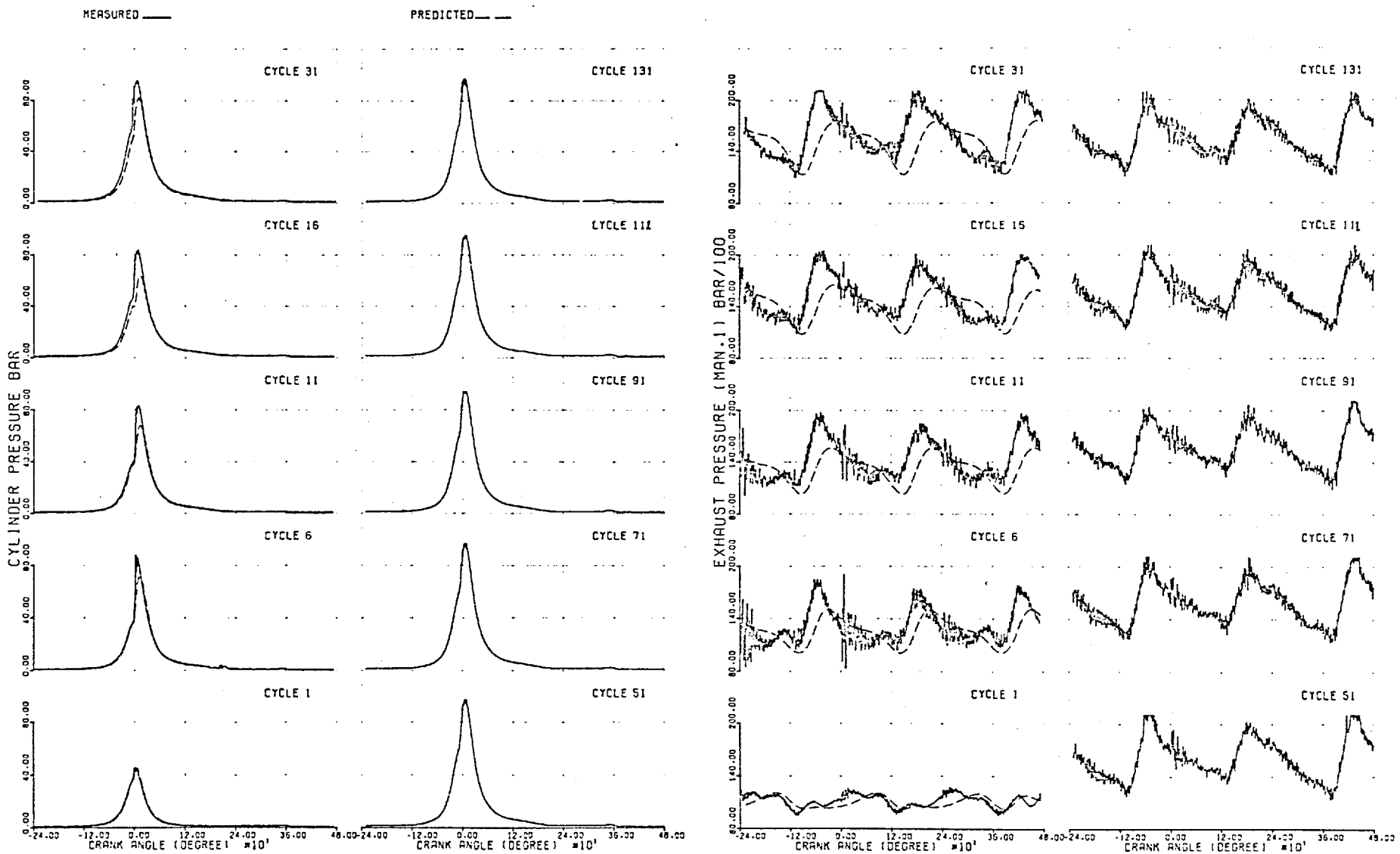


FIG(7.30b)TRANSIENT CASE TR19

| | LOAD (BMEP BAR) | GOV. SETTING | ENG. SPEED (RPM) |
|---|---|---|---|
| INITIAL | 0.1 | -0.200 | 1497.0 |
| FINAL | 8.7 | 0.290 | 2286.0 |

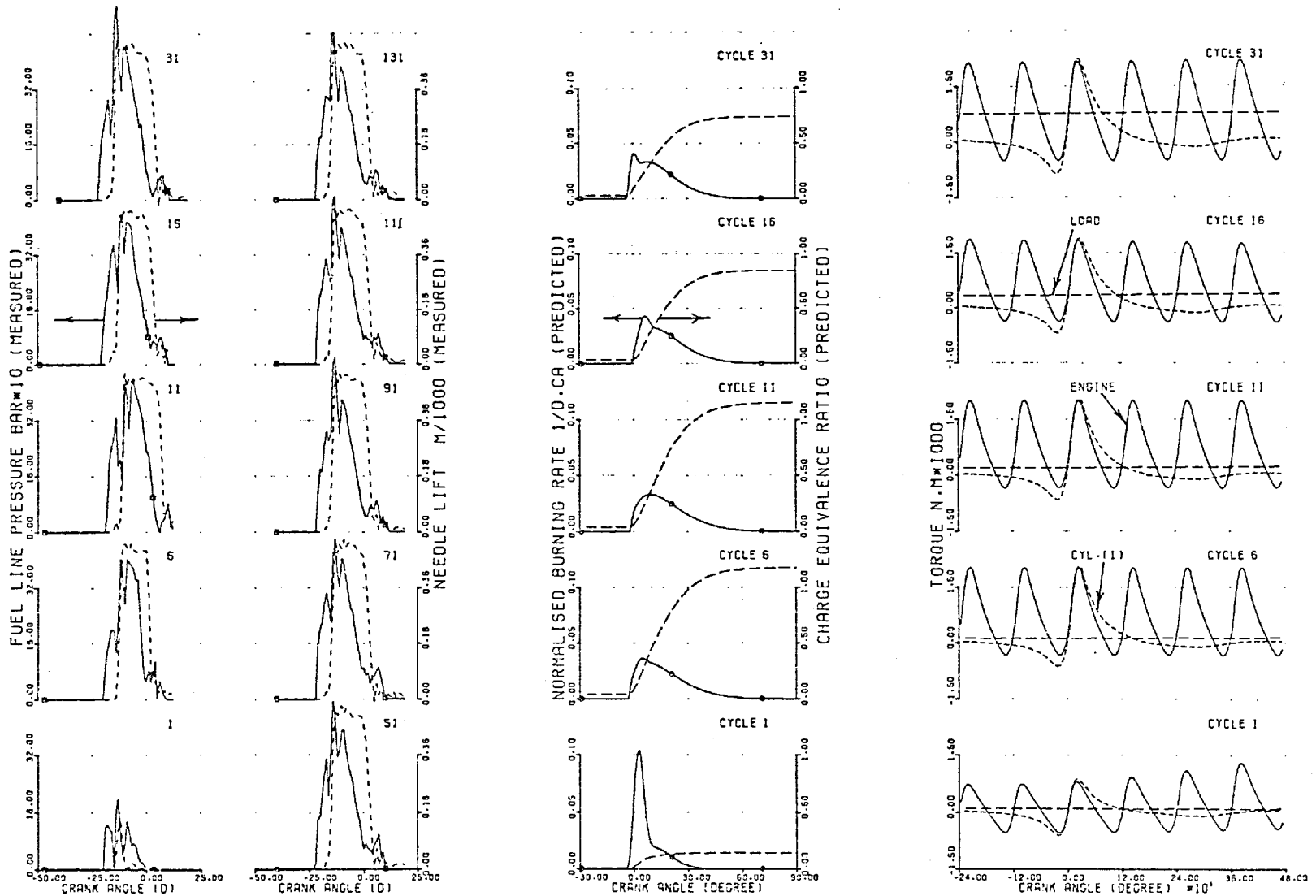


FIG(7.30c)TRANSIENT CASE TR19

| | LOAD (BMEP BAR) | GOV. SETTING | ENG. SPEED (RPM) |
|---|---|---|---|
| INITIAL | 0.1 | -0.200 | 1497.0 |
| FINAL | 8.7 | 0.290 | 2286.0 |

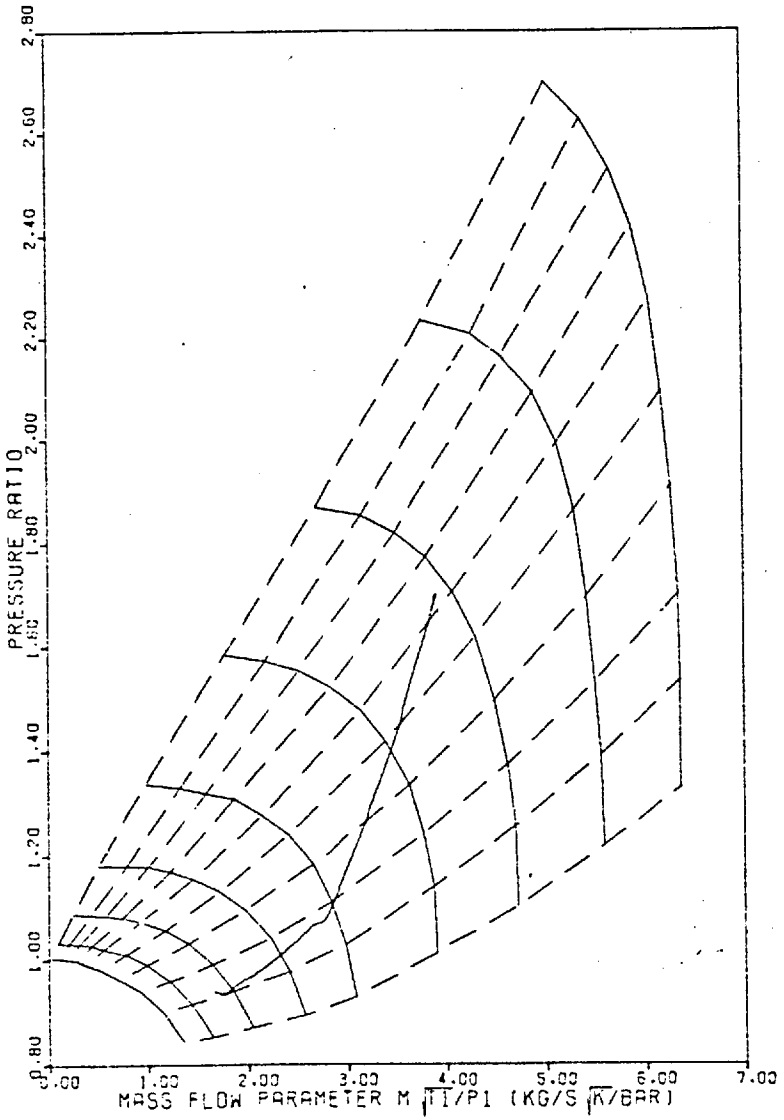


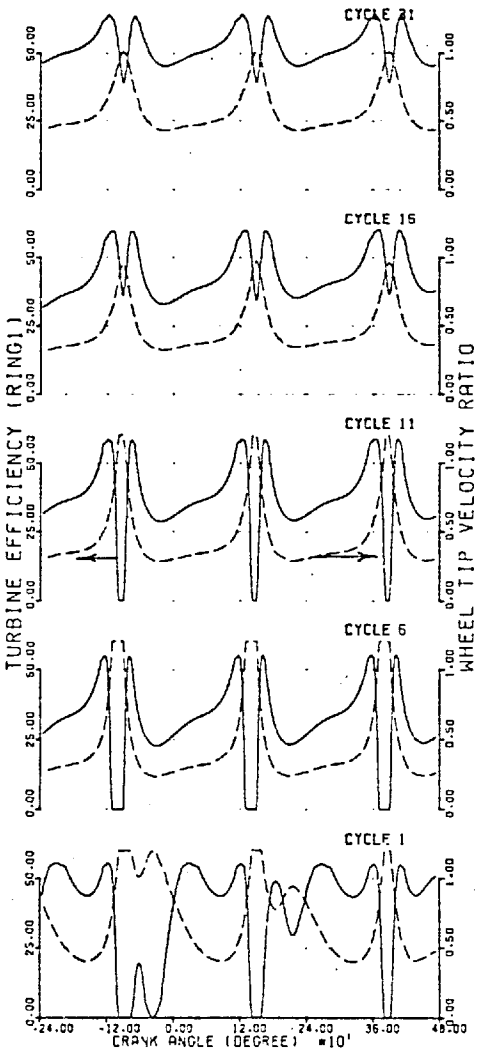


FIG. (7.30,d) TRANSIENT CASE TR19

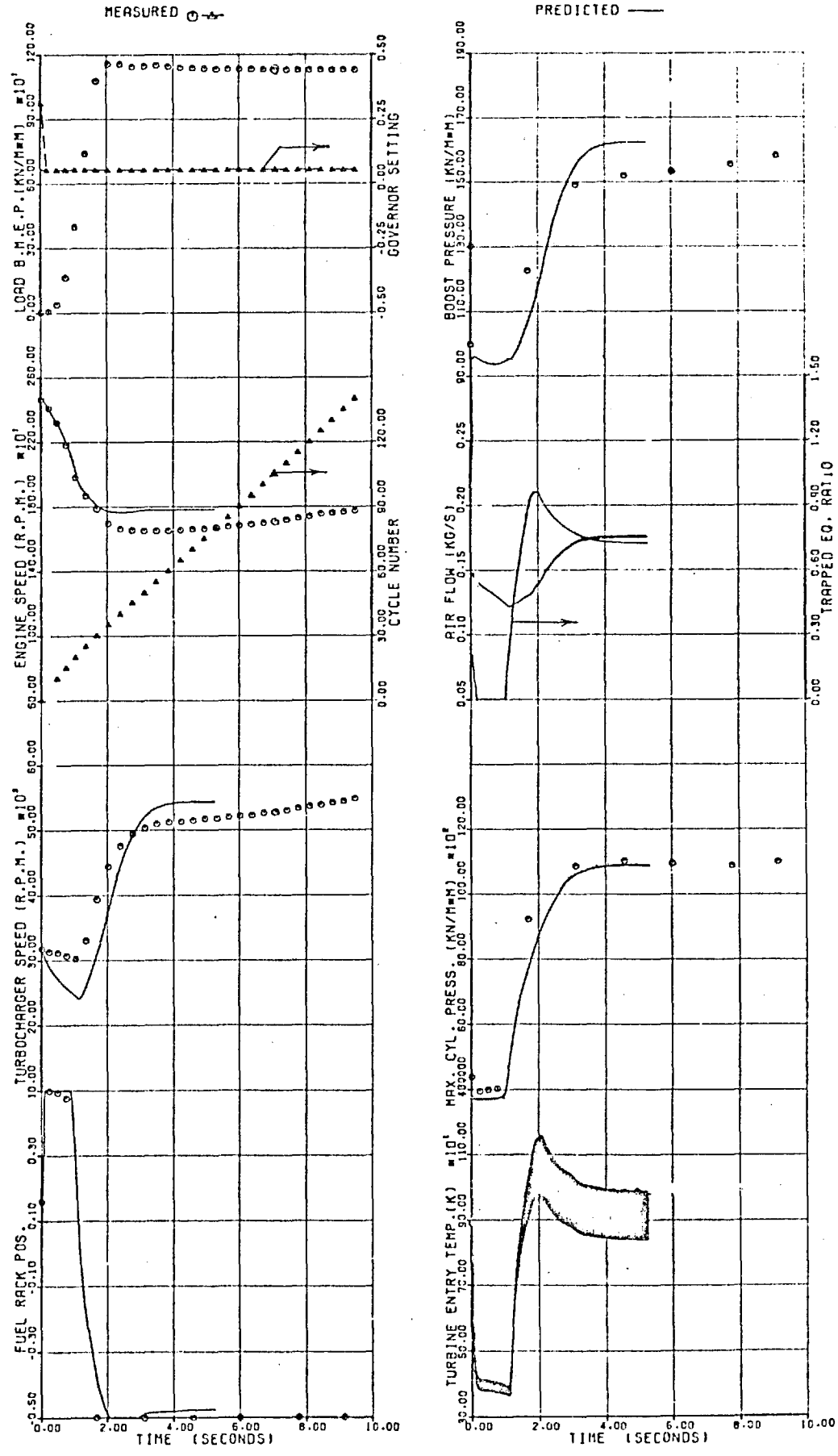


FIG(7.31,a) TRANSIENT CASE TR23

| | LOAD (BMEP BAR) | GOV. SETTING | ENG. SPEED (RPM) |
|---|---|---|---|
| INITIAL | 0.0 | 0.310 | 2463.0 |
| FINAL | 11.3 | 0.052 | 1775.0 |

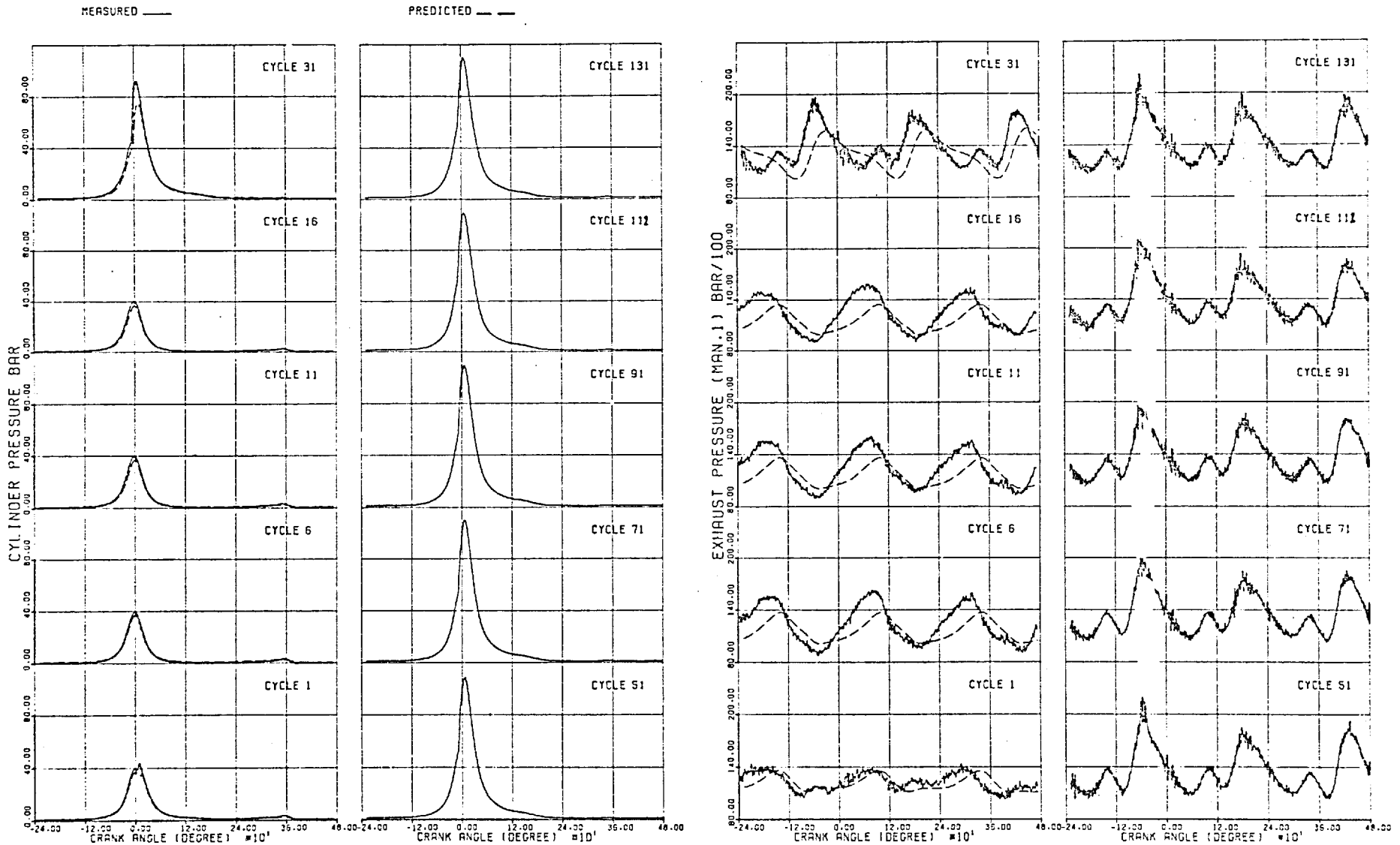


FIG(7.31b)TRANSIENT CASE TR23

| | LOAD (BMEP BAR) | GOV. SETTING | ENG. SPEED (RPM) |
|---|---|---|---|
| INITIAL | 0.0 | 0.310 | 2463.0 |
| FINAL | 11.3 | 0.052 | 1775.0 |

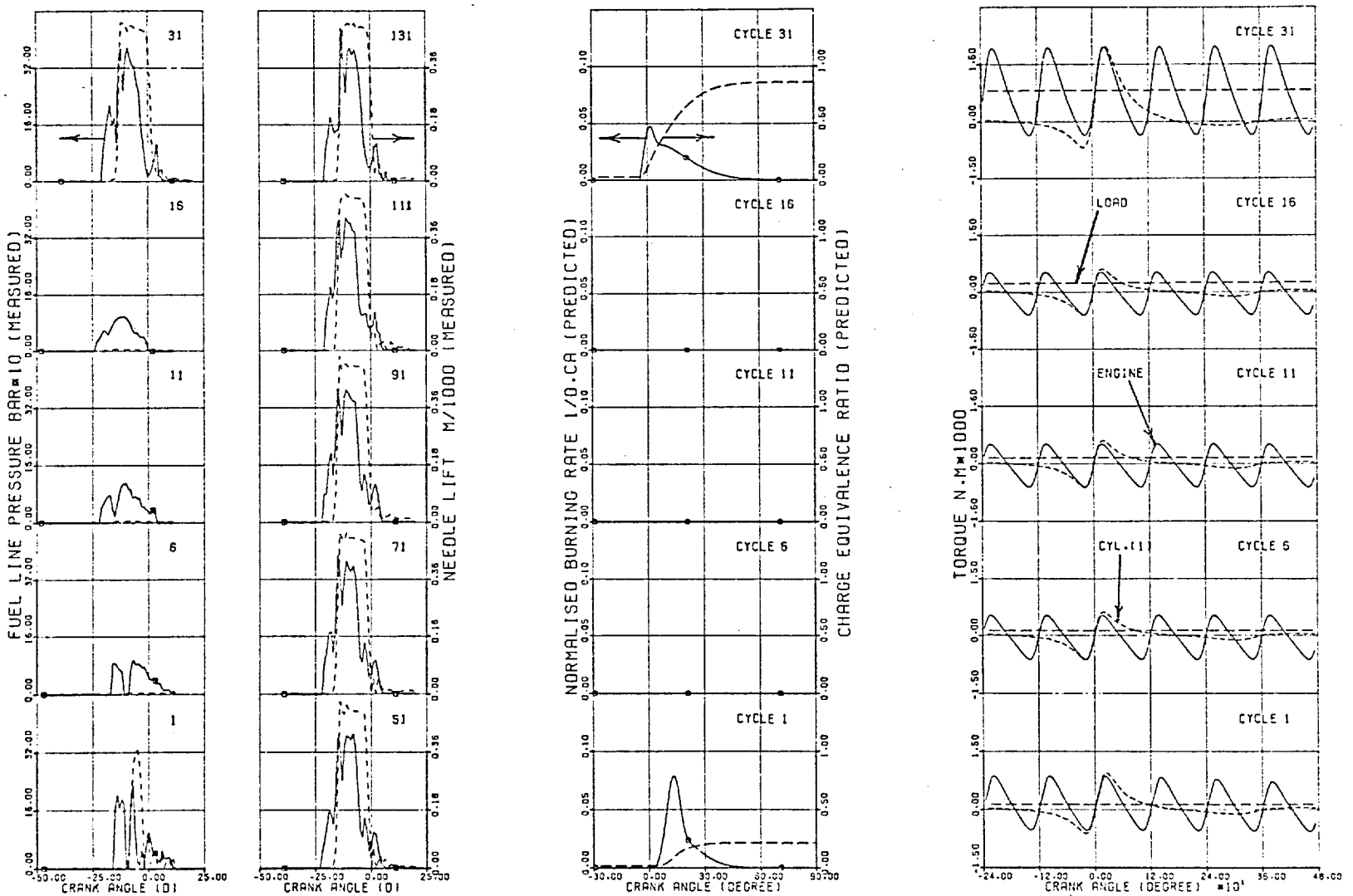


FIG(7.31c)TRANSIENT CASE TR23

| | LOAD (BMEP BAR) | GOV. SETTING | ENG. SPEED (RPM) |
|---|---|---|---|
| INITIAL | 0.0 | 0.310 | 2463.0 |
| FINAL | 11.3 | 0.052 | 1775.0 |

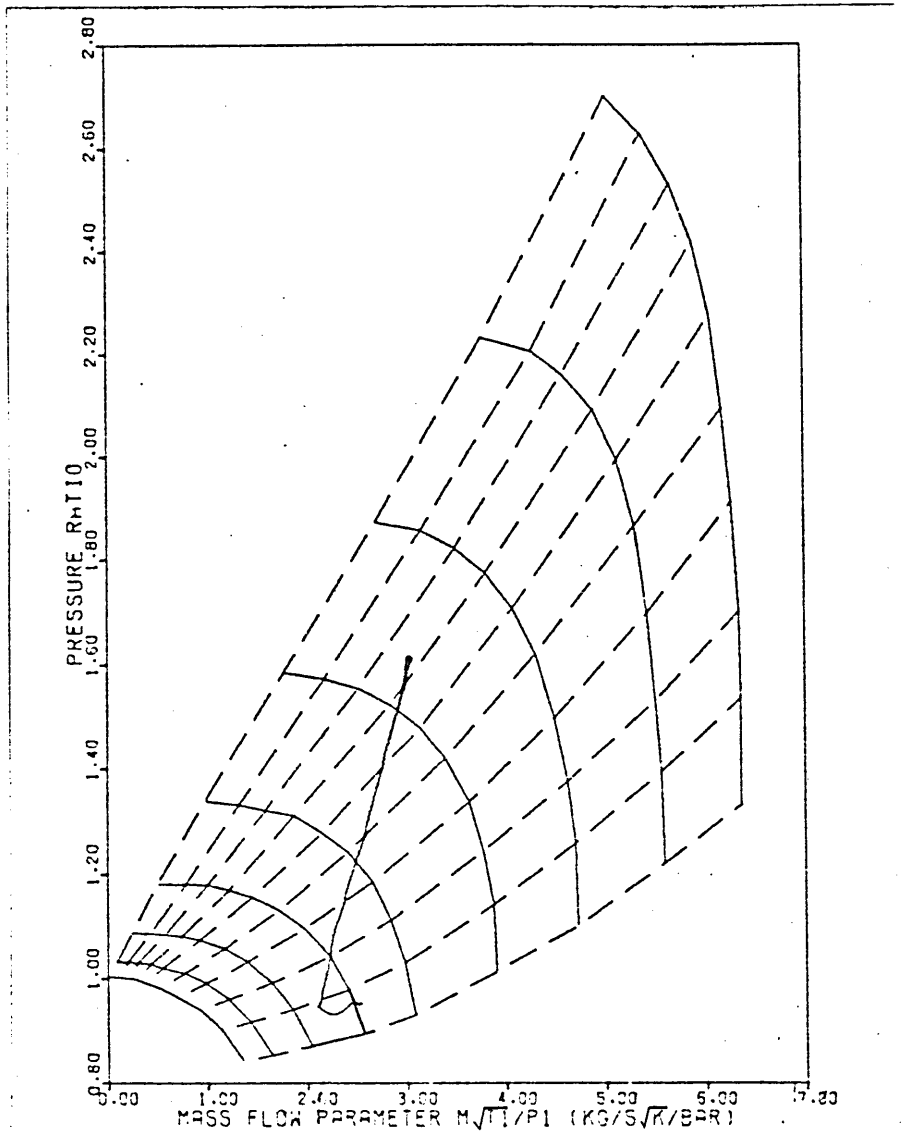


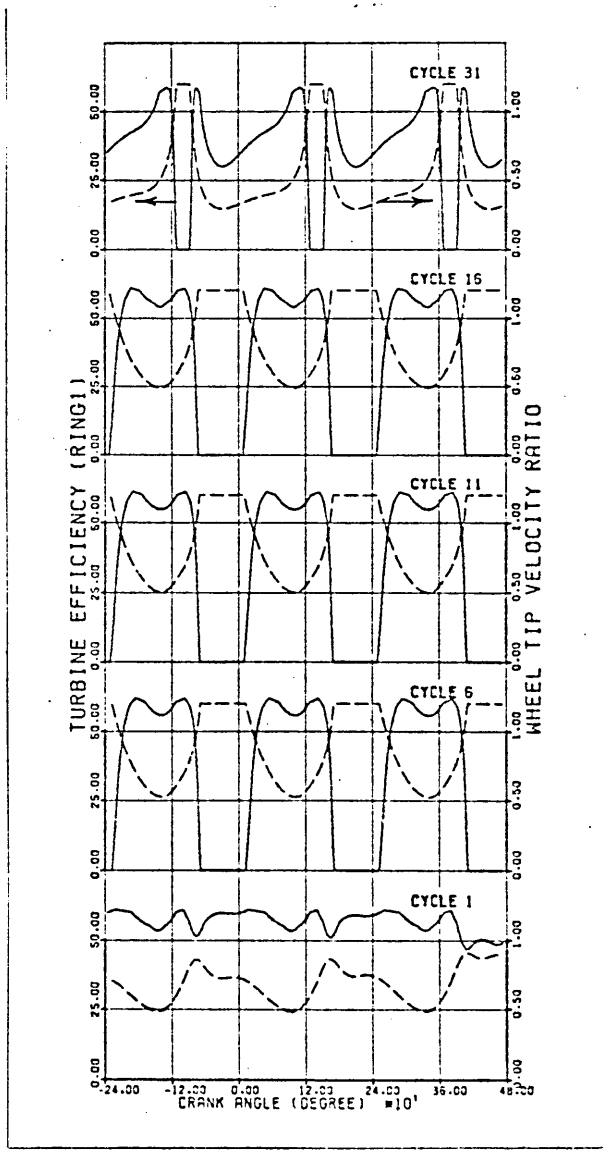


FIG. (7.31,d) TRANSIENT CASE TR23

From the foregoing comparisons it can be concluded that discrepancies between the transient response of the model and the actual engine are small and are caused by one or more of the following factors:

1. Inaccuracies in the turbocharger characteristics.
2. Errors in torque measurements.
3. Overestimation of maximum fuelling.
4. Overrating of governor response to changes in demand speed.
5. Inaccuracies in the calculation of engine friction.

The steady state characteristics of turbochargers vary from one unit to another, mainly due to manufacturing tolerances. This is believed to lead to variations in performance of the order of 5%. Errors are also introduced by the need to extrapolate the data to regions which are not normally tested by the manufacturer. A typical example (which is important to part load operation) is the compressor characteristics at very low pressure ratios. Other errors are introduced when approximating the flow characteristics of the turbine by using one swallowing capacity curve. Provided sufficient data is available, the program is capable of simulating the dependence of turbine flow on its rotational speed.

It was mentioned earlier, in Chapter 4, that fluctuations were observed to exist in the recorded torque signal. This problem was cured during steady state operation via signal filtering. However, the filtering was reduced during transient operation in order to minimise its effect on the signal response. The resulting errors in

torque measurements were found to be less than 4%. An example of the effects of such an error is case TR4. The final torque was underestimated, which led to an over-estimation of the corresponding engine speed.

Figure 7.32 shows the predicted effect of the rate of loading on the response of the engine. A load of 11.3 bar bmep is applied to the model at the same demand speed, but using two rates of loading. It is obvious that the fast loading rate produced a higher deceleration in the engine speed, followed by a larger speed droop. The result is a faster movement of the fuel rack and turbocharger acceleration. However, the rise time of the former is nearly halved against a reduction of about one-third for the latter. This is caused by the nature of the links between the different components of the engine system; mechanical in the case of the governor against thermodynamic for the turbocharger. It also follows that the faster loading rate results in richer fuel/air mixtures and consequently higher exhaust temperatures.

The amount of fuel introduced into the cylinders of the model engine when the fuel rack reached maximum fuelling was checked. This was found to exceed measured values of maximum fuelling by 3.1%. The overestimation was caused by a deviation between the mathematical representation of the fuel injection system and experimental data. The effect of such an error is more pronounced at high loads, particularly when the fuel rack is at the maximum fuelling position, e.g. case TR8. It results in higher steady state values of the engine and turbocharger speeds and hence boost pressure. This can be seen in Fig. 7.33, in

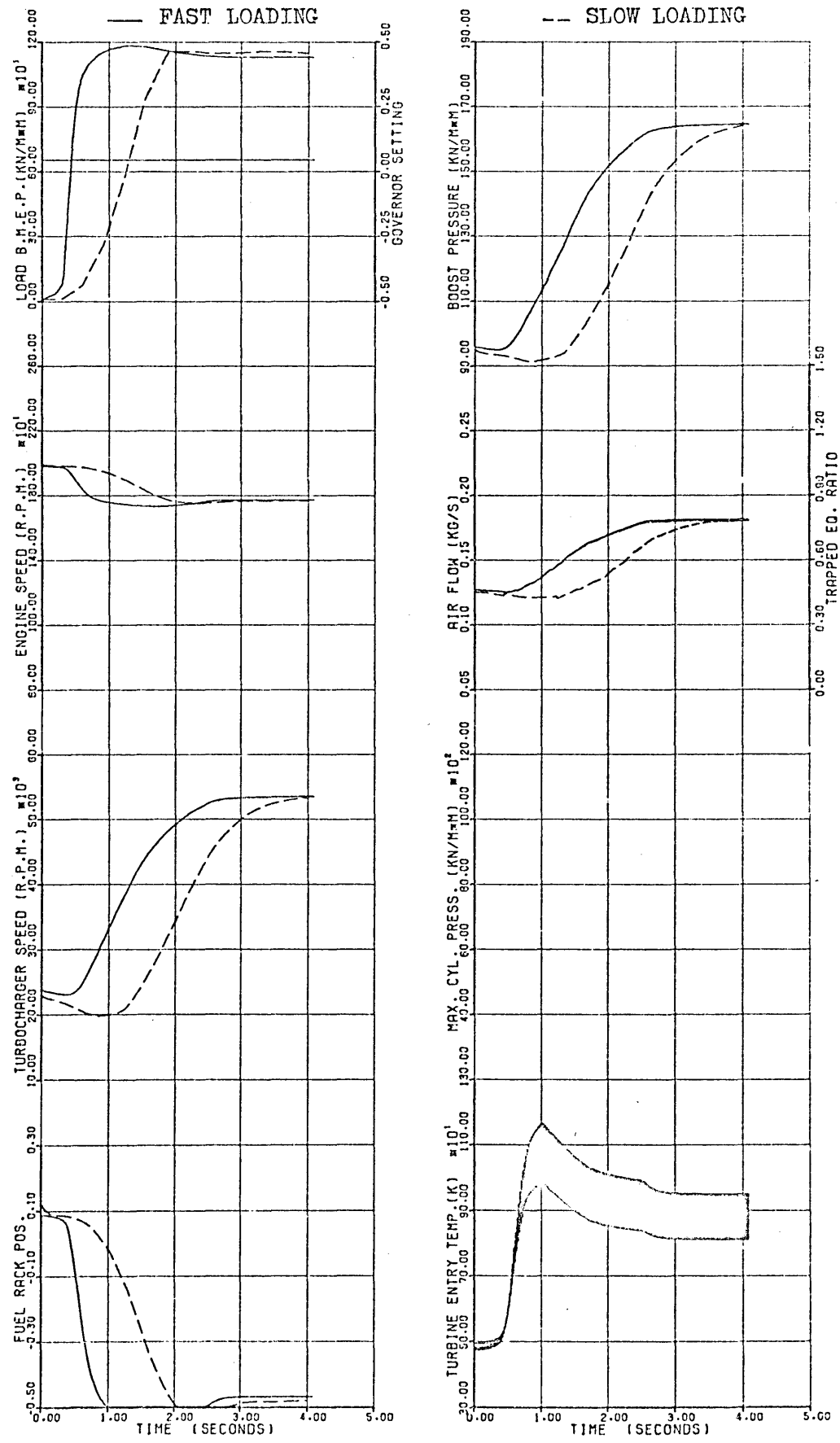


FIG. (7.32) EFFECT OF LOADING RATE

| | LOAD (BMEP BAR) | GOV. SETTING | ENG. SPEED (RPM) |
|---|---|---|---|
| INITIAL | 0.1 | 0.045 | 1980.4 |
| FINAL | 11.3 | 0.045 | 1772.7 |

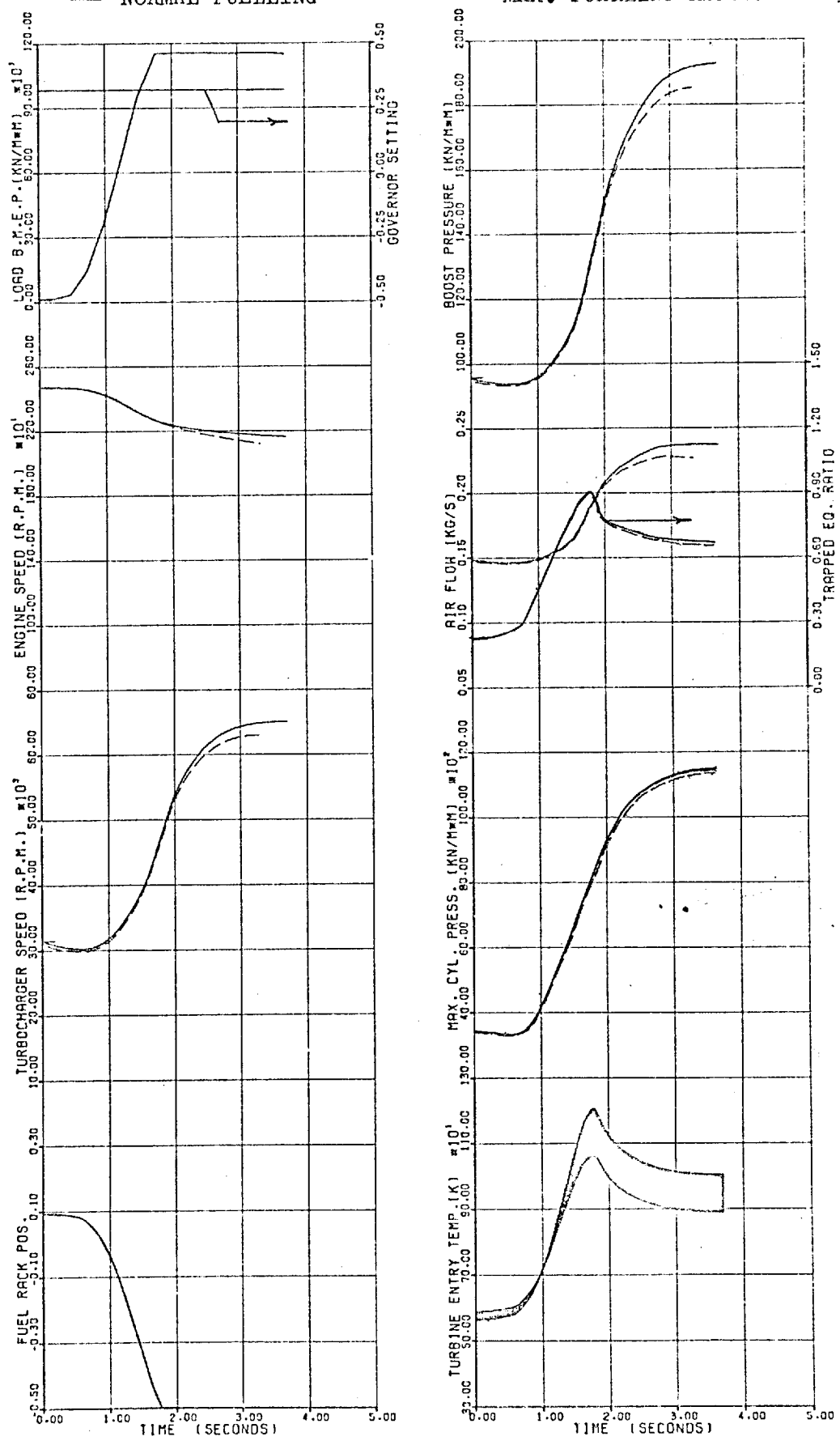


FIG.(7.33) EFFECT OF REDUCING MAXIMUM FUELLING

| | LOAD (BMEP BAR) | GOV. SETTING | ENG. SPEED (RPM) |
|---|---|---|---|
| INITIAL | 0.1 | 0.320 | 2471.6 |
| FINAL | 11.3 | 0.320 | 2163.6 |

which the original response predicted in case TR8 is compared with results obtained after reducing the model maximum fuelling by 3%.

The dynamic performance of the governor is largely influenced by the inertia of its moving parts and the amount of damping involved. It follows that an underestimation of the dynamic terms in the governor differential equation would lead to the prediction of faster response of the fuel rack, in comparison with measurements. This can result from inaccuracies in the determination of the coefficients C1 and C2 in equation (2.46). It is to be noted, that no frequency response data was available for the governor considered, hence engine test data had to be employed (Section 5.2.2).

In Fig. 7.34 the predicted transient response of the engine is compared with that resulting from increasing "friction" by 20% and 50%. The objective of this exercise was twofold, namely: to show the effect of engine friction on transient response and to demonstrate the effect of any inaccuracies in the computation of the friction torque. It can be seen that increased friction at part loads has little effect on engine speed, as this is counteracted by governor action; i.e. increasing fuelling. Accordingly this shows slightly higher turbocharger speeds. At maximum fuelling, higher friction results in lower engine speed.

During steady state operation at full load (maximum fuelling), higher friction losses lead to lower engine and turbocharger speeds. This applies until the sum of the loading and frictional torques emerges outside the maximum indicated torque envelopes of the engine, i.e. the engine cannot develop the required brake torque. A 50% increase

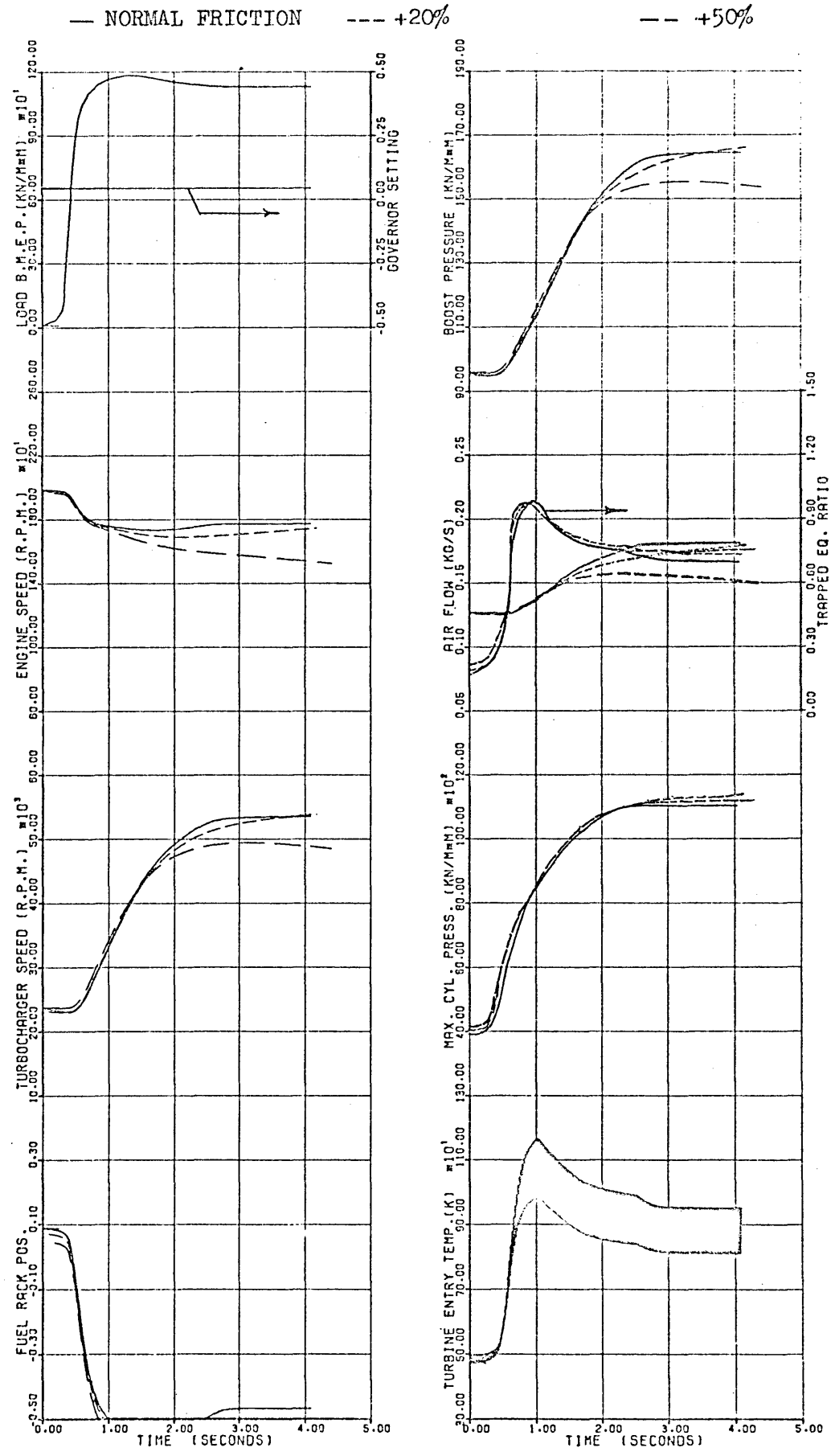


FIG. (7.34) EFFECT OF ENGINE FRICTION

| | LOAD (BMEP BAR) | GOV. SETTING | ENG. SPEED (RPM) |
|---|---|---|---|
| INITIAL | 0.1 | 0.045 | 1980.4 |
| FINAL | 11.3 | 0.045 | 1772.7 |

in friction seems to provide a suitable illustration on the Leyland engine; the simulation program predicts engine stalling (Fig. 7.34). On the other hand, the engine appears to tolerate a 20% increase in friction. Naturally, the rise in friction imposes a faster deceleration, a larger engine speed droop and a slower recovery. It also causes a faster increase in fuelling, hence a slight increase in the initial acceleration of the turbocharger. However, a reduction in the turbocharger acceleration is produced later, due to the lower engine speed. (A low engine speed results in lower exhaust energy.)

As expected, the effect of cylinder wall temperatures on the transient response of the engine has been found to be negligible. Figure 7.35 shows the response curves predicted with two widely different values of the wall time constants (equation 2.58). These were 100 and 0.1 seconds. According to experimental evidence (94), the former value is certainly more realistic.

It may be observed that due to the small reduction of trapped mass in the cylinder (following the rapid rise in wall temperature) the maximum equivalence ratio rose slightly (2.76%). The response in engine and turbocharger speeds was not changed significantly, particularly in the first 2 seconds. Thus, it may be concluded that despite the extremely low time constant used, the response in the cylinder wall temperature has very little influence on the accuracy of the predictions of the simulation program.

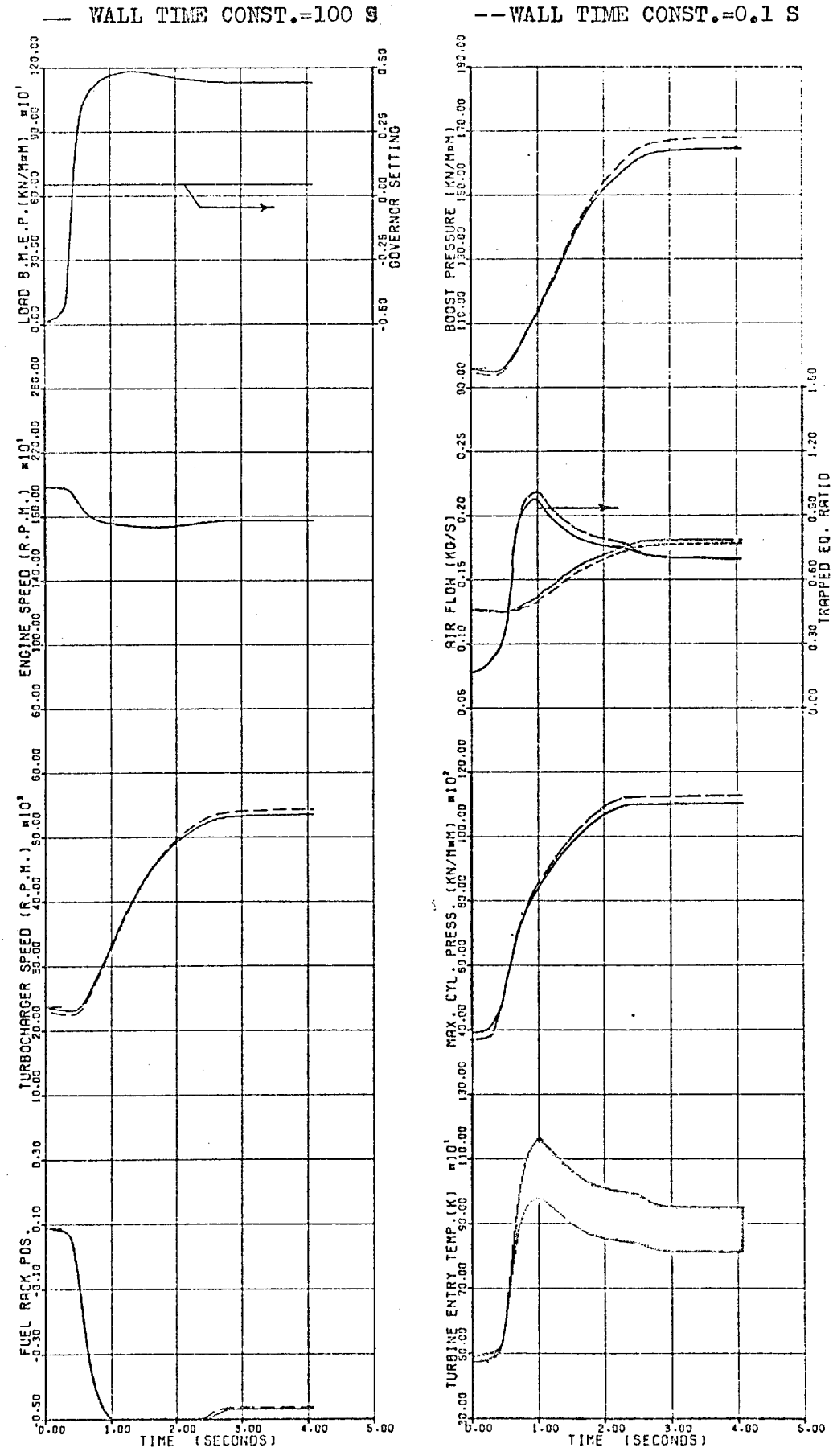


FIG. (7.35a) EFFECT OF CYLINDER WALL TEMPERATURE

| | LOAD (BMEP BAR) | GOV. SETTING | ENG. SPEED (RPM) |
|---|---|---|---|
| INITIAL | 0.1 | 0.045 | 1980.4 |
| FINAL | 11.3 | 0.045 | 1772.7 |

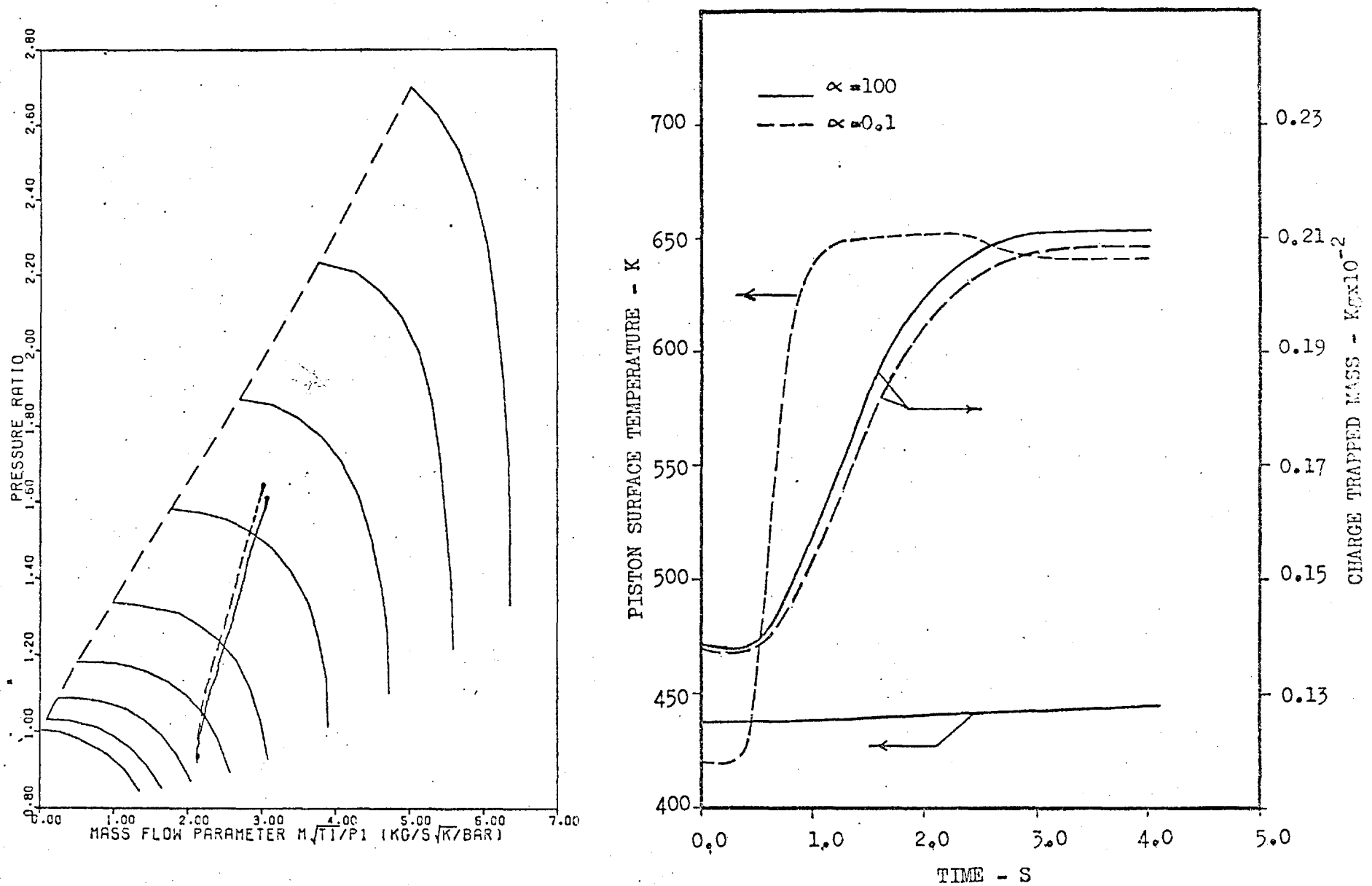


FIG. (7.35,b) EFFECT OF CYLINDER WALL TEMPERATURE

## 7.4 PARAMETRIC VARIATIONS

The transient performance of an engine/turbocharger combination is a result of many interacting factors (e.g. match, dynamics of turbocharger and engine, turbocharger characteristics, exhaust manifold design, governor, etc.). Consequently, the influence of design changes is difficult to assess. The present section demonstrates the value of using the simulation program for this application. The effects of variations in a number of relevant design parameters, on the transient response of the engine, are predicted.

It should be borne in mind that the absolute values of the predictions vary with engine and turbocharger designs, due to their particular component characteristics. However, the results are believed to be representative in general.

### 7.4.1 Effect of engine and turbocharger dynamics

Engine-load inertia:

In most applications, probably with the exception of marine propulsion, the inertia of the load is large in comparison with that of the engine. Accordingly, variations in the former have a more pronounced effect on transient operation. Figure 7.36 illustrates the transient response of the engine to a rapid increase in load, for two values of engine-load inertia; 5.51 and 9.26 $kg.m^2$.

It can be seen that an increase in total inertia reduces the droop in engine speed and results in a more gradual decrease to the final steady state value. Accordingly the governor produces a slower rack travel towards the maximum fuelling stop. This in turn results in a slightly

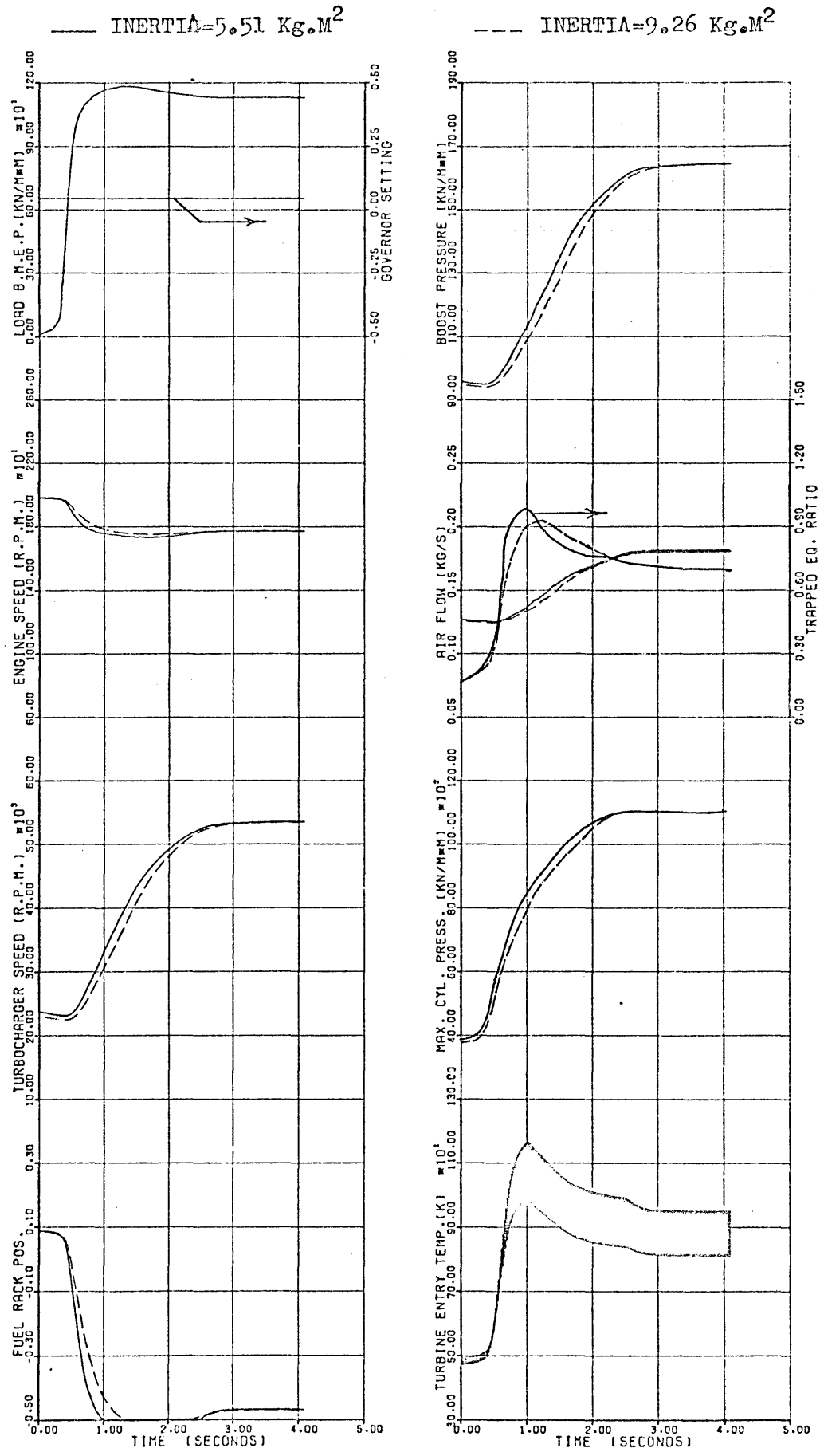


FIG. (7.36) EFFECT OF ENGINE-LOAD INERTIA

| | LOAD (BMEP BAR) | GOV. SETTING | ENG. SPEED (RPM) |
|---|---|---|---|
| INITIAL | 0.1 | 0.045 | 1980.4 |
| FINAL | 11.3 | 0.045 | 1772.7 |

delayed turbocharger response (speed, hence air flow and boost pressure). However, the net outcome is a more gradual rise in the equivalence ratio coupled with a lower peak value. Also the maximum cylinder pressure shows a slower rate of increase as a result of the delayed responses of fuelling and charge trapped mass.

It is concluded that, for a specified maximum droop in engine speed, an increase in total inertia would enable a load to be applied faster. Also the system inertia becomes more important with increase in engine bmep because of its influence on the maximum equivalence ratio. On the other hand, a reverse effect is to be expected in traction applications due to acceleration requirements.

Turbocharger inertia:

The response of the turbocharger is a controlling factor for the transient performance of the engine. In general, faster turbocharger acceleration results in an improvement in transient response, which increases with engine rating. Accordingly, efforts are directed towards reducing the polar moment of inertia of the turbocharger.

The use of lighter metals in conjunction with smaller units is the logical solution, where possible. The effect of reducing the turbocharger inertia by 21% (which is equivalent to reducing the wheel tip diameter by 6%) is shown in Fig. 7.37. No changes were made to the flow and efficiency characteristics of the turbocharger components. However, only a little improvement was shown in the speed response of the engine.

—— INERTIA=$2.262 \times 10^{4} Kg.M^{2}$ --- INERTIA REDUCED BY 21%

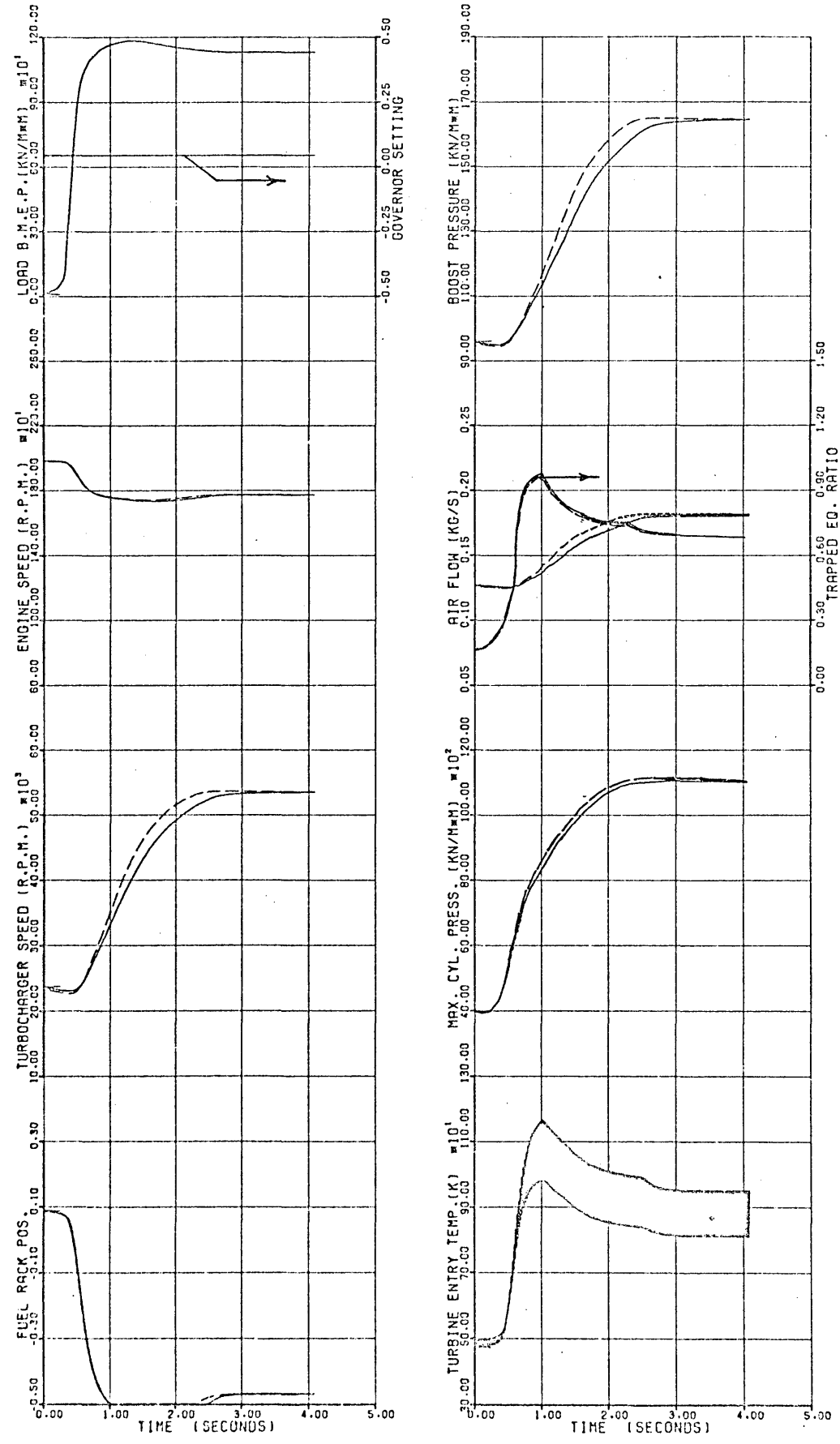


FIG.(7.37) EFFECT OF TURBOCHARGER INERTIA

| | LOAD (BMEP BAR) | GOV. SETTING | ENG. SPEED (RPM) |
|---|---|---|---|
| INITIAL | 0.1 | 0.045 | 1980.4 |
| FINAL | 11.3 | 0.045 | 1772.7 |

### 7.4.2 Effect of manifold volumes

In a pulse turbocharged diesel engine, pressure fluctuations are created in the exhaust manifold due to the intermittent release of high pressure and temperature gases at the beginning of the exhaust valve opening period. At a constant engine speed the amplitude of pressure fluctuations depends on the capacity of the exhaust manifold, the release pressure and turbine area. A decrease in the manifold volume may result in higher peak pressures and temperatures and so augment the useful energy available at the turbine entry. Furthermore, this effect becomes more pronounced with higher release pressures and temperatures. In other words, it increases with the mass of air trapped inside the cylinder, and the amount of heat liberated per cycle (i.e. with fuelling in the case of steady state operation).

The influence of reducing the exhaust manifold volume on the transient response of the engine (to sudden loading) is shown in Fig. 7.38. With a volumetric reduction of 20%, the turbocharger response exhibits a gradually increasing improvement in the later stages of the transient period. The accompanying rise in boost pressure and air flow is not sufficient to affect the peak value of the equivalence ratio curve. However, the maximum cylinder pressure displays an increase at the later stages of the transient period. Obviously this yields higher release pressures, which feed back and push the turbine power up. The resulting increases in final steady state values of the turbocharger speed, boost pressure, air flow and maximum cylinder pressure are 1.9%, 1.98%, 1.5% and 1.3% respectively.

It is interesting to note that engine speed and fuel rack travel show very little change. This results from

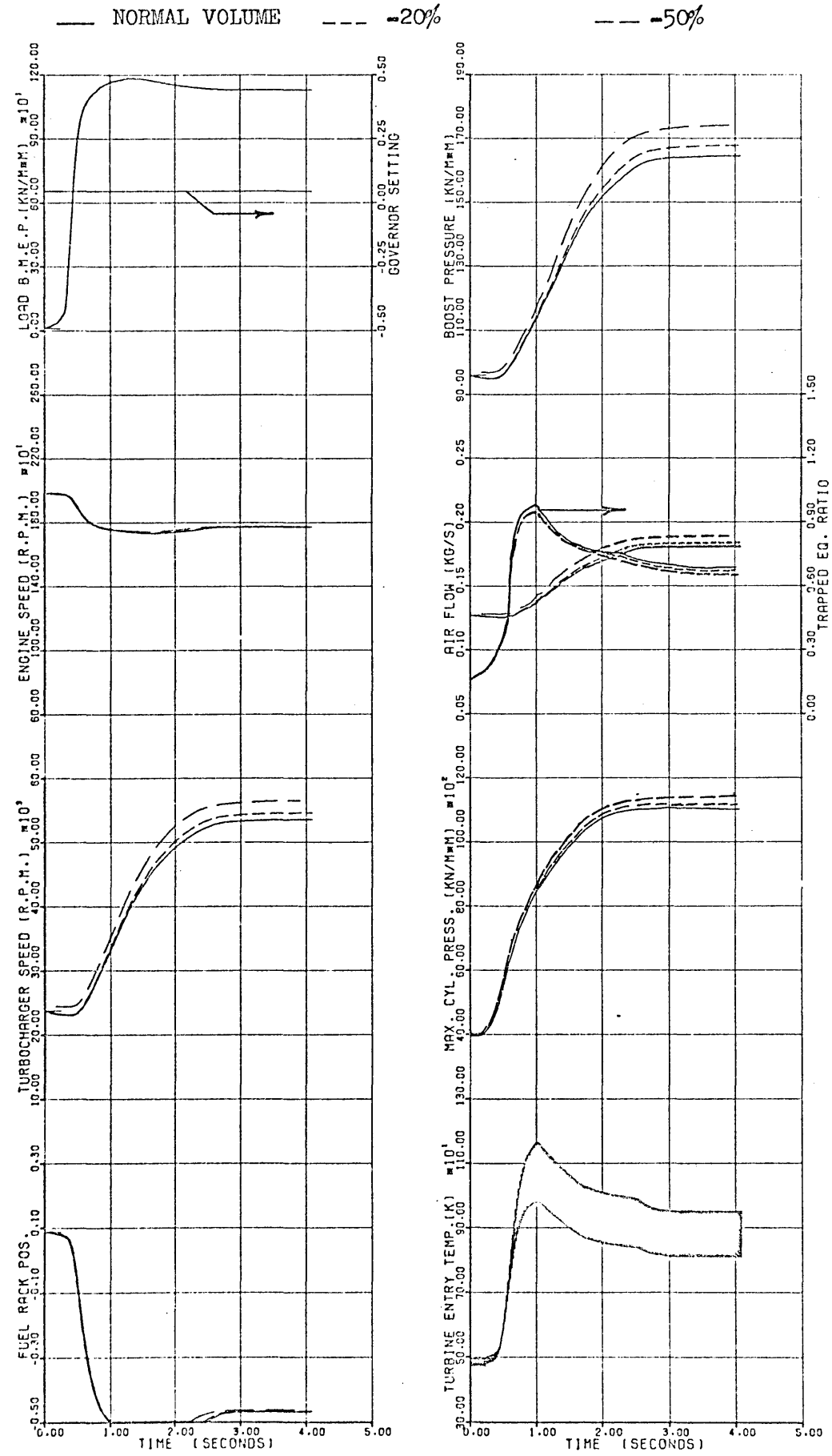


FIG.(7.38) EFFECT EXHAUST MANIFOLD VOLUME

| | LOAD (BMEP BAR) | GOV. SETTING | ENG. SPEED (RPM) |
|---|---|---|---|
| INITIAL | 0.1 | 0.045 | 1980.4 |
| FINAL | 11.3 | 0.045 | 1772.7 |

an increase of 0.4% in friction torque and a reduction of 0.3% in fuelling. To achieve an appreciable improvement in the speed response of the engine, the exhaust manifold must be further reduced until the peak equivalence ratio is significantly lowered by the increase in air flow. This can be visualised from the third set of response curves (Fig. 7.38) in which the exhaust manifold volume is reduced by 50%. However, care must be taken not to reduce the exhaust pipe cross-sectional area (hence volume) beyond an optimum value, since under these circumstances the fluid friction losses might outweigh the gains obtained from a decrease in volume. (Note that the program would not be able to take account of pressure wave reflections which may be important for larger engines; the effect of wave action being governed by diameter and length of the exhaust pipe.)

A 50% reduction in the induction manifold volume was tried. This resulted in very little change in the transient response of all the parameters. Nevertheless, it would appear that the influence of the induction manifold volume becomes more important in the case of large, slower speed and higher bmep engines.

### 7.4.3 Effect of exhaust valve timing

This exercise shows how the simulation program may be used to investigate the effect of exhaust valve timing on the transient response of an engine. An initial comparison between the steady state engine performance for three valve timings is shown in Fig. 7.39. For the particular engine under consideration (Leyland 520), steady state performance can be seen to deteriorate when the exhaust valve timing is advanced by $14^{o}$CA. As the valve overlap period is very

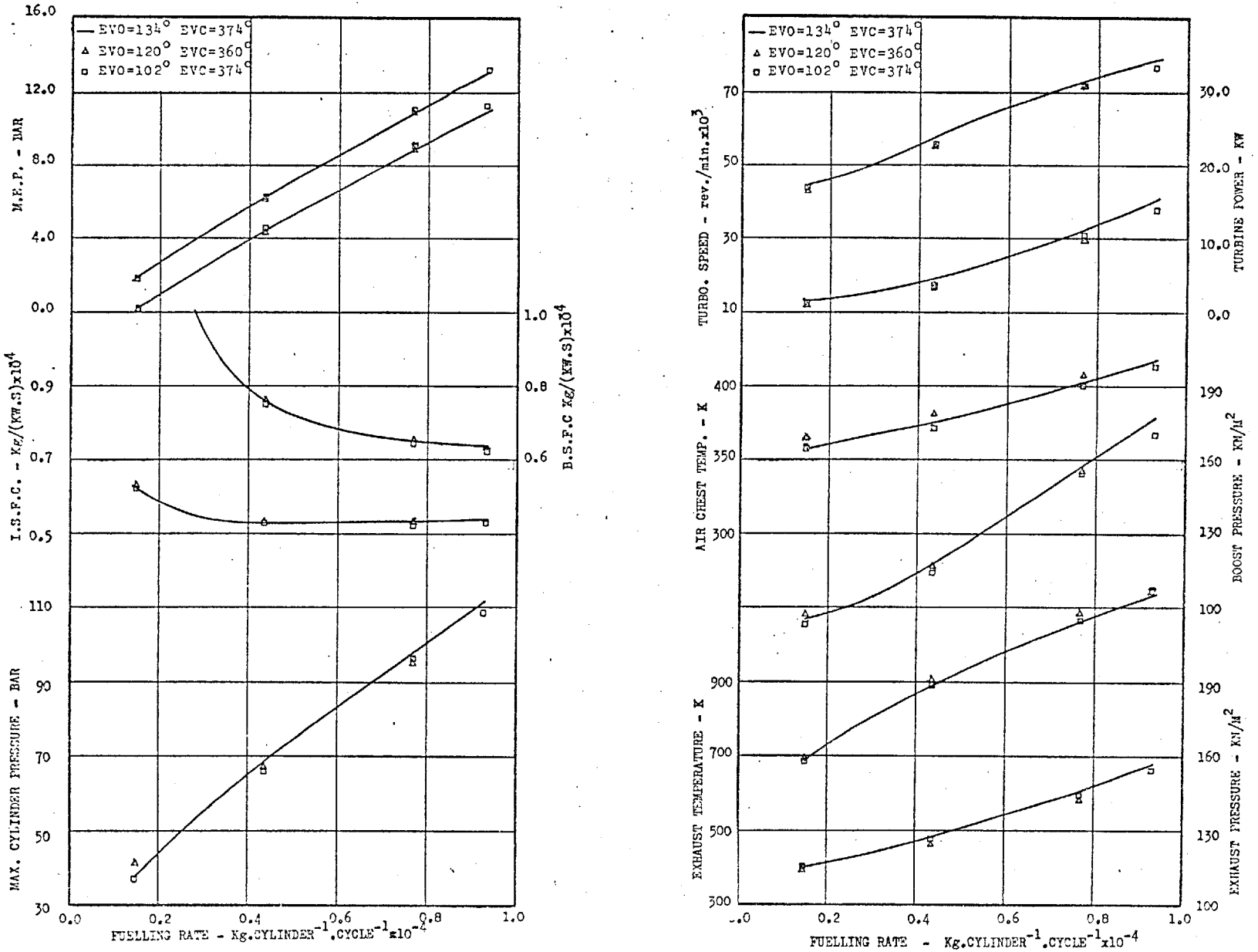


FIG. (7.39) Steady State Performance at Various Exhaust Valve Timings

short originally, advancing the timing causes the exhaust valve to close at TDC. This leads to a rise in cylinder pressure during the exhaust stroke and hence an increase in pumping work. By maintaining the same timing for valve closure and advancing opening by $32^{o}$CA, the maximum bmep (at the same speed) is decreased by 1.7% and the bsfc is reduced by 1.5%. However, boost pressure and air flow (at maximum torque) are reduced by 3.7% and 1.99%, and turbo-charger speed falls by 3.8%. The effects of the three timings on scavenging pressures and valve flow are shown in Fig. 7.40.

Figure 7.41 shows the effect of advancing the exhaust valve opening by $32^{o}$CA (with a fixed closure timing) on the transient response of the engine. It should be noted that the resulting changes in response cannot be generalised due to their dependence on a host of factors pertinent to a particular engine design. It follows that the program should be used to investigate the effect of exhaust valve timing in each particular case. For example, it is likely that a mechanism which advances the exhaust valve timing during transient operation would prove more beneficial in the case of engines with wide valve overlap. In such situations, the reduction in valve overlap could minimise backflow into the induction manifold at the initial stages of the transient (this results from the fast increase in exhaust pressure relative to boost). Hence the trapped mass of air would increase and lead to a reduction in the maximum equivalence ratio. The resulting reduction in scavenge flow would increase the mean exhaust temperature and also reduce the compressor power requirement. Naturally this would be coupled with the expected increase in blowdown exhaust pulsations.

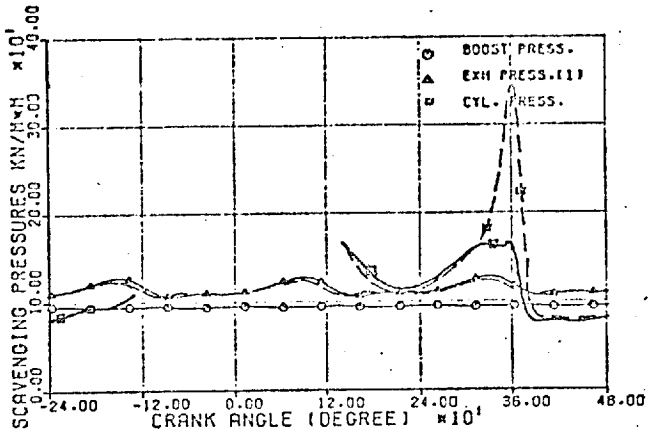


BMEP=0.0 BAR

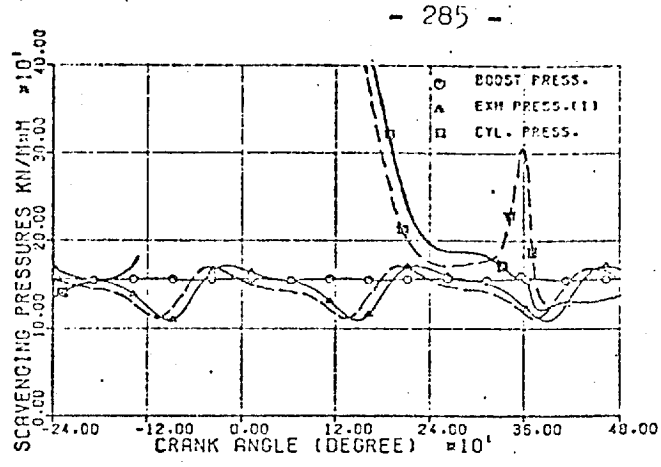


BMEP=9.0 BAR.

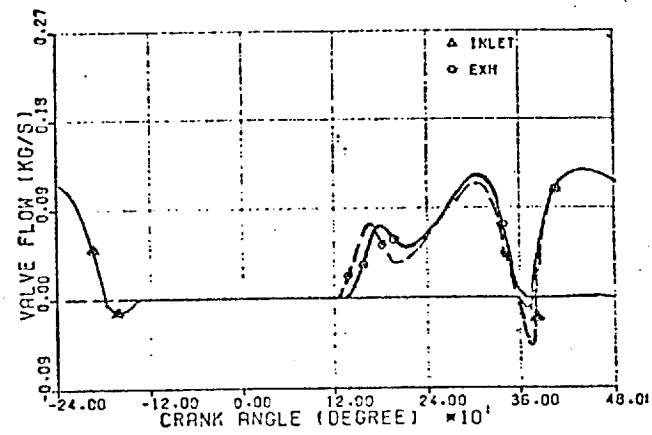


NORMAL TIMING

EVO=134° EVC=374°

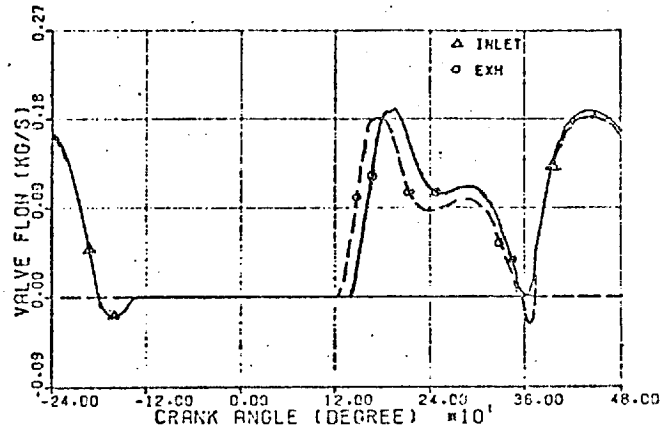


NEW TIMING

EVO=120° EVC=360°

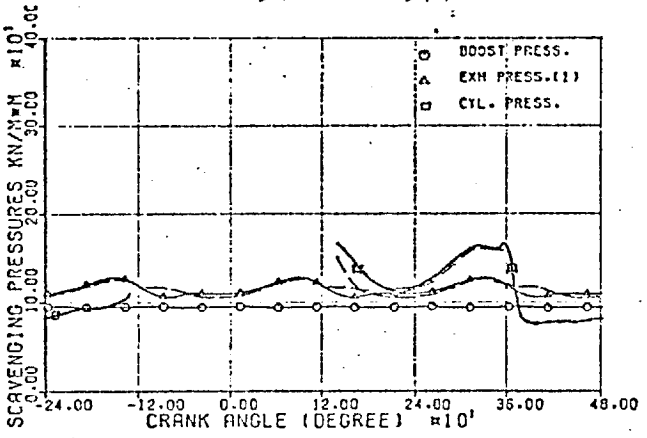


BMEP=0.0 BAR

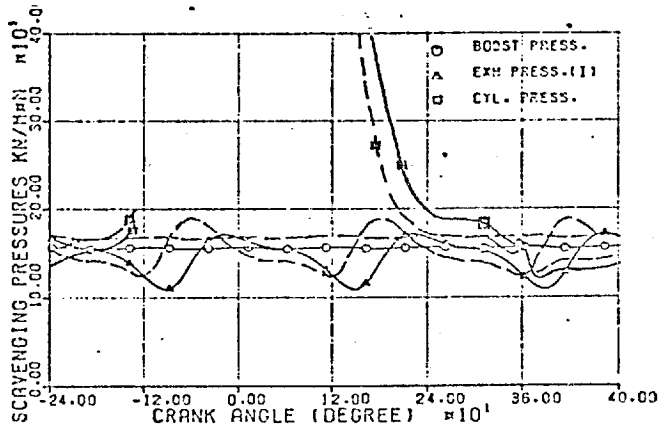


BMEP=9.0 BAR

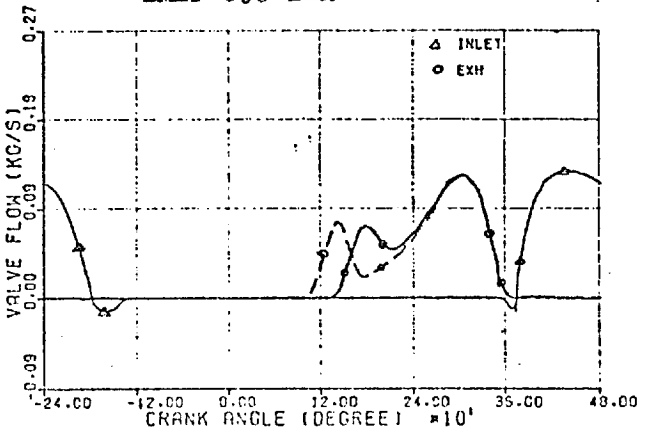


NORMAL TIMING

EVO=134° EVC=374°

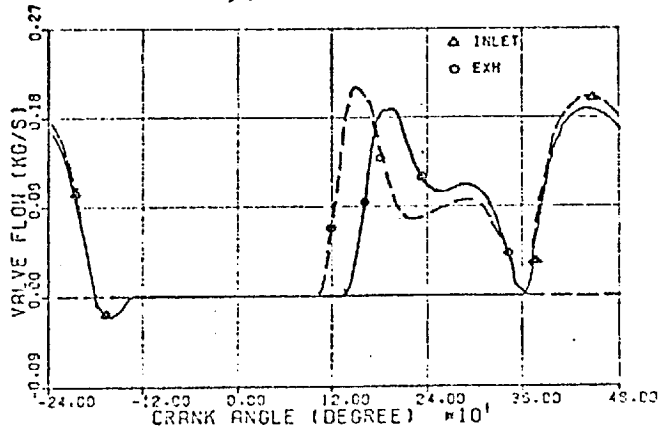


NEW TIMING

EVO=102° EVC=374°

FIG.(7.40) Influence of Exhaust Valve Timing on Gas Exchange.
Engine Speed=2000 rev./min.

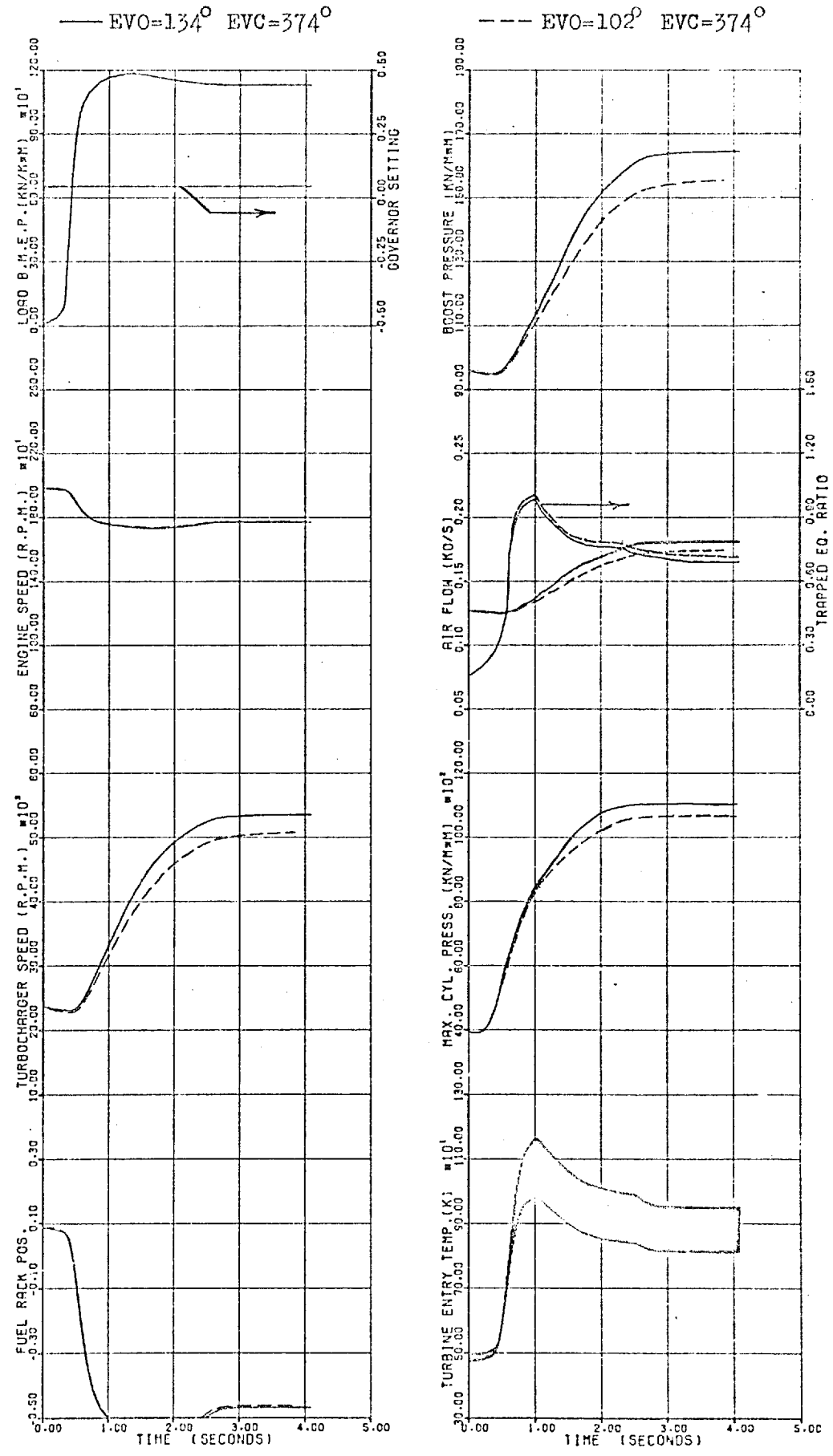


FIG.(7.41) EFFECT EXHAUST VALVE TIMING

| | LOAD (BMEP BAR) | GOV. SETTING | ENG. SPEED (RPM) |
|---|---|---|---|
| INITIAL | 0.1 | 0.045 | 1980.4 |
| FINAL | 11.3 | 0.045 | 1772.7 |

### 7.4.4 Effect of air cooling

Considering constant engine speed operation only, Fig. 7.42c shows significant advantages for the aftercooled engine compared with the non-aftercooled version. In this exercise a zero pressure drop is assumed through the cooler. Also the maximum fuelling, plus the total volume in between the compressor and inlet valves, are fixed for the two engines. Of particular importance is the relatively high air flow with low inlet manifold pressure obtained with cooling and the resultant low exhaust temperatures. Also, the lower heat rejection to the coolant with the aftercooled engine is quite significant. Fuel consumption also shows a slight improvement with aftercooling.

The transient response of the two engines, to the same load application is displayed in Fig. 7.42a. It can be seen that the speed of the aftercooled engine recovers earlier even though the turbocharger shows very little improvement in speed response. This is caused mainly by the reduction in heat rejection to the cylinder walls and the decrease in maximum equivalence ratio (following the increase in air flow). The final steady state values of engine and turbocharger speeds and peak cylinder pressure are increased slightly with aftercooling, whilst boost pressure, fuelling, equivalence ratio and exhaust temperature are reduced. The working line of the aftercooled engine, superimposed on the compressor map (Fig. 7.42b), can be seen to have a lower gradient in relation to the non-aftercooled version. This indicates a higher rate of increase of air flow with boost pressure.

In this exercise the thermal capacity of the cooler is assumed to have no effect. The cooler effectiveness is taken to be 70% and a coolant temperature of 300$^{o}$K

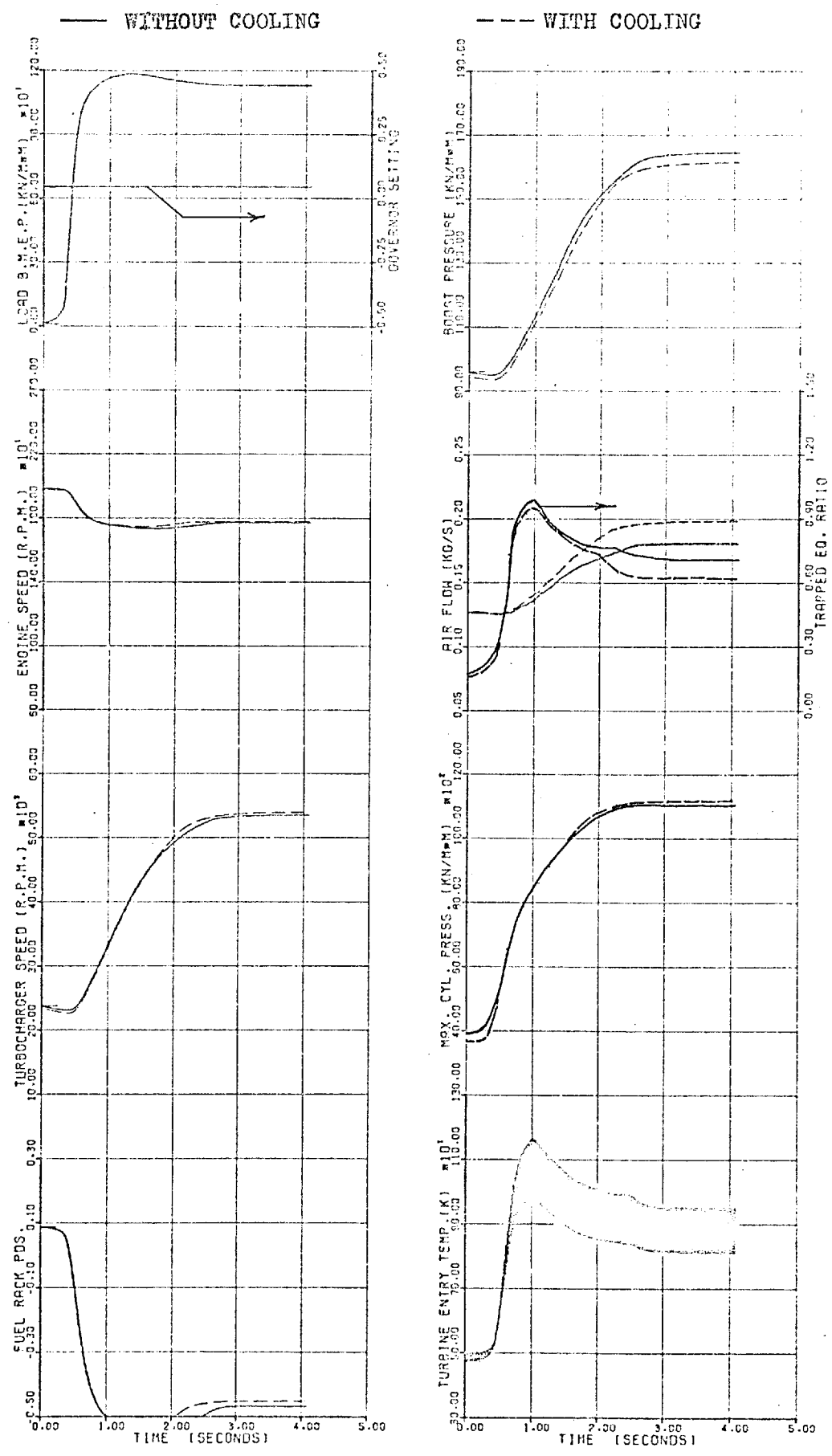


FIG. (7.42,a) EFFECT OF AIR COOLING ($\eta$ = 0.7)

| | LOAD (BMEP BAR) | GOV. SETTING | ENG. SPEED (RPM) |
|---|---|---|---|
| INITIAL | 0.1 | 0.045 | 1980.4 |
| FINAL | 11.3 | 0.045 | 1772.7 |

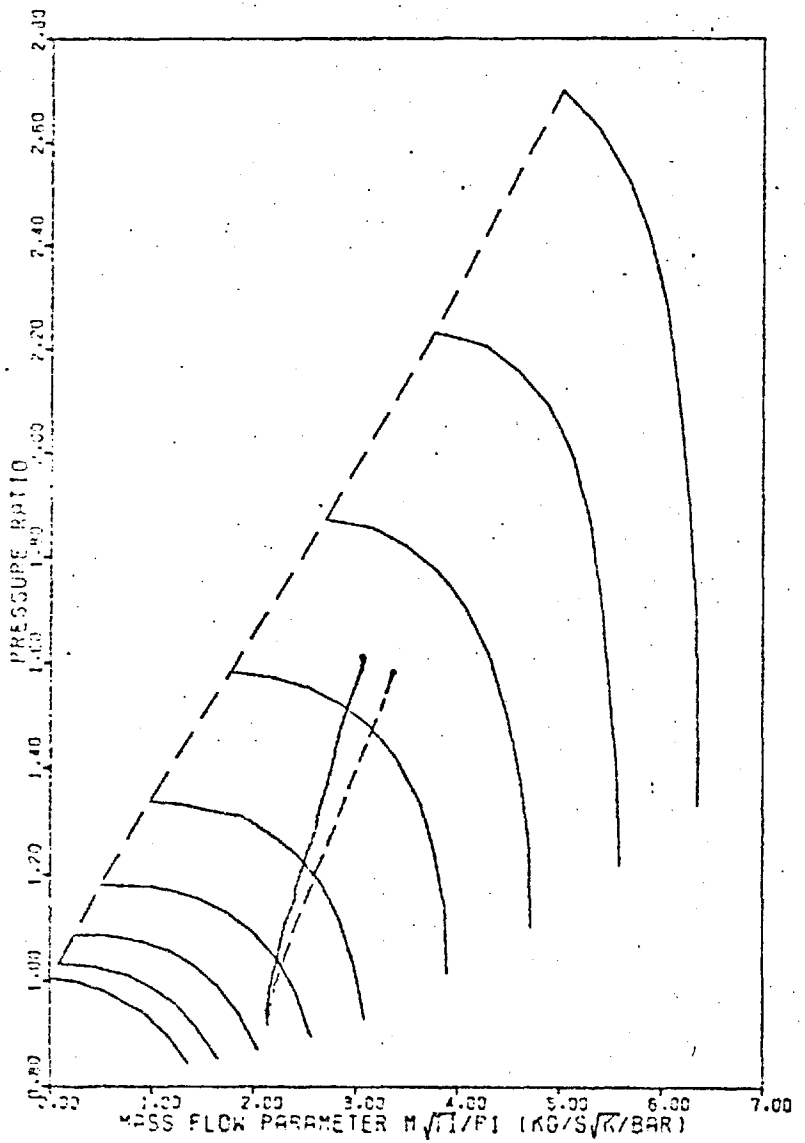


FIG. (7.42,b) EFFECT OF AIR COOLING

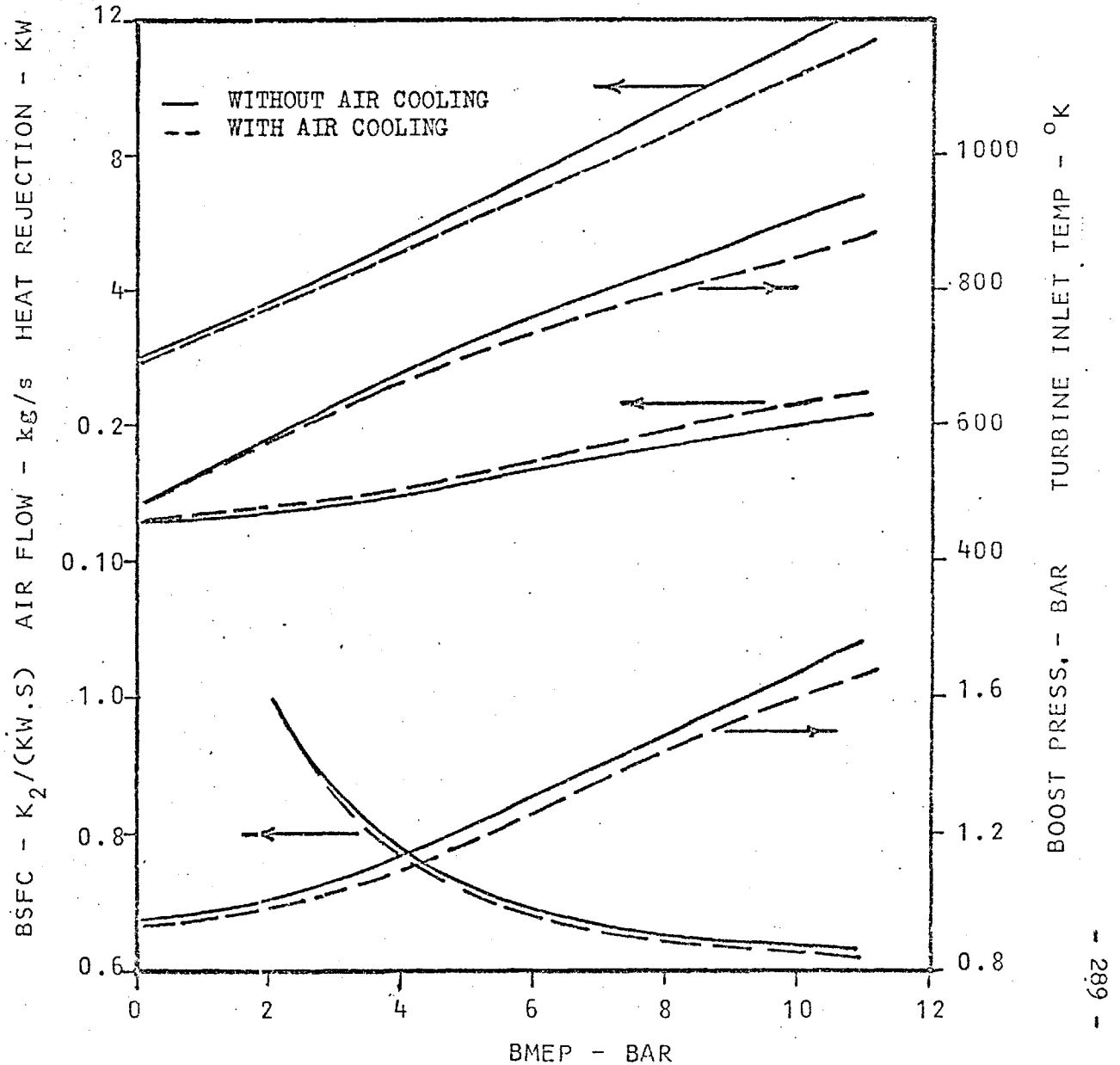


FIG. (7.42C) Effect of Air Cooling on Steady State Performance.
Engine Speed = 2000 rev./min.

is assumed. This is representative of an air to water cooler for stationary engines or an air to air cooler for automotive applications. The problem of obtaining cool inlet air on a vehicle is relatively complex. The simplest cooler for vehicle use is one using the cooling circuit of the engine. Such an arrangement can be shown to lead to a deterioration in the transient response of the aftercooled engine. This results from the decreased initial air mass flow caused by the relatively high coolant temperature (engine water).

### 7.4.5 Effect of variable geometry turbine

In most automotive applications it is necessary to develop high torque at low engine speed to ensure hill climbing power and adequate vehicle acceleration. From the standpoint of the maximum engine torque, it would be desirable to have a variable geometry exhaust turbine. By varying the angle of the inlet nozzles, the effective area of the turbine (and hence energy availability) and its efficiency characteristics both alter. This provides more than adequate air supply at maximum power and improves performance at low engine speeds. A typical design of such a system adjusts the nozzle area according to boost pressure.

The simulation program was employed to model a turbocharged diesel engine, equipped with a variable nozzle turbine. Ideally, the dynamics of the control mechanism should be represented by a second order differential equation of the form:

$$\ddot{x} + C1\dot{x} + C2x = C3f(P_b) \qquad (7.2)$$

where: $x$ = instantaneous nozzle area, as a percentage of the maximum value.

$P_b$ = boost pressure.

C1, C2, C3 = constants which depend on the design.

Equation (7.2) describes the dynamic balance between the force generated by the boost pressure and the opposing forces due to the spring, inertia and damping. It can be resolved into two first order simultaneous differential equations, to be solved in conjunction with the other differential equations of the simulation (Section 3.2).

However, the time-dependent terms were not considered in this exercise, and the percentage change in nozzle area was related to boost pressure as follows:

$$x = 0.8 + \frac{0.2}{70}(P_b - 90.0) \qquad (7.3)$$

This represented a full range variation of nozzle area of 20% (of the maximun area), within boost pressure limits of: $90.0 < P_b < 160$ KN/m$^2$. Hence it resulted in a smaller nozzle area at part loads and also at low engine speeds. Turbine efficiency was taken as independent of nozzle area for this simple exercise. Nevertheless, the program can consider the influence of a changing efficiency with area, provided that data is available.

Fig. 7.43 shows that by fitting a variable geometry turbine to the engine, a significant improvement in the turbocharger response is obtained. This is seen to start very early in the transient period as the maximum reduction in the turbine swallowing capacity occurs at low boost. A similar effect is shown in both the boost pressure and air flow, which results in higher peak cylinder pressures compared with the normal engine. A small reduction in the overall equivalence ratio curve is achieved, but only close to the peak value. The response in engine speed is marginally better.

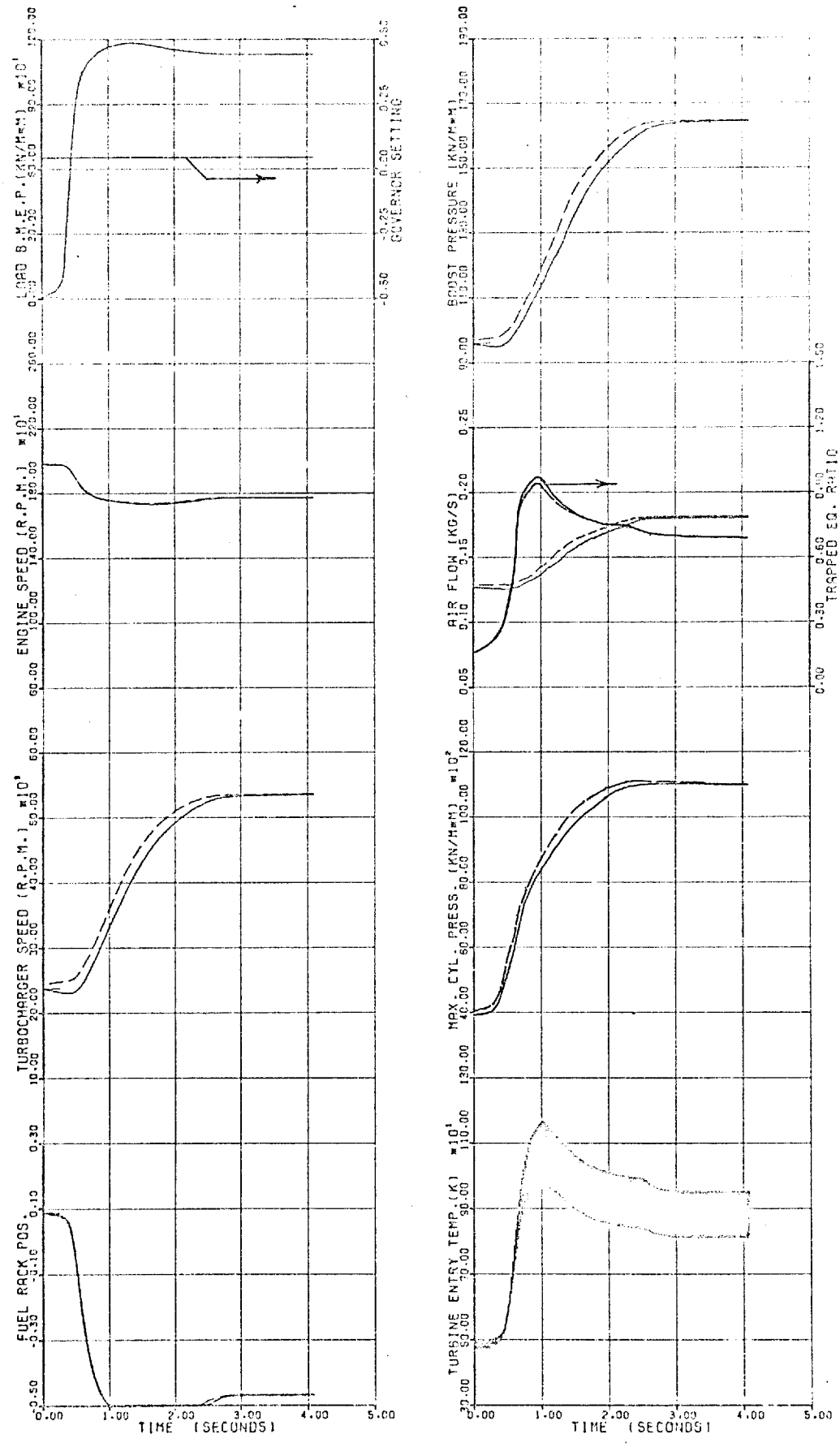


FIG.(7.43) EFFECT OF VARIABLE GEOMETRY TURBINE

| | LOAD (BMEP BAR) | GOV. SETTING | ENG. SPEED (RPM) |
|---|---|---|---|
| INITIAL | 0.1 | 0.045 | 1980.4 |
| FINAL | 11.3 | 0.045 | 1772.7 |

However, this improvement is underestimated by neglecting the time-dependent terms in equation (7.2) and by assuming no reduction in turbine size (hence inertia). This leads to an instantaneous variation of nozzle area with boost pressure.

If the control system were designed to give a sufficient lag between the response in nozzle area and boost pressure, a significant improvement in the transient response of the engine could be obtained. Naturally this would be more pronounced with engines of higher bmep.

### 7.4.6 Effect of rematching to a smaller turbocharger with exhaust waste gate

The variable geometry turbine may be a somewhat complex mechanism, hence expensive and unreliable. However, a substitute which has been in use for many years on turbocharged aircraft engines, is in the form of a controllable by-pass valve around the turbine. This type of control (waste gate) is normally used in conjunction with a smaller turbine nozzle. The exhaust by-pass valve opens sufficiently to prevent turbine overspeed at high engine output. Thus while it does not duplicate the performance of the variable nozzle, it approximates to it via a simpler mechanism.

The exhaust waste gate normally operates according to the boost level, but other alternatives are possible. A simple poppet valve (actuated pneumatically) is a typical design.

Since the use of a smaller turbine nozzle coupled with exhaust waste gating basically increases the specific air consumption of the engine at low speeds, it was felt that it would also improve transient performance. A logical

development would be to employ a smaller turbocharger (rather than a smaller turbine nozzle) so as to augment the improvement in engine response via the additional benefit of a reduced turbocharger inertia. The simulation program was employed to investigate this proposal.

For the purpose of comparison it was decided to employ the standard turbocharger match of the Leyland engine as a baseline. Predicted performance (maximum torque curve) with this match is shown in detail in Fig. 7.44a-c. The baseline performance was obtained using the characteristics of the Holset 4L 456/2.75 turbocharger, details of which are given in Appendix C.

The next step was to predict the engine performance with a smaller frame size of the turbocharger. It proved possible to employ a smaller turbine area and achieve the correct mass-flow characteristics by using a Holset 3LD turbocharger. The engine performance predicted with this turbocharger (fitted with a hypothetical turbine casing having an effective area 22% less than the 4LE unit) is also shown on Fig. 7.44a-c. The fuelling was scaled to maintain the baseline minimum air-fuel ratio. In practice this meant an increase of 5%. As a result of the new match, a 4% increase in maximum torque was obtained. However, this was accompanied by a 1.5% deterioration in specific fuel consumption because of increased pumping work. Note that the maximum turbocharger speed increased from 75500 to 93000 rev./min. (22%) and the peak cylinder pressure rose from 121.4 to 138.5 bar (14.1%).

A waste gate model was then built into the simulation program, permitting each branch of the exhaust manifold to be kept separate (i.e. one by-pass valve per

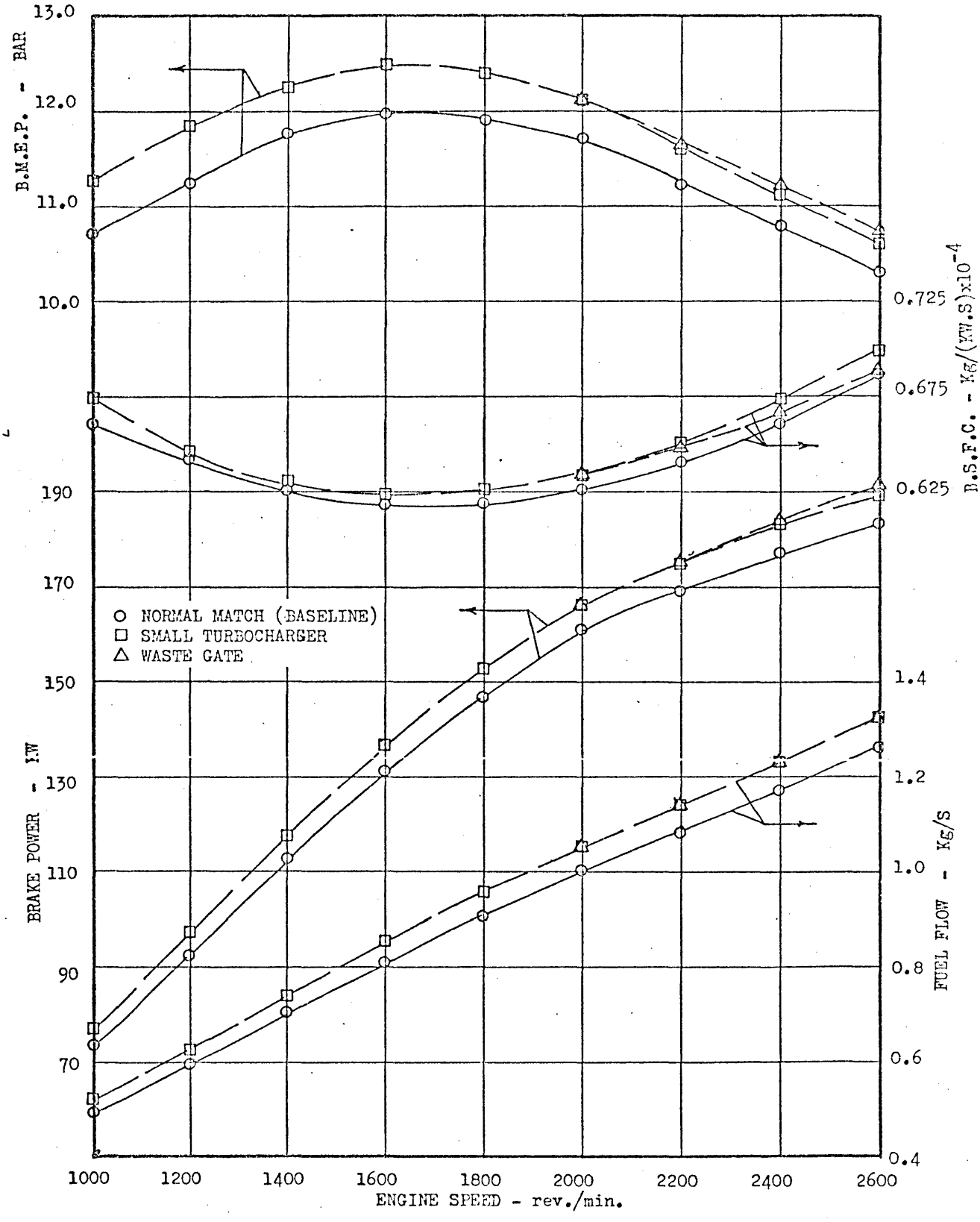


FIG.(7.44a) Steady State Performance of Engine Rematched with Waste Gate

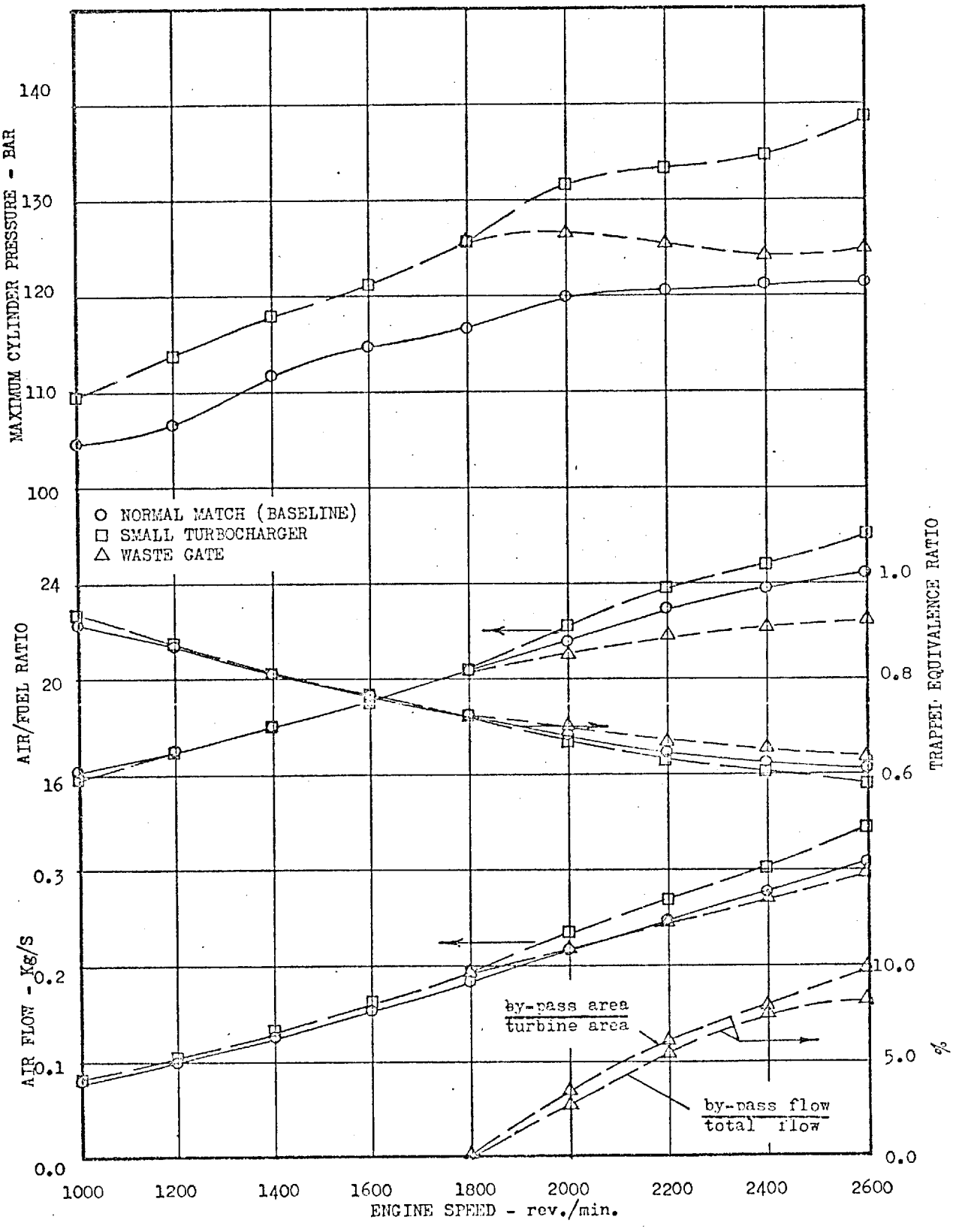


FIG.(7.44b) Steady State Performance of Engine Rematched Waste Gate.

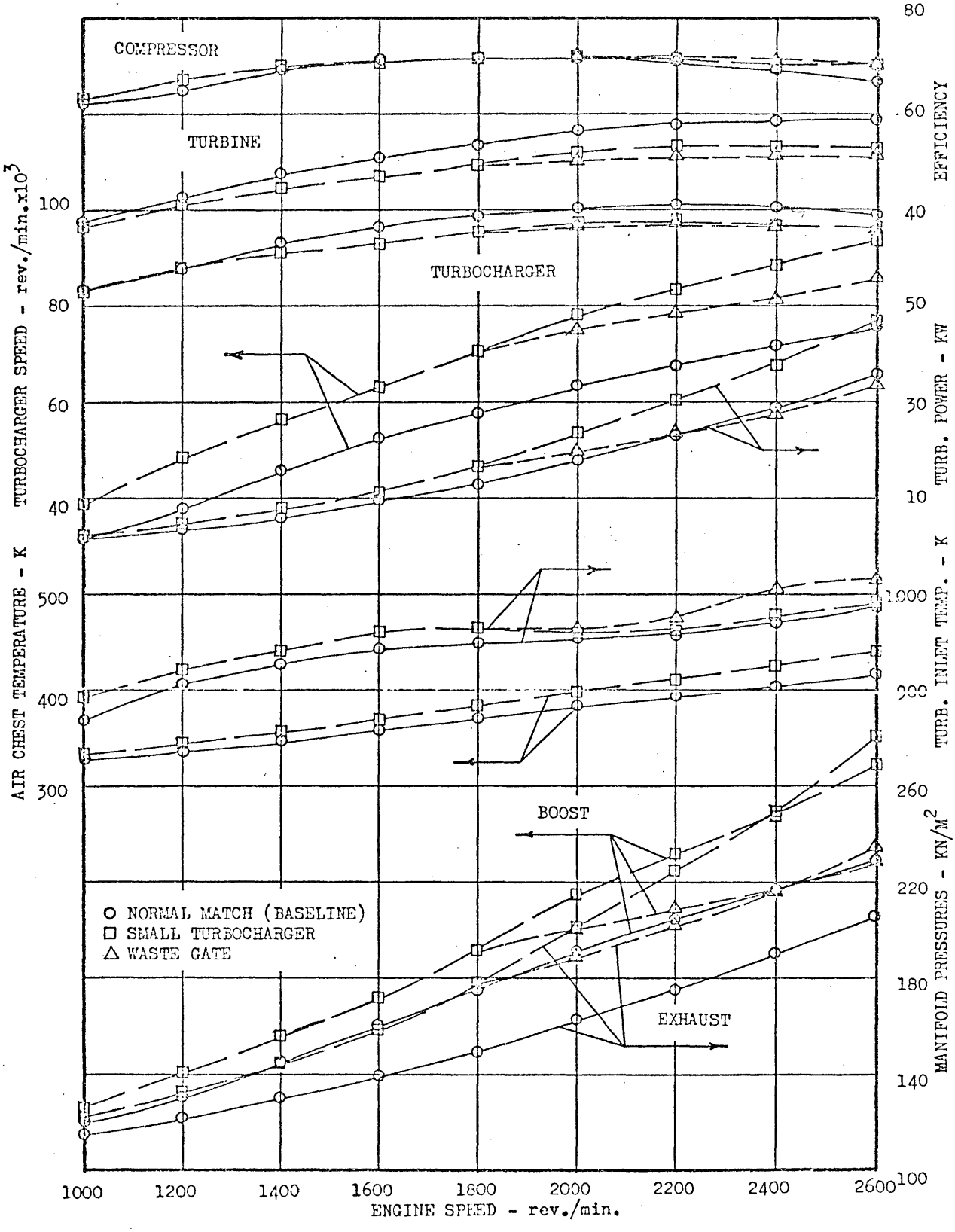


FIG.(7.44c) Steady State Performance of Engine Rematched Waste Gate.

turbine entry). The valve area was chosen such that the boost pressure at maximum power was reduced to the corresponding baseline value. An effective valve area of 1.3 $cm^2$ (i.e. 10% of the turbine area) was found to be sufficient to reduce the maximum boost pressure from 269 to 229 $KN/m^2$. It was also assumed, for convenience, that the valve area varied linearly with boost pressure and closed completely at 190 $KN/m^2$.

Figures 7.44a-c display the engine performance with the new turbocharger match and waste gate. Note that at maximum power, the waste gate passed 8.3% of the total mass flow. The maximum bmep increased by 4% in relation to the baseline value and the specific fuel consumption rose by less than 1%. Also the maximum values of the cylinder pressure and turbocharger speed were not embarrassingly high; 126.5 bar and 86000 rev./min. respectively (i.e. increases of 4.2% and 13.9%).

Comparing predictions with and without the waste gate, but with the same turbocharger match, shows that the valve improved performance via reducing excess pumping work.

The influence of the foregoing design changes on the transient performance of the engine was then investigated. Figure 7.45 compares predicted engine response to a rapid load increase for the two cases: the baseline engine, and rematched with waste gate system. Clearly the response of the turbocharger was dramatically improved by adoption of the waste gate. The resultant difference in the speed response of the engine was dramatic since it was able to accept this load increase without difficulty. However, the speed undershoot was substantially reduced, with the fuel

—— NORMAL TURBOCHARGER --- SMALLER TURBO.& WASTE GATE

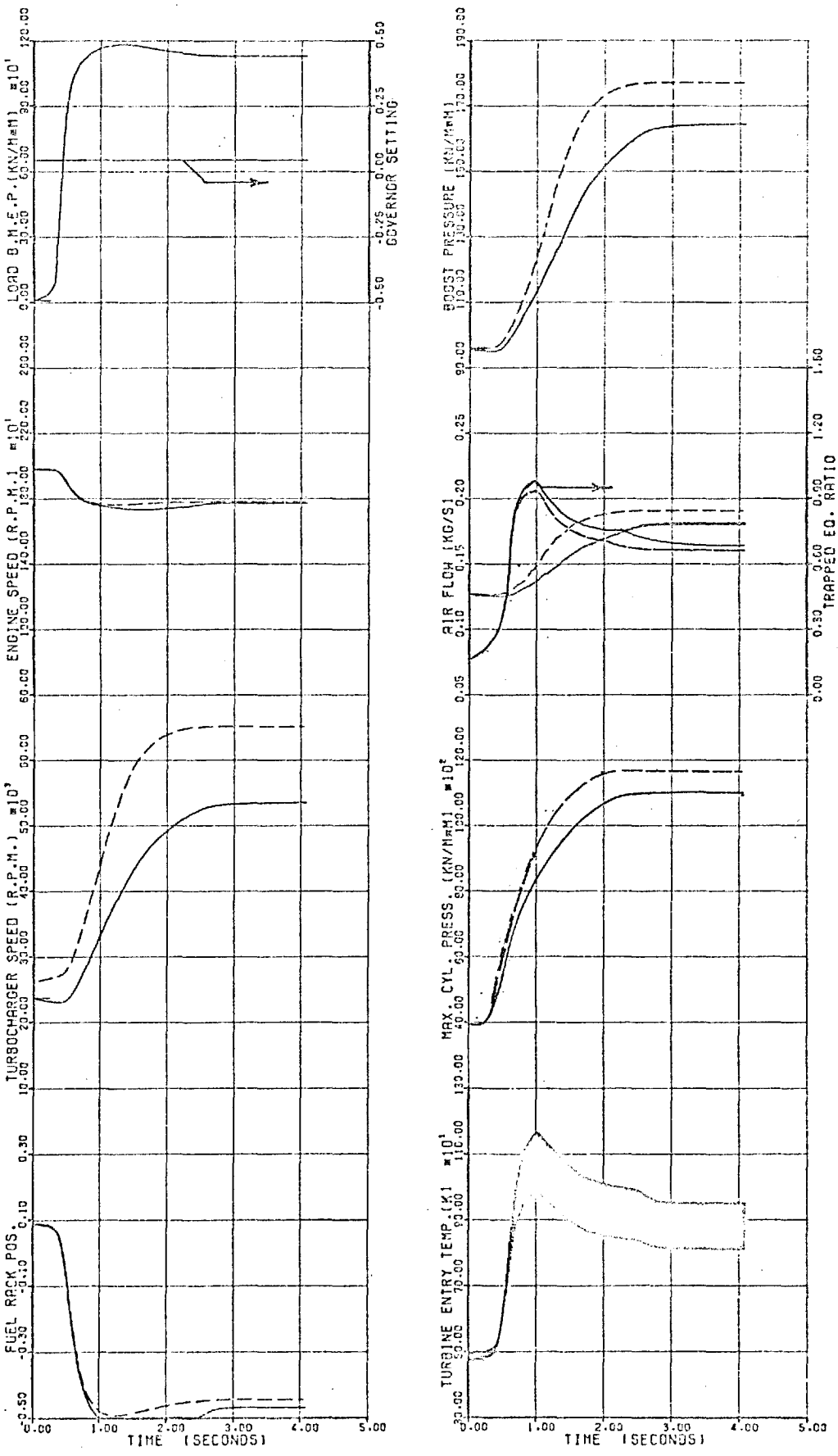


FIG.(7.45) SMALLER SIZE TURBOCHARGER AND WASTE GATE

| | LOAD (BMEP BAR) | GOV. SETTING | ENG. SPEED (RPM) |
|---|---|---|---|
| INITIAL | 0.1 | 0.045 | 1980.4 |
| FINAL | 11.3 | 0.045 | 1772.7 |

rack touching the maximum fuelling stop. This, as well as the increased air flow (following the improvement in turbocharger response) led to a lower maximum equivalence ratio. Consequently, it would be expected that the improvements brought about by the waste gating system would become greater at higher engine ratings.

The improvement in transient response has resulted largely from reduced turbocharger inertia following the adoption of a smaller frame size. The turbine wheel reduction from 0.0914 m. to 0.0762 m. was accompanied by a reduction of about 52% in polar moment of inertia.

### 7.4.7 Effect of limiting fuel rack travel

The need to control fuel input in relation to air flow (in order to avoid undesirable exhaust smoke) is known to increase with engine rating. Boost pressure sensing fuel rack limiters are provided to control the quantity of fuel injected per cycle during periods of rapid increases in injection rates, particularly at low engine speeds. The example presented here demonstrates the ability of the simulation program to predict the effects of such devices on the transient performance of the engine.

The predicted transient response of the engine with and without a rack limiter is presented in Fig. 7.46. Transient case TR11 (Section 7.3) (in which the engine was subjected to a sudden increase in demand speed from an initial condition of 985 rev./min. and 4.5 bar bmep). The dynamic limit on rack travel was taken to vary linearly with boost pressure within minimum and maximum positions, which were attained at 90 and 160 $KN/m^2$ respectively. In other words, the fixed maximum fuelling stop was never

—— FIXED MAX. LIMIT  =-= VARYING MAX. LIMIT

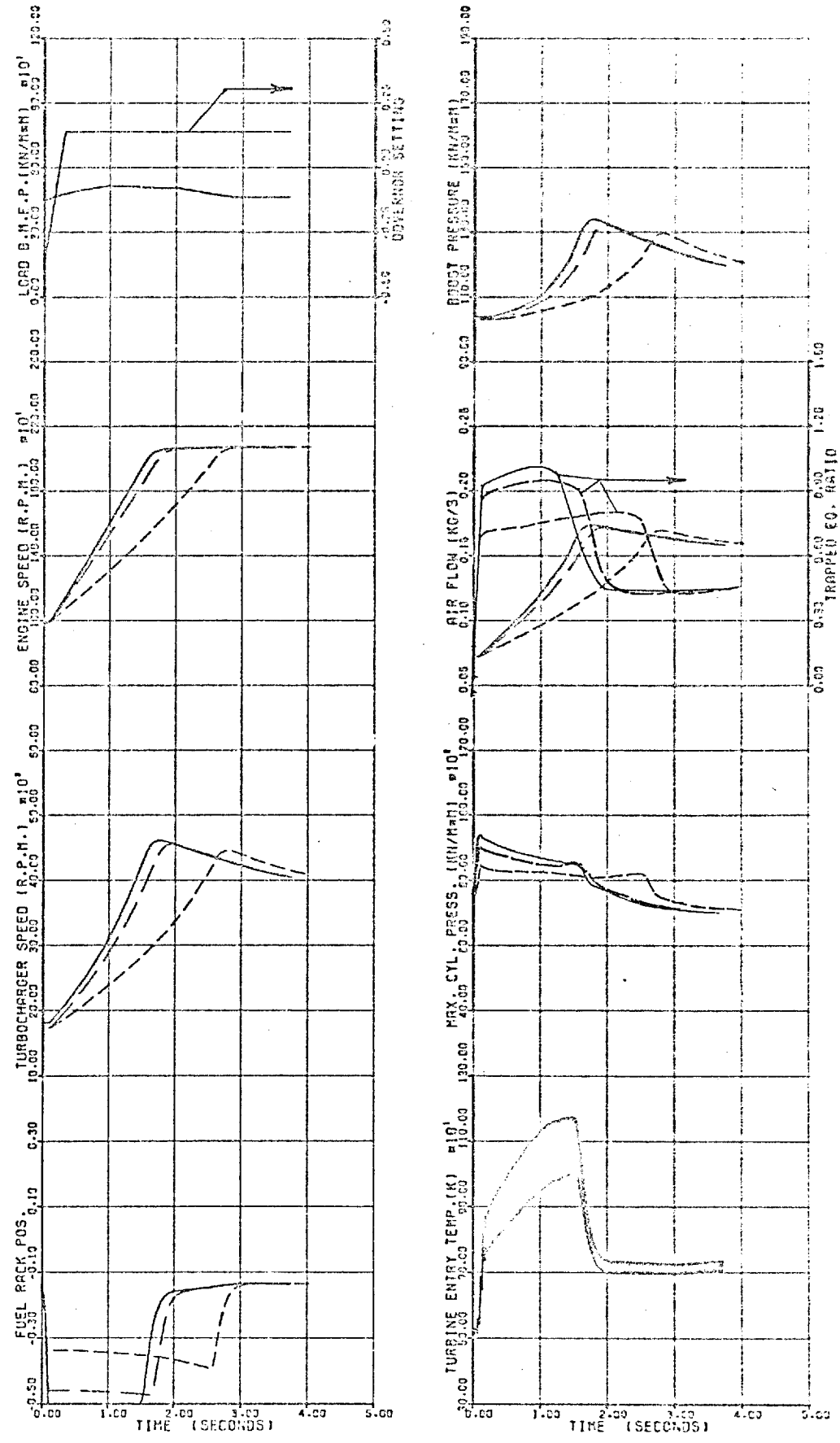


FIG.(7.46) EFFECT OF LIMITING RACK TRAVEL

| | LOAD (BMEP BAR) | GOV. SETTING | ENG. SPEED (RPM) |
|---|---|---|---|
| INITIAL | 4.5 | -0.360 | 984.7 |
| FINAL | 4.6 | 0.138 | 2071.6 |

reached at boost pressures below 160 $KN/m^2$. However, two values for the minimum position of the dynamic rack limit were tried; away from the maximum fuelling stop by 5% and 20% of the full rack travel.

It can be seen, in the case considered, that a 20% reduction in the rack travel (equivalent to 30% of the maximum fuelling) reduced the fuel/air ratio to 18.8; a realistic criterion for the exhaust smoke level. However, a dramatic deterioration in the transient response of the engine (see engine and turbocharger speed curves) resulted. It should be remembered, though, that this may not be so for highly rated engines, in which the instantaneous fuel/air ratios could become excessively rich (i.e. greater than stoichiometric); a rack limiter may then be beneficial to the response.

# CHAPTER 8

## CONCLUSIONS AND RECOMMENDATIONS

Considering the important criteria which influence the transient performance of turbocharged diesel engines, and noting the modelling techniques published to date, it was concluded that a more basic and generalised theoretical approach was needed. The present work was carried out accordingly, and the main objectives (Section 1.1) were achieved.

During transient operation, a turbocharged diesel engine experiences a wide range of normal and off-design conditions. Naturally the steady state relationship between the input fuel and torque developed (at any speed) no longer applies. This arises from the non-linear effects of the thermodynamics and gas flow as well as the dynamic interactions of the individual components of the engine. Hence a continuous analysis of these interactions in conjunction with the thermo and fluid dynamics is essential.

The application of the quasi-steady "filling and emptying" concept in the analysis of the thermo and fluid dynamics during transient operation proved successful. It permitted the simulation to take account of:

1. The time-discrete behaviour of the engine, which is governed by the intermittent fuel injection.
2. The non-linear influence of the combustion process on the torque developed and available exhaust energy.
3. The pulsating nature of gas flow (resulting from valve motion) as well as effects of manifold capacity.

4. The influence of manifold pressures on pumping work (gas exchange period).

Correlating experimental fuel burning rate curves to ignition delay, engine speed and equivalence ratio as well as evaluating heat generation via thermodynamic and chemical equilibrium, provided a dynamic combustion model which was justifiable for the application. The model was successful for steady state as well as transient operation. It was also moderately successful for cases in which over-rich fuel/air mixtures were developed. Further improvements might be achieved by including the effects of charge density, swirl, etc.

The key differential equations of the simulation constitute an initial value problem. A convenient set of state variables was employed to define the instantaneous conditions of the engine system, including thermo and fluid dynamics. By executing the numerical solution along crank-angle (instead of time), the periodic nature of the engine processes was displayed and the programming effort was reduced. Also the application of absolute internal energies and enthalpies greatly simplified thermodynamic computations.

The evaluation and development of the program was aided by obtaining reliable and detailed experimental data. A computer-based testing facility ensured the repeatability of the transient tests and enabled a very large fund of relevant measurements to be recorded. The computer-controlled test bed, instrumentation, plus the data logging system and techniques developed have been described. Even with computer-aided testing, the simultaneous control of engine transient operation and recording of considerable amounts of data (more than 40 K values/tests) requires skillful and competent

techniques. The techniques and test procedures developed in this work involved variable control of engine speed and load, multi-channel high speed data logging (up to 400 KHz), control of test sequence, plus processing and mass storage of data.

Experimental data, obtained from a turbocharged automotive diesel engine (Leyland 500 series) showed that:

(i) The response in peak cylinder pressure follows the rapid response of the governor, despite the resultant development of over-rich fuel/air mixtures (beyond the stoichiometric level).

(ii) The turbocharger response becomes faster with increase in engine speed.

(iii) The response of the engine to increased demand speed is slower at increased loads.

Comparisons of predicted and measured steady state data showed close agreement over the entire operational range of the engine; agreement improved with increase in load. Predicted and experimental transient data were compared for large changes (up to 100%) in load and demand speed as well as combined changes. Fuel/air ratios of 12.7:1 were attained in some cases. These comparisons included crankangle diagrams as well as overall response data. Again favourable agreement (within the accuracy of the measurements and the component characteristics of the engine system) was shown.

Since the transient performance of an engine/turbocharger combination is a result of many interacting factors, the influence of design changes on engine response is difficult to assess. An illustrative study of specific design changes has been completed. It was found that increasing specific air consumption via, (i) air cooling,

(ii) rematching to a smaller turbocharger in conjunction with exhaust waste gating or variable geometry turbine, improved the transient performance of the engine. Reducing the volume of the exhaust manifolds was beneficial, but advancing exhaust valve opening only slightly influenced transient response. The effects of limiting fuel rack travel as well as varying the inertias of the engine-load and turbocharger have also been investigated. These findings may not necessarily be generalised, because of variations in component characteristics of different engines and turbochargers. However, the simulation program can be applied in each specific case to decide its feasibility.

With such a simulation program one must consider its applicability to various engine designs, its limitations and the extent to which actual engine testing can be replaced. An explicit and comprehensive answer was beyond the objectives of this work; however, the conclusions reached so far are given below.

The present structure of the simulation program restricts its use to 4-stroke direct injection diesel engines, with or without turbocharging. It may readily be applied to 2-stroke engines with the assumption of perfect mixing during gas exchange. However, the introduction of a scavenging model should not be difficult. The indirect injection engine can be considered by including an extra thermodynamic control volume to represent the pre-chamber as well as modifying the combustion model. Two-stage turbocharging can be treated with very little modification. Additional control volumes in between low and high pressure components of the two turbochargers, as well as the performance characteristics of the second turbocharger are required. Furthermore, simulation of supercharged and compound engines is relatively

straightforward. These modifications are open for future investigation.

Summarising, it appears that the simulation method is applicable to all cases in which steady state performance prediction programs are currently employed. The present simulation excludes pressure wave reflection phenomena, therefore, the treatment of the exhaust manifold may be less successful with large engines. The resultant influence on accuracy of the predicted transient response may not be crucial; this remains to be assessed. Such a limitation can be alleviated by applying the method of characteristics; however, considerably larger computing requirements (time and core) make it impracticable.

By extending mathematical cycle analysis to engine transient operation, the simulation developed in this work eliminated the major restrictions experienced with earlier models; namely, application of linearised control techniques, oversimplification of component characteristics and extensive reliance on experimental steady state data. Naturally this enhances the value of the simulation program as a research and development tool. However, additional work directed towards improving the modelling of combustion, heat transfer, scavenging, turbocharger performance, and engine friction, would be worthwhile.

The variation of the thermodynamic state variables during the cycle (particularly during valve overlap) dominate the selection of the integration interval. Valve overlap is the most critical part of the cycle, since both the inlet and exhaust valves are partly open, pressures in the cylinder and manifolds are nearly equal, the cylinder volume is close to its maximum value and the piston is changing its direction of motion.

A step size of $1^{o}$CA suited engine speeds down to 1000 rev./min. When this was halved, very little effect on the accuracy of the prediction was seen. However, smaller steps might be necessary at lower speeds, particularly on engines with wide valve overlap. Also, the use of relaxation factors dampened numerical fluctuations and speeded convergence.

The extent to which the simulation program can be relied on to replace actual engine testing is largely dependent on the skill of the user; considerable judgement may be necessary when designing a new engine. Consequently the main application of the program should be to limit the amount of actual testing, rather than predicting absolute values. In other words, it should be used to determine the feasability of a new design option or to study the effect of design changes on the performance (steady state and transient) of an existing engine. The program can also be most useful in investigating different devices employed to improve the transient response of the engine. Testing would then be limited to cases seen from the predictions to be feasible or optimal.

# APPENDIX A

## THE EVALUATION OF FLUID PROPERTIES

Diesel engines undergoing transient operating conditions cover a very wide range of mixture strengths. In some cases the equivalence ratio exceeds unity and the mixture becomes over rich in fuel, which leads to incomplete combustion. In order to obtain a practical and workable model, the treatment of the actual complex heterogeneous state of the combustion products is simplified by assuming thermodynamic equilibrium. This assumption was employed by Borman (21) and many others.

The application of Powell's concept (86) of absolute enthalpy and internal energy energy simplifies the analysis and computation of all processes, including those which involve mixing and combustion:

$$h_{absolute}(T) = \left[\begin{array}{c}\text{heat of formation at} \\ T=0^{o}K \text{ from elements in} \\ \text{their standard reference} \\ \text{states at } 0^{o}K\end{array}\right] + \left[\begin{array}{c}\text{sensible} \\ \text{heat at T} \\ \text{above } 0^{o}K\end{array}\right] \qquad (A.1)$$

Consequently, enthalpies of various systems which are at different thermodynamic states and composition become similar and compatible quantities.

For further simplicity, computational convenience and economy, mathematical expressions can be fitted to the tabulated values of the internal energy and gas constant of the combustion products of air and diesel fuel

### Actual products of combustion

Due to inhomogeneities, the actual combustion process does not necessarily generate the same products of combustion as would result from thermodynamic equilibrium

theory. Under steady running conditions the overall equivalence ratio is normally less than unity, whilst the combustion in various parts of the chamber may occur at much richer fuel-air ratios. The situation is worse during transient operation requiring rapid increases in fuelling. As a result of such over-rich fuel-air ratios and other non-equilibrium effects, some solid carbon may be formed and may be retained in the exhaust (81). Smoke measurements indicate the extent of such carbon formation; however, this is probably only qualitative, during severe transients.

The entire picture becomes very complex if non-equilibrium combustion is considered such that even if a simple single zone model could be developed, the analysis would require enormous computer storage and time. Furthermore, errors introduced by assuming equilibrium are reduced to some extent by the procedure of obtaining the fuel burning rate from the experimental pressure diagram, having made the same assumption.

Formulae for internal energy and the gas constant

The equilibrium thermodynamic properties of the products of combustion of air and diesel fuel (assumed to be $C_nH_{2n}$) were expressed analytically in the form:

$$e = e(T, P, F) \qquad (A.2)$$

$$R = R(T, P, F) \qquad (A.3)$$

The required formulae for lean fuel/air mixtures ($F < 1$) were taken from Krieger (64). For properties of rich mixture products ($1 < F < 1.6$), other formulae were fitted to data published by the General Electric Company (45). These are as follows:

(1) Internal energy:

for $F > 1.0$ and $T < 1333^{o}K$:

$$e = -2888.78 + 595.25(F-1) + 0.66854T + 2.71304 \times 10^{-4}T^{2} - 7.40325 \times 10^{-8}T^{3} + 0.25107(F-1)T \quad (A.4)$$

for $F > 1.1$ and $T > 1333^{o}K$:

$$e_1 = -3466.2 + 903.84 \times (F-1) + 0.65898T - 3.79924 \times 10^{-4}T^{2} + 8.23288 \times 10^{-8}T^{3} \quad (A.5)$$

for $1 < F < 1.1$ and $T > 1333^{o}K$:

$$e = e_1 + 14.2029(T - 1388.89)^{4.5371} \cdot \frac{(1-10(F-1))}{P^{0.46024}} \quad (A.6)$$

(2) Gas constant:

$$R = 0.22751 + 0.063438F - 3.33005 \times 10^{-3}F^{2} \quad (A.7)$$

where:

T = temperature, $^{o}K$.

P = pressure, bar.

F = equivalence ratio.

e = internal energy, KJ/Kg mixture.

R = gas constant, $KJ/K^{o}.Kg$ mixture.

Figure A.1 shows the internal energy and gas constant variation (together with their partial derivatives), with respect to equivalence ratio, covering both sides of the stoichiometric equivalence ratio ($0 < F < 1.6$) and temperatures up to $2000^{o}K$. The appearance of negative internal energies is a characteristic feature when using the absolute zero internal energy reference state. By definition, elements at $0^{o}$ have zero energy content (86) (the main combustion products, $CO_2$, $H_2O$ have large negative heats of formation), while on the other hand the sensible heat of an equilibrium mixture is

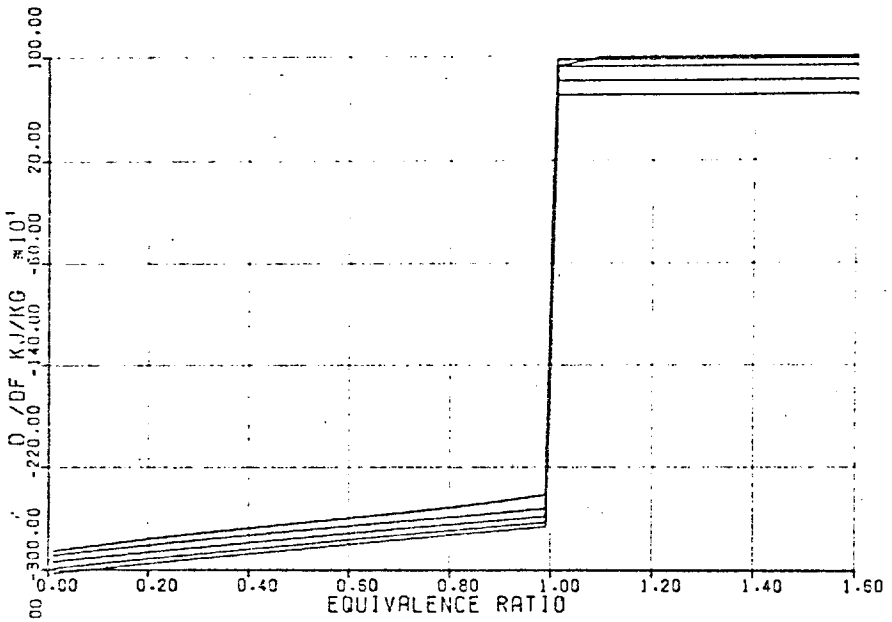


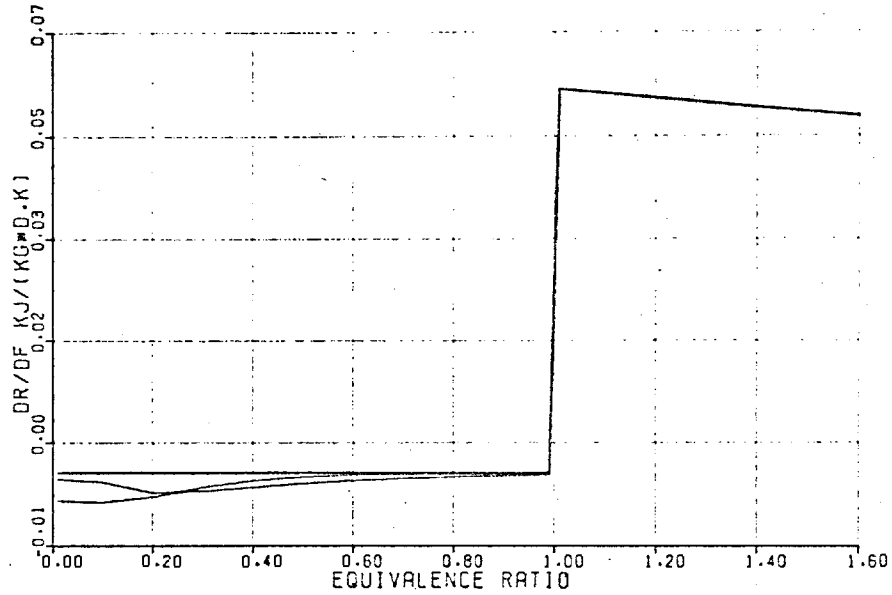


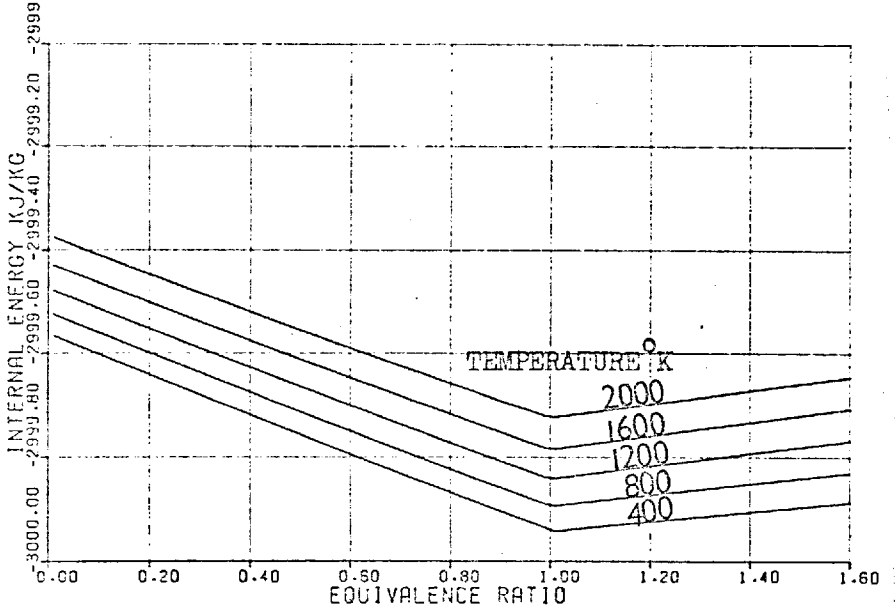


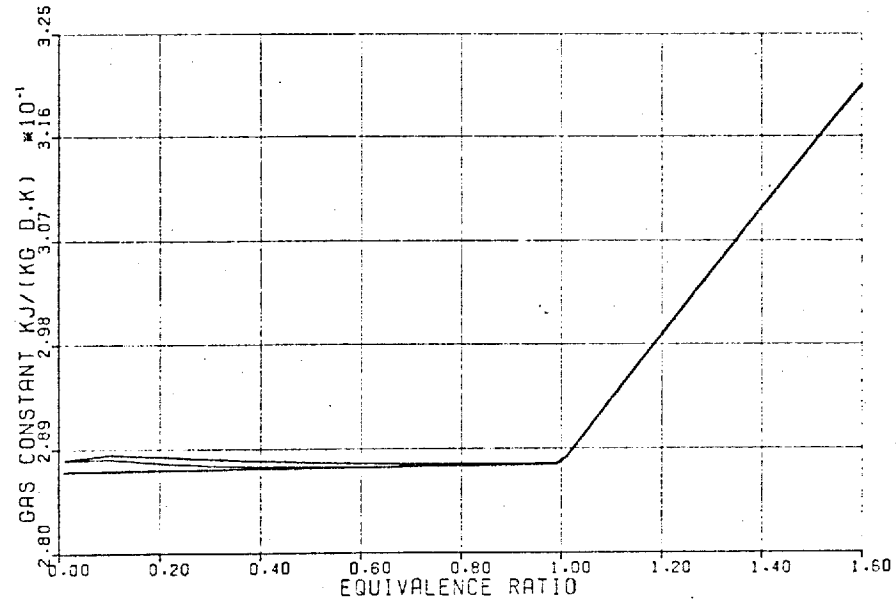


FIG.(A.1) Internal Energy and Gas Constant (together with Partial Derivatives wrt Equiv. Ratio) for Combustion Products of $C_nH_{2n}$ and Air as Function of Equivalence Ratio and Temperature.

always positive. Consequently the resulting absolute internal energy may be positive or negative.

The variation of $\frac{\partial e}{\partial F}\Big)_T$ can be seen to shift from negative (for lean mixtures) to positive (for rich mixtures), with a discontinuity at or near F = 1. Starting with pure air (F = 0), as more fuel is added and burnt, the amounts of $CO_2$ and $H_2O$ (accompanied by their large negative heats of formation) increase. In order to maintain a specified isotherm temperature, more heat has to be removed from the combustion products. At the stoichiometric air/fuel ratio, F = 1, no more free oxygen is theoretically available. Further introduction of fuel would entail the replacement of $CO_2$ and $H_2O$ with other products of lesser oxygen content and hence smaller heats of formation, e.g. CO.

# APPENDIX B

## DESCRIPTION OF INDIVIDUAL SUBROUTINES IN SIMULATION PROGRAM

### 1. Subroutine MAIN:

This is the master sub-program which directs all computations according to the operational mode specified (Section 3.5). It embodies a main loop which generates the crank position (in steps) and hence controls the basic sequence of computations involved in the simulation.

MAIN starts by calling subroutine INPUT to read all the input data and to initialise all variables. It also calls subroutines GEOMET, ETHERM, HT and GOVERN at each crank position. Subroutine PERFOR is called at the end of each steady state cycle to evaluate and print the overall performance data of the engine.

Computation of engine speed, turbocharger speed and fuel injected is executed by MAIN. The computation is allowed to proceed for a number of steady state cycles (NSS) in which the engine and governor dynamics are disabled. This ensures convergence of the thermodynamic conditions in all control volumes at a constant engine speed and fuel input. This is then followed by a number of transient cycles (NTR1) in which the dynamics of the engine and governor are considered under fixed initial values of load and governor setting. This period is necessary to achieve a real initial steady state prior to the application of the external disturbance. Values of NSS, NTR1 together with the number of cycles simulated during the transient response period (NTR2) are fed with input data. NSS and NTR1 were normally taken as 2 and 4 cycles respectively.

2. Subroutine ETHERM:

Thermodynamic and gas flow equations describing the developments inside the engine compartments are solved simultaneously in subroutine ETHERM. It applies the predictor corrector scheme described in Section 3.3 at each crank position $\theta_j$ to determine $M(\theta_j)$, $F(\theta_j)$ and $T(\theta_j)$ in the cylinders and manifolds. This requires instantaneous values of the following variables:

1. Engine and turbocharger speeds.
2. Geometric parameters (cylinders and valves).
3. Rates of burning of fuel.
4. Gas Properties.
5. Rates of gas flow through valves, turbine rings and compressor.
6. Rates of heat transfer from the gas to the surroundings.

Engine and turbocharger speeds are provided as input signals by the master subprogramme MAIN. Subroutines PROP, RFLOW, TURB, COMP and HTR are employed every iteration, to compute the last four items, due to their interaction with conditions inside the compartments. Geometric data of the cylinders and valves in addition to the fuel burning rates are generated every step, prior to starting the thermodynamic iteration (ETHERM).

3. Subroutine FBR:

This subroutine is called by MAIN at each step to compute the instantaneous fuel burning rates inside all the cylinders. Interaction between the combustion model

and the controlling parameters (ignition delay, trapped equivalence ratio and engine speed) is only permitted at the ignition point of each cylinder.

Whenever accessed, FBR performs a series of systematic checks to determine the timing of each cylinder in relation to the following points: static injection, dynamic injection, ignition and end of burning. As the last three points are dynamic values, which vary with the operating conditions, an iterative procedure is conducted in the event of any cylinder being within the static injection and ignition points. Equations (2.48) and (2.20) are applied on a step by step basis (each time FBR is called) in order to determine the dynamic injection point and the ignition point respectively.

The mode of burning proportionality factor and the premixed and diffusion burning shape factors (Chapter 6) are evaluated at the ignition point. Use is made of the corresponding conditions inside the cylinder considered, engine speed, current fuelling and ignition delay.

4. Subroutine GEOMET:

GEOMET generates (for all cylinders) instantaneous values of the following geometric parameters:

- cylinder volume, V
- rate of change of volume, $\frac{dV}{d\theta}$
- liner area exposed to gases, $A_L$
- inlet valve effective flow area, $A_{iv}$
- exhaust valve effective flow area, $A_{ev}$
- velocity term constant for heat transfer correlation.

Cylinder number 1 is taken as a reference, and all events (valve opening and closure, piston motion), are

timed by the angular position of the crankshaft in relation to the firing T.D.C. A relative crank position is also evaluated for each cylinder using its phase angle in relation to cylinder (1).

5. Subroutine HTR:

This subroutine evaluates the following:

1. Instantaneous rates of heat transfer from the gases (cylinders and exhaust manifolds).

2. Cycle-averaged temperatures of the cylinder walls.

Instantaneous values of the temperatures and pressures of the gases, engine speed, and liner exposed area are required in the case of the cylinders. Instantaneous gas temperatures only are required in the exhaust manifolds. Heat transfer to or from the inlet manifold is neglected.

HTR is subdivided into six sections, each of which is assigned a specific task. The first segment is accessed only once (at the beginning of each run) to evaluate the effective liner area (Section 2.7). A fifth order Newton Coates (29) integration formula is employed. The second segment treats the cylinder walls as three different regions (cylinder head, liner and piston crown) and is called at every thermodynamic iteration in any cylinder. It computes the rate of heat transfer to each surface according to the instantaneous values of gas temperature, pressure and engine speed in conjunction with the current mean temperature of the surface. Woschni's correlation (123) is used for evaluating the coefficient of heat transfer.

The third part of HTR executes (at each step) the integrations shown in the numerator of equations (2.51) and (2.52). Segment four applies the equivalent steady heat flow model (Section 2.7) and computes new mean values for the gas side surface temperatures. These are later employed (in segment 2) for the computation of the heat transfer rates in the next steady state cycle.

The variation of wall temperatures during transient operation is computed in segment 5, using equation (2.58) and temperatures evaluated at the previous cycle. Instantaneous rates of heat transfer from exhaust gases to the surroundings are evaluated every thermodynamic iteration in Section 6.

6. Subroutine PROP:

This subroutine provides the simulation program with values of the thermodynamic equilibrium properties of the gas mixtures. It embodies analytical expressions (Appendix A) representing the absolute internal energy and gas constant of dissociated and non-dissociated products of combustion with equivalence ratios varying between 0 and 1.6. Given values of T, F and P of the gas mixture, PROP computes the following: $e$, $\frac{\partial e}{\partial T}$, $\frac{\partial e}{\partial F}$, $\frac{\partial e}{\partial P}$, $R$, $\frac{\partial R}{\partial T}$, $\frac{\partial R}{\partial F}$, $\frac{\partial R}{\partial P}$.

7. Subroutine GOVERN:

Steady state and dynamic behaviour of the governor are evaluated by this subroutine. The initial position of the fuel rack (prior to the application of external disturbances) is determined by applying the steady state form of equation (2.46). During transient operation, GOVERN applies the predictor corrector pair, equations (3.20) and (3.21), to evaluate the new position of the fuel rack. Current

values of engine speed and governor setting are provided by MAIN.

8. Subroutine TURB:

TURB simulates each ring/sector as an individual turbine. It receives values of T, P and F of the exhaust gases, the back pressure, $P_b$, and the turbocharger speed at each thermodynamic iteration. Accordingly it responds by calculating mass flow, available exhaust power (rate of enthalpy transfer), efficiency and torque. Full admission characteristics (swallowing capacity and efficiency-blade ratio curves) are employed in a quasi-steady manner as described in Section 2.3.1.

If the operating point shifts, momentarily, outside the range of the turbine performance characteristics, computation is allowed to proceed using values at the nearest boundary, and cautionary messages are printed out.

9. Subroutine COMP:

COMP evaluates the compressor performance on a quasi-steady basis (Section 2.3.2), yielding the mass flow rate and delivery temperature of the air in addition to shaft torque. The steady flow performance map is represented by a grid formed by lines of constant speed parameter ($N/\sqrt{T_1}$) and an arbitrary family of approximately orthagonal curves, Fig. B.1. Grid points are defined by the pressure ratio $P_2/P_1$ and $N/\sqrt{T_1}$. The mass flow parameter $(\dot{m}\sqrt{T_1})/P_1$ and the compression temperature rise are considered as dependent variables.

Subroutine COMP is called at each thermodynamic iteration (ETHERM) and is fed with instantaneous values of

the boost pressure ratio and turbocharger speed. Subsequently it carries out a searching sequence followed by two-dimensional interpolation to determine corresponding values of $\dot{m}\sqrt{T_1}/P_1$ and $T_c$. The compression power and torque required are then computed. A series of identifying messages are incorporated for cases of choking, surging and pressure ratios below or above the minimum and maximum values on the performance map.

10. Subroutine RFLOW:

This subroutine computes the mass flow rates of gases through the valves (or orifices positioned at the entry of the air chest and exit of the exhaust manifold respectively, when the program is run in the naturally aspirated mode). It requires instantaneous values of the pressure ratio, upstream conditions of the gases (T,P,F,), geometric area and coefficient of discharge.

11. Subroutine INPUT:

This subroutine reads and processes all the input data. It also initialises all the variables and constants of the program.

12. Subroutine PERFOR:

PERFOR is employed at the end of each steady state cycle to compute the overall performance parameters of the engine.

# APPENDIX C

## ENGINE AND TURBOCHARGER DATA

| | | |
|---|---|---|
| Engine make and model: | Leyland, 520 series. | |
| Type | : | 4-stroke, compression-ignition, turbocharged. |
| Combustion chanber | : | open type (direct injection). |
| Number of cylinders | : | 6. |
| Bore | : | 0.118 M. |
| Stroke | : | 0.125 M. |
| Compression ratio | : | 15.1:1. |
| Full load speed range: | 800-2600 rev./min. | |
| Valve timing | : | |

| | Open | Close |
|---|---|---|
| Exhaust valve | 134°CA | 374°CA |
| Inlet valve | 350°CA | 590°CA |

(°CA = degrees crankangle after top dead centre preceding expansion stroke)

| | | |
|---|---|---|
| Static injection timing: | 24°CA before TDC. | |
| Firing order | : | 1, 5, 3, 6, 2, 4. |
| Moment of inertia | : | 3.09 Kg.M$^2$. (load inertia = 2.42 Kg.M$^2$) |
| Turbocharger make and model | : | Holset, 4LE. |
| Turbine type: | : | Double entry, single stage, radial. |
| Outside wheel diameter of turbine | : | 0.09144 M. |
| Compressor type | : | Single stage, centrifugal. |
| Outside wheel diameter: | 0.0938 | |
| Moment of inertia | : | 2.262 x 10$^{-4}$ Kg.M$^2$. |

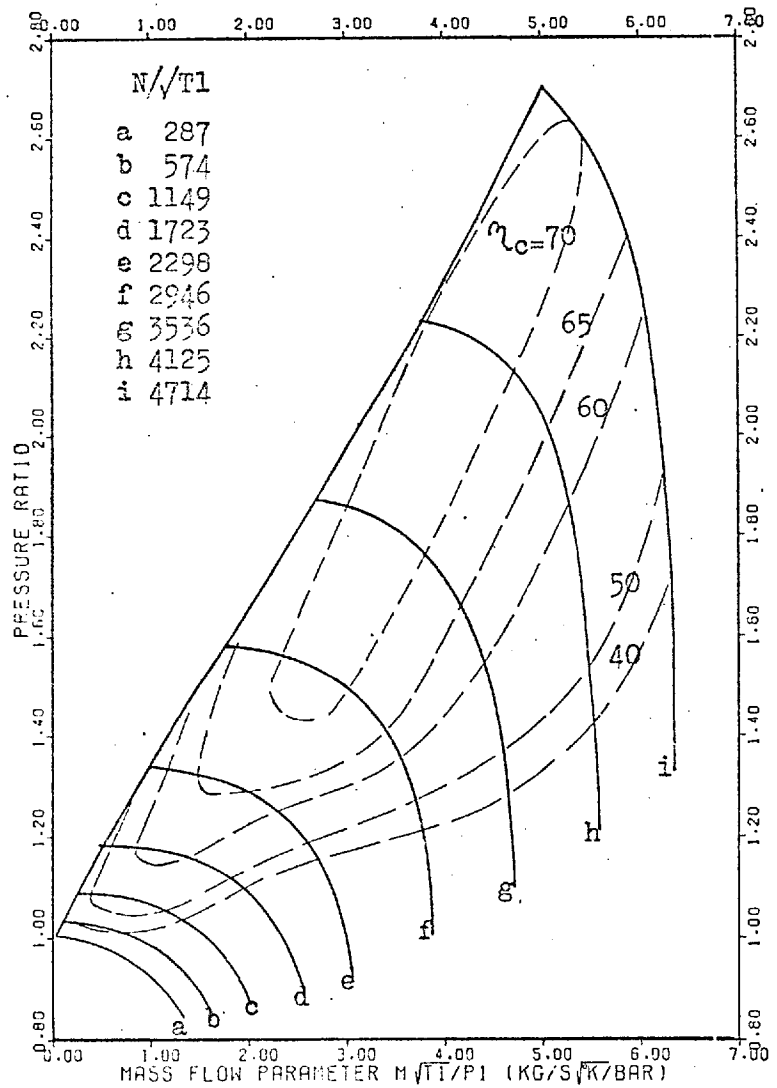


Compressor Performance Map

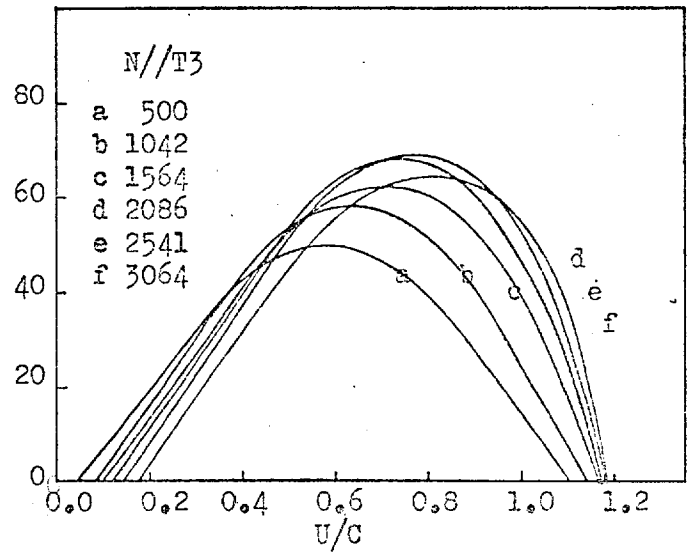


Turbine Efficiency Curves.

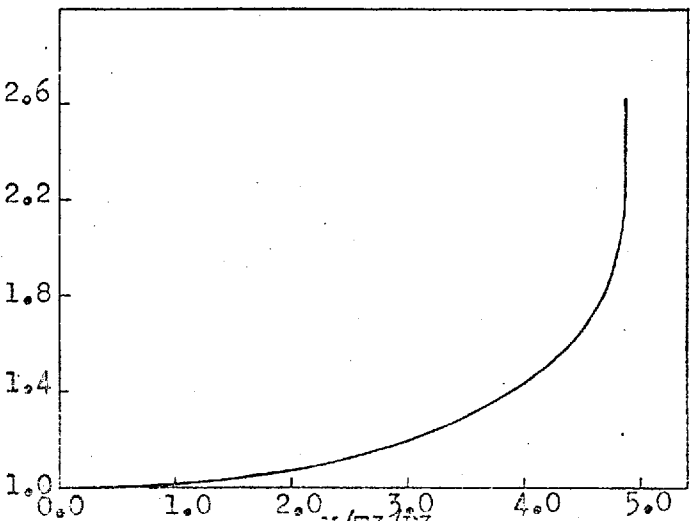


Turbine Swallowing Capacity

FIG.(C.1) Steady State Performance Characteristics of HOLSET 4LE Turbocharger.

# APPENDIX D

## COMPUTATION OF FUEL BURNING RATES FROM EXPERIMENTAL CYLINDER PRESSURE DIAGRAMS: AN ASSESSMENT OF ACCURACY

It has been established that a fuel burning rate curve provides a useful representation of the combustion process in a diesel engine, particularly for engine simulation programs. The calculation of the rate of burning from an experimental cylinder pressure diagram is based on the application of the First Law of Thermodynamics to the contents of the cylinder during combustion (Chapter 6). The factors that have most influence on the overall accuracy of this calculation are discussed below.

### Base line shift of the cylinder pressure diagram

A basic datum shift in the cylinder pressure diagram does not affect the rate of change of pressure. This is fortunate, since the latter is needed for the calculation of the rate of heat release. Drift does, however, make it difficult to establish the exact mass of gas trapped in the cylinder at valve closure.

A useful check on drift is to calculate the standard deviation of a large series of cylinder pressure diagrams, during the intake stroke.

### Temperature sensitivity and thermal shock

Thermal shock can seriously distort the cylinder pressure diagram. This would cause major errors in the fuel burning rate since the calculation relies on the first derivative of cylinder pressure. An effective means of minimizing thermal shock (26) is to recess the pressure

transducers by 3-5 mm. Thermal shielding of the transducer diaphragm is also helpful in this respect, but was not used.

Cylinder volume

The instantaneous volume of the cylinder is normally evaluated via the crank position in relation to T.D.C. The effects of an error of $\pm 2^{o}$CA in the determination of the T.D.C. are shown in Fig. D.1. Apart from the resultant phase shift, the latter part of the fuel burning rate diagram suffers major distortion. Also, the computed total quantity of fuel burnt is in error by $\pm 12\%$. Hence, T.D.C. must be determined accurately.

Figure D.2 illustrates the effect of inaccuracies in values of the clearance volume or compression ratio of the order of $\pm 10\%$. The calculated quantity of fuel burnt has not changed but the burning rate curve is distorted.

Sampling interval

In order to obtain a burning rate curve from a cylinder pressure diagram which is digitised at specific crank angle intervals, numerical differentiation must be used. This is basically an unstable process where accuracy is primarily dependent on interval length. Thus a smaller interval means a more accurate first derivative and a more realistic burning rate curve. Figure D.3 shows the effect of sample interval on burning rate curves. The importance of accurate spacing of the crank angle markers (i.e. accurate and equal intervals) is also implied. Such errors, normally hard to detect, are automatically reproduced in the burning rate curve, and must therefore be reduced at source.

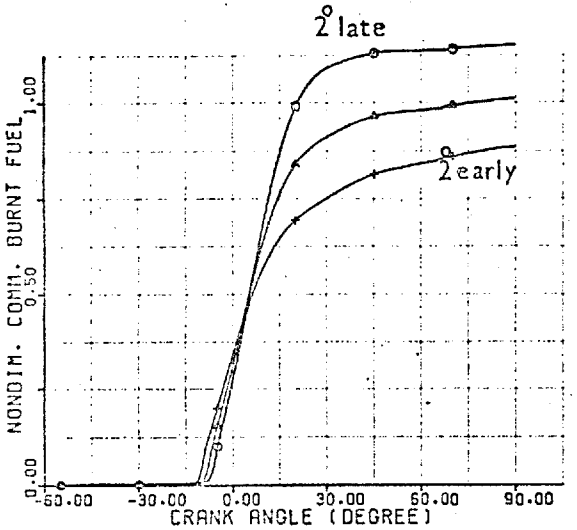


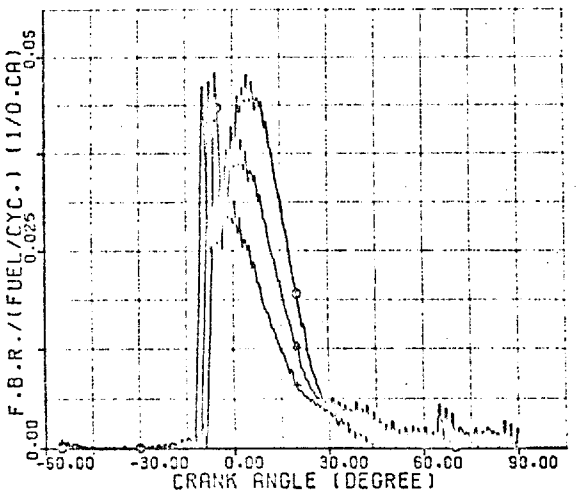


FIG.(D.1) Effect of TDC Position. (±2°CA)

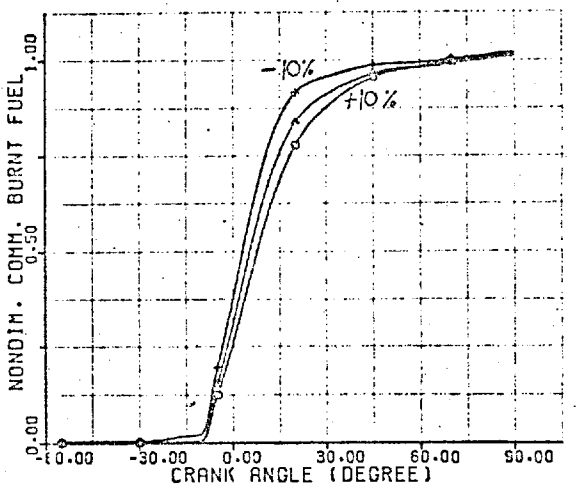


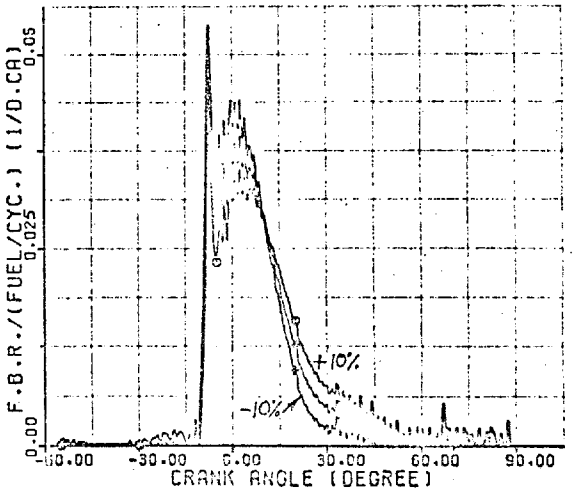


FIG.(D.2) Effect of Errors in Clearance Volume. (±10%)

Cycle averaging

Cyclic variations in combustion in the petrol engine are well known, but similar (although much smaller) variations can occur in diesel engines (120). Since these variations are present, it is important either to record all parameters of interest in a particular engine test during one unique cycle or, for a more representative result, to average over many cycles. Both techniques are easily achieved with computer data logging.

In addition to reducing the effects of cyclic variation, cycle averaging attenuates any random high frequency oscillations, electronic noise, etc., resulting in a more typical diagram.

Quantisation errors

Any data logging system reads off the instantaneous value of a variable at a discrete time (or angular position). The accuracy of the process is governed by the resolution of the analogue to digital convertor (ADC); the choice of which is based on accuracy requirements, computer storage and speed.

With a resolution of 10 binary bits (Chapter 4) quantisation error (expressed in percentage terms) will only become significant at low pressures. This can be reduced by using an offset "zero" and working on a reduced voltage scale, or by employing a low pressure transducer, if possible. Although ADCs of higher resolution have been used by others, there seems little point in doing so. The conversion speed will be reduced and computer storage increased, yet the overall accuracy of the system will probably remain limited by the transducer accuracy.

Smoothing and differentiating the pressure diagram

The rate of change of cylinder pressure has a dominant effect on the burning rate curve. Slight errors in pressure are magnified when the burning rate is computed, hence the differentiation must be conducted with care. It is possible to use an electronic circuit to differentiate the (analogue) cylinder pressure signal, and record the final result digitally, via an ADC. However, the slow response of such circuits may dampen any steep rates present in the pressure curve. As a result, the peak rate of pressure rise may be underestimated. A preferable alternative is numerical differentiation of the digital cylinder pressure diagram.

The quantisation errors, although small, result in spurious derivative values and oscillations in the burning rate curve. Unless the basic (averaged) digital pressure diagram is smoother before differentiation, an oscillating burning rate curve will result. A preferred technique is to fit a smooth curve to the digital pressure diagram and then carry out the differentiation process. However, the following constraints must be imposed on this process:

(a) The error at any point on the curve must be very small and within a specified tolerance (e.g. a fraction of standard deviation).

(b) The curve must be smooth, continuous and non-oscillatory.

(c) The first derivative of the curve must be continuous and stable.

The spline function, as recommended by Streit (99), provides a suitable curve. The extent of smoothing can be adjusted, hence it is simple to achieve a compromise

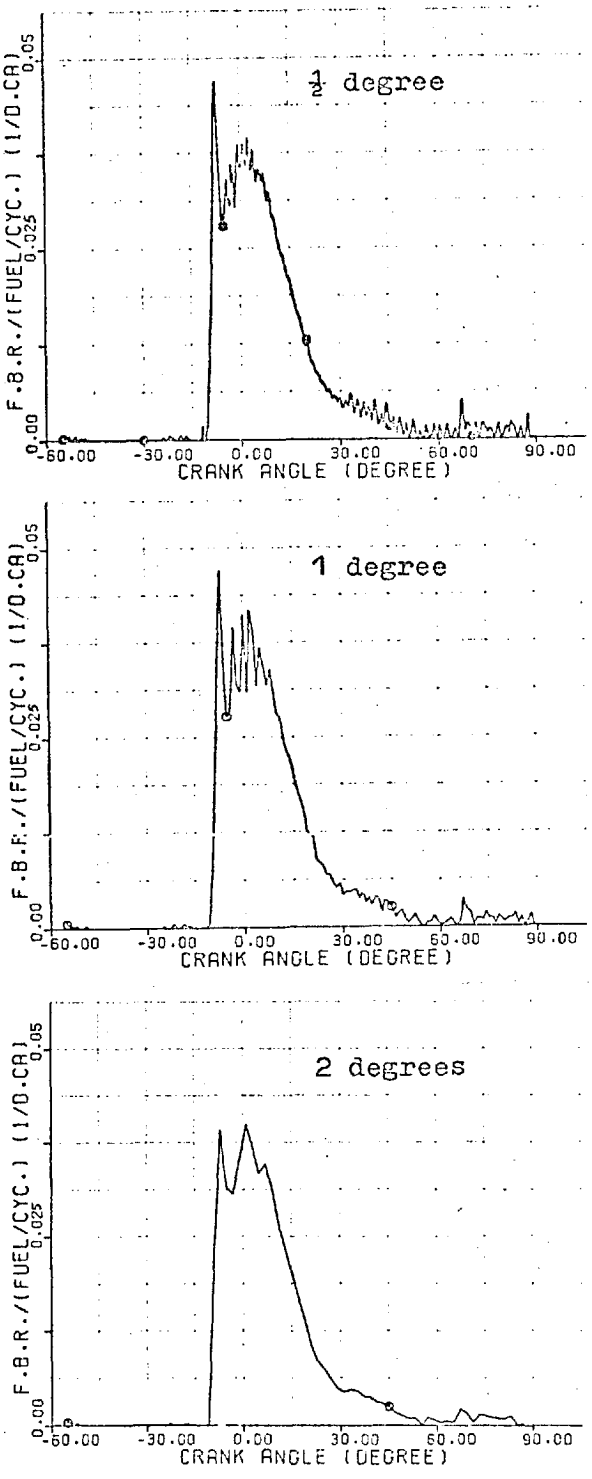


FIG.(D.3) Effect of Sampling Interval.

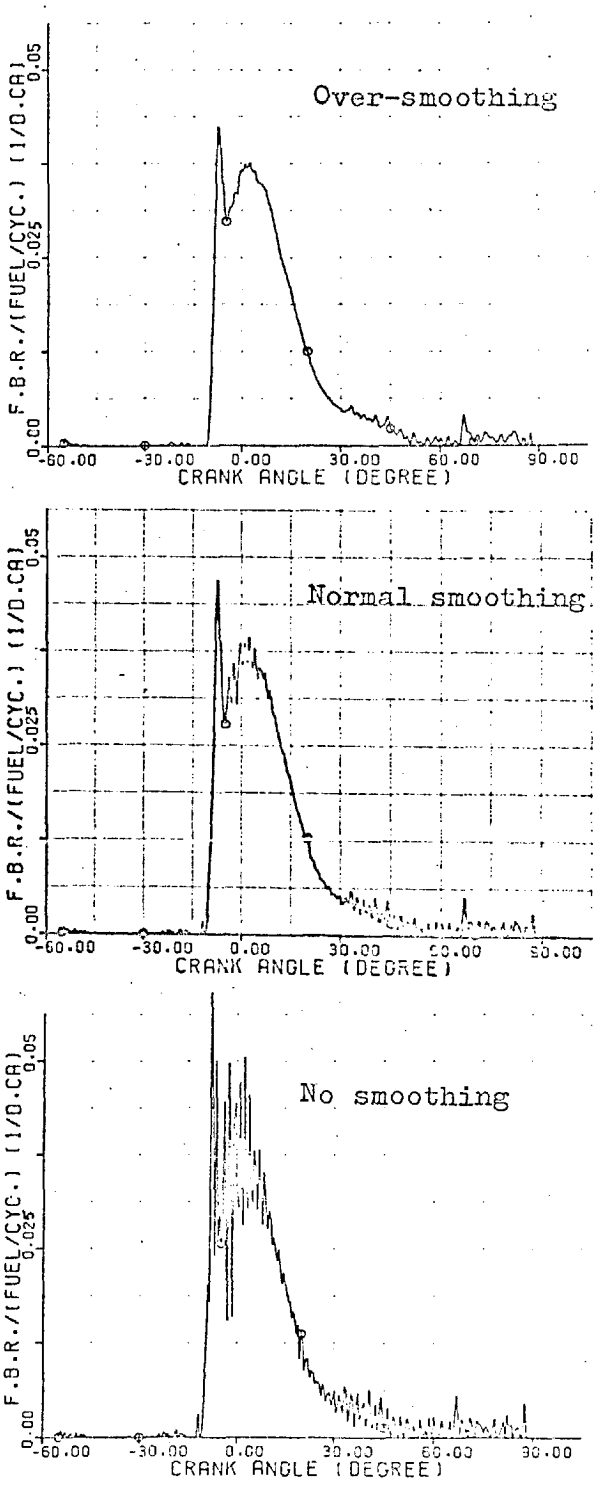


FIG.(D.4) Effect of Smoothing of Cylinder Pressure Diagram.

solution (a non-distorted smooth pressure diagram versus a non-oscillatory fuel burning curve). The effect of smoothing can be seen by comparing the burning rate curves presented in Fig. D.4.

Initial conditions in the cylinder

A reasonably accurate estimate of the mass of charge in the cylinder and, to a lesser extent, its composition, is required for calculating a reliable burning rate. To compute the initial mass, the gas pressure and temperature at valve closure must be known; these being dependent on the intake and exhaust processes (especially in two-stroke engines). At best one can only obtain a reasonable estimate of temperature and pressure and hence trapped mass. Usually the estimate will be within 5%.

Accuracy can be improved by a process of iteration between the burning rate computation and a normal full-cycle analysis programme. Figure D.5 illustrates the effect of a $\pm$5% error in trapped mass on the burning rate calculation. The shape of the burning rate curve remains unchanged, but a small error in the calculated quantity of fuel burnt is introduced. Thus the initial estimate of trapped mass is not a highly sensitive parameter.

Computation of heat transfer

The instantaneous heat transfer rates are computed using semi-empirical heat transfer correlations (Table 2.1). Here, the instantaneous heat transfer coefficient and/or the gas side temperature can be in error. Figure D.6 shows that varying the heat transfer coefficient by $\pm$50% results in little variation in the shape of the burning rate curve. The

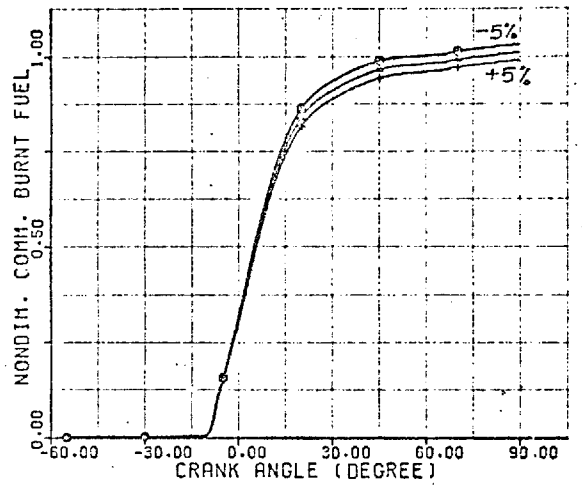


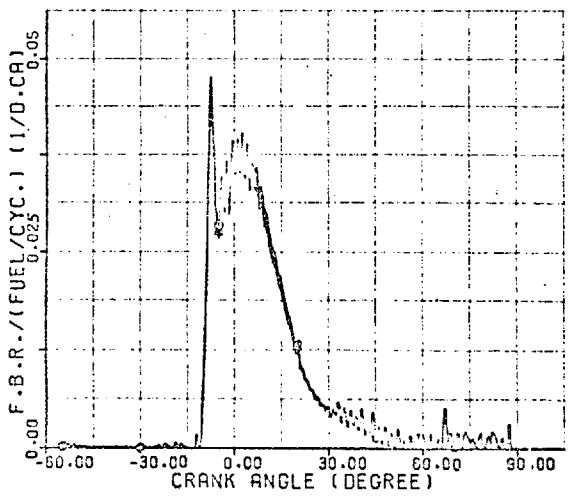


FIG.(D.5) Effect of Errors in Trapped Mass of Charge.($\pm$5%)

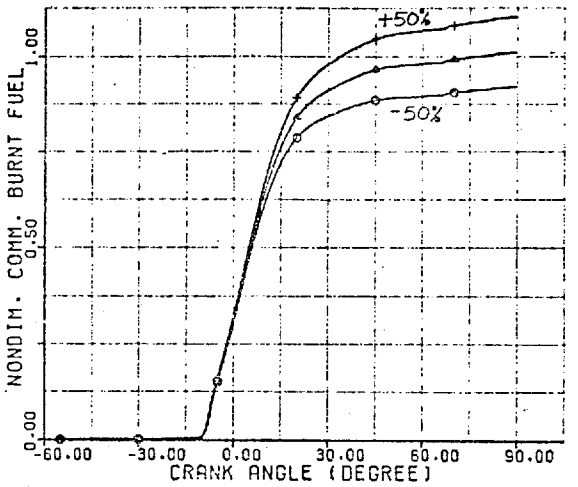


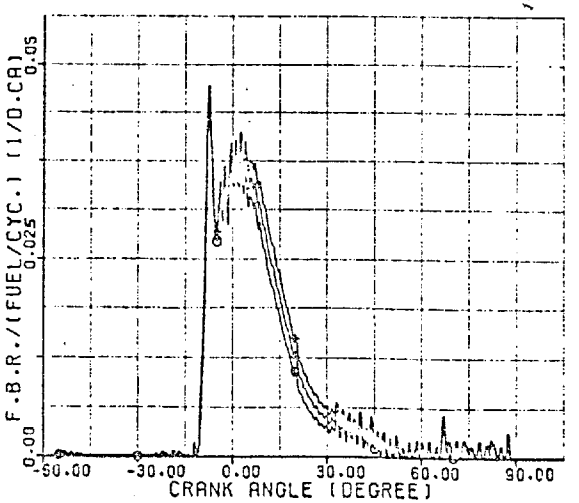


FIG.(D.6) Effect of Errors in the Coefficient of Heat Transfer.($\pm$50%)

calculated quantity of fuel burnt is changed by $\pm 9\%$. Changes in the cylinder wall temperature of $\pm 50^{o}C$ show a negligible effect at the running condition under consideration. However, the effect of wall temperature increases with reduction in engine output.

## PUBLICATIONS

SOME PROBLEMS IN DIESEL ENGINE RESEARCH WITH SPECIAL REFERENCE TO COMPUTER CONTROL AND DATA ACQUISITION

M. MARZOUK
N. WATSON

The Institution of Mechanical Engineers, Combustion Engines Group. Proceedings 1976, Vol. 190 23/76.

Paper presented at a joint Meeting of the Combustion Engines Group and Diesel Engineers and Users Association.

## REFERENCES


1. ALCOCK, J.K. and SCOTT W.M. (1962-63)
   Some more light on Diesel Combustion.
   Proc. Inst. Mech. Eng. (A.D.), (5), p. 179.

2. ANNAND, W.J.D. (1968)
   Choice of a Computing Procedure for Digital Synthesis of Reciprocating Engine Cycles.
   J. of Mech. Eng. Sci., 10, (3), 1968.

3. ANNAND, W.J.D. (1966)
   Compressible Flow through Square-Edged Orifices: An Empirical Approximation for Computer Calculations.
   J. Mech. Eng. Sci., 8, (4), pp. 448-449.

4. ANNAND, W.J.D. (1963)
   Heat Transfer in the Cylinders of Reciprocating Internal Combustion Engines.
   Inst. Mech. Engrs., London, 177, (36).

5. AUSTEN, A.E.W. and LYN, W.T. (1960-1961)
   Relation between Fuel Injection and Heat Release in a Direct-Injection Engine and the Nature of the Combustion Processes.
   Inst. of Mech. Engrs., Auto. Div. Proc.

6. BECCHI, G.A.
   Analytical Simulation of Fuel Injection in Diesel Engines.
   SAE Paper 710568.

7. BENSON, R.S., LEDGER, J.D., WHITEHOUSE, N.D. and WALMSLEY, N.D.
   Comparison of Experimental and Simulated Transient Responses of a Turbocharged Diesel Engine.
   SAE Paper 730666.

8. BENSON, R.S. (1954)
The Flow of Gases in large Two-Stroke Cycle Diesel Engines.
M.Sc. Dissertation (Eng.), University of London.

9. BENSON, R.S. (1955)
Discharge of Gas from a Cylinder to Atmosphere.
Engineer (London), 199, pp. 546, 582, 618.

10. BENSON, R.S. (1957)
Discharge from an Engine Cylinder to Atmosphere.
Engineer (London), 203, pp. 946-949, 976-978.

11. BENSON, R.S. (1959)
Experiments on Two-Stroke Engine Exhaust Ports under Steady and Unsteady Flow Conditions.
Proc. Inst. Mech. Engrs., 173, pp. 511-546.

12. BENSON, R.S. and SCRIMSHAW, K.H. (1965-1966)
An Experimental Investigation of Non-Steady Flow in Radial Gas Turbines.
Proc. Inst. Mech. Engrs., 180, Pt. 3J, pp. 74-88.

13. BENSON, R.S. (1971)
A Comprehensive Computer Programme to simulate a Compression Ignition Engine including Intake and Exhaust Systems.
Paper 71073 presented at SAE Automotive Engineering Congress, Detroit, January 1971..

14. BENSON, R.S.
Prediction of Performance of Radial Gas Turbines in Automotive Turbochargers.
ASME Paper 71-6T-66.

15. BENSON, R.S. and WHITFIELD, A. (1968)
Application of Non-steady Flow in a Rotating Duct to

Pulsating Flow in a Centrifugal Compressor.
Proc. of Inst. Mech. Engrs., 182, Pt. 3H, pp. 184-196.

16. BENSON, R.S. and WHITFIELD, A. (1968)
A Quasi-Steady Flow Representation of Centrifugal Compressor Performance Characteristics in Non-Steady Flow Systems.
Proc. Inst. Mech. Engrs., 182, Pt. 3H, pp. 197-208.

17. BENSON, R.S. (1967-1968)
A Computer Program for calculating the Performance of an Internal Combustion Engine Exhaust System.
Proc. Inst. Mech. Engrs., 182, Pt. 3L, pp. 91-108.

18. BIRMANN, R. and TRENTON, N.J. (1956)
Aerothermodynamic Considerations involved in Turbocharging Four- and Two-Cycle Diesel Engines.
Trans. ASME, January 1956, pp. 171-183.

19. BLOXHAM, R.D. (1972)
Computer Control for I.C. Engines' Development.
CME, 19, (9), October.

20. BODE, E. (1967)
Theoretische Untersuchung der Energieverhältnisse am Abgasturbolader eines turboaufgeladenen Dieselmotors mit pulsierende Beaufschlagung Dieselmotor Nachr.
Rosslau, 1, pp. 21-36.

21. BORMAN, S.L. (1964)
Mathematical Simulation of Internal Combustion Engine Processes and Performance including Comparisons with Experiment.
Ph.D. Thesis, University of Wisconsin.

22. BOWNS, D.E., CAVE, P.R., HARGREAVES, M.R.O. and WALLACE, F.J. (1973)
Transient Characteristics of Turbocharged Diesel Engines.
Inst. Mech. Engrs., Conf. on Engine Performance Modelling, London, May 1973.

23. BOWNS, D.E. (1971)
The Dynamic Characteristics of Reciprocating Engines.
Proc. Inst. Mech. Engrs., 185, (16).

24. BREVES, L. (1938)
Die Fortpflanzung der Verbrennung im Dieselmotor.
VDI-Sonderheft: Dieselmaschinen, VII, pp. 28-36.

25. BRILLING, N.R. (1963)
Investigation of the Heat Transfer in an Internal Combustion Piston Engine.
MIRA Translation No. 25.

26. BROWN, W.L. (1967)
Methods for Evaluating Requirements and Errors in Cylinder Pressure Measurement.
SAE Paper 670008.

27. CHEN, S.K. and FLYN, T. (1965)
Development of a Compression Ignition Research Engine.
SAE Paper 650733.

28. COLIN, R. (1964)
Typical Performance Characteristics of Gas Turbine Radial Compressors.
J. of Engr. for Power, April 1964, pp. 161-175.

29. CONTE, S.D.
Elementary Numerical Analysis.
McGraw-Hill Series in Infoemation Processing and Computers.
McGraw-Hill Book Company, New York, U.S.A.

30. CRAIG, H.R.M., EDWARDS, K.J., HORLOCK, J.H., JANOTA, M., SHAW, R. and WOODS, W.A. (1968-1969)
An Investigation of Steady and Unsteady Flow through a Napier Turboblower Turbine under Conditions of Full and Partial Admission.
Proc. Inst. Mech. Eng., 183, Pt. 1, (30).

31. CRAIG, H. and JANOTA, M. (1965)
The Potential of Turbochargers as applied to Highly Rated Two-Stroke and Four-Stroke Engines.
CIMAC Paper B.14, London.

32. DANESLYAR, H., EDWARDS, K.J., HORLOCK, H.J. JANOTA, M.S., PEARSON, R.D. and SHAW, R. (1969-1970)
A Comparison of the Performance of Three Model Axial Flow Turbines tested under both Steady and Pulse Flow Conditions.
Proc. Inst. Mech. Engrs., 184, Pt. 1, (61).

33. DIGITAL EQUIPMENT CORPORATION (1972)
DOS System Manual: System Architecture, Internal Operation, Maintenance.
Maynard, Massachusetts.

34. DIGITAL EQUIPMENT CORPORATION (1972)
PDP-15 Systems Reference Manual.
Maynard, Massachusetts.

35. DOUDA, P.
Private Communication.
C.V.U.T., Prague, Czechoslovakia.

36. EDGAR, T.F. (1975)
Least Squares Model Reduction using Step Response.
Int. J. Control, 22, (2), pp. 261-270.

37. EGLI, H. (1975)
Transient Torque Responsiveness of Turbocharged Diesel Engines for Vehicles.
The Seminar Technische Akademic Wuppertal, W. Germany.

38. EICHELBERG, G. (1939)
Some new investigations on old Combustion Engine Problems.
Part I Engineering, September 27th, p. 463.

39. ELSER, K. (1954)
Der instantionare Warmübergang in Dieselmotoren.
Mitt. Inst. Thermodyn., Zurich, 15.

40. EL-WAKIL, M.M., MYERS, P.S. and UYEHARA, O.A. (1956)
Fuel Vaporization and Ignition Lag in Diesel Combustion.
Trans. SAE, 64, pp. 712-726.

41. ENGLISH ELECTRIC DIESELS LTD.
Private Communication. (Ruston Paxman Diesels Ltd.)
Lincoln, England.

42. FLOWER, J.O. and GUPTA, R.K. (1974)
Optimal Control Considerations of Diesel Engine
Discrete Models.
Int. J. Control, 19, (6), pp. 1057-1068.

43. GARG, D.P. and BOZIUK, J.S. (1972)
Parameter Estimation of Non-Linear Dynamical Systems.
Int. J. Control, 15, (6), pp. 1121-1127.

44. GEE, D.E. and KARIM, G.A. (1966)
Heat Release in a Compression Ignition Engine.
The Engineer, 222, p. 474.

45. GENERAL ELECTRIC COMPANY (1955)
Properties of Combustion Gases/System: $C_nH_{2n}$-Air.
Volumes 1 and 2 G.E.C. Aircraft Gas Turbine Development
Department, Cincinnati, Ohio, U.S.A.

46. GIBSON, J.E.
Nonlinear Automatic Control.
International Student Edition, McGraw-Hill Book Co.,
New York.

47. GIFFEN, E. and ROWE, A.W. (1939)
Pressure Calculations for Oil Engine Fuel-Injection Systems.
Proc. Inst. Mech. Engrs., 141, p. 519.

48. GILLESPIE, D.A., SMITH, R.N. and TAYLOR, P.J. (1968)
Automatic Control and Associated Problems with High Pressure Charged Engines.
C.I.M.A.C., Brussels Conference.

49. GREENHALGH, R., TOOTH, P. and BICKELY, I.J. (1975)
Application Engineering Techniques related to High Performance, Medium Speed Diesel Engines.
C.I.M.A.C. Congress.

50. GILCHRIST, J.M. (1948)
Chart for the Investigation of Thermodynamic Cycles in Internal Combustion Engines and Turbines.
Proc. Inst. Mech. Engrs., London, 159, p. 335.

51. HAMMING, R.W. (1962)
Numerical Methods for Scientists and Engineers.
McGraw-Hill Book Co.

52. HAZELL, P.A. and FLOWER, J.O. (1971)
Sampled-Data Theory applied to the Modelling and Control Analysis of Compression Ignition Engines. Part I.
Int. J. Control, 13, (3), pp. 549-562.

53. HENEIN, N.A. (1964)
Instantaneous Heat Transfer Rates and Coefficients between the Gas and Combustion Chamber of a Diesel Engine.
SAE Trans.

54. HORLOCK, J.H. and WOODS, W.A. (1966)
The Thermodynamics of Charging and Discharging Processes.
Inst. Mech. Engrs., Thermodynamics and Fluid Mechanics Convention.

55. HORLOCK, J.H. and BENSON, R.S. (1962)
The Matching of Two-Stroke Engines and Turbochargers.
G.IM.A.C. (Copenhagen), A.10.

56. HOWARTH, M.H. (1966)
The Design of High Speed Diesel Engines. Constable & Co., London

57. ILMARI, E.J. (1965)
The Spray Impingement Theory of Ignition Delay in Small Swirl Chamber Diesel Engines.
Thesis for Degree of Doctor of Technology, Institute of Technology, Helsinki, February 1965.

58. IZUMI, S., OMOTEHARA, I., YANO, T. and KUSHIYAMA, T.
Matching of Exhaust Turbochargers to Two-Cycle Diesel Engines.
ASME, Paper 68-DGP-9.

59. JAMOULLE, A. (1973)
Etudes et recherches sur les regimes transitoires des moteurs diesel a 4 temps et a haute suralimentation.
Reveu Universelle des Mines, 4, December 1973.

60. JANOTA, M.S., HALLAM, A.J., BROCK, E.K. and DEXTER, S.G. (1967-1968)
The Prediction of Diesel Engine Performance and Combustion Chamber Component Temperatures using Digital Computers.
Proc. Inst. Mech. Engrs., 182, Pt. 3L.

61. JANOTA, M.S. (1969)
Quasi-Steady Analysis applied to Turbocharged Engine Performance.
Ph.D. Thesis, University of London, 1969.

62. JONES, T.F. and WING, R.D. (1975)
On-line Computer Control for Automatic Testing of I.C. Engines.
Conference on Advances in Automatic Testing Technology, Inst. of Elect. and Radio Engrs., April.

63. KNIGHT, B.E. (1960-1961)
Fuel Injection System Calculations.
Proc. Inst. Mech. Engrs., Automobile Div., 1.

64. KRIEGER, R.B. and BORMAN, G.L. (1966)
The Computation of Apparent Heat Release for Internal Combustion Engines.
ASME Paper, No. 66-WA/DGP-4.

65. LANGE, K. (1969)
Berechnung von Druckverlang und Wirkungsgrad im Verbrennungsmotor.
Motortechnische Zeitschrift, 30, pp. 173-176.

66. LEDGER, J.D. and WALMSLEY, N.D. (1971)
Computer Simulation of a Turbocharged Diesel Engine operating under Transient Load Conditions.
Paper 710177 presented as SAE Automotive Engineering Congress, Detroit, January.

67. LEDGER, J.D., BENSON, R.S. and WHITEHOUSE, N.D. (1973)
Dynamic Modelling of a Turbocharged Diesel Engine.
Inst. Mech. Engrs., Conf. on Engine Performance Modelling, London, May.

68. LEDGER, J.D., BENSON, R.S. and FURUKAWA, H. (1973)
Improvements in Transient Performance of a Turbocharged Diesel Engine by Air Injection into the Compressor.
Paper 730665 presented at SAE combined Commercial Vehicle Engineering and Operations and Powerplant Meetings, Chicago, June.

69. LE FEUVRE, T., MEYRS, P.S. and UYEHARA, O.A.
Experimental Instantaneous Heat Fluxes in a Diesel Engine and their Correlation.
SAE Paper 690464.

70. LYNN, W.T. (1962)
Study of Burning Rate and Nature of Combustion in Diesel Engines.
9th Symposium on Combustion, Cornel Univ.

71. LYNN, W.T. (1960-1961)
Calculations of the Effect of Rate of Heat Release on the Shape of Cylinder Pressure Diagram and Cycle Efficiency.
Proc. Inst. Mech. Engrs., 174, pp. 34-46.

72. LYNN, W.T. and VALDMANIS, E.
The Effects of Physical Factors On Ignition Delay.
Inst. Mech. Engrs.

73. MARZOUK, M. (1972)
On-Line Control of Internal Combustion Engines under Transient Conditions.
M.Sc. Thesis, University of London.

74. MASSAY, A.G. and OLDENBURGER, R. (1958)
Scientific Design of a Diesel Governor.
Trans. ASME, Paper No. 58-OGP-11.

75. MELLINGTON, B.W. and HARTLES, E.R.
Frictional Losses in Diesel Engines.
Ricardo & Co. Engineers (1927) Ltd.
SAE Paper 680590.

76. METZ, J.R., URBER, A., STEIGER, A. (1967-1968)
Contribution to the Investigation of the Diesel Cycle with the Aid of Digital Computers.
Proc. Inst. Mech. Engrs., 182, Pt. 3L.

77. MIYASHITA, T., TOMITA, T. and ISHIHARA, D. (1974)
Performance of Inward Radial Flow Turbine under Unsteady Flow Conditions, Influence of Pulse Frequency.
I.H.I Engineering Review, Vol. 7, (1), January.

78. NAGAO, F., IKEGAMI, M., OSHIMA, K. (1967)
An Analysis of Combustion Known in a Diesel Engine.
Bull. JSME, 10, (39), pp. 531-542.

79. NOTTINGHAM ALGORITHMS GROUP
A Subroutine to minimize a Sum of Squares of m non-linear Functions or Residuals.
Subroutine E04FBF, N.A.G. Library, ICL 1900 System.

80. NUSSELT, W. (1923)
Die Warneübergang in den Verbrennungskraftmachinen.
Z. der Ver. dtsch. Ing., 67, pp. 629-708.

81. OBERT, E.F. (1968)
Internal Combustion Engines.
3rd Edition, International Textbook Co., Scranton, Pa.

82. OGATO, K.
Modern Control Engineering.
Prentice-Hall Inc., Englewood Cliffs, N.J., U.S.A.

83. OUGURI, T. (1960)
On the Coefficient of Heat Tranfer between Gases and Cylinder Walls of the Spark Ignition Engine.
Bull. Japan Soc. Mech. Engrs., 3, p. 363.

84. PEDERSON, P.S. and QVALE, B.
A Model for the Physical Part of the Ignition Delay in a Diesel Engine.
SAE 740716.

85. PFLAUM, W. (1962)
New Investigations and Experience relating to the Turbocharging of large Two-Stroke Engines.
CIMAC, A11.

86. POWELL, H.N. (1956)
Applications of an Enthalpy-Fuel/Air Ratio Diagram to

'First Law' Combustion Problems.
ASME, Gas Turbine Power and Machine Design Divisions, Semi-Annual Meeting, Cleveland, Ohio, 17-21 June.

87. POWELL, M.J.D. (1968)
A Fortran Subroutine for solving Systems of non-linear Algenraic Equations.
Harwell Report. AERE-R5947.

88. REDFIELD, J.A. and MURPHY, J.H.
Sectionalised Compressible and Momentum Integral Models for Channel Hydrodynamics.
ASME 71-HT-14.

89. SCHMIDT, F.A.F. (1938)
Theoretische Untersuchung und Versuche über Zundverzug und Klopfvorgang.
VDI-Forschungsheft, 392, pp. 1-14.

90. SCHWEITZER, P.H. (1926)
The Tangent Method of Analysis for Indicator Cards of Internal Combustion Engines.
Bull. No. 35, Penn. State Exp. Sta., September 1926.

91. SHIPINSKI, J.H., UYEHARA, O.A. and MYERS, P.S.
Experimental Correlation between Rate of Injection and Rate of Heat Release in a Diesel Engine.
ASME Paper 68-DGP-11.

92. SHIPINSKI, J.H., MYERS, P.S. and UYEHARA, O.A. (1970)
A Spray Droplet Model for Diesel Combustion.
Proc. of Inst. Mech. Engrs.

93. SITKEI, G. (1963)
Uber den dieselmotorischen Zundverzug.
MTZ, 24 Jg, 6, June, pp. 190-194.

94. SITKEI, G. (1974)
Heat Transfer and Thermal Loading in Internal

Combustion Engines.
Akademiai Kado, Budapest.

95. SITKEI, G. (1962)
Contribution to the Theory of Heat Transfer in the Internal Combustion Engines.
Konstruktion, 14, (2), pp. 67-71.

96. SMITH, J.M. (1972)
A Fixed-Head Concept Diesel Engine.
Proc. Inst. Mech. Engrs., 186

97. STANITZ, J.D. (1952)
Some Theoretical Aerodynamic Investigations of Impellers in Radial and Mixed Flow Centrifugal Compressors.
Trans. ASME, 74/1952.

98. STREIT, E.E.
Mathematical Simulation of a larger Pulse-Turbocharged Two-Stroke Diesel Engine.
Ph.D. Thesis, University of Wisconsin.

99. STREIT, E.E. and BORMAN, G.L. (1971)
Mathematical Simulation of a large Turbocharged Two-Stroke Diesel Engine.
Trans. SAE, Paper 71076.

100. TANASAWA, Y. (1953)
On the Combustion Rate of a Group of Fuel Particles.
Technology Reports of Tohoku Univ., 18, (1), pp. 61-74.

101. THOMPSON, E.J. Private Communication. Also:
BAKER, R.C. and THOMPSON, E.J. (1975)
A Two Beam Ultrasonic Phase-Shift Flowmeter.
Conf. on Fluid Flow Measurements in the Mid 1970's.
8-10 April, National Engineering Laboratory, East Kilbride, Scotland, U.K.

102. TODA, N., KUSHIYAMA, T. and OYAMA, T. (1969)
On a Method of Calculating Characteristics of Exhaust

Gas Turbocharged Two-Stroke Diesel Engines.
Bull. JSME, Paper 621-436-05.

103. TSAO, K.C., MYERS, P.S. and UYEHARA, O.A. (1962)
Gas Temperature during Compression in Motored and Fired Diesel Engine.
Trans. SAE, 70, 136.

104. WALLACE, F.J., ADGEY, J.M. and BLAIR, G.P. (1969-1960)
Performance of Inward Radial Flow Turbines under Non-Steady Flow Conditions.
Proc. Inst. Mech. Engrs., 184, Pt. 1, (10).

105. WALLACE, F.J. and BLAIR, G.P. (1965)
The Pulsating-Flow Performance of Inward Radial-Flow Turbines.
ASME Paper 65-GTP-21.

106. WALLACE, F.J. and ADGEY, J.M.
Theoretical Assessment of Non-Steady Flow Performance of Inward Radial Flow Turbines.
Proc. Inst. Mech. Engrs., 182, Pt. 3H.

107. WALLACE, F.J. and CAVE, P.R. (1973)
Matching of High-Output Diesel Engines with Associated Turbomachinery.
Proc. Inst. Mech. I., 187, (48).

108. WALLACE, F.J., CAVE, P.R. and MILES, J. (1969-1970)
Performance of Inward Radial Flow Turbines under Steady Flow Conditions with Special Reference to High Pressure Ratios and Partial Admission.
Proc. Inst. Mech. Engrs., 184, Pt. 1, (56).

109. WALLACE, F.J. and MILES, J.
Performance of Inward Flow Turbines under Unsteady Flow Conditions with Full and Partial Admission.

110. WALLACE, F.J. and BOXER, G. (1956)
Wave Action in Diffusers for Exhaust Pipe Systems, with special reference to the Scavenging of Two-Stroke Engines.
Proc. Inst. Mech. Engrs., 170, pp. 1131-1156.

111. WALLACE, F.J. and MITCHELL, R.W.S. (1951)
Wave Action following the Sudden Release of Air through an Engine Port System.
Engineering (London), 172, pp. 423.

112. WALLACE, F.J. and MITCHELL, R.W.S. (1952)
Wave Action and the Sudden Release of Air through an Engine Port System.
Gas and Oil Power, 47, pp. 287-291.

113. WALLACE, F.J. and NASSIF, M.H. (1954)
Air Flow in Naturally Aspirated Two-Stroke Engines.
Proc. Inst. Mech. Engrs., 168, pp. 515-544.

114. WELBOURN, D.B., ROBERTS, D.K. and FULLER, R.A. (1959)
Governing of Compression-Ignition Oil Engines.
Inst. Mech. Engrs., 173, (22).

115. WHITEHOUSE, N.D., STOTTER, A., GOUDIE, G.O. and PRENTICE, B.W. (1962)
Method of Predicting some Aspects of Performance of a Diesel Engine using a Digital Computer.
Proc. Inst. Mech. Engrs., 176, (9).

116. WHITEHOUSE, N.D. and WAY, R. (1969-1970)
Rate of Heat Release in Diesel Engines and its Correlation with Fuel Injection Data.
Proc. Inst. Mech. Engrs., 184, Pt. 3J.

117. WIEBE, I. (1956)
Habempirische Formel für die Verbrennungsgeschwindigkeit.
Verlag der Akademie der Wissenschaften der VdSSR, Moscow.

118. WILLIS, D.N. and JONES, T.F.
Ford Software System.
Internal progress report, Thermal Power Section, Mech. Eng. Dept., Imperial College of Science & Technology, London.

119. WINDETT, G.P. and FLOWER, J.O. (1974)
Sampled-data Frequency Response Measurements of a large Diesel Engine.
Int. J. Control, 19, (6), pp. 1069-1086.

120. WING, R.D Private Communication, and
WING, R.D. (1975)
The Rotary Fuel Injection Pump as a Source of Cyclic Variation in Diesel Engines and its Effects on Nitric Oxide Emissions.
Proc. Inst. Mech. Engrs., 189, (5).

121. WOLFER, H.H. (1938)
Der Zündverzug im Dieselmotor.
VDI-Forschungsheft 392, pp. 15-24.

122. WOODS, W.A. and KHAN, S.R. (1968)
Discharge from a Cylinder through a Poppet Valve to an Exhaust Pipe.
Inst. Mech. Engrs. Thermodynamics and Fluid Mechanics Convention.

123. WOSCHNI, G. (196 )
A Universally Applicable Equation for the Instantaneous Heat Transfer Coefficient in the Internal Combustion Engine.
Paper 670931 presented at SAE Combined National Meetings, Pittsburgh, Pa.

124. WOSCHNI, G. (1965)
Computer Programs to determine the Relationship between Pressure Flow, Heat Release and Thermal Load in Diesel Engines.
SAE Paper 650450 presented at Chicago, Illinois, May 1965.

125. WOSCHNI, G. and ANISITS, F.
Experimental Investigation and Mathematical Presentation of Rate of Heat Release in Diesel Engines dependent upon Engine Operating Conditions.
SAE Paper No. 740086.

126. WYLIE, E.B., BOLT, J.A. and EL-ERIAN, M.F.
Diesel Fuel Injection System Simulation and Experimental Correlation.
SAE Paper 710569.

127. YAMAOKA, K., SAITO, A. and OKAYAKI, M. (1972)
Analysis of By-Pass Control Type Fuel Injection System for Small Diesel Engine by Digital Computer. Parts 1 and 2.
Bull. of JSME, 15, (82).

128. ZAPF, H. (1969)
Beitrag zur Untersuchung des Warmeübergangs während des Ladungswechsels im Viertakt-Dieselmotor.
Motortechnische Zeitschrift, 30, (12), pp. 461-465.

129. ZIMMERMANN, K.D. (1962)
Uber dem Zündverzug bei der dieselmotorischen Verbrennung.
Diss. Karlsruhe, p. 138.

130. ZINNER, K. (1961)
Diagramme zur Bestimmung des Betriebspunktes einstufiger Abgasturbolader.
M.A.N. Forschungsheft, p. 63.